frontiers | Research Topics

Marine omics in a changing ocean: Modelling molecular pathways and networks to understand species acclimation and adaptation

Edited by
Carolina Madeira, Piero Calosi and Diana Sofia Madeira

Published in
Frontiers in Marine Science
Frontiers in Ecology and Evolution

ISSN 1664-8714
ISBN 978-2-8325-5151-6
DOI 10.3389/978-2-8325-5151-6

About Frontiers

Frontiers is more than just an open access publisher of scholarly articles: it is a pioneering approach to the world of academia, radically improving the way scholarly research is managed. The grand vision of Frontiers is a world where all people have an equal opportunity to seek, share and generate knowledge. Frontiers provides immediate and permanent online open access to all its publications, but this alone is not enough to realize our grand goals.

Frontiers journal series

The Frontiers journal series is a multi-tier and interdisciplinary set of open-access, online journals, promising a paradigm shift from the current review, selection and dissemination processes in academic publishing. All Frontiers journals are driven by researchers for researchers; therefore, they constitute a service to the scholarly community. At the same time, the *Frontiers journal series* operates on a revolutionary invention, the tiered publishing system, initially addressing specific communities of scholars, and gradually climbing up to broader public understanding, thus serving the interests of the lay society, too.

Dedication to quality

Each Frontiers article is a landmark of the highest quality, thanks to genuinely collaborative interactions between authors and review editors, who include some of the world's best academicians. Research must be certified by peers before entering a stream of knowledge that may eventually reach the public - and shape society; therefore, Frontiers only applies the most rigorous and unbiased reviews. Frontiers revolutionizes research publishing by freely delivering the most outstanding research, evaluated with no bias from both the academic and social point of view. By applying the most advanced information technologies, Frontiers is catapulting scholarly publishing into a new generation.

What are Frontiers Research Topics?

Frontiers Research Topics are very popular trademarks of the *Frontiers journals series*: they are collections of at least ten articles, all centered on a particular subject. With their unique mix of varied contributions from Original Research to Review Articles, Frontiers Research Topics unify the most influential researchers, the latest key findings and historical advances in a hot research area.

Find out more on how to host your own Frontiers Research Topic or contribute to one as an author by contacting the Frontiers editorial office: frontiersin.org/about/contact

Marine omics in a changing ocean: Modelling molecular pathways and networks to understand species acclimation and adaptation

Topic editors
Carolina Madeira — NOVA University Lisbon, Portugal
Piero Calosi — Université du Québec à Rimouski, Canada
Diana Sofia Madeira — University of Aveiro, Portugal

Citation
Madeira, C., Calosi, P., Madeira, D. S., eds. (2024). *Marine omics in a changing ocean: Modelling molecular pathways and networks to understand species acclimation and adaptation*. Lausanne: Frontiers Media SA.
doi: 10.3389/978-2-8325-5151-6

Table of contents

frontiers | Frontiers in Marine Science

ORIGINAL RESEARCH
published: 28 July 2022
doi: 10.3389/fmars.2022.925845

Genetic Variation in Heat Tolerance of the Coral *Platygyra Daedalea* Indicates Potential for Adaptation to Ocean Warming

Holland Elder[1]*, *Virginia M. Weis*[1], *Jose Montalvo-Proano*[2,3], *Veronique J. L. Mocellin*[2], *Andrew H. Baird*[3], *Eli Meyer*[1†] *and Line K. Bay*[2†]

[1] *Integrative Biology, Oregon State University, Corvallis, OR, United States*, [2] *Australian Institute of Marine Science, AIMS@ James Cook University (JCU), Cape Cleveland, QLD, Australia*, [3] *ARC Centre of Excellence for Coral Reef Studies, James Cook University, Townsville, QLD,, Australia*

OPEN ACCESS

Edited by:
Diana Sofia Madeira, University of Aveiro, Portugal

Reviewed by:
Catarina Vinagre, University of Algarve, Portugal
Marta Andreia Dias, Center for Marine and Environmental Sciences (MARE), Portugal

***Correspondence:**
Holland Elder
hollandelder@gmail.com

[†]*These authors contributed equally and share last authorship*

Specialty section:
This article was submitted to Marine Molecular Biology and Ecology, a section of the journal Frontiers in Marine Science

Received: *22 April 2022*
Accepted: *06 June 2022*
Published: *28 July 2022*

Citation:
Elder H, Weis VM, Montalvo-Proano J, Mocellin VJL, Baird AH, Meyer E and Bay LK (2022) Genetic Variation in Heat Tolerance of the Coral Platygyra Daedalea Indicates Potential for Adaptation to Ocean Warming. Front. Mar. Sci. 9:925845. doi: 10.3389/fmars.2022.925845

Ocean warming represents the greatest threat to the persistence of reef ecosystems. Most coral populations are projected to experience temperatures above their current bleaching thresholds annually by 2050. Adaptation to higher temperatures is necessary if corals are to persist in a warming future. While many aspects of heat stress have been well studied, few data are available for predicting the capacity for adaptive cross-generational responses in corals. Consistent sets of heat tolerant genomic markers that reliably predict thermal tolerance have yet to be identified. To address this knowledge gap, we quantified the heritability and genetic variation associated with heat tolerance in *Platygyra daedalea* from the Great Barrier Reef. We tracked the survival of ten quantitative genetic crosses of larvae produced form six parental colonies in a heat tolerance selection experiment. We also identified allelic shifts in heat-selected (35°C) survivors compared with paired, non-selected controls (27°C). The narrow-sense heritability of survival under heat stress was 0.66 and a total of 1,069 single nucleotide polymorphisms (SNPs) were associated with different survival probabilities. While 148 SNPs were shared between several experimental crosses, no common SNPs were identified for all crosses, which suggests that specific combinations of many markers are responsible for heat tolerance. However, we found two regions that overlap with previously identified loci associated with heat tolerance in Persian Gulf populations of *P. daedalea*, which reinforces the importance of these markers for heat tolerance. These results illustrate the importance of high heritability and the complexity of the genomic architecture underpinning host heat tolerance. These findings suggest that this *P. daedalea* population has the genetic prerequisites for adaptation to increasing temperatures. This study also provides knowledge for the development of high throughput genomic tools which may screen for variation within and across populations to enhance adaptation through assisted gene flow and assisted migration.

Keywords: heritability, genomic markers, allele frequency change, coral reefs, resilience, thermal tolerance

INTRODUCTION

Ocean warming induced by anthropogenic climate change has increased the frequency and severity of coral bleaching events worldwide to the point that it is recognized as the primary threat to coral reefs (Hutchings et al., 2019; Souter et al., 2020). Bleaching is the process in which dinoflagellate symbionts (Family Symbiodiniaceae) are lost or expelled from host corals and/or their pigments per symbiont are lost (e.g. Hoegh-Guldberg and Smith, 1989; Fitt and Warner, 1995; Smith et al., 2005; Hume et al., 2013; Lajeunesse et al., 2018). As symbiont photosynthesis provides the majority of host nutritional requirements, mass coral bleaching caused by marine heat waves can result in rapid and widespread coral mortality (Glynn, 1993). Global and regional bleaching events have resulted in a substantial loss of coral cover worldwide over the last few decades (Hughes et al., 2017; Hughes et al., 2018). Over the last five years alone, 30% of reefs in the Great Barrier Reef (GBR) showed decreases in coral cover (Hughes et al., 2018; Hughes et al., 2019; Long Term Reef Monitoring Program, 2019).

For coral reef ecosystems to persist in an ocean that will continue to warm for the foreseeable future, corals will need to rapidly become more tolerant or resilient to higher temperatures. Consequently, there is an urgent need to understand the adaptive capacity of corals to this threat across ocean basins and populations to inform conventional management approaches. This knowledge is also required for restoration and adaptation programs using assisted gene flow and assisted migration to enhance the tolerance of local populations as adaptive capacity can help determine which populations should be used to stock nursery and breeding programs (van Oppen et al., 2015). Working knowledge of the genomic regions that influence heat tolerance, the extent to which coral host genetics contributes to heat tolerance, and its cross generational persistence in a population will be essential to predict corals' responses to climate change into the future.

Mechanisms of thermal and bleaching tolerance are diverse, and both hosts and symbionts are known to contribute to the holobiont phenotype. For example, different symbiont species can confer different thermal tolerances in the same host species (Fuller et al., 2020). In addition, the shuffling of low background densities of heat tolerant symbiont species can aid in recovery from heat stress by facilitating coral calcification and thus reef accretion (Berkelmans and van Oppen, 2006; Oliver and Palumbi, 2011; Silverstein et al., 2014; Bay et al., 2016; Manzello et al., 2018). Many studies have also documented genetic variation in coral host heat tolerance that supports the potential for adaptation (Meyer et al., 2009; Kenkel et al., 2013; Woolsey et al., 2014; Dixon et al., 2015; Howells et al., 2016; Bay et al., 2017; Matz et al., 2020). Differential gene expression has been associated with heat tolerance in a number of coral species (e.g., Barshis et al., 2013; Kenkel et al., 2016; Ruiz-jones and Palumbi, 2017; Traylor-knowles et al., 2017). While some studies have identified genomic markers in coding and non-coding genes that are associated with a heat tolerant phenotype, no consensus has yet emerged regarding a set of 'candidate genes' (Bay and Palumbi, 2014; Dixon et al., 2015; Jin et al., 2016; Dziedzic et al., 2019; Fuller et al., 2020). Furthermore, the genetic architecture underpinning heat tolerance remains largely unknown.

Coral heat tolerance is likely a complex polygenic trait controlled by many alleles of small effect, which complicates efforts to identify loci in part due to the statistical challenge of distinguishing signal from noise (Fuller et al., 2020). Polygenicity is well documented in diverse traits in agricultural species, model organisms, and humans (reviewed in Sella and Barton, 2019), but remains difficult to detect because most genotyping methods are biased towards detecting loci of large effect (Wellenreuther and Hansson, 2016). Although methodological challenges remain, genome-wide association studies have yielded insight into the genomic basis of key performance traits in a number of species. For example, in plants, allele frequency analysis has identified markers associated with traits such as yield, drought tolerance, and heat tolerance (Venuprasad et al., 2009; Vikram et al., 2012; Singh et al., 2017; Wang et al., 2019). Consequently, great interest remains in identifying and developing genomic marker sets for conservation, restoration and adaptation applications (Baums et al., 2019).

Even in the absence of predictive markers, knowledge of trait heritability can inform breeding programs (Falconer and Mackay, 1996; Lynch and Walsh, 1998) and the development of predictive models (Gienapp et al., 2013). If variation in a fitness-related phenotype is heritable and not otherwise constrained, then selection can act to further propagate it within populations (Charmantier and Garant, 2005). Narrow-sense heritability (h^2) describes the total phenotypic variance in a trait that can be attributed to parental or additive genetics and is used to determine the genetic contribution to traits such as heat tolerance (Falconer and Mackay, 1996; Lynch and Walsh, 1998). To model the persistence of a trait in a population with the breeder's equation, estimates of narrow-sense heritability are essential for calculating selection differentials (Falconer and Mackay, 1996; Lynch and Walsh, 1998). Specifically, estimates of narrow-sense heritability of heat tolerance in corals will allow us to calculate potential rates of adaptation under various selection scenarios.

Current estimates of narrow-sense heritability suggest that the genetic variation to support adaptation of increased heat tolerance is present in coral populations in many different regions. For example, a heritability value of 0.58 was found for bleaching resistance in *Orbicella faveolata* in the Caribbean (Dziedzic et al., 2019) and values between 0.49 and 0.75 for heat tolerance in *Platygyra daedalea* in the Persian Gulf (Kirk et al., 2018). Heritability was similarly high for two *Acropora* species from the GBR: $h^2 = 0.87$ for heat tolerance in the larvae of the coral *A. millepora* (Dixon et al., 2015) and $h^2 = 0.93$ for survival during heat stress in the recruits of *A. spathulata* (Quigley et al., 2020). However, heritability can vary substantially between species, as well as between populations of conspecifics, and is influenced by the environment in which it is measured (Falconer and Mackay, 1996; Lynch and Walsh, 1998). Therefore, a heritability estimate from the Persian Gulf should not be used to estimate selection for heat tolerance or potential for adaptation in a population on the GBR, but a comparison among regions can inform understanding of the evolutionary potential of the species. To understand the heritability of heat tolerance, selection for heat

tolerance, and the potential for adaptation in GBR populations, more heritability estimates of heat tolerance from populations on the GBR are needed (Bairos-Novak et al., 2021).

Cross ocean basin comparisons of heritability and the genetic basis of heat tolerance are important for assessing whether results from one region can be extrapolated to another. *Platygyra daedalea*, an important reef building boulder or massive brain coral, is a good candidate species for this type of study because it is widely distributed in the Indo-Pacific and also occurs in the much warmer Persian Gulf (D'Angelo et al., 2015). The Gulf regularly experiences temperatures of 33 - 34°C in the summer and the bleaching threshold for Gulf populations of *P. daedalea* is between 35 and 36°C (Riegl et al., 2011; Howells et al., 2016). Indeed, the bleaching threshold temperature for the coral assemblages is 3 - 7°C higher in the Gulf than in other regions (29 - 32°C), including the GBR (Hoegh-Guldberg, 1999; Berkelmans, 2002; Coles and Riegl, 2013). In addition, heritability estimates and preliminary data on genomic associations exist for a population of *P. daedalea* in the Persian Gulf (Kirk et al., 2018). This provides a unique opportunity to compare heritability and the genomic basis of heat tolerance between populations from these relatively warmer and cooler environments, which is important for understanding how increased thermal tolerance has evolved and for determining whether the genetic mechanisms underpinning heat tolerance in this species are conserved across ocean basins.

To understand the potential for a GBR population of *P. daedalea* to persist in a warming environment through selection and genetic adaptation we estimated narrow-sense heritability and identified genomic regions associated with heat tolerance. We also compared the genomic basis of heat tolerance in this species on the GBR to those of the Persian Gulf *P. daedalea* (Kirk et al., 2018). Estimating heritability of heat tolerance allowed us to quantify the host genetic contribution to this trait. We identified genomic markers associated with heat tolerant phenotypes by conducting a heat selection experiment and then assessing changes in allele frequency in the survivors. Sequencing our heat-selected pools of bi-parental crosses allowed us to identify markers associated with heat tolerance and examine how widespread these markers were across families in both genic and intergenic genomic regions. This study addresses fundamental questions regarding the adaptive potential of corals to heat stress and provides evidence of their ability to survive and persist in a changing environment.

MATERIALS AND METHODS

Experimental Crosses and Larval Culture

Six colony fragments of *Platygyra daedalea* were collected from Esk Reef, an inshore reef in the central region of the Great Barrier Reef (18° 46'21.95" S, 146° 31' 19.33" E) under Australian Institute of Marine Science, (2020) permit G12/35236.1. The corals were maintained in the National Sea Simulator at AIMS at Esk Reef ambient temperature (27°C) in flow-through sea water aquaria with 25% reduced ambient sunlight. In November 2016 (the 5th night after the full moon, at 18:30) the six parental colonies were isolated in ~60L bins filled with filtered sea water (FSW) that was filtered with a 0.04µm filter (Weeriyanun et al., 2021). Colonies spawned between 18:30-19:00 GMT+10. Gamete bundles were collected and washed with FSW. Sperm and eggs were then separated using 60 µm mesh sieves and eggs were thrice rinsed to eliminate residual sperm. We combined gametes from pairs of colonies according to a partial diallel design (**Figure 1**) to produce 10 families (hereafter termed crosses). A full diallel cross was not possible because colonies D and E did not produce enough eggs for the purposes of this experiment. Each cross was maintained at a density of 0.5 to 1.0 planula larvae per ml in separate 12L culture vessels with flow-through FSW at 27°C and gentle aeration.

Heat Stress Experiments

To quantify the variation in coral heat tolerance, we measured larval survival during controlled heat stress exposure following (Dixon et al., 2015). Six replicates of 20 larvae from each cross were randomly allocated to each of two temperature treatments: ambient reef temperatures from the site of collection (27°C, **Supplemental Data Sheet 1**) or an acute heat stress (35.5°C). Larval replicates were contained in individual 40µm mesh

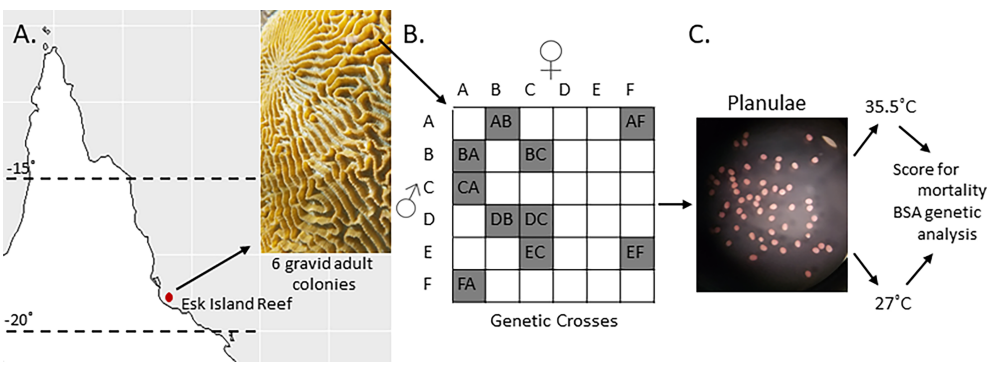

FIGURE 1 | Crossing design and heat stress experiments. **(A)** Six *Platygyra daedalea* colonies were sampled from Esk Reef on the GBR. **(B)** Crossing design used to produce ten crosses among those parental colonies. **(C)** Representative micrograph (10X) of planula larvae used for these experiments (53 hours post-fertilization).

bottomed 20ml wells (to allow for water circulation) within 60L flow through FSW tanks (N = 6 control and N = 6 heat per cross). A ramping rate of 1°C per hour was used to reach 35.5°C and water temperatures were maintained thereafter by computer-controlled heaters. Mortality was monitored by manually counting with a hand counter the number of surviving larvae in each well every 12 hours for the next ten days. Larval survival data can be found at https://github.com/hollandelder/Platygyradaedalea_HeritabiltyandMarkersofThermalTolerance.

Statistical Analysis of Heat Tolerance

Survival under heat stress was modeled using a Kaplan Meier Survival Analysis and a Cox Proportional Hazards (CPH) model that compared larval survival between crosses at 35.5°C and 27°C (Kaplan and Meier, 1958; Cox, 1972) using the Survival package in R (Therneau and Grambsch, 2000). Our model fit individual survival, allowing slopes to vary for temperature, cross, and the interaction of temperature and cross. We also calculated the uncensored survival probabilities as in Kirk et al., 2018. The code for the Kaplan Meier survival plots and CPH model can be referenced at https://github.com/hollandelder/Platygyradaedalea_HeritabiltyandMarkersofThermalTolerance.

CPH in the Survival package in R does not account for random effects, so we also used a generalized linear mixed model (GLMM) to determine if position contributed to variation in survival. Please see the supplemental text for complete GLMM analysis details (**Supplemental Data Sheet 3**).

We used survival fractions at the experimental endpoint and Kaplan Meier survival probabilities to estimate narrow-sense heritability of the variation in heat tolerance (Falconer and Mackay, 1996; Wilson et al., 2010) using a restricted maximum likelihood (REML) mixed-effects model implemented in the software package WOMBAT (Meyer, 2007) with the fixed effects of temperature, sire, and dam.

Heat Stress Selection Experiment to Investigate the Genomic Basis for Heat Stress Tolerance

We conducted a selection experiment to identify changes in allele frequency in response to acute heat exposure. Four replicates of 500 larvae per cross were allocated into 1L flow-through culture containers for a total of 2000 larvae in each of two temperature treatments (27°C and 35.5°C). Treatment conditions and ramping profiles were identical to those described for the survival analysis. We sampled 100 larvae from each replicate for a total of 400 larvae per treatment after 53 h, the time at which more than 50% mortality was evident in most crosses, and larvae were preserved in 100% ethanol for subsequent genetic analysis.

Genomic Library Preparation

Genomic DNA from each replicate pool was extracted from preserved samples using the Omega Bio-tek E.Z.N.A. Tissue Kit (Omega Bio-tek, Norcross, GA) and genotyped using 2bRAD, a sequencing-based approach for SNP genotyping (Wang et al., 2012) that has been previously applied in corals https://github.com/z0on/2bRAD_denovo (Dixon et al., 2015; Howells et al., 2016). Libraries were sequenced on four lanes of Illumina HiSeq2500 (50bp SE) at Ramaciotti Centre for Genomics at the University of New South Wales (Sydney, Australia).

Sequence Processing

Raw reads were quality filtered to remove any that had ten or more bases with a Q-score < 30. This is a stringent filter, but 95% of reads were retained for most samples at this threshold (**Supplemental Table 1**). Reads exhibiting a 12bp match to the Illumina sequencing adaptors were also removed. Remaining high quality reads were mapped against a 2bRAD reference previously developed from larvae of Persian Gulf *P. daedalea* (SRA accession: SRP066627, Howells et al., 2016) to facilitate subsequent cross-region comparisons using the gmapper command of the SHRiMP software package (Rumble et al., 2009) with flags –qv-offset 33 -Q –strata -o 3 -N 1 as in (Kirk et al., 2018). On average, 91% of reads mapped to the reference (**Supplemental Table 1**). After alignment to the reference, we further filtered reads with ambiguous (i.e. those mapping equally well to two or more different regions in the reference) or weak matches (those that did not span at least 33 of a 36 base sequence and matched fewer than 30 bases within that span of a sequence). SNPs were called using the CallGenotype.pl script found at https://github.com/Eli-Meyer/2bRAD_utilities as in (Kirk et al., 2018; Dziedzic et al., 2019) using observed nucleotide frequencies and a minor allele frequency of 0.25 to be considered heterozygous. Monomorphic loci were removed as well as those occurring in fewer than 25% of samples within a cross. From here on, we refer to mapped, quality filtered, and genotyped reads as tags. Samples with too many missing tags (<10,000 remaining) following read filtering were also removed. We required that each tag be genotyped in at least seven out of eight replicates for each cross to compare alleles at that locus across replicates in each treatment. Tags with more than two SNPs were also removed because they are likely to come from repetitive regions (Treangen and Salzberg, 2012). Finally, we down-sampled to one SNP per tag to control for non-independence and linkage but prioritized minimizing the number of missing SNPs. That is to say, the SNP found in most samples for a given tag was the one kept. If a sample did not have a SNP in the same base pair position in the tag compared to other copies of the tag, the SNP in the alternative position was kept. All 2bRAD genotyping and sequence filtering was conducted using scripts available at (https://github.com/Eli-Meyer/2brad_utilities).

Allele Frequency Analysis

We then compared allele frequencies between control larvae and the survivors of heat stress in replicate samples from each treatment within each cross. Since these samples represented pools of large numbers of larvae (100) rather than single diploid individuals, we followed the same general approach previously described as Pool-Seq (Kofler et al., 2017). We applied a stringent coverage threshold of 80x within cross to minimize sampling error that is likely to distort estimates of allele frequencies at lower coverage considering the number of individuals in each

sample (Zhu et al., 2012). To find the percentage of loci not genotyped in all crosses following filtering, we extracted and compared the number of tags to all SNPs genotyped in each cross using scripts available at https://github.com/hollandelder/PlatygyradaedaleaHeritabiltyandMarkersofThermalTolerance.

We interpreted SNP frequencies at a locus as allele frequencies in the pool. To test for differences in allele frequencies between control larvae and those surviving heat stress, we used logistic regression to analyze the number of observations of each allele in each sample with generalized linear models in R (glm with argument "cross=binomial(logit)") where treatment was a fixed effect (R Core Team, 2017). We used a Benjamini-Hochberg false discovery rate (FDR) correction to adjust p-values (Waite and Campbell, 2006). An allele was determined to be significant at an FDR-corrected p-value ≤ 0.05. We also calculated the proportion of alleles that increased or decreased in frequency as a result of heat stress treatment for each cross.

Comparison of Genotyped SNPs Between Crosses

All scripts and code for recreating the analyses described below can be found at https://github.com/hollandelder/PlatygyradaedaleaHeritabiltyandMarkersofThermalTolerance. Pearson correlation tests as implemented in the R package ggpubr (Kassambara, 2020) tested for correlations between the number of significant markers and the number of markers genotyped in each cross, as well as the number of significant markers and the mean survival following ten days of heat stress. We calculated the genetic distance between sets of parents by conducting pairwise comparisons of the high coverage loci using a custom Perl script which tested for numbers of shared markers in each parent set. The number of shared markers determined genetic distance between parents.

We then examined the presence and absence of SNPs between all pairwise combinations of crosses. To determine if the difference in significant SNPs identified between crosses was the result of filtering and genotyping steps, we calculated the percentage of tags missing in all crosses. Tidyverse and dplyr R software packages were used to extract the number of tags before and after all the filtering steps, and at the 80x coverage threshold and to compare those to all tags genotyped in each cross (Wickham et al., 2019; Wickham et al., 2020). To calculate the percentage of tags shared between each pair of crosses we compared the total significant tags genotyped in one cross to the sum of the significant tags genotyped in each focal pair. We also found whether significant tags were found to be insignificant or not genotyped in each cross. For tags with overlap in four or more crosses, we determined whether the allele in the cross was increasing or decreasing in frequency.

Functional Enrichment Analysis

To investigate the functional implications of candidate tolerance loci, we mapped the 2bRAD reference (SRA accession: SRP066627, Howells et al., 2016) to the *P. daedalea* transcriptome (SRA accession: PRJNA403854, Kirk et al., 2018) using Bowtie2 (Langmead et al., 2009) requiring a minimum MAPQ score of 23. Gene names and ontology terms were assigned to mapped 2bRAD tags based on the existing transcriptome annotations (Kirk et al., 2018). For tags that were identified in the transcriptome, we determined if the allele in the tag was increasing or decreasing in frequency. A rank-based gene ontology (GO) enrichment analysis was conducted to identify significantly enriched terms among annotated tags containing significant SNPs as identified in the allele frequency analysis using the GO_MWU suite of scripts (Wright et al., 2015) https://github.com/z0on/GO_MWU). The p-value from the allele frequency analysis was negative log-transformed and used as the continuous variable to identify GO terms enriched among the most significant SNPs using a Mann Whitney U test followed by Benjamini-Hochberg false discovery rate correction.

Ocean Basin Comparison

As reads from our experiment were mapped against the Persian Gulf *P. daedalea* reference (SRA accession: SRP066627, Howells et al., 2016), we were able to compare tags containing significant SNPs identified in this study to the tags containing significant SNPs identified by Kirk and colleagues in their larval heat stress study (Kirk et al., 2018). This was done using dplyr and tidyverse software packages in R to extract all matching significant tags in this study and match them to the subset of tags containing significant SNPs from Kirk and colleagues' study (Wickham et al., 2019; Wickham et al., 2020).

RESULTS

Survival in Heat Stress Experiments

A Cox proportional hazards (CPH) model revealed significant effects of heat on larval survival (p-value < 0.0001) (**Supplemental Data Sheet 2**). Individual factors in the model, temperature and cross, as well as the interaction were significant (p-value < 0.0001). Endpoint survival presented a broader range among crosses at 35.5°C (0.405 to 0.750) than at 27°C (0.861 to 0.975) (**Figure 2**). Cross DB had the highest survival probability at 35.5°C (0.75+/- 0.04), while cross CA had the lowest survival probability (0.41 \+/- 0.04) (**Figure 2**). Coral E provided sperm in both EC and EF, which both rank among the top four crosses, with (0.68+/- 0.04) and (0.64+/- 0.04) probability of survival, respectively. Coral C provided eggs in crosses DC and BC and provided sperm in cross CA, and this coral is associated with the bottom three survival probabilities 0.48 (+/- 0.04), 0.44 (+/- 0.05), and 0.40 (+/- 0.04).

CPH does not allow for testing of random effects. Since position of the net wells were randomly assigned, position could contribute to variation in thermal tolerance and thus we applied a generalized linear mixed model (GLMM) to test for position effects. We found that position did not contribute significantly to variation. Please see supplemental GLMM text for more details (**Supplemental Data Sheet 3**).

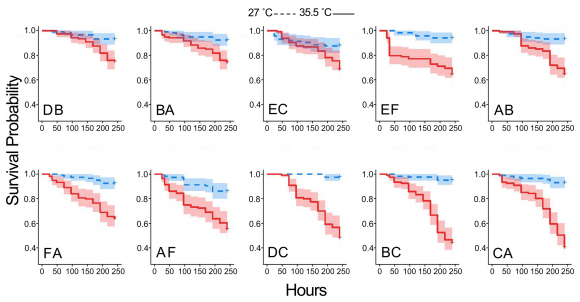

FIGURE 2 | Heat tolerance differs among crosses. Kaplan Meier plots of cumulative probability of survival for each family in control 27.5°C (blue) and elevated 35.5°C (red) temperature. Panels are arranged in order of heat tolerance, based on survival probability at 240 hr. Shaded regions represent 95% confidence intervals.

Quantitative Genetic Analysis of Variation in Heat Tolerance

Variation in survival during heat stress was highly heritable, with additive genetic variation explaining 66% of variation in survival (i.e. h^2 = 0.66; **Table 1**). We also estimated h^2 using the survival probabilities from the Kaplan Meier analysis and recovered a similar estimate (h^2 = 0.64). Both metrics reflect the total mortality over the entire time course (**Table 1**).

Genomic Analysis of Markers Under Selection During Heat Stress

Comparative analysis of larvae surviving an acute heat stress exposure versus paired control larval pools for each cross revealed that experimental treatment altered allele frequencies at hundreds of loci. Logistic regression of multilocus SNP genotypes (**Figure 3**) uncovered tens-to-hundreds of alleles in each cross whose frequencies were significantly altered by heat stress (**Table 2**). Overall, there was a general pattern of increase in major allele frequency in most crosses except for crosses BC, DC, and FA (**Figure 4**). This also meant that minor alleles were decreasing in frequency in most crosses. The number of alleles significantly associated with survival under heat stress differed widely among crosses; however, the number of significant alleles was not correlated with the number of tags genotyped in each sample (P = 0.48, R^2 = -0.26), genetic distance between the parents (P = 0.46, R^2 = -0.27), or the heat tolerance of each cross (P = 0.48, R^2 = -0.27). The variation was also not associated with a particular parent. For example, parents C and D each produced crosses with few SNPs under selection (BC and DB), but the combination of these parents in cross DC had the most, with 336 SNPs associated with survival under heat stress (**Table 2**).

TABLE 1 | Estimates of narrow-sense heritability of thermal tolerance obtained from different survival metrics.

Data	Survival	h^2
Survival at 240hr	59%	0.66
KM Estimate	59%	0.64

Censored and uncensored KM estimates refer to cumulative probability of survival estimated with or without censoring individuals surviving at the experimental endpoint.

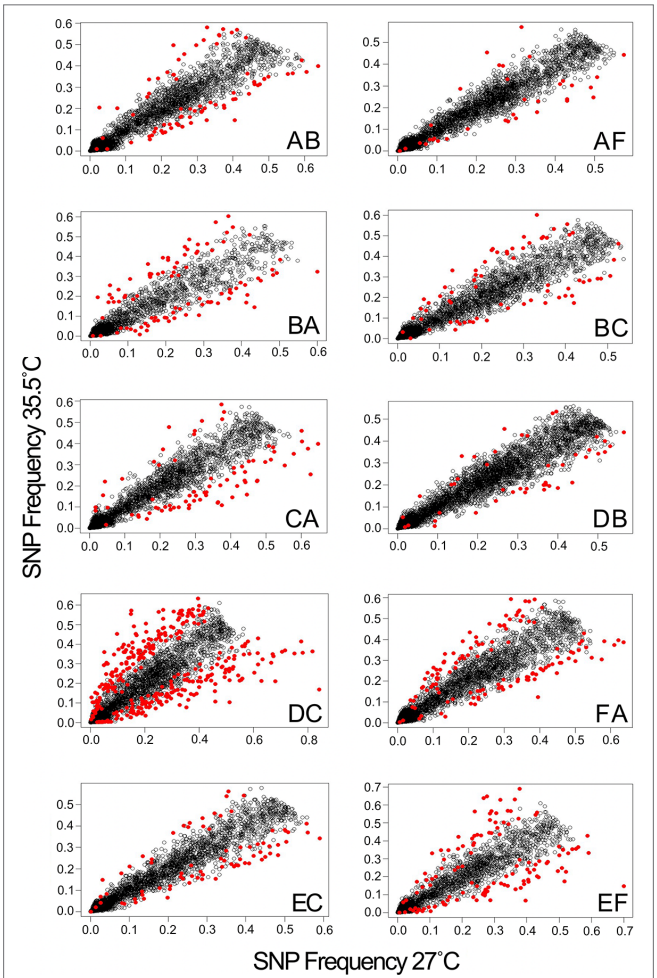

FIGURE 3 | Heat stress alters allele frequencies in surviving larvae. Panels show correlations between the average allele frequencies in survivors of replicate heat stress treatments relative to the corresponding controls. Markers with significantly altered allele frequencies (logistic regression, FDR < 0.05) are highlighted in red.

To evaluate the generalizability of genetic associations we searched for overlap in significant tags among crosses. A proportion of tags were consistently associated with heat stress across multiple crosses. In total, 148 significant tags were found in more than one cross (**Table 3** and **Supplemental Table 2**). A pairwise comparison of the percent of shared significant tags between a focal pair of crosses, revealed that 1-6% of significant tags were found to be significant in another cross (**Figure 5**, **Table 3** and **Supplemental Table 2**). The same two tags were found in seven crosses, a single tag overlapped in six crosses, and the same four tags overlapped in five crosses (**Table 3**). The major allele in six different tags that were found to be significantly changing in frequency in four or more crosses was found to increase in frequency (**Table 3**). Five tags showed mixed change in frequency for

TABLE 2 | The number of loci at which allele frequencies were significantly altered in survivors of thermal stress in each cross.

Cross	Significant markers	Markers genotyped	Parental distance	Survival (10 d)
AB	76	15,217	0.247	0.637
AF	34	19,399	0.245	0.551
BA	95	11,616	0.247	0.742
BC	69	22,820	0.257	0.442
CA	75	23,173	0.246	0.406
DB	44	23,999	0.256	0.758
DC	336	17,548	0.246	0.483
EC	77	16,734	0.262	0.683
EF	124	13,904	0.257	0.654
FA	139	16,691	0.245	0.639

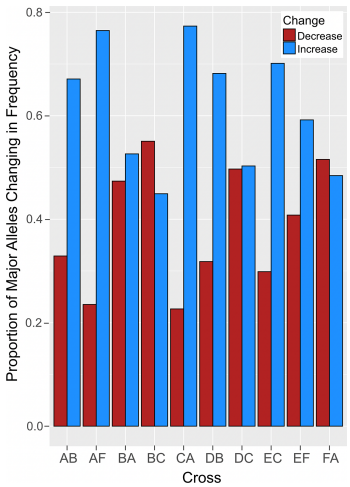

FIGURE 4 | The proportion of major alleles that changed in frequency after heat stress. Crosses are indicated on the x-axis and the proportions of major alleles that increased (blue) and decreased (red) are depicted on the y-axis.

the major allele, in some crosses it increased and in others it decreased (**Table 3**). Only one tag showed consistent decrease in frequency of the major allele across crosses in which it was identified (**Table 3**). However, most tags associated with heat tolerance in one cross were not associated with heat tolerance in unrelated crosses. For example, cross DC shared no parents with crosses EF or FA and 82 - 92% of the tags identified in each cross were not associated with heat stress in the other two.

To determine whether this lack of overlap was a result of the necessarily stringent filtering required for the analysis of pool-seq data (Kofler et al., 2011; Zhu et al., 2012), we investigated overlap in tags among crosses at earlier stages of our analysis. After initial quality filtering, we found only 30 – 63% of tags were genotyped in another cross (median of 52%, **Supplemental Table 3**). This range did not appreciably change after the 80X coverage threshold was applied, with 21 - 66% of tags identified in other crosses (median of 49%, **Supplemental Table 4**) indicating that the coverage threshold was not driving this pattern. However, statistical thresholds did have a moderate impact, as the percentage of significant tags in one focal cross not identified in other pairwise comparisons ranged from 11 - 61% (median of 42%, **Supplemental Table 5**).

We identified whether each significant tag was either not genotyped or was genotyped and found to be insignificant. We found that a majority of significant tags (64%) were genotyped in at least five out of ten crosses (**Supplemental Table 6**). Of the tags that were found to be significant in at least four or more crosses, they were found to be insignificant in at least one and in most cases more than one other cross (**Table 4** and **Supplemental Table 6**).

TABLE 3 | Tags identified as changing in frequency after heat stress in four or more crosses.

Marker	SNP Location	Marker Found in Crosses	v
denovoLocus34739	1, 21	AB, AF, BC, CA, DC, EF, FA	7
denovoLocus44191	16, 17	AB, AF, BA, CA, DB, EF, FA	7
denovoLocus9359	1	AB, BC, CA, DC, EF, FA	6
denovoLocus121909	11	AB, BA, CA, EC, FA	5
denovoLocus1291	4, 6	AB, BA, BC, DB, EF	5
denovoLocus22543	1, 25	BA, CA, EC, EF, FA	5
denovoLocus93322	3, 25	AB, AF, DC, EC, EF	5
denovoLocus13062	26, 36	CA, EC, EF, FA	4
denovoLocus18723	1	BA, DB, DC, EC	4
denovoLocus29413	1	BC, DC, EF, FA	4
denovoLocus36225	1, 4	AB, AF, EC, EF	4
denovoLocus51123	4	AB, AF, DC, EF	4

The color of the cross indicates whether the allele in the tag was increasing in frequency (blue) or decreasing in (red).

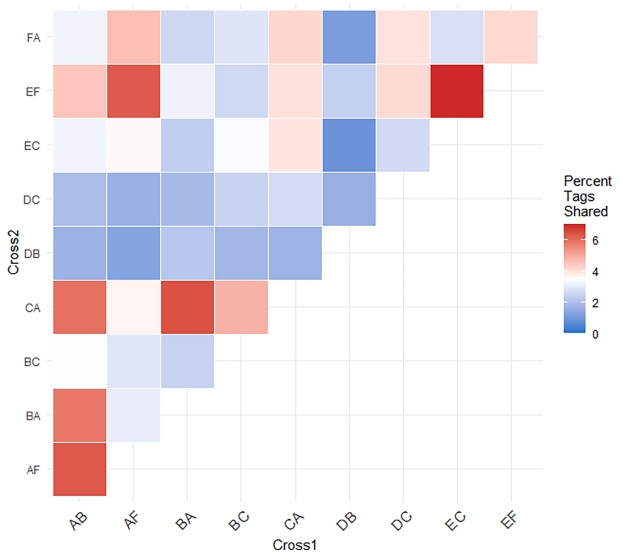

FIGURE 5 | Heatmap of the percent of significant tags shared between pairs of crosses. The percent of shared significant tags for each cross was calculated from the number of significant tags shared between the pair and the total number of potential tags that could have been shared. These comparisons demonstrate independent associations between heat stress and genotype at these loci across different genetic backgrounds.

Functional Significance of Enriched Tags

Seven GO terms were significantly enriched among the nine annotated tags that changed in allele frequency in response to heat stress in any cross (**Figure 6**). Tags in genes regulating cell projection, receptor signaling, regulation of apoptosis, regulation of hydrolase, and negative regulation of metabolism were over-represented among the most significantly differentially represented tags under heat stress conditions (**Table 5**). For the subset of significant tags shared among crosses, nine markers could be unambiguously assigned to a position in the transcriptome, all of which were annotated (**Table 5**). Furthermore, two of these tags, which were identified in three crosses were annotated as genes previously implicated in heat tolerance Monocarboxylate transporter 10 (K1PRR1) and Isocitrate dehydrogenase subunit 1 (E9C6G6) (**Table 5**) (Polato et al., 2010; Kenkel et al., 2013; Drury et al., 2022; Pathmanathan et al., 2021). In two tags that mapped to transcripts and overlapped in other crosses, we found consistent decrease in the major allele for the Monocarboxylate transporter and consistent increase of the major allele for the isocitrate dehydrogenase subunit (**Table 5**).

Ocean Basin Comparison

Finally, we compared significant SNPs arising from any cross with previously identified SNPs enriched in response to heat stress in Persian Gulf *P. daedalea* (Kirk et al., 2018). We found two tags significantly associated with both survival and heat tolerance in our dataset overlapped with sites identified in Kirk et al. (2018) (**Table 6**). The specific SNPs identified in each tag differed among studies (**Table 5**) and the tags did not match any genes in the reference transcriptome, so the potential functional significance of this shared variation remains unknown.

DISCUSSION

Adaptive Potential of Platygyra Daedalea

Our analysis shows that substantial variation in heat tolerance is evident among larval crosses. Moreover, 66% of this variation was attributable to additive genetic effects, indicating significant adaptive potential. Coral parent E was generally associated with crosses that had high survival probabilities and Coral parent C was associated with crosses that had lower survival probabilities (**Figure 2**). Our results add to only four published narrow-sense heritability estimates for heat tolerance in corals, all of which find this trait is highly heritable ranging from 0.58 – 0.87 (Dixon et al., 2015; Kirk et al., 2018; Dziedzic et al., 2019; Quigley et al., 2020; Bairos-Novak et al., 2021). Heritability estimates from different populations can yield valuable information about selection in a given geographic region as estimates are dependent on both the environment and the standing genetic variation in the population for which the estimate is made (Falconer and Mackay, 1996). However, the heritability estimates will be low if all parents express the same phenotype and genetic variation contributing to a trait is low (Falconer and Mackay, 1996). However, the heritability estimates will be high if both the phenotypic and genetic variation contributing to the trait is also high (Falconer

TABLE 4 | The number of crosses a tag was identified as either significant, insignificant, or not genotyped for tags that were found to be significantly changing in frequency in four or more crosses.

Tag	Number Crosses Significant	Number Crosses Insignificant	Number Crosses Not Genotyped
denovoLocus34739	7	1	2
denovoLocus44191	7	0	3
denovoLocus9359	6	3	1
denovoLocus121909	5	4	1
denovoLocus22543	5	3	2
denovoLocus93322	5	3	2
denovoLocus1291	5	1	4
denovoLocus18723	4	5	1
denovoLocus13062	4	4	2
denovoLocus36225	4	4	2
denovoLocus29413	4	3	3
denovoLocus51123	4	1	5

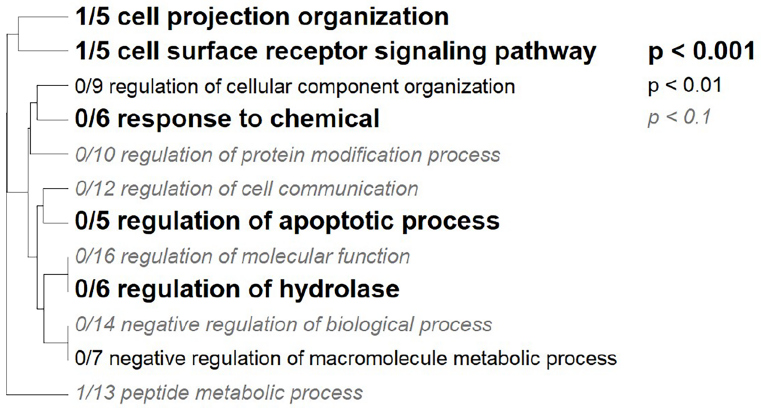

FIGURE 6 | Gene Ontology Tree. Gene ontology categories enriched in significant markers. The size of the font indicates the significance of the category per the inset key. Markers were mapped to the *Platygyra daedalea* transcriptome and the matching transcripts were assigned the log adjusted p-value from the allele frequency logistic regression.

TABLE 5 | Tags mapped to transcripts that changed in frequency after heat stress.

Crosses	Number of Tags Mapped to Transcript	Transcripts	Descriptions (Annotation)
AB, BA, EF	1	c39807	Monocarboxylate transporter 10 (K1PRR1)
AF, BA, CA	1	c15457	Isocitrate dehydrogenase subunit 1 (E9C6G6)
AB	1	c36043	Metalloendopeptidase (A7RVF7)
AB	1	c9426	60S_ribosomal_protein_L6_(Fragment)
BC	1	c10517	3-oxoacyl-[acyl-carrier-protein] reductase (K1QNK4)
DC	1	c7510	Putative dna polymerase type b (A0A069DZN0)
DC	1	c11010	Zinc finger MYM-type protein 3 (K1QD06)
FA	1	c16893	Rab9_effector_protein_with_kelch_motifs
FA	1	c12147	GPI mannosyltransferase 2 (K1PUQ8)

Listed in order of the number of crosses in which the tag was found. Color of the cross indicates the direction in the change of frequency: red represents a decrease and blue represents an increase.

TABLE 6 | Tags shared between the Persian Gulf and GBR populations that are significant to thermal tolerance.

Cross	Tag	SNP Base Pair GBR	SNP Base Pair Persian Gulf	Major Allele GBR	Major Allele Persian Gulf
CA	denovoLocus12624	35	28	T	GT
DC	denovoLocus60661	16	21	T	C

and Mackay, 1996). A novel comparison is the contrast of the heritability estimate for the same phenotype, larval survival in acute heat stress (0.48) found by Kirk and colleagues for *P. daedalea* in the Persian Gulf (Kirk et al., 2018). Persian Gulf *P. daedalea* have survived in a very shallow and warm sea for thousands of years (Purkis and Riegl, 2012), which may mean that a degree of selection for heat tolerance has already taken place resulting in less genetic diversity in the extant population (Falconer and Mackay, 1996). The lower heritability value is evidence to support less genetic diversity in the population. Also, the comparatively higher estimate of heritability for this trait in the central GBR *P. daedalea* population suggests that until very recently, heat stress may not have been the predominant selective pressure on this population, consistent with historical bleaching datasets for this region (Hughes et al., 2018).

Responses to selection depend on genetic variation in traits (Falconer and Mackay, 1996; Lynch and Walsh, 1998). Consequently, our study contributes to the understanding of the quantitative genetic framework necessary to model heat tolerance under various selection regimes. In its simplest form, this can be expressed in the breeder's equation, which describes the response to selection (R) as the product of heritability (h^2) and the selection differential (S) of the trait under selection. Selection differentials have not been widely estimated in corals (Kenkel et al., 2015; Weeriyanun et al., 2021), but considering the widespread reductions in coral populations following coral bleaching (Bellwood et al., 2004; Bruno and Selig, 2007; Hoegh-Guldberg et al., 2007; De'ath et al., 2012), they are likely high for sensitive species. For truncation selection, where all individuals with trait values above a threshold contribute offspring to

the next generation, selection differentials are equal to the difference in mean trait values between the selected population and the original population expressed as standard deviations of the population mean (Falconer and Mackay, 1996; Lynch and Walsh, 1998). If the selection differential equals one standard deviation, all parents with traits one standard deviation above the population mean contribute to phenotypic variation in the next generation. Based on the distribution of cumulative survival probabilities in heat stress from our experiment (0.57 ± 0.18) and the heritability of variation in heat tolerance we estimated from these data (0.66), the Breeder's Equation predicts a response to selection of 0.12. After selection, we would expect that if larvae of the next generation were subjected to the same heat stress treatment, the average mortality would be 0.48 (0.57 - 0.12), a 20% reduction in mortality under acute heat stress in a single generation. If instead of the high h^2 estimated in our study (0.66), we modeled the responses to selection using a minimum h^2 value of 0.1, we would predict only a 3% reduction in mortality in the following generation. While the estimates above are underpinned by many assumptions, the comparison highlights how empirical estimations of narrow-sense heritability can be used to predict adaptive responses. The relevance of these estimates for population responses depends on the extent to which larval survival during heat stress is directly under selection in natural populations, or the effectiveness of larval heat tolerance as a proxy for heat tolerance in adult colonies. Considering the lack of work in multi-generational comparisons, works including several generations would be valuable in future studies.

Allele Frequency Analysis Supports Multilocus Adaptation

Physiological and fitness traits can be determined by single or few loci of large effect, but in general they are underpinned by many loci of small effect (Sella and Barton, 2019). Surveying a larger portion of the population and limiting our detection of allele frequency to within the offspring of two known parents has helped to detect tens-to-hundreds of alleles supporting survival during heat stress. Comparing between crosses allowed us to investigate the generality of these patterns among different genetic backgrounds. This comparison revealed a number of markers with consistent changes in allele frequencies in multiple crosses (**Table 3** and **Supplemental Table 2**). The tags that show allele frequency change in a consistent direction are important targets for future studies of markers of thermal tolerance. Those tags that show inconsistent frequency change direction could be further evidence of the polygenicity of this trait. One allele might be important for thermal tolerance response, but if the right combination of alleles is not found at other sites in the genome, thermal tolerance will not be as high.

However, many of the associations detected in each cross were not shared in comparisons of multiple crosses. Our investigation into the lack of overlap among markers revealed that 49% of markers in a given cross, on average, were not genotyped in other crosses, even before the application of the 80X within cross coverage filter (**Supplementary Tables 3–5**), suggesting that this loss is not a result of bioinformatic filtering applied, but instead may result from aspects of the sequencing methodology and the biology of the animals involved. Null alleles are one common explanation for missing markers during sequencing (e.g. Crooks et al., 2013). Alternatively, bias could also result from the pooled sequencing approach. There were 100 individuals in each of eight replicate pools. Although amplification of libraries was kept to a minimum (no more than 17 cycles of PCR) a certain amount of PCR bias is unavoidable and in a given cross, certain regions may have been amplified more frequently (Dohm et al., 2008). A small number of additional sites were lost through the filtering process, but stringent thresholds are required to reduce false positive allele calls, given the small size of our RAD tags (Kofler et al., 2011). In this study, a pooled sequencing approach was chosen to maximize the resources available to survey as much of the population as possible. However, this is a clear tradeoff of pooled sequencing with this number of individuals per pool and sequencing relatively short fragments of the genome. Sequencing individual larvae may help alleviate this issue (e.g. Dixon et al., 2015).

Statistical thresholds also had an impact. The observation that certain SNPs were found to be significant in some crosses but not others could also result from the underlying distribution of those alleles in our parental population. In isolated populations the loci contributing to a trait are predicted to be fewer and of larger effect size (Savolainen et al., 2013). However, in populations experiencing immigration, the locus effect size and the number of loci that contribute to a trait become more variable (Savolainen et al., 2013). Corals can disperse in their larval phase before metamorphosis into a sedentary juvenile, so it is entirely possible that individuals originating from disparate reefs were among those chosen for our parental population (Davies et al., 2015). The observation that many markers associated with heat stress were specific to individual crosses suggests that many alleles of small effect contribute to variation in heat tolerance and that many different combinations of these small effect alleles can affect heat tolerance as is the growing consensus for thermal tolerance in coral (Bay and Palumbi, 2014; Thomas and Palumbi, 2017; Kirk et al., 2018; Fuller et al., 2020). The fact that many of our significant tags were found to be insignificant in other crosses also supports the conclusions of these other studies (**Table 4** and **Supplemental Table 6**). These differences may also result in part from epistatic interactions where the effects of variation at these loci depend on the interaction of two or more genes and composition of alleles at these genes, which are both dependent on genetic background (Day et al., 2008). The large number of alleles changing in frequency in cross DC could result from an unfortunate combination of parental alleles at many loci producing larvae with multiple deleterious alleles. The large number of alleles changing in frequency could be the result of additive genetic effects, but it could also be an indicator of epistasis, which is harder to detect but found frequently in polygenic traits in model organisms (Soyk et al., 2020). Nevertheless, repeated observation of some of these associations across different genetic backgrounds provides strong evidence that these markers are linked to genetic factors contributing to variation in heat tolerance.

Future studies can use the alleles that increased in frequency and the genomic regions identified in this and other studies to develop biomarkers to identify resilient coral populations for assisted gene flow or use in selective breeding programs. Starting with genetic markers associated with habitat variation in previous studies (Capper et al., 2015), we can test these associations through a combination of laboratory experiments and extensive population surveys of allele frequencies (Jin et al., 2016). These studies revealed that the frequencies of alleles associated with enhanced tolerance for environmental stress range from 0.48 in some populations to 0.92 in others (Jin et al., 2016). Further studies are needed to extend these surveys across species, markers, and geographic regions to develop an ecosystem-scale perspective on the potential for coral adaptive responses to ocean warming.

SNPs Associated With Heat Tolerance Occur in Genes Related to Extracellular Matrix and Metabolism

Among the annotated SNPs exhibiting significant changes in allele frequency in response to experimental selection, a number of functional enrichments were identified in genes associated with the organization of the cellular matrix and cellular components, the regulation of apoptosis, regulation of hydrolase, and metabolism. In addition, we found a subset of tags mapped to genes previously implicated in heat tolerance, two of which were observed in multiple crosses (**Table 5**). These genes are prime candidates for further functional studies aimed at delineating the potential mechanistic role of these polymorphisms (Cleves et al., 2018; Cleves et al., 2020a; Cleves et al. 2020b).

Four markers were associated with genes that play roles in the extracellular matrix, with enrichments in cell projection organization, surface receptor signaling, and cell component organization (**Table 5** and **Figure 6**). GPI Mannosyltransferase 2 functions in the assembly of glycosylphosphatidylinositol (GPI) anchors that attach proteins to cell membranes (Ji et al., 2005). In corals, this protein is in the pathway that changes the mannose content of the extracellular matrix (Lee et al., 2016). The abundance of Gammaproteobacteria is reduced with the change in mannose in coral mucus composition (Lee et al., 2016) Both zinc finger MYM-type protein and metalloendopeptidase, a metal-dependent protease, restructure and organize the extracellular matrix (Lodish et al., 2020). The Rab9 effector with kelch motifs controls docking of endosomes in the process of exocytosis (Díaz et al., 1997). While both metalloendopeptidase and this zinc finger protein were not found in other coral studies, they are found in other invertebrates during heat stress (Zhang et al., 2015; Prieto et al., 2019; Juárez et al., 2021). On the other hand, Rab proteins have been identified as important for signaling the start of phagocytosis mechanisms and cell destruction in anemones during oxidative stress and bleaching (Chen et al., 2005; Downs et al., 2009). In this case, it is likely the Rab 9 effector is involved in signaling the start of the cell death during heat stress. SNPs in these genes indicate that control of cell reorganization and structure is important during heat stress.

Negative regulation of macromolecule metabolic process was also identified as a significant GO category (**Figure 6**). Three coral crosses had a SNP in the Krebs cycle enzyme isocitrate dehydrogenase (IDH) and a monocarboxylate transporter both of which are associated with this annotation. These proteins have been identified in gene expression studies as important to the coral thermal stress response (Polato et al., 2010; Kenkel et al., 2013; Drury et al., 2022; Pathmanathan et al., 2021). IDH participates in reducing reactive oxygen species and is one of the 44 proteins identified as the minimal stress proteome (Kultz, 2005). The monocarboxylate transporter moves lactate, pyruvate, and ketone bodies across plasma membranes, thus it is associated with the regulation of metabolism (Halestrap, 2012). This transporter has been identified as important in recent coral heat stress studies and is upregulated under heat stress (Drury et al., 2022; Pathmanathan et al., 2021). The SNPs in IDH and the monocarboxylate transporter associated with heat tolerance in this study further strengthens their proposed role in the thermal stress response in corals.

Additional genes annotated with GO categories like metabolism, regulation of hydrolase, and regulation of apoptosis, may also be important for handling reactive oxygen species. While the 3oxoacyl (acyl-carrier-protein) reductase has a larger role in fatty acid biosynthesis, it also catalyzes a reduction reaction (Chan and Vogel, 2010). Similarly, IDH is responsible for regulation of metabolism, but the reaction it catalyzes is also a reduction. These genes have been identified as important for controlling reactive oxygen species levels resulting from increased metabolism during heat stress (Dixon et al., 2015) and our results add further evidence of the possible importance of these SNPs to corals' heat stress response.

The consistent change in the frequency of the major alleles in the monocarboxylate transporter and isocitrate dehydrogenase across multiple crosses also suggests that these alleles are important for heat stress survival. They are prime targets for future studies assessing markers of thermal tolerance.

Ocean Basin Comparison

Comparisons of populations of *P. daedalea* in more typical reef temperature conditions (this study) and unusually warm conditions (Kirk et al., 2018) will be important to understand the genomic basis of heat tolerance. Two markers from the present study were significantly associated with heat tolerance in the Persian Gulf population (**Table 6**). Neither of these markers matched genes in the transcriptome, and without a genomic resource it is not possible to identify their location in the genome or proximal genes. However, their repeated identification strongly supports an important role in coral thermal tolerance. Further work could include screening for differential abundance of these alleles among natural thermal gradients and potential validation for gene function through knock-down from CRISPR-Cas9 induced mutagenesis (e.g., Cleves et al., 2018). The lack of shared markers between these cross-ocean basin populations may be further evidence that many alleles of small effect contribute to heat tolerance and that they vary in their distribution across populations.

Conclusions

Our findings demonstrate substantial genetic variation and high heritability of heat tolerance (i.e., > 60%) in the coral *Platygyra daedalea* from the GBR, supporting the potential for adaptation. Our analysis identified hundreds of markers associated with heat tolerance, including markers that were repeatedly associated with heat tolerance across different genetic backgrounds. These results support the conclusion that heat tolerance is a complex polygenic trait determined by many alleles of small effect that are likely to be species and population specific. Despite this complexity, we nevertheless found markers shared in multiple crosses that may be important for heat tolerance in *P. daedalea*. Two markers were also identified in Persian Gulf populations, and a number occurred in genes previously implicated in coral thermal tolerance. Our findings build on the growing body of evidence that natural populations of corals harbor substantial genetic variation in heat tolerance that can support adaptive responses to selection and identify genetic markers for heat tolerance in a globally distributed coral species. These heat tolerance markers are essential to any type of reseeding or assisted gene flow and assisted migration programs, which may be necessary to maintaining reefs in the future as we work to reduce CO_2 emissions and mitigate the effects of climate change.

DATA AVAILABILITY STATEMENT

The datasets presented in this study can be found in online repositories. The names of the repository/repositories and accession number(s) can be found below https://www.ncbi.nlm.nih.gov/, PRJNA542930.

AUTHOR CONTRIBUTIONS

EM, HE, and LB conceived the experiments. HE, VM, JM-P, and LB conducted experiments, LB and AB provided advice and logistical support through the project, HE conducted genetic and statistical analysis and wrote the manuscript. LB and EM helped with genetic and statistical analysis and LB, VW and AB helped write the manuscript. All authors contributed to the article and approved the submitted version.

FUNDING

This research was conducted under Great Barrier Reef Marine Park Authority permit (G11/34671.1) and supported with funding from the National Science Foundation Graduate Research Fellowship to HE, National Science Foundation Graduate Research Opportunities Worldwide to HE and internal grants from AIMS to LB.

ACKNOWLEDGMENTS

We thank the staff of the National Sea Simulator at the Australian Institute of Marine Science for their assistance in the collection and husbandry of the corals used in these experiments. We also thank Ida Bjornsbo for her tireless assistance in counting coral larvae at all hours of the day and night.

SUPPLEMENTARY MATERIAL

The Supplementary Material for this article can be found online at: https://www.frontiersin.org/articles/10.3389/fmars.2022.925845/full#supplementary-material

REFERENCES

Australian Institute of Marine Science. (2020). Annual Summary Report on Coral Reef Condition 2019/20. Available at: www.aims.gov.au

Bairos-Novak, K. R., Hoogenboom, M. O., van Oppen, M. J. H. and Connolly, S. R. (2021). Coral Adaptation to Climate Change: Meta-Analysis Reveals High Heritability Across Multiple Traits. *In Global Change Biol.* 27 (22), 5694–5710). doi: 10.1111/gcb.15829

Barshis, D. J., Ladner, J. T., Oliver, T., Seneca, F. O., Traylor-Knowles, N. and Palumbi, S. R. (2013). Genomic Basis for Coral Resilience to Climate Change. *Proc. Natl. Acad. Sci. U. S. A.* 110 (4), 1387–1392. doi: 10.1073/pnas.1210224110

Baums, I. B., Baker, A. C., Davies, S. W., Grottoli, A. G., Kenkel, C. D., Kitchen, S. A., et al. (2019). Considerations for Maximizing the Adaptive Potential of Restored Coral Populations in the Western Atlantic. *Ecol. Appl.* 29 (8), 1–23. doi: 10.1002/eap.1978

Bay, L. K., Doyle, J., Logan, M. and Berkelmans, R. (2016). Recovery From Bleaching is Mediated by Threshold Densities of Background Thermo-Tolerant Symbiont Types in a Reef-Building Coral. *R. Soc. Open Sci.* 3 (160322). 1–10. doi: 10.1098/rsos.160322

Bay, R. and Palumbi, S. R. (2014). Report Multilocus Adaptation Associated With Heat Resistance in Reef-Building Corals. *Curr. Biol.* 1–5. doi: 10.1016/j.cub.2014.10.044

Bay, R., Rose, N., Logan, C. and Palumbi, S. (2017). Genomic Models Predict Successful Coral Adaptation If Future Ocean Warming Rates are Reduced. *Sci. Adv.* 7, 1-10. doi: 10.1126/sciadv.1701413

Bellwood, D. R., Hughes, T. P., Folke, C. and Nystro, M. (2004). Confronting the Coral Reef Crisis. *Nature* 429 (June), 827–833. doi: 10.1038/nature02691

Berkelmans, R. (2002). Time-Integrated Thermal Bleaching Thresholds of Reefs and Their Variation on the Great Barrier Reef. *Mar. Ecol. Prog. Ser.* 229, 73–82. doi: 10.3354/meps229073

Berkelmans, R. and van Oppen, M. J. H. (2006). The Role of Zooxanthellae in the Thermal Tolerance of Corals: A "Nugget of Hope" for Coral Reefs in an Era of Climate Change. Proceedings. *Biol. Sci. / R. Soc.* 273 (1599), 2305–2312. doi: 10.1098/rspb.2006.3567

Bruno, J. F. and Selig, E. R. (2007). Regional Decline of Coral Cover in the Indo-Pacific: Timing , Extent , and Subregional Comparisons. *PloS One* 8. doi: 10.1371/journal.pone.0000711

Capper, R. L., Jin, Y. K., Lundgren, P. B., Peplow, L. M., Matz, M. V. and van Oppen, ,. M. J. H. (2015). Quantitative High Resolution Melting: Two Methods to Determine SNP Allele Frequencies From Pooled Samples. *BMC Genet.* 16 (62), 1–13. doi: 10.1186/s12863-015-0222-z

Chan, D. I. and Vogel, H. J. (2010). Current Understanding of Fatty Acid Biosynthesis and the Acyl Carrier Protein. *In Biochem. J.* 430 (1), 1–19). doi: 10.1042/BJ20100462

Charmantier, A. and Garant, D. (2005). Environmental Quality and Evolutionary Potential: Lessons From Wild Populations. *Proc. R. Soc.* 272, 1415–1425. doi: 10.1098/rspb.2005.3117

Chen, M. C., Hong, M. C., Huang, Y., Liu, M. C., Cheng, Y. M. and Fang, L. S. (2005). ApRab11, a Cnidarian Homologue of the Recycling Regulatory Protein Rab11, Is Involved in the Establishment and Maintenance of the Aiptasia-Symbiodinium Endosymbiosis. *Biochem. Biophys. Res. Commun.* 338 (3), 1607–1616. doi: 10.1016/j.bbrc.2005.10.133

Cleves, P. A., Shumaker, A., Lee, J. M., Putnam, H. M. and Bhattacharya, D. (2020a). Unknown to Known: Advancing Knowledge of Coral Gene Function. *In Trends Genet.* 36 (2), 93–104). doi: 10.1016/j.tig.2019.11.001. Elsevier Ltd.

Cleves, P. A., Strader, M. E., Bay, L. K., Pringle, J. R. and Matz, M. V. (2018). CRISPR/Cas9-Mediated Genome Editing in a Reef Building Coral. *PNAS*, 115 (20), 5235–5240. doi: 10.1073/pnas.1722151115

Cleves, P. A., Tinoco, A. I., Bradford, J., Perrin, D., Bay, L. K. and Pringle, J. R. (2020b). Reduced Thermal Tolerance in a Coral Carrying CRISPR-Induced Mutations in the Gene for a Heat-Shock Transcription Factor. *PNAS* 117 (46), 28899–28905. doi: 10.1073/pnas.1920779117/-/DCSupplemental

Coles, S. L. and Riegl, B. M. (2013). Thermal Tolerances of Reef Corals in the Gulf : A Review of the Potential for Increasing Coral Survival and Adaptation to Climate Change Through Assisted Translocation. *Mar. Pollut. Bull.* 72 (2), 323–332. doi: 10.1016/j.marpolbul.2012.09.006

Core Team, R. (2017) *R: A Language and Environment for Statistical Computing*. Available at: https://www.r-project.org/.

Cox, D. R. (1972). Regression Models and Life-Tables. Journal of the Royal StatisticalSociety. *Ser. B (Methodological)* 34 (2), 187–220.

Crooks, L., Carlborg, Ö., Marklund, S., and Johansson, A. M. (2013). Identification of Null Alleles and Deletions from SNP Genotypes for an Intercross Between Domestic and Wild Chickens. *G3: Genes, Genomes, Genetics* 3 (8), 1253–1260. doi: 10.1534/g3.113.006643

D'Angelo, C., Hume, B. C. C., Burt, J., Smith, E. G., Achterberg, E. P. and Wiedenmann, J. (2015). Local Adaptation Constrains the Distribution Potential of Heat-Tolerant Symbiodinium from the Persian/Arabian Gulf. *ISME J.* 9 (12), 2551–2560. doi: 10.1038/ismej.2015.80

Davies, S. W., Treml, E. A., Kenkel, C. D. and Matz, M. V. (2015). Exploring the Role of Micronesian Islands in the Maintenance of Coral Genetic Diversity in the Pacific Ocean. *Mol. Ecol.* 24 (1), 70–82. doi: 10.1111/mec.13005

Day, T., Nagel, L., van Oppen, M. J. H. and Caley, M. J. (2008). Factors Affecting the Evolution of Bleaching Resistance in Corals *American Naturalist* 171, 2. doi: 10.1086/524956

De'ath, G., Fabricius, K. E., Sweatman, H. and Puotinen, M. (2012). The 27 – Year Decline of Coral Cover on the Great Barrier Reef and its Causes. *PNAS* 109 (44), 17995–17999. doi: 10.1073/pnas.1208909109

Díaz, E., Schimmöller, F. and Pfeffer, S. R. (1997) 138 (2).

Dixon, G., Davies, S., Aglyamova, G., Meyer, E., Bay, L. K. and Matz, M. V. (2015). Genomic Determinants of Coral Heat Tolerance Across Latitudes. *Science* 348 (6242), 1460–1462. doi: 10.1126/science.1261224

Dohm, J. C., Lottaz, C., Borodina, T. and Himmelbauer, H. (2008). Substantial Biases in Ultra-Short Read Data Sets from High-Throughput DNA Sequencing. *Nucleic Acids Res.* 36 (16), 1–10. doi: 10.1093/nar/gkn425

Downs, C. A., Kramarsky-Winter, E., Martinez, J., Kushmaro, A., Woodley, C. M., Loya, Y., et al. (2009). Symbiophagy as A Cellular Mechanism for Coral Bleaching. *Autophagy* 5 (2), 211–216. doi: 10.4161/auto.5.2.7405

Drury, C., Bean, N. K., Harris, C. I., Hancock, J. R., Hucekba, J., Martin, C. H., et al. (2022). Intrapopulation Adaptive Varience Supports Selective Breeding in A Reef Building Coral. *Comm. Biol.* 5 (1), 1–19. doi: 10.1038/s42003-022-03428-3

Dziedzic, K. E., Elder, H. and Meyer, E. (2019). Heritable Variation in Bleaching Responses and its Functional Genomic Basis in Reef-Building Corals (Orbicella faveolata). *Mol. Ecol.*, 1–16. doi: 10.1111/mec.15081

Falconer, D. S. and Mackay, T. F. C. (1996). *Introduction to Quantitative Genetics*. (Harlow: Pearson).

Fitt, W. K. and Warner, M. E. (1995). Bleaching patterns of four species of Caribbean reef corals. *Biol. Bull.* 189 (3), 298–307. doi: 10.2307/1542147

Fuller, Z. L., Mocellin, V. J. L., Morris, L. A., Cantin, N., Shepherd, J., Sarre, L., et al. (2020). Population Genetics of the Coroal Acropora Millepora: Toward Genomic Prediction of Bleaching. *Science* 369 (6501), 1–9. doi: 10.1126/science.aba4674

Gienapp, P., Lof, M., Reed, T. E., McNamara, J., Verhulst, S. and Visser, M. E. (2013). Predicting Demographically Sustainable Rates of Adaptation: Can Great Tit Breeding Time Keep Pace with Climate Change? *Philos. Trans. R. Soc. B: Biol. Sci.* 368 (1610), 1–10. doi: 10.1098/rstb.2012.0289

Glynn, P. W. (1993). Coral Reef Bleaching: Ecological Perspectives. *Coral Reefs* 12, 1–17. doi: 10.1007/BF00303779

Halestrap, A. P. (2012). The Monocarboxylate Transporter Family-Structure and Functional Characterization. *In IUBMB Life* 64 (1), 1–9). doi: 10.1002/iub.573

Hoegh-Guldberg, O. (1999). Climate Change, Coral Bleaching and the Future of the World's Coral Reefs. *Mar. Freshw. Res.* 50 (8), 839–866. doi: 10.1071/MF99078

Hoegh-Guldberg, O., Harvell, C. D., Sale, P. F., Edwards, A. J., Caldeira, K., Knowlton, N., et al. (2007). Coral Reefs Under Rapid Climate Change and Ocean Acidification. *Science* 318 (5857), 1737–1742. doi: 10.1126/science.1152509

Hoegh-Guldberg, O. and Smith, G. J. (1989). The Effect of Sudden Changes in Temperature, Light and Salinity on the Population Density and Export of Zooxanthellae from The Reef Corals Stylophora Pistillata Esper and Seriatopora hystrix Dana. *J. Exp. Mar. Biol. Ecol.* 129 (3), 279–303. doi: 10.1016/0022-0981(89)90109-3

Howells, E. J., Abrego, D., Meyer, E., Kirk, N. and Burt, J. A. (2016). Host Adaptation and Unexpected Symbiont Partners Enable Reef-Building Corals to Tolerate Extreme Temperatures. *Global Change Biol.* 22, 1–13. doi: 10.1111/gcb.13250

Hughes, T. P., Kerry, J. T., Álvarez-noriega, M., Álvarez-romero, J. G., Anderson, K. D., Baird, A. H., et al. (2017). Global Warming and Recurrent Mass Bleaching of Corals. *Nature* 543, 373–377. doi: 10.1038/nature21707

Hughes, T., Kerry, J., Baird, A., Connolly, S., Chase, T., Dietzel, A., et al. (2019). Global Warming Impairs Stock - Recruitment Dynamics of Corals. *Nature* 568, 387–390. doi: 10.1038/s41586-019-1081-y

Hughes, T. P., Kerry, J. T., Baird, A. H., Connolly, S. R., Dietzel, A., Eakin, C. M., et al. (2018). Global Warming Transforms Coral Reef Assemblages. *Nature* 556, 492–496. doi: 10.1038/s41586-018-0041-2

Hume, B., D'angelo, C., Burt, J., Baker, A. C., Riegl, B. and Wiedenmann, J. (2013). Corals from the Persian/Arabian Gulf as Models for Thermotolerant Reef-Builders: Prevalence of Clade C3 Symbiodinium, Host Fluorescence and Ex Situ Temperature Tolerance. *Mar. pollut. Bull.* 72 (2), 313–322. doi: 10.1016/j.marpolbul.2012.11.032

Hutchings, P., Kingsford, M. and Hoegh-Guldberg, O. (2019). *The Great Barrier Reef: Biology, Environment, and Management* (Sydney: Csiro Publishing).

Ji, Y. K., Hong, Y., Ashida, H., Shishioh, N., Murakami, Y., Morita, Y. S., et al. (2005). PIG-V Involved in Transferring the Second Mannose in Glycosylphosphatidylinositol. *J. Biol. Chem.* 280 (10), 9489–9497. doi: 10.1074/jbc.M413867200

Jin, Y. K., Lundgren, P., Lutz, A., Raina, J. B., Howells, E. J., Paley, A. S., et al. (2016). Genetic Markers for Antioxidant Capacity in A Reef-Building Coral. *Sci. Adv.*, 2 (5). doi: 10.1126/sciadv.1500842

Juárez, O. E., Escobedo-Fregoso, C., Arredondo-Espinoza, R. and Ibarra, A. M. (2021). Development of SNP Markers for Identification of Thermo-Resistant Families of the Pacific Oyster Crassostrea Gigas Based on RNA-SEQ. *Aquaculture* 539. doi: 10.1016/j.aquaculture.2021.736618

Kaplan, E. L. and Meier, P. (1958). Nonparametric Estimation from Incomplete Observations. *J. Am. Stat. Assoc.* 53 (282), 457–481.

Kassambara, A. (2020). Ggpubr R Package: *Create Publication Ready Plots*. Available at: https://rpkgs.datanovia.com/ggpubr/.

Kenkel, C. D., Matz, M., and Tx, A. (2016). Enhanced Gene Expression Plasticity as A Mechanism of Adaptation to A Variable Environment in A Reef-Building Coral. *Nat. Ecol. Evol.* 3, 1–21. doi: 10.1038/s41559-016-0014

Kenkel, C. D., Meyer, E. and Matz, M. V. (2013). Gene Expression Under Chronic Heat Stress in Populations of the Mustard Hill Coral (Porites Astreoides) from Different Thermal Environments. *Mol. Ecol.* 22 (16), 4322–4334. doi: 10.1111/mec.12390

Kenkel, C. D., Setta, S. P. and Matz, M. V. (2015). Heritable Differences in Fitness-Related Traits Among Populations of the Mustard Hill Coral, Porites astreoides. *Heredity* 115 (6), 509–516. doi: 10.1038/hdy.2015.52

Kirk, N., Howells, E., Abrego, D., Burt, J. and Meyer, E. (2018). Genomic and Transcriptomic Signals of Thermal Tolerance in Heat-Tolerant Corals (Platygyra daedalea) of the Arabian/Persian Gulf. *Mol. Ecol.* 27, 5180–5194. doi: 10.1111/mec.14934

Kofler, R., Orozco-terWengel, P., de Maio, N., Pandey, R. V., Nolte, V., Futschik, A., et al. (2011). Popoolation: A Toolbox for Population Genetic Analysis of Next Generation Sequencing Data from Pooled Individuals. *PLoS One* 6 (1). doi: 10.1371/journal.pone.0015925

Kofler, R., Pandey, R. V., Schlötterer, C., Populationsgenetik, I., Vienna, V. and Wien, A. (2017). PoPoolation2: Identifying Differentiation Between Populations Using Sequencing of Pooled DNA Samples (Pool-Seq). *Bioinformatics* 27 (24), 3435–3436. doi: 10.1093/bioinformatics/btr589

Kultz, D. (2005). Molecular And Evolutionary Basis of the Cellular Stress Response. *Annu. Rev. Physiol.* 67, 225–257. doi: 10.1146/annurev.physiol.67.040403.103635

Lajeunesse, T. C., Parkinson, J. E., Gabrielson, P. W., Jeong, H. J., Reimer, J. D., Voolstra, C. R., et al. (2018). Systematic Revision of Symbiodiniaceae Highlights the Antiquity and Diversity of Coral Endosymbionts Article Systematic Revision of Symbiodiniaceae Highlights the Antiquity and Diversity of Coral Endosymbionts. *Curr. Biol.* 28 (16), 2570–2580.e6. doi: 10.1016/j.cub.2018.07.008

Langmead, B., Trapnell, C., Pop, M. and Salzberg, S. L. (2009). Ultrafast and Memory-Efficient Alignment of Short DNA Sequences to the Human Genome. *Genome Biol.* 10 (R25), 1–10. doi: 10.1186/gb-2009-10-3-r25

Lee, S. T. M., Davy, S. K., Tang, S. L. and Kench, P. S. (2016). Mucus Sugar Content Shapes the Bacterial Community Structure in Thermally Stressed Acropora muricata. *Front. Microbiol.* 7 (MAR). doi: 10.3389/fmicb.2016.00371

Lodish, H., Berk, A., Kaiser, C. A., Krieger, M., Bretscher, A., Ploegh, H., et al. (2020). *Molecular Cell Biology*. 9th ed (New York: Freeman).

Long Term Reef Monitoring Program. (2019). Annual Report on Reef Condition: Mixed bill of health for the Great Barrier Reef. https://www.aims.gov.au/reef-monitoring/gbr-condition-summary-2018-2019.

Lynch, M. and Walsh, B. (1998). Genetics and Analysis of Quantitative Traits. (Sinauer Associates, Inc.)

Manzello, D. P., Jankulak, M., Matz, M., Enochs, I. C., Valentino, L., Carlton, R. D., et al. (2018). Role of Host Genetics and Heat - Tolerant Algal Symbionts in Sustaining Populations of the Endangered Coral Orbicella Faveolata in the Florida Keys with Ocean Warming. *Global Change Biol.* 25, 1016–1031. doi: 10.1111/gcb.14545

Matz, M. V., Treml, E. A. and Haller, B. C. (2020). Estimating the Potential for Coral Adaptation to Global Warming Across the Indo-West Pacific. *Global Change Biol.* 26 (6), 3473–3481. doi: 10.1111/gcb.15060

Meyer, K. (2007). WOMBAT — A Tool for Mixed Model Analyses in Quantitative Genetics by Restricted Maximum Likelihood (REML). *J. Zhejiang Univ. Sci. B* 8 (11), 815–821. doi: 10.1631/jzus.2007.B0815

Meyer, E., Davies, S., Wang, S., Willis, B., Abrego, D., Juenger, T., et al. (2009). Genetic Variation in Responses to A Settlement Cue and Elevated Temperature in the Reef-Building Coral Acropora millepora. *Mar. Ecol. Prog. Ser.* 392, 81–92. doi: 10.3354/meps08208

Oliver, T. A. and Palumbi, S. R. (2011). Many Corals Host Thermally Resistant Symbionts in High-Temperature Habitat. *Coral Reefs* 30, 241–250. doi: 10.1007/s00338-010-0696-0

Pathmanathan, J. S., Williams, A., Stephens, T. G., Su, X., Eric, N., Conetta, D., et al. (2021). Multi-Omic Characterization of the Thermal Stress Phenome in The Stony Coral Montipora capitata. *BioRxiv*, 1–25. doi: 10.1101/2021.02.05.429981

Polato, N. R., Voolstra, C. R., Schnetzer, J., DeSalvo, M. K., Randall, C. J., Szmant, A. M., et al. (2010). Location-Specific Responses to Thermal Stress in Larvae of the Reef-Building Coral Montastraea faveolata. *PloS One* 5 (6), e11221. doi: 10.1371/journal.pone.0011221

Prieto, D., Markaide, P., Urrutxurtu, I., Navarro, E., Artigaud, S., Fleury, E., et al. (2019). Gill Transcriptomic Analysis in Fast- and Slow-Growing Individuals of Mytilus galloprovincialis. *Aquaculture* 511. doi: 10.1016/j.aquaculture.2019.734242

Purkis, S. J. and Riegl, B. M. (2012). *Coral Reefs of the Gulf: Adaptation to Climatic Extremes in the World's Hottest Sea*. (London: Springer Science), 33–50. doi: 10.1007/978-94-007-3008-3

Quigley, K. M., Bay, L. K. and van Oppen, M. J. H. (2020). Genome-wide SNP Analysis Reveals an Increase in Adaptive Genetic Variation Through Selective Breeding of Coral. *Mol. Ecol.* 29, 2176–2188. doi: 10.1111/mec.15482

Riegl, B., Purkis, S., Al-cibahy, A., Abdel-moati, M. and Hoegh-Guldberg, O. (2011). Present Limits to Heat-Adaptability in Corals and Population-Level Responses to Climate Extremes. *PloS One* 6 (9). doi: 10.1371/journal.pone.0024802

Ruiz-jones, L. J. and Palumbi, S. R. (2017). Tidal Heat Pulses on A Reef Trigger A Fine-Tuned Transcriptional Response in Corals to Maintain Homeostasis. *Sci. Adv.* 3 (e1601298), 1–11. doi: 10.1126/sciadv.1601298

Rumble, S. M., Lacroute, P., Dalca, A. V., Fiume, M., Sidow, A. and Brudno, M. (2009). SHRiMP: Accurate Mapping of Short Color-Space Reads. *PloS Comput. Biol.* 5 (5), 1–11. doi: 10.1371/journal.pcbi.1000386

Savolainen, O., Lascoux, M. and Merilä, J. (2013). Ecological Genomics of Local Adaptation. *Nat. Rev. Genet.* 14 (November), 807–820. doi: 10.1038/nrg3522

Sella, G. and Barton, N. H. (2019). Thinking about the Evolution of Complex Traits in the Era of Genome-Wide Association Studies. *Annu. Rev. Genomics Hum. Genet.* 20, 461–493. doi: 10.1146/annurev-genom-083115-022316

Silverstein, R. N., Cunning, R. and Baker, A. C. (2014). Change in algal symbiont communities after bleaching, not prior heat exposure, increases heat tolerance of reef corals. *Global Change Biol.* 21, 236–249. doi: 10.1111/gcb.12706

Singh, D., Singh, C. K., Sewak, R., Tomar, S. and Pal, M. (2017). Genetics and Molecular Mapping of Heat Tolerance for Seedling Survival and Pod Set in Lentil. *Crop Sci.* 57, 3059–3067. doi: 10.2135/cropsci2017.05.0284

Smith, D. J., Suggett, D. J. and Baker, N. R. (2005). Is Photoinhibition of Zooxanthellae Photosynthesis the Primary Cause of Thermal Bleaching in Corals? *Global Change Biol.* 11 (1), 1–11.

Souter, D., Planes, S., Wicquart, J., Logan, M., Obura, D. and Staub, F. (2020). Status of Coral Reefs of the World: 2020 Chapter 2. *Status Coral Reefs World*. 1–19.

Soyk, S., Benoit, M., and Lippman, Z. B. (2020). New Horizons for Dissecting Epistasis in Crop Quantitative Trait Variation. *Annu. Rev. Genet.* 54, 287–307. doi: 10.1146/annurev-genet-050720

Therneau, T. M., and Grambsch, P. (2000). Modeling Survival Data: *Extending the Cox Model*. New York: Springer-Verlag.

Thomas, L., and Palumbi, S. R. (2017). The genomics of recovery from coral bleaching. Proceedings of the Royal Society B. *Biol. Sci.* 284 (1865), 1–10. doi: 10.1098/rspb.2017.1790

Traylor-knowles, N., Rose, N. H., Sheets, E. A. and Palumbi, S. R. (2017). Early Transcriptional Responses during Heat Stress in the Coral Acropora hyacinthus. *Biol. Bull.* 232, 91–100. doi: 10.1086/692717

Treangen, T. J. and Salzberg, S. L. (2012). Repetitive DNA and Next-Generation Sequencing: Computational Challenges and Solutions. *Nat. Rev. Genet.* 13 (1), 36–46. doi: 10.1038/nrg3117

van Oppen, M. J. H., Oliver, J. K., Putnam, H. M. and Gates, R. D. (2015). Building coral reef resilience through assisted evolution. *Proc. Natl. Acad. Sci.* 112 (8), 2307–2313. doi: 10.1073/pnas.1422301112

Venuprasad, R., Dalid, C. O., del Valle, M., Zhoa, D., Espiritu, M., Sta Cruz, M. T., et al. (2009). Identification and Characterization of Large-Effect Quantitative Trait Loci for Grain Yield Under Lowland Drought Stress in Rice Using Bulk-Segregant Analysis. *Theor. Appl. Genet.* 120, 177–190. doi: 10.1007/s00122-009-1168-1

Vikram, P., Swamy, B. P. M., Dixit, S., Ahmed, H., Cruz, M. T. S., Singh, A. K, et al. (2012). Field Crops Research Bulk segregant analysis : " An effective approach for mapping consistent-effect drought grain yield QTLs in rice ." *Field Crops Res.* 134, 185–192. doi: 10.1016/j.fcr.2012.05.012

Waite, T. A. and Campbell, L. G. (2006). Controlling the False Discovery Rate and Increasing Statistical Power in Ecological Studies. *Ecoscience* 13 (4), 439–442. doi: 10.2980/1195-6860(2006)13[439:CTFDRA]2.0.CO;2

Wang, M., Liu, W., Jiang, B. and Peng, Q. (2019). Genetic Analysis and Related Gene Primary Mapping of Heat Stress Tolerance in Cucumber Using Bulked Segregant Analysis. *Horticulture Sci.* 54 (3), 423–428. doi: 10.21273/HORTSCI13734-18

Wang, S., Meyer, E., McKay, J. and Matz, M. (2012).). 2B-Rad: A Simple and Flexible Method for Genome-Wide Genotyping. *Nat. Methods* 9 (August), 808–810. doi: 10.1038/nmeth.2023

Weeriyanun, P., Collins, R. B., Macadam, A., Kiff, H., Randle, J. L. and Quigley, K. M. (2021). Predicting Selection-Response Gradients of Heat Tolerance in A Wide-Ranging Reef-Building Coral. *BioRxiv*. doi: 10.1101/2021.10.06.463349

Wellenreuther, M., and Hansson, B. (2016). Detecting Polygenic Evolution: Problems, Pitfalls, and Promises. *Trends Genet*. 32 (3), 155–164. doi: 10.1016/j.tig.2015.12.004

Wickham, H., Averick, M., Byan, J., Chang, W., McGowan, L. D., Francois, R., et al. (2019). Welcome to the Tidyverse. *J. Open Source Software* 4 (43), 1–6. doi: 10.21105/joss.01686

Wickham, H., Francois, R., Henry, L. and Muller, K. (2020) *dplyr: A Grammar of Data Manipulation (R package version 0.8.4)*. Available at: https://cran.r-project.org/package=dplyr.

Wilson, A. J., Réale, D., Clements, M. N., Morrissey, M. M., Postma, E., Walling, C. A., et al. (2010). An Ecologist's Guide to the Animal Model. *J. Anim. Ecol.* 79 (1), 13–26. doi: 10.1111/j.1365-2656.2009.01639.x

Woolsey, E. S., Keith, S. A., Byrne, M., Schmidt-Roach, S. and Baird, ,. A. H. (2014). Latitudinal Variation in Thermal Tolerance Thresholds of Early Life Stages of Corals. *Coral Reefs* 34, 471–478. doi: 10.1007/s00338-014-1253-z

Wright, R. M., Aglyamova, G. V., Meyer, E. and Matz, M. V. (2015). Gene Expression Associated With White Syndromes in A Reef Building

Coral, Acropora hyacinthus. *BMC Genomics* 16 (1), 1–12. doi: 10.1186/s12864-015-1540-2

Zhang, Y., Sun, J., Mu, H., Li, J., Zhang, Y., Xu, F., et al. (2015). Proteomic Basis of Stress Responses in the Gills of the Pacific Oyster Crassostrea gigas. *J. Proteome Res.* 14 (1), 304–317. doi: 10.1021/pr500940s

Zhu, Y., Bergland, A. O., González, J. and Petrov, D. A. (2012). Empirical Validation of Pooled Whole Genome Population Re-Sequencing in Drosophila melanogaster. *PloS One* 7 (7), 1–7. doi: 10.1371/journal.pone.0041901

Conflict of Interest: The authors declare that the research was conducted in the absence of any commercial or financial relationships that could be construed as a potential conflict of interest.

Publisher's Note: All claims expressed in this article are solely those of the authors and do not necessarily represent those of their affiliated organizations, or those of the publisher, the editors and the reviewers. Any product that may be evaluated in this article, or claim that may be made by its manufacturer, is not guaranteed or endorsed by the publisher.

frontiers | Frontiers in Ecology and Evolution

TYPE Original Research
PUBLISHED 20 October 2022
DOI 10.3389/fevo.2022.925648

OPEN ACCESS

EDITED BY
Diana Sofia Madeira,
University of Aveiro, Portugal

REVIEWED BY
Matthew Sasaki,
University of Connecticut,
United States
Anu Vehmaa,
Åbo Akademi University, Finland

*CORRESPONDENCE
Victor M. Aguilera
victor.aguilera@ceaza.cl

SPECIALTY SECTION
This article was submitted to Ecophysiology,
a section of the journal
Frontiers in Ecology and Evolution

RECEIVED 21 April 2022
ACCEPTED 20 September 2022
PUBLISHED 20 October 2022

CITATION
Aguilera VM and Bednaršek N (2022) Variations in phenotypic plasticity in a cosmopolitan copepod species across latitudinal hydrographic gradients. *Front. Ecol. Evol.* 10:925648. doi: 10.3389/fevo.2022.925648

Variations in phenotypic plasticity in a cosmopolitan copepod species across latitudinal hydrographic gradients

Victor M. Aguilera [1,2,3]* and Nina Bednaršek [4,5]

[1]Centro de Estudios Avanzados en Zonas Áridas (CEAZA), Coquimbo, Chile, [2]Facultad de Ciencias del Mar, Departamento de Biología Marina, Universidad Católica del Norte, Coquimbo, Chile, [3]Millennium Institute of Oceanography (IMO), Universidad de Concepción, Concepción, Chile, [4]National Institute of Biology, Marine Biological Station, Piran, Slovenia, [5]Cooperative Institute for Marine Resources Studies, Oregon State University, Newport, OR, United States

Studies assessing latitudinal variations in habitat conditions and phenotypic plasticity among populations yield evidence of the mechanisms governing differentiation in the potential to adapt to current/future habitat changes. The cosmopolitan copepod species *Acartia tonsa* thrives across ocean clines delimiting Seasonal (30–40° S) and Permanent (10–30° S) Upwelling coastal provinces established during the middle–late Pliocene (3.6–1.8 Ma) alongshore the South East Pacific (SEP), nowadays exhibiting contrasting variability features related to several ocean drivers (temperature, salinity, pH, and food availability). Latitudinal variation across the range of environmental conditions of the coastal provinces can contribute toward shaping divergent *A. tonsa's* phenotypes, for example, through specific patterns of phenotypic plasticity in morphological and physiological traits and tolerance to environmental drivers. With the aim of contributing to the understanding of these adaptive processes in a relatively little studied oceanic region, here we compared the expression of parental (i.e., adult size, egg production, and ingestion rate) and offspring (i.e., egg size) traits in relation to variation in environmental habitat conditions across different cohorts of two distant (> 15° latitude) *A. tonsa* populations inhabiting estuarine and upwelling habitats located in the Seasonal and Permanent Upwelling province, respectively. Mean conditions and ranges of variability in the habitat conditions and phenotypic plasticity of parental and offspring traits within and among cohorts of *A. tonsa* populations varied significantly across the different examined regions (i.e., Seasonal vs. Permanent). We also found significant differences in the coupling of habitat variability and trait expression, suggesting that the differences in trait expressions might be related to habitat variability. The phenotypic divergence was translated to cohort-related patterns of trait trade-offs regulating reproduction and tolerance of egg production efficiency that can jointly determine the level of plasticity, genetic structure, or local adaptation. The current findings provide novel evidence of how

divergent phenotypes might sustain *A. tonsa* populations across variable coastal provinces of the SEP.

KEYWORDS

coastal ocean, environmental variability, latitudinal gradient, phenotypic plasticity, copepod

Introduction

The variability in morphological and physiological traits that underlie the phenotypic plasticity of individuals is a fundamental component toward understanding the dynamics and persistence of the wild populations against the fluctuating nature of the habitat (Pianka, 1976; Stearns, 1992). Trait-related phenotypic plasticity (i.e., the genotype to have a broader tolerance) in the variable habitats supports the maintenance of individual fitness despite the shifts in the mean habitat conditions and inherent variability (e.g., Schlichting and Pigliucci, 1998; Pigliucci, 2001, 2005). Phenotypic plasticity is manifested during different ontogenetic stages (Senner et al., 2015) and across multiple life history traits (Langerhans, 2018). The expression of traits can vary with that of other traits through trade-offs (Zera and Harshman, 2001; Ortega-Mayagoitia et al., 2018), which can reveal adaptive costs of plasticity (Stillman, 2003; Sasaki and Dam, 2021). In adults, phenotypic plasticity is also related to the phenotype and fitness of their offspring, through parental anticipatory effects or adaptive plasticity (Morrongiello et al., 2012 and references therein). This is mediated by genetic components contributing to the local adaptation (Sunday et al., 2011), such that genetic polymorphism may promote rapid phenotypic responses as a response to changes in the environment (Bitter et al., 2019; Brennan et al., 2019; Sasaki and Dam, 2020). Studies of the drivers and extent of intraspecific variations in phenotypic plasticity within single marine species can yield essential information in determining the mechanisms of populations resilience under current as well as the potential adaptation to future habitat changes (Porlier et al., 2012; Barley et al., 2021; Sasaki and Dam, 2021).

Climate and geographic milestones consolidated during the middle–late Pliocene (3.6–1.8 Ma) (Lindberg, 1991; Cardenas et al., 2009 and references therein) alongshore the South East Pacific (SEP) nowadays promote different climatic (Tapia et al., 2014) and ecogeographic coastal provinces (Camus, 2001; Escribano et al., 2003; **Supplementary Figure 1**). Each province exhibits contrasting mean conditions and variability ranges in several ocean drivers (temperature, salinity, pH, and food) (Vargas et al., 2017), likely conducting to spatial patterns of local adaptation in contemporary populations (Gaitán-Espitia et al., 2017; Vargas et al., 2022). The Seasonal Upwelling province extends from 30° S to 40° S, corresponding to > 1,000 km of coast widely interrupted by river discharges. The river influence on the coastal ocean is maximal during the rainy austral fall-winter, while an intense upwelling activity becomes more important on local hydrography during spring-summer seasons (Vargas et al., 2016). The physical–chemical gradients occurring along and across-shore in these habitats due to river and upwelling influence also experience high-frequency shifts associated with tidal cycles, yielding a temporarily predictable and spatially variable temperature, salinity, and pH mosaic over relatively small coastal areas (Aguilera et al., 2013; Vargas et al., 2016; Garcés-Vargas et al., 2020; Osma et al., 2020). More than 15° latitude toward the north, the Permanent Upwelling province (18–30° S) is located off the Atacama Desert, where nearshore habitat conditions vary in a less predictable way over the synoptic-temporal scale (García-Reyes et al., 2014; Aguilera et al., 2020). Year-round upwelling of cold (< 14°C) and salty and low pH (< 7.7) subsurface water (Torres et al., 1999; Aguilera et al., 2020) leads to synoptic changes in surface ocean conditions, though individual upwelling events are highly variable depending on wind stress and involved water masses (Song et al., 2011; Oerder et al., 2015). Additionally, El Niño (EN) Southern Oscillation can dramatically disrupt the upwelling variability pattern given its proximity to the Equatorial Pacific (Ulloa et al., 2001; Escribano et al., 2004; Aguilera et al., 2019). Empirical evidence scattered over these provinces accumulated over three decades has established strong signatures of higher variability and likely lower predictability in the upwelling habitats (Tapia et al., 2009; Aguirre et al., 2021). These *in situ* studies are fundamental to the ongoing debates in ecology and evolution, specifically, the extensive theoretical and emerging empirical research investigating how organisms have evolved to cope with high heterogeneous habitats (Vargas et al., 2017, 2022).

The cosmopolitan copepod species *Acartia tonsa* (Chaalali et al., 2013) is contemporarily distributed alongshore the SEP from 54° S in the sub-Antarctic region (Aguirre et al., 2012), to the tropical upwelling (20° S) systems (Aguilera et al., 2011; Ruz et al., 2015). In fact, *A. tonsa* is common and abundant enough to be considered as a foundation species in estuarine and upwelling habitats embedded in the contrasting coastal provinces of the SEP (Peterson et al., 1988; Hidalgo and Escribano, 2007; Vargas et al., 2007; Escribano et al., 2009;

Aguilera et al., 2013). Latitudinal gradients occurring in the average and ranges of environmental drivers can influence the expression of traits in copepods, leading to divergent patterns of phenotypic plasticity within populations on a long-term scale (Dunson and Travis, 1991; Pörtner et al., 2004; Lercari and Defeo, 2006). Investigations of variation in physiological traits across space and time can yield evidence for latitudinal differences in phenotypic plasticity among *A. tonsa* populations (Sasaki and Dam, 2019), including acclimation (Stillman, 2003) and developmental phenotypic plasticity (Pereira et al., 2017), and ultimately shape populations' tolerance to variation in environmental conditions (Dam, 2013). Phenotypic divergence can be assessed by analyzing variation in the expression of parental and offspring traits within and across cohorts of the *A. tonsa* populations inhabiting latitudinally distant and climate different coastal provinces. Body size (BS), egg production (EPR), egg size (ES), and ingestion rate (IR) are fundamental traits shaping phenotypic plasticity and acclimation responses outlining the fitness under variable conditions in a given habitat (Kingsolver and Huey, 1998). Recent studies investigated the factors that determine variations in the expression of the traits in heterogeneous habitats (Moran, 1992; Reed et al., 2010; Bernhardt et al., 2020; Bitter et al., 2021) and showed that more heterogeneous habitats, i.e., characterized by a greater difference in the variation, might favor alternative phenotypes, expanding the phenotypic plasticity. Phenotypic plasticity is often modeled in wild populations as the slope of the reaction norm (Stearns, 1992), which can reveal differences among populations in the tolerance to environmental changes (Sasaki and Dam, 2019). On the other hand, dominant drivers, such as temperature, might also act toward reducing phenotypic plasticity (Barley et al., 2021), determining the impact of multiple factors on the development of the population-level phenotypic plasticity. In order to understand the mechanisms that govern the variation in copepod phenotypic plasticity across latitudinal gradients, we studied variation in the expression of morphometric and physiological traits within and across three different cohorts of the two *A. tonsa* populations sourced from an estuarine and upwelling habitat located at the Seasonal (39.8° S) and Permanent (23.3° S) Upwelling provinces of the SEP, respectively. Our study characterized specific habitat variability and phenotypic plasticity at the inter-daily scale of a comprehensive suite of parental (BS, EPR, and IR), and offspring (ES) reproduction-related traits, established for each cohort. Our fundamental question was to investigate the linkage between environmental conditions and variation in the expression of traits within and among cohorts potentially shaping divergent patterns of phenotypic plasticity in *A. tonsa* populations. We found significant differences in the phenotypic plasticity of parental and offspring traits among cohorts of and between *A. tonsa* populations across two examined regions (i.e., Seasonal vs. Permanent). Environmental–biological coupling and cohort-related patterns of trait trade-offs regulating reproduction also diverged between populations, potentially determining the tolerance to environmental drivers. Our study provides novel evidence of how divergent phenotypes might sustain *A. tonsa* populations across latitudinal coastal gradients in the SEP.

Materials and methods

Two divergent study areas

The estuarine and upwelling habitat are located in two distant (>3,000 km, >15° latitude distant) and contrasting climatic-ecogeographic provinces alongshore the SEP (Camus, 2001; Escribano et al., 2003; Tapia et al., 2014; **Supplementary Figure 1**). The first habitat is an estuarine system in Southern Chile (Valdivia River Estuary, 39.8° S), strongly seasonal and affected year-round by river runoff discharges (average 484 ± 300 m^3 s^{-1}; Pérez et al., 2015). Nearshore, river discharges are partially mixed by coastal circulation (Pino et al., 1994), and temporarily modulated by tidal cycles. Such interaction promotes as a whole a marked alongshore gradient in the average and range of temperature (15 ± 2°C), salinity (33 ± 1 psu), and pH_T (7.93 ± 0.3) (Aguilera et al., 2013; Garcés-Vargas et al., 2020; Osma et al., 2020). The second habitat is the Antofagasta upwelling center (Antofagasta, 23.3° S), situated off the most arid desert in the world, the Atacama Desert, which lacks seasonality (Tapia et al., 2014) and freshwater discharges (Hartley et al., 2005). Equatorward wind prevails year-round at this latitude (Strub et al., 1998), favoring permanent upwelling events at the coast. Depending on the intensity and extent of wind stress, the vertical advection of deep-cold (< 14°C) and low pH_T (< 7.7) water masses synoptically affects the nearshore surface habitat (Torres et al., 1999; Aguilera et al., 2020), with upwelling events highly different from each other. Mean profiles of temperature and salinity illustrate vertical differences between habitats and vertical variations as well (**Supplementary Figure 2**). Importantly, ocean clines delimiting the aforementioned coastal provinces can act as effective dispersal barriers for populations of benthic species (Cardenas et al., 2009 and references therein).

Cohorts' assessment and temporal habitat characterization

The copepod *A. tonsa* is a neritic species distributed over the upper 30 m of the water column (Paffenhöfer and Stearns, 1988). Within this range, the peak of chlorophyll-*a* (i.e., copepods food index) is often placed within the upper 10 m in nearshore habitats alongshore the SEP (Escribano et al., 1997, 2009;

TABLE 1 Sampling information within each coastal habitat and population.

Habitat	Mean sampling freq. (d)	Column depth (m)	Sampling depth (m)	Cohort	Year	Surveys
Estuarine	4	20	7*	I	2010–2011	12
			7–12**	II	2011	9
				III	2012	9
Upwelling	6	40	10*	I	2015	9
			20–10**	II	2015	9
				III	2015	10

Habitat conditions and trait expression of three different cohorts were assessed for each population, whose reproductive cycles are either seasonally (estuarine) or year-round (upwelling). Oceanographic (*) and plankton (**) sampling.

Osma et al., 2020). Depending on habitat depth, variability in environmental conditions (temperature, salinity, pH, and food) was in general characterized at 7 m in the estuarine and 10 m in the upwelling habitat (**Table 1**). Because of specific depth measurements, we could not consider vertical variability in the conditions, however, the large bathymetric gradient occurs at the surface (1 m) and near the bottom due to the influence of less dense and low pH freshwater lens (Osma et al., 2020) and turbulent and sediment enriched tidal currents (Pino et al., 1994; Vargas et al., 2003), respectively (see **Supplementary Figure 2**). In the upwelling habitat, *A. tonsa* displays restricted vertical migrations constrained to the upper 30 m likely due to a shallow oxygen minimum zone (Escribano et al., 2009). Habitat conditions were measured interdaily (i.e., each 4–6 days) through 30 estuarine and 28 upwelling nearshore surveys (**Table 1**). The occurrence and reproduction of the estuarine *A. tonsa* population are restricted to the austral spring–summer season (Aguilera et al., 2013). Thus, sampling distributed from 2010 to 2012 was carried out during the austral spring–summer seasons (**Table 1**), corresponding to the seasonal occurrence of the individuals, with no copepods found during fall–winter periods (Aguilera et al., 2013). Variations in habitat drivers (and thus related copepod traits) at the estuarine habitat were measured under the impact of the flood tides, since during ebb tides, the water column is shallower and the abundance of *A. tonsa* individuals was lower. Temperature (°C) and salinity (psu) were recorded at the sampling depth (± 1 m) by a CTD (Ocean Seven 305 Plus[1]). Discrete water samples were collected at 7 m depth with a Niskin bottle for determination of food availability and pH_T. Food concentration was determined in triplicate as counts of nanoflagellates and phytoplankton cells in carbon units (μg C L^{-1}) with their bio-volumes assessed with an inverted microscope OLYMPUS IX-51. Bio-volumes were converted to carbon units by using carbon:volume conversion factors available in the literature (e.g., Vargas and González, 2004). Within 2 h of water collection, triplicate pH_T measurements were assessed in a closed 25-ml cell thermostated at 25.0°C using a Metrohm 713 pH meter, and a glass combined double junction Ag/AgCl electrode (Metrohm model 6.0219.100) calibrated with Tris buffer at 25°C. By using temperature, salinity, $pH_{25°C}$, and total alkalinity (not shown) data, pH was calculated at total scale (pH_T) through the CO2CYS software v.3.0 (Pierrot et al., 2021).

Reproductive copepods of *A. tonsa* are found throughout the year in the upwelling habitat with several season-independent recruitment episodes with generation times of two weeks to two months (Hidalgo and Escribano, 2007). Discrete samplings in this habitat were carried out throughout 2015 (**Table 1**). Temperature (°C) and salinity (psu) were recorded at the sampling depth (± 1 m) with a SeaBird SBE19 Plus CTD. Discrete water samples were attained at 10 m depth through oceanographic sample collections, for determinations of chlorophyll-*a* concentration (copepod food) and pH_T. For determinations of chlorophyll-*a* (Chl) concentration, seawater was filtered on 200 μm mesh to remove large-sized grazers and debris while maintaining natural food assemblages. Triplicate samples (200 ml) were filtered onto a GF/F filter (nominal pore size = 0.7 μM). Chl was extracted for 24h in 90% acetone v/v and measured in a TD Turner fluorometer (Strickland and Parsons, 1972). Chl concentration (μg Chl L^{-1}) was converted to carbon units by using a Chl:C ratio = 120 (Vargas and González, 2004). Within 2 h of collection, seawater pH_T was measured in triplicate as described above in a closed 25-ml cell thermostated (25°C).

Copepod collection

Parental and offspring traits were assessed in three different cohorts of the estuarine *A. tonsa* population over the period of 2010–2012 (**Table 1**), while in the northern-upwelling habitat, these traits were assessed throughout 2015. Based on intraseasonal changes in temperature and body size observed at the upwelling habitat during sampling, three different cohorts were identified within the upwelling population (see "Results" section). Plankton samples were obtained by gently oblique hauling of a 200-μm mesh size WP2 net equipped with a closing

1 www.idronaut.it

system and non-filtering 1 L cod-end, from 7 to 12 m (estuarine) and 10–15 m (upwelling) depth strata. Each time, the content of the cod-end was gently transferred to a temperature-controlled container containing aquarium bubblers to keep containers well oxygenated over the duration of transport to the laboratory. Within 2 h of collection, mature and visibly healthy adult copepod females were sorted out under a stereomicroscope and transferred in groups of 10 females to 200 ml beakers. Copepods were incubated in natural seawater collected during sampling with the aim of conducting the experiments to estimate phenotypic plasticity in parental and offspring traits as related to the habitat-specific variations in environmental conditions (**Supplementary Figure 2**). Laboratory temperature was maintained at a controlled temperature (14 ± 1°C at the estuarine and 15 ± 1°C at the upwelling habitat), which corresponded to the temperature conditions experienced by the various cohorts in the natural habitats. Given that we infer that the parental and offspring traits are all based on the adult females makes a more scattered sampling in the estuarine area more acceptable.

Copepod traits

The assessed traits in the adult females were the following: body size (BS), mean egg production rate (EPR), egg size, and ingestion rate (IR). For BS estimations, up to 45 copepod females grouped in three batches were immediately preserved in 90% ethanol for further measurements of body size (cephalothorax length, mm). Body length was converted to body mass with the *A. clausi* length–dry weight regressions (Uye, 1982) and to body carbon (BC) assuming that the C content was 45% of dry weight (Kiørboe and Nielsen, 1994). The body mass was then considered to estimate specific reproduction rates. Mean egg production rates (EPR) were estimated based on three groups of 30–40 copepod females, individually incubated at *in situ* temperature for 17–20 h in 200 ml clean crystallizing dishes filled with sieved (<200 μm) natural seawater. Eggs produced over this period by each group were counted under a stereomicroscope, standardized to daily duration (24 h), with the mean EPR expressed as the egg fem^{-1} d^{-1} (± SD). Eggs (30) produced by each female group were randomly sorted and preserved (90% ethanol), and their size (i.e., diameter, μm) was measured using an Olympus IX-51 inverted microscope within two weeks of preservation to diminish ethanol effects on egg size (Moksness and Fossum, 1992). Assuming spherical-shaped eggs and a conversion factor of 0.14×10^{-6} μg C μm^{-3} ratio (Huntley and Lopez, 1992), the diameter of the egg size was converted to mass (μg C). Specific EPR was calculated as the EPR/BC quotient × 100% ($EPR_{\%BC}$).

In parallel, ingestion rates (IR) were estimated through the bottle incubation method (Kiørboe et al., 1982) and expressed in μg C fem^{-1} d^{-1}. Additional copepod (4–5) females were pipetted into three 660-ml borosilicate bottles containing ambient water filled with < 200 μm natural food assemblages. These bottles alongshore another three control bottles without animals (i.e., blank bottles) were placed on a plankton wheel rotated r at 1.2 rpm for 14–16 h at the same temperature as the EPR was estimated. Subsamples were preserved at the beginning (T_0) and at the end of the incubation period (T_f) from experimental and blank bottles. Ingestion rate (IR) (μg C fem^{-1} d^{-1}) was calculated following Frost (1972) and modified by Marín et al. (1986). With data of EPR (μg C fem^{-1} d^{-1}) and IR (μg C fem^{-1} d^{-1}), the egg production efficiency (EPE) was calculated as the EPR/IR quotient.

Defining terms

Due to the abundance of data and multiple analyses across various cohorts, we provide a definition of the measurements and this related interpretation in this study. In this study, we refer to estuarine and upwelling *A. tonsa* populations in the absence of genetic evidence supporting the occurrence of various genotypes. Cohorts of the respective population were sampled in subsequent chronological order, which implies that the latter cohorts inherently contain genetic information in response to environmental conditions experienced by earlier cohorts. However, cohorts, especially those from the estuarine habitat but also those from the upwelling location considering habitat environmental variability, were sampled and correspond to discrete subgroups within a highest-level nominal group or population. Habitat drivers and copepod traits were characterized in terms of mean values and their variability, with reaction norms on different cohorts of both *A. tonsa* populations. For each cohort, habitat conditions and traits were assessed only at the adult stages, which referred to different cohorts between measurements. There are two measures of variability within and among cohorts. The first one is a measure of variations, i.e., the variability experienced by a single cohort. The second is similar to that experienced across generations or among different cohorts, ultimately characterizing each population. We also define the term "trade-off" as a significant correlation between two traits (Zera and Harshman, 2001; Ortega-Mayagoitia et al., 2018).

Data analysis

Habitat environmental and copepod data were examined for requirements of parametric tests, such as normal distribution (Lilliefors test, $p < 0.01$) and homogeneity of variance

(Levene's tests). Variations in nominal environmental drivers and copepod traits were assessed regarding two variability factors: habitats/populations (groups) and cohorts (subgroups). To evaluate changes in a nominal variable among subgroups in relation to a single value of the highest-level nominal variable (the groups), we utilized a nested design ANOVA (Error type III) in which cohorts were nested within their respective habitat/population. To evaluate the potential effects of plasticity on trait differences between habitats, we conducted a linear mixed effects model in which environmental drivers and habitat were considered as fixed effects and cohorts as random effects. Plasticity effects on trait variations were indicated by a significant interaction between environmental drivers and habitat. The correlation or coupling between environmental variability with identified drivers and biological variables was explored in both habitats, first through the Principal Component Analysis (PCA). The numerical relationships of specific $EPR_{\%BC}$ and EPE with environmental drivers were explored with Pearson's correlation tests, such as plastic responses expressed as a mean reaction norm that had a significantly non-zero slope, and were compared between populations (Stearns, 1992). Mechanistic relationships between traits and specific environmental features can yield insights into ecological speciation among populations (Chen and Hare, 2008). Ocean Data View and SURFER packages provided graphical outputs, whereas statistical analyses were performed in STATISTICA package10.

Results

Intrahabitat/population variability

The distribution of environmental conditions (temperature, salinity, pH_T, and food concentration) showed normal distribution and homogeneity of variance in both habitats. Habitat drivers varied widely among cohorts of the estuarine (**Figure 1**) and upwelling (**Figure 2**) population, while also exhibiting fluctuations within cohorts (**Supplementary Figure 3**). The mean temperature range at the estuarine habitat was 12°C–17°C (**Figure 2A**), in which each cohort experienced mean thermal fluctuations of 3.5°C without significant changes among cohorts (**Table 2**). A warmer mean temperature range (14°C–17°C) was observed in the upwelling habitat (**Figure 2A**). The significant changes in temperature were observed among cohorts of the upwelling population (**Table 2**), which in general experienced narrower (2.6°C) thermal fluctuations. Salinity varied between 31.5 and 34 psu at the estuarine (**Figure 1B**) and between 34.6 and 35.1 psu at the upwelling habitat (**Figure 2B**). Cohorts of the estuarine population experienced larger salinity fluctuations, however, salinity varied significantly among cohorts of both populations, especially of the upwelling population (**Table 2**). There was a surprising similarity in the ranges of pH_T variations experienced by cohorts of the estuarine (**Figure 1C**) and upwelling (**Figure 2C**) populations. The significant pH_T variations occurred among cohorts of both populations (**Table 2**) though pH_T ranges were wider for estuarine cohorts. Outliers were detected in food concentration data of the upwelling habitat (Grubbs' test, > 400 μg C L^{-1}). After removing outlier values, food varied between 0 and 350 μg C L^{-1} in the estuarine (**Figure 1D**) and upwelling (**Figure 2D**) habitat. Variations in food concentration were significant among cohorts of the upwelling population (**Table 2**).

The distribution of parental and offspring traits was normally distributed, but egg size failed the test for homogeneity of variance. The expression of parental and offspring traits displayed important variations within the estuarine (**Figure 1**) and upwelling (**Figure 2**) populations. With respect to body size, it varied between 0.85 and 0.99 mm within the estuarine (**Figure 1E**) and between 0.80 and 0.99 mm within the upwelling (**Figure 2E**) population. Variations in BS were significant only among cohorts of the upwelling population (**Table 2**), although BS fluctuations within cohorts were similar between populations. Removing the 0 values (likely related to the incubation of non-egg producing C5 stage with a similar size range as the adults) and outliers (> 70 egg fem^{-1} d^{-1}), the EPR range was 1–57 egg fem^{-1} d^{-1} in the estuarine (**Figure 1F**) and 2–25 egg fem^{-1} d^{-1} in the upwelling (**Figure 2F**) population. There were significant EPR variations among cohorts of both populations (**Table 2**), and larger fluctuations were observed within and among estuarine cohorts. The egg size (ES) varied between 71.3 and 86.2 μm, and 76.5 and 89.5 μm among the cohorts of the estuarine (**Figure 1G**), and the upwelling (**Figure 2G**) population, respectively. Although changes in the ES within cohorts were similar between populations, significant differences in BS were observed among cohorts of the upwelling population (**Table 2**). IR varied between 2 and 7 μg C fem^{-1} d^{-1} among the three cohorts assessed within the estuarine population (**Figure 1H**) and between 3 and 5 μg C fem^{-1} d^{-1} among two cohorts of the upwelling population (**Figure 2H**). IR varied significantly only among cohorts of the estuarine population (**Table 2**).

Significant effects of isolated environmental drivers together with interactions between environmental drivers and habitat explained a relatively lower (28%) to moderate (51%) proportion of the variations accounted for in the expression of copepod traits, according to the linear mixed-effects model (**Table 3**). The interactions between salinity, food, and habitat were important for changes observed in body size. With the exception of food, the interactions between habitat and assessed environmental drivers were significant for EPR variation, whereas only the interaction between habitat and salinity was relevant for changes in egg size. Significant correlations (i.e., trade-offs) between morphometric and physiological traits were detected only in

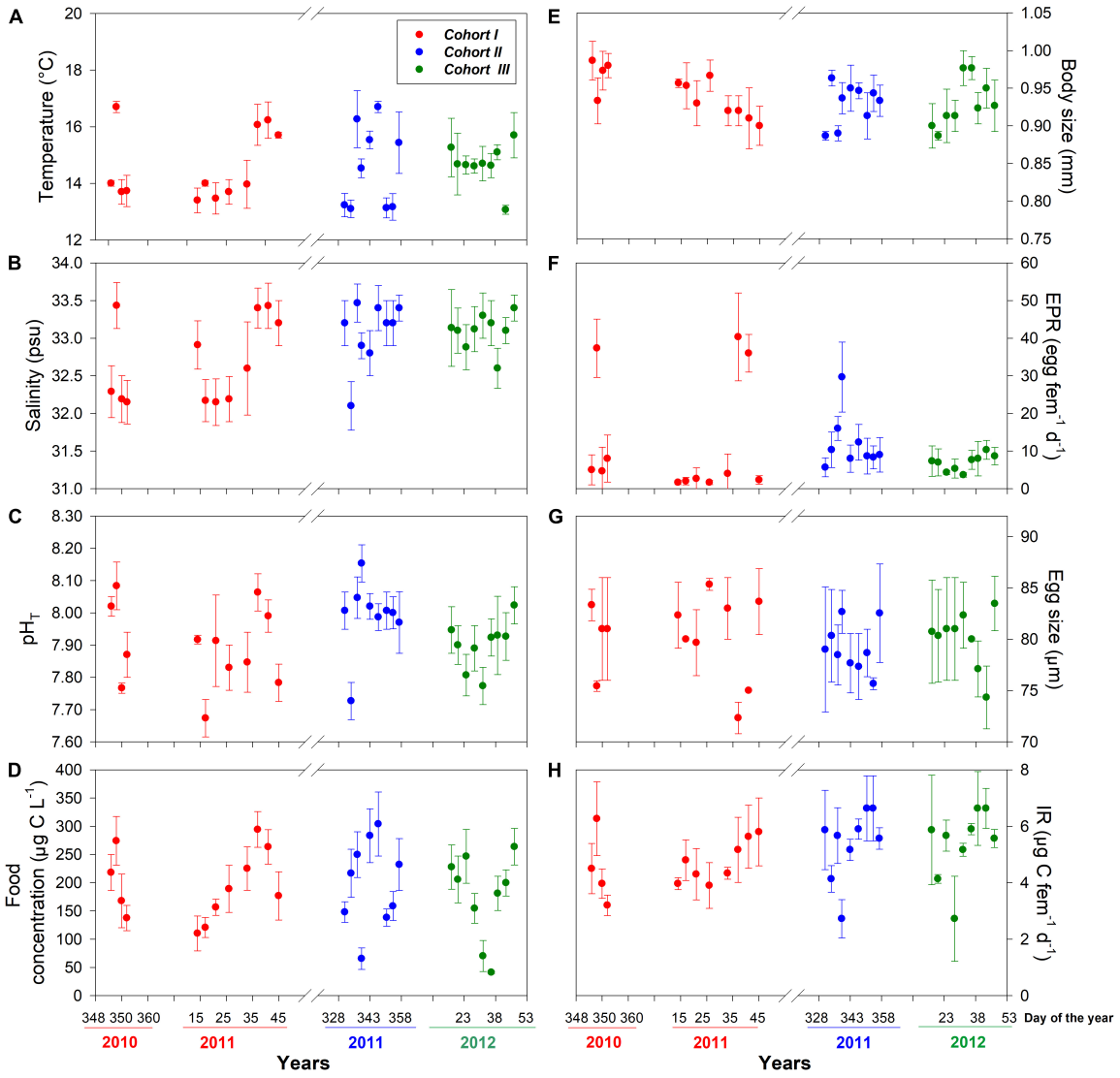

FIGURE 1
Interdaily mean (± SD) values of environmental drivers **(A–D)** and copepod traits **(E–H)** assessed for three different cohorts at the estuarine habitat. Sampling was conducted during the seasonal occurrence and reproductive period of the local *A. tonsa* population.

the estuarine population (Figure 3). Female size was inversely related to EPR (Figure 3A), and EPR was negatively related to eggs (Figure 3B).

Interhabitat/population variability

An average and ranges of environmental conditions and copepod traits were plotted in box plots for comparison between habitats and populations (estuarine and upwelling) (Figure 4). There were significant differences between the two habitats in all assessed environmental conditions except for pH$_T$ (Table 2). The ranges of temperature and salinity were wider, and mean values were significantly higher in the upwelling than estuarine habitat (Figures 4A,B). In contrast to temperature and salinity, pH$_T$ ranges largely overlapped (Figure 4C) with no significant difference in mean pH$_T$ between the habitats (Table 2). Food concentration ranges also overlapped between habitats (Figure 4D), although the mean food concentration in the estuarine (< 150 µg C L^{-1}) was lower than in the upwelling habitat (> 200 µg C L^{-1}) (Table 2). There were significant differences in the expression of parental and offspring traits between the populations, except for EPR (Figure 4). The body size of adult estuarine females was significantly larger than that of their upwelling counterparts (Table 2), though exhibiting a narrower BS range (Figure 4E). Despite mean EPR values not varying significantly between the estuarine and upwelling populations (Table 2), the EPR range was

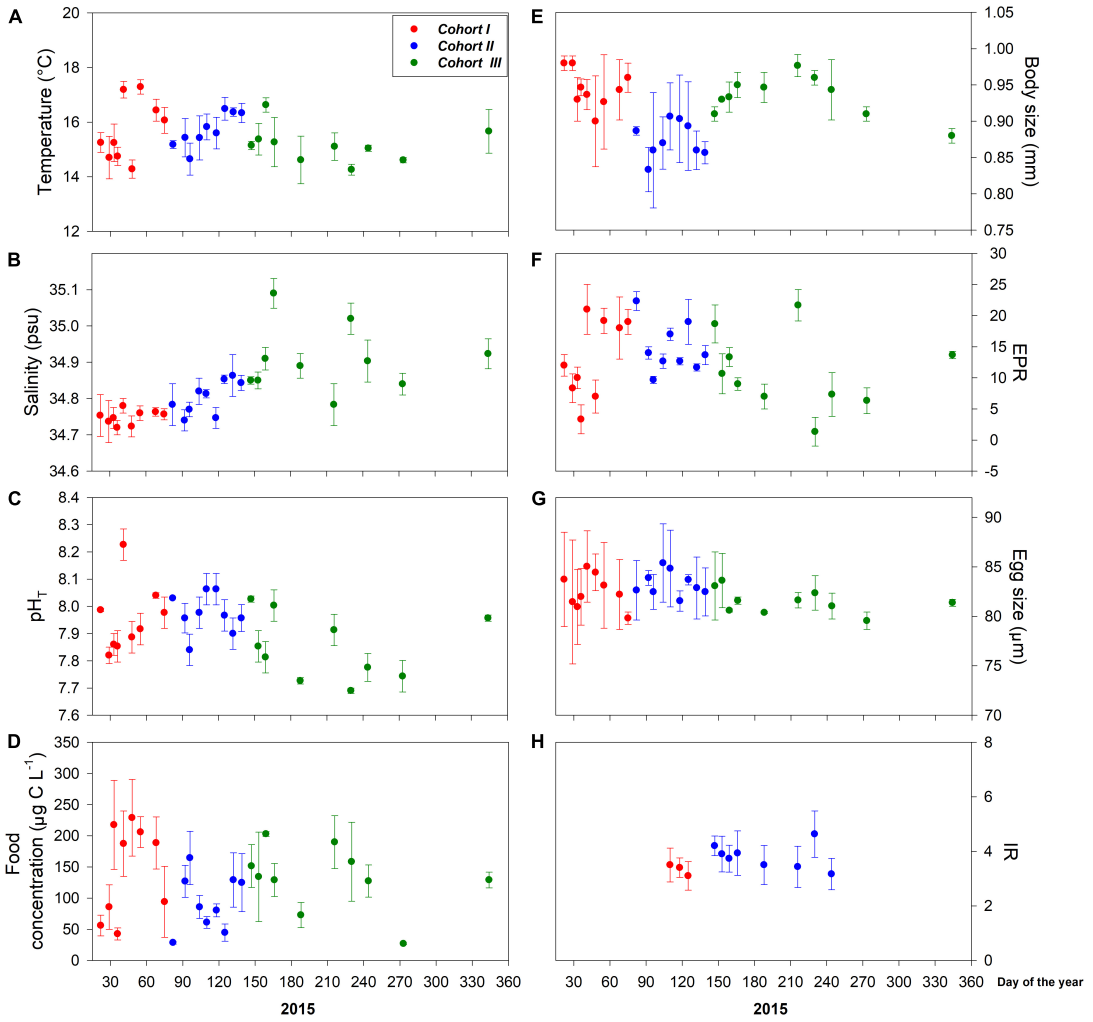

FIGURE 2
Interdaily mean (± SD) values of environmental drivers **(A–D)** and copepod traits **(E–H)** assessed for three different cohorts at the upwelling habitat. Local *A. tonsa* population reproduces year-round under upwelling-dominant environmental conditions, which were strongly disrupted during samplings due to El Niño 2015.

wider within estuarine females (Figure 4F). Among similar ranges of egg size (Figure 4G), the mean value of egg size produced by upwelling females was significantly larger than that produced by estuarine females (Table 2). The IR of estuarine females was significantly higher than that of their upwelling counterparts (Table 2) also exhibiting a wider IR range (Figure 4H).

The association or coupling among nominal environmental drivers and between those with copepod traits was assessed for each habitat with a Principal component analysis (PCA) (Figure 5). Upon assessed abiotic and biotic variables, this analysis accounted for a higher explained variability in the estuarine (R^2 = 69) than in the upwelling (R^2 = 64) habitat. This analysis also revealed a stronger coupling among environmental conditions and between environmental conditions with copepod traits in the estuarine (Figure 5A) than in the upwelling habitat (Figure 5B). Featured variables were salinity, pH_T, EPR, and ES in the estuarine habitat, and salinity, pH_T, BS, and EPR in the upwelling habitat (Supplementary Table 1).

Habitat-specific drivers on the reproduction

Reproduction rates (EPR) were standardized by the body mass of females in carbon units (EPR expressed as a percentage of body mass) (Figure 6). The significant changes in $EPR_{\%BC}$ were observed among cohorts of both populations ($F_{4,168}$ = 14, $p < 0.0001$) (Figure 6A). Such variability in the $EPR_{\%BC}$ was higher among cohorts of the upwelling population, which produced significantly ($F_{1,168}$ = 16, $p < 0.0001$) more carbon

TABLE 2 Comparison of environmental drivers and copepod traits regarding two variability factors: cohorts (3 levels) and habitats (2 levels).

						Among cohorts *Post hoc*		Between habitats *Post hoc*
Variable	**Factor**	**d.f.**	**MS**	**F**	***p*-value**	**Estuarine**	**Upwelling**	**Habitat**
Temperature	Cohorts	4,168	1.4	1.2	< 0.0001	I = II = III	I = II > III	E < U
	Habitat	1,168	36	32	< 0.0001			
Salinity	Cohorts	4,168	1.5	11	< 0.0001	I<II = III	I < II < III	E < U
	Habitat	1,168	162	1191	< 0.0001			
pH_T	Cohorts	4,168	0.1	8.0	< 0.0001	I = III < II	I = II > III	E = U
	Habitat	1,168	0.01	0.1	0.8			
Food	Cohorts	4,168	> 10000	2.3	0.1	I = II = III	I = III > II	E > U
	Habitat	1,168	> 10000	38	< 0.0001			
Body size	Cohorts	4,168	0.02	14	< 0.0001	I = II = III	I = III > II	E > U
	Habitat	1,168	0.01	8.5	0.004			
EPR	Cohorts	4,168	169	2	0.1	I = II > III	I = II > III	E = U
	Habitat	1,168	231	3	0.1			
Egg size	Cohorts	4,168	160	1.2	0.3	I = II = III	I = II > III	E < U
	Habitat	1,168	290	23	< 0.0001			
IR	Cohorts	3,118	8.2	6.8	0.0003	I = II > III	II = III	E > U
	Habitat	1,118	24.0	20.3	< 0.0001			

Cohorts were nested within their respective habitats. Environmental and biological traits passed tests of normal distribution and homogeneity of variance. *Post hoc* test (Tukey) denotes the comparison among cohorts and between populations.

TABLE 3 Results of the linear mixed effects model.

Trait	**Factor**	**Effect(F/R)**	**SS**	**d.f.**	**MS**	**F**	***P***
Body size	Cohort	Random	0.08	4	0.02	15.7	< 0.0001
	Habitat × Environ Sal	Fixed	0.02	2	0.008	5.7	0.004
	Habitat × Environ Food	Fixed	0.01	2	0.005	4.1	0.02
	Error		0.22	162	0.001		
					$R^2 = 0.38$		
EPR	Cohort	Random	1012.0	4	253.0	5.2	0.001
	Habitat	Fixed	349.8	1	349.8	7.2	0.01
	Temperature	Fixed	751	1	751	15.1	0.0001
	pH	Fixed	1905	1	1905	39.2	< 0.0001
	Habitat × Environ Temp	Fixed	765.5	2	382.7	7.9	0.0005
	Habitat × Environ Sal	Fixed	394.1	2	197.0	4.0	0.02
	Habitat × Environ pH	Fixed	2193.6	2	1096.8	22.6	< 0.0001
	Error		7777.5	160	48.6		
					$R^2 = 0.51$		
Egg size	Habitat × Environ Sal	Fixed	89.7	2	44.8	3.9	0.02
	Error		1826.0	160	11.4		
					$R^2 = 0.28$		
IR	Cohort	Random	20.3	3	6.8	7.2	0.0002
	Food	Fixed	1.7	1	1.7	3.3	0.04
	Habitat × Environ Temp	Fixed	6.6	2	3.3	3.5	0.03
	Habitat × Environ Sal	Fixed	18.8	2	9.4	10.0	0.0001
	Habitat × Environ Food	Fixed	10.2	2	5.1	5.4	0.006
	Error		103.2	110	0.9		
					$R^2 = 0.46$		

Only significant terms were included after straightforward analyses in which the adjusted correlation coefficient (R^2) did not vary. EPR and IR correspond to egg production and ingestion rate, respectively.

eggs at a similar body size than their estuarine counterparts (Figure 6B). In addition, the egg production efficiency (EPE), corresponding to the EPR/IR ratio was significantly correlated (i.e., reaction norms), with environmental conditions in both habitats (Figure 7). These correlations demonstrate the impact (i.e., mitigating/aggravating) of habitat conditions and potential differences in the tolerance (i.e., slope) to environmental drivers between populations (Table 4). Temperature exerted a

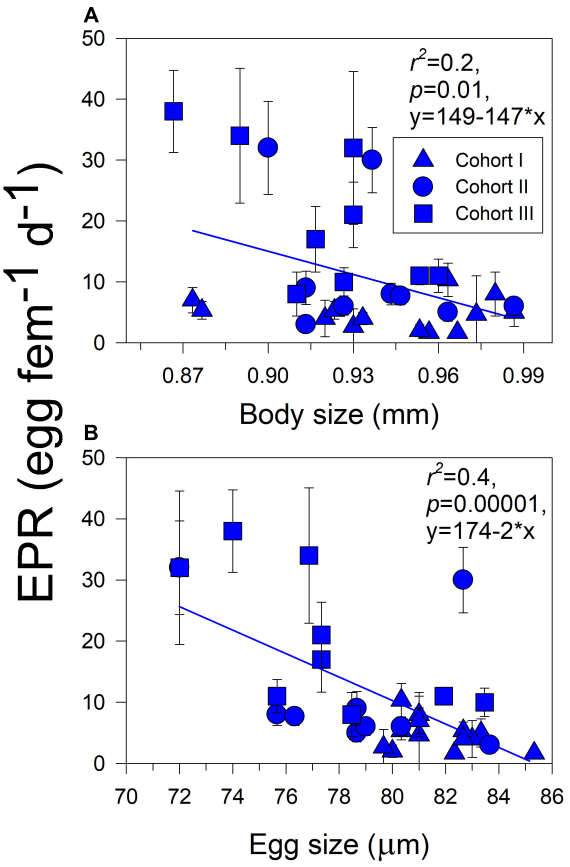

FIGURE 3
Correlations (i.e., trade-offs) between parental **(A)** and offspring **(B)** traits with reproductive trait in the estuarine *A. tonsa* population. Dots represent the average (± SD) value of each trait at a given sampling survey.

mitigating (i.e., positive) effect on the EPE of both populations (Figure 7A), though the EPE of the estuarine population was less tolerant to thermal changes (Table 4). Salinity showed contrasting effects on EPE, mitigating in the estuarine, and aggravating (i.e., negative) in the upwelling population (Figure 7B). The pH_T exerted mitigating effects on the EPE of both populations (Figure 7C), and the estuarine population was less tolerant (slope = 0.8) than the upwelling (slope = 0.12) population to pH changes. Food concentration was only related to EPE in the estuarine population, where it exerted a positive effect (Figure 7D).

Discussion

This study comprehensively captured patterns of variability in the expression of parental and offspring traits within and among cohorts of *A. tonsa* populations sourced from latitudinal distant habitats located in contrasting climatic provinces alongshore the SEP. Understanding the variation in phenotypic plasticity within the species in the wild conferring the acclimation and adaptation to climate change provides central insights for evolutionary ecology (Porlier et al., 2012; Sasaki and Dam, 2020; Barley et al., 2021). One of the aspects is variability across different habitats as it provides cues on different habitat-specific variability that shapes different phenotypes. The information gathered in this study allowed us to compare the habitats' variability manifested as mean values and environmental temporal heterogeneity, environmental–biological coupling, and its relationship with patterns of phenotypic plasticity in parental and offspring traits. In understanding and interpreting these results, contrasting life strategies related to the timing of occurrence to cope with seasonal (estuarine) or synoptic (upwelling) temporal variability affecting habitat conditions can be considered. Under such selective pressure(s), we focused on parental traits that largely predict tactical variation in offspring fitness among populations concerning the environmental quality or variability (Morrongiello et al., 2012 and references therein). The estuarine habitat located in the seasonal ocean seascape exhibited lower temporal variability in habitat drivers among cohorts of the local

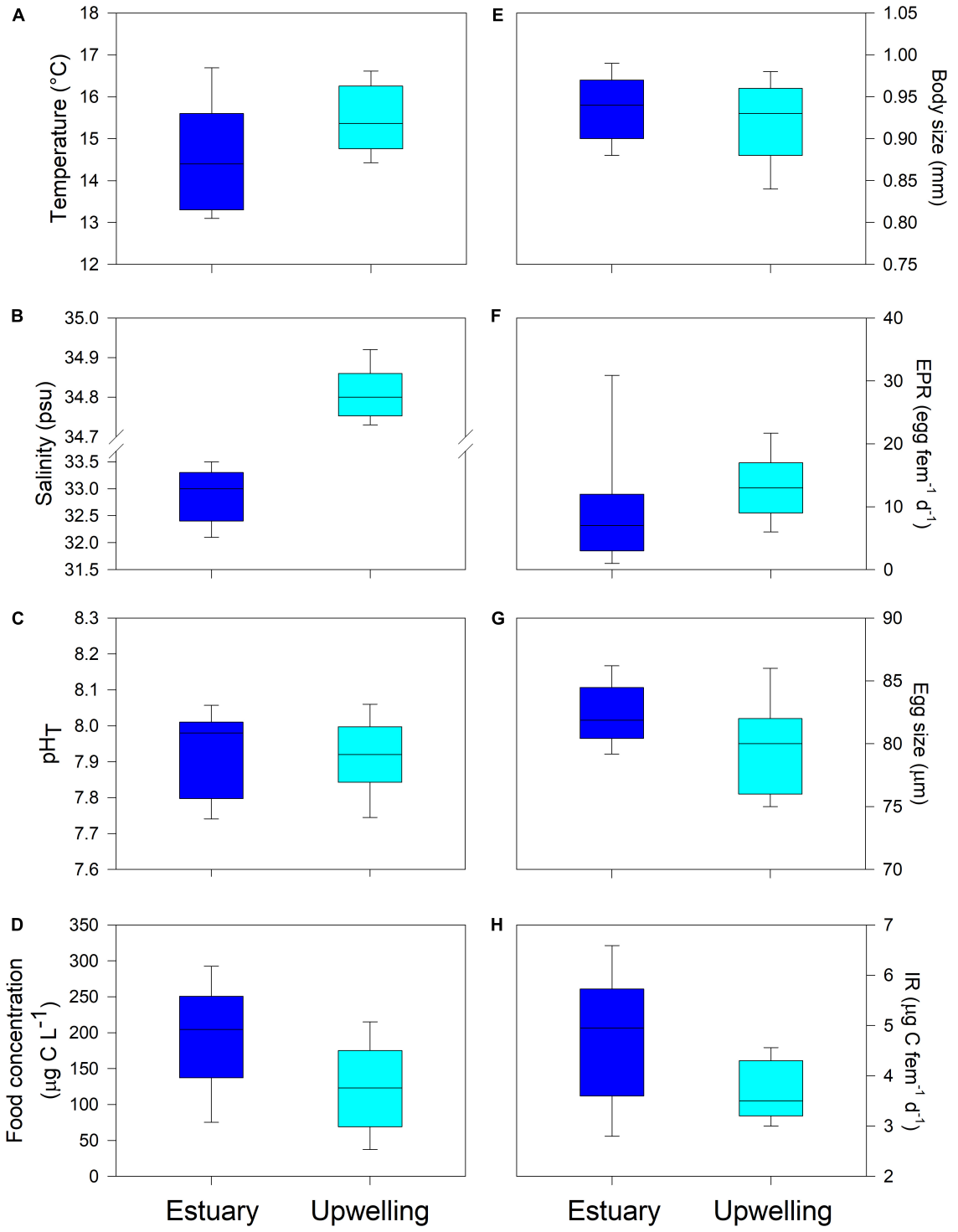

FIGURE 4
Comparison of box plots of environmental drivers **(A–D)** and copepod traits **(E–H)** between examined estuarine and upwelling populations. Statistical results are provided in **Table 2**.

population. The relationship between habitat variability and related traits was higher in the estuarine habitat, suggesting how the extent of habitat variability impacts phenotypic plasticity. The phenotypic divergence was translated to cohort-related patterns of trait trade-offs regulating reproduction and population-specific tolerance

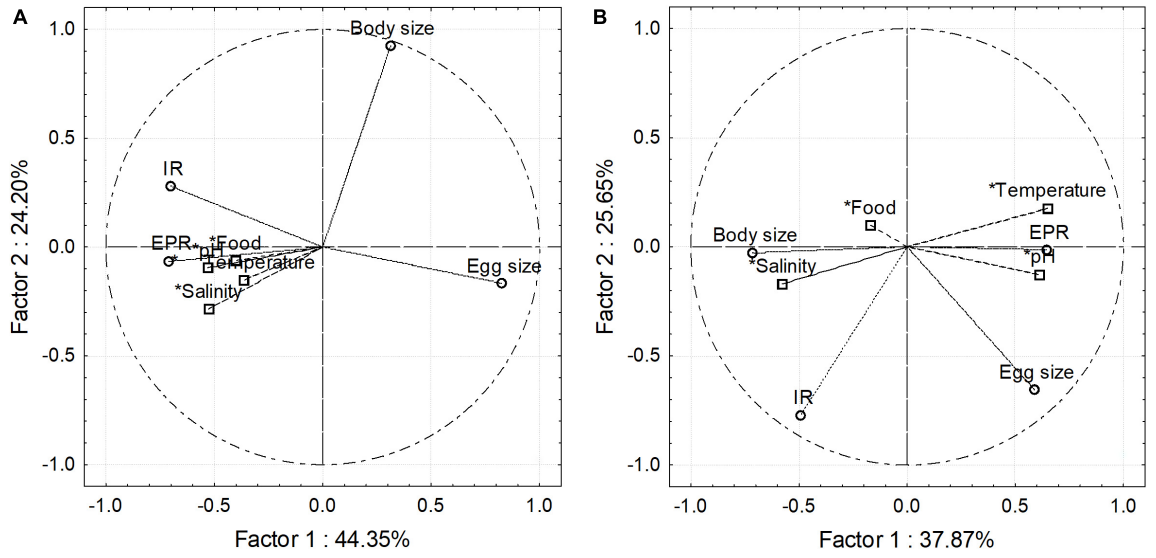

FIGURE 5
Environmental–biological coupling in the estuarine **(A)** and upwelling **(B)** habitat explored through Principal Component Analysis. Besides explaining a higher proportion of the observed variance, PCA in the estuarine habitat also indicates biological cues, especially physiological ones correlated among them.

to environmental changes. Current findings provide novel evidence of how divergent phenotypes might sustain the population of *A. tonsa* across variable coastal provinces of the SEP.

Characterization of cohorts and habitat variability

The assessment of discrete cohorts is well supported in the population inhabiting the seasonal estuarine habitat. Temperate populations exhibit seasonal–biological dynamics (Uye, 1982), and the estuarine population was sampled seasonally across different spring–summer periods from 2010 to 2012. At a mean habitat temperature of 14.6 ± 1.2°C, the local *A. tonsa* population should complete its ontogenetic development within 17–18 days and thus, several recruitment events can occur in the estuarine habitat during the seasonal reproductive cycle over approximately four months between the austral spring (September to October) and summer (December to February) period. In contrast, the upwelling population that reproduces year-round (Hidalgo and Escribano, 2007) was sampled throughout 2015. As with the most wild populations, age distribution among copepod cohorts might be stable or change over time (i.e., true cohort) (Landry, 1978; Durbin and Durbin, 1981). Copepod populations, including *A. tonsa*, grow in a temperature-dependent way in the permanent upwelling habitat (Hidalgo and Escribano, 2007). Furthermore, species of the genus *Acartia* can complete each molt-to-molt phase of the life cycle at a constant time (i.e., isochronal development), which depends on habitat temperature. At a mean temperature of 15.6 ± 0.8°C, the upwelling *A. tonsa* population should complete its life cycle within 17 days (Miller et al., 1977). Given the high likelihood of collecting females belonging to the same cohorts, we assigned Cohort I to those females collected at the beginning of 2015. Although upwelling-driven hydrographic variability prevailed throughout the study period, El Niño 2015 also impacted hydrographic conditions in the upwelling habitat during the fall–winter. In this sense, El Niño 2015 shifted the subsurface temperature range from 14.0°C to 15.3°C, prevailing because of the upwelling dynamics, to warmer (> 16°C) water under El Niño which separated the year into three different hydrographic regimes, each lasting around 2–3 months (Aguilera et al., 2019). By analyzing accumulated (over 4 consecutive sampling days) changes in the body size of reproducing females, we detected significant changes after periods of roughly 100 days matching the above described hydrographic regimes (**Figure 2E**). Although females belonging to subsequent cohorts (true cohorts) might have overlapped during consecutive samplings, the integrated analysis of changes in female body size allowed us to distinguish among different female cohorts, each exhibiting specific plasticity patterns related to a specific thermal experience. Indeed, females sampled during El Niño 2015 were relatively smaller than females sampled before and after El Niño.

Both estuarine and upwelling habitats were characterized by interdaily variability of the suite of environmental conditions, such as temperature, pH, salinity, and food availability (Henson et al., 2017). We acknowledge that our sampling might have underestimated higher frequency variability (i.e., hours-day)

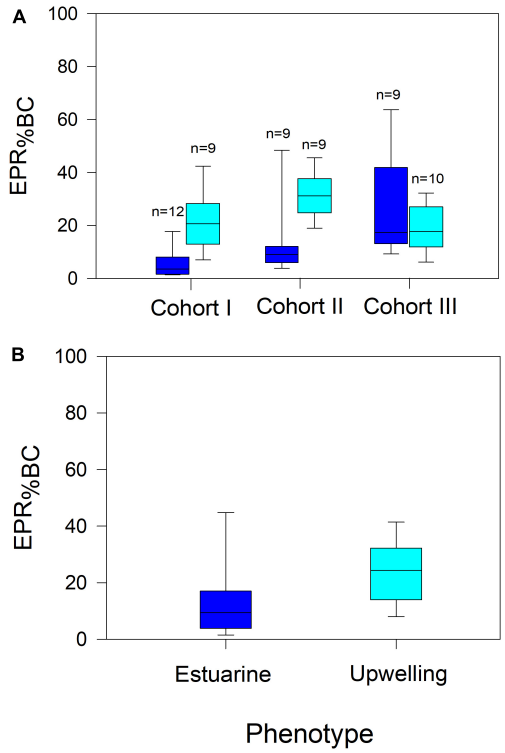

FIGURE 6
Among cohorts **(A)** and between populations **(B)** comparison of specific EPR ($EPR_{\%BC}$). Significant $EPR_{\%BC}$ variations were found among cohorts of both populations, in which upwelling females produced comparatively more eggs per body carbon than estuarine females. n denotes the number of observations for each cohort.

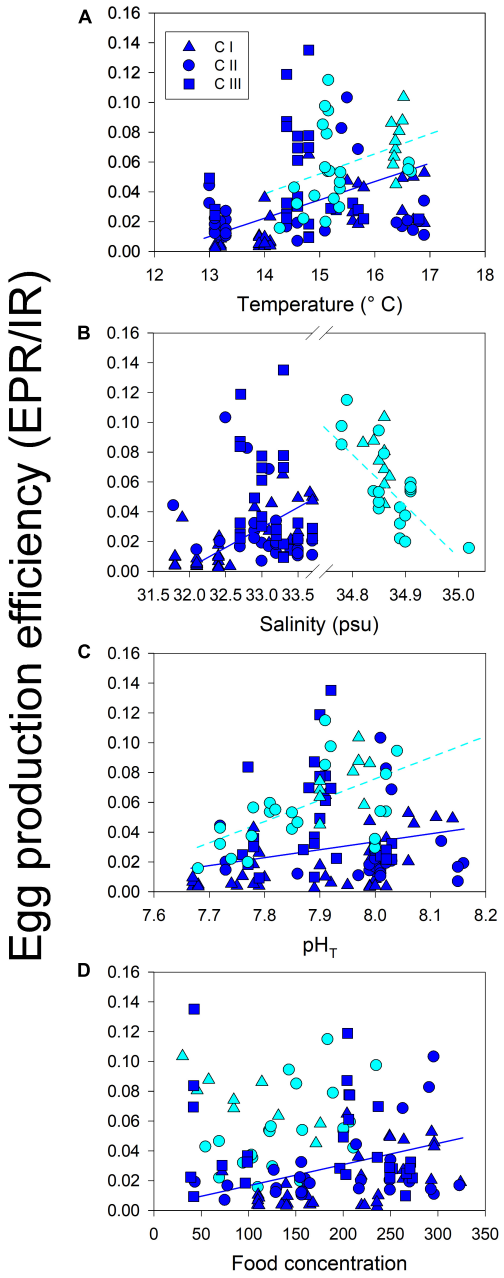

FIGURE 7
Phenotypic plasticity of EPE (EPR/IR quotient) to sampling temperature **(A)**, salinity **(B)**, pH_T **(C)** and food **(D)** in each habitat. Plastic responses were expressed as a mean reaction norm that had a significantly non-zero slope. The slope denotes the EPE tolerance to the respective driver.

affecting physical–chemical conditions (see e.g., Hofmann et al., 2011. Bednaršek et al., 2022). For short life-cycle copepods (i.e., month-months), this high-frequency variability might be critical in shaping the biological plasticity and tolerance to changing habitat conditions (Gaitán-Espitia et al., 2017; Vargas et al., 2017; Sasaki and Dam, 2020) and needs to be further assessed. In addition, there were clear differences in the temporal characterization of environmental variability between habitats. The estuarine habitat variability was characterized only during spring–summer periods, while the variability at the upwelling location was characterized throughout the annual cycle. This difference in habitat characterization might likely have underestimated the range of both environmental conditions and phenotypic plasticity within the estuarine population. However, the seasonal occurrence and biological productivity of the estuarine population are likely restricted to spring-summer periods, like the other mid-high latitude copepod species (Uye, 1982). In addition, copepod vertical migrations can extend the range of environmental conditions experienced within and among cohorts. Contrary to large-sized species, the vertical distribution of *A. tonsa* in coastal provinces of the SEP is restricted to the upper vertical layers. Within this range, constrained in the estuarine habitat by the surface freshwater lens (Osma et al., 2020), tidal currents (Vargas et al., 2003) in the estuarine habitats, and shallow oxygen-poor water in the upwelling habitat (Escribano et al., 2009); habitat and cohorts' characterization were assessed in this study at a mean

TABLE 4 Significant correlations (i.e., phenotypic plasticity) between EPE and environmental drivers for each population.

Habitat	Estuarine			Upwelling		
Driver	***r***	***p*-value**	**equation**	***r***	***p*-value**	**equation**
Temperature	0.4	0.001	$y = -1.14 + 0.12 \times x$	0.4	0.03	$y = -1.15 + 0.01 \times x$
Salinity	0.5	0.0001	$y = -11 + 0.3 \times x$	−0.6	0.0003	$y = 6.6 - 0.19 \times x$
pH_T	0.2	0.03	$y = -5.6 + 0.8 \times x$	0.6	0.001	$y = -1.1 + 0.14 \times x$
Food	0.2	0.05	$y = 0.46 + 0.001 \times x$			

The slope of the regressions denotes the sensitivity of EPE to the respective driver. *r* denotes the Pearson correlation coefficients.

depth likely representing the most prevalent environmental conditions affecting cohorts' traits (**Supplementary Figure 2**). In the case of seasonal observations in the estuarine habitat, a similar thermal range (4°C) was reported during the seasonal reproductive occurrence of *A. tonsa* and *A. hudsonica* in Narragansett Bay (41° N) (Sullivan and McManus, 1986), and *Oithona nana* in temperate (39° S) coastal waters of Argentina (Temperoni et al., 2011). The subsurface (10 m depth) thermal range (14°C–17°C) observed in the upwelling habitat was consistent with the reported annual cycle achieved in the same site at a higher (i.e., weekly) frequency (Hidalgo et al., 2005), and a subtropical (20° S) upwelling loci in the northern Benguela upwelling system (Bode et al., 2014). In this sense, laboratory temperature was 1°C above and below the lower and upper edge, respectively, of the thermal range in the estuarine habitat, and 1°C below the upper edge in the upwelling habitat. However, these cases corresponded to only 14% (estuarine) and 6% (upwelling) of incubations, which might have introduced a negligible effect on estimations of copepod traits. All this suggests that the conducted estuarine characterization might have covered environmental variations experienced within generations. This is important when we consider the importance of fluctuating selection on genetic polymorphism of the local population (Sasaki and Dam, 2020).

Intrapopulation variability in traits and plasticity

There were significant variations in the expression of parental and offspring traits within cohorts of the estuarine population (**Supplementary Figure 3**) and among cohorts of the upwelling population (**Table 2**). Significant effects of single drivers on the expression of trait suggest there is an effect of plasticity, while the effect of habitat–environmental driver interactions indicates such plasticity diverged between populations (**Table 3**). In terms of environmental conditions, members of the same cohort experienced greater variations in the estuarine habitat, conditions that tended to prevail across the different cohorts. In turn, environmental conditions seem to be relatively more homogeneous during the development of a single cohort in the upwelling population, which, however, were environmentally decoupled from other cohorts. The divergent pattern in phenotypic plasticity between both *A. tonsa* populations can be related to genetic polymorphism among cohorts (Sasaki and Dam, 2020) and habitat variability (Pigliucci, 2005; Reed et al., 2010). For example, temperature and food abundance modulate phenotypic changes in the body size/weight of copepods (McLaren, 1963; Huntley and Lopez, 1992). Temperature and food abundance varied across the cohorts alongshore the body size of copepods in the upwelling habitat (**Figure 3**). In the upwelling seascape, changes in the body size of copepods have been related to temperature increases either experimentally (Escribano and McLaren, 1999) or in the field due to El Niño (Ulloa et al., 2001; Escribano et al., 2004). However, plasticity in morphometric traits was not related to habitat–temperature but habitat–salinity interaction, whereas physiological traits did relate to habitat-specific temperature conditions. Morphometric traits are settled in the early ontogeny of copepods in a tight relationship with habitat temperature (Miller et al., 1977), which might not necessarily correspond to the sampling temperature. Furthermore, the narrow temperature range associated with either seasonal thermal changes or vertical migrations over a restricted (30 m) depth range shaping the phenotypic plasticity (and genetic diversity) of the upwelling *A. tonsa* population was disrupted during this study by drastic thermal changes associated with El Niño 2015. Along with explaining the lack of correlation between variations in the expression of traits and habitat temperature, El Niño 2015 experienced among cohorts of the upwelling population could have changed the relative allele frequency and favored the selection of different alleles, for example, related to the phenotypic responses (Sasaki and Dam, 2020). Changes in the body size further translate to and influence the expression of reproductive traits (Durbin et al., 1983; Roff, 2002). In fact, EPR and egg size also varied significantly among cohorts in the upwelling population (**Table 2**). As the environment experienced by earlier generations can transgenerationally interact with the future generations, this can predetermine the phenotype, and thus related plasticity against future conditions (Donelson et al., 2018 and references therein); these findings suggest a reduced capacity in adult females for sensing habitat cues early in the season period, to better anticipate or fit their own and offspring

traits through anticipatory maternal effects (Marshall et al., 2008). In the case of the estuarine population, the expression of body and egg size remained constant among cohorts while physiological EPR and IR traits varied among cohorts (**Figure 2** and **Table 2**). The expression of these physiological traits is also strongly dependent on the food-driven phenotypic changes through food composition and quality (Kleppel and Burkart, 1995; Jónasdóttir et al., 2009). Although we did not evaluate changes in food quality, there were significant variations in food abundance among cohorts of the estuarine population, responding to the observed temporal and alongshore changes in the estuarine habitat (Aguilera et al., 2013; Osma et al., 2020). The relatively larger phenotypic plasticity observed in the expression of physiological traits might have rendered a reduced tolerance to environmental drivers (see below) in the estuarine population.

Variability in traits and plasticity between populations

The significant differences in the expression of parental and offspring traits were found between examined *A. tonsa* populations (**Figure 4** and **Table 2**), overall, indicating variations in parental phenotypic plasticity (Burgess and Marshall, 2014). Adult females from the estuarine habitat were significantly larger than their upwelling counterparts, although the EPR of each population was similar. However, standardized by body size, the $EPR_{\%BC}$ of upwelling was higher than that of estuarine females (**Figure 6**). This suggests that the upwelling population is allocating a greater proportion of their energy intake to reproduction. Furthermore, since female body size is positively correlated with the number of eggs produced (Durbin et al., 1983; Hopcroft and Roff, 1998), observed differences in body size and $EPR_{\%BC}$ can have strong implications for population growth rates and ecosystem processes (Bassar et al., 2010; Gianuca et al., 2016). The slower growth in the colder estuarine environment, with no increment in fecundity related to the body size and lower gross reproductive output, might represent a handicap for the estuarine population (Stearns, 1989, 1992). This seems to be in part countered by a stronger phenological regulation manifested in higher fecundity in smaller females, as suggested by the trade-off between body size and EPR observed consistently among cohorts of the estuarine population (**Figure 3A**). The EPR varied within upwelling females without any obvious phenological cycles. Females from the upwelling habitat produced larger eggs (**Table 2**), which varied (trade-off) inversely with EPR in estuarine females (**Figure 3B**). Larger eggs in upwelling females cannot be explained phenologically as the upwelling females have a relatively smaller body size. Alternatively, the offspring size could evolve to reflect the optimal compromise between the positive fitness effects of increased size on offspring survival and the reduced/increased number of offspring produced (Smith and Fretwell, 1974; Brockelman, 1975). Increased EPR in smaller estuarine females might be related to elevated IR, which was phenotypically mediated by food variations in the estuarine habitat. Variation in habitat conditions can indeed determine phenotype variations among populations as demonstrated by the linear mixed-effects model (**Table 3**). In terms of fluctuations and correlations among points of a given variable, and between points of different variables in each habitat, the estuarine habitat seemed less variable with lower heterogeneity in the environmental conditions (**Figure 5**). In the estuarine habitat, the environmental drivers strongly covary, which was also reflected in strongly coupled environmental–biological variables (**Figure 5**), suggesting a significant role of habitat variability on phenotypic plasticity. Our current results in spatial patterns of variability in environmental conditions and reproduction-related traits agree that divergent phenotype variations, for example, parental anticipatory effects, take place in response to different environmental pressures alongshore climate-spatial gradients (Marshall et al., 2008; Burgess and Marshall, 2014).

Tolerance to habitat drivers between populations

Significant correlations found between EPE (EPR/IR quotient) and environmental conditions might correspond to the effect of simultaneous drivers on EPE (**Figure 7**). Building upon different and discrete cohorts of both *A. tonsa* populations, mechanistic relationships between EPE and environmental drivers can also reflect ecological specialization and local adaptation, for example, disentangling individual mechanisms that can be assessed later through multifactorial experimental approaches (Boyd et al., 2018). Furthermore, significant non-zero slopes indicate phenotypic plasticity in EPE and variation in the tolerance (sensitivity) to environmental changes. Both populations exhibited roughly the same tolerance to temperature which exerted positive effects on the EPE of both populations (**Table 4**). The mean temperature was higher at the upwelling habitat, whereas wider ranges and drastic thermal fluctuations were observed among cohorts of the estuarine population. Thermal fluctuations can strongly modulate selection on plasticity and thermal tolerance (Stillman, 2003; Sasaki and Dam, 2020), in which the mean temperature experienced by a population corresponds to tolerance, whereas phenotypic plasticity should evolve in response to temperature variability (Stevens, 1989). Salinity exerted population-specific effects on the EPE. The positive effect on the estuarine population might be related to the high natural variability of salinity in estuarine habitats (Kinne, 1966). In fact, elevated EPE levels were evident among cohorts of the local *A. tonsa* population when high salinity values prevailed. In contrast, the salinity range and fluctuations typically prevailing at the

upwelling habitat were dramatically disrupted in timing and magnitude by the 2015 El Niño-related hydrographic shifts (Aguilera et al., 2020). Under upwelling influence, salinity in the upper water column varies over a narrow (0.01 psu) range forced by upwelling-driven replacement of water masses with slightly different salinity values (Silva et al., 2009). Larger (> 0.4 psu) salinity shifts were observed in the upwelling habitat due to El Niño (Aguilera et al., 2020) together with other unpredictable hydrographic changes significantly affecting the distribution and physiology of upwelling populations (Escribano et al., 2004; Riascos et al., 2009; Aguilera et al., 2019). Interestingly, both populations showed relatively similar tolerance to salinity and pH_T. In the case of pH_T, this promoted a positive effect on EPE of both populations, such that elevated EPE levels were evident when high pH_T prevailed. The significant changes in pH_T were observed within and among cohorts of both populations. However, phenotypic plasticity in physiological traits was higher in the estuarine population. These findings suggest that higher phenotypic plasticity can render the population less tolerant to changes in the environmental drivers (Stillman, 2003; Sasaki and Dam, 2019), which could decrease its overall adaptive variability (Leung et al., 2020).

Other potential factors structuring phenotypic plasticity

Our study is limited in the way that it only considers the impact of habitat variability in structuring phenotypic plasticity across two divergent habitats. However, we strongly emphasize that habitat-related parameters are only one aspect, while genetic structure, local adaptation, and gene flow include additional parameters that simultaneously impact the overall determination of the level of plasticity. A comprehensive interpretation of all observed parameters provides novel evidence of how divergent phenotypes might sustain the population of *A. tonsa* across variable coastal provinces of the SEP. Preliminary results based on (COI) mtDNA sequence data indicate the occurrence of different clades alongshore the SEP with higher haplotype diversity in the southern population, and the presence of a common haplotype with reduced frequency in the upwelling population (pers. work in progress). Ocean clines delimiting coastal provinces alongshore the SEP tend to act as effective dispersal barriers for populations of benthic species (Cardenas et al., 2009 and references therein). Comparatively, pelagic copepods exhibit higher dispersal potential that erodes ocean clines and manifested ecological speciation (Chen and Hare, 2008), preventing selection and local adaptation across large spatial scales in the presence of ocean connectivity. Despite evident differences in mean values and ranges of environmental conditions between the estuarine and upwelling habitat, patterns of phenotypic plasticity in the tolerance to environmental variations tended to overlap between populations. This might suggest there was or is a south-to-north gene flow which can posit some antagonist influence in the phenotypic plasticity and adaptive genetic differentiation between *A. tonsa* populations. Common garden experiments would help to clarify the role of habitat variability, genetic structure, and adaptations on phenotypic plasticity to fluctuations in other combined habitat drivers.

Conclusion

Our results underline the role of habitat-related variability between the estuarine and upwelling habitat toward shaping the distribution of the expression of trait and subsequent plasticity. The significant differences in patterns of environmental variability and phenotypic plasticity were found between both *A. tonsa* populations, in parental and offspring morphological and physiological traits, traits trade-offs regulating reproduction, and sensitivity to environmental drivers. Such differences in plasticity and tolerance related to temperature, pH and other ocean drivers are concerning if considering the species role in trophodynamics and biogeochemical cycles, and that both upwelling (Sydeman et al., 2014) and El Niño (Cai et al., 2021) intensity are projected to increase in the SEP due to global warming. Despite the absence of genetic evidence supporting the occurrence of various genotypes, our findings strongly indicate divergent *A. tonsa* phenotypes to be currently distributed across specific climate and ecogeographic provinces alongshore the SEP.

Data availability statement

Publicly available datasets were analyzed in this study. This data can be found here: doi: 10.1007/s12237-013-9615-2 and doi: 10.1594/PANGAEA.925450.

Author contributions

VA performed field campaigns and experiments. VA and NB analyzed and interpreted the data and led the writing of the manuscript. Both authors contributed critically to the drafts and gave final approval for publication.

Funding

VA was supported by the Chilean Scientific and Technologic Agency (ANID) through the Millennium Scientific Initiative Grant IC120019 and Proyecto ANILLOS ACT210071. NB was supported by the Slovene Research Agency (ARRS J1-2468 "Biomarkers of subcellular stress in the Northern Adriatic under global environmental change").

Acknowledgments

We would like to thank Mr. Mauricio Vegas, Mr. Miguel Barrientos, Mr. Jose Martel, and Mr. Boris Aqueveque for their help during field surveys and experiments. We would also like to thank Paulo and Borja Aguilera for keeping hope of better times alive.

Conflict of interest

The authors declare that the research was conducted in the absence of any commercial or financial relationships that could be construed as a potential conflict of interest.

Publisher's note

Supplementary material

The Supplementary Material for this article can be found online at: https://www.frontiersin.org/articles/10.3389/fevo.2022.925648/full#supplementary-material

References

Aguilera, V. M., Donoso, K., and Escribano, R. (2011). Reproductive performance of small-sized dominant copepods with a highly variable food resource in the coastal upwelling system off the Chilean Humboldt Current. *Mar. Biol. Res.* 7, 235–249. doi: 10.1080/17451000.2010.499437

Aguilera, V. M., Vargas, C. A., Manríquez, P. H., Navarro, J. M., and Duarte, C. (2013). Low-pH freshwater discharges drive spatial and temporal variations in life history traits of neritic copepod *Acartia tonsa*. *Estuaries Coasts* 36, 1084–1092. doi: 10.1007/s12237-013-9615-2

Aguilera, V. M., Escribano, R., Vargas, C. A., and González, M. T. (2019). Upwelling modulation of functional traits of a dominant planktonic grazer during "warm-acid" El Niño 2015 in a year-round upwelling area of Humboldt Current. *PLoS One* 14:e0209823. doi: 10.1371/journal.pone.0209823

Aguilera, V. M., Vargas, C. A., and Dewitte, B. (2020). Intraseasonal hydrographic variations and nearshore carbonates system off northern Chile during the 2015 El Niño event. *J. Geophys. Res. Biogeosci.* 125:e2020JG005704. doi: 10.1029/2020JG005704

Aguirre, C., Garreaud, R., Belmar, L., Farías, L., Ramajo, L., and Barrera, F. (2021). High-frequency variability of the surface ocean properties off central Chile during the upwelling season. *Front. Mar. Sci.* 8:702051. doi: 10.3389/fmars.2021.702051

Aguirre, G. E., Capitanio, F. L., Lovrich, G. A., and Esnal, G. B. (2012). Seasonal variability of metazooplankton in coastal sub-Antarctic waters (Beagle Channel). *Mar. Biol. Res.* 8, 341–353. doi: 10.1080/17451000.2011.627922

Barley, J. M., Cheng, B. S., Sasaki, M., Gignoux-Wolfsohn, S., Hays, C. G., Putnam, A. B., et al. (2021). Limited plasticity in thermally tolerant ectotherm populations: evidence for a trade-off. *Proc. R. Soc. B* 288:20210765. doi: 10.1098/rspb.2021.0765

Bassar, R. D., Marshall, M. C., López-Sepulcre, A., Zandonà, E., Auer, S. K., Travis, J., et al. (2010). Local adaptation in *Trinidadian guppies* alters ecosystem processes. *Proc. Natl. Acad. Sci. U S A.* 107, 3616–3621. doi: 10.1073/pnas.0908023107

Bednarsšek, N., Beck, M. W., Pelletier, G., Applebaum, S. L., Feely, R. A., Butler, R., et al. (2022). Natural analogues in pH variability and predictability across the coastal pacific estuaries: extrapolation of the increased oyster dissolution under increased pH amplitude and low predictability related to ocean acidification. *Environ. Sci. Technol.* 56, 9015–9028. doi: 10.1021/acs.est.2c00010

Bernhardt, J. R., O'Connor, M. I., Sunday, J. M., and Gonzalez, A. (2020). Life in fluctuating environments. *Philos. Trans. R. Soc. B* 375:20190454. doi: 10.1098/rstb.2019.0454

Bitter, M. C., Kapsenberg, L., Gattuso, J. P., and Pfister, C. A. (2019). Standing genetic variation fuels rapid adaptation to ocean acidification. *Nat. Commun.* 10:5821. doi: 10.1038/s41467-019-13767-1

Bitter, M. C., Kapsenberg, L., Silliman, K., Gattuso, J. P., and Pfister, C. A. (2021). Magnitude and predictability of pH fluctuations shape plastic responses to ocean acidification. *Am. Nat.* 197, 486–501. doi: 10.1086/712930

Bode, M., Kreiner, A., van der Plas, A. K., Louw, D. C., Horaeb, R., Auel, H., et al. (2014). Spatio-temporal variability of copepod abundance along the 20° S monitoring transect in the northern Benguela upwelling system from 2005 to 2011. *PLoS One* 9:e97738. doi: 10.1371/journal.pone.0097738

Boyd, P. W., Collins, S., Dupont, S., Fabricius, K., Gattuso, J. P., Havenhand, J., et al. (2018). Experimental strategies to assess the biological ramifications of multiple drivers of global ocean change—a review. *Global Change Biol.* 24, 2239–2261. doi: 10.1111/gcb.14102

Brennan, R. S., Garrett, A. D., Huber, K. E., Hargarten, H., and Pespeni, M. H. (2019). Rare genetic variation and balanced polymorphisms are important for survival in global change conditions. *Proc. R. Soc. B* 286:20190943. doi: 10.1098/rspb.2019.0943

Brockelman, W. Y. (1975). Competition, the fitness of offspring, and optimal clutch size. *Am. Nat.* 109, 677–699. doi: 10.1086/283037

Burgess, S. C., and Marshall, D. J. (2014). Adaptive parental effects: the importance of estimating environmental predictability and offspring fitness appropriately. *Oikos* 123, 769–776. doi: 10.1111/oik.01235

Cai, W., Santoso, A., Collins, M., Dewitte, B., Karamperidou, C., Kug, J. S., et al. (2021). Changing El Niño-Southern Oscillation in a warming climate. *Nat. Rev. Earth Environ.* 2, 628–644. doi: 10.1038/s43017-021-00199-z

Camus, P. A. (2001). Biogeografía marina de Chile continental. *Rev. Chilena Historia Nat.* 74, 587–617. doi: 10.4067/S0716-078X2001000300008

Cardenas, L., Castilla, J. C., and Viard, F. (2009). A phylogeographical analysis across three biogeographical provinces of the south-eastern Pacific: the case of the marine gastropod *Concholepas concholepas*. *J. Biogeography* 36, 969–981. doi: 10.1111/j.1365-2699.2008.02056.x

Chaalali, A., Beaugrand, G., Raybaud, V., Goberville, E., David, V., Boët, P., et al. (2013). Climatic facilitation of the colonization of an estuary by *Acartia tonsa*. *PLoS One* 8:e74531. doi: 10.1371/journal.pone.0074531

Chen, G., and Hare, M. P. (2008). Cryptic ecological diversification of a planktonic estuarine copepod. *Acartia tonsa*. *Mol. Ecol.* 17, 1451–1468. doi: 10.1111/j.1365-294X.2007.03657.x

Dam, H. G. (2013). Evolutionary adaptation of marine zooplankton to global change. *Ann. Rev. Mar. Sci.* 5, 349–370. doi: 10.1146/annurev-marine-121211-172229

Donelson, J. M., Salinas, S., Munday, P. L., and Shama, L. (2018). Transgenerational plasticity and climate change experiments: where do we go from here? *Global Change Biol.* 24, 13–34. doi: 10.1111/gcb.13903

Dunson, W. A., and Travis, J. (1991). The role of abiotic factors in community organization. *Am. Nat.* 138, 1067–1091. doi: 10.1086/285270

Durbin, A. G., and Durbin, E. G. (1981). Standing stock and estimated production rates of phytoplankton and zooplankton in Narragansett Bay, Rhode Island. *Estuaries* 4, 24–41. doi: 10.2307/1351540

Durbin, E. G., Durbin, A. G., S-mayda, T. J., and Verity, P. G. (1983). Food limitation of production by adult Acartia tonsa in Narragansett Bay, Rhode Island. *Limnol. Oceanography* 28, 1199–1213. doi: 10.4319/lo.1983.28.6.1199

Escribano, R., Daneri, G., Farías, L., Gallardo, V. A., González, H. E., Gutiérrez, D., et al. (2004). Biological and chemical consequences of the 1997–1998 El Niño in the Chilean coastal upwelling system: a synthesis. *Deep Sea Res. Part II: Top. Stud. Oceanography* 51, 2389–2411. doi: 10.1016/j.dsr2.2004.08.011

Escribano, R., Fernández, M., and Aranís, A. (2003). Physical-chemical processes and patterns of diversity of the Chilean eastern boundary pelagic and benthic marine ecosystems: an overview. *Gayana (Concepción)* 67, 190–205. doi: 10.4067/S0717-65382003000200008

Escribano, R., Hidalgo, P., and Krautz, C. (2009). Zooplankton associated with the oxygen minimum zone system in the northern upwelling region of Chile during march 2000. *Deep Sea Res. Part II: Top. Stud. Oceanography* 56, 1083–1094. doi: 10.1016/j.dsr2.2008.09.009

Escribano, R., Irribarren, C., and Rodriguez, L. (1997). Influence of food quantity and temperature on development and growth of the marine copepod *Calanus chilensis* from northern Chile. *Mar. Biol.* 128, 281–288. doi: 10.1007/s002270050093

Escribano, R., and McLaren, I. (1999). Production of Calanus chilensis in the upwelling area of Antofagasta, northern Chile. *Mar. Ecol. Prog. Series* 177, 147–156. doi: 10.3354/meps177147

Frost, B. W. (1972). Effects of size and concentration of food particles on the feeding behavior of the marine planktonic copepod *Calanus pacificus*. *Limnol. Oceanography* 17, 805–815. doi: 10.4319/lo.1972.17.6.0805

Gaitán-Espitia, J. D., Marshall, D., Dupont, S., Bacigalupe, L. D., Bodrossy, L., and Hobday, A. J. (2017). Geographical gradients in selection can reveal genetic constraints for evolutionary responses to ocean acidification. *Biol. Lett.* 13:20160784. doi: 10.1098/rsbl.2016.0784

Garcés-Vargas, J., Schneider, W., Pinochet, A., Piñones, A., Olguin, F., Brieva, D., et al. (2020). Tidally forced saltwater intrusions might impact the quality of drinking water, the Valdivia River (40° S), Chile estuary case. *Water* 12:2387. doi: 10.3390/w12092387

García-Reyes, M., Largier, J. L., and Sydeman, W. J. (2014). Synoptic-scale upwelling indices and predictions of phyto- and zooplankton populations. *Prog. Oceanography* 120, 177–188. doi: 10.1016/j.pocean.2013.08.004

Gianuca, A. T., Pantel, J. H., and De Meester, L. (2016). Disentangling the effect of body size and phylogenetic distances on zooplankton top-down control of algae. *Proc. R. Soc. B: Biol. Sci.* 283:20160487. doi: 10.1098/rspb.2016.0487

Hartley, A. J., Chong, G., Houston, J., and Mather, A. E. (2005). 150 Million years of climatic stability: evidence from the Atacama Desert, northern Chile. *J. Geol. Soc.* 162, 421–424. doi: 10.1144/0016-764904-071

Henson, S. A., Beaulieu, C., Ilyina, T., John, J. G., Long, M., Séférian, R., et al. (2017). Rapid emergence of climate change in environmental drivers of marine ecosystems. *Nat. Commun.* 8:14682. doi: 10.1038/ncomms14682

Hidalgo, P., and Escribano, R. (2007). Coupling of life cycles of the copepods *Calanus chilensis* and *Centropages brachiatus* to upwelling induced variability in the central-southern region of Chile. *Prog. Oceanography* 75, 501–517. doi: 10.1016/j.pocean.2007.08.028

Hidalgo, P., Escribano, R., and Morales, C. E. (2005). Ontogenetic vertical distribution and diel migration of the copepod *Eucalanus inermis* in the oxygen minimum zone off northern Chile (20–21° S). *J. Plankton. Res.* 27, 519–529. doi: 10.1093/plankt/fbi025

Hofmann, G. E., Smith, J. E., Johnson, K. S., Send, U., Levin, L. A., Micheli, F., et al. (2011). High-frequency dynamics of ocean pH: a multi-ecosystem comparison. *PLoS One* 6:e28983. doi: 10.1371/journal.pone.0028983

Hopcroft, R. R., and Roff, J. C. (1998). Zooplankton growth rates: the influence of female size and resources on egg production of tropical marine copepods. *Mar. Biol.* 132, 79–86. doi: 10.1007/s002270050373

Huntley, M., and Lopez, M. (1992). Temperature-dependent production of marine copepods: a global synthesis. *Am. Nat.* 140, 201–242. doi: 10.1086/285410

Jónasdóttir, S. H., Visser, A. W., and Jespersen, C. (2009). Assessing the role of food quality in the production and hatching of *Temora longicornis* eggs. *Mar. Ecol. Prog. Series* 382, 139–150. doi: 10.3354/meps07985

Kingsolver, J. G., and Huey, R. B. (1998). Evolutionary analyses of morphological and physiological plasticity in thermally variable environments. *Am. Zool.* 38, 545–560. doi: 10.1093/icb/38.3.545

Kinne, O. (1966). Physiological aspects of animal life in estuaries with special reference to salinity. *Netherlands J. Sea Res.* 3, 222–244. doi: 10.1016/0077-7579(66)90013-5

Kiørboe, T., Møhlenberg, F., and Nicolajsen, H. (1982). Ingestion rate and gut clearance in the planktonic copepod *Centropages hamatus* (Lilljeborg) in relation to food concentration and temperature. *Ophelia* 21, 181–194. doi: 10.1080/00785326.1982.10426586

Kiørboe, T., and Nielsen, T. G. (1994). Regulation of zooplankton biomass and production in a temperate, coastal ecosystem. 1. copepods. *Limnol. Oceanography* 39, 493–507. doi: 10.4319/lo.1994.39.3.0493

Kleppel, G. S., and Burkart, C. A. (1995). Egg production and the nutritional environment of *Acartia tonsa*: the role of food quality in copepod nutrition. *ICES J. Mar. Sci.* 52, 297–304. doi: 10.1016/1054-3139(95)80045-X

Landry, M. R. (1978). Population dynamics and production of a planktonic marine copepod, *Acartia clausii*, in a small temperate lagoon on San Juan Island, Washington. *Int. Rev. Gesamten Hydrobiol. Hydrographie* 63, 77–119. doi: 10.1002/iroh.19780630106

Langerhans, R. B. (2018). Predictability and parallelism of multitrait adaptation. *J. Heredity* 109, 59–70. doi: 10.1093/jhered/esx043

Lercari, D., and Defeo, O. (2006). Large-scale diversity and abundance trends in sandy beach macrofauna along full gradients of salinity and morphodynamics. *Estuarine Coastal Shelf Sci.* 68, 27–35. doi: 10.1016/j.ecss.2005.12.017

Leung, C., Rescan, M., Grulois, D., and Chevin, L. M. (2020). Reduced phenotypic plasticity evolves in less predictable environments. *Ecol. Lett.* 23, 1664–1672. doi: 10.1111/ele.13598

Lindberg, D. R. (1991). Marine biotic interchange between the northern and southern hemispheres. *Paleobiology* 17, 308–324. doi: 10.1017/S0094837300010629

Marín, V., Huntley, M. E., and Frost, B. (1986). Measuring feeding rates of pelagic herbivores: analysis of experimental design and methods. *Mar. Biol.* 93, 49–58. doi: 10.1007/BF00428654

Marshall, D. J., Allen, R. M., and Crean, A. J. (2008). The ecological and evolutionary importance of maternal effects in the sea. *Oceanography Mar. Biol. Ann. Rev.* 46, 203–250. doi: 10.1201/9781420065756.ch5

McLaren, I. A. (1963). Effects of temperature on growth of zooplankton, and the adaptive value of vertical migration. *J. Fisheries Board Canada* 20, 685–727. doi: 10.1139/f63-046

Miller, C. B., Johnson, J. K., and Heinle, D. R. (1977). Growth rules in the marine copepod genus Acartia. *Limnol. Oceanography* 22, 326–335. doi: 10.4319/lo.1977.22.2.0326

Moksness, E., and Fossum, P. (1992). Daily growth rate and hatching-date distribution of Norwegian spring-spawning herring (*Clupea harengus* L.). *ICES J. Mar. Sci.* 49, 217–221. doi: 10.1093/icesjms/49.2.217

Moran, N. A. (1992). The evolutionary maintenance of alternative phenotypes. *Am. Nat.* 139, 971–989. doi: 10.1086/285369

Morrongiello, J. R., Bond, N. R., Crook, D. A., and Wong, B. B. (2012). Spatial variation in egg size and egg number reflects trade-offs and bet-hedging in a freshwater fish. *J. Animal Ecol.* 81, 806–817. doi: 10.1111/j.1365-2656.2012.01961.x

Oerder, V., Colas, F., Echevin, V., Codron, F., Tam, J., and Belmadani, A. (2015). Peru-Chile upwelling dynamics under climate change. *J. Geophys. Res. Oceans* 120, 1152–1172. doi: 10.1002/2014JC010299

Ortega-Mayagoitia, E., Hernández-Martínez, O., and Ciros-Pérez, J. (2018). Phenotypic plasticity of life-history traits of a calanoid copepod in a tropical lake: is the magnitude of thermal plasticity related to thermal variability? *PLoS One* 13:e0196496. doi: 10.1371/journal.pone.0196496

Osma, N., Latorre-Melín, L., Jacob, B., Contreras, P. Y., von Dassow, P., and Vargas, C. A. (2020). Response of phytoplankton assemblages from naturally acidic coastal ecosystems to elevated pCO2. *Front. Mar. Sci.* 7:323. doi: 10.3389/fmars.2020.00323

Paffenhöfer, G. A., and Stearns, D. E. (1988). Why is *Acartia tonsa* (Copepoda: Calanoida) restricted to nearshore environments? *Mar. Ecol. Prog. Series* 42, 33–38. doi: 10.3354/meps042033

Pereira, R. J., Sasaki, M. C., and Burton, R. S. (2017). Adaptation to a latitudinal thermal gradient within a widespread copepod species: the contributions of genetic divergence and phenotypic plasticity. *Proc. R. Soc. B: Biol. Sci.* 284:20170236. doi: 10.1098/rspb.2017.0236

Pérez, C. A., DeGrandpre, M. D., Lagos, N. A., Saldías, G. S., Cascales, E. K., and Vargas, C. A. (2015). Influence of climate and land use in carbon biogeochemistry in lower reaches of rivers in central southern Chile: implications for the carbonate system in river-influenced rocky shore environments. *J. Geophys. Res. Biogeosci.* 120, 673–692. doi: 10.1002/2014JG002699

Peterson, W. T., Arcos, D. F., McManus, G. B., Dam, H., Bellantoni, D., Johnson, T., et al. (1988). The nearshore zone during coastal upwelling: daily variability and coupling between primary and secondary production off central Chile. *Prog. Oceanography* 20, 1–40. doi: 10.1016/0079-6611(88)90052-3

Pianka, E. R. (1976). Natural selection of optimal reproductive tactics. *Am. Zool.* 16, 775–784. doi: 10.1093/icb/16.4.775

Pierrot, D., Epitalon, J.-M., Orr, J. C., Lewis, E., and Wallace, D. W. R. (2021). *MS Excel program developed for CO_2 system calculations.* Available online at: https://github.com/dpierrot/co2sys_xl

Pigliucci, M. (2001). *Phenotypic Plasticity: Beyond Nature and Nurture*. Baltimore, MD: JHU Press. doi: 10.1093/oso/9780195131543.003.0009

Pigliucci, M. (2005). Evolution of phenotypic plasticity: Where are we going now? *Trends Ecol. Evol.* 20, 481–486. doi: 10.1016/j.tree.2005.06.001

Pino, M. Q., Perillo, G. M. E., and Santamarina, P. (1994). Residual fluxes in a cross-section of the Valdivia river estuary, Chile. *Estuarine Coastal Shelf Sci.* 38, 491–505. doi: 10.1006/ecss.1994.1034

Porlier, M., Charmantier, A., Bourgault, P., Perret, P., Blondel, J., and Garant, D. (2012). Variation in phenotypic plasticity and selection patterns in blue tit breeding time: between-and within-population comparisons. *J. Animal Ecol.* 81, 1041–1051. doi: 10.1111/j.1365-2656.2012.01996.x

Pörtner, H. O., Langenbuch, M., and Reipschläger, A. (2004). Biological impact of elevated ocean CO2 concentrations: lessons from animal physiology and earth history. *J. Oceanography* 60, 705–718. doi: 10.1007/s10872-004-5763-0

Reed, T. E., Waples, R. S., Schindler, D. E., Hard, J. J., and Kinnison, M. T. (2010). Phenotypic plasticity and population viability: the importance of environmental predictability. *Proc. R. Soc. B: Biol. Sci.* 277, 3391–3400. doi: 10.1098/rspb.2010.0771

Riascos, J. M., Carstensen, D., Laudien, J., Arntz, W. E., Oliva, M. E., Güntner, A., et al. (2009). Thriving and declining: climate variability shaping life-history and population persistence of Mesodesma donacium in the Humboldt Upwelling System. *Mar. Ecol. Prog. Series* 385, 151–163. doi: 10.3354/meps08042

Roff, D. A. (2002). *Life History Evolution*. Sunderland: Sinauer Associates. doi: 10.1016/B978-0-12-384719-5.00087-3

Ruz, P. M., Hidalgo, P., Yáñez, S., Escribano, R., and Keister, J. E. (2015). Egg production and hatching success of Calanus chilensis and *Acartia tonsa* in the northern Chile upwelling zone (23 S), Humboldt Current System. *J. Mar. Systems* 148, 200–212. doi: 10.1016/j.jmarsys.2015.03.007

Sasaki, M. C., and Dam, H. G. (2019). Integrating patterns of thermal tolerance and phenotypic plasticity with population genetics to improve understanding of vulnerability to warming in a widespread copepod. *Global Change Biol.* 25, 4147–4164. doi: 10.1111/gcb.14811

Sasaki, M. C., and Dam, H. G. (2020). Genetic differentiation underlies seasonal variation in thermal tolerance, body size, and plasticity in a short-lived copepod. *Ecol. Evol.* 10, 12200–12210. doi: 10.1002/ece3.6851

Sasaki, M. C., and Dam, H. G. (2021). Negative relationship between thermal tolerance and plasticity in tolerance emerges during experimental evolution in a widespread marine invertebrate. *Evol. Appl.* 14, 2114–2123. doi: 10.1111/eva.13270

Schlichting, C., and Pigliucci, M. (1998). *Phenotypic Evolution: a Reaction Norm Perspective*. Wallingford: CABI.

Senner, N. R., Conklin, J. R., and Piersma, T. (2015). An ontogenetic perspective on individual differences. *Proc. R. Soc. B: Biol. Sci.* 282:20151050. doi: 10.1098/rspb.2015.1050

Silva, N., Rojas, N., and Fedele, A. (2009). Water masses in the Humboldt Current System: Properties, distribution, and the nitrate deficit as a chemical water mass tracer for Equatorial Subsurface Water off Chile. *Deep Sea Res. II Top. Stud. Oceanogr.* 56, 1004–1020. doi: 10.1016/j.dsr2.2008.12.013

Smith, C. C., and Fretwell, S. D. (1974). The optimal balance between size and number of offspring. *Am. Nat.* 108, 499–506. doi: 10.1086/282929

Song, H., Miller, A. J., Cornuelle, B. D., and Di Lorenzo, E. (2011). Changes in upwelling and its water sources in the California current system driven by different wind forcing. *Dyn. Atmospheres Oceans* 52, 170–191.

Stearns, S. C. (1989). The evolutionary significance of phenotypic plasticity. *Bioscience* 39, 436–445. doi: 10.2307/1311135

Stearns, S. C. (1992). *The Evolution of Life Histories*. Oxford: Oxford University Press.

Stevens, G. (1989). The latitudinal gradient in geographical range: how so many species coexist in the tropics. *Am. Nat.* 133, 240–256. doi: 10.1086/284913

Stillman, J. H. (2003). Acclimation capacity underlies susceptibility to climate change. *Science* 301:65. doi: 10.1126/science.1083073

Strickland, J. D. H., and Parsons, T. R. (1972). *A Practical Handbook of Seawater Analysis*. Ottawa: Fisheries Research Board of Canada.

Strub, P. T., Mesías, J. M., Montecino, V., Rutlant, J., and Salinas, S. (1998). Coastal ocean circulation off western South America. *Coast. Segment* 273–313.

Sullivan, B. K., and McManus, L. T. (1986). Factors controlling seasonal succession of the copepods *Acartia hudsonica* and *A. tonsa* in Narragansett Bay, Rhode Island: temperature and resting egg production. *Mar. Ecol. Prog. Ser.* 28, 121–128. doi: 10.3354/meps028121

Sunday, J. M., Crim, R. N., Harley, C. D., and Hart, M. W. (2011). Quantifying rates of evolutionary adaptation in response to ocean acidification. *PLoS One* 6:e22881. doi: 10.1371/journal.pone.0022881

Sydeman, W. J., García-Reyes, M., Schoeman, D. S., Rykaczewski, R. R., Thompson, S. A., Black, B. A., et al. (2014). Climate change and wind intensification in coastal upwelling ecosystems. *Science* 345, 77–80. doi: 10.1126/science.1251635

Tapia, F. J., Largier, J. L., Castillo, M., Wieters, E. A., and Navarrete, S. A. (2014). Latitudinal discontinuity in thermal conditions along the nearshore of central-northern Chile. *PLoS One* 9:e110841. doi: 10.1371/journal.pone.0110841

Tapia, F. J., Navarrete, S. A., Castillo, M., Menge, B. A., Castilla, J. C., Largier, J., et al. (2009). Thermal indices of upwelling effects on inner-shelf habitats. *Prog. Oceanography* 83, 278–287. doi: 10.1016/j.pocean.2009.07.035

Temperoni, B., Viñas, M. D., Diovisalvi, N., and Negri, R. (2011). Seasonal production of *Oithona nana* Giesbrecht, 1893 (Copepoda: Cyclopoida) in temperate coastal waters off Argentina. *J. Plankton Res.* 33, 729–740. doi: 10.1093/plankt/fbq141

Torres, R., Turner, D. R., Silva, N., and Rutllant, J. (1999). High short-term variability of CO2 fluxes during an upwelling event off the Chilean coast at 30 S. *Deep Sea Res. Part I: Oceanographic Res. Papers* 46, 1161–1179. doi: 10.1016/S0967-0637(99)00003-5

Ulloa, O., Escribano, R., Hormazabal, S., Quinones, R. A., González, R. R., and Ramos, M. (2001). Evolution and biological effects of the 1997–98 El Niño in the upwelling ecosystem off northern Chile. *Geophys. Res. Lett.* 28, 1591–1594. doi: 10.1029/2000GL011548

Uye, S. I. (1982). Length-weight relationships of important zooplankton from the Inland Sea of Japan. *J. Oceanograph. Soc. Japan* 38, 149–158. doi: 10.1007/BF02110286

Vargas, C. A., Araneda, S. E., and Valenzuela, G. (2003). Influence of tidal phase and circulation on larval fish distribution in a partially mixed estuary, Corral Bay, Chile. *J. Mar. Biol. Assoc. U K* 83, 217–222. doi: 10.1017/S0025315403006994h

Vargas, C. A., Contreras, P. Y., Pérez, C. A., Sobarzo, M., Saldías, G. S., and Salisbury, J. (2016). Influences of riverine and upwelling waters on the coastal carbonate system off central Chile and their ocean acidification implications. *J. Geophys. Res. Biogeosci.* 121, 1468–1483. doi: 10.1002/2015JG003213

Vargas, C. A., Cuevas, L. A., Broitman, B. R., San Martin, V. A., Lagos, N. A., Gaitán-Espitia, J. D., et al. (2022). Upper environmental pCO_2 drives sensitivity to ocean acidification in marine invertebrates. *Nat. Clim. Chang.* 12, 200–207. doi: 10.1038/s41558-021-01269-2

Vargas, C. A., and González, H. E. (2004). Plankton community structure and carbon cycling in a coastal upwelling system. I. Bacteria, microprotozoans and phytoplankton in the diet of copepods and appendicularians. *Aquatic Microbial Ecol.* 34, 151–164. doi: 10.3354/ame034151

Vargas, C. A., Lagos, N. A., Lardies, M. A., Duarte, C., Manríquez, P. H., Aguilera, V. M., et al. (2017). Species-specific responses to ocean acidification should account for local adaptation and adaptive plasticity. *Nat. Ecol. Evol.* 1:84. doi: 10.1038/s41559-017-0084

Vargas, C. A., Martínez, R. A., Cuevas, L. A., Pavez, M. A., Cartes, C., González, H. E., et al. (2007). The relative importance of microbial and classical food webs in a highly productive coastal upwelling area. *Limnol. Oceanography* 52, 1495–1510. doi: 10.4319/lo.2007.52.4.1495

Zera, A. J., and Harshman, L. G. (2001). The physiology of life history trade-offs in animals. *Ann. Rev. Ecol. Systematics* 32, 95–126. doi: 10.1146/annurev.ecolsys.32.081501.114006

frontiers | Frontiers in Marine Science

TYPE Original Research
PUBLISHED 30 November 2022
DOI 10.3389/fmars.2022.1011663

OPEN ACCESS

EDITED BY
Carolina Madeira,
NOVA University Lisbon, Portugal

REVIEWED BY
Mickael Le Gac,
Institut Français de Recherche pour l'Exploitation de la Mer, France
Kieng Soon Hii,
University of Malaya, Malaysia

*CORRESPONDENCE
Zhenghong Sui
suizhengh@ouc.edu.cn

†These authors have contributed equally to this work

SPECIALTY SECTION
This article was submitted to Marine Molecular Biology and Ecology, a section of the journal Frontiers in Marine Science

RECEIVED 04 August 2022
ACCEPTED 14 November 2022
PUBLISHED 30 November 2022

CITATION
Qi J, Zhu Z, Liu Y and Sui Z (2022) First insight into H3K4me3 modification in the rapid growth of *Alexandrium pacificum* (dinoflagellates). *Front. Mar. Sci.* 9:1011663. doi: 10.3389/fmars.2022.1011663

First insight into H3K4me3 modification in the rapid growth of *Alexandrium pacificum* (dinoflagellates)

Juan Qi[1†], Zhimei Zhu[1†], Yuan Liu[1,2] and Zhenghong Sui[1*]

[1]Key Laboratory of Marine Genetics and Breeding of Ministry of Education of China, College of Marine Life Sciences, Ocean University of China, Qingdao, China, [2]College of Agronomy, Qingdao Agricultural University, Qingdao, China

Background: *Alexandrium pacificum* is a dinoflagellate species notorious for its rapid growth resulting in large-scale blooms. This study aimed to investigate the molecular mechanisms of A. pacificum under laboratory-simulated rapid growth conditions from the perspective of H3K4me3 modification regulation.

Methods and results: Western blot was used to detect the modification abundance of H3K4me3 in *A. pacificum* cultured under different conditions, including high light (HL), high nitrogen (HN), and f/2 medium (control, CT), in the rapid growth exponential phase. The results showed that the modification abundance of H3K4me3 under HL or HN was greater than that under CT. Chromatin immunoprecipitation-sequencing was used to explore the acting genes of H3K4me3 under different conditions for the first time. Nitrogen metabolism and endocytosis were significantly associated with H3K4me3 regulation under HL. Furthermore, H3K4me3 was also significantly associated with the vitamin metabolism pathway under HN.

Conclusions: These findings demonstrate that H3K4me3 plays a potentially important role in the regulation of the rapid growth of *A. pacificum*. Such knowledge of a histone modification regulatory network in this dinoflagellate, lays a necessary foundation for future research in related fields.

KEYWORDS

***Alexandrium pacificum*, H3K4me3, histone, ChIP-seq, epigenetics, HABs**

Highlights

- The regulatory mechanism of H3K4me3 was studied for the first time in *Alexandrium pacificum* under different growth conditions.

- ChIP-seq analysis of species without genomic data was performed using a close species.
- Nitrogen metabolism and endocytosis were related to H3K4me3 regulation in *A. pacificum* under high light conditions.
- Vitamin metabolism was related to H3K4me3 regulation under high nitrogen conditions.

Introduction

Alexandrium pacificum is one of the main blooming microalgae species in many coastal areas. Paralytic shellfish toxin produced by *A. pacificum* can significantly harm or kill marine organisms, and ultimately human, through food chain transfer *via* bivalve mollusks (Grattan et al., 2016). Variations in nutrient concentrations, especially nitrogen, are closely related to the occurrence and termination of blooms, and the accumulation of nitrogencan induce the rapid growth of algal cells (Yu et al., 2020; Baek et al., 2021). The biomass of *Alexandrium tamarense* under high nitrogen concentrations (2,646 μmol L^{-1}) was greater than that observed under low nitrogen concentrations when f/2 medium was used for culturing (Zhang et al., 2006). Irradiance is another factor that plays a vital role in stimulating growth (Laabir et al., 2011). It was found that the increase of illumination from 10 to 90 μmol photons m^{-2} s^{-1} was directly proportional to the growth rate of *A. pacificum* (Cao et al., 2011; Karabashev and Evdoshenko, 2016). However, knowledge of the intercellular mechanisms underlying the rapid growth of *A. pacificum* is limited. Previous studies have focused on the gene expression *A. pacificum* under different conditions through transcriptome technology (Zhang et al., 2014; Liu et al., 2021). Proteins related to environmental stress (nutrients, light, and temperature) at different growth stages of *A. pacificum* have also been identified, including, S-adenosylmethionine synthetase (AdoMetS), ribulose-1,5-bisphosphate carboxylase/oxygenase (RuBisCO), and heat shock proteins (HSPs)which are involved in macromolecular biosynthesis, photosynthesis, stress response, and cell cycle regulation (Uribe et al., 2008; Wang et al., 2012). However, the research into the growth mechanisms of *A. pacificum*, including the epigenetic regulation of molecular mechanisms, remains limited.

The genomic structure of dinoflagellates is unique; the genome is immense, and the DNA display a status of liquid crystal, and the chromosomes are permanently condensed (Hackett et al., 2004; Chow et al., 2010). Moreover, there appears to be a high degree of DNA redundancy in the dinoflagellate genome. Noncoding repetitive sequences comprise up to 60% of dinoflagellate genomes (Jaeckisch et al., 2011). In genome structure, non-coding sequences generally comprise promoters, enhancers, cis-acting elements, and trans-acting factors that regulate downstream genes to respond to biological needs. These non-coding regulatory regions are usually combined with transcription factors and epigenetic modifiers (histone modifications, DNA methylation, RNA methylation, and chromatin remodeling) to respond to environmental signals through the regulation of downstream gene expression (Koenecke et al., 2016). In dinoflagellates, these non-coding sequences comprise 60% of the genome, indicating that the existence of a prodigious and complex regulatory network. Therefore, the study of this regulatory role in dinoflagellates is very important for researching physiological activity and response mechanisms to the environment.

In dinoflagellates, histones exist with a very low protein/DNA ratio (1:10) (Hamkalo and Rattner, 1977; Hou and Lin, 2009; Lin, 2011), which is significantly lower than the ratio close to 1:1 in other eukaryotes. However, unlike in other eukaryotes, histones in dinoflagellates are not involved in nucleosome assembly (Figueroa et al., 2014). This leads to questions regarding the role that histones play in dinoflagellates. A previous study reported that several genes are responsible for histone modification in *A. pacificum*, including histone acetyltransferases, deacetylases, methylases, and demethylases (Riaz and Sui, 2018). The presence of histone modifying enzymes indicates that histone modifications may play an important role in *A. pacificum*. In higher plants, histone modification plays an important role in regulating the expression of genes at the epigenetic level, in response to the environment and stress, as well as being involved in a variety of biological processes such as growth and development (Yamamoto et al., 2020; Moreno-Perez et al., 2021). Therefore, it is reasonable to expect that histone modifications also play an essential role in *A. pacificum*.

Histone modifications, as a form of epigenetic regulation, play an important role in plant growth, development, and stress response (Liu et al., 2010). However, their effects on algae remain poorly understood, especially in dinoflagellates. In microalgae, studies on histone modifications have focused on marine diatoms and green algae. For example, in *Nannochloropsis* spp., H3K27me3, H3K27ac, and H3K9me3 showed different modification levels under different carbon dioxide conditions (Wei and Xu, 2018). In the macroalgae *Ectocarpus*, Bourdareau et al. (2021) identified 47 histone modifications and a new histone modification, H2AZR38me1; however, H3K27me3 modification, which is common in higher plants, and a corresponding multi-comb complex, were absent. This indicated that there are differences in histone modification and regulation mechanisms between algae and higher plants (Bourdareau et al., 2021).

Previous studies have reported various modification types such as histone methylation, acetylation, phosphorylation, and ubiquitination (Riaz et al., 2019; Zhu et al., 2022). Among the histone modifications studied previously, H3K4me3 modification was the most conservative site (Marinov and Lynch, 2015), which

provided a great advantage for using commercial H3K4me3 antibodies in subsequent studies. H3K4me3 is an activator of gene expressions in multiple biological processes, as well as a flexible modification in response to the environment in plants (Lauberth et al., 2013; Yan et al., 2019). Genes occupied by H3K4me3 in plants, especially in the absence of H3K4me1 and H3K4me2, generally display low tissue specificity but high levels of constitutive expression in *Arabidopsis* (Ha et al., 2011). However, H3K4me3 distribution broadened considerably along with differentially expressed genes during drought stress in *Arabidopsis* (Dijk et al., 2010), and showed differential trimethylation for a proportion of genes differentially expressed during drought stress in rice (Zong et al., 2013). This suggests that H3K4me3 may also be associated with tightly regulated pathways. Ngan et al. (2015) explored the relationship between the lipid production capacity of *Chlamydomonas reinhardtii* under nitrogen and sulfur starvation, and the regulation of five histone modifications including H3K4me3, and found that these histone modifications showed differential modification levels under nitrogen and sulfur restriction. H3K4me3 modification in soybean was found to promote carbon and nitrogen metabolism in rhizobia, supporting effective nitrogen fixation and promote material exchange between the and rhizobia (Wang et al., 2020). This suggests that H3K4me3 modification plays an important role in the growth and development of plants. Therefore, it is speculated that H3K4me3 may also play an important role in the growth of *A. pacificum*. In this study, epigenomicprofiles of H3K4me3 were employed to investigate its involvement in the responses of *A. pacificum* rapid growth to high light and high nitrogen. This study aimed to generate the first global H3K4me3 profile in *A. pacificum* through chromatin-immunoprecipitation (ChIP) followed by ChIP-sequencing (ChIP-seq) to disclose the regulation mechanism of H3K4me3 sustaining bloom progression and to decipher the regulation networks behind the utilization of light and nutrients in rapid growth.

Materials and methods

Algal culture and treatment conditions

Alexandrium pacificum was obtained from the Key Laboratory of Marine Genetics and Breeding, Ministry of Education, Ocean University of China. The algal cells were grown at 20 ± 1°C in a f/2 medium (Guillard and Ryther, 1962; Guillard, 1975) under a 12 hr light: 12 hr dark photo cycle using cool white fluorescent lights at a set intensity of 30 µmol photon m^{-2} s^{-1} (Guillard, 1975).

Alexandrium pacificum was initially inoculated at 4,000 cells/mL into 3 L Erlenmeyer flasks containing 2 L of modified f/2 medium for processing. The three treatment conditions were high light (HL), high nitrogen (HN), and control (CT), as shown in Table 1. Cell growth was then followed for 25 days. Samples (1 mL) for cell counting were fixed in 2% Lugol's iodine solution every 2 days, and then a micro-slide under a microscope (Nikon YS-100, Tokyo, Japan) was used to enumerate the cell concentration. The growth curve of *A. pacificum* was established to observe its growth state and help to determine sampling time. For counting, the samples were collected at a fixed time (between 11:00 and 12:00 pm) every day. Before each sampling, the cells were evenly distributed by gently shaking the flask. For each treatment condition, there were three biological replicates and three technical replicates.

Detection of H3K4me3 modification abundance

The abundance of H3K4me3 in *A. pacificum* at the exponential phase (12 days) under the different treatment conditions (HN, HL, and CT) was detected by Western blot with three biological replicates (Liu et al., 2022). The histone was extracted following the nucleoprotein extraction method, and quantified by the Bradford protein quantification kit (P0006, Beyotime Biotechnology, Haimen, China). Given that *A. pacificum* histone H3 sequences are very similar to human H3 sequences and show conservation, including the H3K4 locus (Riaz et al., 2019), a H3K4me3 commercial antibody raised from human H3 (PTM-613, Jingjie Biotechnology Co., Ltd. Hangzhou, China) was used in the western blot assay to determine H3K4me3 abundance under the different treatment conditions, with H3 as the internal reference (Chen et al., 2013).

ChIP

Alexandrium pacificum was grown in 2 L of f/2 medium under the three treatment conditions. Samples at the exponential phase (12 days, ~ 4 × 10^7cells) under the three treatment conditions were collected in a 50 mL centrifuge tube. Formaldehyde (final concentration: 1%) was added for cross-linking reaction at 25°Cand maintained for 30 min. Glycine (final concentration of 0.125 M) was added to quench the cross-linking reaction for 10 min at 25°C. The collected cells were washed with the sterilized water three times and centrifugated at 3,000 rpm for 5 min at 4°C to remove the formaldehyde. The

TABLE 1 Treatment conditions of *A. pacificum*.

Sample	Treatments
High nitrogen (HN)	Nitrate nitrogen concentration: 2.646 mmol L^{-1}, 30 µmol photos m^{-1} s^{-1}
High light (HL)	Nitrate nitrogen concentration: 882 µmol L^{-1}, 60 µmol photos m^{-1} s^{-1}
Control (CT)	Nitrate nitrogen concentration: 882 µmol L^{-1}, 30 µmol photos m^{-1} s^{-1}

cross-linked *A. pacificum* cells were frozen with liquid nitrogen and stored at -80°C. Chromatin extraction was carried out (Gendrel et al., 2005), and then the chromatin was sheared into 200–500 bp fragments using a chromatin shearing non-contact ultrasound instrument (S220 focused-ultrasonicator, Covaris, USA). Reverse cross-linking and gel electrophoresis (1.5% agarose gel) was performed to examine the effect of sonication. The ChIP kit of Abcam (ab117137, ABCAM, Cambridge, UK) and H3K4me3 antibody (PTM-613, PTM, Hangzhou, China) were used for immunoprecipitation. Reverse cross-linking and DNA purification was carried out following the kit instructions. Qubit2.0 (Invitrogen, Waltham, USA) was employed to quantify DNA concentration. Library construction and sequencing were performed by Wuhan IGENEBOOK Biotechnology Co., Ltd.

Sequencing and data analysis

The DNA library was sequenced with the HiSeq 2000 system for 50 nt single-end sequencing. Respectively, low-quality reads were filtered out with Trimmomatic (v. 0.4, Bolger et al., 2014). The clean reads were mapped to the symbiosis dinoflagellate (*Fugacium kawagutii*) genome (PRJNA630740) by BWA (v.: 0.7.15-r1140). Potential polymerase chain reaction (PCR) duplicates were removed with the software Samtools (v.1.3.1, Danecek et al., 2021). The software MACS2 (v. 2.1.1.20160309, Zhang et al., 2008) was used to call peaks using default parameters (model fold, 5, 50; bandwidth, 300 bp; q value, 0.05) and then the peak result was obtained for the subsequent analysis.

To further explore the binding site characteristics of H3K4me3 and to investigate the mechanism of H3K4me3 regulation on gene expression, the gene corresponding to the nearest transcription start site was found from the peak summit position (if there was no summit site, the midpoint was taken) for Gene Ontology (GO) and Kyoto Encyclopedia of Genes and Genomes (KEGG) annotation (Ashburner et al., 2000; Kanehisa and Goto, 2000). A diagram of the number of genes associated with H3K4me3 under the different conditions was then generated using a webtool (https://www.omicshare.com/tools). To determine the interval of up-regulation or down-regulation difference modification between samples, the number of reads in the peak region was counted using the DiffBind package (v.1.16.3, Wang et al., 2008), and the difference analysis was performed on two different groups of samples (Stark and Brown, 2011). The standard condition for screening the difference peak is a false discovery rate < 0.05 and a fold change > 0. From the summit position of the significant difference peak (if there is no summit site, the midpoint was taken), the nearest gene was selected for GO and KEGG annotation.

To study the unique mechanism of H3K4me3 regulation on the rapid growth of *A. pacificum* under the conditions of HL and HN, the genes associated with H3K4me3 only in HL or HN, but not in CT, were further analyzed using KEGG enrichment (Kanehisa and Goto, 2000). The genes enriched in the top 10 KEEG items were used to draw KEEG bubble diagrams, (https://www.omicshare.com/tools). The metabolic pathways and related genes with a number of genes > 3 and p-value < 0.05 in the enriched metabolic pathways were then further analyzed through a network of pathways and genes.

ChIP-qPCR

To validate the ChIP-Seq results, nine genes associated with H3K4me3 were selected from the ChIP-Seq data for ChIP-quantitative qPCR. The peak sequences (Supplementary 1) of the selected genes were used for primers design. The PCR primers of the genes were designed using Premier 5.0 software (https://www.PremierBiosoft.com) and presented in Table 2. The ChIP-qPCR was performed in 20 µl reactions using Universal Blue qPCR SYBR Green Master Mix (Ye Sen Biotech Co., Ltd., Shanghai, China). The reactions consisted of 10 µl of Universal Blue qPCR SYBR Green Master Mix, 0.4 µl of forward and reverse primer (10 µmol L^{-1}), 1 µl of immunoprecipitated DNA or input DNA, and 8.2 µl of H_2O. ChIP-qPCR was performed with three biological replicates, and the results were calculated as the percentage of input DNA (Haring et al., 2007; Solomon et al., 2021).

Results

Physiological responses of *A. pacificum* under different conditions

To observe the growth status and determine the sampling time, counting and growth curves were carried out for *A. pacificum* under three treatment conditions. It was found that cells of *A. pacificum* exhibited a low growth rate from days 1 to 3, then grew rapidly from 5 to 15 days (Figure 1). After 15 days the algae growth tends to stabilize. The results showed that high irradiation and nitrogen conditions will promote the growth of *Alexandrium pacificum*. The 12th day of the rapid growth period was selected as the sampling time for subsequent experiments.

H3K4me3 abundance of *A. pacificum* under different conditions

The modification abundance of H3K4me3 of *A. pacificum* under the different treatment conditions is shown in Figure 2. The abundance of H3K4me3 under HN and HL was greater than that under CT during the exponential rapid growth period of *A. pacificum*.

TABLE 2 ChIP-qPCR primers.

Gene name	Forward	Reverse
RibBA	TCCGCTCCAGTTCTGAGATGGTTGT	AAGGATTGGCTTTGAGGGTTGGGTA
Euk	ACAACACCAAACGAAACCACACCA	TTGTGATGTGTTGAGTTGTCGCGTG
Mok12	CGGTCATCCTCAACAGAAATCCAAC	ACAAGAAATAACAATACAGGGCATCC
L14	TCTTGGCAAATGCTTTCGCAGTAGT	ATGATTGATAGGGATAGTTGGGGGC
E1	GTAAGCAGAACTGGCGATGAGGGAT	CGTCCTGCTGTCAAAATGAACCAAC
RNA gene	GTCATCCTCAACAGAAATCCAACTACG	GACAAGAAATAACAATACAGGGCATCC
cytochrome b gene	TTTGGCACAGCTTTTAACATAGCATATTG	ATTCATTTCGGTTTCTCTTATTTCTCACA
ATP synthase CF1	AGGAGGAATTGTTTGGAATCTTTGGT	TGCTTTTTGCTTGACGGGCAGTATG
18S rRNA	GGCGATGAGGGATGAACCTACCG	GACCACCGTCCTGCTGTCAAAAT

H3K4me3 associated genes of *A. pacificum* under different conditions

Over 30 million uniquely mapped reads were obtained per library. More than 35% of the ChIP-Seq reads could be aligned to the *Fugacium kawagutii* genome. In total, around 2,878–7,822 peaks were called under each condition; and 156 genes from HL, 254 genes from HN, and 803 from CT were found to be specifically associated with H3K4me3 (Figure 3). A total of 36 genes were associated with H3K4me3 modification under HN and HL, but not under CT.

ChIP-qPCR

ChIP-qPCR was performed to confirm the results of ChIP-Seq, as shown in Figure 4. A total of nine genes (from 156 + 36 +254+219 in Figure 3) involved in various biological processes were selected for ChIP-qPCR, including riboflavin biosynthesis protein RibBA (RibBA), eukaryotic translation initiation factor 2 (Euk), cell wall alpha-1,3-glucan synthase mok12 (Mok12), ribosomal protein L14 (L14), ubiquitin-activating enzyme E1 (E1), small subunit ribosomal RNA gene (RNA gene), cytochrome b gene (CB), ATP synthase CF1 subunit alpha

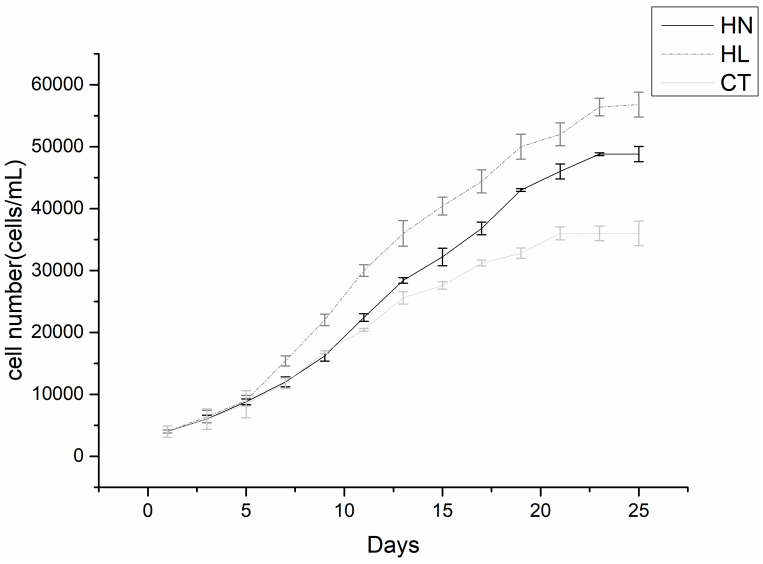

FIGURE 1
Growth curves of *Alexandrium pacificum* under different conditions. High light (HL), high nitrogen (HN), and f/2 normal medium condition (control [CT]). Each point is the mean of three independent experiments.

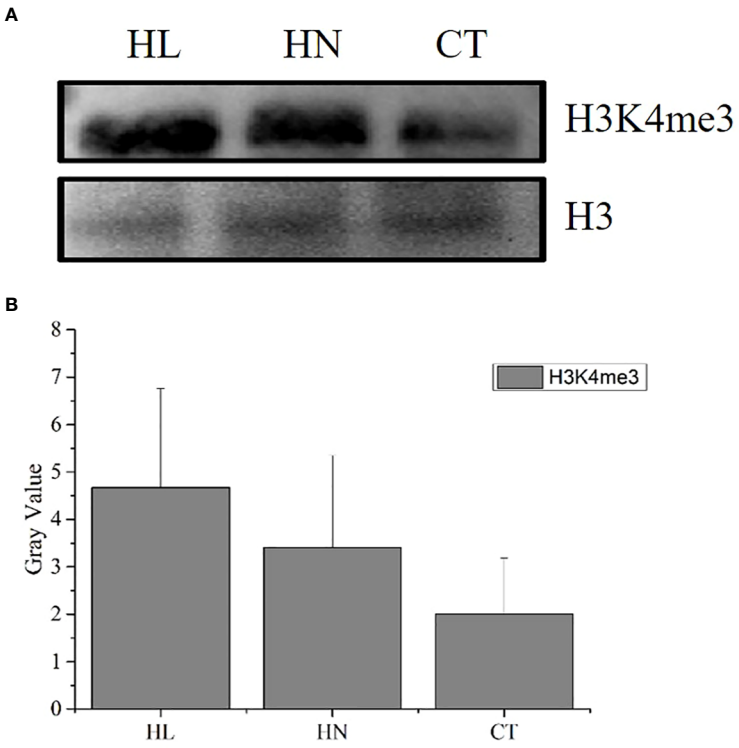

FIGURE 2
H3K4me3 abundance detection of *Alexandrium pacificum* under different conditions. **(A)** Western blot results of H3K4me3 modification in *A pacificum* under HN, HL, and CT; **(B)** Bar graph of the blot-spot density. Each column is the mean of three independent experiments, statistically significant differences were assessed using SPSS Statistics (v. 17.0; IBM Corp., Armonk, NY, USA) based on Tukey's test at $p < 0.05$.

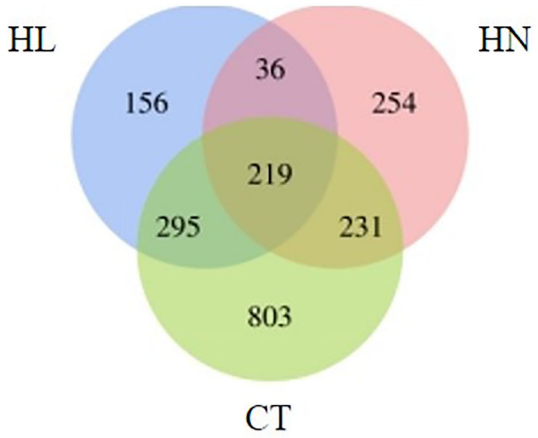

FIGURE 3
Venn diagram of the number of genes associated with H3K4me3 under different conditions: high light (HL), high nitrogen (HN), and normal f/2 medium condition (CT).

(ATP), and 18S rRNA gene (18S). Sample immunoglobulin G was used as the negative control in the ChIP-qPCR assay. Most selected genes displayed significant enrichment under HL and HN compared to under CT. The relative enrichment of immunoprecipitated DNA and immunoglobulin G (negative control) of each gene was more than 10-fold.

Analysis of H3K4me3-associated genes unique to the HL condition in *A. pacificum*

KEGG enrichment analysis showed that pathways related to growth and nutrient uptake, such as nitrogen metabolism, endocytosis, glyoxylate, and dicarboxylate metabolism, folate biosynthesis, phenylalanine metabolism, and protein processing in the endoplasmic reticulum, were all significantly enriched (Figure 5). In these enriched pathways, H3K4me3-associated genes unique to the HL condition, such as nitrate reductase and glutamine synthetase, were involved in nitrogen metabolism. In

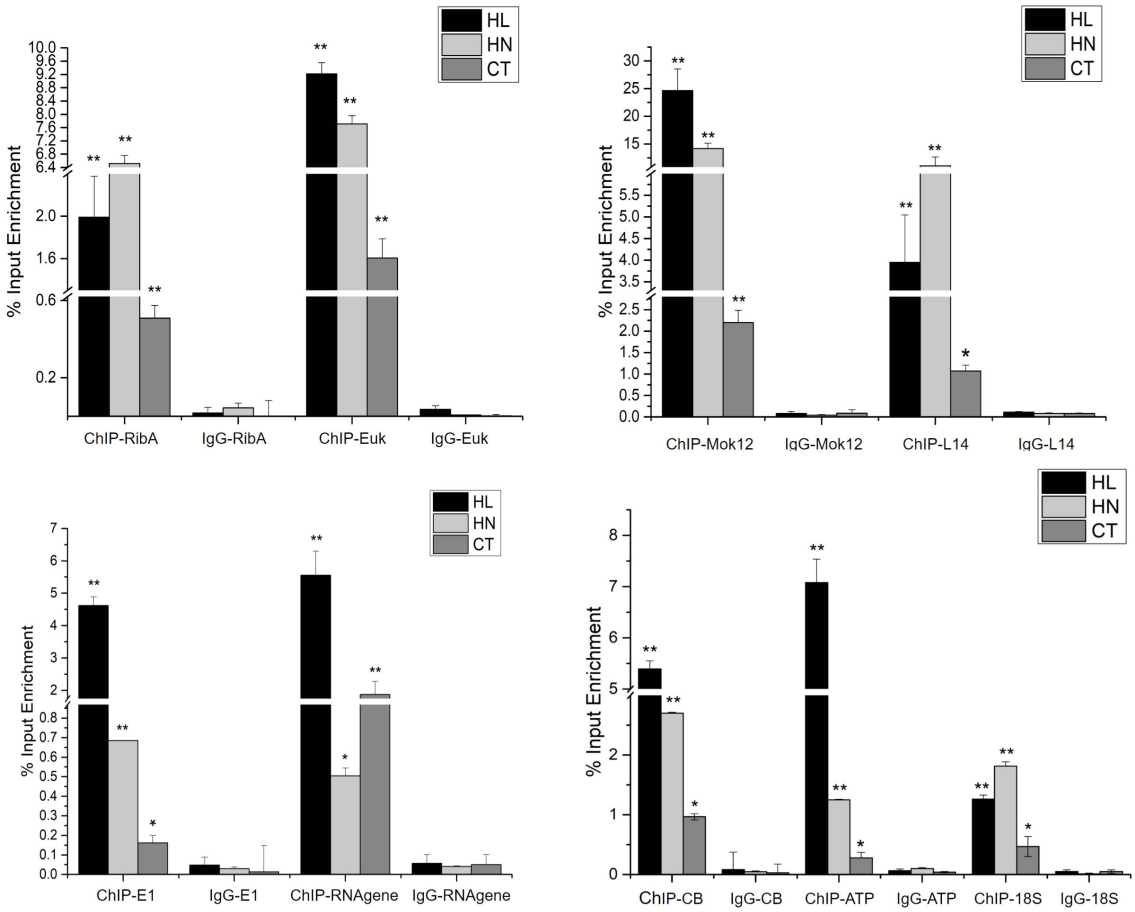

FIGURE 4
The result of ChIP-qPCR under high light (HL), high nitrogen (HN), and normal (CT) conditions. IP DNA was the experimental group and IgG DNA was the negative control group. Each column is the mean of three independent experiments. Significant differences are indicated by asterisks (**$p < 0.01$; *$p < 0.05$).

addition, several H3K4me3-related genes such as protein 26, E3 ubiquitin-protein ligase, and heat shock protein 70 (HSP70) were involved in the endocytosis pathway (Supplementary 2).

Analysis of H3K4me3 associated genes unique to the HN condition in *A. pacificum*

H3K4me3-associated genes unique to the HN condition were analyzed by KEGG enrichment. Vitamin B6 metabolism was significantly enriched. Furthermore, other pathways related to vitamin metabolism including folate, thiamine, pantothenate, and coenzyme A biosynthesis, and nicotinate and nicotinamide metabolism, were also enriched. In addition, the citrate cycle, mitogen–activated protein kinase signaling, plant hormone signal transduction, and RNA polymerase inositol phosphate metabolism pathways were also enriched (Figure 6). KEGG analysis revealed that the most affected pathway in *A. pacificum* under the HN condition was the vitamin metabolic pathway. The three genes of phosphoserine aminotransferase, exosome complex exonuclease RRP6, and pyridoxine 4-dehydrogenase involved in vitamin B6 metabolism were significantly enriched (Supplementary 2).

Discussion

H3K4me3 antibody selection and genome mapping protocol

For H3K4me3 modification, approximately 5.5% of the homologous sequences are covered by H3K4me3 peaks in the human genome (effective genome) and rhesus macaque genome, accounting for 132,294 homologous pairs. Additionally, there is a total of 79,865 human-mouse (more evolutionary distant)

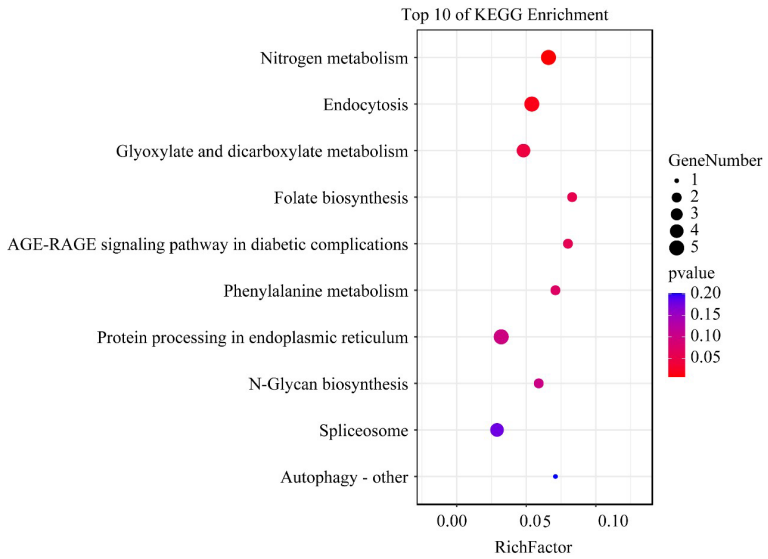

FIGURE 5
The top 10 enriched KEGG pathway terms of H3K4me3 associated genes unique to the HL condition in *Alexandrium pacificum*. RichFactor represents the ratio of the number of genes located in the KEGG term to the total number of genes located in the KEGG term in all annotated genes. The size of the circle represents the number of genes enriched in the term. The gradient of color from blue to red represents the size of the *p*-value changes.

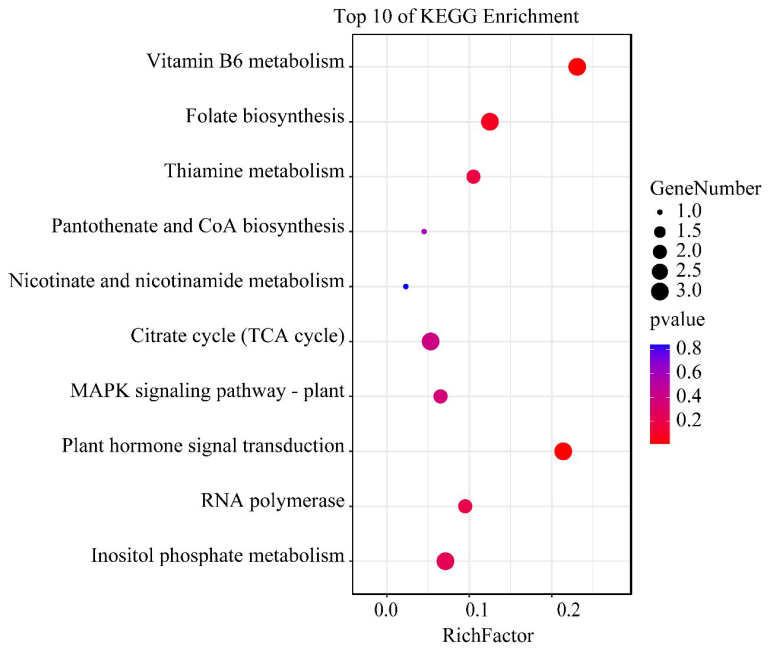

FIGURE 6
The top 10 enriched KEGG pathway terms of H3K4me3 associated genes unique to the HN condition in *Alexandrium pacificum*. RichFactor represents the ratio of the number of genes located in the KEGG term to the total number of genes located in the KEGG term in all annotated genes. The size of the circle represents the number of genes enriched in the term. The gradient of color from blue to red represents the size of the *p* value changes.

homologous region pairs with H3K4me3 signals (Lu et al., 2018), which indicate that H3K4me3 modification is highly conservative. The conservatism of H3K4me3 is important in the selection of commercial antibodies in ChIP. The antibody is the most critical factor in ChIP-seq, and directly affects the success of the ChIP experiment. The selection of the human H3K4me3 antibody is supported by several aspects. First, the N-terminal of the *A. pacificum* histone is conservative and divergent, and the two H3 variants are similar to human H3 sequences, both have conserved all the key residues (including the H3K4) of the histone code except H3K18 and H3S28 (Liu et al., 2019; Riaz et al., 2019). In addition, the human histone H3 antibody has been successfully used to detect histone H3 of *A. pacificum* (Liu et al., 2019). Moreover, mass spectrometry on the protein at the position of the H3 antibody was performed and the conserved modification site of H3K4 was found (Zhu et al., 2022). This led to the successful use of the H3K4me3 commercial antibody raised from human H3 for chromatin immunoprecipitation.

Due to the large size of the dinoflagellate genome, which contains highly redundant and repetitive sequences (Davidson et al., 2002; Hou and Lin, 2009), complete sequencing, assembly, and annotation of the dinoflagellate genome is nearly impossible within the constraints of current technology and expenditure. To date, less than 250 of the more than 8 million estimated eukaryotic species have been fully sequenced at the chromosome level (He et al., 2015). Nevertheless, information from several related species is often required to determine common processes and their evolutionary plasticity in order to understand the overarching principles of developmental biology. While detailed maps of developmental gene regulatory networks are well established for the sea urchin, *Stronglyocentrotus purpuratus*, a model organism, comparative studies using related species including sea stars and sea cucumbers, which have not been fully sequenced to date, are required to resolve longstanding questions related to factors involved in sea urchin development (Davidson et al., 2002). The genome of the dinoflagellate, *F. kawagutii*, was previously completed alongside the assembly, annotation, and uploading of the genome (Lin et al., 2015). In the present study, the genome of *F. kawagutii* was used to complete the genome-matching process. Finally, approximately 35% of the ChIP-seq reads were aligned to the genome of *F. kawagutii*. The results were verified by ChIP-qPCR, indicating that the results of the ChIP-seq had a certain credibility, and that the single gene in the results (including the target genes of interest in the subsequent analysis) had a high reliability. The analysis of the ChIP-seq results can help us acquire knowledge of H3K4me3-related genes under different conditions.

However, 65% of the reads were not aligned with the genome of *F. kawagutii*, leading to the omission of a large amount of relevant information from the results and making it impossible to judge the most important regulatory information of H3K4me3 overall. In addition, most of the peak sequences obtained by H3K4me3 were in gene regulatory regions. The gene information obtained by this alignment method cannot be correlated with the transcriptome data of *A. pacificum*, which introduces significant difficulties in the follow-up study of H3K4me3-related genes. Moreover, the method of the comparing genomes of other species may also have a large impact on the accuracy of the peak annotation and results analysis. For example, the annotation information of the peak sequence is the annotation information of *F. kawagutii* obtained by aligning the genome of *F. kawagutii*, and although the peak sequence is conservative, it does not exclude the possibility that the gene in which it is located is not conservative, which may also cause deviation in the subsequent gene analysis results. Therefore, it is necessary to continue the search for more suitable alignment genomes or more appropriate research methods to solve them.

H3K4me3 participates in nitrogen metabolism and endocytosis in *A. pacificum* under HL

The growth curves showed that *A. pacificum* grew more rapidly under HL than under the other conditions. H3K4me3 modification abundance was greater in the fast-growing log-phase under this condition than under the other conditions, indicating that H3K4me3 modification may be involved in the regulation of the rapid growth of *A. pacificum*. ChIP-seq results showed that among the H3K4me3-related genes specific to the HL condition, genes related to nitrogen metabolism, endocytosis, and mitogen-activated protein kinase signal transduction were significantly enriched. Therefore, these metabolic pathways and related genes may be involved in the regulation of the rapid growth of *A.pacificum* under HL in response to the change of H3K4me3.

Nitrogen is essential for the growth of marine phytoplankton (Li et al., 2021). The rapid growth of algae is closely related to an increase in nitrogen metabolic rate under HL. A previous study showed that the influence of light is very important on the activity of nitrate reductase; nitrate reductase activity increased with increasing light in the range of 10–90 μmol m^{-2} s^{-1} (Li et al., 2013). Therefore, under the condition of HL, nitrate reductase should play a major role in nitrogen metabolism. In our study, the genes related to H3K4me3 unique to HL, encoding metabolic enzymes within the nitrogen metabolism, especially those governing the rate-limiting steps, including nitrate reductase and glutamine synthetase gene, suggesting that H3K4me3 may contribute to the rapid growth of *A. pacificum* cells under HL conditions by nitrogen metabolism pathway.

Autotrophic, heterotrophic, and mixotrophic nutrition are the three main ways for dinoflagellates to uptake nutrients (Legrand and Carlsson, 1998). Studies have shown that dinoflagellate can ingest carbohydrates, some heterotrophic bacteria, and cyanobacteria through endocytosis (Feinstein et al., 2002; Zhang et al., 2011). Endocytosis plays an important role in the uptake of extracellular nutrients, the regulation of cell surface receptor expression, plasma

membrane homeostasis, and antigen presentation (Couto and Zipfel, 2016; Liao et al., 2017). HSP70 plays an important role in transmembrane transport, and E3 ubiquitin ligase-mediated ubiquitination regulates plasma membrane-resident receptor-like kinase endocytosis and intracellular degradation (Zhou et al., 2018). E3 ubiquitin ligase-mediated endocytosis of the plasma membrane receptor BR INSENSITIVE1 is mainly needed for signaling attenuation because the blocking of its internalization resulted in the enhancement of brassinosteroid responses in *Arabidopsis thaliana* (Irani et al., 2012). Regarding the present ChIP-seq results, the genes related to endocytosis affected by H3K4me3, including vacuolar sorting-related protein 26, HSP70, and E3 ubiquitin ligase, were significantly enriched. Previously, it has been reported that *Prorocentrum shikokuense*, when forming blooms, can ingest *Synechococcus*, *Isochrysis galbana*, and *Skeletonema* to acquire nutrients (Jeong et al., 2005). This indicates that endocytosis may be an important approach for the uptake of external nutrients and intracellular nutrient signal transduction during the rapid growth of *A. pacificum*, and may be conducive to maintaining a sufficient nutrient supply for the rapidly growing algal cells.

H3K4me3 participates in vitamin metabolism in *A. pacificum* under HN

The growth curves showed that *A.pacificum* grew faster under HN than under CT (normal f/2 condition). The H3K4me3 modification abundance was greater in the fast-growing algae under this condition than under CT, indicating that H3K4me3 may also be involved in the regulation of the rapid growth of *A. pacificum* under HN. The results of the differential analysis of H3K4me3-related genes between HN and CT showed that genes involved in vitamin metabolism were significantly enriched. The vitamin metabolism pathway is closely related to dinoflagellate growth (Lin et al., 2019).

Vitamin B6 is an important coenzyme in over 100 different cellular reactions and processes including those of amino acid metabolism, heme and chlorophyll biosynthesis, ethylene biosynthesis, fatty acid metabolism, transcriptional regulation, and response to oxidative stress (Rueschhoff, 2009; Colinas et al., 2016). The growth of dinoflagellates requires vitamin B, for example, *Prorocentrum donghaiense* and *Lingulodinium polyedrum* need vitamin B12 during tbloomings (Lin et al., 2014). Furthermore, microalgae growth can require different combinations of three types of vitamins B: vitamin B12 (cobalamin), B1 (thiamine), and B7 (biotin) (Fischer and Bacher, 2011). Thiamine plays an important role in carbon metabolism, and is a coenzyme factor of various carbohydrate-related enzymes in primary metabolism and amino acid-related enzymes (Tang et al., 2010). The active form of thiamine is thiamine pyrophosphate, which is essential for all organisms. The cofactor is associated with several enzymes involved in primary carbohydrate and branched-chain amino acid metabolism, including pyruvate dehydrogenase, transketolase, α-keto-acid decarboxylase, and α-ketoacid oxidase (Suzuki et al., 2010). Pantothenate (vitamin B5) is essential for fatty acid and anabolic steroids. It is also involved in steroid violet, melatonin,

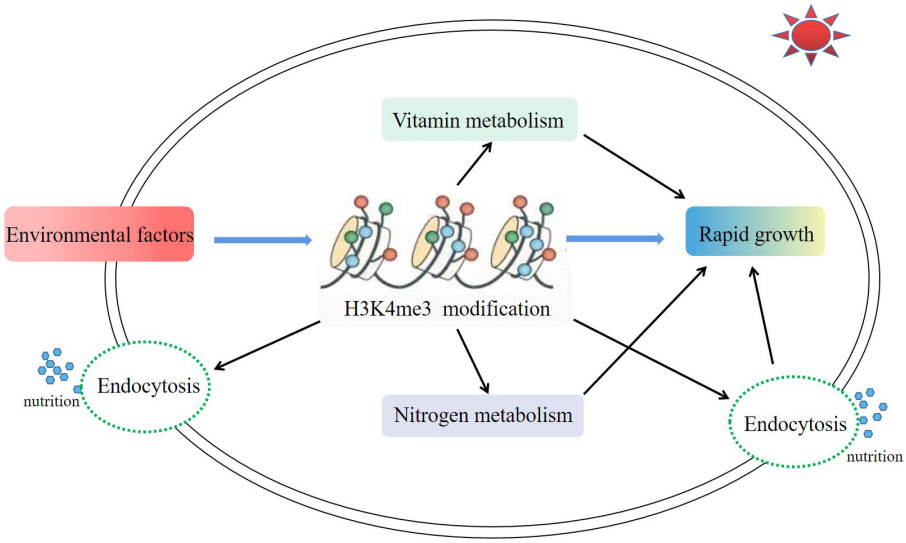

FIGURE 7
Major metabolic pathways associated with H3K4me3 in *Alexandrium pacificum* under high light and high nitrogen conditions. Environmental factors (high nitrate and high light intensity) enhanced the modification enrichment of H3K4me3. A higher enrichment level of H3K4me3 further promoted the vitamin metabolism, nitrogen metabolism, and endocytosis pathways, and finally promoted the rapid growth of *A. pacificum*.

and heme synthesis, the citric acid cycle, choline acetylation, antibodies, and other necessary intermediate metabolites (Webb and Smith, 2011). However, there are no reports of vitamin B6 utilization in dinoflagellates, and the enrichment of the vitamin B6 metabolic pathway in *A. pacificum* suggested that this may be a unique form of vitamin utilization and synthesis, which may contribute to the formation and succession of its red tide.

Conclusion

In this study, H3K4me3-associated genes of *A.pacificum* under the conditions of HL and HN were investigated. H3K4me3 was involved in the rapid growth of *A. pacificum* under HL and HN conditions, including acting on genes related to nitrogen metabolism, endocytosis, and vitamin metabolism (Figure 7). To the best of the authors' knowledge, this study revealed the epigenetic regulatory network of a red tide microalgae which induced red tide outbreak for the first time, providing important information for further understanding the mechanisms of harmful algal blooms. However, the detailed mechanisms behind the involvement of these metabolic pathways in algal growth need to be further investigated and explored.

Data availability statement

The datasets presented in this study can be found in online repositories. The names of the repository/repositories and accession number(s) can be found below: BioProject, accession number PRJNA881615.

Author contributions

JQ and ZS mainly designed the experimental protocol and participated in the wrote of the paper. JQ was responsible for the experiment and date analysis. ZZ participated in the experiment and revised the writing. YL participated in the design of the experimental scheme. All authors contributed to the article and approved the submitted version.

Funding

This work was supported by the National Natural Science Foundation of China (grant numbers 41676091 and 41176098).

Acknowledgments

Thanks to Professor Senjie Lin from Xiamen University for generously providing the genomic information of *Fugacium kawagutii*.

Conflict of interest

The authors declare that the research was conducted in the absence of any commercial or financial relationships that could be construed as a potential conflict of interest.

Publisher's note

Supplementary material

The Supplementary Material for this article can be found online at: https://www.frontiersin.org/articles/10.3389/fmars.2022.1011663/full#supplementary-material

References

Ashburner, M., Ball, C. A., Blake, J. A., Botstein, D., Butler, H., Cherry, J. M., et al. (2000). Gene ontology: Tool for the unification of biology. the gene ontology consortium. *Nat. Genet.* 25 (1), 25–29. doi: 10.1038/75556

Baek, S. S., Kwon, Y. S., Pyo, J., Choi, J., Kim, Y. O., and Cho, K. H. (2021). Identification of influencing factors of *A. catenella* bloom using machine learning and numerical simulation. *Harmful Algae* 103, 102007. doi: 10.1016/j.hal.2021.102007

Bolger, A., Lohse, M., and Usadel, B. (2014). Trimmomatic: A flexible trimmer for illumine sequence data. *Bioinformatics* 30 (15), 2114–2120. doi: 10.1093/bioinformatics/btu170

Bourdareau, S., Tirichine, L., Lombard, B., Loew, D., Scornet, D., Wu, Y., et al. (2021). Histone modifications during the life cycle of the brown alga *Ectocarpus*. *Genome Biol.* 22 (1), 12. doi: 10.1186/s13059-020-02216-8

Cao, C., Zheng, B., Chen, Z., Huang, M., and Zhang, J. (2011). Eutrophication and algal blooms in channel type reservoirs: A novel enclosure experiment by changing light intensity. *J. Environ. Sci.* 23 (10), 1660–1670. doi: 10.1016/s1001-0742(10)60587-6

Chen, Q., Chen, X., Wang, Q., Zhang, F., Lou, Z., Zhang, Q., et al. (2013). Structural basis of a histone H3 lysine 4 demethylase required for stem elongation in rice. *PloS Genet.* 9 (1), e1003239. doi: 10.1371/journal.pgen.1003239

Chow, M. H., Yan, K. T., Bennett, M. J., and Wong, J. T. (2010). Birefringence and DNA condensation of liquid crystalline chromosomes. *Eukaryot Cell* 9 (10), 1577–1587. doi: 10.1128/EC.00026-10

Colinas, M., Eisenhut, M., Tohge, T., Pesquera, M., Fernie, A. R., Weber, A. P. M., et al. (2016). Balancing of B_6 vitamers is essential for plant development and metabolism in arabidopsis. *Plant Cell* 28, 439–453. doi: 10.1105/tpc.15.01033

Couto, D., and Zipfel, C. (2016). Regulation of pattern recognition receptor signalling in plants. *Nat. Rev. Immunol.* 16 (9), 537–552. doi: 10.1038/nri.2016.77

Danecek, P., Bonfield, J. K., Liddle, J., Marshall, J., Ohan, V., Pollard, M. O., et al. (2021). Twelve years of SAMtools and BCFtools. *Gigascience* 10 (2), 1–4. doi: 10.1093/gigascience/giab008

Davidson, E. H., Rast, J. P., Oliveri, P., Ransick, A., Calestani, C., Yuh, C. H., et al. (2002). A genomic regulatory network for development. *Science* 295 (5560), 1669–1678. doi: 10.1126/science.1069883

Dijk, K., Ding, Y., Malkaram, S., Riethoven, J., Liu, R., Yang, J., et al. (2010). Dynamic changes in genome-wide histone H3 lysine 4 methylation patterns in response to dehydration stress in *Arabidopsis thaliana*. *BMC Plant Biol.* 10, 238. doi: 10.1186/1471-2229-10-238

Feinstein, T. N., Traslavina, R., Sun, M. Y., and Lin, S. J. (2002). Effects of light on photosynthesis, grazing, and population dynamics of the heterotrophic dinoflagellate *Pfiesteria piscicida* (Dinophyceae). *J. Phycol.* 38 (4), 659–669. doi: 10.1046/j.1529-8817.2002.01175.x

Figueroa, R. I., Cuadrado, A., Stüken, A., Rodríguez, F., and Fraga, S. (2014). Ribosomal DNA organization patterns within the dinoflagellate genus *Alexandrium* as revealed by FISH: Life cycle and evolutionary implications. *Protist* 165 (3), 343–363. doi: 10.1016/j.protis.2014.04.001

Fischer, M., and Bacher, A. (2011). Biosynthesis of vitamin B2 and flavocoenzymes in plants. *Adv. Bot. Res.* 58, 93–152. doi: 10.1016/B978-0-12-386479-6.00003-2

Gendrel, A., Lippman, Z., Martienssen, R., and Vincent, C. (2005). Profiling histone modification patterns in plants using genomic tiling microarrays. *Nat. Methods* 2 (3), 213–218. doi: 10.1038/nmeth0305-213

Grattan, L. M., Holobaugh, S., and Morris, J. G. (2016). Harmful algal blooms and public health. *Harmful Algae* 57, 2–8. doi: 10.1016/j.hal.2016.05.003

Guillard, R. R. L. (1975). "Culture of phytoplankton for feeding marine invertebrates," in *Culture of marine invertebrate animals*. Eds. W. L. Smith and M. H. Chanley (New York: Plenum Press), 26–60.

Guillard, R. R. L., and Ryther, J. H. (1962). Studies of marine planktonic diatoms. i. cyclotella nana hustedt and detonula confervacea cleve. *Can. J. Microbiol.* 8, 229–239. doi: 10.1139/m62-029

Hackett, J. D., Anderson, D. M., Erdner, D. L., and Bhattacharya, D. (2004). Dinoflagellates: a remarkable evolutionary experiment. *Am. J. Bot.* 91 (10), 1523–1534. doi: 10.3732/ajb.91.10.1523

Hamkalo, B. A., and Rattner, J. (1977). The structure of a mesokaryote chromosome. *Chromosoma* 60 (1), 39–47. doi: 10.1007/BF00330409

Ha, M., Ng, D. W. K., Li, W. H., and Chen, Z. J. (2011). Coordinated histone modifications are associated with gene expression variation within and between species. *Genome Res.* 21 (4), 590–598. doi: 10.1101/gr.116467.110

Haring, M., Offermann, S., Danker, T., Horst, I., Peterhansel, C., and Stam, M. (2007). Chromatin immunoprecipitation: optimization, quantitative analysis and data normalization. *Plant Methods* 3 (1), 11. doi: 10.1186/1746-4811-3-11

He, X., Cicek, A. E., Wang, Y., Schulz, M. H., Le, H. S., and Bar-Joseph, Z. (2015). *De novo* ChIP-seq analysis. *Genome Biol.* 16, 205. doi: 10.1186/s13059-015-0756-4

Hou, Y., and Lin, S. (2009). Distinct gene number-genome size relationships for eukaryotes and non-eukaryotes: gene content estimation for dinoflagellate genomes. *PloS One* 4 (9), e6978. doi: 10.1371/journal.pone.0006978

Irani, N. G., Rubbo, S. D., Mylle, E., Begin, J., Schneider-Pizoń,, Hniliková, J., et al. (2012). Fluorescent castasterone reveals BRI1 signaling from the plasma membrane. *Nat. Chem. Biol.* 8 (6), 583–589. doi: 10.1038/nchembio.958

Jaeckisch, N., Yang, I., Wohlrab, S., Glockner, G., Kroymann, J., Vogel, H., et al. (2011). Comparative genomic and transcriptomic characterization of the toxigenic marine dinoflagellate *Alexandrium ostenfeldii*. *PloS One* 6 (12), e28012. doi: 10.1371/journal.pone.0028012

Jeong, H. J., Park, J. Y., Nho, J. H., Park, M. O., Ha, J. H., Seong, K. A., et al. (2005). Feeding by red-tide dinoflagellates on the cyanobacterium *Synechococcus*. *Aquat. Microb. Ecol.* 41, 131–143. doi: 10.3354/ame041131

Kanehisa, M., and Goto, S. (2000). KEGG: kyoto encyclopedia of genes and genomes. nucleic acids research. *Nucleic Acids Res.* 28 (1), 27–30. doi: 10.1093/nar/28.1.27

Karabashev, G. S., and Evdoshenko, M. A. (2016). Narrowband shortwave minima in spectra of backscattered light from the sea obtained from ocean color scanners as a remote indication of algal blooms. *Oceanologia* 58 (4), 279–291. doi: 10.1016/j.oceano.2016.05.001

Koenecke, N., Johnston, J., Gaertner, B., Natarajan, M., and Zeitlinger, J. (2016). Genome-wide identification of drosophila dorso-ventral enhancers by differential histone acetylation analysis. *Genome Biol.* 17 (1), 196. doi: 10.1186/s13059-016-1057-2

Laabir, M., Jauzein, C., Genovesi, B., Masseret, E., Grzebyk, D., Cecchi, P., et al. (2011). Influence of temperature, salinity and irradiance on the growth and cell yield of the harmful red tide dinoflagellate *Alexandrium catenella* colonizing Mediterranean waters. *J. Plankton Res.* 33 (10), 1550–1563. doi: 10.1093/plankt/fbr050

Lauberth, S. M., Nakayama, T., Wu, X., Ferris, A. L., Tang, Z., Hughes, S. H., et al. (2013). H3K4me3 interactions with TAF3 regulate preinitiation complex assembly and selective gene activation. *Cell* 152 (5), 1021–1036. doi: 10.1016/j.cell.2013.01.052

Legrand, C., and Carlsson, P. (1998). Uptake of high molecular weight dextran by the dinoflagellate *Alexandrium catenella*. *Aquat. Microbial. Ecol.* 16, 81–86. doi: 10.3354/ame016081

Liao, D., Cao, Y., Sun, X., Espinoza, C., Nguyen, C. T., Liang, Y., et al. (2017). *Arabidopsis* E3 ubiquitin ligase PLANT U-BOX13 (PUB13) regulates chitin receptor lysin motif receptor Kinase5 (LYK5) protein abundance. *New Phytol.* 214 (4), 1646–1656. doi: 10.1111/nph.14472

Lin, S. (2011). Genomic understanding of dinoflagellates. *Res. Microbiol.* 162 (6), 551–569. doi: 10.1016/j.resmic.2011.04.006

Lin, S., Cheng, F., Song, B., Zhong, X., Lin, X., Li, W., et al. (2015). The *Symbiodinium kawagutii* genome illuminates dinoflagellate gene expression and coral symbiosis. *Science* 350 (6261), 691–694. doi: 10.1126/science.aad0408

Lin, S. J., Ji, N. J., and Luo, H. (2019). Recent progress in marine harmful algal bloom research. *Oceanol. Et Limnol. Sin.* 50 (03), 495–510. doi: 10.11693/hyhz20180800191

Lin, J. N., Yan, T., Zhang, Q. C., Wang, Y. F., Liu, Q., and Zhou, M. J. (2014). *In situ* detrimental impacts of *Prorocentrum donghaiense* blooms on zooplankton in the East China Sea. *Mar. pollut. Bull.* 88 (1-2), 302–310. doi: 10.1016/j.marpolbul.2014.08.026

Li, H. M., Shi, X. Y., Ding, Y. Y., and Tang, H. J. (2013). Illumination's effect on the growth and nitrate reductase activity of typical red-tide algae in the East China Sea. *Huan Jing Ke Xue* 34 (9), 3391–3397. doi: 10.13227/j.hjkx

Liu, C., Lu, F., Cui, X., and Cao, X. (2010). Histone methylation in higher plants. *Annu. Rev. Plant Biol.* 61, 395–420. doi: 10.1146/annurev.arplant.043008.091939

Liu, Y., Zhu, Z., Qi, J., Sui, Z., Shang, E., Zhang, S., et al. (2021). Comparative transcriptome profiling reveals insights into the mechanisms related to explosive growth of *Alexandrium pacificum*. *Front. Mar. Sci.* 8. doi: 10.3389/fmars.2021.751851

Liu, Y., Zhu, Z., Sui, Z., Liu, H., and Riaz, S. (2022). Calmodulin and its interactive proteins participate in regulating the explosive growth of *Alexandrium pacificum* (dinoflagellate). *Int. J. Mol. Sci.* 23, 145. doi: 10.3390/ijms23010145

Liu, H., Riaz, S., Liu, Y., Khurshid, A., Zhang, W., Sui, Z., et al (2019). Cloning and expression analysis of histone H3 in *Alexandrium catenella* during the growth process. *Marine Sci.* 43 (11), 19–27. doi: 10.11759/hykx20190401001

Li, X. Y., Yu, R. C., Geng, H. X., and Li, Y. F. (2021). Increasing dominance of dinoflagellate red tides in the coastal waters of yellow Sea. *China Mar. pollut. Bull.* 168, 112439. doi: 10.1016/j.marpolbul.2021.112439

Lu, J., Cao, X., and Zhong, S. (2018). A likelihood approach to testing hypotheses on the co-evolution of epigenome and genome. *PloS Comput. Biol.* 14 (12), e1006673. doi: 10.1371/journal.pcbi.1006673

Marinov, G. K., and Lynch, M. (2015). Diversity and divergence of dinoflagellate histone proteins. *G3 (Bethesda)* 6 (2), 397–422. doi: 10.1534/g3.115.023275

Moreno-Perez, A. J., Santos-Pereira, J. M., Martins-Noguerol, R., DeAndres-Gil, C., Troncoso-Ponce, M. A., Venegas-Caleron, M., et al. (2021). Genome-wide mapping of histone H3 lysine 4 trimethylation (H3K4me3) and its involvement in fatty acid biosynthesis in sunflower developing seeds. *Plants (Basel)* 10 (4), 706. doi: 10.3390/plants10040706

Ngan, C. Y., Wong, C. H., Choi, C., Yoshinaga, Y., Louie, K., Jia, J., et al. (2015). Lineage-specific chromatin signatures reveal a regulator of lipid metabolism in microalgae. *Nat. Plants* 1 (8), 15107. doi: 10.1038/nplants.2015.107

Riaz, S., Niaz, Z., Khan, S., Liu, Y., and Sui, Z. (2019). Detection, characterization and expression dynamics of histone proteins in the dinoflagellate *Alexandrium pacificum* during growth regulation. *Harmful Algae* 87, 101630. doi: 10.1016/j.hal.2019.101630

Riaz, S., and Sui, Z. (2018). Molecular cloning, transcriptome profiling, and characterization of histone genes in the dinoflagellate *Alexandrium pacificum*. *J. Microbiol. Biotechnol.* 28 (7), 1185–1198. doi: 10.4014/jmb.1802.01075

Rueschhoff, E. E. (2009). Vitamin B6 metabolism in arabidopsis thaliana. dissertations and theses - gradworks. (Raleigh, North Carolina: North Carolina State University).

Solomon, E., Caldwell, K., and Allan, A. (2021). A novel method for the normalization of ChIP-qPCR data. *MethodX* 8, 101504. doi: 10.1016/j.taap.2020.114920

Stark, R., and Brown, G. (2011). *DiffBind: differential binding analysis of ChIP-seq peak data. r package version* (Cambridge: University of Cambridge, Cancer Research UK- Cambridge Institute.), Vol. 100. 4–3.

Suzuki, R., Katayama, T., Kim, B. J., Wakagi, T., Shoun, H., Ashida, H., et al. (2010). Crystal structures of phosphoketolase: thiamine diphosphate-dependent dehydration mechanism. *J. Biol. Chem.* 285 (44), 34279–34287. doi: 10.1074/jbc.M110.156281

Tang, Y. Z., Koch, F., and Gobler, C. J. (2010). Most harmful algal bloom species are vitamin B1 and B12 auxotrophs. *Proc. Natl. Acad. Sci. United States America* 107 (48), 20756–20761. doi: 10.1073/pnas.1009566107

Uribe, P., Fuentes, D., Valdés, J., Shmaryahu, A., Zúñiga, A., Holmes, D., et al. (2008). Preparation and analysis of an expressed sequence tag library from the toxic dinoflagellate *Alexandrium catenella*. *Mar. Biotechnol.* 10 (6), 692–700. doi: 10.1007/s10126-008-9107-8

Wang, H., Hernandez, J. M., and Van Mieghem, P. (2008). Betweenness centrality in a weighted network. *Phys. Rev. E Stat. Nonlin. Soft Matter Phys.* 77, 46105. doi: 10.1103/PhysRevE.77.046105

Wang, D., Lin, L., Wang, M., Li, C., and Hong, H. (2012). Proteomic analysis of a toxic dinoflagellate *Alexandrium catenella* under different growth phases and conditions. *Chin. Sci. Bull.* 57 (25), 3328–3341. doi: 10.1007/s11434-012-5160-9

Wang, Q., Yung, W. S., Wang, Z., and Lam, H. M. (2020). The histone modification H3K4me3 marks functional genes in soybean nodules. *Genomics* 112 (6), 5282–5294. doi: 10.1016/j.ygeno.2020.09.052

Webb, M. E., and Smith, A. G. (2011). Pantothenate biosynthesis in higher plants. *Adv. Bot. Res.* 58, 203–255. doi: 10.1016/B978-0-12-386479-6.00001-9

Wei, L., and Xu, J. (2018). Optimized methods of chromatin immunoprecipitation for profiling histone modifications in industrial microalgae nannochloropsis spp. *J. Phycol.* 54, 358–367. doi: 10.1111/jpy.12623

Yamamoto, J., Han, Q., Inubushi, S., Sugisawa, N., Hamada, K., Nishino, H., et al. (2020). Histone methylation status of H3K4me3 and H3K9me3 under methionine restriction is unstable in methionine-addicted cancer cells, but stable in normal cells. *Biochem. Biophys. Res. Commun.* 533 (4), 1034–1038. doi: 10.1016/j.bbrc.2020.09.108

Yan, H., Liu, Y., Zhang, K., Song, J., Xu, W., and Su, Z. (2019). Chromatin state-based analysis of epigenetic H3K4me3 marks of *Arabidopsis* in response to dark stress. *Front. Genet.* 10. doi: 10.3389/fgene.2019.00306

Yu, L., Zhang, Y., Li, M., Wang, C., Lin, X., Li, L., et al. (2020). Comparative metatranscriptomic profiling and microRNA sequencing to reveal active metabolic pathways associated with a dinoflagellate bloom. *Sci. Total Environ.* 699, 134323. doi: 10.1016/j.scitotenv.2019.134323

Zhang, Y. J., Cao, Y., Wang, Z., Han, B., and Yang, Y. (2006). Effects of limitation of nitrogen and phosphorus on the growth of *Alexandrium tamarense*. *J. Trop. Subtrop. Bot.* 14 (006), 482–486. doi: 10.1186/gb-2008-9-9-r137

Zhang, Y., Liu, T., Meyer, C. A., Eeckhoute, J., Johnson, D. S., Bernstein, B. E., et al. (2008). Model-based analysis of ChIP-seq (MACS). *Genome Biol.* 9, R137. doi: 10.1186/gb-2008-9-9-r137

Zhang, S., OU, L., and Lu, S. (2011). Effects of light and nutrients on the phagotrophic behaviors of three harmful dinoflagellates. *Jinan Univ. (MA thesis)* 35 (4), 94–99. doi: 10.1088/1674-1137/35/2/019

Zhang, S., Sui, Z., Chang, L., Kang, K., Ma, J., Kong, F., et al. (2014). Transcriptome *de novo* assembly sequencing and analysis of the toxic dinoflagellate *Alexandrium catenella* using the illumina platform. *Gene* 537 (2), 285–293. doi: 10.1016/j.gene.2013.12.041

Zhou, J., Liu, D., Wang, P., Ma, X., Lin, W., Chen, S., et al. (2018). Regulation of *Arabidopsis* brassinosteroid receptor BRI1 endocytosis and degradation by plant U-box PUB12/PUB13-mediated ubiquitination. *Proc. Natl. Acad. Sci. U.S.A.* 115 (8), E1906–E1915. doi: 10.1073/pnas.1712251115

Zhu, Z., Liu, Y., Qi, J., and Sui, Z. (2022). Identification of epigenetic histone modifications and analysis of histone lysine methyltransferases in *Alexandrium pacificum*. *Harmful Algae* 119, 102323. doi: 10.1016/j.hal.2022.102323

Zong, W., Zhong, X., You, J., and Xiong, L. (2013). Genome-wide profiling of histone H3K4-tri-methylation and gene expression in rice under drought stress. *Plant Mol. Biol.* 81 (1-2), 175–188. doi: 10.1007/s11103-012-9990-2

frontiers | Frontiers in Marine Science

TYPE Original Research
PUBLISHED 02 December 2022
DOI 10.3389/fmars.2022.1010319

OPEN ACCESS

EDITED BY
Carolina Madeira,
NOVA University Lisbon, Portugal

REVIEWED BY
Michael Ginger,
University of Huddersfield,
United Kingdom
Pedro M. Costa,
New University of Lisbon, Portugal

*CORRESPONDENCE
Ying Zhang
yingzhang@uri.edu
Joan M. Bernhard
jbernhard@whoi.edu

SPECIALTY SECTION
This article was submitted to Marine Molecular Biology and Ecology, a section of the journal Frontiers in Marine Science

RECEIVED 02 August 2022
ACCEPTED 09 November 2022
PUBLISHED 02 December 2022

CITATION
Powers C, Gomaa F, Billings EB, Utter DR, Beaudoin DJ, Edgcomb VP, Hansel CM, Wankel SD, Filipsson HL, Zhang Y and Bernhard JM (2022) Two canonically aerobic foraminifera express distinct peroxisomal and mitochondrial metabolisms. *Front. Mar. Sci.* 9:1010319. doi: 10.3389/fmars.2022.1010319

Two canonically aerobic foraminifera express distinct peroxisomal and mitochondrial metabolisms

Christopher Powers[1], Fatma Gomaa[2,3], Elizabeth B. Billings[1], Daniel R. Utter[3], David J. Beaudoin[2], Virginia P. Edgcomb[2], Colleen M. Hansel[4], Scott D. Wankel[4], Helena L. Filipsson[5], Ying Zhang[1]* and Joan M. Bernhard[2]*

[1]Department of Cell and Molecular Biology, College of the Environment and Life Sciences, University of Rhode Island, Kingston, RI, United States, [2]Department of Geology and Geophysics, Woods Hole Oceanographic Institution, Woods Hole, MA, United States, [3]Department of Organismic and Evolutionary Biology, Harvard University, Cambridge, MA, United States, [4]Department of Marine Chemistry and Geochemistry, Woods Hole Oceanographic Institution, Woods Hole, MA, United States, [5]Department of Geology, Lund University, Lund, Sweden

Certain benthic foraminifera thrive in marine sediments with low or undetectable oxygen. Potential survival avenues used by these supposedly aerobic protists include fermentation and anaerobic respiration, although details on their adaptive mechanisms remain elusive. To better understand the metabolic versatility of foraminifera, we studied two benthic species that thrive in oxygen-depleted marine sediments. Here we detail, *via* transcriptomics and metatranscriptomics, differential gene expression of *Nonionella stella* and *Bolivina argentea*, collected from Santa Barbara Basin, California, USA, in response to varied oxygenation and chemical amendments. Organelle-specific metabolic reconstructions revealed these two species utilize adaptable mitochondrial and peroxisomal metabolism. *N. stella*, most abundant in anoxia and characterized by lack of food vacuoles and abundance of intracellular lipid droplets, was predicted to couple the putative peroxisomal beta-oxidation and glyoxylate cycle with a versatile electron transport system and a partial TCA cycle. In contrast, *B. argentea*, most abundant in hypoxia and contains food vacuoles, was predicted to utilize the putative peroxisomal gluconeogenesis and a full TCA cycle but lacks the expression of key beta-oxidation and glyoxylate cycle genes. These metabolic adaptations likely confer ecological success while encountering deoxygenation and expand our understanding of metabolic modifications and interactions between mitochondria and peroxisomes in protists.

KEYWORDS

protists, mitochondria, peroxisomes, chemocline, anoxia, benthic foraminifera, Santa Barbara Basin

Introduction

Foraminifera are widely distributed across the marine realm, where they can constitute large proportions of the benthos (Bernhard et al., 2000; Gooday et al., 2000). This diverse protistan group is broadly implicated in biogeochemical cycling, where some foraminifera and/or their symbionts perform approximately two-thirds of total denitrification (Risgaard-Petersen et al., 2006; Piña-Ochoa et al., 2010; Bernhard et al., 2012a), with some studies noting all (Choquel et al., 2021). Others are involved in sulfur cycling (Nomaki et al., 2016) and exhibit physiological responses, such as increased adenosine triphosphate (ATP) concentrations, to reactive oxygen species (ROS) (Bernhard and Bowser, 2008). Certain foraminiferan species, while exhibiting lower abundance in oxygenated habitats, thrive in hypoxic or anoxic sediments that are characterized by low oxygen or absence of dissolved oxygen, respectively (Bernhard et al., 1997; Bernhard et al., 2003; Levin et al., 2009).

Robust foraminiferan populations occur across the oxygen gradient within chemoclines. Chemoclines are often coupled with complex gradients of reduction-oxidation chemistry (Reimers et al., 1996) and considerable concentrations of hydrogen sulfide (Bernhard et al., 2003). Reactive oxygen species, such as oxygen radicals and hydrogen peroxide, can be produced in chemoclines *via* abiotic means such as the interaction of O_2 with reduced metals, sulfide, or dissolved organic carbon, or through biotic means mediated by transmembrane NADPH oxidases (Hansel and Diaz, 2021). Certain chemocline-associated foraminifera contain masses of peroxisomes, often correlated with the presence of endoplasmic reticulum (Bernhard and Bowser, 2008). It has been hypothesized that peroxisomes can mediate foraminiferal aerobic respiration through catalase-induced O_2 production (Bernhard and Bowser, 2008), but this hypothesis requires further investigation.

Protists inhabiting hypoxic or anoxic environments have been shown to modify the functions of their mitochondria and peroxisomes (Müller et al., 2012; Burki et al., 2013; Stairs et al., 2015; Gawryluk et al., 2016; Verner et al., 2021; Záhonová et al., 2022). The mitochondria related organelles (MROs), reduced forms of mitochondria characterized by the loss of key enzymes involved in oxygen-dependent metabolism, are often specialized for anaerobic energy generation through pyruvate fermentation, hydrogen production, substrate-level phosphorylation, and malate dismutation (Müller et al., 2012; Stairs et al., 2015; Leger et al., 2017), or known to abandon their roles in energy metabolism entirely (Jedelský et al., 2011; Burki et al., 2013; Leger et al., 2017). The metabolism of MROs can be evolutionarily linked to metabolic modifications of peroxisomes. In some obligate anaerobic protists, the peroxisomes are often absent, as in the cases of *Giardia* and *Trichomonas* (Gabaldón et al., 2016), or highly modified, as observed in *Entamoeba histolytica, Pelomyxa schiedti*, and *Mastigameoba balamuthi* (Le et al., 2020; Verner et al., 2021; Záhonová et al., 2022). Modifications to peroxisomal metabolism in anaerobes often entail loss of the O_2-involving catalase and beta-oxidation functions (Le et al., 2020; Verner et al., 2021; Záhonová et al., 2022).

The known metabolic capacity in benthic foraminifera may include denitrification (Risgaard-Petersen et al., 2006; Woehle et al., 2018; Gomaa et al., 2021), ammonium assimilation (LeKieffre et al., 2018b; Gomaa et al., 2021), fermentation (Orsi et al., 2020; Gomaa et al., 2021), and utilization of dissolved organic matter (DeLaca et al., 1981; Orsi et al., 2020). Our recent findings, based on transcriptomic and metatranscriptomic analysis of two foraminiferan species, *Nonionella stella* and *Bolivina argentea*, collected from the oxygen-depleted Santa Barbara Basin (SBB), USA, provided insights into metabolic functions related to the survival of these two species in anoxia, such as anaerobic pyruvate metabolism and denitrification (Gomaa et al., 2021). Here, we performed additional analysis on the (meta)transcriptomes of these two species by computationally reconstructing metabolic responses of intracellular organelles to chemical amendments, which has not been elucidated in the two foraminifera.

N. stella and *B. argentea* inhabit distinct niches within the SBB (Table 1). *N. stella* is most abundant in severely hypoxic to euxinic (anoxic plus sulfidic) conditions, and is the sole calcareous foraminifer documented to survive long-term anoxia within the basin (Bernhard et al., 1997; Bernhard et al., 2006). *N. stella* sequesters chloroplasts (Bernhard and Bowser, 1999; Grzymski et al., 2002; Gomaa et al., 2021), likely from prey, proliferates peroxisome-endoplasmic reticulum (P-ER) complexes (Bernhard and Bowser, 2008), and apparently lacks food vacuoles (Gomaa et al., 2021). In contrast, *B. argentea* is abundant at the basin's flanks, rarely occurring in the most oxygen-depleted conditions (Bernhard et al., 1997), contains

TABLE 1 Distinctive cytology and ecophysiology of *N. stella* and *B. argentea*.

	Peroxisomes	Kleptoplasty	Food Vacuoles	Denitrification	Habitat
N. stella	Peroxisome-ER Complexes (Bernhard and Bowser, 2008)	Yes (Bernhard and Bowser, 1999)	Not observed (Gomaa et al., 2021)	Yes (Risgaard-Petersen et al., 2006; Gomaa et al., 2021)	Hypoxia to Euxinia (Bernhard et al., 1997; Bernhard et al., 2003)
B. argentea	Sparse Distribution (Bernhard et al., 2012a)	No (Bernhard et al., 2012a)	Yes (Bernhard et al., 2012a)	Yes (Bernhard et al., 2012a; Gomaa et al., 2021)	Hypoxia (Bernhard et al., 1997)

solitary to small groups of peroxisomes, and exhibits evidence of digestion of chloroplasts and other organics (Bernhard et al., 2012a). Given their contrasting physiological features, we hypothesize these two species would demonstrate distinct metabolic responses to variable biogeochemistry, which is known to occur episodically within the SBB (Reimers et al., 1996; Kuwabara et al., 1999; Bernhard et al., 2003). Based on the identification of potential metabolic connectivity between peroxisomes and mitochondria, we illustrate the organelle-specific metabolic responses of *N. stell*a and *B. argentea* to the addition of hydrogen peroxide (H_2O_2), nitrate (NO_3^-), and/or hydrogen sulfide (H_2S) amendments under anoxia or hypoxia, thereby providing insights into the metabolic adaptations of foraminifera to chemocline biogeochemistry.

Results

Production and maintenance of peroxisomes

Genes related to the function and biogenesis of peroxisomes were identified in the (meta)transcriptomes of *N. stella* and *B. argentea* (Figure 1). Specifically, transcripts were found encoding a transmembrane protein (Pex11) linked to remodeling of the peroxisome membrane for proliferation of peroxisomes (Koch et al., 2010; Williams et al., 2015), transport of fatty acids for peroxisomal beta-oxidation (Mindthoff et al., 2016), and initiation of contact between mitochondria and peroxisomes (Mattiazzi Ušaj et al., 2015). Transcripts of three receptor proteins (i.e. Pex5, Pex7, Pex19) that recognize signals for peroxisomal protein import were also identified (Brown and Baker, 2003). Further, expression of genes encoding AAA ATPases (i.e. Pex1, Pex6) and ubiquitination proteins (i.e. Pex4, Pex2, Pex10) demonstrated activities in the release of peroxisomal imported proteins from signal receptors and the recycling of receptor proteins, respectively (Brown and Baker, 2003). It is notable that transcription of all the *Pex* genes was observed in *N. stella*, while transcription of the *Pex11* and *Pex19* genes was not identified in *B. argentea* under any treatment (Figure 1; SI Table S1).

Metabolism of the peroxisomes and mitochondria

A reconstruction of metabolic pathways, based on transcripts identified in the (meta)transcriptomes of *N. stella* and *B. argentea*, revealed an overall distinction in the metabolism of the two species (Figure 2). Protein localizations to the peroxisome were predicted based on a consensus of four motif identification procedures for each of the three peroxisome targeting signals, peroxisome targeting signal 1 (PTS1), peroxisome targeting signal 2 (PTS2), and the peroxisomal membrane protein import signal (PMP) (SI Table S2). Protein localizations for mitochondrial functions were predicted based on the consensus of multiple probabilities for mitochondrial localization signals (SI Table S3; **Materials and Methods**). The resulting localization predictions represent hypothesized final cellular locations based on our bioinformatics approaches and are summarized below.

Proteins involved in beta-oxidation and the glyoxylate cycle were predicted to localize in the peroxisome. Beta-oxidation, which has not been previously described in foraminifera, is linked to the detoxification of H_2O_2 or superoxide radicals by catalase/peroxidase (e.g. CAT, KATG) or superoxide dismutase (SOD), respectively. Beta-oxidation breaks down fatty acids for the production of acetyl-CoA, which in turn serves as a precursor metabolite for the glyoxylate cycle, leading to the production of central carbon metabolites, such as malate and oxaloacetate (OAA) (Figure 2). All genes associated with the above-mentioned peroxisomal pathways were expressed in *N. stella*, while transcripts that encode 3-hydroxyacyl-CoA dehydrogenase (HCoADH) of the beta-oxidation pathway and malate synthase (MS) of the glyoxylate cycle were not identified in *B. argentea* across all conditions examined (Figure 3). Similarly, genes encoding Pex11, which supports the transport of fatty acids for enabling beta-oxidation in the peroxisomes (Mindthoff et al., 2016), were expressed in *N. stella* but not in *B. argentea* (Figure 1).

Transcripts encoding fructose bisphosphatase (FBP), a committed step of gluconeogenesis, were identified and predicted to localize in the peroxisome of both *N. stella* and *B. argentea*. However, the predicted peroxisomal gluconeogenic pathways in the two species had distinct entry points using metabolites from the cytosol: 1,3-bisphospho-D-glycerate (1,3DPG) for *N. stella*; phosphoenolpyruvate (PEP) for *B. argentea* (Figure 2). Similarly, the oxidative pentose phosphate pathway was predicted to localize in the peroxisome of both species, but it appeared to be active in *B. argentea* but not in *N. stella* because *N. stella* lacked expression of genes encoding the peroxisome-localized 6-phosphogluconolactonase (6PGL) or glucose-6-phosphate isomerase (G6PI) (Figures 2, 3).

The prediction of protein localization in mitochondria also revealed distinct transcription of metabolic pathways in *N. stella* and *B. argentea*. Expression of genes for mitochondrial substrate-level phosphorylation was observed in both species, with transcripts encoding acetyl-CoA hydrolase (ACoAH) identified in *N. stella* but not *B. argentea*, and transcripts encoding succinate: acetate CoA transferase (SCoAT) found in *B. argentea* but not *N. stella*. Related to the utilization of acetyl-CoA, genes encoding pyruvate:NADP oxidoreductase (mPNO) were expressed in both species and genes encoding pyruvate:ferredoxin oxidoreductase (mPFOR) were expressed in *B. argentea*. Further, transcripts encoding the sulfide-oxidizing sulfide:quinone oxidoreductase (SQOR) were detected in *N. stella*, but not in *B. argentea* (SI

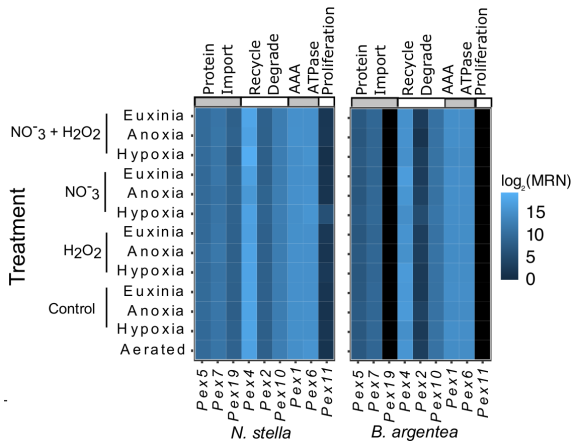

FIGURE 1
Heatmap presented by species showing the $\log_2$ transformed median ratio normalization (MRN) values for all the identified peroxisome biogenesis genes. Black indicates no expression.

Figure S1). Finally, a complete mitochondrial tricarboxylic acid (TCA) cycle was identified from the (meta)transcriptomes of *B. argentea*, while only a truncated TCA cycle, from oxaloacetate (OAA) to succinyl-CoA, was detected in the *N. stella* (meta) transcriptomes (Figure 2).

Core subunits of the electron transport chain (ETC) Complexes I-V were identified in both species. However, variations were observed in the subunit compositions of Complex II (CII) (SI Figure S1). Specifically, characterization of succinate dehydrogenase (SDH) was based on the overall sequence similarity to experimentally verified reference proteins and the presence of an isoleucine and other common variants in the quinone-binding site of the large cytochrome subunit (CII-SDHC) (Zhou et al., 2011). The characterization of quinol: fumarate oxidoreductase (QFR) was based on the presence of a glycine in a key position of the quinone-binding pocket, which indicated an essential modification in the QFR large cytochrome subunit (CII-QFRC) for the binding of rhodoquinone, an electron carrier required for anaerobic energy metabolism through fumarate reduction (Zhou et al., 2011; Del Borrello et al., 2019) (Figure 4A). While transcripts encoding the CII-SDHC were detected in both *N. stella* and *B. argentea*, putative transcripts of the CII-QFRC were identified solely in *N. stella* (Figure 4B). The putative CII-SDH and CII-QFR formed a monophyletic group with other foraminifera (e.g. *Rosalina*, *Reticulomyxa*, *Sorites*, *Elphidium*, *Ammonia*). Presence of the same QFR-conserved glycine mutation was observed among other taxa known to exhibit anaerobic metabolism (i.e. *Mastigamoeba balamuthi*, *Blastocystis hominis*, and the metazoans *Ascaris suum*, *Caenorhabditis elegans*, *Ancylostoma ceylanicum*) (Figure 4A). The biosynthesis of rhodoquinone was putatively identified in both *N. stella* and *B. argentea* based on the detection of transcripts encoding rhodoquinone biosynthesis protein A (RQUA) (Figure 4B), which catalyzes the conversion of ubiquinone to rhodoquinone (Bernert et al., 2019). Multiple sequence alignment revealed a conservation of quinone binding site residues between the RQUA proteins of foraminifera and other eukaryotes that perform fumarate reduction during exposure to anoxia (Figure 4C) (Bernert et al., 2019).

The mitochondrial electron transport system of both *N. stella* and *B. argentea* was complemented by alternative oxidase (AOX), which is known to mediate redox state of the quinone pool (Millenaar et al., 1998), and denitrification proteins (composed of pNR, NirK, and Nor/Nod) (Woehle et al., 2018; Gomaa et al., 2021). The *AOX* and denitrification genes were constitutively expressed in both foraminifers (SI Table S1).

Proteins that were not predicted to locate in any specific organelles were classified as cytosolic proteins. Transcripts encoding cytosolic proteins, such as malate dehydrogenase (cMDH), malic enzyme (ME), and acetyl-CoA ligase (ACoAL), were identified from the (meta)transcriptomes of both *N. stella* and *B. argentea* (Figure 2). Finally, transcripts encoding the cytosolic pyruvate carboxylase (PC) and assimilatory sulfite reductase (aSR) were identified in *B. argentea* but not in *N. stella* (Figure 2; SI Table S1).

Differential gene expressions

N. stella responses to the addition of chemical amendments were revealed by the identification of differentially expressed metabolic genes under exposure to H_2O_2 and NO_3^-, particularly within the anoxic condition (SI Table S4; Figure 5). The H_2O_2 amendment produced no significant differential expression of genes compared to the anoxia control (without either H_2O_2 or NO_3^- amendment) or the amendment of both H_2O_2 and NO_3^-. However, significant differential gene expression was observed between the H_2O_2 and the NO_3^- only amendment (Figure 5A). Specifically, genes associated with denitrification (*pNR*, *NirK*, and *Nor/Nod*), sulfite oxidation (*SO*), and Complex V ATP synthase (*CV*) were up-regulated in the H_2O_2 amendment. In contrast, genes associated with subunits of Complex II (*CII*) were down-regulated in H_2O_2 compared to the NO_3^- amendment. Genes related to several peroxisomal processes, such as the acyl-CoA importer (*PXA*), beta-oxidation of fatty acids (enoyl-CoA hydratase - *ECoAH* and 3-hydroxyacyl-CoA dehydrogenase - *HCoADH*), the glyoxylate cycle (*cACON* - cytosolic aconitase), gluconeogenesis (*FBP*), and *Pex7*, which encodes a receptor for peroxisomal matrix proteins, were also upregulated in the H_2O_2 amendment. Additional up-regulation of genes was observed among the cytosolic Enolase (*cPPH*) and glyceraldehyde-3-phosphate dehydrogenase (*cGAPDH*).

The transcriptional responses of *N. stella* to the addition of NO_3^- under anoxia included the up-regulation of genes related to fumarate reduction (*CII* and *RQUA*) and the down-regulation of

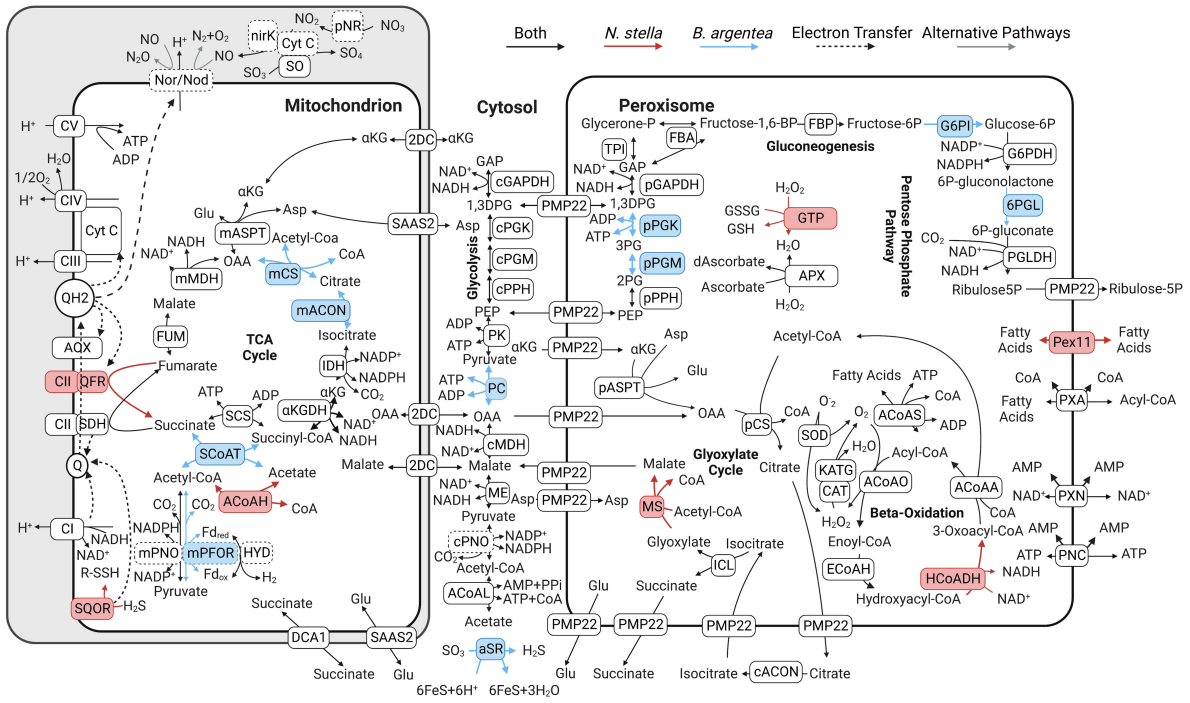

FIGURE 2
Pathway map of the predicted peroxisomal and mitochondrial metabolic processes in *N. stella* and *B. argentea*. Unique genes expressed in *N. stella* are shown with pink shade with the corresponding metabolic reactions indicated as red arrows. Unique genes expressed in *B. argentea* are shown with blue shade with the corresponding metabolic reactions indicated as blue arrows. Genes expressed in both species are shown in black boxes with the corresponding metabolic reactions indicated as black arrows. Biochemical conversions between metabolites are annotated with the abbreviation of corresponding genes, as defined in SI Table S1. Boxes with a dotted outline indicate genes that have been described previously (Gomaa et al., 2021). Gray arrows represent alternative pathways for the same genes, specifically with respect to the currently uncertain role of Nor/Nod (Gomaa et al., 2021). Q represents quinones/rhodoquinones and QH2 represents quinols/rhodoquinols. Cyt C represents Cytochrome (C) CI, CII, CIII, CIV, and CV, represent Complex I, II, III, IV, and V, respectively, of the electron transport chain. Dashed arrows indicate the flow of electrons.

genes associated with denitrification (*pNR*, *NirK*, *Nor/Nod*) and Complex III (*CIII*) (Figure 5B). Several genes related to carbon metabolism, including the cytosolic malate dehydrogenase (*cMDH*), mitochondrial and peroxisomal aspartate transaminase (*mASPT* and *pASPT*), mitochondrial 2-oxodicarboxylate carrier (*2DC*) and peroxisomal glycolysis (fructose-bisphosphate aldolase - *FBA*), were also up-regulated in the NO_3^- amendment. Lastly, the NO_3^- amendment also stimulated up-regulation of genes associated with peroxisome biogenesis (*Pex19* and *Pex2*) and ROS response (ascorbate peroxidase - *APX* and glutathione peroxidase - *GTP*).

N. stella exhibited similar responses to the H_2O_2 and NO_3^- amendments under hypoxia as compared to anoxia, but with modifications. The NO_3^- amendment in hypoxia induced the up-regulation of *CII*, *CIV*, and genes encoding the peroxisome transmembrane protein Pex11 (SI Figure S3A). The combined amendment of both NO_3^- and H_2O_2 induced the up-regulation of denitrification gene *NirK* and carbon metabolism genes, such as 2-oxoglutarate dehydrogenase (*aKGDH*), *cGAPDH*, and *cPPH* (SI Figure S3B).

Besides the H_2O_2 and NO_3^- amendments, differential expression of metabolic genes was observed in *N. stella* in the presence or absence of oxygen and with or without the addition of H_2S. For example, significant up-regulation of Complex IV (*CIV*) was identified in the aerated treatment compared to the hypoxic, anoxic, and euxinic treatments (SI Figure S2). Similarly, genes related to ROS responses, such as *APX*, *GTP*, and catalase-peroxidase (*KATG*), and the peroxisome biogenesis (*Pex19*), were up-regulated in the aerated condition (SI Table S4). Interestingly, the addition of H_2S to the NO_3^- amendment of anoxia (SI Figure S4) induced a similar response as the H_2O_2 amendment of anoxia (Figure 5A), with the up-regulation of genes for denitrification (*pNR*, *NirK*, *Nor/Nod*), beta-oxidation (*ECoAH* and *HCoADH*), the glyoxylate cycle (*cACON*), gluconeogenesis (*FBP*), and peroxisome receptor gene *Pex7* in the NO_3^- amendment under euxinia.

In contrast to the diverse transcriptional responses of *N. stella* to deoxygenation and chemical amendments, *B. argentea* exhibited up-regulation of genes only under the NO_3^- amendment in hypoxia. Specifically, genes related to the assimilatory sulfite reductase (*aSR*), glutathione reductase

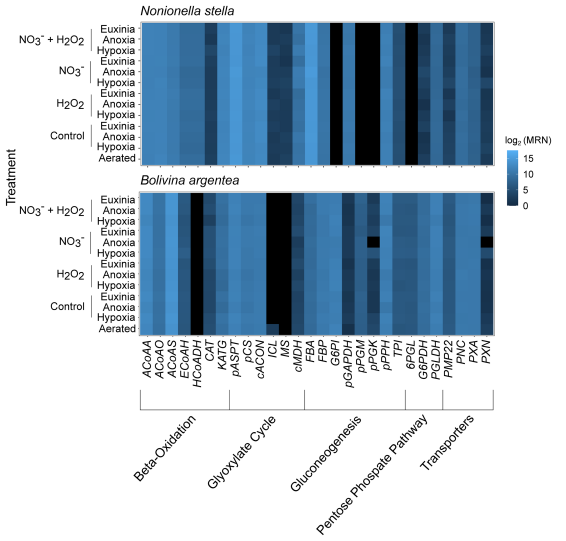

FIGURE 3
Heatmap showing the $\log_2$ transformed median ratio normalization (MRN) values for all genes involved in the peroxisomal pathways of each species. Black indicates no expression. Abbreviations align with those in SI Table S1.

(*GTR*), and Complex I (*CI*) were up-regulated in the NO_3^- amendment compared to the hypoxia control and the H_2O_2 amendment (SI Figure S5). Several carbon metabolism genes, including the mitochondrial *mMDH*, cytosolic *PC*, and peroxisomal *pPGK*, were also upregulated in the NO_3^- amendment compared to the H_2O_2 amendment, but not in comparison to the hypoxia control (SI Figure S5). Unlike the active regulation of *Pex* genes in *N. stella*, no differential expression of the *Pex* genes was detected in *B. argentea* under the examined conditions.

Discussion

Microbial eukaryotes have evolved variable combinations of carbon and energy metabolism in their organelles consistent with their ecological specialization, such as modifications observed in mitochondria (Shiflett and Johnson, 2010; Müller et al., 2012) and peroxisomes (Müller et al., 1968; Michels et al., 2005). Our (meta)transcriptomic analysis of two cytologically and ecophysiologically distinct foraminifera from the SBB, *N. stella* and *B. argentea* (Table 1), revealed contrasting utilization of these organelles. As expected from the peroxisome-ER complexes observed in previous cytological analyses (Bernhard and Bowser, 2008), our analysis showed *N. stella* actively expressed a wide range of genes regulating the function and proliferation of peroxisomes (Figure 1). However, *B. argentea* lacked the expression of key genes related to peroxisome protein localization (*Pex19*) and metabolite transport and peroxisome proliferation (*Pex11*), indicating reduced peroxisomal activities consistent with the sparse distribution of peroxisomes in *B. argentea* (Table 1).

The identification of transcripts encoding beta-oxidation and the glyoxylate cycle revealed that *N. stella* may use intracellular lipid droplets as a primary carbon source. This is consistent with the dearth of observed food vacuoles and the abundance of lipid droplets in *N. stella* (Gomaa et al., 2021) and in closely related species, such as *Nonionellina labradorica* (LeKieffre et al., 2018a). The predicted integration of beta-oxidation and the glyoxylate cycle in *N. stella* peroxisomes is similar to the glyoxysomes in vascular plants, which are specialized peroxisomes that break down fatty acids to support central carbon metabolism and are linked to the metabolism of mitochondria in germinating seeds (Eastmond and Graham, 2001; Ma et al., 2016). In contrast, *B. argentea* lacked the expression of key genes in beta-oxidation and the glyoxylate cycle (Figures 2, 3).

B. argentea instead were predicted to employ gluconeogenesis and the oxidative pentose phosphate pathway in the peroxisome (Figures 2, 3), indicating an active central carbon metabolism likely driven by digestion of phagocytosed organic materials. The predicted peroxisomal localization of gluconeogenesis in *B. argentea* could allow the simultaneous carbon metabolism in both the glycolytic and the gluconeogenic directions. This may serve as an alternative to allosteric regulation that prevents toxic accumulation of metabolic intermediates (Haanstra et al., 2008; Gualdrón-López et al., 2012), similar to that which may occur in the glycosomes described in diplonemids (Morales et al., 2016).

Based on predictions of protein localizations, the categorization of *N. stella* and *B. argentea* peroxisomes into a glyoxysome-like and a glycosome-like metabolism, respectively, is consistent with their different cytological traits and ecological distributions (Table 1). The predicted localization of the glyoxylate cycle to the peroxisomes of *N. stella* may represent an adaptation of protistan peroxisomes to use H_2O_2 for lipid metabolism in the SBB chemocline. The predicted compartmentalization of glycolysis and gluconeogenesis in *B. argentea* suggests this adaptation could be widespread in microeukaryotes and may reflect convergent evolution associated with hypoxia tolerance (Morales et al., 2016; Škodová-Sveráková et al., 2021).

The electron transport system of *B. argentea* and *N. stella* appeared to be an integration of oxygen-dependent and nitrate-dependent metabolisms, likely reflecting adaptations to hypoxic and/or anoxic environments. Diverse electron transport machinery in the mitochondria, including denitrification (Gomaa et al., 2021), alternative oxidase (AOX), and sulfide: quinone oxidoreductase (SQOR), was identified among the gene transcripts in either or both foraminifera (Figure 2; SI Figure S1).

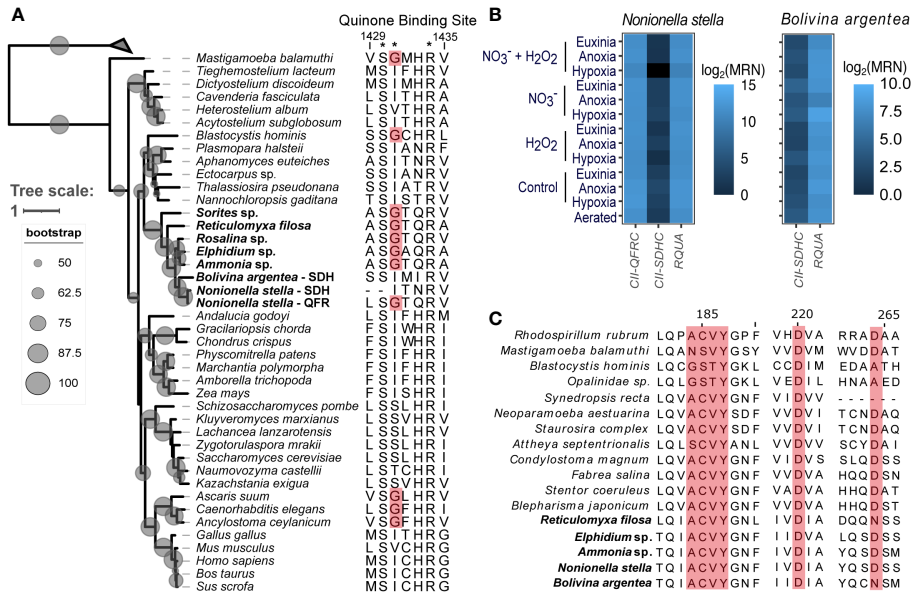

FIGURE 4
(A) Phylogenetic reconstruction of concatenated protein sequences from Complex II showing phylogenetic placement of the putative CII-QFR and CII-SDH from *N. stella* and *B. argentea*, with bootstrapping support values represented as scaled, gray-shaded circles. This phylogeny is rooted using bacterial fumarate reductase sequences. Leaves belonging to foraminifera are highlighted with bold font. The amino acid sequences to the right of the tree shows an alignment of the quinone-binding site in the CII large cytochrome C subunit. Asterisks indicate amino acids implicated in quinone binding. Sites highlighted in red background are QFR-specific mutations associated with the binding of rhodoquinone. **(B)** Expression of the *CII-QFRC*, *CII-SDHC*, and *RQUA* genes of *N. stella* and/or *B. argentea* represented as a heatmap for each species based on the $\log_2$ transformed median ratio normalization (MRN) values. **(C)** Multiple sequence alignment of the RQUA protein from foraminifera and other eukaryotes. Amino acid residues highlighted in red background indicate functional sites in the quinone-binding pocket. Sequences belonging to foraminifera are labeled with bold font.

Genes encoding SQOR have been reported before in other foraminifers, such as *Reticulomyxa filosa, Ammonia* sp., and *Elphidium margaritaceum* (Stairs et al., 2018). The presence of enzymes associated with denitrification has been discussed in depth for both *N. stella* and *B. argentea* (Gomaa et al., 2021), as well as in other foraminifers (Woehle et al., 2018; Orsi et al., 2020). Additionally, the AOX contributes to redox balance by serving as an alternative path to the proton-pumping machinery (Complex III/IV) of the ETC (Millenaar et al., 1998), alleviating potential ROS or reactive nitrogen species (RNS) stress caused by the intracellular production of H_2O_2, oxygen radicals, and/or nitric oxide from electron leakage of the ETC (Zhao et al., 2019).

Despite oxygen being a common terminal electron acceptor for AOX, genes encoding this protein were expressed across all treatments, including both the anoxic and euxinic conditions (Orsi et al., 2020). Constitutive expression of this gene could have resulted from adaptations to rapid fluctuations of oxygen (Chaudhuri et al., 2006), endogenously sourced oxygen hypothetically produced by catalases in the anoxic treatment (Bernhard and Bowser, 2008) or oxygenic denitrification by Nor/Nod (Gomaa et al., 2021). Interestingly, recent evidence has shown that nitrite can serve as an alternative electron acceptor for AOX under hypoxia and anoxia in some plants (Vishwakarma et al., 2018), suggesting a potential mechanism for the activation of foraminiferan AOX under anoxia that deserves dedicated biochemical investigation. The observation of SQOR transcripts solely in *N. stella* indicates its capacity to use H_2S as an electron donor to fuel respiration. The SQOR contributes to a reduced quinol pool that can be used by Nor/Nod to drive denitrification. This is corroborated by the upregulation of denitrification genes in *N. stella* with NO_3^- amendment under euxinia compared to anoxia (SI Figure S4). The expansion of *N. stella*'s electron transport system to utilize H_2S as an alternative electron donor reflects an adaptive feature for the conservation of carbon sources in *N. stella*, which may be carbon limited as this SBB population of *N. stella* lacks evidence of digestion (Gomaa et al., 2021) and utilizes a truncated TCA cycle (Figure 2).

Quinol:fumarate oxidoreductase (QFR) is commonly considered an adaptive mechanism for anaerobic respiration in eukaryotic organisms under anoxic conditions (Del Borrello et al., 2019). We found constitutive expression of genes encoding QFR solely in *N. stella* (Figure 4B), suggesting potential adaptations of this species to an anaerobic lifestyle.

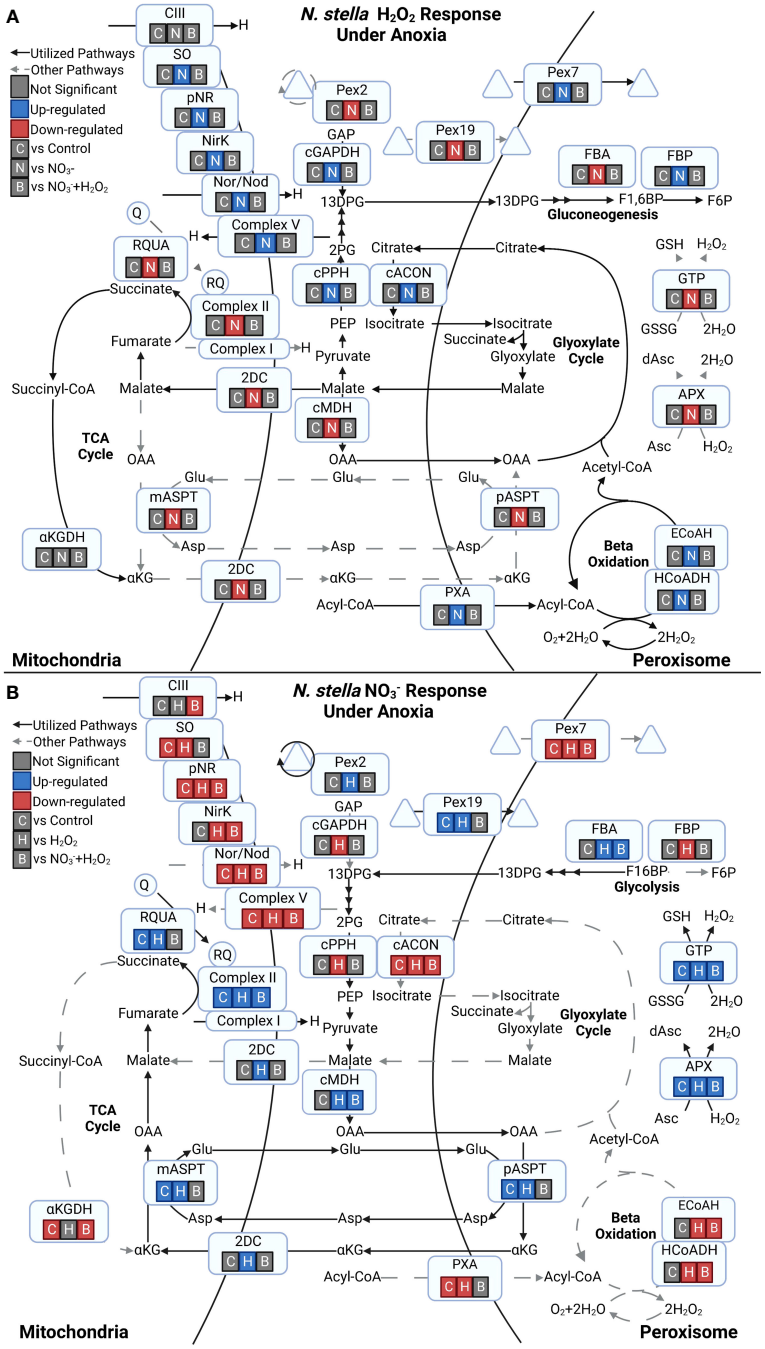

FIGURE 5
Responses to chemical amendments under anoxia for proteins predicted to the peroxisome and mitochondria in *N. stella*. **(A)** Differential expression of genes under the H_2O_2 amendment in contrast to the control (C), NO_3^- (N), and combined H_2O_2 + NO_3^- **(B)** amendments. **(B)** Differential expression of genes under the NO_3^- amendment in contrast to the control (C), H_2O_2 (H), and combined H_2O_2 + NO_3^- **(B)** amendments. Triangles in both panels represent transported and recycled proteins. Significant differential gene expressions between contrasts (adjusted p-value< 0.05) are highlighted in green (Up-regulated) or red (Down-regulated). Contrasting conditions with no significant differential gene expression are indicated in gray (Not Significant).

The conservation of QFR based on the presence of a glycine residue in the large cytochrome subunit of foraminifers (Figure 4A) indicates an ancestral state of this taxon that may have evolved in an anoxic milieu. In *N. stella*, transcripts encoding RQUA of the rhodoquinone biosynthesis pathway further supports the potential presence of fumarate reduction (Stairs et al., 2018; Salinas et al., 2020). Interestingly, transcripts of succinate dehydrogenase (SDH) were observed in both *N. stella* and *B. argentea*. The SDH formed a monophyletic group with the QFR, suggesting that both the QFR and SDH may have originated from a common foraminiferal ancestor capable of fumarate reduction. Given the prevalence of QFR in other foraminifera and the expression of the RQUA gene in *B. argentea*, a QFR could be encoded in the *B. argentea* genome, although it was not detected in the (meta)transcriptomes represented in this study.

B. argentea additionally demonstrated potential capacities for substrate-level phosphorylation through the coupling of succinate:acetate CoA transferase (SCoAT) and succinyl-CoA synthetase (SCS). Genes encoding SCS and SCoAT have been previously identified in related species (Orsi et al., 2020), but this is the first documentation of the expression of the *SCoAT* gene in foraminifera. Carbon conservation was inferred from the predicted mitochondrial PFOR, the cytosolic PNO, and the cytosolic acetyl-CoA ligase (ACoAL), another gene previously not documented in foraminifera (Figure 2). The utilization of substrate-level phosphorylation and the constitutive expression of denitrification pathways by *B. argentea* under hypoxia indicated the potential lifestyle of a facultative anaerobe. The up-regulation of *aSR* and *GTR* by *B. argentea* in hypoxia NO_3^- amendment (SI Figure S5) was consistent with an increased tolerance of ROS stress for maintaining active carbon metabolism (Gill et al., 2013; Wang et al., 2016).

In contrast, *N. stella* demonstrated a wider range of metabolic responses to the H_2O_2, NO_3^-, and H_2S amendments under both hypoxia and anoxia by using a combination of peroxisomal and mitochondrial pathways. The H_2O_2 amendment induced the up-regulation of genes associated with beta-oxidation and the glyoxylate cycle in *N. stella*, likely linked to the utilization of intracellular lipid droplets that are abundant in this species (Gomaa et al., 2021). The release of carbon substrates by beta-oxidation and the glyoxylate cycle appears to be coupled with carbon storage *via* gluconeogenesis (i.e. up-regulation of *FBP*) and a more active electron transport system, based on the up-regulation of the denitrification and *SO* genes (Figure 5A). The H_2O_2 amendment also stimulated up-regulation of ATP-producing Complex V genes, which was consistent with the experimentally measured increases in intracellular ATP production of *N. stella* with the addition of H_2O_2 (Bernhard and Bowser, 2008). The metabolism of *N. stella* under the H_2O_2 amendment may reflect its native metabolic state in the SBB sediments, as no differential gene expression was identified between the H_2O_2 amendments under anoxia or hypoxia versus their corresponding control (without amendment) conditions (Figure 5A; SI Table S4).

The NO_3^- amendment of *N. stella* induced differential gene expression compared to both the control and the H_2O_2 amendment. The down-regulation of *FBP* and the up-regulation of *FBA* in anoxia NO_3^- amendment may indicate the activation of carbon metabolism in the glycolytic direction, which can be an adaptive mechanism in response to the lack of carbon substrates due to down-regulation of the beta-oxidation (Figure 5B). The up-regulation of both *RQUA* and Complex II genes indicates the potential activation of fumarate reduction. This is coordinated with the down-regulation of denitrification genes and likely reflects a metabolism limited by electron donors, as denitrification competes with fumarate reduction for the quinone pool. Further evidence for limited availability of electron donors was observed under the anoxic NO_3^- amendment in comparison to the euxinic NO_3^- amendment. With H_2S as an alternative electron donor *via* SQOR, *N. stella* showed an up-regulation of genes involved in denitrification, beta-oxidation, the glyoxylate cycle, and gluconeogenesis (SI Figure S4). This reflects an adaptive feature for the conservation of carbon sources in *N. stella*, which may be carbon limited as this species lacks evidence for digestion through the presence of food vacuoles (Gomaa et al., 2021). Lastly, the up-regulation of ROS response genes (e.g. *APX*, *GTP*) in the NO_3^- amendment of *N. stella* likely indicates cellular mitigation of the effects of electron leakage during fumarate reduction (Gawryluk and Stairs, 2021).

The evolution of mitochondria and peroxisomes are often coupled in eukaryotes (Le et al., 2020; Verner et al., 2021; Záhonová et al., 2022) and represents a spectrum of metabolic phenotypes (Müller et al., 2012; Stairs et al., 2015). Combinations of metabolic pathways known in MROs were predicted to localize in the mitochondria of *N. stella* and *B. argentea* (Figure 2); however, mitochondria of these foraminifers still maintain the oxygen-dependent ETC (CIII, CIV, AOX) (Figure 2) and may perform anaerobic respiration through denitrification (Gomaa et al., 2021). These unique metabolic capabilities have not been identified in any other protists and may allow our two benthic foraminifera to survive in both oxygen depleted and aerated conditions. The organelle-specific metabolic flexibility documented in this study offers a contrast to the mitochondrial metabolism of conventional MROs found in anaerobic protists. These differences suggest that the mitochondria of these two benthic foraminifera have evolved specialized metabolic tools that support their ability to respond to varied oxygen concentrations and milieu chemistry. The plasticity observed in the mitochondria was enhanced by the peroxisomes in both species, which are metabolically distinct not only from each other, but also from known anaerobic peroxisomes (Le et al., 2020; Verner et al., 2021; Záhonová

et al., 2022). The selective pressures associated with survival in highly variable habitats have conferred our two foraminifera with diverse metabolic toolkits of mitochondrial and peroxisomal metabolism that enables survival in SBB chemoclines.

Overall, the two foraminifers demonstrated distinct metabolic adaptations to hypoxia and anoxia, and had different capacities to use compounds often abundant in SBB pore water (Risgaard-Petersen et al., 2006; Gomaa et al., 2021). This indicates benthic foraminiferal metabolism is not uniform across species. While the ability to perform denitrification and anaerobic energy metabolism are established for *N. stella* (Risgaard-Petersen et al., 2006; Gomaa et al., 2021), we show here that *N. stella* of the SBB are adept at surviving anoxia, having metabolically flexible mitochondria that function in coordination with the predicted metabolism of its peroxisomes. The metabolism predicted for *B. argentea* suggested the capacity to digest food vacuole contents as a facultative anaerobe. These species represent only two examples of the unique cytologies that occur along the SBB chemocline. Additional cytological diversity is known among other foraminifera, such as *Bulminella tenuata*, an endobiont-bearing species that also exhibits close associations between mitochondria and peroxisomes (Bernhard and Bowser, 2008), or an as-yet undescribed agglutinated foraminifer with coccoid endosymbionts that lacks peroxisome-ER complexes in favor of few peroxisomes (Bernhard et al., 2006; Bernhard et al., 2012b). The highly variable cytology observed among foraminifera of the SBB chemocline and elsewhere, such as hydrocarbon seeps (Bernhard et al., 2010), implies potential distinctions in their metabolic capacity, which may influence biogeochemical cycling and calcite biomineralization, as the presence of symbionts likely shifts $\delta^{13}C_{calcite}$ values in one foraminifera species (Bernhard, 2003). Further understanding the highly variable metabolic adaptations that can occur across foraminifera will allow for more informed reconstructions of paleoceanographic conditions and strengthen biogeochemical and ecological predictions of shifts in organismal and metabolic niches under future ocean deoxygenation. Lastly, these findings provide additional insights into the biogeochemical roles and the evolution of this ecologically significant protistan taxon that diversified in the Neoproterozoic.

Materials and methods

(Meta)Transcriptome data

Transcriptome and metatranscriptome data were obtained from the NCBI BioProject PRJNA714124. Details of the experimental settings were described in (Gomaa et al., 2021). Briefly, surface sediments containing either *N. stella* or *B. argentea* of the Santa Barbara Basin were subjected to laboratory treatments under four oxygen conditions (i.e. aerated, hypoxic, anoxic, and euxinic) and four chemical amendments: the no amendment (Control), nitrate (NO_3^-), hydrogen peroxide (H_2O_2), nitrate and hydrogen peroxide ($NO_3^- + H_2O_2$), with 2-3 replicates in ~75 cm^2 polypropylene containers for each species given each combination of the oxygen and amendment conditions. Following a treatment period of three days, *N. stella* or *B. argentea* were picked into pools of 25 (cleaned) conspecifics, and each pool was counted as a biological replicate for transcriptomic or metatranscriptomic sequencing using the PolyA- or Total RNA-based library preparation, respectively (Gomaa et al., 2021). Quality and integrity of each RNA sample were assessed with Nanodrop and Bioanalyzer (Agilent 2100), only samples with nanodrop values of 260:280 and 260:230 higher than 1.8 and 2.0, respectively, and Bioanalyzer RNA integrity numbers above 5 were selected for library preparation. Bar-coded library samples were quantified with Bioanalyzer (Agilent 2100) and TapeStation (Agilent 2200), and each sample was amplified with 11 to 15 rounds of PCR cycles in preparation for sequencing. Paired-end sequencing was performed using two sequencing runs on an Illumina NovaSeq platform for the polyA selected mRNA library and two sequencing runs on an Illumina NextSeq platform for the total RNA library, resulting in approximately 8 billion and 1.9 billion reads, respectively, from the two platforms. Overall, between 3-7 biological replicates per amendment/treatment were analyzed, with each biological replicate represented by pooling all sequences from its two sequencing runs. Detailed information of all samples referenced in this study and their corresponding data in the National Center for Biotechnology Information (NCBI) Sequence Read Archive (SRA) database are summarized in SI Table S5.

Transcriptome assembly and annotation

The *N. stella* and *B. argentea* transcriptomes and metatranscriptomes were quality checked and processed as described previously (Gomaa et al., 2021). Briefly, reads were quality checked with TrimGalore (Krueger, 2015), a wrapper script built around Cutadapt (Martin, 2011) and FastQC (Andrews, 2010). Each (meta)transcriptome was assembled individually using the *de novo* transcriptome assembly functions in rnaSPAdes v3.14.1 with default parameters (Bushmanova et al., 2019).

Due to the large size of the nucleotide dataset (greater than fifty million contigs), the lin-clust clustering algorithm from MMSEQS2 was used to cluster nucleotide sequences with a minimum sequence identity of 97% using default settings (Steinegger and Söding, 2018). Coding sequences (CDS) within a representative contig from each cluster were identified using geneMarkS-T with default settings (Tang

et al., 2015) and the protein sequences encoded by the resulting CDS were further clustered using the Cluster Database at High Identity with Tolerance (CD-HIT) (Fu et al., 2012) with a minimum sequence identity of 99% and 95% to identify representative sequences for further annotations and taxonomic assignments, respectively. Representative protein sequences from the 99% CD-HIT clustering were annotated with EggNOG V.2 (Huerta-Cepas et al., 2019) to assign enzyme commission (EC) numbers using default settings. The EggNOG annotation did not capture all subunits of mitochondrial electron transport chain complexes. Therefore, targeted identification of these subunits was performed by examining the presence and organization of protein domains based on matches to hidden markov models (HMM) from the Pfam 27.0 database (Finn et al., 2014) using HMMER 3.1 (Eddy, 2011) with an independent e-value under 1E-5. Genes identified as missing or as expressed in only one species were further searched for using a homology-based approach by mapping reference proteins against the assembled contigs using tblastn (Zhang et al., 2000). Three sets of protein sequences were used as the reference database for this search: foraminifera proteins identified from the automated prediction of coding sequences for genes that were missing in one species, sequences of the ETC complexes from the Protein Data Bank (PDB IDs: SRFR, 3VRB, 1NTZ, and 5B3S for CII, CII, CIII, and CIV respectively), and the RQUA sequence from *Reticulomyxa filosa* (Accession: ETO28810.1). Sequences that shared 60% identity and 70% coverage to the reference proteins and were not already identified in the CDS predictions were added to the list of annotated genes. Two RQUA transcripts found through this search were included in the analysis despite sharing a sequence identity of 47.6% and 45.5% to the RQUA sequence from *Reticulomyxa filosa* based on the identification of binding sites known for RQUA (Figure 4C).

Representative protein sequences from the 95% CD-HIT clustering were mapped against the NCBI non-redundant protein database using the DIAMOND BLASTP (Buchfink et al., 2021). If a sequence had an alignment to foraminifera out of the top 25 best hits, it was taxonomically assigned to the foraminifera group. If a representative protein sequence had a majority of the top 25 hits assigned to diatoms, other eukaryotes, bacteria, or archaea, the sequence was taxonomically assigned based on the majority mapping.

Organelle localization predictions

Peroxisome localization was predicted using a consensus approach that combined motif-based identification of targeting signals with homology-based search of well-curated peroxisomal proteins (SI Figure S6). The *Pex5*, *Pex7*, and *Pex19* genes were identified in the foraminiferal (meta) transcriptomes and the Pex5, Pex7, and Pex19 proteins recognize peroxisome targeting signal 1 (PTS1), peroxisome targeting signal 2 (PTS2), and peroxisomal membrane protein import signal (PMP), respectively. Correspondingly, these three signals were used to predict peroxisomal localization. The predictions were informed by a consensus of four strategies (SI Figure S6) using tools from the MEME Suite, version 5.1.1 (Bailey et al., 2009). All four strategies used the FIMO software (Grant et al., 2011) to scan translated proteins from the foraminifera transcriptome, using custom MEME motifs derived from different sets of putative peroxisomal proteins (SI Table S6; SI Figure S6). Strategy one used the MEME motif constructed from whole sequences that showed exact matches to the canonical PTS1 (Rucktäschel et al., 2011), PTS2 (Petriv et al., 2004), or PMP (Rottensteiner et al., 2004) signals, Strategy two was similarly initiated based on the exact matches of canonical motifs, but made site-specific constructions using Sites2Meme (Bailey et al., 2009). Strategy three used reference motif sequences from the peroxisomeDB to construct the MEME motif profiles using Sites2Meme. Strategy four aligned the peroxisomeDB reference sequences using MAFFT version 7.453 (Katoh et al., 2002) and converted them to the MEME motif using Sites2Meme. Each protein sequence identified from this pipeline was assigned a consensus score from one to four for each of the peroxisomal import signals by counting the number of strategies that resulted in a motif match to the target sequence. Confidence levels of peroxisome localization prediction were evaluated based on the number of strategies that support the motif-based mapping and a homology search to the peroxisomeDB reference database, a database of peroxisomal proteins from diverse organisms, including protists (Schlüter et al., 2010), using DIAMOND BLASTP (Buchfink et al., 2021) (SI Table S7).

Mitochondrion localization was predicted based on homology and a consensus of three predictors: MitoFates version 1.2, TargetP version 2.0, and PredSL (Petsalaki et al., 2006; Fukasawa et al., 2015; Armenteros et al., 2019), combinations of which have been utilized with success in putatively anaerobic protists previously (Eme et al., 2017; Stairs et al., 2021). Combined probabilities of mitochondrion localization were calculated by multiplying the probabilities from all three predictors to provide an aggregated estimation. In parallel, DIAMOND BLASTP (Buchfink et al., 2021) was used to identify homology from our assembly to a reference database consisting of mitochondrial proteins from OrganelleDB (Wiwatwattana et al., 2007), Mitocarta (Calvo et al., 2016), the *Acanthomoeba castellanii* mitochondrial proteome (Gawryluk et al., 2014), the *Andalucia godoyi* proteome (Gray et al., 2020), and mitochondrial sequences from the plant proteome database (Sun et al., 2009). Confidence levels were assigned to the putative

mitochondrial proteins by integrating the combined probability of localization and the homology identifications to the reference mitochondrial protein database (SI Table S7).

Taxonomic assignments were additionally used for the filtering of peroxisomal and mitochondrial pathways. Only proteins taxonomically assigned to foraminifera or other eukaryotes were included in the metabolic reconstruction. A number of metabolic processes were placed to mitochondria because they represent known or proposed genes in mitochondria. These included subunits of the electron transport chain complexes and mitochondrial transporters (SI Table S1) identified through homology to the above-mentioned mitochondrial protein reference database and the transporter classification database (TCDB) (Saier et al., 2021) using DIAMOND BLASTP with a sequence identity cutoff of at least 30% and a reference coverage cutoff of at least 50%.

Similarly, some proteins were assigned to the peroxisome because they represent peroxisomal-relevant processes and/or were shown to co-localize with other peroxisomal proteins, including Pex proteins, transmembrane transporters, catalase, peroxidase, and isocitrate lyase (SI Table S1). Pex proteins were identified based on the EggNOG annotations using default settings and/or homology searches to the peroxisomeDB using DIAMOND BLASTP (Buchfink et al., 2021) with a sequence identity of at least 30% and a reference coverage of at least 50%. The presence and organization of protein domains in the Pex proteins were analyzed based on matches to HMMs from the Pfam 27.0 database (Finn et al., 2014) using HMMER 3.1 (Eddy, 2011) with an e-value under 1E-5. Transport of small soluble metabolites such as malate and succinate across the peroxisomal membrane was included in our prediction, as the transport of small metabolites is commonly mediated by a variety of non-selective channels through which these compounds can freely diffuse (Antonenkov and Hiltunen, 2012). Specific transporters for cofactors such as NAD, CoA, ATP, acyl-CoA, and fatty acids were identified through homology searches to known peroxisomal transporters from the Swiss-Prot database, release-2021_01 (Boeckmann et al., 2003), and the peroxisomeDB using DIAMOND BLASTP (Buchfink et al., 2021) with a sequence identity cutoff of at least 30% and a reference coverage cutoff of at least 50%. The catalase and peroxidase proteins are commonly known to localize in the peroxisome. Further, the peroxisomal localization of catalase in *N. stella* is seen through the presence of the crystalline cores formed by the catalase aggregates in its peroxisomes (Bernhard and Bowser, 2008). Isocitrate lyase was included because previous research showed that this protein can be localized without import signals to the peroxisome by co-importing as oligomeric proteins (Lee et al., 1997). The isocitrate lyases in our data are also homologous to the isocitrate lyases in the peroxisomeDB. Catalases are known to have a modified peroxisomal import signal, which may explain why they were not identified in our analysis (Oshima et al., 2008). While little support was found for the localization of the denitrification proteins (pNR, NirK, and Nor/Nod) to the mitochondria, its involvement in respiration may require an association with the mitochondria. This was proposed in previous studies by our group and others (Woehle et al., 2018; Gomaa et al., 2021), so these proteins were included in our reconstruction of mitochondrial metabolism.

Proteins not localized to peroxisome or mitochondrion were classified as cytosolic and were included in the metabolic reconstruction for the completion of central carbon metabolism. Metabolic connections among the peroxisomal, mitochondrial, and cytosolic compartments were examined by tracing the carbon flow in the metabolic network using the *findprimarypairs* function in the PSAMM software package version 1.0 (Steffensen et al., 2016).

Identification of succinate dehydrogenase/quinol:fumarate oxidoreductase

Binding sites relevant to the function of Complex II were analyzed based on multiple sequence alignments (MSA), generated using the PROfile Multiple Alignment with predicted Local Structures and 3D constraints (PROMALS3D) (Pei et al., 2008). Each subunit of Complex II was aligned to reference sequences from the protein data bank, marine microbial eukaryotic transcriptome sequencing project (MMETSP) (Keeling et al., 2014), Swiss-Prot (Boeckmann et al., 2003), NCBI RefSeq non-redundant protein database (O'Leary et al., 2016), and from eukaryotes known to live in anoxic conditions (Gawryluk and Stairs, 2021). Three-dimensional protein structures of the Complex II from *Ascaris suum* (PDB ID 3VR8), *Sus scrofa* (PDB ID 3FSD), and *Gallus gallus* (PDB ID 2H89) were used in PROMALS3D (Pei et al., 2008) to guide the MSA construction for each subunit. Alignments of the four core subunits (CII-SDHA, CII-SDHB, CII-SDHC/QFRC, CII-SDHD) were concatenated and used as input for the phylogenetic reconstruction using RAxML version 8.2 (Stamatakis, 2014). A concatenated alignment of all subunits resulted in an alignment with 39.28% gaps and 1677 distinct alignment positions. No trimming was performed on the MSA. An optimal substitution model was selected by RAxML using the automatic model selection under Akaike Information Criterion (AIC) (Burnham and Anderson, 2007). The best model, LG substitution with the GAMMA model of rate heterogeneity and empirical base frequencies, was applied for the phylogenetic reconstruction of Complex II using 100 bootstraps. Specific amino acid residues relevant to the functions of QFR and SDH were identified following previous studies on the quinone-binding pocket of these proteins (Del Borrello et al., 2019).

Differential expression analysis

Differentially expressed genes were identified using representative transcripts from the assembly after clustering at 99% minimum amino acid sequence identity (described above). Quality controlled sequencing reads from each sample were mapped to these representative transcripts using BBMap from the BBTools package (Bushnell, 2014). Briefly, read mapping files from each sample were sorted, indexed with the SAMtools package version 1.7 (Danecek et al., 2021), and used for the calculation of transcript abundance using the Pileup function in BBTools version 37.36 (Bushnell, 2014). The species-specific mapping of transcripts was achieved by counting the abundance of a transcript across all treatments of a species. A denoising step was applied to remove sporadic mappings of reads by exclusively assigning each transcript to a species (i.e. *N. stella* or *B. argentea*) if the read mapping was dominated (e.g. with a 10 times higher abundance) by samples from that species. If a transcript received a similar number of mapped reads from both species, the transcript was assigned to both species if greater than 60 reads were mapped across all samples of each species. Transcripts mapped to less than 60 reads in both species were removed from further consideration, as having less than 60 reads would on average represent only around one read mapped per sample in each species. Count data were summed for all transcripts mapped to the same species and annotated as the same gene, and this combined count data were used as inputs for the differential gene expression analysis using DESeq2 version 1.26.0 in R (Love et al., 2014). Each combination of chemical amendments and oxygen conditions was used as an experimental treatment for the modeling of differential gene expression. Additionally, a variable was introduced to the statistical model with two factor levels to control for the potential variation introduced from the use of two different library preparation techniques: (1) polyA selection that targets the polyadenylated mRNA from eukaryotes, and (2) total RNA preparation that targets all mRNA molecules from eukaryotes and prokaryotes (Gomaa et al., 2021). Statistical significance was based on the Wald test by estimating variation in log-fold change (LFC) using differences between experimental treatments. Results from the Wald test were further considered if the two sets of samples represented the same oxygenation treatment but different chemical amendment, or if they represented the same chemical amendment but different oxygenation treatments. For example, the non-amended hypoxic treatment and the NO_3^- amended hypoxic treatment reflected a comparison of chemical-driven responses. In contrast, the NO_3^- amended hypoxic treatment and the NO_3^- amended anoxic treatment reflected a comparison of oxygen-driven responses. A significance threshold less than 0.05 was used on the adjusted p-values based on a Benjamin Hochberg correction for false discovery rates. The expression of genes in a treatment was calculated by taking the mean of the median ratio normalization (MRN) values across all biological replicates of a given treatment followed by $\log_2$ transformations. Heatmaps were created based on the $\log_2$ transformed MRN values using ggplot2, version 3.3.2 (Ginestet, 2011). Differential expression of genes was similarly plotted using ggplot2.

Data availability statement

Publicly available datasets were analyzed in this study. This data can be found here: https://www.ncbi.nlm.nih.gov/bioproject/?term=PRJNA714124. Assemblies, annotations, and abundance mapping of the (meta)transcriptomes can be accessed following doi: 10.6084/m9.figshare.16632259.

Author contributions

JB, YZ, CH, and VE conceived the study. JB, DB, CH, SW, and HF contributed to sample collection. FG, JB, and DB performed the experiment. CP, YZ, FG, EB, DU, SW, CH, and JB analyzed and interpreted the data. CP, YZ, FG, and JB composed the manuscript. All authors gave feedback on the manuscript.

Funding

This project was funded by the U.S. National Science Foundation IOS 1557430 and 1557566. CP acknowledges partial support from the U.S. National Science Foundation DBI 1553211. EB acknowledges support from the URI MARC U*STAR grant from the National Institute of General Medical Sciences of the National Institutes of Health under grant number T34GM131948 (Niall G. Howlett, PI). HF acknowledges support from the Swedish Research Council VR (grant number 2017-04190). JB acknowledges partial support from the Investment in Science Program at WHOI.

Acknowledgments

The authors acknowledge that this work has appeared previously online as a preprint at biorxiv (DOI: https://doi.org/10.1101/2022.07.20.500910). We thank the captain, crew, and science parties of the R/V *Robert Gordon Sproul* cruises SP1703, SP1718, and SP1811. Figures 2, 5, S3, S4, and S5 were created with BioRender.com.

Conflict of interest

The authors declare that the research was conducted in the absence of any commercial or financial relationships that could be construed as a potential conflict of interest.

Publisher's note

All claims expressed in this article are solely those of the authors and do not necessarily represent those of their affiliated organizations, or those of the publisher, the editors and the reviewers. Any product that may be evaluated in this article, or claim that may be made by its manufacturer, is not guaranteed or endorsed by the publisher.

Supplementary material

The Supplementary Material for this article can be found online at: https://www.frontiersin.org/articles/10.3389/fmars.2022.1010319/full#supplementary-material

References

Andrews, S. (2010) *FastQC: a quality control tool for high throughput sequence data*. Available at: https://www.bioinformatics.babraham.ac.uk/projects/fastqc/.

Antonenkov, V. D., and Hiltunen, J. K. (2012). Transfer of metabolites across the peroxisomal membrane. *Biochim. Biophys. Acta* 1822, 1374–1386. doi: 10.1016/j.bbadis.2011.12.011

Armenteros, J. J. A., Salvatore, M., Emanuelsson, O., Winther, O., Von Heijne, G., Elofsson, A., et al. (2019). Detecting sequence signals in targeting peptides using deep learning. *Life Sci. Alliance* 2:e201900429. doi: 10.26508/lsa.201900429

Bailey, T. L., Boden, M., Buske, F. A., Frith, M., Grant, C. E., Clementi, L., et al. (2009). MEME SUITE: tools for motif discovery and searching. *Nucleic Acids Res.* 37, W202–W208. doi: 10.1093/nar/gkp335

Bernert, A. C., Jacobs, E. J., Reinl, S. R., Choi, C. C. Y., Roberts Buceta, P. M., Culver, J. C., et al. (2019). Recombinant RquA catalyzes the *in vivo* conversion of ubiquinone to rhodoquinone in *Escherichia coli* and *Saccharomyces cerevisiae*. *Biochim. Biophys. Acta Mol. Cell Biol. Lipids* 1864, 1226–1234. doi: 10.1016/j.bbalip.2019.05.007

Bernhard, J. M. (2003). Potential symbionts in bathyal foraminifera. *Science* 299, 861. doi: 10.1126/science.1077314

Bernhard, J. M., and Bowser, S. S. (1999). Benthic foraminifera of dysoxic sediments: chloroplast sequestration and functional morphology. *Earth-Sci. Rev.* 46, 149–165. doi: 10.1016/S0012-8252(99)00017-3

Bernhard, J. M., and Bowser, S. S. (2008). Peroxisome proliferation in foraminifera inhabiting the chemocline: an adaptation to reactive oxygen species exposure? *J. Eukaryot. Microbiol.* 55, 135–144. doi: 10.1111/j.1550-7408.2008.00318.x

Bernhard, J. M., Buck, K. R., Farmer, M. A., and Bowser, S. S. (2000). The Santa Barbara basin is a symbiosis oasis. *Nature* 403, 77–80. doi: 10.1038/47476

Bernhard, J. M., Casciotti, K. L., McIlvin, M. R., Beaudoin, D. J., Visscher, P. T., and Edgcomb, V. P. (2012a). Potential importance of physiologically diverse benthic foraminifera in sedimentary nitrate storage and respiration. *J. Geophys. Res.* 117:G03002. doi: 10.1029/2012jg001949

Bernhard, J. M., Edgcomb, V. P., Casciotti, K. L., McIlvin, M. R., and Beaudoin, D. J. (2012b). Denitrification likely catalyzed by endobionts in an allogromiid foraminifer. *ISME J.* 6, 951–960. doi: 10.1038/ismej.2011.171

Bernhard, J. M., Habura, A., and Bowser, S. S. (2006). An endobiont-bearing allogromiid from the Santa Barbara basin: Implications for the early diversification of foraminifera. *J. Geophys. Res.* 111:G03002. doi: 10.1029/2005jg000158

Bernhard, J. M., Martin, J. B., and Rathburn, A. E. (2010). Combined carbonate carbon isotopic and cellular ultrastructural studies of individual benthic foraminifera: 2. toward an understanding of apparent disequilibrium in hydrocarbon seeps. *Paleoceanography* 25:PA4206. doi: 10.1029/2010pa001930

Bernhard, J. M., Sen Gupta, B. K., and Borne, P. F. (1997). Benthic foraminiferal proxy to estimate dysoxic bottom-water oxygen concentrations; Santa Barbara basin, US pacific continental margin. *J. Foraminiferal Res.* 27, 301–310. doi: 10.2113/gsjfr.27.4.301

Bernhard, J. M., Visscher, P. T., and Bowser, S. S. (2003). Submillimeter life positions of bacteria, protists, and metazoans in laminated sediments of the Santa Barbara basin. *Limnol. Oceanogr.* 48, 813–828. doi: 10.4319/lo.2003.48.2.0813

Boeckmann, B., Bairoch, A., Apweiler, R., Blatter, M.-C., Estreicher, A., Gasteiger, E., et al. (2003). The SWISS-PROT protein knowledgebase and its supplement TrEMBL in 2003. *Nucleic Acids Res.* 31, 365–370. doi: 10.1093/nar/gkg095

Brown, L.-A., and Baker, A. (2003). Peroxisome biogenesis and the role of protein import. *J. Cell. Mol. Med.* 7, 388–400. doi: 10.1111/j.1582-4934.2003.tb00241.x

Buchfink, B., Reuter, K., and Drost, H.-G. (2021). Sensitive protein alignments at tree-of-life scale using DIAMOND. *Nat. Methods* 18, 366–368. doi: 10.1038/s41592-021-01101-x

Burki, F., Corradi, N., Sierra, R., Pawlowski, J., Meyer, G. R., Abbott, C. L., et al. (2013). Phylogenomics of the intracellular parasite *Mikrocytos mackini* reveals evidence for a mitosome in rhizaria. *Curr. Biol.* 23, 1541–1547. doi: 10.1016/j.cub.2013.06.033

Burnham, K. P., and Anderson, D. R. (2007). *Model selection and multimodel inference: A practical information-theoretic approach* (New York, NY, USA: Springer Science & Business Media).

Bushmanova, E., Antipov, D., Lapidus, A., and Prjibelski, A. D. (2019). rnaSPAdes: A *de novo* transcriptome assembler and its application to RNA-seq data. *Gigascience* 8:giz100. doi: 10.1093/gigascience/giz100

Bushnell, B. (2014) *BBTools software package*. Available at: http://sourceforge.net/projects/bbmap.

Calvo, S. E., Clauser, K. R., and Mootha, V. K. (2016). MitoCarta2.0: an updated inventory of mammalian mitochondrial proteins. *Nucleic Acids Res.* 44, D1251–D1257. doi: 10.1093/nar/gkv1003

Chaudhuri, M., Ott, R. D., and Hill, G. C. (2006). Trypanosome alternative oxidase: from molecule to function. *Trends Parasitol.* 22, 484–491. doi: 10.1016/j.pt.2006.08.007

Choquel, C., Geslin, E., Metzger, E., Filipsson, H. L., Risgaard-Petersen, N., Launeau, P., et al. (2021). Denitrification by benthic foraminifera and their contribution to n-loss from a fjord environment. *Biogeosciences* 18, 327–341. doi: 10.5194/bg-18-327-2021

Danecek, P., Bonfield, J. K., Liddle, J., Marshall, J., Ohan, V., Pollard, M. O., et al. (2021). Twelve years of SAMtools and BCFtools. *Gigascience* 10:giab008. doi: 10.1093/gigascience/giab008

DeLaca, T. E., Karl, D. M., and Lipps, J. H. (1981). Direct use of dissolved organic carbon by agglutinated benthic foraminifera. *Nature* 289, 287–289. doi: 10.1038/289287a0

Del Borrello, S., Lautens, M., Dolan, K., Tan, J. H., Davie, T., Schertzberg, M. R., et al. (2019). Rhodoquinone biosynthesis in *C. elegans* requires precursors generated by the kynurenine pathway. *Elife* 8:e48165. doi: 10.7554/eLife.48165

Eastmond, P. J., and Graham, I. A. (2001). Re-examining the role of the glyoxylate cycle in oilseeds. *Trends Plant Sci.* 6, 72–78. doi: 10.1016/S1360-1385(00)01835-5

Eddy, S. R. (2011). Accelerated profile HMM searches. *PloS Comput. Biol.* 7, e1002195. doi: 10.1371/journal.pcbi.1002195

Eme, L., Gentekaki, E., Curtis, B., Archibald, J. M., and Roger, A. J. (2017). Lateral gene transfer in the adaptation of the anaerobic parasite *Blastocystis* to the gut. *Curr. Biol.* 27, 807–820. doi: 10.1016/j.cub.2017.02.003

Finn, R. D., Bateman, A., Clements, J., Coggill, P., Eberhardt, R. Y., Eddy, S. R., et al. (2014). Pfam: the protein families database. *Nucleic Acids Res.* 42, D222–D230. doi: 10.1093/nar/gkt1223

Fukasawa, Y., Tsuji, J., Fu, S.-C., Tomii, K., Horton, P., and Imai, K. (2015). MitoFates: improved prediction of mitochondrial targeting sequences and their cleavage sites. *Mol. Cell. Proteomics* 14, 1113–1126. doi: 10.1074/mcp.M114.043083

Fu, L., Niu, B., Zhu, Z., Wu, S., and Li, W. (2012). CD-HIT: accelerated for clustering the next-generation sequencing data. *Bioinformatics* 28, 3150–3152. doi: 10.1093/bioinformatics/bts565

Gabaldón, T., Ginger, M. L., and Michels, P. A. M. (2016). Peroxisomes in parasitic protists. *Mol. Biochem. Parasitol.* 209, 35–45. doi: 10.1016/j.molbiopara.2016.02.005

Gawryluk, R. M. R., Chisholm, K. A., Pinto, D. M., and Gray, M. W. (2014). Compositional complexity of the mitochondrial proteome of a unicellular eukaryote (*Acanthamoeba castellanii*, supergroup amoebozoa) rivals that of animals, fungi, and plants. *Proteomics J.* 109, 400–416. doi: 10.1016/j.jprot.2014.07.005

Gawryluk, R. M. R., Kamikawa, R., Stairs, C. W., Silberman, J. D., Brown, M. W., and Roger, A. J. (2016). The earliest stages of mitochondrial adaptation to low oxygen revealed in a novel rhizarian. *Curr. Biol.* 26, 2729–2738. doi: 10.1016/j.cub.2016.08.025

Gawryluk, R. M. R., and Stairs, C. W. (2021). Diversity of electron transport chains in anaerobic protists. *Biochim. Biophys. Acta Bioenerg.* 1862, 148334. doi: 10.1016/j.bbabio.2020.148334

Gill, S. S., Anjum, N. A., Hasanuzzaman, M., Gill, R., Trivedi, D. K., Ahmad, I., et al. (2013). Glutathione and glutathione reductase: a boon in disguise for plant abiotic stress defense operations. *Plant Physiol. Biochem.* 70, 204–212. doi: 10.1016/j.plaphy.2013.05.032

Ginestet, C. (2011). ggplot2: elegant graphics for data analysis. *J. R Stat. Soc. Ser. A Stat. Soc.* 174, 245–245. doi: 10.1111/j.1467-985X.2010.00676_9.x

Gomaa, F., Utter, D. R., Powers, C., Beaudoin, D. J., Edgcomb, V. P., Filipsson, H. L., et al. (2021). Multiple integrated metabolic strategies allow foraminiferan protists to thrive in anoxic marine sediments. *Sci. Adv.* 7:eabf1586. doi: 10.1126/sciadv.abf1586

Gooday, A. J., Bernhard, J. M., Levin, L. A., and Suhr, S. B. (2000). Foraminifera in the Arabian Sea oxygen minimum zone and other oxygen-deficient settings: taxonomic composition, diversity, and relation to metazoan faunas. *Deep-Sea Res. II: Top. Stud. Oceanogr.* 47, 25–54. doi: 10.1016/s0967-0645(99)00099-5

Grant, C. E., Bailey, T. L., and Noble, W. S. (2011). FIMO: scanning for occurrences of a given motif. *Bioinformatics* 27, 1017–1018. doi: 10.1093/bioinformatics/btr064

Gray, M. W., Burger, G., Derelle, R., Klimeš, V., Leger, M. M., Sarrasin, M., et al. (2020). The draft nuclear genome sequence and predicted mitochondrial proteome of *Andalucia godoyi*, a protist with the most gene-rich and bacteria-like mitochondrial genome. *BMC Biol.* 18. doi: 10.1186/s12915-020-0741-6

Grzymski, J., Schofield, O. M., Falkowski, P. G., and Bernhard, J. M. (2002). The function of plastids in the deep-sea benthic foraminifer, *Nonionella stella*. *Limnol. Oceanogr.* 47, 1569–1580. doi: 10.4319/lo.2002.47.6.1569

Gualdrón-López, M., Brennand, A., Hannaert, V., Quiñones, W., Cáceres, A. J., Bringaud, F., et al. (2012). When, how and why glycolysis became compartmentalised in the kinetoplastea. a new look at an ancient organelle. *Int. J. Parasitol.* 42, 1–20. doi: 10.1016/j.ijpara.2011.10.007

Haanstra, J. R., van Tuijl, A., Kessler, P., Reijnders, W., Michels, P. A. M., Westerhoff, H. V., et al. (2008). Compartmentation prevents a lethal turbo-explosion of glycolysis in trypanosomes. *PNAS* 105, 17718–17723. doi: 10.1073/pnas.0806664105

Hansel, C. M., and Diaz, J. M. (2021). Production of extracellular reactive oxygen species by marine biota. *Ann. Rev. Mar. Sci.* 13, 177–200. doi: 10.1146/annurev-marine-041320-102550

Huerta-Cepas, J., Szklarczyk, D., Heller, D., Hernández-Plaza, A., Forslund, S. K., Cook, H., et al. (2019). eggNOG 5.0: a hierarchical, functionally and phylogenetically annotated orthology resource based on 5090 organisms and 2502 viruses. *Nucleic Acids Res.* 47, D309–D314 doi: doi: 10.1093/nar/gky1085.

Jedelský, P. L., Doležal, P., Rada, P., Pyrih, J., Šmíd, O., Hrdý, I., et al. (2011). The minimal proteome in the reduced mitochondrion of the parasitic protist *Giardia intestinalis*. *PloS One* 6, e17285. doi: 10.1371/journal.pone.0017285

Katoh, K., Misawa, K., Kuma, K.-I., and Miyata, T. (2002). MAFFT: a novel method for rapid multiple sequence alignment based on fast Fourier transform. *Nucleic Acids Res.* 30, 3059–3066. doi: 10.1093/nar/gkf436

Keeling, P. J., Burki, F., Wilcox, H. M., Allam, B., Allen, E. E., Amaral-Zettler, L. A., et al. (2014). The marine microbial eukaryote transcriptome sequencing project (MMETSP): illuminating the functional diversity of eukaryotic life in the oceans through transcriptome sequencing. *PloS Biol.* 12, e1001889. doi: 10.1371/journal.pbio.1001889

Koch, J., Pranjic, K., Huber, A., Ellinger, A., Hartig, A., Kragler, F., et al. (2010). PEX11 family members are membrane elongation factors that coordinate peroxisome proliferation and maintenance. *J. Cell Sci.* 123, 3389–3400. doi: 10.1242/jcs.064907

Krueger, F. (2015). Trim galore. a wrapper tool around cutadapt and FastQC to consistently apply quality and adapter trimming to FastQ files 516, 517. Available at: https://www.bioinformatics.babraham.ac.uk/projects/trim_galore/.

Kuwabara, J. S., van Geen, A., McCorkle, D. C., and Bernhard, J. M. (1999). Dissolved sulfide distributions in the water column and sediment pore waters of the Santa Barbara basin. *Geochim. Cosmochim. Acta* 63, 2199–2209. doi: 10.1016/s0016-7037(99)00084-8

Lee, M. S., Mullen, R. T., and Trelease, R. N. (1997). Oilseed isocitrate lyases lacking their essential type 1 peroxisomal targeting signal are piggybacked to glyoxysomes. *Plant Cell* 9, 185–197 doi: doi: 10.1105/tpc.9.2.185.

Leger, M. M., Kolisko, M., Kamikawa, R., Stairs, C. W., Kume, K., Čepička, I., et al. (2017). Organelles that illuminate the origins of *Trichomonas* hydrogenosomes and *Giardia* mitosomes. *Nat. Ecol. Evol.* 1:0092. doi: 10.1038/s41559-017-0092

LeKieffre, C., Bernhard, J. M., Mabilleau, G., Filipsson, H. L., Meibom, A., and Geslin, E. (2018a). An overview of cellular ultrastructure in benthic foraminifera: New observations of rotalid species in the context of existing literature. *Mar. Micropaleontol.* 138, 12–32. doi: 10.1016/j.marmicro.2017.10.005

LeKieffre, C., Jauffrais, T., Geslin, E., Jesus, B., Bernhard, J. M., Giovani, M.-E., et al. (2018b). Inorganic carbon and nitrogen assimilation in cellular compartments of a benthic kleptoplastic foraminifer. *Sci. Rep.* 8:10140. doi: 10.1038/s41598-018-28455-1

Levin, L. A., Ekau, W., Gooday, A. J., Jorissen, F., Middelburg, J. J., Naqvi, S. W. A., et al. (2009). Effects of natural and human-induced hypoxia on coastal benthos. *Biogeosciences* 6, 2063–2098. doi: 10.5194/bg-6-2063-2009

Le, T., Žárský, V., Nývltová, E., Rada, P., Harant, K., Vancová, M., et al. (2020). Anaerobic peroxisomes in *Mastigamoeba balamuthi*. *PNAS* 117, 2065–2075. doi: 10.1073/pnas.1909755117

Love, M. I., Huber, W., and Anders, S. (2014). Moderated estimation of fold change and dispersion for RNA-seq data with DESeq2. *Genome Biol.* 15, 550. doi: 10.1186/s13059-014-0550-8

Ma, Z., Marsolais, F., Bernards, M. A., Sumarah, M. W., Bykova, N. V., and Igamberdiev, A. U. (2016). Glyoxylate cycle and metabolism of organic acids in the scutellum of barley seeds during germination. *Plant Sci.* 248, 37–44. doi: 10.1016/j.plantsci.2016.04.007

Martin, M. (2011). Cutadapt removes adapter sequences from high-throughput sequencing reads. *EMBnet.journal* 17, 10–12. doi: 10.14806/ej.17.1.200

Mattiazzi Ušaj, M., Brložnik, M., Kaferle, P., Žitnik, M., Wolinski, H., Leitner, F., et al. (2015). Genome-wide localization study of yeast Pex11 identifies peroxisome–mitochondria interactions through the ERMES complex. *J. Mol. Biol.* 427, 2072–2087. doi: 10.1016/j.jmb.2015.03.004

Michels, P. A. M., Moyersoen, J., Krazy, H., Galland, N., Herman, M., and Hannaert, V. (2005). Peroxisomes, glyoxysomes and glycosomes (review). *Mol. Membr. Biol.* 22, 133–145. doi: 10.1080/09687860400024186

Millenaar, F. F., Benschop, J. J., Wagner, A. M., and Lambers, H. (1998). The role of the alternative oxidase in stabilizing the *in vivo* reduction state of the ubiquinone pool and the activation state of the alternative oxidase. *Plant Physiol.* 118, 599–607. doi: 10.1104/pp.118.2.599

Mindthoff, S., Grunau, S., Steinfort, L. L., Girzalsky, W., Hiltunen, J. K., Erdmann, R., et al. (2016). Peroxisomal Pex11 is a pore-forming protein homologous to TRPM channels. *Biochim. Biophys. Acta* 1863, 271–283. doi: 10.1016/j.bbamcr.2015.11.013

Morales, J., Hashimoto, M., Williams, T. A., Hirawake-Mogi, H., Makiuchi, T., Tsubouchi, A., et al. (2016). Differential remodelling of peroxisome function underpins the environmental and metabolic adaptability of diplonemids and kinetoplastids. *Proc. Biol. Sci.* 283:20160520. doi: 10.1098/rspb.2016.0520

Müller, M., Hogg, J. F., and De Duve, C. (1968). Distribution of tricarboxylic acid cycle enzymes and glyoxylate cycle enzymes between mitochondria and peroxisomes in *Tetrahymena pyriformis*. *J. Biol. Chem.* 243, 5385–5395. doi: 10.1016/S0021-9258(18)91961-7

Müller, M., Mentel, M., van Hellemond, J. J., Henze, K., Woehle, C., Gould, S. B., et al. (2012). Biochemistry and evolution of anaerobic energy metabolism in eukaryotes. *Microbiol. Mol. Biol. Rev.* 76, 444–495. doi: 10.1128/MMBR.05024-11

Nomaki, H., Bernhard, J. M., Ishida, A., Tsuchiya, M., Uematsu, K., Tame, A., et al. (2016). Intracellular isotope localization in ammonia sp. (Foraminifera) of oxygen-depleted environments: Results of nitrate and sulfate labeling experiments. *Front. Microbiol.* 7. doi: 10.3389/fmicb.2016.00163

O'Leary, N. A., Wright, M. W., Brister, J. R., Ciufo, S., Haddad, D., McVeigh, R., et al. (2016). Reference sequence (RefSeq) database at NCBI: current status, taxonomic expansion, and functional annotation. *Nucleic Acids Res.* 44, D733–D745. doi: 10.1093/nar/gkv1189

Orsi, W. D., Morard, R., Vuillemin, A., Eitel, M., Wörheide, G., Milucka, J., et al. (2020). Anaerobic metabolism of foraminifera thriving below the seafloor. *ISME J.* 14, 2580–2594. doi: 10.1038/s41396-020-0708-1

Oshima, Y., Kamigaki, A., Nakamori, C., Mano, S., Hayashi, M., Nishimura, M., et al. (2008). Plant catalase is imported into peroxisomes by Pex5p but is distinct from typical PTS1 import. *Plant Cell Physiol.* 49, 671–677. doi: 10.1093/pcp/pcn038

Pei, J., Kim, B.-H., and Grishin, N. V. (2008). PROMALS3D: a tool for multiple protein sequence and structure alignments. *Nucleic Acids Res.* 36, 2295–2300. doi: 10.1093/nar/gkn072

Petriv, O. I., Tang, L., Titorenko, V. I., and Rachubinski, R. A. (2004). A new definition for the consensus sequence of the peroxisome targeting signal type 2. *J. Mol. Biol.* 341, 119–134. doi: 10.1016/j.jmb.2004.05.064

Petsalaki, E. I., Bagos, P. G., Litou, Z. I., and Hamodrakas, S. J. (2006). PredSL: a tool for the n-terminal sequence-based prediction of protein subcellular localization. *Genomics Proteomics Bioinf.* 4, 48–55. doi: 10.1016/S1672-0229(06)60016-8

Piña-Ochoa, E., Høgslund, S., Geslin, E., Cedhagen, T., Revsbech, N. P., Nielsen, L. P., et al. (2010). Widespread occurrence of nitrate storage and denitrification among foraminifera and gromiida. *PNAS* 107, 1148–1153. doi: 10.1073/pnas.0908440107

Reimers, C. E., Ruttenberg, K. C., Canfield, D. E., Christiansen, M. B., and Martin, J. B. (1996). Porewater pH and authigenic phases formed in the uppermost sediments of the Santa Barbara basin. *Geochim. Cosmochim. Acta* 60, 4037–4057. doi: 10.1016/S0016-7037(96)00231-1

Risgaard-Petersen, N., Langezaal, A. M., Ingvardsen, S., Schmid, M. C., Jetten, M. S. M., Op den Camp, H. J. M., et al. (2006). Evidence for complete denitrification in a benthic foraminifer. *Nature* 443, 93–96. doi: 10.1038/nature05070

Rottensteiner, H., Kramer, A., Lorenzen, S., Stein, K., Landgraf, C., Volkmer-Engert, R., et al. (2004). Peroxisomal membrane proteins contain common Pex19p-binding sites that are an integral part of their targeting signals. *Mol. Biol. Cell* 15, 3406–3417. doi: 10.1091/mbc.e04-03-0188

Rucktäschel, R., Girzalsky, W., and Erdmann, R. (2011). Protein import machineries of peroxisomes. *Biochim. Biophys. Acta* 1808, 892–900. doi: 10.1016/j.bbamem.2010.07.020

Saier, M. H., Reddy, V. S., Moreno-Hagelsieb, G., Hendargo, K. J., Zhang, Y., Iddamsetty, V., et al. (2021). The transporter classification database (TCDB): 2021 update. *Nucleic Acids Res.* 49, D461–D467. doi: 10.1093/nar/gkaa1004

Salinas, G., Langelaan, D. N., and Shepherd, J. N. (2020). Rhodoquinone in bacteria and animals: Two distinct pathways for biosynthesis of this key electron transporter used in anaerobic bioenergetics. *Biochim. Biophys. Acta Bioenerg.* 1861, 148278. doi: 10.1016/j.bbabio.2020.148278

Schlüter, A., Real-Chicharro, A., Gabaldón, T., Sánchez-Jiménez, F., and Pujol, A. (2010). PeroxisomeDB 2.0: an integrative view of the global peroxisomal metabolome. *Nucleic Acids Res.* 38, D800–D805 doi: doi: 10.1093/nar/gkp935.

Shiflett, A. M., and Johnson, P. J. (2010). Mitochondrion-related organelles in eukaryotic protists. *Annu. Rev. Microbiol.* 64, 409–429. doi: 10.1146/annurev.micro.62.081307.162826

Škodová-Sveráková, I., Záhonová, K., Juricová, V., Danchenko, M., Moos, M., Baráth, P., et al. (2021). Highly flexible metabolism of the marine euglenozoan protist *Diplonema papillatum*. *BMC Biol.* 19, 251. doi: 10.1186/s12915-021-01186-y

Stairs, C. W., Eme, L., Muñoz-Gómez, S. A., Cohen, A., Dellaire, G., Shepherd, J. N., et al. (2018). Microbial eukaryotes have adapted to hypoxia by horizontal acquisitions of a gene involved in rhodoquinone biosynthesis. *Elife* 7:e34292. doi: 10.7554/eLife.34292

Stairs, C. W., Leger, M. M., and Roger, A. J. (2015). Diversity and origins of anaerobic metabolism in mitochondria and related organelles. *Philos. Trans. R. Soc Lond. B Biol. Sci.* 370, 20140326. doi: 10.1098/rstb.2014.0326

Stairs, C. W., Táborský, P., Salomaki, E. D., Kolisko, M., Pánek, T., Eme, L., et al. (2021). Anaeramoebae are a divergent lineage of eukaryotes that shed light on the transition from anaerobic mitochondria to hydrogenosomes. *Curr. Biol.* 31, 5605–5612.e5. doi: 10.1016/j.cub.2021.10.010

Stamatakis, A. (2014). RAxML version 8: a tool for phylogenetic analysis and post-analysis of large phylogenies. *Bioinformatics* 30, 1312–1313. doi: 10.1093/bioinformatics/btu033

Steffensen, J. L., Dufault-Thompson, K., and Zhang, Y. (2016). PSAMM: A portable system for the analysis of metabolic models. *PloS Comput. Biol.* 12, e1004732. doi: 10.1371/journal.pcbi.1004732

Steinegger, M. , and Söding, J. (2018). Clustering huge protein sequence sets in linear time. *Nat. Commun.* 9, 2542. doi: 10.1038/s41467-018-04964-5

Sun, Q., Zybailov, B., Majeran, W., Friso, G., Olinares, P. D. B., and van Wijk, K. J. (2009). PPDB, the plant proteomics database at Cornell. *Nucleic Acids Res.* 37, D969–D974. doi: 10.1093/nar/gkn654

Tang, S., Lomsadze, A., and Borodovsky, M. (2015). Identification of protein coding regions in RNA transcripts. *Nucleic Acids Res.* 43, e78. doi: 10.1093/nar/gkv227

Verner, Z., Žárský, V., Le, T., Narayanasamy, R. K., Rada, P., Rozbeský, D., et al. (2021). Anaerobic peroxisomes in *Entamoeba histolytica* metabolize myo-inositol. *PloS Pathog.* 17, e1010041. doi: 10.1371/journal.ppat.1010041

Vishwakarma, A., Kumari, A., Mur, L. A. J., and Gupta, K. J. (2018). A discrete role for alternative oxidase under hypoxia to increase nitric oxide and drive energy production. *Free Radic. Biol. Med.* 122, 40–51. doi: 10.1016/j.freeradbiomed.2018.03.045

Wang, M., Jia, Y., Xu, Z., and Xia, Z. (2016). Impairment of sulfite reductase decreases oxidative stress tolerance in *Arabidopsis thaliana*. *Front. Plant Sci.* 7, 1843. doi: 10.3389/fpls.2016.01843

Williams, C., Opalinski, L., Landgraf, C., Costello, J., Schrader, M., Krikken, A. M., et al. (2015). The membrane remodeling protein Pex11p activates the GTPase Dnm1p during peroxisomal fission. *Proc. Natl. Acad. Sci. U. S. A.* 112, 6377–6382. doi: 10.1073/pnas.1418736112

Wiwatwattana, N., Landau, C. M., Cope, G. J., Harp, G. A., and Kumar, A. (2007). Organelle DB: an updated resource of eukaryotic protein localization and function. *Nucleic Acids Res.* 35, D810–D814. doi: 10.1093/nar/gkl1000

Woehle, C., Roy, A.-S., Glock, N., Wein, T., Weissenbach, J., Rosenstiel, P., et al. (2018). A novel eukaryotic denitrification pathway in foraminifera. *Curr. Biol.* 28, 2536–2543.e5. doi: 10.1016/j.cub.2018.06.027

Záhonová, K., Treitli, S. C., Le, T., Škodová-Sveráková, I., Hanousková, P., Čepička, I., et al. (2022). Anaerobic derivates of mitochondria and peroxisomes in the free-living amoeba *Pelomyxa schiedti* revealed by single-cell genomics. *BMC Biol.* 20. doi: 10.1186/s12915-022-01247-w

Zhang, Z., Schwartz, S., Wagner, L., and Miller, W. (2000). A greedy algorithm for aligning DNA sequences. *J. Comput. Biol.* 7, 203–214. doi: 10.1089/10665270050081478

Zhao, R.-Z., Jiang, S., Zhang, L., and Yu, Z.-B. (2019). Mitochondrial electron transport chain, ROS generation and uncoupling. *Int. J. Mol. Med.* 44, 3–15. doi: 10.3892/ijmm.2019.4188

Zhou, Q., Zhai, Y., Lou, J., Liu, M., Pang, X., and Sun, F. (2011). Thiabendazole inhibits ubiquinone reduction activity of mitochondrial respiratory complex II *via* a water molecule mediated binding feature. *Protein Cell* 2, 531–542. doi: 10.1007/s13238-011-1079-1

frontiers | Frontiers in Marine Science

TYPE Original Research
PUBLISHED 01 March 2023
DOI 10.3389/fmars.2023.1113278

OPEN ACCESS

EDITED BY
Diana Sofia Madeira,
University of Aveiro, Portugal

REVIEWED BY
Kai Xu,
Jimei University, China
Amit Kumar,
Sathyabama Institute of Science and Technology, India
Gretty Villena,
National Agrarian University, Peru

*CORRESPONDENCE
Weiye Li
liweiye1999@sina.com

†These authors have contributed equally to this work and share first authorship

SPECIALTY SECTION
This article was submitted to Marine Molecular Biology and Ecology, a section of the journal Frontiers in Marine Science

RECEIVED 01 December 2022
ACCEPTED 08 February 2023
PUBLISHED 01 March 2023

CITATION
Tian K, Li Q, Zhang X, Guo H, Wang Y, Cao P, Xu S and Li W (2023) Analysis of the expression and function of the CBL-CIPK network and MAPK cascade genes in *Kandelia obovata* seedlings under cold stress.
Front. Mar. Sci. 10:1113278.
doi: 10.3389/fmars.2023.1113278

Analysis of the expression and function of the CBL-CIPK network and MAPK cascade genes in *Kandelia obovata* seedlings under cold stress

Kuo Tian[1†], Qi Li[1†], Xiumei Zhang[1], Haoyu Guo[1], Yihang Wang[1], Pinglin Cao[1], Shengyong Xu[1] and Weiye Li[2*]

[1]School of fishery, Zhejiang Ocean University, Zhoushan, Zhejiang, China, [2]Zhoushan Fisheries Research Institute, Zhoushan, Zhejiang, China

Mangroves are an important component of coastal wetland ecosystems, and low temperature is the main factor that limits their extension to higher latitudes. *Kandelia obovata* as one of the most cold-tolerant species in mangrove ecosystems can provide basis for the northward migration of mangrove ecosystems. We took *K. obovata* seedlings from Zhoushan (Zhoushan, Zhejiang, China) as the research object in this study. Transcriptome sequencing based on the Illumina HiSeqTM 2500 platform was performed to compare the transcriptome changes of roots, stems, and leaves before and after freezing and to reveal the molecular mechanisms of frost resistance. A total of 1560, 370, and 416 genes were differentially expressed in the roots, stems, and leaves before and after cold snaps, respectively. Among these differentially expressed genes, 13 positive and negative regulators were attributed to the CBL-CIPK signaling network and MAPK cascade, which might be related to the frost resistance mechanism of *K. obovata* Transcription factors such as AP2/EREBP and bHLH were involved in regulating the synthesis pathways of ethylene, cytokinin, growth hormone, and flavonoids. Results provide new insights into the frost resistance mechanism of *K. obovata* seedlings.

KEYWORDS

***Kandelia obovata* seedlings, transcriptome, cold stress, CBL-CIPK network, MAPK cascade**

1 Introduction

Mangrove forests are woody plant communities that are naturally distributed throughout the tropics and subtropics and are a unique ecosystem in the sea-land transition zone, in which marine organisms, such as birds, fish, shrimps, and shellfish thrive. Moreover, mangroves can promote siltation, protect beaches and purify the

environment (Wang et al., 2011). Mangrove ecosystems play an irreplaceable role in protecting coastal wetland ecosystems and biodiversity and maintaining coastal ecological balance. They are also important ecological security systems in the coastal region of southeastern China (Wang et al., 2011; Su et al., 2019). Among mangrove plants, *Kandelia obovata* has the highest natural distribution latitude in China and is one of the most cold-resistant mangrove species (Wang et al., 2011). In the 1950s, this species was successfully transplanted from the northernmost part of its natural distribution in Fujian Province (27° 17′ N) to further up north in Yueqing in the Zhejiang Province (28° 20′ N) (Su et al., 2019; Fei et al., 2021b). However, the persistent phenomenon of climate change has led to a tendency for mangrove species to expand to higher latitudes. The introduction of mangrove *K. obovata* has been recorded in the Zhoushan of Zhejiang Province (29°30′N) (Osland et al., 2013; Zheng C. et al., 2016). During their northward journey, mangroves are susceptible to extreme weather conditions.

In the context of global climate change, the frequency and intensity of extreme weather, particularly in the tropical-temperate transition zone, limits plant productivity and affects species distribution, ecosystem structure, and ecosystem function (Chen et al., 2017). The tendency of North Atlantic and East Asian mangroves to spread northward is significantly influenced by the frequency and severity of cold snaps (Cavanaugh et al., 2014; Cavanaugh et al., 2015; Osland et al., 2017). Cold stress is divided into chilling stress (0 °C-15 °C) or freezing stress (<0 °C). Chilling stress may impede the growth and development of plants, and extended exposure to temperatures below 0 °C can cause ice crystals to accumulate in the cytoplasm of plant cells. This phenomenon can dehydrate cells or rupture cell membranes or walls, causing irreparable harm to the plant (Shi et al., 2018). The various physiological and metabolic processes that occur in plants at low temperatures are very intricate regulatory processes (Guy, 1990). Numerous investigations into the physiological and molecular processes underlying the hypothermic response of *K. obovata* have been conducted and yielded insightful results (Peng et al., 2015; Liu et al., 2019; Wang et al., 2019; Fei et al., 2021a). For example, the KoWRKY40 gene in WRKY transcription factors plays key roles in responses to biotic and abiotic stresses (Liu et al., 2019; Du Z. K. et al., 2022). Among the C-repeat binding factor (CBF), KoCBF1 and KoCBF3 may have functions in plant growth and cold resistance and are involved in responses to salinity and heavy metal stress (Peng et al., 2020). Ko-Aquaporins (KoAQPs) aid in the transport of water and solutes for adaptation to coastal intertidal habitats and have complex responses to environmental factors, such as salt and temperature (Guo et al., 2022). KoOsmotin, a class of proteins with osmotic functions, is highly induced in *K. obovata* leaves during cold stress (Fei et al., 2021a). KoHsp70, stress-inducible heat shock protein gene, plays a role in protective response to cold stress in *K. obovata* (Fei et al., 2015). Moreover, the photosynthetic system, enzymes, and non-enzymatic antioxidants of *K. obovata* are extensively involved in stress response at low temperatures to increase the plant's potential for cold adaptation (Peng et al., 2015; Chen et al., 2017). Gene expression regulation tends to respond rapidly to external environmental changes by regulating protein abundance. The six levels of plant gene expression control include mRNA degradation control, protein activity control, RNA processing control, RNA transport, localization control, transcriptional control, and translational control. As transcriptional regulation is a multi-faceted, deep-level process, further research is needed in this field (Alberts, 2015). Although the gene expression profiles of many tissues have been disclosed by sequencing of critical genes for cold adaptation in adult *K. obovata*, information on the two important cold stress nodes of the B-like protein-interacting protein kinase (CBL-CIPK) network and mitogen-activated protein kinase (MAPK) cascade has not been completely reported (Su et al., 2019).

The CBL-CIPK network plays a key role in cold stress response, where CBL proteins interact with CBL-interacting protein kinases (CIPK) or SOS Ras/Rho Guanine Nucleotide Exchange Factor 2 (SOS2) protein kinase to form different signaling cascades. A complex CBL-CIPK network can regulate Ca^{2+} transport in response to low temperatures and freezing injury to plant cells (Batistic and Kudla, 2004; Kolukisaoglu et al., 2004; Buchwal et al., 2020). Ca^{2+} affects the cold tolerance of plant cells by improving the stability of the cell wall and promoting the secretion of peroxidase (Batistic and Kudla, 2004; Kolukisaoglu et al., 2004). The typical MAPK cascade signaling network is composed of three specific protein kinases, namely, MAPK kinase kinases (MKKKs), MAPK kinases (MKKs), and MAPKs. These protein kinases are activated by sequential phosphorylation at conserved activation sites, and the interaction between SaMKK2 and SaMAPK4/7 increases the plant's resistance to cold temperatures (Teige et al., 2004; Chen et al., 2022). Currently, the CBL-CIPK network and the MARK cascade have been isolated from many plants, and their regulatory pathways have been well studied. However, the regulated transcriptional signaling pathways of *K. obovata* are still poorly understood, especially during its seedling growth phase.

Due to large-scale ecological restoration operations along the Chinese coast, *K. obovata* has been introduced as a non-native species in Zhoushan beyond the limits of their natural range. However, the area is more susceptible to extreme cold snaps. Extreme cold events have a significant effect on the abundance and productivity of mangrove plants. However, as plants grow and mature, adults have stronger resistance and recovery from cold events than seedlings. Given that the survival and development of seedlings often determine the rate at which the population grows, additional research is required on mechanisms by which *K. obovata* withstand cold events during northern migration (Coldren and Proffitt, 2017). In this context, field-based experiments will be more helpful in understanding how *K. obovata* seedlings react to cold events or freezing damage because extreme cold snap events are relatively rare. It is difficult to replicate a natural environment similar to freezing stress on *K. obovata* seedlings in an artificial environment. (Osland et al., 2015). In this study, transcriptome changes were examined in the root, stem, and leaf tissues of *K. obovata* seedlings transplanted in the Zhoushan intertidal zone before and after a cold snap. Given the relevance of CBL-CIPK network and MAPK signaling pathways on the cold tolerance of plants, we then identified the genes involved in these pathways in *K. obovata* and compared in detail the gene expression of these two

pathways before and after the cold snap to provide insights into the freezing resistance mechanisms of *K. obovata* seedlings under extremely cold events.

2 Materials and methods

2.1 Material collection

K. obovata embryos were collected from Lei Zou of Guangdong in March 2020 and temporarily nurtured in an outdoor nursery in the Zhoushan area for 6 months before being moved to the intertidal zone of the Zhoushan main island in September 2020 (Figure S1). We transplanted 300 seedlings on about 600 m^2 of tidal flat. We determined the sampling time range according to Zhoushan's local historical meteorological data. To predict the best sampling times, we followed the weather forecast to know when a cold snap would occur. Three tissues including the root, stem, and leaf were freshly sampled from different healthy *K. obovata* seedlings on December 29 and December 31 before and after the cold snaps (Figure S2). The lowest temperature registered during the cold snap was -2.10°C, measured with an automatic temperature recorder (HOBO MX2201) placed on the sampling sites for the period (2020.12.16-2021.01.13). After collection, samples were washed with water, dried with paper, and stored in liquid nitrogen in an ultra-low temperature refrigerator at -80°C. At least three biological replicates were collected from the field at each sampling time, with each plant representing an independent biological replicate. In total, we analyzed 18 samples (3 biological replicates × 2 sampling times × 3 tissues).

2.2 RNA extraction, library preparation, and RNA-Seq

Extraction was performed according to the manufacturer's instructions using the RNeasy Plant RNA Extraction Kit (Qiagen, Dusseldorf, Germany) to extract RNA from each of the six unique tissues mentioned above. RNA concentration was measured using an Agilent 2100 Bioanalyzer (Agilent Technologies, Santa Clara, CA, USA). NanoPhotometer® spectrophotometer (IMPLEN, CA, USA) was used to check RNA purity.

We constructed cDNA library and conducted RNA sequences at Biomarker Biotechnology Corporation in Beijing, China. About 3 μg of RNA per sample was used for RNA preparation. A poly-T oligo-attached magnetic bead method was used to purify mRNA from total RNA. Dividing the mRNA with divalent cations was conducted at elevated temperatures using NEBNext First-Strand Synthesis Reaction Buffer (5×). The first-strand cDNA was synthesized using random hexamer primers and M-MuLV reverse transcriptase (RNase H-). DNA polymerase I and RNase H were used to synthesize cDNA on the second strand while exonucleases and polymerases were used to turn the remaining overhangs into blunt ends. To prepare samples for hybridization, the 3′ ends of the DNA fragments were adenylated and ligated to NEBNext adaptors with hairpin loop structures. In the following step, 150–200 bp-long cDNA fragments were selected from the library and purified using a Beckman Coulter Agencourt AMPure XP system (Brea, California, USA). The size-selected, adaptor-ligated cDNA was added with 3 μL of USER enzyme (New England Biolabs, Ipswich, MA, USA) at 37 °C for 15 min followed by 5 min at 95 °C. PCR analysis was performed using Phusion High-Fidelity DNA polymerase (Thermo Fisher, Waltham, MA, USA), universal PCR primers, and index (X) primer. A Bioanalyzer 2100 was used to evaluate the quality of the library constructed from the PCR products purified with the AMPure XP system. Clustering of index-coded samples was performed using a cBot Cluster Generation System and a TruSeq PE Cluster Kit v3-cBot-HS (Illumina, San Diego, CA, USA). The manufacturer's instructions were followed for all experimental procedures. Using the Illumina Hiseq 2000 platform, paired-end reads were generated from the library preparations.

2.3 Differential expression analysis

Raw data in fastq format were processed using in-house Perl scripts. Clean data were obtained by removing low-quality reads and those containing the adapters or poly-N sequences. We checked the quality of the unassembled read dataset by examining Q20, Q30, GC-content, and sequence duplication. All the downstream analyses were performed using high-quality clean data.

Genes from 18 transcriptomes were previously annotated in seven public databases including NR (NCBI, Non-Redundant Protein Database), Swiss-Prot, GO (Gene Ontology), Pfam database, KOG database, COG (Clusters of Orthologous Groups), and KEGG (Kyoto Encyclopedia of Genes and Genomes). Based on the annotation results of 18 transcriptomes, the unigene annotation information of the *K. obovata* seedling transcriptome was screened and analyzed. FPKM method was used to calculate gene expression based on the annotation results. The relative measure of transcript abundance was fragmented per kilobase of transcript per million mapped reads (FPKM) (Florea et al., 2013). Correlation and principal component (PCA) analyses were also performed for the 18 transcriptomes of genes by using the latic, cluster package.

Differentially expressed genes (DEGs) were analyzed using the DESeq 2 package to visualize the results, with FDR < 0.01 and $|\log2FoldChange| \geq 2.00$ as the screening criteria to obtain the set of DEGs among samples. DEGs were classified as up- or down-regulated genes based on significant positive or negative log changes in their values. The screened DEGs were subjected to GO and KEGG pathway enrichment analyses, where q-value < 0.05 indicated the significant enrichment of the DEGs.

2.4 Identification of transcription factor

The TF family of *K. obovata* seedlings was predicted in different tissue samples by using the Plant Transcription Factor Database (version 3.0). The DEGs were submitted to iTAK software for prediction and further classification. The dataset of the TFs of *K. obovata* seedlings was used as reference, and the default values of

the parameters “substitution matrix” and “E-value” were used (Zheng Y. et al., 2016).

2.5 Identification of CBL-CIPK network and MAPK cascade genes in *K. obovata* seedlings

The NGDC website (https://ngdc.cncb.ac.cn) contains information on the sequences of *K. obovata* genes. The CBL-CIPK network and MAPK cascade genes of *K. obovata* can be identified by comparing the protein sequences generated by the genes of *K. obovata* seedlings in the database with those in the experiment. When the similarity of gene sequences was higher than 80% compared with the database, it was identified as the corresponding genes with the close homology relationship in the *k. obovata*.

2.6 Gene expression analysis of CBL-CIPK network and MAPK cascade in *K. obovata* seedlings

The expression of 13 key genes in the CBL-CIPK network and MAPK cascade in *K. obovata* seedling was studied under control and cold stress conditions. The fpkm values of gene expression were normalized by z-score, and the expression was plotted using the stats package for heat mapping. We performed Pearson correlation analysis to obtain correlation matrices between gene pairs. The network relationship graph between 13 genes was determined using the igraph package in R language.

3 Results

3.1 Creation of databases and functional annotation of the transcriptome of *K. obovata* seedlings

We generated 18 cDNA libraries in 18 samples of various tissues of *K. obovata* seedlings at different temperatures by using RNA-seq technique. A total of 117.37 Gb of raw data were obtained to gain insights into the response network of genes in the root, stem, and leaf of *K. obovata* seedlings before and after cold stress. After removing low-quality sequences and adapter sequences from the raw data obtained by sequencing, the GC rates of the 18 samples were 45.58%–46.5%, and all Q30s were greater than 90%, indicating the sufficient accuracy and quality of the sequencing data for further analysis. The general sequencing statistics are shown in Table S1. On the PCA of the gene expression profiles of the 18 samples, three biological replicates of each tissue clustered together (Figure S3), indicating the reliability of all mRNA sequence library replicates. The Pearson correlation analysis of the dataset revealed gene expression patterns and significant tissue specificity, with identical tissues clustered together (Figure S4), consistent with the phenomenon in Figure S3. To gain insight into single genes, GO was classified using WEGO, resulting in 53 GO terms in a three-level ontology (Figure 1A) (Ye et al., 2018). The category of

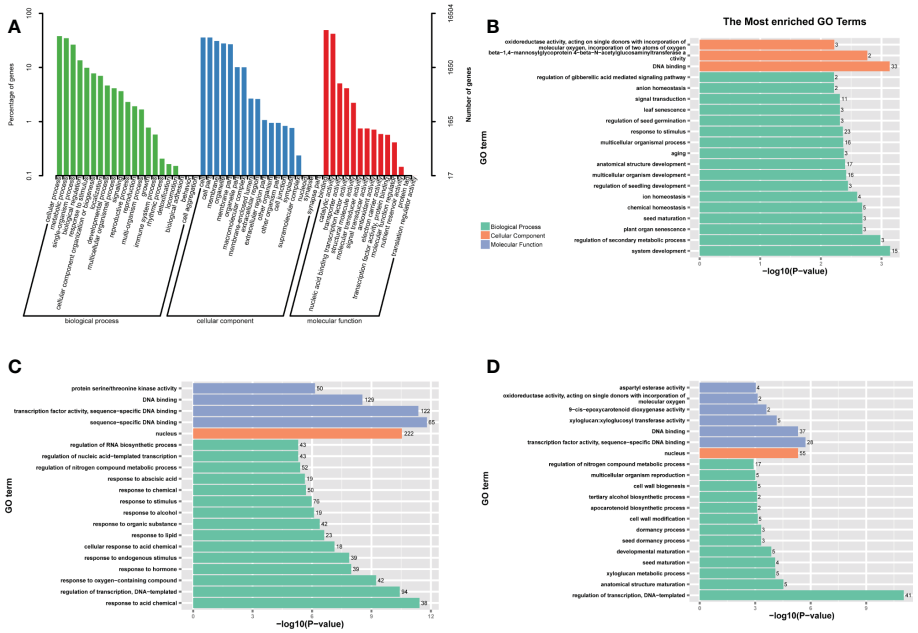

FIGURE 1
(A) Gene ontology (GO) belonging to the functional classification of all unigenes of the *K. obovata* seedlings transcriptome, the right y-axis indicates the number of genes in each category and the left y-axis indicates the percentage of genes. **(B-D)** Gene ontology (GO) enrichment analysis of differentially expressed genes (DEG) in three tissues under cold stress conditions. **(B)** Representative enrichment (p-value < 0.05) GO terms in **(B)** leaf **(C)** root **(D)** stem DEGs, three colors indicate three different categories and horizontal coordinates indicate p-values.

biological process was dominated by "cellular process" (GO:0009987, 6249 unigenes), "metabolic process" (GO:0008152, 5723 unigenes), "single-organism process" (GO:0044699, 4353 unigenes) dominated. In the category of cellular component, "cell" (GO:0005623, 5901 unigenes), "cellular part" (GO:0044464, 5901 unigenes), "membrane" (GO:0016020, 5088 unigenes), "organelle" (GO:0043226, 4583 unigenes), and "membrane part" (GO: 0044425, 4445 unigenes) had important roles. In the GO molecular function, a large number of single genes were annotated as "binding" (GO:0005488, 8107 unigenes) and "catalytic activity" (GO:0 003824, 6915 unigenes).

The KEGG pathway annotations were used to identify biochemical pathways in the *K. obovata* seedling transcriptome. A total of 6,902 single genes were matched to 136 pathways. The major pathways included "plant hormone signal transduction" (524 single genes), "plant–pathogen interaction" (494 single genes), "MAPK signaling pathway–plant" (318 single genes), and "carbon metabolism" (311 single genes) pathways (Table S2).

3.2 Identification and functional enrichment analysis of DEGs in different tissues under cold stress

RNAseq was used to identify DEGs in different tissues of *K. obovata* seedlings before and after the cold snaps. According to the RNA-seq results, gene expression in the seedlings changed significantly before and after the cold snap, with a total of 1560, 370, and 416 DEGs in the root, stem, and leaf respectively. The Volcano map and Differential genetic Wayne plots showed the aggregation of DEGs in the roots, stems, and leaves, respectively (Figures 2 and S5). The DEGs included 346 up-regulated genes and 1214 down-regulated genes in the roots, 183 up-regulated genes and 187 down-regulated genes in the stems, and 281 up-regulated genes and 135 down-regulated genes in the leaves (Figure 2).

The DEGs of each tissue were subjected to GO and KEGG pathway enrichment analyses to determine the possible functions of the cold response genes. In GO enrichment, the leaf response annotations were mainly focused on biological processes, with "system development" and "regulation of secondary metabolic processes" as the most abundant. The most abundant GO terms in molecular functions were related to "DNA binding." The root and stem response annotations tended to be consistent, and the molecular function of "transcription factor activity" dominated. The cellular component was mainly annotated as "nuclear," and the "management of transcription factors" was highly represented in biological processes. The terms "sequence-specific DNA binding" and "response to acidic chemicals" were unique to the root (Figures 2B-D). Among the KEGG pathway enrichments, circadian-vegetative (ko04712), taurine, and hypotaurine metabolism (ko00430) were significantly enriched in the leaves. Plant–pathogen interactions (ko04626), MAPK signaling pathway (ko04016), biosynthesis of scopolamine, piperidine, and pyridine alkaloids (ko00960), beta-Alanine metabolism (ko00410), and amino and nucleotide sugar metabolism (ko00520) were significantly enriched in the roots. Starch and sucrose metabolism (ko00500), phenylpropanoid biosynthesis (ko00940), and carotenoid biosynthesis (ko00906) were enriched in the stems. Phytohormone signaling (ko04075) was enriched in all tissues (Figures 3A-C).

3.3 Transcription factors in response to cold stress in *K. obovata* seedlings

Transcription factors regulate gene expression and are thus regulators of cellular processes and environmental responses. Transcription factors can control the expression of many target genes by specifically binding to their various promoters (Nakashima et al., 2009). To clarify the transcriptional regulation of cold stress-responsive genes, we identified DEGs encoding TFs under cold stress. Among transcription factors, AP2/ERF, WRKY, C2H2, and NAC were concentrated at the root. And the enrichment of these transcription factors in the root was much higher than in the stem and leaves. The major transcription factors in the stems were the same as in the roots, except for the increase in HD-ZIP transcription factors. WRKY did not appear in the stems. The transcription factors NAC, AP2/ERF, bHLH, and GARP were mainly present in the leaves (Figures 4A-C).

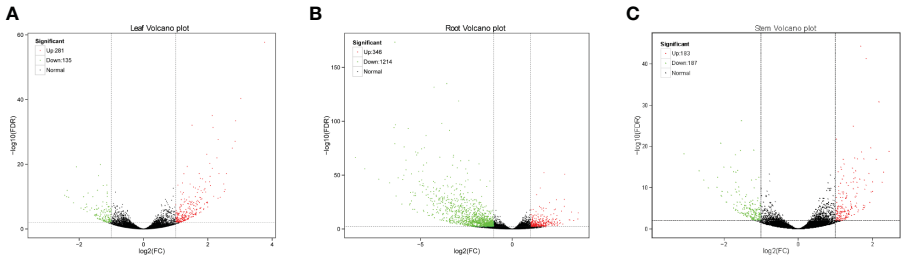

FIGURE 2
Volcano plot showing the numbers of DEGs among the three *K.obovata* seedlings organizations. The x-axis represents the fold-change (FC) of gene expression among samples. The more different genes are at either end. The y-axis represents the significance of the shift in gene expression, which is indicated by -log10. The y is the P-value (t-test) negative log, as adjusted by the false discovery rate (FDR). Genes that were significantly differentially expressed are represented by red dots (up-regulated) and green dots (down-regulated), while insignificantly differentially expressed genes are represented by black dots. Leaf: 281 up-regulated genes and 135 down-regulated genes. Root: 346 up-regulated genes and 1214 down-regulated genes. Stem: 183 up-regulated genes and 187 down-regulated genes.

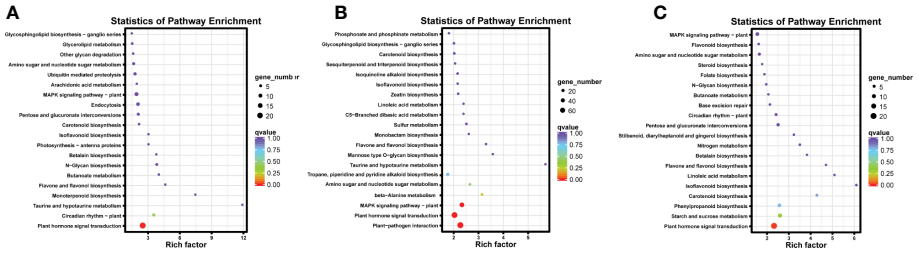

FIGURE 3
Results of gene and genome enrichment analysis of DEGs in leaves **(A)** and roots **(B)** and stems **(C)** of *K. obovata* seedlings before and after the cold snaps and Kyoto Encyclopedia of Genes and Genomes (KEGG) pathway. The horizontal coordinates represent the degree of enrichment, the different colors represent the size of the p-value, and the size of the dots represents the number of genes.

3.4 Identification and functional analysis of CBL-CIPK network and MAPK cascade genes

Research has concentrated on the CBL-CIPK network and MAPK cascade of *Arabidopsis thaliana* and some model plants. No study has been conducted on thorough identification and functional analysis of the expression and regulation of the CBL-CIPK network and MAPK cascade-related genes in *K. obovata* seedlings under cold stress. In the present work, we found that *K. obovata* seedlings contain 13 CBL-CIPK networks and MAPK cascade-related genes (Figure 5A). The heat map shows that CBL4, CBL3, and CIPK2 are grouped together, but they are separated from CBF1, meanwhile, CBL2, CBL3, and MAPK6 are grouped together. The gene functions of the CBL-CIPK network and MAPK cascade are connected in the *K. obovata* seedlings. The co-expression regulatory network of the 13 genes in *K. obovata* was established using this dataset, and the mutual regulatory relationships between among the genes were visualized. The gray line represents the negative regulatory relationship between genes, the blue line represents the positive regulatory relationship between genes, and the increase in line thickness represents a stronger prediction relationship (Figure 5B). Among the co-expression regulatory networks, genes in the CBL-CIPK network and MAPK cascade, for instance CRLK1 with MEKK1 and MEKK1 with MAPK3/6, had strong correlations. The co-expression relationship among the 13 genes could provide insights into the correlation between the CBL-CIPK network and MAPK cascade genes in *K. obovata* seedlings under cold stress.

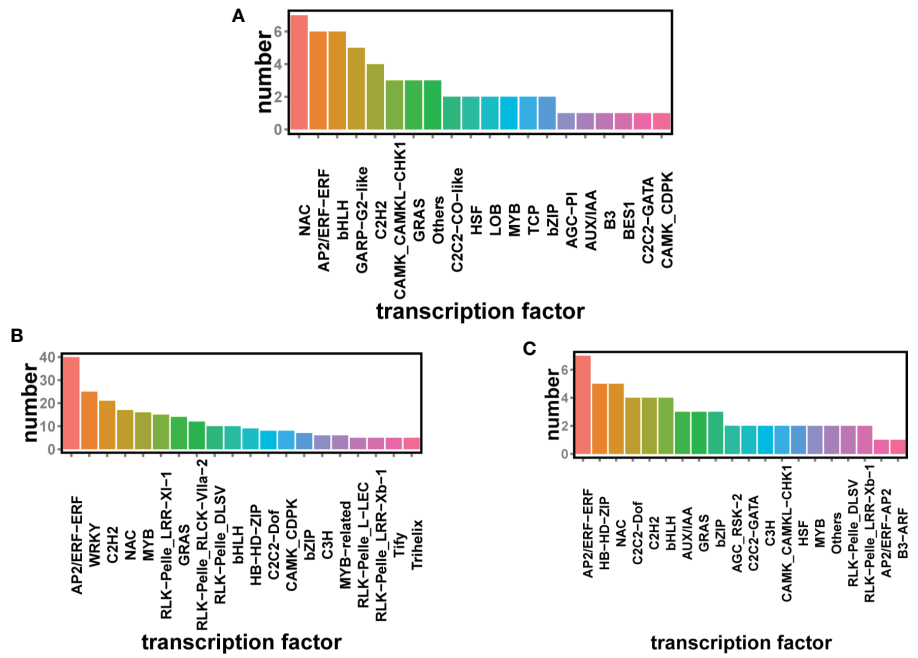

FIGURE 4
Significant transcription factor (TF) classification in three tissues of *K. obovata* seedlings, leaves **(A)** and roots **(B)** and stems **(C)**, before and after chilling, with vertical coordinates representing the number of transcription factors ($P < 0.05$ and $|LOG2FC| > 2$).

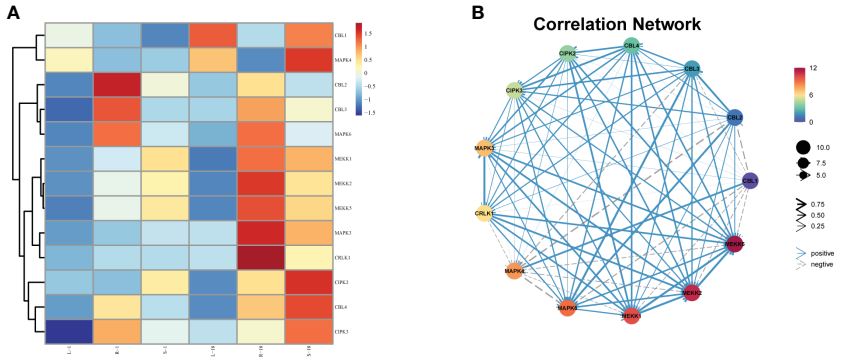

FIGURE 5
Identification of CBL-CIPK network and MAPK cascade gene genes in different tissues of *K. obovata* seedlings and visualization of their co-expression networks. **(A)** Hierarchical clustering analysis of 13 CBL-CIPK networks and MAPK cascade genes. The values in the heat map indicate the z-normalized values of FPKM in different samples. Red and blue colors indicate high and low expression levels, respectively. **(B)** Thirteen ICE- CBL-CIPK network and MAPK cascade gene co-expression networks.

4 Discussion

4.1 Signal-mediated cold stress response

Under cold stress, plants can trigger the expression of genes involved in multiple signal transduction pathways and further activate downstream regulatory processes related to physiological adaptation. Cold stress generates downstream responses in plants by modifying membrane flow in plant cells (Orvar et al., 2000). Important processes, such as nutrient and ion transport, solute uptake, and osmotic pressure, are affected by the properties of cell membranes, particularly their structure and composition, proper membrane fluidity is necessary to maintain the structure and function of the membrane (Valerica Raicu, 2008). According to our studies, there were 463 DEGs related to membrane composition altered in various tissues (101, 367, and 64 in the leaves, roots, and stems, respectively), among which 69 were up-regulated in the leaves, 46 in the roots, and 27 in the stems. This finding suggests that different tissues of *K. obovata* seedlings respond differently to cold stress. The membrane fluidity increases in the leaves but decreases in the roots and stems. Changes in membrane fatty acid composition and content can affect membrane fluidity, thereby influencing the adaptation of *K. obovata* seedlings to cold stress (Zhao et al., 2012). Membrane fluidity initiates cold signaling by affecting the transport of ions and metabolites (Jeon and Kim, 2013). Ion transport mainly affects Ca^{2+} ions released from apoplastic, endomembrane systems, and organelles, and CIPK acts as a Ca^{2+} ions sensor in response to elevated cellular solute Ca^{2+} levels (Tähtiharju et al., 1997). Under cold stress, four genes associated with Ca^{2+} signaling were found in *K. obovata* seedlings, consistent with the expected role of Ca^{2+} in early cold signaling. The results are in line with Su's findings in his study of adult hardiness (Su et al., 2019). Ca^{2+} induces intracellular biochemical responses through sensing and transduction of downstream CDPKs, thereby regulating plant responses to various abiotic stress signals (Boudsocq and Sheen, 2013). CBL is a specific calcium sensor with non-classical EF-hand domains that can capture calcium signals in different plant species, including *Arabidopsis* (Ma X. et al., 2022). These CBLs/SCaBPs do not have enzymatic activity of their own, but CBLs are triggered by changes in Ca^{2+} characteristics and interact precisely with CIPK (CBL-interacting protein kinase) or SOS2 protein kinase (Ma X. et al., 2022). Increasing lines of evidence indicate that the CBL-CIPK network plays a key role in cold stress response. In the present study, one CDPK, twoCMLs, three CBLs, and three CIPKswere found to be up-regulated, indicating the critical function of Ca^{2+}-mediated signaling pathways in the response of *K. obovata* seedlings to cold stress.

4.2 Metabolic pathways involved in cold stress

Plants produce metabolites to adapt to a stressful, changing growing environment, which may involve interactions through signaling processes and pathways (Edreva et al., 2008). In the present study, the term "regulation of secondary metabolic processes" was a rich category in GO classification. The results of the KEGG pathway enrichment analysis showed that starch and sucrose metabolism, amino saccharide, and nucleotide sugar metabolism were enriched in different tissues. Plant responses to cold stress include sucrose accumulation due to the induction of sucrose phosphate synthase and sucrose catabolic enzymes (convertases and sucrose synthases) (Coleman et al., 2009). Moreover, nucleotide sugars are key intermediates in the starch and sucrose biosynthesis pathways (Coleman et al., 2009; Figueroa et al., 2021). At low temperatures, starch hydrolyzes into soluble sugars (sucrose), improving the osmotic pressure in cells and preventing protoplasm from dehydration and solidification. Dissolution of sucrose increases the concentration of the cell fluid, reducing the freezing point, avoiding the possibility of protein precipitation and solidification and salting, and simultaneously increasing the cell's structural stability (Sun et al.,

2015). We found the enrichment of metabolic pathways for starch and sucrose metabolism as well as amino and nucleotide sugars in the stems and roots. These metabolic pathways are significantly enriched in cold-domesticated *K. obovata* and play an important role in its resistance to cold stress.

4.3 Transcription factors involved in the cold stress response

To resist and adapt to cold stress, plants form complex and efficient regulatory networks, with transcriptional regulation playing a key role. Transcription factors regulate gene expression by binding to cis-acting elements in the promoter region and have an important function in the plant abiotic stress response network (Wang et al., 2020). Furthermore, TFs highlight the role of multiple transcriptional mechanisms in stress signaling pathways and are linked to the regulation of various abiotic stress signals and gene transcription (Shanker and Venkateswarlu, 2011). Many TF families, including AP2/EREBP, bHLH, WRKY, MYB, NAC, and MYC, coordinate the signals transduced by plants in response to different environmental stresses (Liu et al., 2014). According to our results, the largest TF families induced by cold stress are AP2-ERF and bHLH, which consist of 20 members, respectively. AP2-ERF and bHLH-TFs are involved in a variety of physiological processes, and overexpression of AP2/ERF in red pine and PtrbHLH in lemon and tobacco can enhance the cold tolerance of plants at freezing temperatures (Huang et al., 2013; Wang et al., 2020). According to Hajar's research results, the expression level of plant AP2/ERF transcription factors in roots was higher than that in stems and leaves under cold stress, which is similar to our research results (Alberts, 2015). WRKY is the largest TF family in plants, and it controls plant growth and development and plays a critical part in many stress responses. NAC is a class of transcription factors that are unique to plants.It is involved in various cold stress regulatory pathways, particularly ABA-dependent signaling pathways, which interact with the gibberellin and Auxin signaling pathways and control lateral root development (Nakashima et al., 2012; Wang et al., 2018). Since the samples we collected were seedlings, the over-expression of WRKY and NAC transcription factors in the roots might improve the plant's cold tolerance and promote root development (Du Z. et al., 2022; Fei et al., 2022; Sun et al., 2022). Cold stress in plants first damages the structure of the cell membrane, thus affecting its function of the cell membrane. C2H2-ZF transcription factors can enhance the ability of plants to resist cold stress by maintaining the stability of cell membranes (Ma L. et al., 2022). At the same time, C2H2-ZF transcription factors contain cis-elements related to plant hormones or abiotic stress, which are involved in tissue and organ development, especially root and flower (Liu et al., 2015). Therefore, C2H2-ZF transcription factors were highly enriched in roots. Other TFs, including DEGs of the GRAS, bZIP, MYB, and WHSF families, also respond to cold stress in *K. obovata* seedlings. Hence, these TFs may be essential regulators that drive downstream gene expression cascades.

4.4 CBL-CIPK network and MAPK cascade involved in cold stress response

The MAPK cascade is a crucial plant response to abiotic stress. The MAPK1-MKK4/5-MAPK3/6 module of *Arabidopsis thaliana* was the first MAPK signaling module identified in a plant. It mediates the transcriptional up-regulation of genes encoding transcription factors WRKY22 and WRKY29 in response to fungal and bacterial pathogen assault (Asai et al., 2002; Galletti et al., 2011). The MKK4/5-MAPK3/6, MKK1-MAPK3/6, and MKK6-MAPK4 modules are key players in plant response to cold stress (Wang et al., 2021). We identified 13 genes in the CBL-CIPK network and MAPK cascade signaling module of *K. obovata* seedlings and investigated their relevance under cold stress. When subjected to cold stress conditions, MEKK1-MKK2-MPK4 confers cold sensitivity and freezing tolerance in *K. obovata* seedlings (Zhao et al., 2017). Low temperatures change the fluidity of the cell membrane, which Ca^{2+} channels and proteins can sense on the membrane. The calcium response protein and MAPK cascade genes are then activated, leading to downstream modulation of genes that regulate the low-temperature response (Zhao et al., 2017). MAPK contains a group of tertiary phosphorylation-dependent kinases: MEKK or MKKK, MEK or Mkk, and MPK. The MAPK cascade activates and mediates signals from the cell membrane to the nucleus, regulating physiological activity (Furuya et al., 2013). When *K. obovata* seedlings are exposed to cold stress conditions, ca2+/cams regulate the activity of receptor-like kinases (CRLK1 and CRLK2) and phosphorylates MEKK1, thereby activating the MeKK1-MKK2-MPK4 cascade. Activated MEKK1-MKK2-MPK4 inhibits the protein abundance and kinase activity of Mpk3 and MPK6, actively modulating the hypothermia response, inhibiting cold-mediated activation, and enhancing the cold resistance of plants. (Furuya et al., 2013; Zhao et al., 2017).

5 Conclusion

Mangroves are an important component of the wetland ecosystem. *Kandelia. obovata*, as one of the cold-resistant mangrove species, will experience more severe extreme low temperatures as it moves north. We compared gene expression differences in three tissues of *K. obovata* seedlings before and after cold snaps and found 1,560, 370, and 416 DEGs in the roots, stems, and leaves, respectively. The gene expression strategies of *K. obovata* seedlings in response to winter cold snaps are summarized as follows: (1)In regulating transcription factors in various tissues, AP2-ERF, NAC, and C2H2 are the most involved transcription factor families in the cold stress response. In addition, bHLH, WRKY, GRAS, bZIP, MYB, and WHSF also participate in the cold stress response. (2)The fluidity of cell membranes in different seedling tissues varies in response to cold pressure, being faster in leaves and slower in roots and stems. Changes in the membrane composition affect Ca^{2+} ion transport and, therefore, the CBL-CIPK network. Moreover, (3) the upregulation of secondary metabolism-related genes resulted in the accumulation of starch

and sucrose in a seedling's root and stem tissues. In *K. obovata* seedlings, 13 cold stress-responsive CBL-CIPK network and MAPK cascade genes were identified and used to construct a paired co-expression network model. The findings provide insights into molecular regulatory mechanisms governing the cold stress response of *K. obovata* seedlings. This study can be used as an empirical reference for further research into the CBL-CIPK network and MAPK cascade in plants.

Data availability statement

The data presented in the study are deposited in the NCBI repository, accession number PRJNA927281. https://www.ncbi.nlm.nih.gov/sra/PRJNA927281.

Author contributions

KT, and QL: conceptualization, investigation, validation, data analysis, methodology, and visualization, writing-original draft. XZ, PC, SX, HG, and YW: conceptualization, experiment design, reviewing and revising the manuscript. WL: collection of samples, funding acquisition. All authors contributed to the article and approved the submitted version.

Funding

This research was supported by Zhejiang Provincial Natural Science Foundation of China under Grant NO. LGN18D060001, LGN20C190002.

Acknowledgments

We thank Dr. Zhiqiang Han for his writing guidance on this manuscript. Dr. Zhiqiang Han and multiple reviewers were especially helpful in shaping this manuscript.

Conflict of interest

The authors declare that the research was conducted in the absence of any commercial or financial relationships that could be construed as a potential conflict of interest.

Publisher's note

All claims expressed in this article are solely those of the authors and do not necessarily represent those of their affiliated organizations, or those of the publisher, the editors and the reviewers. Any product that may be evaluated in this article, or claim that may be made by its manufacturer, is not guaranteed or endorsed by the publisher.

Supplementary material

The Supplementary Material for this article can be found online at: https://www.frontiersin.org/articles/10.3389/fmars.2023.1113278/full#supplementary-material

References

Alberts, B. (2015). *Molecular biology of the cell, sixth edition* (W.W. Norton & Company), 131–135. doi: 10.1201/9781315735368/molecular-biology-cell-bruce-alberts

Asai, T., Tena, G., Plotnikova, J., Willmann, M. R., Chiu, W. L., Gomez-Gomez, L., et al. (2002). MAP kinase signalling cascade in arabidopsis innate immunity. *Nature* 415, 977–983. doi: 10.1038/415977a

Batistic, O., and Kudla, J. (2004). Integration and channeling of calcium signaling through the CBL calcium sensor/CIPK protein kinase network. *Planta* 219, 915–924. doi: 10.1007/s00425-004-1333-3

Boudsocq, M., and Sheen, J. (2013). CDPKs in immune and stress signaling. *Trends Plant Sci.* 18, 30–40. doi: 10.1016/j.tplants.2012.08.008

Buchwal, A., Sullivan, P. F., Macias-Fauria, M., Post, E., Myers-Smith, I. H., Stroeve, J. C., et al (2020). Divergence of *Arctic shrub* growth associated with sea ice decline. *Proc. Natl. Acad. Sci. U. S. A.* 117, 33334–33344. doi: 10.1073/pnas.2013311117

Cavanaugh, K. C., Kellner, J. R., Forde, A. J., Gruner, D. S., Parker, J. D., Rodriguez, W., et al (2014). Poleward expansion of mangroves is a threshold response to decreased frequency of extreme cold events. *Proc. Natl. Acad. Sci. U. S. A.* 111, 723–727. doi: 10.1073/pnas.1315800111

Cavanaugh, K. C., Parker, J. D., Cook-Patton, S. C., Feller, I. C., Williams, A. P., and Kellner, J. R. (2015). Integrating physiological threshold experiments with climate modeling to project mangrove species' range expansion. *Global Change Biol.* 21, 1928–1938. doi: 10.1111/gcb.12843

Chen, Y., Chen, L., Sun, X. M., Kou, S., Liu, T. T., Dong, J. K., et al. (2022). The mitogen-activated protein kinase kinase MKK2 positively regulates constitutive cold resistance in the potato. *Environ. Exp. Botany* 194, 10. doi: 10.1002/ecs2.1865

Chen, L. Z., Wang, W. Q., LI, Q. S. Q., Zhang, Y. H., Yang, S. C., Osland, M. J., et al. (2017). Mangrove species' responses to winter air temperature extremes in China. *Ecosphere* 8, 14. doi: 10.1002/ecs2.1865

Coldren, G. A., and Proffitt, C. E. (2017). Mangrove seedling freeze tolerance depends on salt marsh presence, species, salinity, and age. *Hydrobiologia* 803, 159–171. doi: 10.1007/s10750-017-3175-6

Coleman, H. D., Yan, J., and Mansfield, S. D. (2009). Sucrose synthase affects carbon partitioning to increase cellulose production and altered cell wall ultrastructure. *Proc. Natl. Acad. Sci. U. S. A.* 106, 13118–13123. doi: 10.1073/pnas.0900188106

Du, Z., You, S., Yang, D., Tao, Y., Zhu, Y., Sun, W., et al (2022). Comprehensive analysis of the NAC transcription factor gene family in *Kandelia obovata* reveals potential members related to chilling tolerance. *Front. Plant Sci.* 13. doi: 10.3389/fpls.2022.1048822

Du, Z. K., You, S. X., Zhao, X., Xiong, L. H., and Li, J. M. (2022). Genome-wide identification of WRKY genes and their responses to chilling stress in *Kandelia obovata*. *Front. Genet.* 13. doi: 10.3389/fgene.2022.875316

Edreva, A., Velikova, V., Tsonev, T., Dagnon, S., Gurel, A., Aktas, L., et al. (2008). Stress protective role of secondary metabolite: Diversity of functions and mechanisms. *Gen. Appl. Plant Physiol.* Special issue, 34 (1-2), 67–78. Available at: https://www.researchgate.net/publication/251847574.

Fei, J., Wang, Y. S., Cheng, H., Su, Y. B., Zhong, Y. J., and Zheng, L. (2021a). Cloning and characterization of KoOsmotin from mangrove plant *Kandelia obovata* under cold stress. *BMC Plant Biol.* 21, 12. doi: 10.1186/s12870-020-02746-0

Fei, J., Wang, Y. S., ChenG, H., Su, Y. B., Zhong, Y. J., and Zheng, L. (2022). The *Kandelia obovata* transcription factor KoWRKY40 enhances cold tolerance in transgenic arabidopsis. *BMC Plant Biol.* 22, 15. doi: 10.1186/s12870-022-03661-2

Fei, J., Wang, Y. S., Cheng, H., Sun, F. L., and Sun, C. C. (2021b). Comparative physiological and proteomic analyses of mangrove plant *Kandelia obovata* under cold stress. *Ecotoxicology* 30, 1826–1840. doi: 10.1007/s10646-021-02483-6

Fei, J., Wang, Y. S., Zhou, Q., and Gu, J. D. (2015). Cloning and expression analysis of HSP70 gene from mangrove plant *Kandelia obovata* under cold stress. *Ecotoxicology* 24, 1677–1685. doi: 10.1007/s10646-015-1484-y

Figueroa, C. M., Lunn, J. E., and Iglesias, A. A. (2021). Nucleotide-sugar metabolism in plants: the legacy of Luis f. leloir. *J. Exp. Botany* 72, 4053–4067. doi: 10.1093/jxb/erab109

Florea, L., Song, L., and Salzberg, S. L. (2013). Thousands of exon skipping events differentiate among splicing patterns in sixteen human tissues. *F1000Research* 2, 188. doi: 10.12688/f1000research.2-188.v2

Furuya, T., Matsuoka, D., and Nanmori, T. (2013). Phosphorylation of *Arabidopsis thaliana* MEKK1 *via* Ca^{2+} signaling as a part of the cold stress response. *J. Plant Res.* 126, 833–840. doi: 10.1007/s10265-013-0576-0

Galletti, R., Ferrari, S., and De Lorenzo, G. (2011). Arabidopsis MPK3 and MPK6 play different roles in basal and oligogalacturonide- or flagellin-induced resistance against botrytis cinerea. *Plant Physiol.* 157, 804–814. doi: 10.1104/pp.111.174003

Guo, Z. J., Ma, D. N., LI, J., Wei, M. Y., Zhang, L. D., Zhou, L. C., et al. (2022). Genome-wide identification and characterization of aquaporins in mangrove plant *Kandelia obovata* and its role in response to the intertidal environment. *Plant Cell Environ.* 45, 1698–1718. doi: 10.1111/pce.14286

Guy, C. L. (1990). Cold-acclimation and freezing stress tolerance - role of protein-metabolism. *Annu. Rev. Plant Physiol. Plant Mol. Biol.* 41, 187–223. doi: 10.1146/annurev.pp.41.060190.001155

Huang, X.-S., Wang, W., Zhang, Q., and Liu, J.-H. (2013). A basic helix-Loop-Helix transcription factor, ptrbhlh, of poncirus trifoliata confers cold tolerance and modulates peroxidase-mediated scavenging of hydrogen peroxide. *Plant Physiol.* 162, 1178–1194. doi: 10.1104/pp.112.210740

Jeon, J., and Kim, J. (2013). Cold stress signaling networks in arabidopsis. *J. Plant Biol.* 56, 69–76. doi: 10.1007/s12374-013-0903-y

Kolukisaoglu, U., Weinl, S., Blazevic, D., Batistic, O., and Kudla, J. (2004). Calcium sensors and their interacting protein kinases: Genomics of the arabidopsis and rice CBL-CIPK signaling networks. *Plant Physiol.* 134, 43–58. doi: 10.1104/pp.103.033068

Liu, J. H., Peng, T., and Dai, W. S. (2014). Critical cis-acting elements and interacting transcription factors: Key players associated with abiotic stress responses in plants. *Plant Mol. Biol. Reporter* 32, 303–317. doi: 10.1007/s11105-013-0667-z

Liu, Q., Wang, Z., Xu, X., Zhang, H., and LI, C. (2015). Genome-wide analysis of C2h2 zinc-finger family transcription factors and their responses to abiotic stresses in poplar (*Populus trichocarpa*). *PloS One* 10, e0134753. doi: 10.1371/journal.pone.0134753

Liu, W. C., Zheng, C. F., Chen, J. N., Qiu, J. B., Huang, Z. X., Wang, Q., et al. (2019). Cold acclimation improves photosynthesis by regulating the ascorbate-glutathione cycle in chloroplasts of *Kandelia obovata*. *J. Forest. Res.* 30, 755–765. doi: 10.1007/s11676-018-0791-6

Ma, X., Gai, W. X., Li, Y., Yu, Y. N., Ali, M., and Gong, Z. H. (2022). The CBL-interacting protein kinase CaCIPK13 positively regulates defence mechanisms against cold stress in pepper. *J. Exp. Botany* 73, 1655–1667. doi: 10.1093/jxb/erab505

Ma, L., Xu, J., Tao, X., Wu, J., Wang, W., Pu, Y., et al. (2022). Genome-wide identification of C2H2 ZFPs and functional analysis of BRZAT12 under low-temperature stress in winter rapeseed (*Brassica rapa*). *Int. J. Mol. Sci.* 23 (20), 12218. doi: 10.3390/ijms232012218

Nakashima, K., ITO, Y., and Yamaguchi-Shinozaki, K. (2009). Transcriptional regulatory networks in response to abiotic stresses in arabidopsis and grasses. *Plant Physiol.* 149, 88–95. doi: 10.1104/pp.108.129791

Nakashima, K., Takasaki, H., Mizoi, J., Shinozaki, K., and Yamaguchi-SHinozaki, K. (2012). NAC transcription factors in plant abiotic stress responses. *Biochim. Biophys. Acta* 1819, 97–103. doi: 10.1016/j.bbagrm.2011.10.005

Orvar, B. L., Sangwan, V., Omann, F., and Dhindsa, R. S. (2000). Early steps in cold sensing by plant cells: the role of actin cytoskeleton and membrane fluidity. *Plant J.* 23, 785–794. doi: 10.1046/j.1365-313x.2000.00845.x

Osland, M. J., Day, R. H., From, A. S., Mccoy, M. L., Mcleod, J. L., and Kelleway, J. J. (2015). Life stage influences the resistance and resilience of black mangrove forests to winter climate extremes. *Ecosphere* 6, 15. doi: 10.1890/ES15-00042.1

Osland, M. J., Day, R. H., Hall, C. T., Brumfield, M. D., Dugas, J. L., and Jones, W. R. (2017). Mangrove expansion and contraction at a poleward range limit: climate extremes and land-ocean temperature gradients. *Ecology* 98, 125–137. doi: 10.1002/ecy.1625

Osland, M. J., Enwright, N., Day, R. H., and Doyle, T. W. (2013). Winter climate change and coastal wetland foundation species: salt marshes vs. mangrove forests in the southeastern united states. *Global Change Biol.* 19, 1482–1494. doi: 10.1111/gcb.12126

Peng, Y. L., Wang, Y. S., Fei, J., and Sun, C. C. (2020). Isolation and expression analysis of two novel c-repeat binding factor (CBF) genes involved in plant growth and abiotic stress response in mangrove *Kandelia obovata*. *Ecotoxicology* 29, 718–725. doi: 10.1007/s10646-020-02219-y

Peng, Y. L., Wang, Y. S., Fei, J., Sun, C. C., and Cheng, H. (2015). Ecophysiological differences between three mangrove seedlings (*Kandelia obovata*, aegiceras corniculatum, and avicennia marina) exposed to chilling stress. *Ecotoxicology* 24, 1722–1732. doi: 10.1007/s10646-015-1488-7

Shanker, A. K., and Venkateswarlu, B. (2011). Abiotic stress response in plants-physiological, biochemical and genetic perspectives. London, UK: IntechOpen. *Abiotic Biotic Stress Response Crosstalk Plants* 1, 3–26. doi: 10.5772/1762

Shi, Y. T., Ding, Y. L., and Yang, S. H. (2018). Molecular reculation of CBF sicnalinc in colc acclimation. *Trends Plant Sci.* 23, 623–637. doi: 10.1016/j.tplants.2018.04.002

Su, W. Y., Ye, C. T., Zhang, Y. H., Hao, S. Q., and Li, Q. S. Q. (2019). Identification of putative key genes for coastal environments and cold adaptation in mangrove *Kandelia obovata* through transcriptome analysis. *Sci. Total Environ.* 681, 191–201. doi: 10.1016/j.scitotenv.2019.05.127

Sun, Y. M., Liu, L. J., Feng, M. F., Wang, J. H., Cang, ,. J., Li, S., et al. (2015). Research progress of sugar metabolism of plants under cold stress. *J. Northeast Agric. Univ.* 46 (7), 95–102. doi: 10.3969/j.issn.1005-9369.2015.07.015

Sun, M. M., Liu, X., Huang, X. J., Yang, J. J., Qin, P. T., Zhou, H., et al. (2022). Genome-wide identification and expression analysis of the NAC gene family in *Kandelia obovata* , a typical mangrove plant. *Curr. Issues Mol. Biol.* 11, 5622–5637. doi: 10.3390/cimb44110381

Tähtiharju, S., Sangwan, V., Monroy, A. F., Dhindsa, R. S., and Borg, M. (1997). The induction of kin genes in cold-acclimating *Arabidopsis thaliana*. evidence of a role for calcium. *Planta* 203, 442–447. doi: 10.1007/s004250050212

Teige, M., Scheikl, E., Eulgem, T., Doczi, F., Ichimura, K., Shinozaki, K., et al. (2004). The MKK2 pathway mediates cold and salt stress signaling in arabidopsis. *Mol. Cell.* 15, 141–152. doi: 10.1016/j.molcel.2004.06.023

Valerica Raicu, A. P. (2008). "Cell membrane: Structure and physical properties," in *Integrated molecular and cellular biophysics* (Dordrecht: Springer). doi: 10.1007/978-1-4020-8268-9_3

Wang, F., Chen, S., Liang, D. Y., Qu, G. Z., Chen, S., and Zhao, X. Y. (2020). Transcriptomic analyses of *Pinus koraiensis* under different cold stresses. *BMC Genomics* 21, 14. doi: 10.1186/s12864-019-6401-y

Wang, Z., Wan, Y. Y., Meng, X. J., Zhang, X. L., Yao, M. N., Miu, W. J., et al. (2021). Genome-wide identification and analysis of MKK and MAPK gene families in brassica species and response to stress in brassica napus. *Int. J. Mol. Sci.* 22, 21. doi: 10.3390/ijms22020544

Wang, W. Q., You, S. Y., Wang, Y. B., Huang, L., and Wang, M. (2011). Influence of frost on nutrient resorption during leaf senescence in a mangrove at its latitudinal limit of distribution. *Plant Soil* 342, 105–115. doi: 10.1007/s11104-010-0672-z

Wang, Z., Yu, D., Zheng, C., Wang, Y., Cai, L., Guo, J., et al. (2019). Ecophysiological analysis of mangrove seedlings *Kandelia obovata* exposed to natural low temperature at near 30°N. *J. Mar. Sci. Engineering* 7, 292. doi: 10.3390/jmse7090292

Wang, P., Zhao, Y., Li, Z., Hsu, C. C., Liu, X., Fu, L., et al. (2018). Reciprocal regulation of the TOR kinase and ABA receptor balances plant growth and stress response. *Mol. Cell.* 69, 100–112.e6. doi: 10.1016/j.molcel.2017.12.002

Ye, J., Zhang, Y., Cui, H., Liu, J., Wu, Y., Cheng, Y., et al. (2018). WEGO 2.0: a web tool for analyzing and plotting GO annotations 2018 update. *Nucleic Acids Res.* 46, W71–W75. doi: 10.1093/nar/gky400

Zhao, Z. G., Tan, L. L., Dang, C. Y., Zhang, H., Wu, Q. B., and An, L. Z. (2012). Deep-sequencing transcriptome analysis of chilling tolerance mechanisms of a subnival alpine plant, *Chorispora bungeana*. *BMC Plant Biol.* 12, 17. doi: 10.1186/1471-2229-12-222

Zhao, C. Z., Wang, P. C., Si, T., Hsu, C. C., Wang, L., Zayed, O., et al. (2017). MAP kinase cascades regulate the cold response by modulating ICE1 protein stability. *Dev. Cell.* 43, 618–629. doi: 10.1016/j.devcel.2017.09.024

Zheng, Y., Jiao, C., Sun, H. H., Rosli, H. G., Pombo, M. A., Zhang, P. F., et al. (2016). iTAK: A program for genome-wide prediction and classification of plant transcription factors, transcriptional regulators, and protein kinases. *Mol. Plant* 9, 1667–1670. doi: 10.1016/j.molp.2016.09.014

Zheng, C., Ye, Y., Liu, W., Tang, J., Zhang, C., Qiu, J., et al. (2016). Recovery of photosynthesis, sucrose metabolism, and proteolytic enzymes in *Kandelia obovata* from rare cold events in the northernmost mangrove, China. *Ecol. Processes* 5, 9. doi: 10.1186/s13717-016-0047-3

frontiers | Frontiers in Ecology and Evolution

TYPE Original Research
PUBLISHED 03 March 2023
DOI 10.3389/fevo.2023.1125134

OPEN ACCESS

EDITED BY
Vera Maria Fonseca Almeida-Val,
National Institute of Amazonian Research (INPA), Brazil

REVIEWED BY
Richelle Li Tanner,
Chapman University,
United States
Luciana Fé,
Fundação de Vigilância em Saúde–Dra. Rosemary Costa Pinto (FVS-RCP), Brazil

*CORRESPONDENCE
Christelle Leung
✉ christelle.leung@dfo-mpo.gc.ca
Geneviève J. Parent
✉ geneviève.parent@dfo-mpo.gc.ca

SPECIALTY SECTION
This article was submitted to Ecophysiology, a section of the journal Frontiers in Ecology and Evolution

RECEIVED 15 December 2022
ACCEPTED 13 February 2023
PUBLISHED 03 March 2023

CITATION
Leung C, Guscelli E, Chabot D, Bourret A, Calosi P and Parent GJ (2023) The lack of genetic variation underlying thermal transcriptomic plasticity suggests limited adaptability of the Northern shrimp, *Pandalus borealis*.
Front. Ecol. Evol. 11:1125134.
doi: 10.3389/fevo.2023.1125134

The lack of genetic variation underlying thermal transcriptomic plasticity suggests limited adaptability of the Northern shrimp, *Pandalus borealis*

Christelle Leung[1]*, Ella Guscelli[2], Denis Chabot[3], Audrey Bourret[1], Piero Calosi[2] and Geneviève J. Parent[1]*

[1]Laboratory of Genomics, Maurice Lamontagne Institute, Fisheries and Oceans Canada, Mont-Joli, QC, Canada, [2]Marine Ecological and Evolutionary Physiology Laboratory, Département de Biologie, Chimie et Géographie, Université du Québec à Rimouski, Rimouski, QC, Canada, [3]Maurice Lamontagne Institute, Fisheries and Oceans Canada, Mont-Joli, QC, Canada

Introduction: Genetic variation underlies the populations' potential to adapt to and persist in a changing environment, while phenotypic plasticity can play a key role in buffering the negative impacts of such change at the individual level.

Methods: We investigated the role of genetic variation in the thermal response of the northern shrimp *Pandalus borealis*, an ectotherm species distributed in the Arctic and North Atlantic Oceans. More specifically, we estimated the proportion transcriptomic responses explained by genetic variance of female shrimp from three origins after 30 days of exposure to three temperature treatments.

Results: We characterized the *P. borealis* transcriptome (170,377 transcripts, of which 27.48% were functionally annotated) and then detected a total of 1,607 and 907 differentially expressed transcripts between temperatures and origins, respectively. Shrimp from different origins displayed high but similar level of transcriptomic plasticity in response to elevated temperatures. Differences in transcript expression among origins were not correlated to population genetic differentiation or diversity but to environmental conditions at origin during sampling.

Discussion: The lack of genetic variation explaining thermal plasticity suggests limited adaptability in this species' response to future environmental changes. These results together with higher mortality observed at the highest temperature indicate that the thermal niche of *P. borealis* will likely be restricted to higher latitudes in the future. This prediction concurs with current decreases in abundance observed at the southern edge of this species geographical distribution, as it is for other cold-adapted crustaceans.

KEYWORDS

phenotypic plasticity, climate change, ocean warming, crustacean, decapod, fisheries, RNA-seq

1. Introduction

Increasing temperature is one major manifestation of global changes. To cope with increasing temperatures, some species may shift their distribution tracking their thermal niche, while others may persist in their local habitat (Perry et al., 2005; Lima et al., 2007;

Bonebrake et al., 2018). Predicting a species' ability to cope with global changes requires attaining an in-depth critical understanding of the mechanisms underpinning acclimatization and adaptation allowing species to persist and thrive in changing environments (Román-Palacios and Wiens, 2020). Acclimatization relies on phenotypic plasticity, the capacity of a given genotype to change its phenotypes according to the environment (Levins, 1963; Bradshaw, 1965). Phenotypic plasticity can act as a buffer for the negative effect of environmental changes on the performance and fitness of organisms (Ghalambor et al., 2007). Phenotypic plasticity is adaptive in environments that change predictably, i.e., when the cues for the development of a phenotype are reliable (Gavrilets and Scheiner, 1993; Reed et al., 2010; Scheiner and Holt, 2012). It represents a key mechanism for individuals and populations to persist in changing environments, and ultimately influencing both population dynamics and extinction risk (Reed et al., 2010; Ashander et al., 2016; Rescan et al., 2020).

Global changes are characterized by increased mean temperature, amplified environmental variation, and greater frequency and intensity of extreme thermal events (Alley, 2000; Rahmstorf and Coumou, 2011; Hobday et al., 2016; IPCC, 2022). These phenomena result in increasing environmental unpredictability and new selection horizons for living organisms. Under unpredictable changes, the reliability of environmental cues required to trigger the development of a given phenotype will diminish. In those conditions, phenotypic plasticity may be maladaptive, favorizing the evolution toward alternative strategies (Gavrilets and Scheiner, 1993; Reed et al., 2010; Scheiner and Holt, 2012; Tufto, 2015; Dey et al., 2016; Leung et al., 2020). For instance, individuals from multiple populations may evolve to a single phenotype that represents the optimal compromise among environmental conditions (e.g., Scheiner and Yampolsky, 1998). The lack of variation in plasticity levels may have for consequence to reduce the potential for evolutionary responses to climate changes (Oostra et al., 2018). Characterizing a species plasticity to temperature and the genetic variation underpinning these responses may help to predict a species' vulnerability to global changes (Landy et al., 2020).

Genomic tools can help to improve prediction of organisms' response to global changes by disentangling the molecular mechanisms involved in acclimatization and adaptation (De Wit et al., 2016; Kelly, 2019; Waldvogel et al., 2020). Gene expression is considered as a molecular phenotype to study phenotypic plasticity (Aubin-Horth and Renn, 2009; Pavey et al., 2010). Changes in gene expression underly phenotypic plasticity, as most changes in mRNA expression are associated with changes in protein production and abundance. It is shaped by both environmental and genetic components and evolves in response to selective pressures (Gerken et al., 2015; Leder et al., 2015). Alternatively, genome sequencing allows the inference of the evolutionary potential of a population, by characterizing and contrasting genetic compositions. Higher levels of genetic variation across a species distribution usually enable greater levels of phenotypic variation (Hansen, 2006), and a higher capacity of a species to undergo further adaptation *via* natural selection (Fisher, 1930; Hughes et al., 2008). Combined, these genomics tools help shedding light on the role of phenotypic plasticity and its genetic variation in the mechanisms of species' responses to global changes.

Marine ectotherms are models of choice to understand the role of phenotypic plasticity and genetic variation in a species vulnerability to global changes (Huey et al., 2012; Paaijmans et al., 2013; Seebacher et al., 2014; Pinsky et al., 2019). In fact, ectotherms are particularly sensitive to temperature fluctuations due to their limited ability to use metabolic heat and maintain their body temperature (Angilletta, 2009). The adjustment of their body temperature to environmental conditions is therefore usually coupled with physiological and behavioral plasticity (Huey and Stevenson, 1979; Stevenson, 1985; Amarasekare and Savage, 2012; Abram et al., 2017). However, the level of plasticity varies largely among ectotherms (e.g., Somero, 2005, 2010; Logan et al., 2015).

The northern shrimp *Pandalus borealis* (Krøyer, 1838) is a circumboreal species distributed in the colder regions of North Atlantic Ocean. Adults and juveniles experience temperatures ranging from−1.7 to 11.1°C but are found to be most abundant between 0 and 5°C in the northwest Atlantic (Allen, 1959; Haynes and Wigley, 1969; Shumway et al., 1985; Garcia, 2007). Previous studies have shown that *P. borealis* is sensitive to increasing temperature, resulting in reduced survival, lowered recruitment, increased growth and metabolism rates (Chabot and Ouellet, 2005; Ouellet and Chabot, 2005; Daoud et al., 2007, 2010; Richards, 2012; Arnberg et al., 2013; Dupont-Prinet et al., 2013; Chemel et al., 2020). As a consequence, an important reduction in abundance has been observed over the last decade in the species southern distribution (Apollonio et al., 1986; Koeller, 2000; DFO, 2021, 2022; Richards and Hunter, 2021). This together with the high economic value of the species highlight the urgency of understanding the vulnerability of the northern shrimp to increasing temperatures of populations at higher latitudes.

In this study, we investigated the effect of elevated temperature to shed light on the molecular mechanisms underlying thermal plasticity in *P. borealis* and predict its vulnerability to ocean warming. We hypothesize a high level of transcriptomic plasticity in the northern shrimp in response to temperature, as an adaptation to the predictable variation of temperature that the species encounters on an annual or a life-cycle basis (Koeller et al., 2009). We thus predicted differences in plasticity among populations from contrasted environments and underlay by genetic variation. To test these hypotheses, we collected shrimp from three origins in a study area in the northwest Atlantic, with one origin close to a steep climatic gradient (Stanley et al., 2018). We exposed shrimp to three temperatures under laboratory conditions, mimicking current conditions, and future ocean warming scenarios. We built a reference transcriptome and identified differentially expressed transcripts (DETs) associated with temperature treatment, shrimp origin, or their interaction. The DETs were grouped in modules of expression profiles and their functions were explored to understand the molecular mechanisms underlying response to temperature. We also assessed the standing genetic variation and how it could explain temperature transcriptomic response to clarify the role of acclimatization and adaptation in thermal plasticity of *P. borealis*.

2. Materials and methods

2.1. Specimen collection, transport and experimental design

Female *P. borealis* were collected from three different origins along the northwest Atlantic representing different oceanographic conditions:

St. Lawrence Estuary (SLE), Eastern Scotian Shelf (ESS) and Northeast Newfoundland Coast (NNC) (Figure 1; Supplementary Table S1). Collection, transport and maintenance were conducted as described in Guscelli et al. (*submitted for review*). Briefly, shrimp were collected using a rigid frame trawl (SLE), shrimp traps (ESS), or commercial shrimp trawl (NNC). Supplementary Table S1 provides dates and positions. Live shrimp were transported to the Maurice Lamontagne Institute (MLI) in 750 L tank filled with 2–3°C water. The only long-distance transportation that took place when air temperature was above 5°C (NNC to MLI) used a refrigerated truck. Air bubbling kept water well oxygenated during transport. Upon arrival at MLI, shrimp were transferred into shallow (40–50 cm depth) rectangular tanks (1700 L) filled with sea water at a temperature of 4.5°C, pH of 7.9 (total scale), salinity of 32 PSU (Practical Salinity Unit) and 100% O_2 saturation relative to air. Shrimp were fed *ad libitum* with a mixture of capelin (*Mallotus villosus*, Müller, 1776) and shrimp (*Pandalus* spp.) three times a week prior the beginning of the experiments.

After approximately eight weeks, female shrimp were transferred into experimental tanks kept at 2, 6 or 10°C (two replicate tanks *per* temperature treatment) for 30 days. As this experiment was part of a project also dealing with ocean acidification, all tanks were maintained at a slightly acidified pH, 7.75 (total scale), matching current conditions of the deep waters of the Gulf of St. Lawrence (Mucci et al., 2011, 2018). The coldest temperature, 2°C, represents the temperature where shrimp are most abundant along the Labrador and Newfoundland coast (Orr and Sullivan, 2013) and within the range where most SLE shrimp were found in 2008–2021 (1–5.5°C; DFO, 2022). The intermediate temperature represents a predicted 4°C increase by the end of this century according to the RCP 8.5 scenario (IPCC, 2014) for shrimp living close to 2°C presently, and it is also the current temperature (5–7°C) in the deep waters of the Gulf of St. Lawrence, where shrimp populations are found (Bourdages et al., 2022). The highest temperature, 10°C, represents predicted conditions at the end of the century for populations that are already exposed to 6°C (Lavoie et al., 2020). Dead and moulting individuals were counted daily. Dead individuals were frozen until waste collection according to MLI policy. Shrimp from different origins were exposed to the same experimental conditions but they could not be exposed simultaneously, due to space limitations within the experimental system and also to keep the period between capture and the beginning of the experimentation constant. Consequently, exposure to all the three experimental temperatures occurred in August 2018, April 2019, and December 2019 for shrimp from SLE, ESS, and NNC, respectively. After 30 days of exposure, six randomly chosen individuals (three from each tank) were collected from the experimental system and immediately flash-frozen in liquid nitrogen. Samples were then stored at−80°C until nucleic acid extraction was conducted. The duration of exposure was chosen to mimic northern latitude deep-water temperature fluctuation where intra-seasonal variability occurs at a period of 10–30 days (Fischer et al., 2004). At the end of the experiment, we did not find any differences in shrimp size (cephalothorax length = 23.91 mm, s.d. = 1.50) among temperature ($F_{(2,47)} = 2.097$, $p = 0.134$) or origin ($F_{(2,47)} = 1.845$, $p = 0.169$).

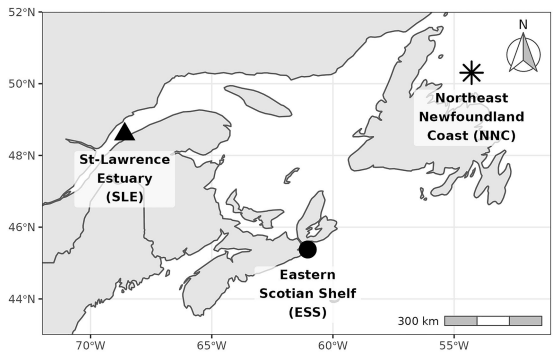

FIGURE 1
Pandalus borealis collection sites. Map of the southeast of Canada with the three geographic locations where shrimp used in this study originated from. Collection conditions are described in Supplementary Table S1.

2.2. DNA/RNA extraction, sequencing and bioinformatics preprocessing

We assessed genetic variation and gene expression levels among individuals by generating ddRAD-sequencing and RNA-sequencing (seq), respectively. Genomic DNA and RNA extraction of the 54 shrimp (three temperature treatments × three origins × six shrimp, combining three from each replicate tank) was carried out on *ca.* 2 g of muscle tissue from shrimp abdomen, using QIAGEN DNeasy Blood & Tissue kit and Qiazol RNA extraction reagent (Qiagen), respectively, following the manufacturer's protocol. Muscle was chosen to ensure enough material was available as input for sequencing, and because this tissue displayed metabolic changes in response to temperature changes in studies of other shrimp species, in addition to be responsible for general locomotion and escape-behavior responses in decapods (e.g., Rosa et al., 2014; Madeira et al., 2020). RNA-seq methodology was selected to investigate the changes in the entire transcriptome, with no *a priori* and less bias manner than selecting specific genes, in addition to displaying more power in revealing gene expression changes that could be difficult to discerned through more targeted approaches.

Preparation of ddRAD-seq libraries for the genomic DNA was carried out by the *Institut de Biologie Intégrative et des Systèmes* (IBIS at Université Laval, Quebec City, QC, Canada) with *PstI* and *MspI* restriction enzymes, and using the procedure described by Poland et al. (2012), with the following exceptions. First, a blue Pippin (SAGE sciences) was used to size libraries before PCR amplification (elution set between 50 and 65 min, on a 2% agarose gel); second, plate barcoding was used to enable sequencing on a shared Illumina NovaSeq 6,000 S4 PE150 lane, as described in Colston-Nepali et al. (2019). The 54 DNA samples were added to a larger pool of samples (total 1858 samples), and split into 20 libraries of 96 samples. Libraries were sequenced at Génome Québec (Montreal, QC, Canada).

For the RNA samples, library construction was performed by Génome Québec, using NEB mRNA stranded library preparation kit. In addition to the 54 libraries (one *per* individual), a supplemental library was constructed from a pool of 120 shrimp exposed in different environmental conditions and from various populations (Supplementary Table S2), to maximize the number of detected genes during *de novo* transcriptome assembly. Finally, high-throughput sequencing steps for all libraries (Illumina NovaSeq 6,000 S4 PE100) were performed by Génome Québec.

For the resulting DNA sequencing dataset, adapters were removed with Trimmomatic v0.39 (Bolger et al., 2014), and three base pairs were removed from the R2 (the *MspI* restriction site) to account for lower quality in the first nucleotides. Demultiplexing and quality filtering were performed with the *process_radtags* module of STACKS v2.4 (Catchen et al., 2013; Rochette et al., 2019), with a truncation at 135 pb and a check for the *PstI* restriction site. Cleaned reads were aligned to a *P. borealis* reference genome (newly assembled by C3G–McGill University, Montreal, QC, Canada) with *mem* from BWA-MEM with default parameters. Aligned paired-end reads were assembled with the *gstacks* modules and only samples with a mean depth of coverage of at least 5× were kept in the analysis. SNPs were first filtered with *populations* module of STACKS to only include SNPs present in all three origins, for at least 75% of individuals and with a minimum minor allele frequency of 5%. Furthermore, SNPs with more than 10% missingness and in Hardy–Weinberg disequilibrium in more than one origin were removed. Only the first SNP by loci was kept to avoid linkage disequilibrium. The ddRAD-seq final dataset consisted of 22,227 SNPs over 54 individuals.

Transcriptome assembly and annotation, and isoform count matrix estimation, were performed by C3G. *De novo* transcriptome assembly was performed following the pipeline described by Haas et al. (2013) and based on the Trinity assembly software suite. In brief, raw reads were trimmed using Trimmomatic from the 3′ end to have a minimum *Phred* score of 30 and a minimum length of 50 bp. Normalization was performed using the Trinity normalization utility v2.0.4 (Haas et al., 2013). An abundance estimate was computed using RNA-Seq by Expectation Maximization (RSEM) v1.2.12 (Li and Dewey, 2011) *via* Trinity *align_and_estimate_abundance.pl* utility. Expected count values from RSEM were used for downstream analysis. Transcripts were annotated with the Trinotate suite v2.0.2 (Haas et al., 2013), based on a homology search to known sequence data (BLAST+/SwissProt/Uniref90), protein domain identification (HMMER/PFAM), protein signal peptide and transmembrane domain prediction (signalP/tmHMM), comparison to currently curated annotation databases (EMBL UniProt eggNOG/GO Pathways databases). Each transcript was aligned against a custom protein database of the Pacific white shrimp *Penaeus vannamei* (Boone, 1931, GenBank: QCYY00000000.1). An annotation was assigned to the longest putative coding transcript based on the best BLAST hit with an associated gene name and an Expect (E) value cut-off $<1e^{-5}$ whenever possible. All of the above described analyzes were performed using the GenPipes pipeline framework [PMID: 31185495].

2.3. Statistical analyzes

All statistical analyzes were carried out using R software, version 4.1.0 (R Core Team, 2020).

2.3.1. Mortality and molting rates

Mortality data used in this study originate from Chemel et al. (2020) and Guscelli et al. (*submitted for review*). We performed an univariate two-ways ANOVA test on arcsin square-root transformed percentage values (Sokal and Rohlf, 1995) to investigate how temperature affected shrimp mortality and molting rates per day, with *Origin* and *Temperature* as fixed factor tested in isolation and combined (*Origin* × *Temperature*). In addition, a Tukey's Honestly Significant Difference (HSD) test was used to conduct *post-hoc* analyzes, when significant effects were detected by the ANOVA.

2.3.2. Differential transcript expression analysis

Variation partitioning of gene expression and differential expression analyzes were performed using the R package *vegan* version 2.6–2 (Oksanen et al., 2022) and the Bioconductor's package DESeq2 version 1.36 (Love et al., 2014). Expected read count values from RSEM were used to identified differentially expressed transcripts (DETs). The count matrix was first pre-filtered to remove every transcripts not or sparsely expressed according to the criterion based on Chen et al. (2016). Briefly, a transcript was considered expressed if it had a count of at least 10–15 in at least some libraries, but basing the filtering on count-per-million (CPM) values so as to avoid favoring genes that are expressed in larger libraries over those expressed in smaller libraries. We used a cutoff = $10/L$ where L is the minimum library size in millions. From the 118,609 identified transcripts, the pre-filtering process retained a total of 39,065 transcripts. To quantify the proportion of the total gene expression variation that was explained by the main factors or their interactions, we applied partial redundancy analyzes (RDA; Borcard et al., 1992), using the normalized count matrix (i.e., applying a variance stabilizing transformation (VST) to the count data, as implemented in DESeq2) as the response variable and the *Origin* and *Temperature* as categorical explanatory factors. Note that the six randomly chosen individuals were combining individuals from two tank replicates. Prior to this variation partitioning, we have tested for the tank effect on gene expression by performing a partial RDA adding tank identity as an explanatory variable.

We also identified any transcripts that showed changes in expression across the same three terms (i.e., *Origin*, *Temperature* and *Origin* × *Temperature* interaction), by building a general linear model, as implemented in DESeq2. Significance of each explanatory factor was assessed by applying a *Likelihood Ratio Test* (LRT) approach, comparing the full model to reduced ones (Love et al., 2014). Transcripts with FDR < 0.001 [value of p after Benjamini-Hochberg (BH) adjustment] were considered as differentially expressed. For all identified DETs, we assessed how expression levels varied across the three temperatures and origins by identifying modules of co-expressed transcripts. Transcripts whose expression profiles were highly correlated were grouped within a given module, using the *WGCNA* version 1.71 (Langfelder and Horvath, 2008). Enriched gene ontology (GO) terms were then identified, using Fisher's exact test as implemented in the *topGO* version 2.48 (Alexa and Rahnenfuhrer, 2022), to assess the functional role of DETs among origins or according to temperature treatment. For each GO term with FDR < 0.05, we calculated the proportion of identified co-expressed module.

2.3.3. Origin effect on gene expression

The origin effect on the measured gene expression could arise from different sources: 1–genetic differences among sampling sites, or 2–environmental conditions in shrimp natural habitat (as individuals were sampled as adults, each of them might express specific genes programmed during their development). We attempted to clarify the role

of these two potential sources of shrimp gene expression by comparing the effect of population genetic variation, and environmental conditions at origins on transcript expression. Genetic variation was assessed using 22,227 SNPs called from ddRAD-seq dataset, and comparing the same 54 individuals as transcriptomic analysis. We assessed intra-population genetic diversity by calculating the expected heterozygosity (H_E) for each origin, using *poppr* version 2.9.3 (Kamvar et al., 2014), and genetic differentiation among collection sites with pairwise F_{ST}, using *dartR* version 2.0.4 (Gruber et al., 2018). Environmental conditions at origins were characterized by monthly mean salinity and temperature for both surface and bottom sea water, obtained from Bedford Institute of Oceanography North Atlantic Model (BNAM) that averaged values over 1990 to 2015 period (Wang et al., 2018) and selected by removing highly correlated variables ($|r| > 0.90$; Supplementary Figure S2). To disentangle the different sources of gene expression that could explain the origin effect, we performed a variation partitioning (Peres-Neto et al., 2006; Legendre, 2008) of the transcriptomic response. This enabled us to assess the proportion of transcript expression explained by the terms *Temperature*, *Environmental conditions at origin* (hereafter *Environment*) and *Genetic Differentiation* (hereafter *Genetics*).

Factors explaining shrimp transcript expression were also determined by a model selection analysis using the function *ordiR2step* from *vegan* R package. We performed a model selection to obtain a parsimonious model maximizing the adjusted R^2 and *p*-value of a constrained ordination (Blanchet et al., 2008). We used the gene expression normalized count matrix as the response variable, and PCoA coordinates from pairwised F_{ST} matrix (for genetic differentiation) and *Environment* as the explanatory variables, in addition to the interaction terms *Temperature* × *Genetics* and *Temperature* × *Environment*, to test for standing genetic variation for plasticity and effect of past environmental memory on gene expression, respectively.

3. Results

3.1. Mortality and molting rates variation

Variation in mortality and molting rates were observed for female *P. borealis* collected from three origins and exposed to 2, 6, or 10°C temperatures. Mean mortality rates increased proportionally with temperature ($F_{2, 9} = 6.917$; $p = 0.015$), independently of origin ($F_{4, 9} = 1.835$; $p = 0.206$). Mean percentages of death *per* day differed between 2°C (0.084 ± 0.009) and 10°C (0.180 ± 0.018; $p < 0.05$) but not with 6°C (0.110 ± 0.023; Figure 2A).

Molting rates varied between 0.00 ± 0.00 (at 2°C in NNC) and 0.022 ± 0.001 (at 10°C in ESS). Mean molting rates differed with increasing temperatures for shrimp from the three origins, as indicated by the presence of an interaction between the terms *Origin* and *Temperature* ($F_{4, 9} = 16.412$; $p < 0.001$; Figure 2B). Shrimp from NNC and SLE displayed no significant changes along the temperature gradient tested, but shrimp from NNC, and not those from SLE, displayed a *quasi*-absence of molt during the whole experiment (Figure 2B). For ESS, molting rate increased with temperature (Figure 2B).

3.2. Reference transcriptome

The reference transcriptome of *P. borealis* was built using RNA from pooled individuals in various physiological conditions and samples from the current study experiment (Supplementary Table S2), maximizing thereby the number of detected genes. We obtained a total of 2.81×10^9 raw paired reads, from which 97.48% remained after the trimming step. The *de novo* assembly resulted in 170,377 transcriptome isoforms that could be grouped into 118,609 components loosely representing genes. Transcript contig length ranged from 224 to 28,419 bp, with a N50 value of 1820 bp.

Functional annotations were performed on homology search to known sequence data based on the protein database of another shrimp species, *P. vannamei*. About 27.48% of the transcripts were successfully annotated to a specific function. Filtration of assembled transcriptome based on the functional annotation resulted in high quality contigs, composed of 46,828 transcript groups into 24,122 genes. Transcripts lengths from this filter assembled transcriptome ranged from 224 bp to 28,419 bp, with a N50 value of 3,049 bp.

3.3. Differential gene expression analysis revealed extensive transcriptomic plasticity

For shrimp collected from the temperature experiment, a total of 39,065 transcripts were expressed at a count greater than 10 reads in at least one sample. Variation partitioning analysis revealed marginal effects of *Temperature* (*adj.* $R^2 = 0.87\%$; $p = 0.015$), *Origin* (*adj.* $R^2 = 1.75\%$; $p = 0.001$) and their interaction (*adj.* $R^2 = 1.34\%$; $p = 0.006$) on gene expression levels. Differential expression analysis detected a higher number of DETs across the temperatures tested ($n = 1{,}607$; 4.11%), than across origins ($n = 907$; 2.32%), and a very low number of significantly DETs were detected for the interaction term ($n = 13$; 0.03%). Ordination plot of distance-based RDA (Figure 3A) showed that the gene expression level gradually changed with increasing temperature (db-RDA 1: 22.50%; $p = 0.001$). In addition, the gene expression level of shrimp from NNC differed markedly from those reported for shrimp from SLE and ESS (db-RDA 2: 20.11%; $p = 0.001$).

The patterns of expression profiles of DETs identified through co-expression module analysis differed between *Temperature* and *Origin* effects. A total of 1,583 (98.51%) and 845 (93.16%) DETs were grouped across temperatures and origins, respectively, into modules of co-expressed transcripts (Figures 3B,C). We identified three and seven modules for DETs across temperatures and origins, respectively (Figures 3B,C). For temperature, gene expression levels increased (module T_2) or decreased (modules T_1 and T_3) linearly with increasing temperature for all three modules identified (Supplementary Figure S1A). For origin, six out of the seven modules identified showed SLE and ESS displaying similar expression levels (modules O_2 and O_7), but differing from those of NNC (Figure 3C).

GO enrichment analyzes revealed that DETs associated with temperature treatments or origins involved distinct functions. For instance, *Temperature* affected the expression of genes belonging to the three ontology categories (i.e., biological processes, cellular components and molecular functions), whereas *Origin* affected the expression of genes associated only to cellular components and molecular functions (Supplementary Figure S1A).

For biological processes affected by temperature, a large proportion of transcripts belonging to the largest module, T_1, involved catabolic activities (88.47%, s.d. 2.76%; Supplementary Figure S1B), where catabolic activities mostly decreased with increasing temperatures. In contrast, the gene

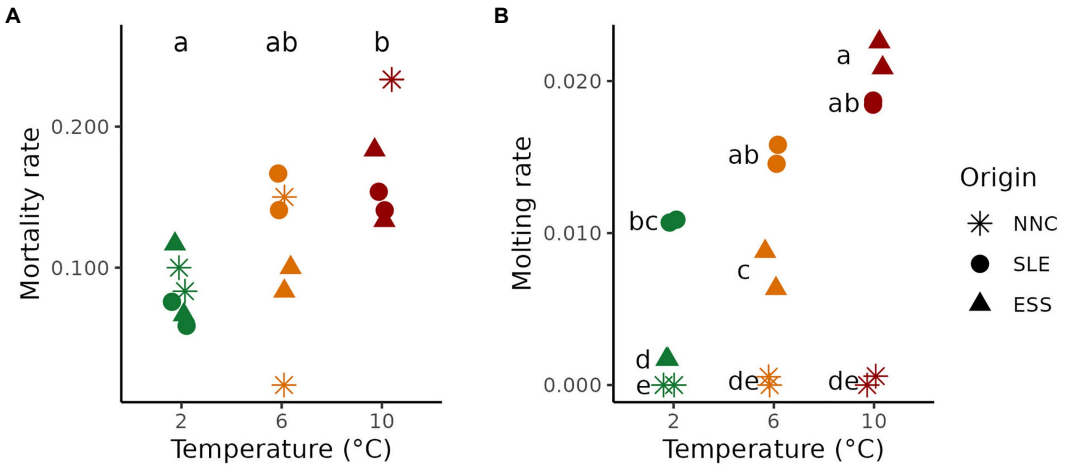

FIGURE 2
Pandalus borealis mortality and molting rates as function of Temperature and Origin. **(A)** Mortality rate at each treatment temperature (green, orange and red for 2, 6 and 10°C, respectively) for shrimp from different origins (shape). **(B)** Molting rate at each treatment temperature for shrimp from different origins. The results of Tukey HSD *post hoc* test are displayed as letters, with different letters representing a significant difference between means ($p<0.05$). ESS=Eastern Scotian Shelf, SLE=St. Lawrence Estuary, NNC=Northeast Newfoundland Coast. Both replicate tanks for each treatment are shown.

expression of module T_2 increased with increasing temperatures. This module has a larger proportion of genes involved in metabolic activities (30.27%, s.d. 2.81%; Supplementary Figure S1B) compared to those involved in catabolic activities (11.53%, s.d. 2.76%; Supplementary Figure S1B).

In terms of cellular components, transcripts associated to protein, catalytic and channel complexes were mostly downregulated with increasing temperature whereas those involved in cell structures, such as actin and myosin, differed significantly among shrimp from different origins. Most cellular components associated with DETs across shrimp origins were part of module O_1 with the expression of these specific transcripts being higher in shrimp from ESS and progressively lower in shrimp from SLE and from NNC (Supplementary Figure S1B), except extracellular functions. These latter functions were represented by up to five modules characterized by similar expression levels for shrimp from ESS and SLE, which were different from NNC. Some DETs with extracellular functions were associated with cytoskeleton and non-membrane-bounded organelle. In terms of molecular functions, *Temperature* modified the expression of genes associated with nucleic and amino acid activities, whereas *Origin* involved DETs associated with structural activities. For temperature, transcripts associated with threonine related activities decreased with increasing temperature.

3.4. Identifying factors affecting *Pandalus borealis* transcriptomic plasticity

3.4.1. Genetics differences among origins

Shrimp displayed genetic differences among origins. Individuals from SLE had lower genetic diversity compared to shrimp from NNC and ESS (Tukey HSD, $p<0.001$; Figure 4A) but differences in gene diversities were small (H_E ranging from 0.215 to 0.223). No genetic differentiation was detected between NNC and SLE ($F_{ST}=0$, $p=0.940$), whereas ESS was differentiated from the two other origins ($F_{ST}>0.003$, $p<0.001$; Figure 4B).

3.4.2. Environmental conditions at origins

Environmental conditions at origins (hereafter *Environment*) were contrasted. We used only the January and July bottom temperatures since these two variables characterized female shrimp habitat and were not strongly correlated ($r=0.32$), unlike other variables (Supplementary Figure S2 and see method section for more details about variables selection). The NCC origin had the most different environmental conditions (Euclidean distance with SLE and ESS > 4.04) compared to SLE and ESS, which were more similar (Euclidean distance between SLE and ESS = 2.93). The origin NNC was characterized by cold temperatures compared to ESS and SLE (Figure 5).

3.4.3. Temperature treatment and environmental conditions at origin affected *Pandalus borealis* plasticity but not genetic differentiation

We did not detect any tank effect on gene expression (partial RDA analysis; adjusted $R^2=0.047\%$; $p=0.429$), and consequently tank identity was not taken into account in the subsequent analyzes. A variation partitioning analysis identified marginal effects of *Temperature* (*adj.* $R^2=2.98\%$; $p=0.001$) and *Environment* (*adj.* $R^2=2.22\%$; $p=0.001$) explaining transcript expression levels (Figure 6). However, genetic differentiation among origins did not explain transcript expression levels (Figure 6). In addition, model selection retained *Temperature*, *Environment* and the *Temperature* × *Environment* as terms explaining transcript expression (Table 1). The terms *Genetics* and the interaction between *Temperature* and *Genetics* were not selected.

4. Discussion

Understanding the molecular mechanisms underlying ectotherms' responses to elevated temperature is paramount to improve our ability to predict their vulnerability to the ongoing global change. Genomic tools can help to improve prediction of organisms' response to changing environments. In this study, we provides a first reference transcriptome of

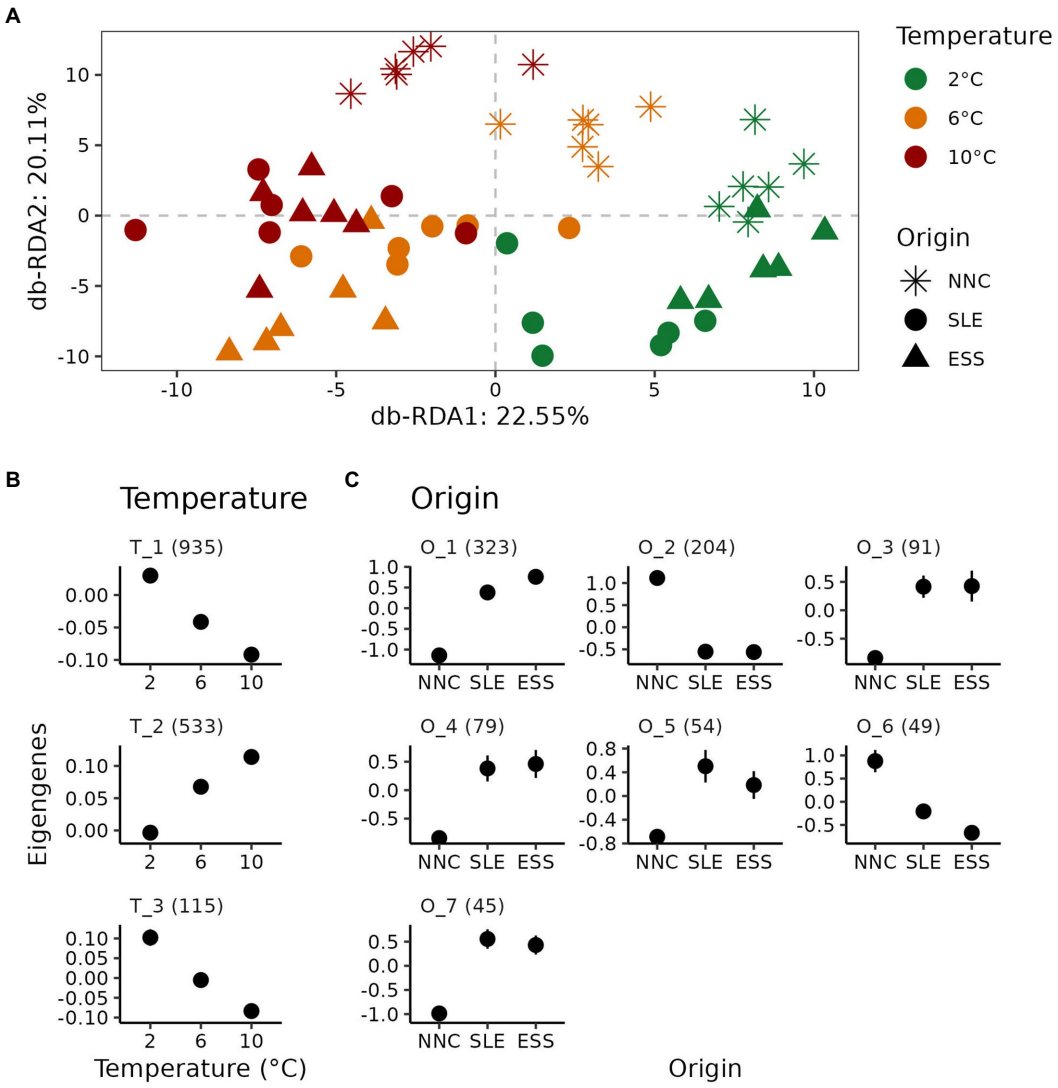

FIGURE 3
Gene expression response to temperature exposure of *P. borealis* shrimp from three different origins. **(A)** Variation of gene expression levels. Distance-based redundancy analysis (db-RDA) plot performed on gene expression levels according to origins (shapes) and temperature treatments (colors). **(B,C)** Relative expression level for each co-expression modules for differentially expressed transcripts (DETs) among temperatures (T) and origins (O), respectively. Means with their standard errors are represented as dots and error bars, respectively. Numbers in parentheses indicate the number of transcripts belonging to each co-expression module.

an important marine ectotherm species, *Pandalus borealis*. Using this new resource, we showed that changes in transcript levels are mainly explained by temperature exposure and environmental conditions at origin. The lack of genetics or genetics-by-temperature interaction effects on transcript expression levels suggested limited evolutionary potential in the species' transcriptomic plasticity in response to temperature changes.

4.1. Temperature drove transcriptomic plasticity

Our results showed that *P. borealis* displays a high level of plasticity in gene expression with changing temperatures. The observed transcriptomic response supports the hypothesis that this species possesses an elevated degree of plasticity to cope with the temperature variation it could encounter throughout its life-time. Temperature-mediated gene expression changes have been reported in several ectotherm species (e.g., Gleason and Burton, 2015; Veilleux et al., 2015; Oostra et al., 2018; Sirovy et al., 2021; Valenza-Troubat et al., 2022). Our results are also in agreement with previous studies showing physiological responses of *P. borealis* to temperature, including changes in cellular energetic metabolism, and metabolic and growth rates (Chabot and Ouellet, 2005; Ouellet and Chabot, 2005; Arnberg et al., 2013; Dupont-Prinet et al., 2013; Chemel et al., 2020).

The linear transcriptomic response we reported across the three temperatures suggests that the northern shrimp can cope with increasing temperatures up to 10°C, at least within 30 days of exposure. This result confirms the suggestion that the temperature levels used for the plasticity assay were within the northern shrimp range of thermal tolerance (Chabot et al., 2013; Guscelli et al. *submitted for review*). However, the greater mortality observed at 10°C compared to 2°C (10%) supports the idea that the highest temperature level used in this study is close to the

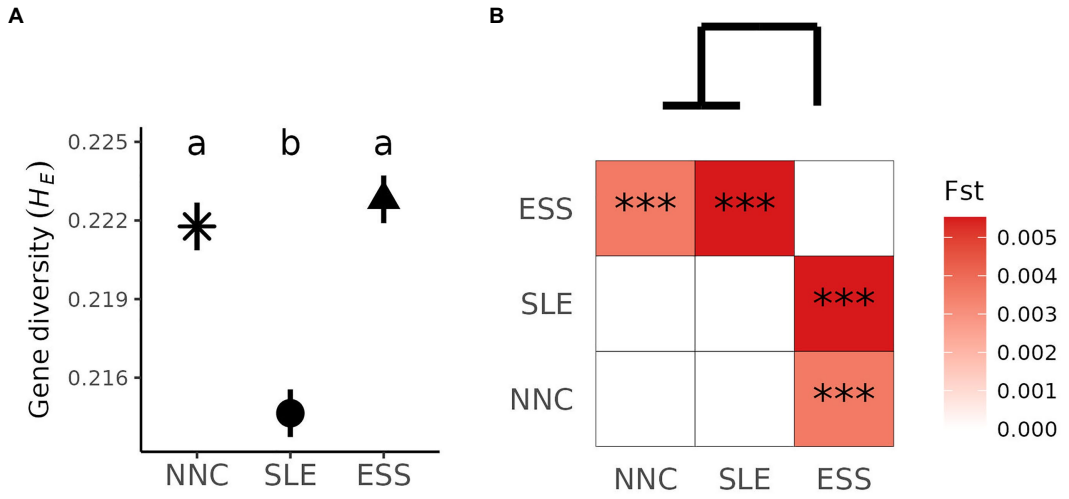

FIGURE 4
Pandalus borealis genetic variation. **(A)** Within origin genetic variation. Mean and standard error of gene diversity (H_E) for each origin. The result of Tukey HSD (honest significant difference) *post hoc* tests are displayed as letters, with different letters representing significant differences among origins' mean values (p<0.001). **(B)** Among origins genetic variation. Pairwise genetic differentiation (F_{ST}) among shrimp's origin varied from white (zero) to red (high), as shown on the right-hand side of the heat-map and values significantly different from zero are denoted by *** for p<0.001. The dendrogram on the top resulted from hierarchical cluster analysis based on the pairwise F_{ST}. ESS=Eastern Scotian Shelf, SLE=St. Lawrence Estuary, NNC=Northeast Newfoundland Coast.

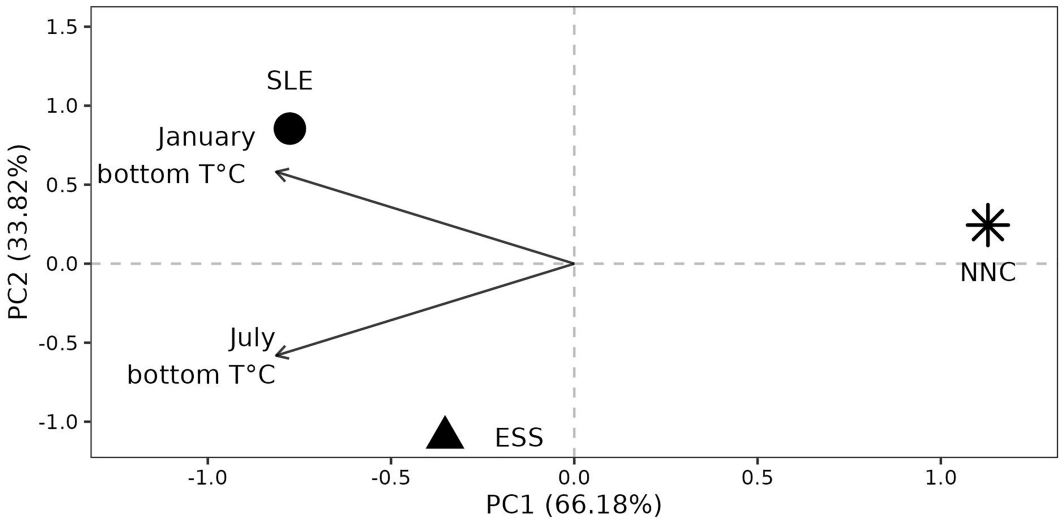

FIGURE 5
Environmental conditions at origin. Principal Component Analysis (PCA) using two monthly environmental variables that are not highly correlated (see methods for more details). ESS=Eastern Scotian Shelf, SLE=St. Lawrence Estuary, NNC=Northeast Newfoundland Coast, PC=Principal Component.

upper limit of thermal tolerance of *P. borealis* (Guscelli et al. *submitted for review*). Such incongruence in the responses to temperature between the mortality rates and the linearity of gene expression may be explained by the fact that only survivors could be analyzed for gene expression. Besides, other tissues than the abdominal muscle analyzed in this study, such as the gills and heart, may show thermal transcriptomic responses more closely associated to survival given their vital physiological functions (Buckley et al., 2006; Liu et al., 2013; Valenza-Troubat et al., 2022). The analysis of such tissues could extend our understanding of mechanisms involved in *P. borealis* responses to global changes.

We also reported changes in biological functions of differentially expressed transcripts (DETs) with increasing temperatures in *P. borealis*. Lipid catabolic activities have been shown to decrease with increasing temperatures in polar fishes (Pörtner, 2002). Similarly, we also observed catabolic activities decreasing with increasing temperature. For *P. borealis*, we identified protein catabolism at low temperatures which may be specific to this species (Supplementary Figure S1). We also observed increasing expression of genes associated to metabolic activities with increasing temperature, which supports previous observations of increased metabolic rate of *P. borealis* at higher temperatures (Ouellet and Chabot, 2005; Arnberg et al., 2013; Dupont-Prinet et al., 2013; Guscelli et al. *submitted for review*).

Our study also identified a molecular mechanism possibly involved in cold tolerance in *P. borealis*. Transcripts associated with

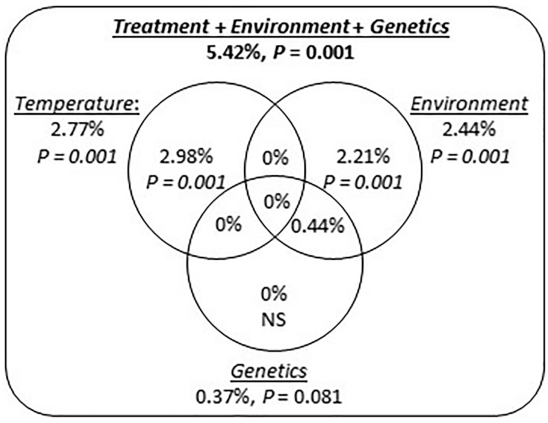

FIGURE 6
Factors influencing transcript expression in *P. borealis*. Venn diagram representing the proportion (*adj.* R^2) of gene expression level explained by exposure temperature (*Temperature*), environmental conditions at origin (*Environment*) and population genetic differentiation (*Genetics*, i.e., pairwise F_{ST} between origins). Number outside circles refer to total percentage of variation explained by each underlined factor. Numbers inside circles indicate the marginal contribution to transcript expression by each factor. Percentages within intersections indicate shared contribution across different variables. Significance of total and marginal contribution to gene expression was tested by permutations test, using 999 randomizations.

TABLE 1 ANOVA table for db-RDA models selection for factors explaining gene expression level.

	Adjusted R^2	Df	F	*p*-value	Adjusted *p*-value[1]
Transcript expression					
Treatment	2.77%	2	1.7538	0.001	0.001
Environment	5.42%	2	1.7151	0.001	0.001
Treatment × Environment	6.76%	4	1.1765	0.006	0.010
All variables	6.76%				

Models were constructed using the forward selection process, maximizing the adjusted R^2 and *p*-value (ordiR2step function from the R package vegan). Genetic variation among origins and its interaction with treatments were also included in the initial model, but were not selected, and therefore not included in the table. [1]*p*-value were adjusted following Holm's correction for multiple testing.

threonine related activities decreased with increasing temperature. In Atlantic salmon *Salmo salar* (Linnaeus, 1758), threonine-type proteins were shown to be involved in low temperature conditioning (Silva et al., 2020). These proteins were also observed in response to cold treatment in the Pacific white shrimp *P. vannamei* (Huang et al., 2017), where threonine-type proteins are downregulated in the warmest temperatures, as for *P. borealis*.

4.2. Variation in gene expression was associated with environmental factors, but not genetic variation

The origin of northern shrimp was associated with contrasting transcriptomic patterns, with shrimp from NNC showing more distinctive gene expression patterns when compared to the SLE and ESS origins. Such difference could be due to acclimatization (environment) or local adaptation (genetics) effects. We used a model selection analysis with temperature, environmental conditions at origin, and genetic differentiation to disentangle acclimatization and adaptation effects on transcript expression levels. Our results showed that experimental temperature and environmental conditions at origin are the two factors explaining differences in transcript levels.

Local adaptation can translate into differential gene expression patterns in distinct populations. In this study, we confirmed the existence of different populations in *P. borealis* in northwest Atlantic by detecting significant genetic differentiation among origins. Our results also showed that shrimp from SLE display the smallest genetic diversity compared to other origins. Despite such genetic differences, we failed to detect any genetic effect on gene expression, either qualitatively with genetic diversity or quantitatively with genetic differentiation (variation partitioning and model selection analyzes). Our results suggest that local adaptation do not underly differential gene expression for shrimp from these three origins. Yet, single or a few loci might be associated with local adaptation and contribute to the geographic variation in gene expression (Whitehead and Crawford, 2006). This hypothesis is now under investigation in a distinct study.

The similarity in transcriptomic patterns and environmental conditions at origins observed in this study may suggest acclimation of shrimp to temperature at origins. However, the interpretation of these results is not straight forward. The variable developmental status of female shrimp was also highlighted with difference in molting rates across origins in this. The SLE shrimp were tested in early fall, when molting occurs in the field, whereas the ESS shrimp were tested in spring, close to hatching and before molting. In contrast, NNC shrimps were tested in winter and adult females are not molting during this season (DFO, 2012, 2021; Bourdages et al., 2022). Consequently, the effect of environmental conditions at origins also included difference in developmental status of female shrimp. Note that differences in transcript levels among shrimp from distinct origins also mirror those we report for molting rates. In addition, most gene functions involved in DETs across origins were associated with cell structures. Transcripts involved in actin and myosin production, cytoskeletal motor activity, and cuticle structural components were also upregulated in SLE and ESS. Such gene functions were previously associated to the molting process in shrimp (de Oliveira Cesar et al., 2006; Corteel et al., 2012; Zhang et al., 2019).

4.3. Limited potential of adaptation to global changes of northern shrimp

Ecologically divergent populations can evolve different transcriptomic plasticity, as observed in the redband trout *Oncorhynchus mykiss gairdneri* (Richardson, 1836) from desert and montane climates (Narum and Campbell, 2015), and in the threespine stickleback *Gasterosteus aculeatus* (Linnaeus, 1758) from marine and freshwater environments (Morris et al., 2014). However, we did not observed different thermal transcriptomic platicity in *P. borealis* among genetically different populations. This result indicates that this species did not evolve locally adapted transcriptomic plasticity in response to the temperature range tested. Furthermore, this lack of

genetic variation underlying transcriptomic responses to changing temperature suggests a limited evolutionary potential of *P. borealis* thermal plasticity, at least at the transcriptional level. It is unclear to what extent this limited evolutionary potential of thermal plasticity at the transcriptomic level reflects a limited evolutionary potential for the plasticity of integrative traits such as growth and reproduction. However, plastic response of gene expression could be adaptive (Koch and Guillaume, 2020), and the evolution of plasticity for the transcriptional phenotypes could propagate across hierarchical levels of the organisms (from gene expression to integrative phenotypes), as observed in another organism (Leung et al., 2022). Our results would also suggest a limited evolutionary potential of integrative traits plasticity.

In conclusion, understanding the molecular mechanisms underpinning a species' thermal plasticity and its vulnerability to global change drivers can ultimately help developing appropriate conservation and management plans, this being paramount also for species of commercial importance that supports the socio-economic development of coastal communities, including first nation ones. Our results show that individuals of *P. borealis* surviving 30 days exposure to elevated temperature are able to buffer the immediate impact of ongoing ocean warming by altering their gene expression. However, the lack of standing variation underlying phenotypic plasticity in response to temperature suggests a limited potential for the evolution of its plasticity. Our results emphasise its vulnerability under future global changes scenarios, as observed in other ectotherm organisms (Gunderson and Stillman, 2015; Sirovy et al., 2021). Consequently, the higher mortality reported at the highest temperature in this study also supports that the thermal niche of *P. borealis* will be progressively restricted to higher latitudes with the ongoing ocean warming (Hobday et al., 2016; Kleisner et al., 2017; Morley et al., 2018; McHenry et al., 2019). This prediction concurs with current decreases in abundance already observed at lower latitudes for this species, prediction also based on modeling (Barria et al. *submitted for review*) and other cold-adapted crustaceans (Neumann et al., 2013; Lenoir et al., 2020; Melo-Merino et al., 2020; Simões et al., 2021).

Data availability statement

The datasets presented in this study can be found in online repositories. The names of the repository/repositories and accession number(s) can be found below: https://www.ncbi.nlm.nih.gov/, PRJNA909194 and https://github.com/GenomicsMLI-DFO/PANOMICS_Transcripto_manuscript.

Ethics statement

The Canadian Council for Animal Care does not require that projects using invertebrates other than cephalopods be approved by an Animal Care Committee.

Author contributions

GP obtained the funding for the genomic analyzes. DC and PC obtained the funding for the experimental work. CL and GP conceived the tested hypothesis. EG, DC, and PC conceived, designed, and ran experiment. AB performed the bioinformatic analyzes of ddRADseq data. CL analyzed the transcriptomic data, prepared figures and tables, and wrote the original draft. All authors contributed to the article and approved the submitted version.

Funding

The experimental work was funded by: (i) an OURANOS grant (554023) to DC and PC; (ii) a DFO Strategic Program for Ecosystem-Based Research and Advice grant and an Aquatic Climate Change Adaptation Services Program grant to DC; (iii) a FIR UQAR grant, a Canada Foundation for Innovation (CFI) grant and a Natural Sciences and Engineering Research Council of Canada (NSERC) Discovery grants (RGPIN-2015-06500 and RGPIN-2020-05627) and a MITACS-Ouranos Accelerate grant, all granted to PC. EG is supported by a Fonds de Recherche du Québec - Nature et Technologies (FRQNT) scholarship (PBEEE, 289597) and a Réal-Decoste Ouranos scholarship (286109).

The genomic work was funded by: Genomics R&D Initiative (GRDI), Government of Canada.

Acknowledgments

We thank T. Hansen, J. Gagnon, and D. Picard for technical support during the experiments and the molecular work at Maurice Lamontagne Institute (DFO, Canada). We are grateful to G. Leveque (C3G) for the RNA-seq bioinformatic preprocessing and G. Cortial and L.-A. Dumoulin for RNA/DNA extractions (DFO, Canada). GP, EG, DC, and PC are working under the FRQ-NT funded research networks of excellence Québec-Océans or Ressources Aquatiques Québec.

Conflict of interest

As PC was a Topic Editor of this special issue, he did not participate in any form to editorial decision nor the editorial processing of this article.

The remaining authors declare that the research was conducted in the absence of any commercial or financial relationships that could be construed as a potential conflict of interest.

Publisher's note

Supplementary material

The Supplementary material for this article can be found online at: https://www.frontiersin.org/articles/10.3389/fevo.2023.1125134/full#supplementary-material

References

Abram, P. K., Boivin, G., Moiroux, J., and Brodeur, J. (2017). Behavioural effects of temperature on ectothermic animals: unifying thermal physiology and behavioural plasticity. *Biol. Rev.* 92, 1859–1876. doi: 10.1111/BRV.12312

Alexa, A., and Rahnenfuhrer, J. (2022). *topGO: Enrichment Analysis for Gene Ontology*. R Packag Version 2.0.

Allen, J. A. (1959). On the biology of *Pandalus borealis* Krøyer, with reference to a population off the Northumberland coast. *J. Mar. Biol. Assoc. U. K.* 38, 189–220. doi: 10.1017/S002531540001568X

Alley, R. B. (2000). Ice-core evidence of abrupt climate changes. *Proc. Natl. Acad. Sci. U. S. A.* 97, 1331–1334. doi: 10.1073/PNAS.97.4.1331/ASSET/F6F66AAD-E997-44E8-9C57-6F4F4C372A73/ASSETS/GRAPHIC/PQ0103809001.JPEG

Amarasekare, P., and Savage, V. (2012). A framework for elucidating the temperature dependence of fitness. *Am. Nat.* 179, 178–191. doi: 10.1086/663677/SUPPL_FILE/52973APE.PDF

Angilletta, M. J. (2009). *Thermal Adaptation: A Theoretical and Empirical Synthesis*. Oxford: Oxford University Press.

Apollonio, S., Stevenson, D. K., and Dunton, J. E. E. (1986). *Effects of Temperature on the Biology of the Northern Shrimp, Pandalus borealis, in the Gulf of Maine*. NOAA Technical Report NMFS; 42. Available at: https://repository.library.noaa.gov/view/noaa/23116 (Accessed August 4, 2022).

Arnberg, M., Calosi, P., Spicer, J. I., Tandberg, A. H. S., Nilsen, M., Westerlund, S., et al. (2013). Elevated temperature elicits greater effects than decreased pH on the development, feeding and metabolism of northern shrimp (*Pandalus borealis*) larvae. *Mar. Biol.* 160, 2037–2048. doi: 10.1007/S00227-012-2072-9/FIGURES/5

Ashander, J., Chevin, L. M., and Baskett, M. L. (2016). Predicting evolutionary rescue via evolving plasticity in stochastic environments. *Proc. R. Soc. B Biol. Sci.* 283:20161690. doi: 10.1098/RSPB.2016.1690

Aubin-Horth, N., and Renn, S. C. P. (2009). Genomic reaction norms: using integrative biology to understand molecular mechanisms of phenotypic plasticity. *Mol. Ecol.* 18, 3763–3780. doi: 10.1111/J.1365-294X.2009.04313.X

Blanchet, F. G., Legendre, P., and Borcard, D. (2008). Forward selection of explanatory variables. *Ecology* 89, 2623–2632. doi: 10.1890/07-0986.1

Bolger, A. M., Lohse, M., and Usadel, B. (2014). Trimmomatic: a flexible trimmer for Illumina sequence data. *Bioinform.* 30, 2114–2120.

Bonebrake, T. C., Brown, C. J., Bell, J. D., Blanchard, J. L., Chauvenet, A., Champion, C., et al. (2018). Managing consequences of climate-driven species redistribution requires integration of ecology, conservation and social science. *Biol. Rev.* 93, 284–305. doi: 10.1111/BRV.12344

Borcard, D., Legendre, P., and Drapeau, P. (1992). Partialling out the spatial component of ecological variation. *Ecology* 73, 1045–1055. doi: 10.2307/1940179

Bourdages, H., Roux, M.-J., Marquis, M.-C., Galbraith, P., and Isabel, L. (2022). *Assessment of Northern Shrimp Stocks in the Estuary and Gulf of St. Lawrence in 2021: Commercial Fishery and Research Survey Data*. DFO Canadian Science Advisory 2022/027.197.

Bradshaw, A. D. (1965). Evolutionary significance of phenotypic plasticity in plants. *Adv. Genet.* 13, 115–155. doi: 10.1016/S0065-2660(08)60048-6

Buckley, B. A., Gracey, A. Y., and Somero, G. N. (2006). The cellular response to heat stress in the goby *Gillichthys mirabilis*: a cDNA microarray and protein-level analysis. *J. Exp. Biol.* 209, 2660–2677. doi: 10.1242/JEB.02292

Catchen, J., Hohenlohe, P. A., Bassham, S., Amores, A., and Cresko, W. A. (2013). Stacks: an analysis tool set for population genomics. *Mol. Ecol.* 22, 3124–3140. doi: 10.1111/mec.12354

Chabot, D., Guénette, S., and Stortini, C. (2013). "A review of the physiological susceptibility of commercial species of fish and crustaceans of the Northwest Atlantic to changes in water temperature, dissolved oxygen, pH and salinity" in *Climate Change Impacts, Vulnerabilities and Opportunities Analysis of the Marine Atlantic Basin*. eds. N. L. Shackell, B. J. W. Greenan, P. Pepin, D. Chabot and A. Warburton (Canadian Manuscript Report of Fisheries and Aquatic Sciences), 83–168.

Chabot, D., and Ouellet, P. (2005). Rearing *Pandalus borealis* larvae in the laboratory: II. Routine oxygen consumption, maximum oxygen consumption and metabolic scope at three temperatures. *Mar. Biol.* 147, 881–894. doi: 10.1007/s00227-005-1626-5

Chemel, M., Noisette, F., Chabot, D., Guscelli, E., Leclerc, L., and Calosi, P. (2020). Good news–bad news: combined ocean change drivers decrease survival but have no negative impact on nutritional value and organoleptic quality of the northern shrimp. *Front. Mar. Sci.* 7:611. doi: 10.3389/fmars.2020.00611

Chen, Y., Lun, A. T. L., Smyth, G. K., Burden, C. J., Ryan, D. P., Khang, T. F., et al. (2016). From reads to genes to pathways: differential expression analysis of RNA-Seq experiments using Rsubread and the edgeR quasi-likelihood pipeline. *F1000 Res.* 5:1438. doi: 10.12688/f1000research.8987.2

Colston-Nepali, L., Tigano, A., Boyle, B., and Friesen, V. (2019). Hybridization does not currently pose conservation concerns to murres in the Atlantic. *Conserv. Genet.* 20, 1465–1470. doi: 10.1007/s10592-019-01223-y

Corteel, M., Dantas-Lima, J. J., Wille, M., Alday-Sanz, V., Pensaert, M. B., Sorgeloos, P., et al. (2012). Moult cycle of laboratory-raised *Penaeus* (Litopenaeus) *vannamei* and *P. monodon*. *Aquac. Int.* 20, 13–18. doi: 10.1007/s10499-011-9437-9

Daoud, D., Chabot, D., Audet, C., and Lambert, Y. (2007). Temperature induced variation in oxygen consumption of juvenile and adult stages of the northern shrimp, *Pandalus borealis*. *J. Exp. Mar. Bio. Ecol.* 347, 30–40. doi: 10.1016/J.JEMBE.2007.02.013

Daoud, D., Lambert, Y., Audet, C., and Chabot, D. (2010). Size and temperature-dependent variations in intermolt duration and size increment at molt of northern shrimp, *Pandalus borealis*. *Mar. Biol.* 157, 2655–2666. doi: 10.1007/s00227-010-1526-1

de Oliveira Cesar, J. R., Zhao, B., Malecha, S., Ako, H., and Yang, J. (2006). Morphological and biochemical changes in the muscle of the marine shrimp *Litopenaeus vannamei* during the molt cycle. *Aquaculture* 261, 688–694. doi: 10.1016/J.AQUACULTURE.2006.08.003

De Wit, P., Dupont, S., and Thor, P. (2016). Selection on oxidative phosphorylation and ribosomal structure as a multigenerational response to ocean acidification in the common copepod *Pseudocalanus acuspes*. *Evol. Appl.* 9, 1112–1123. doi: 10.1111/EVA.12335

Dey, S., Proulx, S. R., and Teotónio, H. (2016). Adaptation to temporally fluctuating environments by the evolution of maternal effects. *PLoS Biol.* 14:e1002388. doi: 10.1371/JOURNAL.PBIO.1002388

DFO. (2012). *Assessment of Northern Shrimp on the Eastern Scotian Shelf (SFAs 13-15)*. DFO Canadian Science Advisory Secretariat Maritimes Region Science Advisory Report, No. 2012/114.

DFO. (2021). *An Assessment of Northern Shrimp (Pandalus borealis) in Shrimp Fishing Areas 4–6 and of Striped Shrimp (Pandalus montagui) in Shrimp Fishing Area 4 in 2020*. DFO Canadian Science Advisory Secretariat Maritimes Region Science Advisory Report, No. 2021/049.

DFO. (2022). *Assessment of Northern Shrimp Stocks in the Estuary and Gulf of St. Lawrence in 2021*. DFO Canadian Science Advisory Secretariat Maritimes Region Science Advisory Report, No. 2022/006.

Dupont-Prinet, A., Pillet, M., Chabot, D., Hansen, T., Tremblay, R., and Audet, C. (2013). Northern shrimp (*Pandalus borealis*) oxygen consumption and metabolic enzyme activities are severely constrained by hypoxia in the estuary and gulf of St. *Lawrence J. Exp. Mar. Bio. Ecol.* 448, 298–307. doi: 10.1016/J.JEMBE.2013.07.019

Fischer, J., Schott, F. A., and Dengler, M. (2004). Boundary circulation at the exit of the Labrador Sea. *J. Phys. Oceanogr.* 34, 1548–1570. doi: 10.1175/1520-0485(2004)034<1548:BCATEO>2.0.CO;2

Fisher, R. A. (1930). *The Genetical Theory of Natural Selection*. Oxford: Clarendon Press.

Garcia, E. G. (2007). The northern shrimp (*Pandalus borealis*) offshore fishery in the Northeast Atlantic. *Adv. Mar. Biol.* 52, 147–266. doi: 10.1016/S0065-2881(06)52002-4

Gavrilets, S., and Scheiner, S. M. (1993). The genetics of phenotypic plasticity. V. Evolution of reaction norm shape. *J. Evol. Biol.* 6, 31–48. doi: 10.1046/J.1420-9101.1993.6010031.X

Gerken, A. R., Eller, O. C., Hahn, D. A., and Morgan, T. J. (2015). Constraints, independence, and evolution of thermal plasticity: probing genetic architecture of long– and short-term thermal acclimation. *Proc. Natl. Acad. Sci.* 112, 4399–4404. doi: 10.1073/PNAS.1503456112

Ghalambor, C. K., McKay, J. K., Carroll, S. P., and Reznick, D. N. (2007). Adaptive versus non-adaptive phenotypic plasticity and the potential for contemporary adaptation in new environments. *Funct. Ecol.* 21, 394–407. doi: 10.1111/J.1365-2435.2007.01283.X

Gleason, L. U., and Burton, R. S. (2015). RNA-seq reveals regional differences in transcriptome response to heat stress in the marine snail *Chlorostoma funebralis*. *Mol. Ecol.* 24, 610–627. doi: 10.1111/MEC.13047

Gruber, B., Unmack, P. J., Berry, O. F., and Georges, A. (2018). Dartr: an r package to facilitate analysis of SNP data generated from reduced representation genome sequencing. *Mol. Ecol. Resour.* 18, 691–699. doi: 10.1111/1755-0998.12745

Gunderson, A. R., and Stillman, J. H. (2015). Plasticity in thermal tolerance has limited potential to buffer ectotherms from global warming. *Proc. R. Soc. B Biol. Sci.* 282:20150401. doi: 10.1098/RSPB.2015.0401

Haas, B. J., Papanicolaou, A., Yassour, M., Grabherr, M., Blood, P. D., Bowden, J., et al. (2013). *De novo* transcript sequence reconstruction from RNA-seq using the trinity platform for reference generation and analysis. *Nat. Protoc.* 8, 1494–1512. doi: 10.1038/nprot.2013.084

Hansen, T. F. (2006). The evolution of genetic architecture. *Annu. Rev. Ecol. Evol. Syst.* 37, 123–157. doi: 10.1146/annurev.ecolsys.37.091305.110224

Haynes, E. B., and Wigley, R. L. (1969). Biology of the northern shrimp, *Pandalus borealis*, in the Gulf of Maine. *Trans. Am. Fish. Soc.* 98, 60–76. doi: 10.1577/1548-8659

Hobday, A. J., Alexander, L. V., Perkins, S. E., Smale, D. A., Straub, S. C., Oliver, E. C. J., et al. (2016). A hierarchical approach to defining marine heatwaves. *Prog. Oceanogr.* 141, 227–238. doi: 10.1016/J.POCEAN.2015.12.014

Huang, W., Ren, C., Li, H., Huo, D., Wang, Y., Jiang, X., et al. (2017). Transcriptomic analyses on muscle tissues of *Litopenaeus vannamei* provide the first profile insight into

the response to low temperature stress. *PLoS One* 12:e0178604. doi: 10.1371/JOURNAL.PONE.0178604

Huey, R. B., Kearney, M. R., Krockenberger, A., Holtum, J. A. M., Jess, M., and Williams, S. E. (2012). Predicting organismal vulnerability to climate warming: roles of behaviour, physiology and adaptation. *Philos. Trans. R. Soc. B Biol. Sci.* 367, 1665–1679. doi: 10.1098/RSTB.2012.0005

Huey, R. B., and Stevenson, R. D. (1979). Integrating thermal physiology and ecology of ectotherms: a discussion of approaches. *Integr. Comp. Biol.* 19, 357–366. doi: 10.1093/ICB/19.1.357

Hughes, A. R., Inouye, B. D., Johnson, M. T. J., Underwood, N., and Vellend, M. (2008). Ecological consequences of genetic diversity. *Ecol. Lett.* 11, 609–623. doi: 10.1111/J.1461-0248.2008.01179.X

IPCC. (2014). *Summary for Policy Makers*. Geneva, Szwitzerland: IPCC.

IPCC. (2022). *Climate change 2022: Impacts Adaptation and Vulnerability*. Geneva, Szwitzerland: IPCC.

Kamvar, Z. N., Tabima, J. F., and Gŕunwald, N. J. (2014). Poppr: an R package for genetic analysis of populations with clonal, partially clonal, and/or sexual reproduction. *PeerJ* 2014, 1–14. doi: 10.7717/PEERJ.281/TABLE-6

Kelly, M. (2019). Adaptation to climate change through genetic accommodation and assimilation of plastic phenotypes. *Philos. Trans. R. Soc. B* 374:20180176. doi: 10.1098/RSTB.2018.0176

Kleisner, K. M., Fogarty, M. J., McGee, S., Hare, J. A., Moret, S., Perretti, C. T., et al. (2017). Marine species distribution shifts on the U.S. northeast continental shelf under continued ocean warming. *Prog. Oceanogr.* 153, 24–36. doi: 10.1016/J.POCEAN.2017.04.001

Koch, E. L., and Guillaume, F. (2020). Additive and mostly adaptive plastic responses of gene expression to multiple stress in *Tribolium castaneum*. *PLoS Genet.* 16:e1008768. doi: 10.1371/journal.pgen.1008768

Koeller, P. A. (2000). Relative importance of abiotic and biotic factors to the Management of the Northern Shrimp (*Pandalus Borealis*) fishery on the Scotian shelf. *J. Northwest Atl. Fish. Sci.* 27, 21–33. doi: 10.2960/J.v27.a3

Koeller, P., Fuentes-Yaco, C., Platt, T., Sathyendranath, S., Richards, A., Ouellet, P., et al. (2009). Basin-scale coherence in phenology of shrimps and phytoplankton in the North Atlantic Ocean. *Science* 80, 791–793. doi: 10.1126/SCIENCE.1170987/SUPPL_FILE/KOELLER.SOM.PDF

Landy, J. A., Oschmann, A., Munch, S. B., and Walsh, M. R. (2020). Ancestral genetic variation in phenotypic plasticity underlies rapid evolutionary changes in resurrected populations of waterfleas. *Proc. Natl. Acad. Sci. U. S. A.* 117, 32535–32544. doi: 10.1073/pnas.2006581117

Langfelder, P., and Horvath, S. (2008). WGCNA: an R package for weighted correlation network analysis. *BMC Bioinformatics* 9, 1–13. doi: 10.1186/1471-2105-9-559/FIGURES/4

Lavoie, D., Lambert, N., Rousseau, S., Dumas, J., Chassé, J., Long, Z., et al. (2020). *Projections of Future Physical and Biogeochemical Conditions in the Gulf of St. Lawrence, on the Scotian Shelf and in the Gulf of Maine*. Canadian Technical Report of Hydrography and Ocean Sciences.

Leder, E. H., McCairns, R. J. S., Leinonen, T., Cano, J. M., Viitaniemi, H. M., Nikinmaa, M., et al. (2015). The evolution and adaptive potential of transcriptional variation in sticklebacks—signatures of selection and widespread heritability. *Mol. Biol. Evol.* 32, 674–689. doi: 10.1093/MOLBEV/MSU328

Legendre, P. (2008). Studying beta diversity: ecological variation partitioning by multiple regression and canonical analysis. *J. Plant Ecol.* 1, 3–8. doi: 10.1093/jpe/rtm001

Lenoir, J., Bertrand, R., Comte, L., Bourgeaud, L., Hattab, T., Murienne, J., et al. (2020, 2020). Species better track climate warming in the oceans than on land. *Nat. Ecol. Evol.* 48, 1044–1059. doi: 10.1038/s41559-020-1198-2

Leung, C., Grulois, D., Quadrana, L., and Chevin, L. M. (2022). The molecular basis of phenotypic plasticity evolves in response to environmental predictability. *bioRxiv* 2022:514467. doi: 10.1101/2022.10.31.514467

Leung, C., Rescan, M., Grulois, D., and Chevin, L. M. (2020). Reduced phenotypic plasticity evolves in less predictable environments. *Ecol. Lett.* 23, 1664–1672. doi: 10.1111/ELE.13598

Levins, R. (1963). Theory of fitness in a heterogeneous environment. II. Developmental flexibility and niche selection. *Am. Nat.* 97, 75–90. doi: 10.1086/282258

Li, B., and Dewey, C. N. (2011). RSEM: accurate transcript quantification from RNA-Seq data with or without a reference genome. *BMC Bioinformatics* 12, 1–16. doi: 10.1186/1471-2105-12-323

Lima, F. P., Ribeiro, P. A., Queiroz, N., Hawkins, S. J., and Santos, A. M. (2007). Do distributional shifts of northern and southern species of algae match the warming pattern? *Glob. Chang. Biol.* 13, 2592–2604. doi: 10.1111/J.1365-2486.2007.01451.X

Liu, S., Wang, X., Sun, F., Zhang, J., Feng, J., Liu, H., et al. (2013). RNA-Seq reveals expression signatures of genes involved in oxygen transport, protein synthesis, folding, and degradation in response to heat stress in catfish. *Physiol. Genomics* 45, 462–476. doi: 10.1152/PHYSIOLGENOMICS.00026.2013/ASSET/IMAGES/LARGE/ZH70121338400004.JPEG

Logan, C. A., Buckley, B. A., Podrabsky, J. E., Stillman, J. H., and Tomanek, L. (2015). Transcriptomic responses to environmental temperature in eurythermal and stenothermal fishes. *J. Exp. Biol.* 218, 1915–1924. doi: 10.1242/JEB.114397

Love, M. I., Huber, W., and Anders, S. (2014). Moderated estimation of fold change and dispersion for RNA-seq data with DESeq2. *Genome Biol.* 15, 1–21. doi: 10.1186/S13059-014-0550-8/FIGURES/9

Madeira, D., Araújo, J. E., Madeira, C., Mendonça, V., Vitorino, R., Vinagre, C., et al. (2020). Seasonal proteome variation in intertidal shrimps under a natural setting: connecting molecular networks with environmental fluctuations. *Sci. Total Environ.* 703:134957. doi: 10.1016/j.scitotenv.2019.134957

McHenry, J., Welch, H., Lester, S. E., and Saba, V. (2019). Projecting marine species range shifts from only temperature can mask climate vulnerability. *Glob. Chang. Biol.* 25, 4208–4221. doi: 10.1111/GCB.14828

Melo-Merino, S. M., Reyes-Bonilla, H., and Lira-Noriega, A. (2020). Ecological niche models and species distribution models in marine environments: a literature review and spatial analysis of evidence. *Ecol. Model.* 415:108837. doi: 10.1016/J.ECOLMODEL.2019.108837

Morley, J. W., Selden, R. L., Latour, R. J., Frölicher, T. L., Seagraves, R. J., and Pinsky, M. L. (2018). Projecting shifts in thermal habitat for 686 species on the north American continental shelf. *PLoS One* 13:e0196127. doi: 10.1371/JOURNAL.PONE.0196127

Morris, M. R., Richard, R., Leder, E. H., Barrett, R. D., Aubin-Horth, N., and Rogers, S. M. (2014). Gene expression plasticity evolves in response to colonization of freshwater lakes in threespine stickleback. *Mol. Ecol.* 23, 3226–3240.

Mucci, A., Levasseur, M., Gratton, Y., Martias, C., Scarratt, M., Gilbert, D., et al. (2018). Tidally induced variations of pH at the head of the Laurentian Channel. *Can. J. Fish. Aquat. Sci.* 75, 1128–1141. doi: 10.1139/cjfas-2017-0007

Mucci, A., Starr, M., Gilbert, D., and Sundby, B. (2011). Acidification of lower St. Lawrence estuary bottom waters. *Atmosphere-Ocean* 49, 206–218. doi: 10.1080/07055900.2011.599265

Narum, S. R., and Campbell, N. R. (2015). Transcriptomic response to heat stress among ecologically divergent populations of redband trout. *BMC. Genom.* 16, 1–12.

Neumann, H., De Boois, I., Kröncke, I., and Reiss, H. (2013). Climate change facilitated range expansion of the non-native angular crab *Goneplax rhomboides* into the North Sea. *Mar. Ecol. Prog. Ser.* 484, 143–153. doi: 10.3354/MEPS10299

Oksanen, J., Simpson, G. L., Blanchet, F. G., Kindt, R., Legendre, P., Minchin, P. R., et al. (2022). *Egan: Community Ecology Package Version 2.6-2 from CRAN*. Available at: https://rdrr.io/cran/vegan/ (Accessed July 29, 2022).

Oostra, V., Saastamoinen, M., Zwaan, B. J., and Wheat, C. W. (2018). Strong phenotypic plasticity limits potential for evolutionary responses to climate change. *Nat. Commun.* 91, 1–11. doi: 10.1038/s41467-018-03384-9

Orr, D., and Sullivan, D. (2013). *The February 2013 Assessment of Northern Shrimp (Pandalus borealis) off Labrador and Northeastern Newfoundland*. DFO Canadian Science Advisory Secretariat Research Document, 2013/055. p. 144.

Ouellet, P., and Chabot, D. (2005). Rearing *Pandalus borealis* (Krøyer) larvae in the laboratory: I. development and growth at three temperatures. *Mar. Biol.* 147, 869–880. doi: 10.1007/S00227-005-1625-6/FIGURES/10

Paaijmans, K. P., Heinig, R. L., Seliga, R. A., Blanford, J. I., Blanford, S., Murdock, C. C., et al. (2013). Temperature variation makes ectotherms more sensitive to climate change. *Glob. Chang. Biol.* 19, 2373–2380. doi: 10.1111/GCB.12240

Pavey, S. A., Collin, H., Nosil, P., and Rogers, S. M. (2010). The role of gene expression in ecological speciation. *Ann. N. Y. Acad. Sci.* 1206, 110–129. doi: 10.1111/J.1749-6632.2010.05765.X

Peres-Neto, P. R., Legendre, P., Dray, S., and Borcard, D. (2006). Variation partitioning of species data matrices: estimation and comparison of fractions. *Ecology* 87, 2614–2625. doi: 10.1890/0012-9658(2006)87[2614:VPOSDM]2.0.CO;2

Perry, A. L., Low, P. J., Ellis, J. R., and Reynolds, J. D. (2005). Ecology: climate change and distribution shifts in marine fishes. *Science* 80, 1912–1915. doi: 10.1126/SCIENCE.1111322/SUPPL_FILE/PERRY.SOM.REVISED.PDF

Pinsky, M. L., Eikeset, A. M., McCauley, D. J., Payne, J. L., and Sunday, J. M. (2019). Greater vulnerability to warming of marine versus terrestrial ectotherms. *Nature* 569, 108–111. doi: 10.1038/s41586-019-1132-4

Poland, J. A., Brown, P. J., Sorrells, M. E., and Jannink, J. L. (2012). Development of high-density genetic maps for barley and Wheat using a novel two-enzyme genotyping-by-sequencing approach. *PLoS One* 7:e32253. doi: 10.1371/JOURNAL.PONE.0032253

Pörtner, H. O. (2002). Physiological basis of temperature-dependent biogeography: trade-offs in muscle design and performance in polar ectotherms. *J. Exp. Biol.* 205, 2217–2230. doi: 10.1242/JEB.205.15.2217

R Core Team. (2020). *R: A Language and Environment for Statistical Computing*. Vienna, Austria: R Foundation for Statistical Computing.

Rahmstorf, S., and Coumou, D. (2011). Increase of extreme events in a warming world. *Proc. Natl. Acad. Sci. U. S. A.* 108, 17905–17909. doi: 10.1073/PNAS.1101766108/ASSET/45E632EF-D52B-4B90-8492-5D7B773D3028/ASSETS/GRAPHIC/PNAS.1101766108EQ10.JPEG

Reed, T. E., Waples, R. S., Schindler, D. E., Hard, J. J., and Kinnison, M. T. (2010). Phenotypic plasticity and population viability: the importance of environmental predictability. *Proc. R. Soc. B Biol. Sci.* 277, 3391–3400. doi: 10.1098/rspb.2010.0771

Rescan, M., Grulois, D., Ortega-Aboud, E., and Chevin, L. M. (2020). Phenotypic memory drives population growth and extinction risk in a noisy environment. *Nat. Ecol. Evol.* 42, 193–201. doi: 10.1038/s41559-019-1089-6

Richards, R. A. (2012). Phenological shifts in hatch timing of northern shrimp *Pandalus borealis*. *Mar. Ecol. Prog. Ser.* 456, 149–158. doi: 10.3354/MEPS09717

Richards, R. A., and Hunter, M. (2021). Northern shrimp *Pandalus borealis* population collapse linked to climate-driven shifts in predator distribution. *PLoS One* 16:e0253914. doi: 10.1371/JOURNAL.PONE.0253914

Rochette, N. C., Rivera-Colón, A. G., and Catchen, J. M. (2019). Stacks 2: analytical methods for paired-end sequencing improve RADseq-based population genomics. *Mol. Ecol.* 28, 4737–4754. doi: 10.1111/mec.15253

Román-Palacios, C., and Wiens, J. J. (2020). Recent responses to climate change reveal the drivers of species extinction and survival. *Proc. Natl. Acad. Sci. U. S. A.* 117, 4211–4217. doi: 10.1073/pnas.1913007117

Rosa, R., Lopes, A. R., Pimentel, M., Faleiro, F., Baptista, M., Trübenbach, K., et al. (2014). Ocean cleaning stations under a changing climate: biological responses of tropical and temperate fish-cleaner shrimp to global warming. *Glob. Chang. Biol.* 20, 3068–3079. doi: 10.1111/gcb.12621

Scheiner, S. M., and Holt, R. D. (2012). The genetics of phenotypic plasticity. X. Variation versus uncertainty. *Ecol. Evol.* 2, 751–767. doi: 10.1002/ece3.217

Scheiner, S. M., and Yampolsky, L. Y. (1998). The evolution of *Daphnia pulex* in a temporally varying environment. *Genet. Res.* 72, 25–37. doi: 10.1017/S0016672398003322

Seebacher, F., White, C. R., and Franklin, C. E. (2014). Physiological plasticity increases resilience of ectothermic animals to climate change. *Nat. Clim. Chang* 51, 61–66. doi: 10.1038/nclimate2457

Shumway, S. E., Perkins, H. C., Schick, D. F., and Stickney, A. P. (1985). *Synopsis of Biological Data on the Pink Shrimp, Pandalus borealis Krøyer, 1838*. FAO Fisheries Synopsis No. 144, p. 57.

Silva, A. M. M., Ige, T., Goonasekara, C. L., and Heeley, D. H. (2020). Threonine-77 is a determinant of the Low-temperature conditioning of the Most abundant isoform of tropomyosin in Atlantic Salmon. *Biochemistry* 59, 2859–2869. doi: 10.1021/ACS.BIOCHEM.0C00416/ASSET/IMAGES/LARGE/BI0C00416_0006.JPEG

Simões, M. V. P., Saeedi, H., Cobos, M. E., and Brandt, A. (2021). Environmental matching reveals non-uniform range-shift patterns in benthic marine *Crustacea*. *Clim. Chang.* 168, 1–20. doi: 10.1007/S10584-021-03240-8/FIGURES/3

Sirovy, K. A., Johnson, K. M., Casas, S. M., La Peyre, J. F., and Kelly, M. W. (2021). Lack of genotype-by-environment interaction suggests limited potential for evolutionary changes in plasticity in the eastern oyster, *Crassostrea virginica*. *Mol. Ecol.* 30, 5721–5734. doi: 10.1111/MEC.16156

Sokal, R. R., and Rohlf, F. J. (1995). "Biometry: the principles and practice of statistics" in *Biological Research*. ed. W. H. Freeman. *3rd* ed (New York: WH Freeman and Company)

Somero, G. N. (2005). Linking biogeography to physiology: evolutionary and acclimatory adjustments of thermal limits. *Front. Zool.* 2, 1–9. doi: 10.1186/1742-9994-2-1/FIGURES/3

Somero, G. N. (2010). The physiology of climate change: how potentials for acclimatization and genetic adaptation will determine 'winners' and 'losers.' *J. Exp. Biol.* 213, 912–920. doi: 10.1242/JEB.037473

Stanley, R. R. E., DiBacco, C., Lowen, B., Beiko, R. G., Jeffery, N. W., Van Wyngaarden, M., et al. (2018). A climate-associated multispecies cryptic cline in the Northwest Atlantic. *Sci. Adv.* 4:eaaq0929. doi: 10.1126/sciadv.aaq0929

Stevenson, R. D. (1985). The relative importance of behavioral and physiological adjustments controlling body temperature in terrestrial ectotherms. *Am. Nat.* 126, 362–386. doi: 10.1086/284423

Tufto, J. (2015). Genetic evolution, plasticity, and bet-hedging as adaptive responses to temporally autocorrelated fluctuating selection: a quantitative genetic model. *Evolution* 69, 2034–2049. doi: 10.1111/evo.12716

Valenza-Troubat, N., Davy, M., Storey, R., Wylie, M. J., Hilario, E., Ritchie, P., et al. (2022). Differential expression analyses reveal extensive transcriptional plasticity induced by temperature in New Zealand silver trevally (*Pseudocaranx georgianus*). *Evol. Appl.* 15, 237–248. doi: 10.1111/EVA.13332

Veilleux, H. D., Ryu, T., Donelson, J. M., Van Herwerden, L., Seridi, L., Ghosheh, Y., et al. (2015). Molecular processes of transgenerational acclimation to a warming ocean. *Nat. Clim. Chang.* 512, 1074–1078. doi: 10.1038/nclimate2724

Waldvogel, A. M., Feldmeyer, B., Rolshausen, G., Exposito-Alonso, M., Rellstab, C., Kofler, R., et al. (2020). Evolutionary genomics can improve prediction of species' responses to climate change. *Evol. Lett.* 4, 4–18. doi: 10.1002/EVL3.154

Wang, Z., Lu, Y., Greenan, B., Brickman, D., and DeTracey, B. (2018). *BNAM: An Eddy Resolving North Atlantic Ocean Model to Support Ocean Monitoring*. Canadian Technical Report of Hydrography and Ocean Sciences 327, p. 18.

Whitehead, A., and Crawford, D. L. (2006). Neutral and adaptive variation in gene expression. *Proc. Natl. Acad. Sci. U. S. A.* 103, 5425–5430. doi: 10.1073/PNAS.0507648103/SUPPL_FILE/07648TABLE2.XLS

Zhang, X., Yuan, J., Sun, Y., Li, S., Gao, Y., Yu, Y., et al. (2019). Penaeid shrimp genome provides insights into benthic adaptation and frequent molting. *Nat. Commun.* 101, 1–14. doi: 10.1038/s41467-018-08197-4

frontiers | Frontiers in Marine Science

TYPE Original Research
PUBLISHED 23 May 2023
DOI 10.3389/fmars.2023.1170451

OPEN ACCESS

EDITED BY
Jonathan Y.S. Leung,
University of Adelaide, Australia

REVIEWED BY
Gisela Lannig,
Alfred Wegener Institute Helmholtz Centre for Polar and Marine Research (AWI), Germany
Liqiang Zhao,
Guangdong Ocean University, China

*CORRESPONDENCE
Ella Guscelli
ella.guscelli@uqar.ca

†These authors have contributed equally to this work and share last authorship

RECEIVED 20 February 2023
ACCEPTED 09 May 2023
PUBLISHED 23 May 2023

CITATION
Guscelli E, Chabot D, Vermandele F, Madeira D and Calosi P (2023) All roads lead to Rome: inter-origin variation in metabolomics reprogramming of the northern shrimp exposed to global changes leads to a comparable physiological status.
Front. Mar. Sci. 10:1170451.
doi: 10.3389/fmars.2023.1170451

All roads lead to Rome: inter-origin variation in metabolomics reprogramming of the northern shrimp exposed to global changes leads to a comparable physiological status

Ella Guscelli[1]*, Denis Chabot[2], Fanny Vermandele[1], Diana Madeira[3†] and Piero Calosi[1†]

[1]Marine Ecological and Evolutionary Physiology Laboratory, Département de Biologie, Chimie et Géographie, Université du Québec à Rimouski, Rimouski, QC, Canada, [2]Institut Maurice-Lamontagne, Fisheries and Oceans Canada, Mont-Joli, QC, Canada, [3]ECOMARE-Laboratory for Innovation and Sustainability of Marine Biological Resources, CESAM-Centre for Environmental and Marine Studies, Department of Biology, University of Aveiro, Aveiro, Portugal

Impacts of global ocean changes on species have historically been investigated at the whole-organism level. However, acquiring an in-depth understanding of the organisms' cellular metabolic responses is paramount to better define their sensitivity to environmental challenges. This is particularly relevant for species that experience highly different environmental conditions across their distribution range as local acclimatization or adaptation can influence their responses to rapid global ocean changes. We aimed at shedding light on the cellular mechanisms underpinning the sensitivity to combined ocean warming (OW) and acidification (OA) in the northern shrimp *Pandalus borealis*, from four different geographic origins defined by distinctive environmental regimes in the northwest Atlantic: i.e. St. Lawrence Estuary (SLE), Eastern Scotian Shelf (ESS), Esquiman Channel (EC) and Northeast Newfoundland Coast (NNC). We characterized targeted metabolomics profiles of the muscle of shrimp exposed to three temperatures (2, 6 or 10°C) and two pH levels (7.75 or 7.40). Overall, shrimp metabolomics profiles were modulated by a significant interaction between temperature, pH and origin. Temperature drove most of the metabolomics reprogramming, confirming that *P. borealis* is more sensitive to OW than OA. Inter-origin differences in metabolomics profiles were also observed, with temperature*pH interactions impacting only shrimp from SLE and ESS, pH affecting only shrimp from SLE and temperature impacting shrimp from all origins. Temperature influenced metabolomics pathways related to the tricarboxylic acid cycle (TCA) and amino acid metabolism, resulting mainly in an accumulation of TCA intermediates and tyrosine. Temperature*pH and pH in isolation only affected amino acid metabolism, leading to amino acids accumulation under low pH. However, the ratio of ATP : ADP remained constant across conditions in shrimp from all origins suggesting that their energetic status is not affected by OW and OA. Still, the accumulation of TCA intermediates and tyrosine suggests the possible enhancement of immune

10.3389/fmars.2023.1170451

responses under future OW and OA conditions. Our findings suggest that shrimp from SLE are more sensitive at the molecular level, compared to others, to future complex environmental conditions. This underlines the importance of investigating intraspecific variation in mechanisms of responses to combined drivers when trying to define species' sensitivity to global ocean changes.

KEYWORDS

Metabolomics (OMICS), macrophysiology, conservation physiology, crustaceans, Pandalus borealis, pathways, stress, immunity

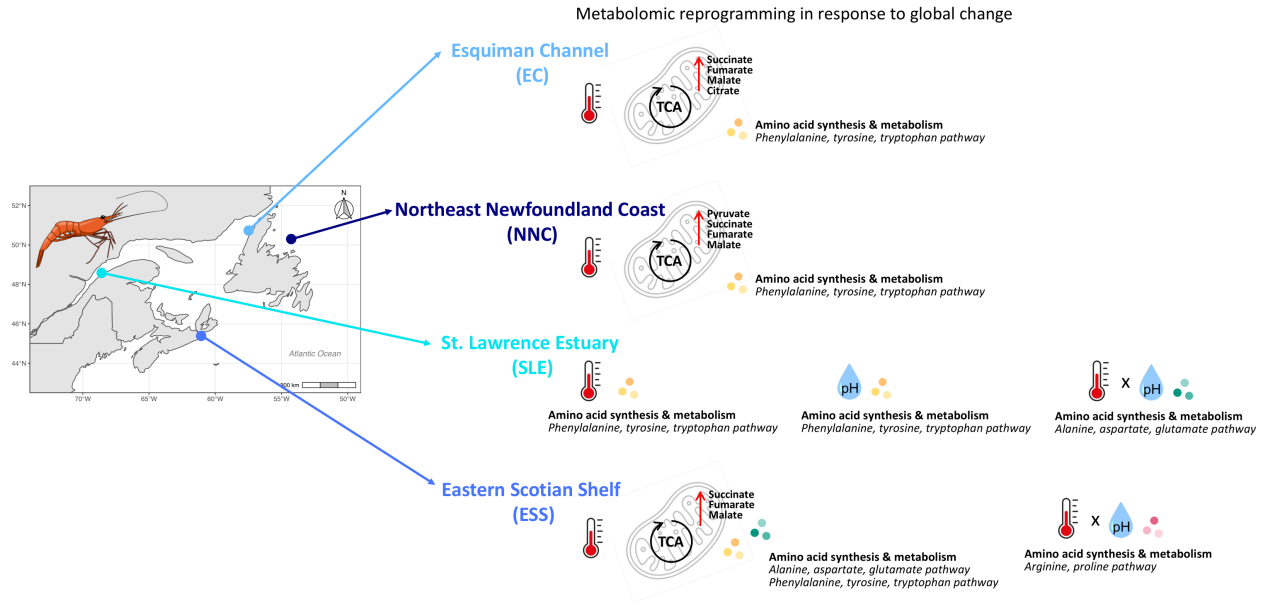

1 Introduction

The rising concentration of anthropogenically emitted carbon dioxide (CO_2) in the atmosphere directly affects the marine environment *via* the decrease of global mean seawater pH and change in carbonate chemistry (ocean acidification, OA) (Caldeira and Wickett, 2003; IPCC, 2022). Indirectly, the increase of greenhouse gasses leads to rising seawater temperatures, a phenomenon known as ocean warming (OW) (IPCC, 2022). According to the most pessimistic, but also most realistic, scenario of the Intergovernmental Panel on Climate Change (IPCC, 2022), both OA and OW are predicted to worsen by the end of the century (+4°C and -0.3 pH units mean globally) posing a major threat to marine biodiversity, particularly to calcifying organisms and ectotherms (Orr et al., 2005; Paaijmans et al., 2013; Lefevre, 2016). Survival, metabolism, growth, reproduction and behaviour are some of the traits affected by OW and OA, as observed at the whole-organism level: which happen to be the most studied traits in global change biology to define species' sensitivity to global changes. However, to better understand the mechanisms underlying the responses to environmental changes at higher levels of biological organization (from whole-organism to species, communities and ecosystems), it is necessary to elucidate and integrate the responses at lower levels of biological organization, i.e. cellular and molecular levels (Bartholomew, 1964; Harvey et al., 2014). In this context, the use of state-of-the-art molecular tools, such as -omics techniques, are of great interest as they allow the determination of which molecules and ultimately which cellular pathways play an important role in the response of organisms exposed to different climate change scenarios (Jones et al., 2013; Pinu et al., 2019; Cappello, 2020; Ebner, 2021). In particular, metabolites are the end products of cellular regulatory processes

that involve multiple interactions among genes, transcripts, proteins and the environment. Therefore, metabolites are considered to be representative of cellular, organs, and organism phenotypes (Fiehn, 2002). Recently, the use of metabolomics analyses, i.e. the identification and quantification of targeted or all metabolites of a biological system (Bundy et al., 2009), has increased in studies investigating the responses of organisms to environmental changes (Williams et al., 2009; Mayor et al., 2015; Aru et al., 2017; Wu et al., 2017; Li et al., 2020a; Li et al., 2020b), and specifically to global change drivers such as OW, OA and ocean deoxygenation, in isolation or combined (e.g. Ellis et al., 2014; Wei et al., 2015; Zhang et al., 2017; Huo et al., 2019). Indeed, in multiple cases, global change drivers have been shown to induce a shift in metabolic pathways, phenomenon known as metabolic reprogramming, and to affect the energy metabolism of organisms (Lannig et al., 2010; Liu et al., 2020; Noisette et al., 2021; Dong et al., 2022; Thor et al., 2022). Elevated levels of succinate, fumarate and malate suggest a disruption of the tricarboxylic acid cycle (TCA) that, together with elevated levels of lactate, support the hypothesis of a shift from aerobic to anaerobic metabolism (Williams et al., 2009; Wei et al., 2015; Clark et al., 2017; Huo et al., 2019; Noisette et al., 2021). However, metabolism not only changes in response to the effect of ocean global drivers, but it is also shown to vary among populations of the same species. For example, populations of the common periwinkle *Littorina littorea* in the northeast Atlantic appeared metabolically adapted to the regional environmental conditions they experience. This was shown by differences in their metabolic rates and metabolomics profiles that influenced their whole-organism response to OA (Calosi et al., 2017). Differences in metabolic rates among populations, and in their response to OW and OA, have been shown in a number of marine species (Di Santo, 2015; Vargas et al., 2017; Thor et al., 2018). Therefore, multi-population studies need to be conducted to accurately and reliably determine species' sensitivity to future ocean conditions, to help identifying the mechanisms underpinning known whole-organism physiological responses. This is especially true for species with a wide range of distribution and of ecological and commercial relevance. A good example is the northern shrimp *Pandalus borealis*. This species is widely distributed in the north Atlantic (Bergström, 2000), where it is a major prey for many fish and marine mammal predators of these ecosystems and supports important fisheries (Hammill and Stenson, 2000; Dawe et al., 2012; Jónsdóttir et al., 2012). In particular, it is the third most lucrative marine fishery in the Canadian waters of the northwest Atlantic (DFO, 2021a). The northern shrimp has been shown to be sensitive to both OW and OA (Brillon et al., 2005; Chabot and Ouellet, 2005; Daoud et al., 2007; Bechmann et al., 2011; Arnberg et al., 2013; Hammer and Pedersen, 2013; Chemel et al., 2020). In addition, it appears to be potentially long-term acclimatized or adapted to regional environmental conditions throughout the northwest Atlantic (Koeller et al., 2009; Ouellet et al., 2017). Indeed, average bottom waters, where shrimp are most abundant, are characterized by higher temperatures and lower pH levels (~6-7°C, ~7.6 pH units) in the Gulf of St. Lawrence compared to the deep waters outside the St. Lawrence system (~0-3°C, ~7.8-8 pH units) (DFO, 2021b; Bourdages et al., 2022; Cyr et al., 2022; DFO, 2022a; DFO, 2022b). Our study aimed at shedding light on the cellular mechanisms underpinning the physiological responses of the northern shrimp from different geographic origins with distinctive environmental conditions, under combined OW and OA scenarios predicted to occur at the end of the century, to characterize the intraspecific variation in metabolic pathways across conditions. To do so, we exposed female shrimp from four different geographic origins within the northwest Atlantic (i.e. St. Lawrence Estuary, Eastern Scotian Shelf, Esquiman Channel and Northeast Newfoundland Coast) to different combinations of OW and OA, and we identified key metabolites associated to the aerobic and anaerobic metabolism to perform targeted metabolomics analyses. Based on our current knowledge, we hypothesize that shrimp from different origins will show different metabolomics profiles under exposure to combined OW and OA, but all possibly showing a shift from aerobic to anaerobic metabolism.

2 Material and methods

2.1 Ethical statement

All procedures complied with Canadian legislation for animal experimentation as the Canadian Council for Animal Care does not require projects using crustaceans to be approved by an Animal Care Committee, thus an ethics approval was not required for this study.

2.2 Shrimp collection and experimental design

The analyses of key targeted metabolites associated to the aerobic and anaerobic metabolism was carried out on abdominal muscle samples of female shrimp *P. borealis* previously exposed to isolated and combined OW and OA scenarios (Guscelli et al. *under review*). Female shrimp were selected because they are the main target of the fishery, they have a greater role in defining population demography and are more sensitive compared to males to ocean global change drivers (Dupont-Prinet et al., 2013). Moreover, we selected only non-ovigerous females to avoid any potential confounding effect linked to differences in reproductive stages and the oxygen consumption of the egg mass. Briefly, shrimp were collected from four different geographic origins within the northwest Atlantic: i.e. St. Lawrence Estuary (SLE, 48° 35' N, 68° 35' W; May 2018), Eastern Scotian Shelf (ESS, 45° 23' N, 61° 04' W; February 2019), Esquiman Channel (EC, 50° 44' N, 57°29' W; July 2019) and Northeast Newfoundland Coast (NNC, 50° 18' N, 54° 16' W; November 2019) with shrimp trawls or traps. At depths where shrimp were sampled temperature and pH conditions are stable year-round, but subjected to slow inter-annual changes. Shrimp were then transported to the Maurice-Lamontagne Institute (MLI), Fisheries and Oceans Canada (Mont-Joli, QC, Canada) where they were maintained in rearing tanks (1700 L) for approximately eight weeks before the beginning of the experiment. Average conditions

during this period were 4.5°C, pH 7.9, 100% oxygen saturation relative to air and salinity 32. Shrimp were then exposed for 30 d to one of six treatments (with two replicate tanks *per* treatment) combining temperatures and pH levels representing the favourable, actual, or future scenario in the northwest Atlantic. In detail, 2°C was chosen as favourable temperature for this species (Shumway et al., 1985), while 6°C represents the recent temperature of shrimp habitat in the Gulf of St. Lawrence (GSL) (Bourdages et al., 2022) and a +4°C predicted globally for the end of the century (RCP 8.5 scenario, IPCC, 2014) for other origins, such as ESS and NNC, and 10°C corresponds to the +4°C increase for GSL shrimp (IPCC, 2014). A pH of 7.75 was selected based on the current conditions of the deep waters of the Estuary and Gulf of St. Lawrence (Mucci et al., 2011; Mucci et al., 2018) and approximatively the -0.3 pH units decrease scenario predicted to occur globally by the year 2100 (RCP 8.5 scenario, IPCC, 2014) for other origins, such as ESS and NNC, while the pH of 7.40 was chosen to correspond to the -0.3 pH units drop for GLS shrimp (IPCC, 2014). Treatments were identified as low temperature and current pH (2C: 2°C, pH 7.75), low temperature and low pH (2A: 2° C, pH 7.40), intermediate temperature and current pH (6C: 6°C, pH 7.75), intermediate temperature and low pH (6A: 6°C, pH 7.40), elevated temperature and current pH (10C: 10°C, pH 7.75), elevated temperature and low pH (10A: 10°C, pH 7.40). At the end of the exposure period, we measured shrimp oxygen uptake as a proxy for metabolic rates *via* intermittent-flow respirometry on five individual *per* tank (10 *per* treatment) (results are presented in Guscelli et al. *under review*). At the end of the respirometry trials we rapidly dissected shrimp on ice and the abdomen muscle was carefully placed in microtubes (Eppendorf, Germany) and flash-frozen in liquid nitrogen to instantly interrupt all biochemical reactions. This procedure was conducted rigorously and rapidly, lasting less than a minute, in order to minimize the negative effects of handling and standardise them (if any) across all treatment and origin combinations. Samples were then stored at -80°C pending analyses.

Shrimp that moulted and/or died during respirometry measurements were considered as unstable samples for metabolomics analysis and they were thus removed from the dataset.

Maintenance of shrimp from all geographic origins and monitoring of temperature and pH in the experimental setup were similar to those detailed for shrimp of SLE in Chemel et al. (2020). For details on the physico-chemical parameters for the duration of the 30-d experiment see Guscelli et al. (*under review*).

2.3 Metabolite extraction and quantification

Metabolite extraction was carried out by Les laboratoires Iso-BioKem Inc. following the method established in their laboratory. Briefly, samples were first freeze-dried for 24 h and then divided in two centrifugal PP tubes (1.5 mL) to carry out the extraction for positive and negative analyses separately. Each part was then weighted, to later normalize metabolite concentration, and homogenized at 6000 rpm for 30 s at −4°C (Precellys 24 with cryolis cooling unit, Bertin corporation, Montigny-le-Bretonneux, France). Once the extraction solution was added, samples were vortexed for 10 s and centrifuged at 30130 ×*g* for 5 min at 5°C to collect and transfer 250 µL of supernatant in an amber HPLC vial with insert (Wheaton, NJ, USA) to analyse the fresh extract. Finally, 225 µL of the supernatant were injected in a high-performance liquid chromatography system (HPLC 1260 Infinity II, Agilent Technologies, Santa Clara, CA, USA) coupled to a mass spectrometer (6420 Triple Quad, Agilent Technologies) to detect targeted metabolites. The absolute quantification of these metabolites (in ng mL^{-1}) was assessed with the MassHunter QQQ quantitative (Quant-my-Way) software (Agilent Technologies) using a calibration curve previously created using Phenylalanine-d8 and Fumarate-d4 standards (Cambridge Isotope Laboratories, Tewksbury, MA, USA).

2.4 Data pre-processing

Raw data matrices were normalized by wet weight and final concentration values were expressed as ng metabolite mg^{-1} wet weight. As LC-MS metabolomics datasets can contain a high amount of missing values (Wei et al., 2018), the matrices were first imported in the web tool MetImp 1.2 (https://metabolomics.cc.hawaii.edu/software/MetImp/, accessed in September 2021) for missing data imputation. As our missing data were due to limit of quantification (LOQ) of the technique, we followed the protocol proposed by Wei et al. (2018) for the 'Missing not at random (MNAR)' type of missing values. Briefly, we used the QRILC algorithm (Quantile Regression Imputation of Left-Censored Data) with 40% group wise missing filtering to input missing values (seed 1234). We decided to increase the threshold to 40% missing values in order to keep more metabolites for the statistical analyses and only rejected 14 metabolites out of 48 identified. Finally, the database was imported into Metaboanalyst 5.0 (http://www.metaboanalyst.ca/, accessed in October 2021) to be log-transformed, to reduce lack of normality and heteroscedasticity in the data, and auto-scaled, to adjust for differences in fold-changes between metabolites.

2.5 Data analysis

Unsupervised principal components analysis (PCA) was applied to explore data structure (FactoMineR package, Husson et al., 2010) and one outlier was removed from the complete dataset. Then, to test the isolated and combined effects of elevated seawater temperature, low pH and geographic origin on metabolomics profiles of shrimp muscle tissue, we performed a three-way Permutational Multivariate Analysis of Variance (PERMANOVA). The PERMANOVA was applied to the data resemblance matrix (based on Euclidean distance) and was run

using type III sums of squares and permutation of residuals under a reduced model (9999 permutations) using the PERMANOVA + add-on in Primer-E v6 (Anderson et al., 2008).

Multivariate and univariate analyses were performed to identify metabolites that discriminate between different temperatures and pH levels, within each geographic origin. Four PCAs were carried out to explore data structure, one *per* geographic origin. Additionally, to test for the effect of temperature, pH and their interaction within each geographic origin, a two-way analysis of variance (ANOVA) with a False Discovery Rate (FDR) cut-off set at 0.05 for significance was carried out for each metabolite on the database (specimen package, Costa et al., 2017). As commonly done when a high number of comparisons exists, the FDR was applied to correct *p*-values (separately for each origin and each factor) for 34 tests. When one of these tests was significant according to FDR, Tukey *post-hoc* tests were used to identify significant differences using the HSD.test or the glht function for isolated or interactive effects respectively (Hothorn et al., 2008; Bretz et al., 2016). Analyses were performed using the software R 4.1.1 version (R Core Team, 2020). Finally, significant metabolites identified by the ANOVAs were then used for pathway analysis to assess the most relevant metabolic pathways involved in the response of shrimp from different geographic origins to temperature increases and pH decreases. To do so, the chosen metabolites were imputed in the "Pathway Analysis" tool of the MetaboAnalyst software. As there are no libraries available for shrimp, we chose the pathway library of a model organism within the same phylum (Arthropoda), namely *Drosophila melanogaster* (fruit fly). Pathway analysis was carried out based on functional enrichment, assessed using hypergeometric tests for over-representation analysis ($p < 0.05$), and pathway topology analysis, implemented using the relative betweenness centrality (> 0.1). Pathways were considered relevant according to either over-representation $p < 0.05$ or pathway topology analysis with impact > 0.1 and most relevant according to the combination of both.

Finally, linear models were used to test the effects of isolated and combined seawater temperature and pH, and geographic origin (fixed factors) on shrimp ATP : ADP ratio, which was calculated and analysed *a posteriori* to verify the cellular energetic status.

3 Results

3.1 Whole metabolome

The overall PCAs, applied to explore the general data structure by factor (geographic origin, temperature, pH and temperature*pH treatments), did not show clear group separation (Supplementary Figure 1).

However, temperature and pH significantly and differently modulated the metabolomics profiles of shrimp from the four geographic origins as indicated by the presence of a significant interaction among origin, temperature and pH (Table 1).

3.2 Origins

For each origin, the PCAs did not show a clear group separation as some overlapping was found among temperature*pH treatments (Figure 1). However, some differences in metabolomics profiles of shrimp exposed to current and low pH levels were shown for shrimp from the SLE (Figure 1), while some differences between the lowest and highest temperatures were shown for the metabolomics profiles of shrimp from the three other origins (Figure 1). Furthermore, for all geographic origins, between seven and 12 metabolites were found to change significantly among temperature, pH and temperature*pH treatments (Supplementary Table 1). Three metabolites of shrimp from the SLE and one metabolite of shrimp from ESS differed among temperature*pH treatments as indicated by the presence of a significant interaction between temperature and pH (Table 2). However, no effect of this interaction was found to be significant on metabolomics profiles of shrimp from EC and NNC (Table 2). Additionally, temperature alone was found to significantly affect the metabolomics profiles of shrimp from all geographic origins whilst pH in isolation was found to significantly affect the metabolomics profiles of shrimp from SLE (Table 2).

3.2.1 SLE

i) The concentration of three metabolites differed significantly among temperature*pH treatments as indicated by the presence of a significant interaction between temperature and pH (Table 2). Pathway analysis showed that these metabolites were involved in five relevant pathways, including: amino acid and pyruvate metabolism and arginine biosynthesis (Figure 2A). The most relevant pathway was the alanine, aspartate and glutamate metabolism (Figure 2A). In this pathway, aspartate mean concentration increased between current and low pH at the intermediate temperature (Figure 2A). Despite the fact that significant effects were evidenced by the ANOVA on pyruvate, multiple comparisons tests between treatments failed to detect significant differences among groups.

ii) The concentration of three metabolites differed significantly between pH treatments (Table 2), and pathway analysis showed that these metabolites were involved in six relevant pathways, including: amino acid biosynthesis and metabolism, aminoacyl-tRNA biosynthesis, ubiquinone and other terpenoid-quinone biosynthesis and biotin metabolism (Figure 2B). The most relevant pathway was the phenylalanine, tyrosine and tryptophan biosynthesis (Figure 2B). In this pathway, tyrosine mean concentration increased at low pH (Figure 2B).

iii) The concentration of two metabolites differed significantly among temperature treatments (Table 2), and the pathway analysis showed that these metabolites were involved in four relevant pathways, including: amino acid biosynthesis and metabolism and ubiquinone and other terpenoid-quinone biosynthesis (Figure 2C). The most relevant pathway was the phenylalanine, tyrosine and tryptophan biosynthesis (Figure 2C). Within this pathway, tyrosine mean concentration increased with increasing temperature being

10.3389/fmars.2023.1170451

TABLE 1 Summary of the results of the PERMANOVA test employed to investigate the effects of origin, temperature and pH and their interactions on the northern shrimp muscle metabolomics profiles.

Source	df	SS	MS	Pseudo-F	P (perm)	Unique perms
Origin (O)	3	881.92	293.97	11.74	**0.0001**	9863
Temperature (T)	2	395.17	197.58	7.89	**0.0001**	9885
pH	1	76.45	76.45	3.05	**0.0002**	9905
O*T	6	294.49	49.08	1.96	**0.0001**	9795
O*pH	3	91.91	30.64	1.22	0.1239	9861
T*pH	2	72.89	36.44	1.46	**0.0475**	9887
O*T*pH	6	241.27	40.21	1.61	**0.0003**	9831
Residuals	196	4907.80	25.04			
Total	219	6957				

The analysis was based on a Euclidean distance matrix, 9999 permutations and type III sums of squares. Numbers in bold indicate significant p-values.

the highest and similar at the two highest temperature treatments (Figure 2C).

3.2.2 ESS

i) Only the concentration of hydroxyproline differed significantly among temperature*pH treatments as indicated by the presence of a significant interaction between temperature and pH (Table 2), and the pathway analysis showed that this metabolite was involved in the arginine and proline metabolism, despite the fact that MetaboAnalyst was unable to produce a pathway figure due to the input metabolite list being only one metabolite. Moreover, multiple comparisons tests between treatments failed to detect significant differences in hydroxyproline concentrations among groups.

ii) The concentration of 12 metabolites differed significantly among temperature treatments (Table 2), and the pathway analysis showed that these metabolites were involved in eight relevant pathways, including: citrate cycle, amino acid biosynthesis and metabolism, aminoacyl-tRNA biosynthesis and pyruvate metabolism (Figure 3). Among these, four were the most relevant pathways: the citrate cycle, the alanine, aspartate and glutamate metabolism, the phenylalanine, tyrosine and tryptophan biosynthesis and the tyrosine metabolism (Figure 3). Within these most relevant pathways, malate, fumarate and succinate mean concentrations increased with increasing temperature being the highest and similar at the two highest temperature treatments (Figure 3). Conversely, tyrosine mean concentrations measured at the two lowest temperatures tested were similar but lower than

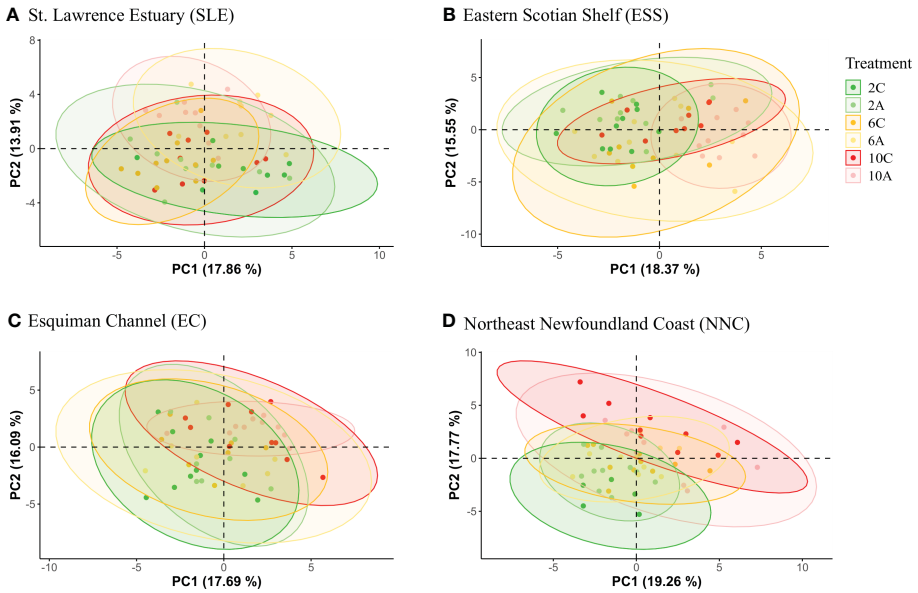

FIGURE 1
PCA 2D score plot with 95% confidence ellipse representing the variation in metabolomics profiles in the northern shrimp *Pandalus borealis* according to temperature*pH treatments: 2C (2°C, pH 7.75), 2A (2°C, pH 7.40), 6C (6°C, pH 7.75), 6A (6°C, pH 7.40), 10C (10°C, pH 7.75) and 10A (10°C, pH 7.40) for **(A)** St. Lawrence Estuary (SLE), **(B)** Eastern Scotian Shelf (ESS), **(C)** Esquiman Channel (EC) and **(D)** Northeast Newfoundland Coast (NNC).

TABLE 2 Summary of the results of the ANOVA tests used to investigate the effects of temperature and pH and their interaction on metabolites quantified in the northern shrimp muscle samples.

		Temperature			pH			Temperature*pH		
Origin	Metabolite	F value	p value	FDR	F value	p value	FDR	F value	p value	FDR
SLE	Betaine	0.339	0.714	0.905	4.996	0.030	0.136	8.512	0.001	**0.011**
SLE	Tyrosine	10.305	0.000	**0.003**	21.395	< 0.001	**0.001**	0.368	0.694	0.787
SLE	Hydroxyproline	0.553	0.579	0.905	15.241	0.000	**0.005**	0.124	0.884	0.911
SLE	Serine	11.841	< 0.001	**0.002**	0.618	0.436	0.549	4.851	0.012	0.101
SLE	Aspartate	0.333	0.719	0.905	5.084	0.029	0.136	10.503	0.000	**0.005**
SLE	Lysine	3.086	0.054	0.236	14.176	0.000	**0.005**	2.653	0.080	0.241
SLE	Pyruvate	0.420	0.659	0.905	0.684	0.412	0.539	6.450	0.003	**0.037**
ESS	Tryptophan	19.920	< 0.001	**0.000**	1.773	0.189	0.611	1.204	0.308	0.552
ESS	Tyrosine	7.507	0.001	**0.010**	2.929	0.093	0.452	2.107	0.132	0.552
ESS	Hydroxyproline	0.076	0.927	0.927	0.147	0.703	0.886	7.929	0.001	**0.034**
ESS	Threonine	6.629	0.003	**0.011**	0.008	0.931	0.931	0.008	0.304	0.552
ESS	Serine	15.735	< 0.001	< **0.001**	4.339	0.042	0.287	2.245	0.116	0.552
ESS	α Aminoadipic acid	5.532	0.007	**0.023**	9.040	0.004	0.069	0.251	0.779	0.855
ESS	Aspartate	10.194	0.000	**0.002**	0.950	0.334	0.757	2.603	0.084	0.474
ESS	Cystine	4.617	0.014	**0.044**	0.669	0.417	0.757	2.674	0.078	0.474
ESS	Glucose	6.519	0.003	**0.011**	0.019	0.892	0.920	0.737	0.483	0.632
ESS	Succinate	6.850	0.002	**0.011**	5.881	0.019	0.213	1.441	0.246	0.552
ESS	Fumarate	7.397	0.001	**0.010**	0.325	0.571	0.809	0.747	0.479	0.632
ESS	Malate	7.036	0.002	**0.011**	0.485	0.490	0.774	1.643	0.203	0.552
EC	Tyrosine	12.535	< 0.001	**0.001**	3.785	0.058	0.492	2.297	0.112	0.615
EC	*β* Aminoisobutyric	7.273	0.002	**0.007**	0.149	0.702	0.822	0.967	0.388	0.791
EC	α Aminobutyric acid	20.310	< 0.001	< **0.001**	0.253	0.618	0.822	1.909	0.160	0.615
EC	Threonine	9.664	0.000	**0.003**	1.900	0.175	0.609	0.210	0.811	0.869
EC	Serine	20.890	< 0.001	< **0.001**	2.632	0.112	0.516	0.253	0.778	0.869
EC	α Aminoadipic acid	4.724	0.014	**0.042**	1.047	0.311	0.688	1.826	0.173	0.615
EC	Succinate	7.181	0.002	**0.007**	4.832	0.033	0.374	0.277	0.759	0.869
EC	Fumarate	8.581	0.001	**0.003**	0.271	0.605	0.822	0.946	0.396	0.791
EC	Malate	8.705	0.001	**0.003**	0.540	0.466	0.822	0.236	0.791	0.869
EC	ADP	9.377	0.000	**0.003**	0.215	0.645	0.822	5.116	0.010	0.168
EC	Citrate	6.502	0.003	**0.011**	1.673	0.202	0.625	0.572	0.569	0.869
NNC	Phenylalanine	50.640	< 0.001	< **0.001**	0.589	0.447	0.805	0.125	0.883	0.968
NNC	Isoleucine	6.171	0.004	**0.016**	0.447	0.507	0.805	0.397	0.675	0.900
NNC	Tyrosine	13.309	< 0.001	**0.000**	0.881	0.353	0.805	0.641	0.531	0.838
NNC	α Aminobutyric acid	5.213	0.009	**0.030**	1.817	0.184	0.805	1.163	0.321	0.761
NNC	α Aminoadipic acid	9.510	0.000	**0.002**	0.609	0.439	0.805	0.308	0.736	0.900
NNC	Histidine	5.089	0.010	**0.031**	0.026	0.873	0.885	0.032	0.969	0.991
NNC	Cystine	12.279	< 0.001	**0.000**	0.231	0.633	0.828	3.667	0.033	0.280

(Continued)

TABLE 2 Continued

Origin	Metabolite	Temperature			pH			Temperature*pH		
		F value	p value	FDR	F value	p value	FDR	F value	p value	FDR
NNC	Pyruvate	8.259	0.001	**0.004**	0.113	0.738	0.839	0.928	0.402	0.765
NNC	Succinate	13.599	< 0.001	**0.000**	0.572	0.453	0.805	3.891	0.027	0.280
NNC	Fumarate	19.579	< 0.001	**< 0.001**	0.330	0.568	0.805	5.248	0.009	0.280
NNC	Malate	20.494	< 0.001	**< 0.001**	0.135	0.715	0.839	4.071	0.023	0.280

Origins: St. Lawrence Estuary (SLE), Eastern Scotian Shelf (ESS), Esquiman Channel (EC) and Northeast Newfoundland Coast (NNC). Only significant metabolites are included in the table. Numbers in bold indicate significant p-values.

mean concentration at the highest temperature condition (Figure 3). Similarly, aspartate mean concentration significantly increased between 6 and 10°C and the mean concentration measured at the lowest temperature was comparable to the one measured at the two highest temperatures tested (Figure 3).

3.2.3 EC

The concentration of 11 metabolites differed significantly among temperature treatments (Table 2), and the pathway analysis showed that these metabolites were involved in six relevant pathways, including: citrate cycle, amino acid biosynthesis and metabolism, pyruvate metabolism and glyoxylate and dicarboxylate metabolism (Figure 4). Among these, three were the most relevant pathways: the citrate cycle, the phenylalanine, tyrosine and tryptophan biosynthesis and the tyrosine metabolism (Figure 4). Within these pathways, malate, fumarate, succinate, citrate and tyrosine mean concentrations all increased with increasing temperature. In more detail, malate, fumarate and citrate mean concentrations measured at the two lowest temperatures tested were similar and the lowest compared to the mean reported at the highest temperature condition (Figure 4). Differently, tyrosine mean concentrations measured at the two highest temperatures were significantly higher than that reported at the lowest temperature condition, but comparable to each other (Figure 4). Finally, succinate mean concentration measured at the highest and lowest temperatures were significantly different from each other, and both comparable to the mean measured at the intermediate temperature (Figure 4).

3.2.4 NNC

The concentration of 11 metabolites differed significantly among temperature treatments (Table 2), and the pathway analysis showed that these metabolites were involved in nine relevant pathways, including: citrate cycle, amino acid biosynthesis and metabolism, aminoacyl-tRNA biosynthesis and pyruvate metabolism (Figure 5). Among these, five were the most relevant pathways: the citrate cycle, the phenylalanine, tyrosine and tryptophan biosynthesis, the tyrosine metabolism, phenylalanine metabolism and the pyruvate metabolism (Figure 5). In these pathways, metabolites such as malate, fumarate, succinate, pyruvate, phenylalanine and tyrosine mean concentrations increased with increasing temperature. In more detail, succinate and pyruvate mean concentration were similar at the two lowest temperatures tested, but lower than the mean concentration at the highest temperature condition (Figure 5), whilst mean concentration for all other metabolites significantly differed among all temperatures tested (Figure 5).

3.3 ATP : ADP ratio

No significant effect of temperature, pH and their interaction was found on the ATP : ADP ratio of shrimp from any origin (minimum *p*-value = 0.6339).

4 Discussion

Here, we show that the ecologically and economically important northern shrimp undergoes metabolomics reprogramming under future global change scenarios, shrimp from different origin responding differently to the combined exposure to temperature and pH. This said, temperature drives most of the responses, followed by a modest effect of the interaction between temperature and pH and almost no effect of pH. These results confirm that the northern shrimp is more sensitive to OW than to OA, similarly to what has been reported for other marine organisms (e.g. Schalkhausser et al., 2014; Noisette et al., 2016; Matoo et al., 2021). Additionally, inter-origin differences are observed, as combined effects of temperature and pH are only detected in SLE and ESS shrimp, and the isolated effect of pH is only evident in SLE shrimp. Despite these inter-origin differences, the metabolomics changes observed are comparable and all related to the regulation of the aerobic energy production pathway and amino acid metabolism, with environmental drivers mostly impacting metabolites of the tricarboxylic acid cycle (TCA). While these metabolites are intrinsically linked to energy metabolism, recent studies emphasize that TCA intermediates participate in a wide range of cellular processes (Martínez-Reyes and Chandel, 2020; Choi et al., 2021). Based on our previous results on *P. borealis* physiological responses to global change drivers (Guscelli et al. *under review*) and the present study, we propose that modulation of TCA intermediates and amino acids may be an important mechanism regulating immune and stress responses of shrimp under global change scenarios.

10.3389/fmars.2023.1170451

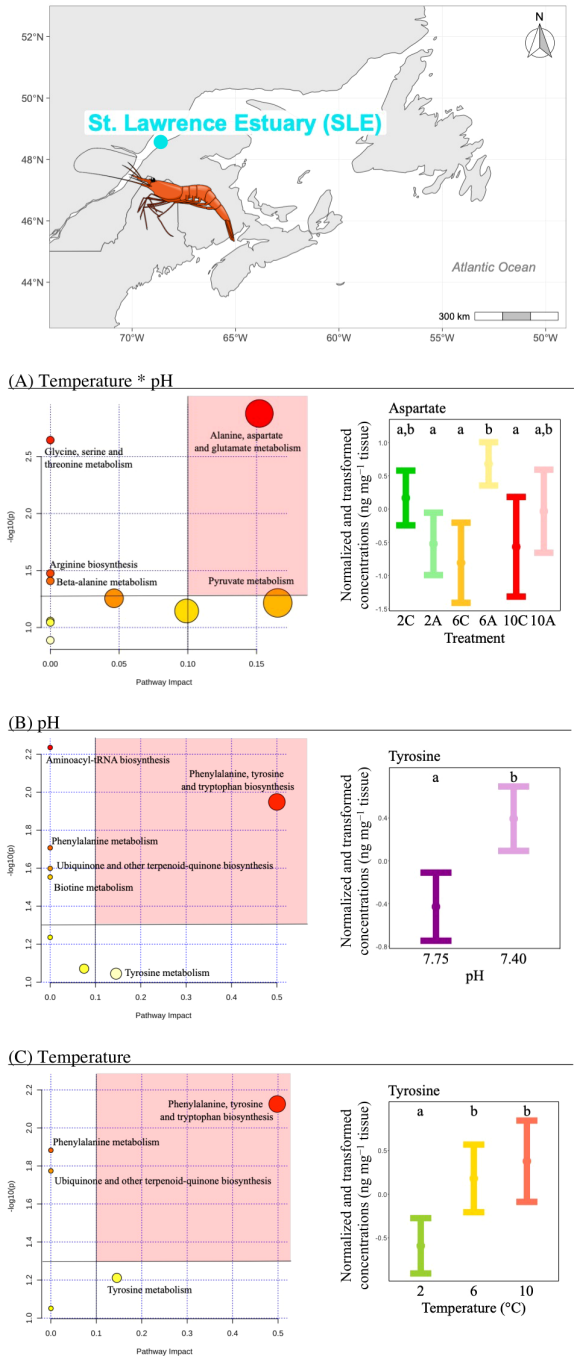

FIGURE 2
Metabolomics differences due to isolated and combined effects of seawater temperature and pH in the northern shrimp *P. borealis* from the St. Lawrence Estuary (SLE). In more detail, at the top of the figure, we show the map representing the collection site and at the left results for the pathway analysis of metabolic changes carried out with the statistically significant metabolites (ANOVA $p < 0.05$) due to **(A)** the combined effect of seawater temperature and pH, **(B)** the isolated effect of seawater pH and **(C)** the isolated effect of seawater temperature. Pathways within the red area were considered the most relevant as they have $p < 0.05$ and impact > 0.1. On the right, **(A)** mean and 95% CI for aspartate concentration for each temperature*pH treatments: 2C (green, N=9), 2A (light green, N=10), 6C (yellow, N=10), 6A (light yellow, N=9), 10C (red, N=9) and 10A (light red, N=9); **(B)** mean and 95% CI for tyrosine concentration for each pH treatment: 7.75 (purple, N=28) and 7.40 (light purple, N=28), combining all temperatures; **(C)** mean and 95% CI for tyrosine concentration for each temperature treatment: 2 (green, N=19), 6 (yellow, N=19) and 10°C (red, N=18), combining all pH levels. Lower case letters identify significant differences ($p < 0.05$) among treatments.

10.3389/fmars.2023.1170451

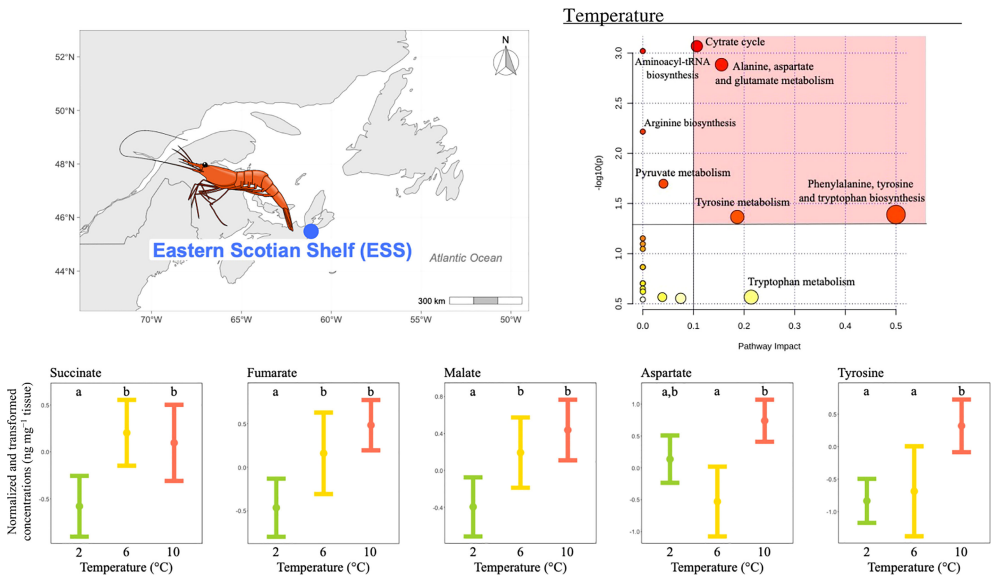

FIGURE 3
Metabolomics differences among temperatures in the northern shrimp *P. borealis* from the Eastern Scotian Shelf (ESS). In more detail, at the top left of the figure we show the map representing the collection site and at the top right of the figure we show the pathway analysis of metabolic changes carried out with the statistically significant metabolites (ANOVA $p < 0.05$). Pathways within the red area were considered the most relevant as they have $p < 0.05$ and impact > 0.1. At the bottom of the figure we show the mean concentration and 95% CI for succinate, fumarate, malate, aspartate and tyrosine for each temperature treatment: 2 (green, N=20), 6 (yellow, N=19) and 10°C (red, N=19), combining all pH levels. Lower case letters identify significant differences ($p < 0.05$) among treatments.

Overall, the northern shrimp metabolomics profiles are mainly affected by temperature. Indeed, only metabolites concentrations of shrimp from SLE changed under exposure to low pH or its combination with temperature, suggesting that shrimp from SLE are more sensitive to OA than shrimp from other origins, at the molecular level. These results are coherent with the results obtained previously at higher levels of biological organization, which confirm that overall adults of *P. borealis* are more sensitive to OW than OA

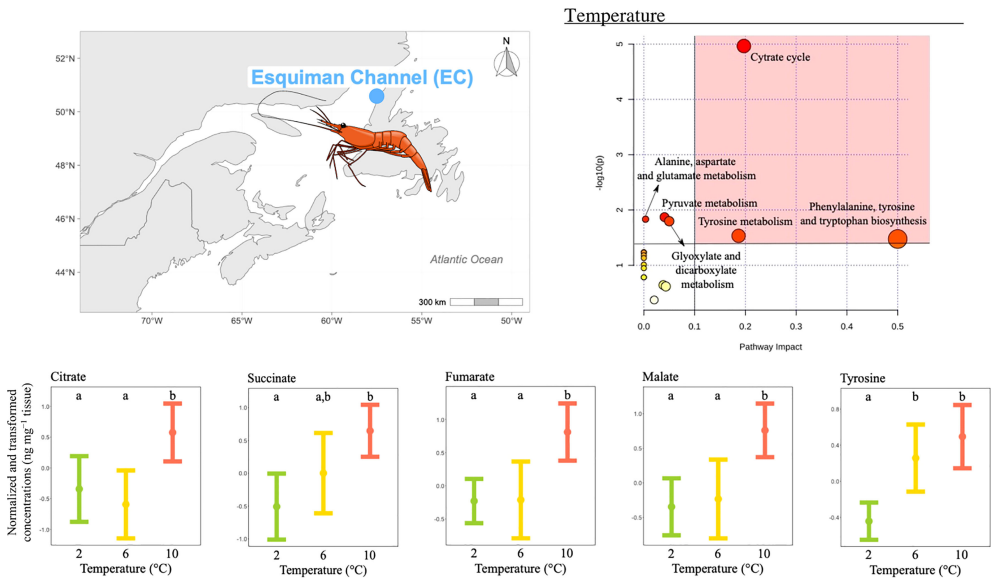

FIGURE 4
Metabolomics differences among temperatures in the northern shrimp *P. borealis* from the Esquiman Channel (EC). In more detail, at the top left of the figure we show the map representing the collection site and at the top right of the figure we show the pathway analysis of metabolic changes carried out with the statistically significant metabolites (ANOVA $p < 0.05$). Pathways within the red area were considered the most relevant as they have $p < 0.05$ and impact > 0.1. At the bottom of the figure we show the mean concentration and 95% CI for citrate, succinate, fumarate, malate and tyrosine for each temperature treatment: 2 (green, N=18), 6 (yellow, N=14) and 10°C (red, N=20), combining all pH levels. Lower case letters identify significant differences ($p < 0.05$) among treatments.

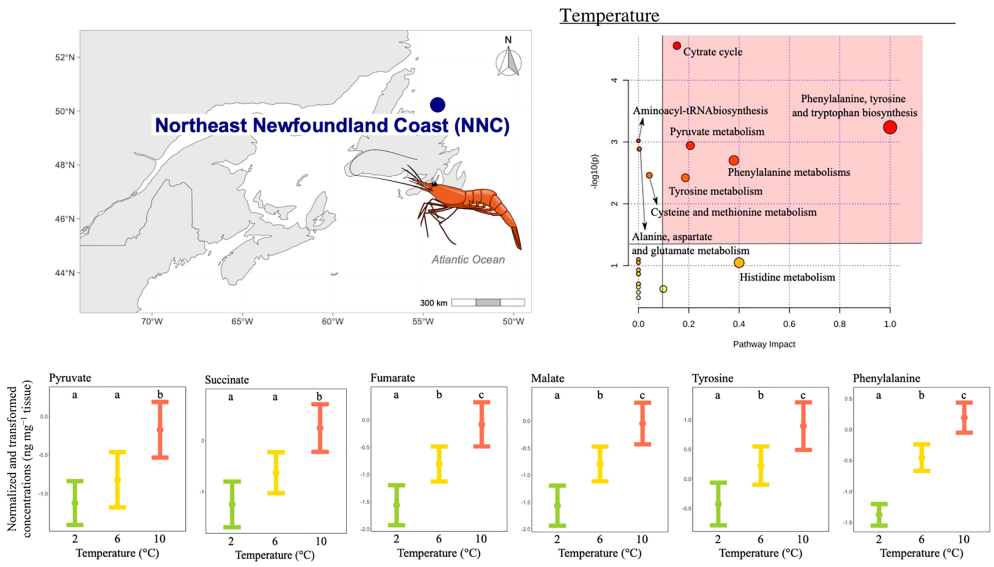

FIGURE 5
Metabolomics differences among temperatures in the northern shrimp *P. borealis* from the Northeast Newfoundland Coast (NNC). In more detail, at the top left of the figure we show the map representing the collection site and at the top right of the figure we show the pathway analysis of metabolic changes carried out with the statistically significant metabolites (ANOVA $p < 0.05$). Pathways within the red area were considered the most relevant as they have $p < 0.05$ and impact > 0.1. At the bottom of the figure we show the mean concentration and 95% CI for pyruvate, succinate, fumarate, malate, tyrosine and phenylalanine for each temperature treatment: 2 (green, N=15), 6 (yellow, N=20) and 10°C (red, N=19), combining all pH levels. Lower case letters identify significant differences ($p < 0.05$) among treatments. .

(Chemel et al., 2020; Guscelli et al. *under review*; Hammer and Pedersen, 2013). Interestingly, the SLE shrimp response to OW and OA is the most divergent when compared to those of shrimp from all other origins. In fact, in shrimp from SLE, the alanine, aspartate and glutamate metabolism pathway is affected but the TCA pathway is not. These results suggest that the responses of shrimp from SLE differ from the ones of shrimp from other origins at multiple levels of biological organization: metabolic, cellular and whole-organism. Indeed, we previously reported that shrimp from SLE possess the worst general physiological condition as they show the highest maximum metabolic rate associated to the lowest cellular energetic capacity (Guscelli et al. *under review*). Moreover, the differences in metabolomics profiles of shrimp from different origins exposed to combined global change drivers, support the previous suggestion of a long-term acclimatization or adaptation of this species to different regional environmental conditions (Guscelli et al. *under review*). Although we recognize that inter-origin differences could be influenced by the potential effect of seasonality on the physiological responses of shrimp to global change drivers, its influence was minimized to a very marginal effect by ensuring similar (approximately eight weeks) and stable pre-exposure laboratory conditions and by selecting only non-ovigerous females. Variation in the metabolome among populations as sign of local adaptation has been shown in other marine invertebrates (e.g. Calosi et al., 2017; Vohsen et al., 2019). However, to our knowledge this is the first study that provides evidence of an inter-origin metabolomics reprogramming under combined OW and OA.

Interestingly, our results show an increase in concentration of TCA intermediates in shrimp from ESS, EC and NNC exposed to increasing temperature. Specifically, we show an increase of succinate, fumarate and malate concentrations in shrimp from these three origins and an increase in citrate and pyruvate concentrations in shrimp from EC and NNC, respectively, with increasing temperature. Usually, the accumulation of TCA metabolites suggests a disruption of the TCA cycle and a consequent shift from aerobic to anaerobic metabolism, as previously shown for example in the saltwater clam *Laternula elliptica* exposed to acute warming and in the olive flounder *Paralichthys olivaceus*, exposed to low salinity (Clark et al., 2017; Wu et al., 2017). In the olive flounder, the accumulation of lactate under low salinity exposure further supports the shift to anaerobic metabolism. However, in our study lactate concentrations are under the limit of detection, which do not allow us to confirm that shrimp shift their energy production to anaerobic metabolism, limiting our further discussion of this hypothesis. Moreover, previous results on the cellular energetic capacity of the northern shrimp exposed to combined OW and OA showed that activities of enzymes catalysing reactions of the oxidative phosphorylation pathway remained stable and that shrimp aerobic scope increased with increasing temperature between 2 and 10°C suggesting that shrimp can tolerate this range of temperatures and sustain an aerobic metabolism (Guscelli et al. *under review*). In the present study AMP, ADP and ATP levels remained stable and comparable among shrimp from different origins in all treatments, further suggesting that shrimp can maintain aerobic respiration even under exposure to high temperatures. This led us to *a posteriori* investigate if temperature, pH and/or origin affect the ATP : ADP ratio as it is a relevant indicator of energy consumption and changes in cellular energy status (Metallo and Vander Heiden, 2013; Tantama et al.,

2013; Yuan et al., 2013). Higher levels of ATP : ADP ratio indicate that organisms possess enough energy to sustain oxidative metabolism while lower levels of ATP : ADP ratio indicates that glycolysis needs to be enhanced. In our study, ATP : ADP ratio is not affected by global change drivers and does not differ among origins, further suggesting that most shrimp can maintain their energy status and possibly sustain aerobic metabolism, confirming that the northern shrimp can tolerate temperatures up to 10°C and low pH conditions, but survival is reduced under these conditions (Guscelli et al. *under review*).

The release of TCA metabolites by mitochondria has been recently linked to the regulation of cell fate and function as they are also involved in controlling chromatin modifications, DNA methylation ultimately affecting protein functions (Martínez-Reyes and Chandel, 2020). TCA metabolites, in particular succinate, have been shown to exert signalling functions and to regulate immune and inflammatory responses, regulating tissue damage (Mills and O'Neill, 2014; Choi et al., 2021). Succinate is a substrate for reactive oxygen species (ROS) production as it provides electrons to the respiratory chain, thus its accumulation can promote the production of ROS linked to oxidative stress and immune response (Murphy, 2009; Lushchak, 2011; Li et al., 2020a; Zhang et al., 2020). However, ROS production was not measured here, and we are unable to validate whether the accumulation of TCA metabolites in the abdominal muscle is linked to oxidative stress in the northern shrimp exposed to OW and OA. Additionally, the antioxidant defence response previously measured on *P. borealis* exposed to low dissolved oxygen levels is unclear (Dupont-Prinet et al., 2013; Pillet et al., 2016). However, the increase in tyrosine concentration in shrimp from all origins under elevated temperature and low pH further supports the suggestion of the enhancement of the immune response. Indeed, metabolites derived from the phenylalanine, tyrosine and tryptophan biosynthesis and degradation play key roles in plants and animals' immune responses (Parthasarathy et al., 2018). Recently, the regulation of phenylalanine, tyrosine and tryptophan biosynthesis and the tyrosine accumulation in the thick shell mussels *Mytilus coruscus*, exposed to OA have been suggested to potentially be linked to the immune response (Shang et al., 2022), although this needs to be investigated in the northern shrimp. We therefore suggest future studies to explore the effect of global ocean changes on *P. borealis* oxidative stress (for example measuring ROS production and antioxidant enzymes activity) and immune response. To do so, multiple tissues should be examined to acquire a more complete understanding of the northern shrimp response to OW and OA, especially hepatopancreas that is considered as the most sensitive tissue to oxidative stress (Ruppert et al., 2004). Nonetheless, as the northern shrimp low response of antioxidant enzymes (Dupont-Prinet et al., 2013; Pillet et al., 2016) could be due to the investigation of such response over short exposure, we suggest developing experiments employing longer exposure periods, as in the present study. Finally, to further acquire information on the potential immune response of shrimp, it would be interesting to measure the itaconate concentration as it is a key immune-responsive metabolite, stemming from diversion of TCA flux, that has been linked to disease in mussels (Li et al., 2020a). Confirming that global change drivers induce oxidative stress in the northern shrimp and enhance their immune response could lead to the re-evaluation of shrimp sensitivity and vulnerability to OW and OA. Indeed, although our results do not support a switch to anaerobiosis, the accumulation of TCA intermediates in shrimp exposed to the highest temperature and the potential enhancement of an immune response confirm that 10°C is a temperature close to the northern shrimp thermal tolerance limit (Guscelli et al. *under review*). This is also confirmed by the increase in free amino acid levels with increasing temperature, which can be indicative of altered protein synthesis/breakdown, possibly to use amino acids as energy sources to feed the TCA cycle. Additionally, amino acids have been increasingly recognised for their function in the immune response and tissue repair of crustaceans and other marine animals, suggesting their importance in coping with stress (Herrera et al., 2019; Huang et al., 2020).

In conclusion, our study confirms that *P. borealis* is overall tolerant to OW and OA conditions predicted to occur by 2100 as the cellular energetic status of shrimp from all origins is maintained. However, OW exposure, and in minor proportion OA, induce the accumulation of metabolites capable of regulating cell physiology and enhancing immune responses, suggesting signs of stress under OW and OA exposure in shrimp from all origins. Our results highlight the importance of investigating cellular mechanisms underpinning whole-organism physiological responses, to better estimate species' sensitivity to future complex environmental conditions (Bartholomew, 1964; Harvey et al., 2014). Finally, the inter-origin differences shown in the metabolic response of shrimp exposed to OW and OA, and the intraspecific similitudes shown in form of the potential enhancement of immune response, highlight the importance of conducting macrophysiological studies to define species' sensitivity to future environmental conditions (Chown and Gaston, 2008).

Data availability statement

The original contributions presented in this study are included in Figure S1 and Table S1 in the Supplementary Material. The dataset generated for this study will be available in the online repository PANGEA. Further inquiries can be directed to the corresponding author.

Ethics statement

Ethical review and approval was not required for the animal study because all procedures complied with Canadian legislation for

animal experimentation as the Canadian Council for Animal Care does not require projects using crustaceans to be approved by an Animal Care Committee.

Author contributions

DC provided the installations for the experimental setups and the live shrimp for the study and EG carried out the experiments, the sample collection and the sample preparation for analysis. PC provided the fundings to support the samples analysis at Les laboratoires Iso-BioKem Inc. EG prepared the dataset and conducted the bioinformatics analyses with support from DM and FV, and discussions with DM and PC. EG conducted the interpretation of the results and prepared figures and tables. EG wrote the manuscript and all authors contributed to its final version. All authors contributed to the article and approved the submitted version.

Funding

Our work has been funded by: (i) an OURANOS grant (554023) to DC and PC; (ii) a DFO Strategic Program for Ecosystem-Based Research and Advice grant and an Aquatic Climate Change Adaptation Services Program grant to DC; (iii) a FIR UQAR grant, a MITACS-Ouranos Accelerate grant, a Canada Foundation for Innovation (CFI) grant and a Natural Sciences and Engineering Research Council of Canada (NSERC) Discovery grants (RGPIN-2015-06500 and RGPIN-2020-05627) to PC; (iv) a Fundação para a Ciência e Tecnologia (Portugal) through a Scientific Employment Stimulus researcher contract granted to DM (CEECIND/01250/2018) and the financial support to CESAM (UIDP/50017/2020+UIDB/50017/2020+LA/P/0094/2020); (v) a MITACS-Ouranos Accelerate grant to support EG; (vi) a Fonds de Recherche du Québec - Nature et Technologies (FRQNT) scholarship (Doctoral PBEEE, 289597) and a Réal-Decoste Ouranos scholarship (286109) to EG; and (vii) a FRQNT scholarship (Doctoral, 274427) and a Vanier Canada Graduate Scholarships (433956) to FV.

Acknowledgments

The authors are especially grateful to Bertrand Genard, Judith Savoie, Anthony Schmutz and Mathieu Millour from Les laboratoires Iso-BioKem Inc. EG, FV and PC are members of the inter-institutional strategic research network Québec-Océan. DC is member of the inter-institutional strategic research network Ressources Aquatiques Québec.

Conflict of interest

The authors declare that the research was conducted in the absence of any commercial or financial relationships that could be construed as a potential conflict of interest.

Publisher's note

Supplementary material

The Supplementary Material for this article can be found online at: https://www.frontiersin.org/articles/10.3389/fmars.2023.1170451/full#supplementary-material

References

Anderson, M., Gorley, R. N., and Clarke, R. K. (2008). Permanova+ for primer: guide to software and statisticl methods. *Primer-E Limited*.

Arnberg, M., Calosi, P., Spicer, J. I., Tandberg, A. H. S., Nilsen, M., Westerlund, S., et al. (2013). Elevated temperature elicits greater effects than decreased pH on the development, feeding and metabolism of northern shrimp (*Pandalus borealis*) larvae. *Mar. Biol.* 160, 2037–2048. doi: 10.1007/s00227-012-2072-9

Aru, V., Engelsen, S. B., Savorani, F., Culurgioni, J., Sarais, G., Atzori, G., et al. (2017). The effect of season on the metabolic profile of the European clam *Ruditapes decussatus* as studied by 1H-NMR spectroscopy. *Metabolites* 7, 1–14. doi: 10.3390/metabo7030036

Bartholomew, G. A. (1964). The roles of physiology and behavior in the maintenance of homeostasis in the desert environment. *Symp. Soc Exp. Biol.* 18, 7–29.

Bechmann, R. K., Taban, I. C., Westerlund, S., Godal, B. F., Arnberg, M., Vingen, S., et al. (2011). Effects of ocean acidification on early life stages of shrimp (*Pandalus borealis*) and mussel (*Mytilus edulis*). *J. Toxicol. Environ. Heal. - Part A* 74, 424–438. doi: 10.1080/15287394.2011.550460

Bergström, B. I. (2000). The biology of *Pandalus*. *Adv. Mar. Biol.* 38, 55–245. doi: 10.1016/S0065-2881(00)38003-8

Bourdages, H., Roux, M.-J., Marquis, M.-C., Galbraith, P., and Isabel, L. (2022). Assessment of northern shrimp stocks in the estuary and gulf of st. Lawrence in 2021: commercial fishery and research survey data. *DFO Can. Sci. Advis. Sec. Res. Doc.* 2022/027, xiv + 195.

Bretz, F., Hothorn, T., and Westfall, P. (2016). *Multiple comparisons using R*. CRC press doi: 10.1201/9781420010909-f

Brillon, S., Lambert, Y., and Dodson, J. (2005). Egg survival, embryonic development, and larval characteristics of northern shrimp (*Pandalus borealis*) females subject to different temperature and feeding conditions. *Mar. Biol.* 147, 895–911. doi: 10.1007/s00227-005-1633-6

Bundy, J. G., Davey, M. P., and Viant, M. R. (2009). Environmental metabolomics: a critical review and future perspectives. *Metabolomics* 5, 3–21. doi: 10.1007/s11306-008-0152-0

Caldeira, K., and Wickett, M. E. (2003). Anthropogenic carbon and ocean pH. *Nature* 425, 365. doi: 10.1038/425365a

Calosi, P., Melatunan, S., Turner, L. M., Artioli, Y., Davidson, R. L., Byrne, J. J., et al. (2017). Regional adaptation defines sensitivity to future ocean acidification. *Nat. Commun.* 8 (1), 1–10. doi: 10.1038/NCOMMS13994

Cappello, T. (2020). NMR-based metabolomics of aquatic organisms. *EMagRes* 9, 81–100. doi: 10.1002/9780470034590.emrstm1604

Chabot, D., and Ouellet, P. (2005). Rearing *Pandalus borealis* larvae in the laboratory: II. routine oxygen consumption, maximum oxygen consumption and metabolic scope at three temperatures. *Mar. Biol.* 147, 881–894. doi: 10.1007/s00227-005-1626-5

Chemel, M., Noisette, F., Chabot, D., Guscelli, E., Leclerc, L., and Calosi, P. (2020). Good news {[/amp]]mdash; bad news: combined ocean change drivers decrease survival but have no negative impact on nutritional value and organoleptic quality of the northern shrimp. *Front. Mar. Sci.* 7. doi: 10.3389/fmars.2020.00611

Choi, I., Son, H., and Baek, J. H. (2021). Tricarboxylic acid (TCA) cycle intermediates: regulators of immune responses. *Life* 11, 1–19. doi: 10.3390/life11010069

Chown, S. L., and Gaston, K. J. (2008). Macrophysiology for a changing world. *Proc. R. Soc B Biol. Sci.* 275, 1469–1478. doi: 10.1098/rspb.2008.0137

Clark, M. S., Sommer, U., Sihra, J. K., Thorne, M. A. S., Morley, S. A., King, M., et al. (2017). Biodiversity in marine invertebrate responses to acute warming revealed by a comparative multi-omics approach. *Glob. Change Biol.* 23, 318–330. doi: 10.1111/gcb.13357

Costa, C., Afonso, T., Cardoso, S., Maraschin, M., and Rocha, M. (2017). *Specmine: an R package for metabolomics and spectral data analysis and mining*. In BOOK OF ABSTRACTS OF (p. 63)

Cyr, F., Snook, S., Bishop, C., Galbraith, P. S., Chen, N., and Han, G. (2022). Physical oceanographic conditions on the Newfoundland and Labrador shelf during 2021. *Can. Sci. Advis. Secr. Res. Doc*.

Daoud, D., Chabot, D., Audet, C., and Lambert, Y. (2007). Temperature induced variation in oxygen consumption of juvenile and adult stages of the northern shrimp, *Pandalus borealis*. *J. Exp. Mar. Bio. Ecol.* 347, 30–40. doi: 10.1016/j.jembe.2007.02.013

Dawe, E. G., Koen-Alonso, M., Chabot, D., Stansbury, D., and Mullowney, D. (2012). Trophic interactions between key predatory fishes and crustaceans: comparison of two Northwest Atlantic systems during a period of ecosystem change. *Mar. Ecol. Prog. Ser.* 469, 233–248. doi: 10.3354/meps10136

DFO (2021a) *2020 value of Atlantic & pacific coast commerical landings, by province*. Available at: https://www.dfo-mpo.gc.ca/stats/commercial/land-debarq/sea-maritimes/s2020pv-eng.htm?

DFO (2021b). Oceanographic conditions in the Atlantic zone in 2020. *Can. Sci. Advis. Secr. Sci. Advis. Rep.* 2021/026.

DFO (2022a). 2021 assessment of northern shrimp on the Eastern scotian shelf (SFAS 13–15). *Can. Sci. Advis. Secr. Sci. Advis. Rep.* 2022/033.

DFO (2022b). Oceanographic conditions in the Atlantic zone in 2021. *Can. Sci. Advis. Secr. Sci. Advis. Rep.* 2022/025.

Di Santo, V. (2015). Ocean acidification exacerbates the impacts of global warming on embryonic little skate, *Leucoraja erinacea* (Mitchill). *J. Exp. Mar. Bio. Ecol.* 463, 72–78. doi: 10.1016/j.jembe.2014.11.006

Dong, X., Yang, Z., Liu, Z., Wang, X., Yu, H., Peng, C., et al. (2022). Metabonomic analysis provides new insights into the response of zhikong scallop (*Chlamys farreri*) to heat stress by improving energy metabolism and antioxidant capacity. *Antioxidants* 11 (6), 1084. doi: 10.3390/antiox11061084

Dupont-Prinet, A., Pillet, M., Chabot, D., Hansen, T., Tremblay, R., and Audet, C. (2013). Northern shrimp (*Pandalus borealis*) oxygen consumption and metabolic enzyme activities are severely constrained by hypoxia in the estuary and gulf of st. Lawrence. *J. Exp. Mar. Bio. Ecol.* 448, 298–307. doi: 10.1016/j.jembe.2013.07.019

Ebner, J. N. (2021). Trends in the application of "omics" to ecotoxicology and stress ecology. *Genes (Basel).* 12 (10), 1481. doi: 10.1007/978-94-007-2072-5

Ellis, R. P., Spicer, J. I., Byrne, J. J., Sommer, U., Viant, M. R., White, D. A., et al. (2014). 1H NMR metabolomics reveals contrasting response by male and female mussels exposed to reduced seawater pH, increased temperature, and a pathogen. *Environ. Sci. Technol.* 48, 7044–7052. doi: 10.1021/es501601w

Fiehn, O. (2002). Metabolomics – the link between genotypes and phenotypes. *Plant Mol. Biol.* 48, 155–171. doi: 10.1023/A:1013713905833

Hammer, K. M., and Pedersen, S. A. (2013). Deep-water prawn *Pandalus borealis* displays a relatively high pH regulatory capacity in response to CO2-induced acidosis. *Mar. Ecol. Prog. Ser.* 492, 139–151. doi: 10.3354/meps10476

Hammill, M. O., and Stenson, G. B. (2000). Estimated prey consumption by harp seals (*Phoca groenlandica*), hooded seals (*Cystophora cristata*), grey seals (*Halichoerus grypus*) and harbour seals (*Phoca vitulina*) in Atlantic Canada. *J. Northwest Atl. Fish. Sci.* 26, 1–23. doi: 10.2960/J.v26.a1

Harvey, B. P., Al-Janabi, B., Broszeit, S., Cioffi, R., Kumar, A., Aranguren-Gassis, M., et al. (2014). Evolution of marine organisms under climate change at different levels of biological organisation. *Water* 6, 3545–3574. doi: 10.3390/w6113545

Herrera, M., Mancera, J. M., and Costas, B. (2019). The use of dietary additives in fish stress mitigation: comparative endocrine and physiological responses. *Front. Endocrinol. (Lausanne).* 10. doi: 10.3389/fendo.2019.00447

Hothorn, T., Bretz, F., and Westfall, P. (2008). Simultaneous inference in general parametric models. *Biometrical J.* 50 (3), 346–363. doi: 10.1002/bimj.200810425

Huang, Z., Aweya, J. J., Zhu, C., Tran, N. T., Hong, Y., Li, S., et al. (2020). Modulation of crustacean innate immune response by amino acids and their metabolites: inferences from other species. *Front. Immunol.* 11. doi: 10.3389/fimmu.2020.574721

Huo, D., Sun, L., Zhang, L., Ru, X., Liu, S., and Yang, H. (2019). Metabolome responses of the sea cucumber *Apostichopus japonicus* to multiple environmental stresses: heat and hypoxia. *Mar. pollut. Bull.* 138, 407–420. doi: 10.1016/j.marpolbul.2018.11.063

Husson, F., Le, S., and Pages, J. (2010). *Exploratory multivariate analysis by example using r, Chapman and hall*. CRC Computer Science & Data Analysis. *CRC Press*, 30, 101–102.

IPCC (2014). *Summary for policy makers*. (Geneva, Szwitzerland: IPCC). doi: 10.1016/j.renene.2009.11.012

IPCC (2022). *The ocean and cryosphere in a changing climate*. Geneva, Szwitzerland: IPCC doi: 10.1017/9781009157964

Jones, O. A. H., Maguire, M. L., Griffin, J. L., Dias, D. A., Spurgeon, D. J., and Svendsen, C. (2013). Metabolomics and its use in ecology. *Austral Ecol.* 38, 713–720. doi: 10.1111/aec.12019

Jónsdóttir, I. G., Björnsson, H., and Skúladóttir, U. (2012). Predation by Atlantic cod *Gadus morhua* on northern shrimp *Pandalus borealis* in inshore and offshore areas of Iceland. *Mar. Ecol. Prog. Ser.* 469, 223–232. doi: 10.3354/meps09977

Koeller, P., Fuentes-Yaco, C., Platt, T., Sathyendranath, S., Richards, A., Ouellet, P., et al. (2009). Basin-scale coherence in phenology of shrimps and phytoplankton in the north Atlantic ocean. *Sci. (80-.).* 324, 791–793. doi: 10.1126/science.1170987

Lannig, G., Eilers, S., Pörtner, H. O., Sokolova, I. M., and Bock, C. (2010). Impact of ocean acidification on energy metabolism of oyster, *Crassostrea gigas* - changes in metabolic pathways and thermal response. *Mar. Drugs* 8, 2318–2339. doi: 10.3390/md8082318

Lefevre, S. (2016). Are global warming and ocean acidification conspiring against marine ectotherms? a meta-analysis of the respiratory effects of elevated temperature, high CO2 and their interaction. *Conserv. Physiol.* 4, 1–31. doi: 10.1093/conphys/cow009

Li, S., Alfaro, A. C., Nguyen, T. V., Young, T., and Lulijwa, R. (2020a). An integrated omics approach to investigate summer mortality of new Zealand Greenshell™ mussels. *Metabolomics* 16, 1–16. doi: 10.1007/s11306-020-01722-x

Li, Y., Yin, W., Zhan, Y., Jia, Y., Cui, D., Zhang, W., et al. (2020b). Comparative metabolome analysis provides new insights into increased larval mortality under seawater acidification in the sea urchin *Strongylocentrotus intermedius*. *Sci. Total Environ.* 747, 141206. doi: 10.1016/j.scitotenv.2020.141206

Liu, Z., Zhang, Y., Zhou, Z., Zong, Y., Zheng, Y., Liu, C., et al. (2020). Metabolomic and transcriptomic profiling reveals the alteration of energy metabolism in oyster larvae during initial shell formation and under experimental ocean acidification. *Sci. Rep.* 10, 1–11. doi: 10.1038/s41598-020-62963-3

Lushchak, V. I. (2011). Environmentally induced oxidative stress in aquatic animals. *Aquat. Toxicol.* 101, 13–30. doi: 10.1016/j.aquatox.2010.10.006

Martínez-Reyes, I., and Chandel, N. S. (2020). Mitochondrial TCA cycle metabolites control physiology and disease. *Nat. Commun.* 11, 1–11. doi: 10.1038/s41467-019-13668-3

Matoo, O. B., Lannig, G., Bock, C., and Sokolova, I. M. (2021). Temperature but not ocean acidification affects energy metabolism and enzyme activities in the blue mussel, *Mytilus edulis*. *Ecol. Evol.* 11, 3366–3379. doi: 10.1002/ece3.7289

Mayor, D. J., Sommer, U., Cook, K. B., and Viant, M. R. (2015). The metabolic response of marine copepods to environmental warming and ocean acidification in the absence of food. *Sci. Rep.* 5, 1–12. doi: 10.1038/srep13690

Metallo, C. M., and Vander Heiden, M. G. (2013). Understanding metabolic regulation and its influence on cell physiology. *Mol. Cell* 49, 388–398. doi: 10.1016/j.molcel.2013.01.018

Mills, E., and O'Neill, L. A. J. (2014). Succinate: a metabolic signal in inflammation. *Trends Cell Biol.* 24, 313–320. doi: 10.1016/j.tcb.2013.11.008

Mucci, A., Levasseur, M., Gratton, Y., Martias, C., Scarratt, M., Gilbert, D., et al. (2018). Tidally induced variations of ph at the head of the laurentian channel. *Can. J. Fish. Aquat. Sci.* 75, 1128–1141. doi: 10.1139/cjfas-2017-0007

Mucci, A., Starr, M., Gilbert, D., and Sundby, B. (2011). Acidification of lower st. Lawrence estuary bottom waters. *Atmos. - Ocean* 49, 206–218. doi: 10.1080/07055900.2011.599265

Murphy, M. P. (2009). How mitochondria produce reactive oxygen species. *Biochem. J.* 417, 1–13. doi: 10.1042/BJ20081386

Noisette, F., Bordeyne, F., Davoult, D., and Martin, S. (2016). Assessing the physiological responses of the gastropod *Crepidula fornicata* to predicted ocean acidification and warming. *Limnol. Oceanogr.* 61, 430–444. doi: 10.1002/lno.10225

Noisette, F., Calosi, P., Madeira, D., Chemel, M., Menu-Courey, K., Piedalue, S., et al. (2021). Tolerant larvae and sensitive juveniles: integrating metabolomics and whole-organism responses to define life-stage specific sensitivity to ocean acidification in the American lobster. *Metabolites* 11 (9), 584. doi: 10.3390/metabo11090584

Orr, J. C., Fabry, V. J., Aumont, O., Bopp, L., Doney, S., Feely, R. A., et al. (2005). Anthropogenic ocean acidification over the twenty-first century and its impact on calcifying organisms. *Nature* 437 (7059), 681–686. doi: 10.1038/nature04095

Ouellet, P., Chabot, D., Calosi, P., Orr, D., and Galbraith, P. S. (2017). Regional variations in early life stages response to a temperature gradient in the northern shrimp *Pandalus borealis* and vulnerability of the populations to ocean warming. *J. Exp. Mar. Bio. Ecol.* 497, 50–60. doi: 10.1016/j.jembe.2017.09.007

Paaijmans, K. P., Heinig, R. L., Seliga, R. A., Blanford, J. I., Blanford, S., Murdock, C. C., et al. (2013). Temperature variation makes ectotherms more sensitive to climate change. *Glob. Change Biol.* 19, 2373–2380. doi: 10.1111/gcb.12240

Parthasarathy, A., Cross, P. J., Dobson, R. C. J., Adams, L. E., Savka, M. A., and Hudson, A. O. (2018). A three-ring circus: metabolism of the three proteogenic aromatic amino acids and their role in the health of plants and animals. *Front. Mol. Biosci.* 5. doi: 10.3389/fmolb.2018.00029

Pillet, M., Dupont-Prinet, A., Chabot, D., Tremblay, R., and Audet, C. (2016). Effects of exposure to hypoxia on metabolic pathways in northern shrimp (*Pandalus borealis*) and Greenland halibut (*Reinhardtius hippoglossoides*). *J. Exp. Mar. Bio. Ecol.* 483, 88–96. doi: 10.1016/j.jembe.2016.07.002

Pinu, F. R., Beale, D. J., Paten, A. M., Kouremenos, K., Swarup, S., Schirra, H. J., et al. (2019). Systems biology and multi-omics integration: viewpoints from the metabolomics research community. *Metabolites* 9, 1–31. doi: 10.3390/metabo9040076

R Core Team (2020). *R: a language and environment for statistical computing* (Vienna, Austria: R Found. Stat. Comput).

Ruppert, E. E., Fox, R. S., and Barnes, R. D. (2004). *Invertebrate zoology: a functional evolutionary approach* (No. 592 RUPi).

Schalkhausser, B., Bock, C., Pörtner, H. O., and Lannig, G. (2014). Escape performance of temperate king scallop, *Pecten maximus* under ocean warming and acidification. *Mar. Biol.* 161, 2819–2829. doi: 10.1007/s00227-014-2548-x

Shang, Y., Wang, X., Shi, Y., Huang, W., Sokolova, I., Chang, X., et al. (2022). Ocean acidification affects the bioenergetics of marine mussels as revealed by high-coverage quantitative metabolomics. *Sci. Total Environ.* 858, 160090. doi: 10.1016/j.scitotenv.2022.160090

Shumway, S. E., Perkins, H. C., Schick, D. F., and Stickney, A. P. (1985). *Synopsis of biological data on the pink shrimp*, Pandalus borealis Krøyer. FAO Fisheries Synopsis No. 1838. 144, 57.

Tantama, M., Martínez-François, J. R., Mongeon, R., and Yellen, G. (2013). Imaging energy status in live cells with a fluorescent biosensor of the intracellular ATP-to-ADP ratio. *Nat. Commun.* 4, 2550. doi: 10.1038/ncomms3550

Thor, P., Bailey, A., Dupont, S., Calosi, P., Søreide, J. E., De Wit, P., et al. (2018). Contrasting physiological responses to future ocean acidification among Arctic copepod populations. *Glob. Change Biol.* 24 (1), e365–e377. doi: 10.1111/gcb.13870

Thor, P., Vermandele, F., Bailey, A., Guscelli, E., Loubet-Sartrou, L., Dupont, S., et al. (2022). Ocean acidification causes fundamental changes in the cellular metabolism of the Arctic copepod *Calanus glacialis* as detected by metabolomic analysis. *Sci. Rep.* 12, 22223. doi: 10.1038/s41598-022-26480-9

Vargas, C. A., Lagos, N. A., Lardies, M. A., Duarte, C., Manríquez, P. H., Aguilera, V. M., et al. (2017). Species-specific responses to ocean acidification should account for local adaptation and adaptive plasticity. *Nat. Ecol. Evol.* 1 (4), 1–7. doi: 10.1038/s41559-017-0084

Vohsen, S. A., Fisher, C. R., and Baums, I. B. (2019). Metabolomic richness and fingerprints of deep-sea coral species and populations. *Metabolomics* 15, 1–13. doi: 10.1007/s11306-019-1500-y

Wei, L., Wang, Q., Ning, X., Mu, C., Wang, C., Cao, R., et al. (2015). Combined metabolome and proteome analysis of the mantle tissue from pacific oyster *Crassostrea gigas* exposed to elevated pCO2. *Comp. Biochem. Physiol. - Part D Genomics Proteomics* 13, 16–23. doi: 10.1016/j.cbd.2014.12.001

Wei, R., Wang, J., Su, M., Jia, E., Chen, S., Chen, T., et al. (2018). Missing value imputation approach for mass spectrometry-based metabolomics data. *Sci. Rep.* 8, 1–10. doi: 10.1038/s41598-017-19120-0

Williams, T. D., Wu, H., Santos, E. M., Ball, J., Katsiadaki, I., Brown, M. M., et al. (2009). Hepatic transcriptomic and metabolomic responses in the stickleback (*Gasterosteus aculeatus*) exposed to ethinyl-estradiol. *Environ. Sci. Technol.* 43 (16), 6341–6348. doi: 10.1021/es9008689

Wu, H., Liu, J., Lu, Z., Xu, L., Ji, C., Wang, Q., et al. (2017). Metabolite and gene expression responses in juvenile flounder *Paralichthys olivaceus* exposed to reduced salinities. *Fish Shellfish Immunol.* 63, 417–423. doi: 10.1016/j.fsi.2017.02.042

Yuan, H. X., Xiong, Y., and Guan, K. L. (2013). Nutrient sensing, metabolism, and cell growth control. *Mol. Cell* 49, 379–387. doi: 10.1016/j.molcel.2013.01.019

Zhang, Y., Wu, H., Wei, L., Xie, Z., and Guan, B. (2017). Effects of hypoxia in the gills of the Manila clam *Ruditapes philippinarum* using NMR-based metabolomics. *Mar. pollut. Bull.* 114, 84–89. doi: 10.1016/j.marpolbul.2016.08.066

Zhang, Y., Zhang, M., Zhu, W., Yu, J., Wang, Q., Zhang, J., et al. (2020). Succinate accumulation induces mitochondrial reactive oxygen species generation and promotes status epilepticus in the kainic acid rat model. *Redox Biol.* 28, 101365. doi: 10.1016/j.redox.2019.101365

frontiers | Frontiers in Ecology and Evolution

TYPE Original Research
PUBLISHED 21 June 2023
DOI 10.3389/fevo.2023.1113357

OPEN ACCESS

EDITED BY
Carolina Madeira,
NOVA University Lisbon, Portugal

REVIEWED BY
Alison Gould,
California Academy of Sciences,
United States
Tessa M. Page,
University of Southampton,
United Kingdom

*CORRESPONDENCE
Kate M. Quigley
katemarie.quigley@my.jcu.edu.au

RECEIVED 01 December 2022
ACCEPTED 02 June 2023
PUBLISHED 21 June 2023

CITATION
Terrell AP, Marangon E, Webster NS, Cooke I and Quigley KM (2023) The promotion of stress tolerant Symbiodiniaceae dominance in juveniles of two coral species under simulated future conditions of ocean warming and acidification.
Front. Ecol. Evol. 11:1113357.
doi: 10.3389/fevo.2023.1113357

The promotion of stress tolerant Symbiodiniaceae dominance in juveniles of two coral species under simulated future conditions of ocean warming and acidification

Alyx P. Terrell[1,2,3], Emma Marangon[1,2,3], Nicole S. Webster[1,4,5], Ira Cooke[6,7] and Kate M. Quigley[2,8]*

[1]Australian Institute of Marine Science, Townsville, QLD, Australia, [2]College of Science and Engineering, James Cook University, Townsville, QLD, Australia, [3]AIMS@JCU, Townsville, QLD, Australia, [4]Australian Centre for Ecogenomics, University of Queensland, Brisbane, QLD, Australia, [5]Australian Antarctic Division, Hobart, TAS, Australia, [6]Department of Molecular and Cell Biology, James Cook University, Townsville, QLD, Australia, [7]Centre for Tropical Bioinformatics and Molecular Biology, James Cook University, Townsville, QLD, Australia, [8]Flourishing Oceans, Minderoo Foundation, Perth, WA, Australia

The symbiotic relationship between coral and its endosymbiotic algae, Symbiodiniaceae, greatly influences the hosts' potential to withstand environmental stress. To date, the effects of climate change on this relationship has primarily focused on adult corals. Uncovering the effects of environmental stress on the establishment and development of this symbiosis in early life stages is critical for predicting how corals may respond to climate change. To determine the impacts of future climate projections on the establishment of symbionts in juvenile corals, ITS2 amplicon sequencing of single coral juveniles was applied to *Goniastrea retiformis* and *Acropora millepora* before and after exposure to three climate conditions of varying temperature and pCO_2 levels (current and RCP8.5 in 2050 and 2100). Compared to ambient conditions, juvenile corals experienced shuffling in the relative abundance of *Cladocopium* (C1m, decrease) to *Durusdinium* (D1 and D1a, increase) over time. We calculated a novel risk metric incorporating functional redundancy and likelihood of impact on host physiology to identify the loss of D1a as a "low risk" to the coral compared to the loss of "higher risk" taxa like D1 and C1m. Although the increase in stress tolerant *Durusdinium* under future warming was encouraging for *A. millepora*, by 2100, *G. retiformis* communities displayed signs of symbiosis de-regulation, suggesting this acclimatory mechanism may have species-specific thresholds. Whilst this study cannot specifically disentangle the individual effects of temperature and pCO_2, it does provide valuable insights into the impacts of both stressors combined. These results emphasize the need for understanding of long-term effects of climate change induced stress on coral juveniles, and their potential for increased acclimation to heat tolerance through changes in symbiosis.

KEYWORDS

coral reefs, acclimation, symbiosis, Symbiodiniaceae, recruit, warming, acidification, bleaching

Introduction

Increasing global temperatures due to anthropogenic climate change is currently the greatest threat to coral survival and has resulted in three global mass bleaching events since the 1980s (1998, 2010, 2014–2017), with bleaching becoming ever more prevalent and extreme (Hughes et al., 2017b). Coral bleaching occurs when endosymbiotic dinoflagellates (family Symbiodiniaceae) are lost from the host coral tissue. This stress response is seen as a loss of the endosymbiont due to a breakdown of the symbiotic relationship (Brown, 1997). As Symbiodiniaceae support their host's energy demands through the provisioning of photosynthates, the prolonged loss of this relationship may cause starvation, and lead to coral mortality (Brown, 1997; Suggett et al., 2017).

Known stressors of coral symbioses include, but are not limited to, increased sea surface temperatures, and increased partial pressure of carbon dioxide (pCO_2). Elevated temperatures are linked to damage of the photosystems of coral endosymbionts, shifting the energetic demands and outputs of the symbiont (Fitt et al., 2001; Robison and Warner, 2006). This can take on a similar form to "parasitism" (*sensu* Baker et al., 2018), as it reduces the photosynthates translocated to the host (Baker et al., 2018). As a result, the host physiology suffers as the coral works to make up for a lack of energy by reaching into other energy storages. While the coral host can turn to heterotrophy to meet some energy demands, there is variation across coral species as to the level to which it is able to accommodate symbiont loss (Anthony et al., 2009). In addition, the increase in pCO_2 into the oceans has been predicted to impact various physiological responses in both the coral host and Symbiodiniaceae (Cohen and Holcomb, 2009; Schoepf et al., 2013). While decreased calcification rates have been well-studied, other responses such as changes in respiration, and metabolism of the host and symbiont may also be impacted by increases in pCO_2 similar, to other phenotypic measures when examined under predicted future climate scenarios (Anthony et al., 2008).

Both stressors have grave implications for coral early life history stages, where energy demands are potentially high during skeletal development and growth as well as during symbiosis establishment. For example, calcification may also be more critical and at-risk during this stage when a coral juvenile is first recruiting and secreting skeletal structures (Foster et al., 2016). The high rates of ocean warming and pCO_2 coupled with the high incidence of bleaching events may be too rapid to allow for natural adaptation to occur (Hoegh-Guldberg et al., 2007; Schoepf et al., 2013; Hughes et al., 2017a). Understanding the effects of climate change on coral–Symbiodiniaceae interactions in early life stages is therefore critical for understanding growth and recovery potentials on reefs, and predicting coral reef resilience to future climate.

Due to the critical role of the endosymbiotic Symbiodiniaceae in energy translocation within the coral host, there has been an emphasis on increased taxonomic resolution of the Symbiodiniaceae present in the host using genetic markers such as the internal transcribed spacer 2 (ITS2) region (Pochon et al., 2014; LaJeunesse et al., 2018; Davies et al., 2022). Symbiodiniaceae are comprised of 9 currently identified genera (formerly clades), each of which is subset into species (formerly "types") (LaJeunesse et al., 2018). Host environmental sensitivity often varies according to the predominant algal symbiont or community (Rowan et al., 1997). For example, colonies with different dominant Symbiodiniaceae communities experienced different bleaching patterns in locations that correlated to predicted limits of symbiont distributions (Rowan et al., 1997; Quigley et al., 2017; Claar et al., 2020; Quigley et al., 2022). These predicted limits of coral symbionts are based on observations where some Symbiodiniaceae taxa are shown to out-perform others, e.g. *Durusdinium* showing greater thermal tolerance than *Cladocopium*. In one example, adults of *Acropora millepora* exhibited changes in Symbiodiniaceae relative abundance towards *Durusdinium* that corresponded to an increase in host heat tolerance by 1–1.5°C (Berkelmans and van Oppen, 2006). Despite few studies assessing the independent role of pCO_2 on Symbiodiniaceae communities, there have been indications of the physiological effects to coral hosts which may be attributed to differences in symbiont taxa and community composition (Howe-Kerr et al., 2020). Finally, the dominance of specific Symbiodiniaceae genera within the coral host can also promote greater resilience under environmental stressors like increased sea surface temperatures or to other stressors present in the environment (Baker et al., 2004; Berkelmans and van Oppen, 2006; Stat and Gates, 2008; Stat et al., 2008; Oliver and Palumbi, 2011).

While the change in relative abundances (termed shuffling) of specific symbiont taxa may improve adult coral tolerance to environmental stress, it is less understood if symbiont shuffling is pervasive in coral early life-history stages (Reich et al., 2017; Quigley et al., 2019). Coral juveniles generally establish their initial endosymbiont community either through direct transmission from the maternal colony (vertical transmission), or *via* environmental acquisition (horizontal transmission) (Baird et al., 2009) or a combination of the two (mixed-mode transmission) (Quigley et al., 2018b). Vertical symbiont establishment provides the opportunity for larvae and subsequent juveniles to acquire a potentially advantageous community of endosymbionts best suited for the local, maternal environment through parental adaptation (Padilla-Gamiño et al., 2012; Quigley et al., 2016; Poland and Coffroth, 2017). Conversely, horizontal transmission can occur through other environmental sources, and it allows for more flexibility to acquire novel symbionts that could be advantageous under changing environmental conditions or after large dispersal distances (Lewis and Coffroth, 2004; Yuyama et al., 2016). Horizontal transmission can occur through the water column, sediment, or other environmental means (McIlroy and Coffroth, 2017; Ali et al., 2019; Umeki et al., 2020). Some research has indicated that coral larvae are capable of selecting and integrating new symbionts from their environment into their endosymbiotic community (LaJeunesse, 2002; Rohwer et al., 2002; Coffroth et al., 2006; LaJeunesse et al., 2009) which may promote greater rates of symbiont acquisition in early life stages (Nitschke et al., 2015;

Poland and Coffroth, 2017; Quigley et al., 2017). This ability of symbiont selection *via* environmental uptake allows for the transfer of beneficial symbiotic traits, and the improvement of coral tolerance to environmental stressors (Baker et al., 2004; Adams et al., 2009; Poland and Coffroth, 2017). Different Symbiodiniaceae taxa also provide the host with distinct benefits. For example, *Durusdinium* may provide increased survival to juveniles under simulated bleaching events (Quigley et al., 2020b; Quigley et al., 2020c). Further, growth rates vary in juveniles between those dominated by either *Cladocopium* or *Durusdinium* (Cantin et al., 2009; Yuyama and Higuchi, 2014; Quigley et al., 2020c), linked to differences in carbon translocation between genera (Cantin et al., 2009). Physiological differences also exist at finer taxonomic scales, for example, within *Durusdinium* "D1a" compared to "D1" might promote slightly greater photosystem II activity (Suggett et al., 2015).

Symbiont diversity varies across coral early life-history stages, in which the diversity of the symbiont community during coral juvenile development may also be important for growth, and survival. For example, there is some evidence that the acquisition of diverse communities of endosymbionts may promote higher growth rates, and increase survival (Yuyama and Higuchi, 2014). Compared to adult corals, early life-history stages (within 1 month of settlement) generally have more diverse endosymbiont communities (Quigley et al., 2017), which eventually winnow to a more stable, lower diversity community (Abrego et al., 2009; Lee et al., 2016; Rouzé et al., 2019). In some cases, symbiont communities in juvenile corals may be impacted by environmental factors. This includes the combined but not necessarily additive effects of temperature and pCO_2, as well as increased temperature, and light (Abrego et al., 2012) or completely halted by increased temperatures with minimal impacts of pCO_2 (Sun et al., 2020). Moreover, the acquisition of symbionts during coral early life-history stages has been assessed only for a limited number of coral species (Cantin et al., 2009; Yorifuji et al., 2017; Quigley et al., 2019; Quigley et al., 2020a), and the effects of elevated temperature and pCO_2 on this process are poorly understood. Combined, these results highlight the importance of Symbiodiniaceae community diversity for the fitness of coral adult and early life-history stages, and highlight an increased need for a better understanding of fine-scale host–symbiont interactions.

To assess changes in Symbiodiniaceae acquisition during coral developmental stages under future climate scenarios, two horizontally transmitting coral species, *Goniastrea retiformis* and *Acropora millepora*, were exposed to varying levels of temperature and pCO_2 predicted for the years 2050 (+1°C offset, pCO_2 685 ± 60ppm) and 2100 (+2°C offset, pCO_2 940 ± 60ppm) under the IPCC RCP 8.5 pathway for projected greenhouse gas concentrations, and compared to present day levels (28.5°C, pCO_2 400 ± 60ppm). These coral species represent different known stress tolerance levels of both stressors, as *G. retiformis* is recognized as being thermally tolerant compared to stress-sensitive *A. millepora* and so were selected to better understand how different coral species may respond to future climate conditions. Juveniles were sampled and the ITS2 region of the symbionts was targeted using amplicon sequencing. The dynamics of symbiont community changes (prevalence, relative abundance, and diversity) were assessed under exposure to these multiple climate treatments for these coral juveniles and further assessed over time (0, 10 days and 4 weeks) for stress-tolerant *G. retiformis* or only at the final timepoint for *A. millepora*.

Materials and methods

Experimental design and coral sampling

In October 2017, gravid colonies of *G. retiformis* and *A. millepora* were collected from Geoffrey Bay at Magnetic Island (S 19°09.326′, E 146°51.861′; Great Barrier Reef Marine Park Authority Permit Number: G13/36318.1), and transported to holding outdoor mesocosm tanks at the National Sea Simulator (SeaSim) at the Australian Institute of Marine Science as per details outlined in (Botté et al., 2020; Uthicke et al., 2020). Corals were acclimated to the following conditions (~27°C, pCO_2 400 ± 60ppm) until spawning (*G. retiformis*: 8th of November 2017; *A. millepora*: 12th December 2017). Multiple colonies were collected, spawned during the spawning night, and mixed in bulk cultures (exact numbers per culture were not recorded). Following spawning, gametes were collected, mixed for fertilization, and larvae were reared in mass culture tanks for 3–4 weeks. Larval culturing followed established methods (Quigley et al., 2016; Pollock et al., 2017) after fertilization success was checked by visually inspecting embryos every hour for up to three hours under the magnification of a benchtop microscope. Larvae were maintained in 500 L flow-through culture tanks at a density of 1–1.2 larva mL^{-1}, filled with 0.2 µm filtered seawater (Pollock et al., 2017).

Larvae (n = 20 per well, 60 per plate) were then distributed to sterile, 6-well plates filled with 0.2 µm filtered seawater containing autoclaved crustose coralline algae (CCA) to induce larval settlement. These plates were not exposed to flow-through conditions, instead they were filled with water, larvae added, and then lid replaced, and left overnight in the dark for larvae to settle. At the first sampling time point of newly settled recruits (T0), individuals were sampled using a sterile scalpel, preserved in absolute ethanol in Eppendorf tubes with minimal water transfer to ensure adequate preservation, and minimize any chance of transfer of symbionts in the water (n = 3 individuals per tube). Following initial sampling, the 6-well plates were placed in outdoor mesocosm tanks (n = 3 tank replicates per treatment; 2 × 6-well plates per tank for each species) representing ambient (present day ~28.5°C, pCO_2 400 ± 60ppm), 2050 (+1°C offset, pCO_2 685 ± 60ppm), and 2100 (+2°C offset, pCO_2 940 ± 60ppm) conditions forecast under RCP 8.5 (Meinshausen et al., 2011; Collins et al., 2013) (Supplementary Table 1). As outlined in previous studies (Botté et al., 2020; Uthicke et al., 2020), these mesocosm tanks had a

range of flora and fauna, including fish, corals, seagrasses, and benthic sediments. Sampling was repeated across each tank after 10 days for both of the coral species in this study, at T1 (*G. retiformis, A. millepora*), and 4 weeks (*G. retiformis*) or 5 weeks (*A. millepora*) (T2) of exposure to simulated climate conditions. All samples were stored at −80°C prior to DNA extraction and ITS2 amplicon sequencing of Symbiodiniaceae communities. However, due to lack of gel electrophoresis bands present in T0 and T1 *A. millepora* samples following PCR amplification, these time points were not sequenced (see "DNA extraction and sequencing" section). No other samples (e.g. water or sediment samples) were collected for sequencing. Juvenile survival was not monitored in this study.

The ambient treatment in this experiment represented average reef conditions over the past ~20 years at a well-studied central Great Barrier Reef site (Davies Reef), allowing for comparisons of symbiont acquisition under elevated temperatures and pCO_2 expected by 2050, and 2100 under RCP 8.5. Corals generally live close to their thermal maximums, and +1 and +2 degrees of temperature increases impact coral offspring physiology and that of their symbionts (Abrego et al., 2012) suggesting that these treatments represent a "stress" for coral offspring.

DNA extraction and sequencing

Genomic DNA was extracted from *G. retiformis* and *A. millepora* samples across three sampling times (T0, T1 and T2), and treatments (ambient, 2050, 2100). Note that the T0 sampling timepoint occurred immediately before juveniles were placed into the three experimental treatments. DNA extractions were performed on individual coral juveniles using a KOH-EDTA method following (Sun et al., 2014), with increased incubation time (15 minutes at 70°C) to enhance cellular lysis.

Polymerase Chain Reaction (PCR) amplification of the ITS-2 locus were conducted using MyTaq DNA Polymerase (Bioline) following manufacturer's protocols with an addition of 1µl 50mM magnesium. The ITS-2 locus was amplified using ITS2alg-F (5'-TCGTCGGCAGCGTCAGATGTGTATAAGAGACAGGTGAATTGCAGAACTCCGTG) and ITS2alg-R(3'-TTCGTATATTCATTCGCCTCCGACAGAGAATATGTGTAGAGGCTCGGGTGCTCTG-5') primers. PCR was performed in 25µl reactions (2µL template) per sample. PCR conditions were the following: initial denaturation at 95°C for 10 minutes, 32 cycles at 95°C for 30 sec, 59°C for 60 sec, 72°C for 30 sec, and a final elongation at 72°C for 7 minutes. PCR amplification products were delivered to the Ramaciotti Centre for Genomics (UNSW, Sydney) for Miseq amplicon sequencing of the 300 bp ITS-2 region (LaJeunesse, 2001; LaJeunesse, 2002). No bands were retrieved during PCR amplification in *A. millepora* samples at T0 and T1 although optimizations were attempted. This was likely due to the extremely low densities of symbionts in these first days of symbiosis establishment, as low density has been demonstrated in other studies of *A. millepora* symbiosis at 40 days (Quigley et al., 2018a). Sequencing was therefore only conducted on *A. millepora* samples for T2.

Bioinformatics and data analysis

A total of 135 individual juvenile samples were successfully sequenced (some samples were removed if PCRs did not result in bands). Of these successfully sequenced juveniles, 27 samples belonged to *A. millepora*, and 110 belonged to *G. retiformis* (see Supplementary Table 2).

Symbiodiniaceae taxonomy is currently undergoing an extensive revision (LaJeunesse et al., 2018) with substantial effort to understand how sequence diversity links with species, genus, and family designations, and most importantly, the functional significance of the symbiont within the coral. Presently, there are generally two analysis pipelines. The first groups sequences within genera (Symportal; Hume et al., 2019), and is generally good for high-abundance taxa and making broad inferences across treatments. The other is based on characterizing individual sequence variants using DADA2 (ASVs; Callahan et al., 2016; Quigley et al., 2019), and provides a higher resolution at the sequence level for exploration of potential diversity at both high and low abundances. The choice of method depends on the question being asked, where both will not render species – or functional – level designations with a formal taxonomic description. Here we chose to use the DADA2 method given our questions about the earliest uptake of symbiont cells and acknowledge that some of the ASVs discovered may be spurious sequence variants and may not represent actual Symbiodiniaceae "species" per-se. The pros and cons of each method and the justification for their use are outlined more fully in (Davies et al., 2022), and a formal comparison of the methods can be found in (Quigley et al., 2022). The DADA2 pipeline generates amplicon sequence variants based on ITS2 sequencing libraries. The ITS2 gene is highly replicated in Symbiodiniaceae and has high levels of intragenomic variation (see Quigley et al., 2014 for full discussion). The calling of ASVs therefore results in the recovery of a diversity of unique ASVs from each Symbiodiniaceae species, resulting in potentially artificially inflated diversity data (discussed in Davies et al., 2022), but offers a higher resolution approach compared to Symportal. Symportal (by design) collapses relevant species diversity when many congeneric Symbiodiniaceae species co-occur within many samples. This therefore represents an overall conservative approach, especially where we are principally focused on low-abundance, highly rare diversity given the life-stage and experimental question. However, to minimize the impact of spurious sequences, most of the analysis collapses diversity to higher levels and primarily focusses on the ten most abundant Symbiodiniaceae ASVs (>4.2% relative abundance cut-off). Neither the authors of this work nor the workshop participants formally endorse either pipeline. The full pipeline and scripts are described in (Quigley et al., 2019) and links therein. Briefly, fastq files were first filtered to

remove any reads with retained sequencing adapters using BBDuk (BBMap, package 38.63 http://sourceforge.net/projects/bbmap/) (Bushnell, 2017) in R (R Core Team, 2013). Based on quality filtering using BBDuk, reads were then assessed for low quality were trimmed by removing reads without an overlap of 30 bp and one expected error. Dereplication of reads grouped unique sequences, which eliminates any redundant comparisons in the pipeline. Culling spurious sequence variants by merging denoised forward and reverse reads and removing none-overlapping paired reads further helps to remove spurious sequences. Error rates for forward and reverse reads are learnt, both ends are merged and used as input into the DADA2 naive RDP's Bayesian classifier to assign amplicon sequence variants (hereafter ASVs). After chimera removal of 2 samples (135 remaining), the assigned taxonomy function within DADA2 was used to classify ASVs to known Symbiodiniaceae sequences from the updated GeoSymbio ITS2 database (Franklin et al., 2012). In essence, this procedure groupings are based on sequence similarity, with names derived from the literature as represented in the updated GeoSymbio database, but do not correspond with strict taxonomic designations, i.e. no binomial species name. Bootstrapping at a threshold of 50 allowed for maximum retention of sequences while minimizing low quality matches. Here we refer to ASVs when discussing the sequence level, and "types" when discussing multiple ASVs that are assigned to the same Symbiodiniaceae taxa (i.e "ASVs" ASV1_C1 and ASV2_C1 are collapsed into "type" C1). On average, 100,801.90 ± 4,212.15 sequences were retained in each sample after quality filtering.

Percent relative abundances of each ASV given the total number of cleaned reads were calculated per sample using the *abundance* (compositional) function in the package "microbiome" (v. 1.10.0) (Lahti et al., 2017). Alpha and beta diversity metrics were calculated using the relative abundance data in "Phyloseq" (v. 1.30.0, McMurdie and Holmes, 2013). Alpha diversity was measured using the Shannon index, and linear mixed models were performed to test differences in diversity across time, treatments and species using the R package lmerTest (Kuznetsova et al., 2017). The assumptions of normality, homogeneity of variance and linearity were tested using the DHARMA (Hartig and Hartig, 2021). To test for differences in diversity across time (T0, T1, T2) and treatments (ambient, 2050, 2100) in *G. retiformis*, a linear mixed model that included time and treatment as fixed effects (and their interactions) and tank as a random effect were performed. For *A. millepora*, the effect of climate treatment on diversity was tested using a linear mixed model using treatment as fixed factor and tank as random factor on square-root transformed data. To test for differences in alpha diversity between species at T2, a linear mixed model with species and treatment (and their interaction) as fixed factors and tank as random factor was run. Post-hoc multiple comparisons adjusted by the False Discovery Rate (Benjamini and Hochberg, 1995) were run in case of significant interactions (or factors) using the R package multcomp (Hothorn et al., 2008). To test for significant differences in the relative abundances of each ASV across treatments, the packages DESeq (v. 1.39.0) and DESeq2 (v. 1.26.0) (Love et al., 2014) were used. Generalized linear models with time (T0, T1, T2) and treatment (ambient, 2050, 2100) as factors were run for 30 iterations, where then non-converging models were filtered prior to multiple test correcting. Significantly differential abundant ASVs were then aligned using Clustal Omega (Sievers et al., 2011).

Risk metric calculation

A risk metric was developed to better understand how the loss or gain of different Symbiodiniaceae taxa could impact host functioning. Taxa of interest were selected based on their total average abundance, overall function profile that included significant shifts between timepoints (ranked redundancy value) and heat tolerance using a "thermal sensitivity" rating (Rk value) determined by (Swain et al., 2016). First, 16 most abundant ASVs were selected. Abundance was determined for each by taking the average sequence reads across the dataset and then selecting the highest average 16 scores.

The ranked redundancy profile was determined by first assigning a function profile for each of the 16 most abundant taxa. To do this, a review of the literature was performed for those selected 16 ASVs to determine a functional redundancy ranking. This literature review rendered health-associated measurements derived from 17 published experimental studies. Source of stress were calculated for each type based on measurements from the literature from these 17 publications (Supplementary Table 3). These health-associated measurements included: Fv/Fm, chlorophyll content, lipid assessment, Photosystem I function relative to photosystem II function, dark oxygen consumption, ratio of photosynthesis to respiration, DMSP concentration, DMSO activity, glutanthione activity, catalase-like activity, superoxide dismutase activity, bleaching response, light pressure response, rate of photosynthesis, experiment type, maximum excitation pressure, and growth. For those publications which measured a value both before and after a stress treatment, the average change across each measurement for each taxon was calculated to assign a rank value. For example, this rendered the difference in Fv/Fm values for D1a before and after a stress treatment. If the study associated this difference with a positive outcome for the symbiont or the host, this change in value was ranked positive ("healthy" or "resilient" host–symbiont interaction). Therefore, each measurement was associated with an average change value, where a change of −0.1 (the smallest change value calculated) was ranked as "1st" (less change) and a change of −0.51 (the largest change value calculated) was ranked as "13th" (more change). Therefore, we define a positive experimental outcome with a small change, compared to a large change, to indicate a greater resilience to stress. For publications with single measurements (only a before or after measurement), ranks were based on the value measurements only. For example, chlorophyll content (Chl a + *c2*) was ranked from high to low values. To address differences in the number of observations for each measurement and for each taxon, a "point" was given per observation and then the total number of observations for each measurement was divided by the total number of observations to render a relative point score. Taking the example of Fv/Fm and D1a above, this rendered a final

relative score of 0.333. This resulted in a ranked redundancy score that included the functional profile, the relative change in measurements that make up the functional profile, and a positive or negative outcome associated with that change. We assume that if the experimental outcome was positive, a higher change is representative of a shift towards greater tolerance.

Thermal sensitivity scores (R_k values) were derived from Swain et al. (2016). The Borda Rank method (Borda, 1781) was used to calculate the final ranking of R_k values and averaged to result in a relative ranking per function per taxa (from "1" being an important taxon in terms of function to "21", being a less important taxa for function) (Supplementary Tables 4, 5). Finally, with these two derived metrics (ranked redundancy and R_k), taxa were categorized into 4 risk categories: High Function, High Sensitivity (High Risk, red points), Low Function, High Sensitivity or High Function (Medium Risk, green points), Low Sensitivity (Medium Risk, green points), and Low Function, Low Sensitivity (Low Risk, blue points). Therefore, a taxon that is considered high risk of loss (lower left) are those taxa that contribute to a large number of functions that are unique (low redundancy) in the coral and that also tend to undergo a large change in thermal sensitivity under heat stress. If lost from the coral, these taxa would potentially have the greatest impact on host function due to their low redundancy and high functional importance. Taxa colored in black were ranked based on only one value for the calculation of the R_k value.

Results and discussion

Changes in relative abundance of *Goniastrea retiformis* juveniles

Adult *G. retiformis* are typically dominated by Symbiodiniaceae of the genus *Cladocopium* with the lowered abundance of *Durusdinium* as "background" taxa (Leveque et al., 2019). However, studies conducted on other coral species suggest that under elevated temperatures, an increase in more thermally tolerant *Durusdinium* could occur (Baker et al., 2004; Claar et al., 2020; Quigley et al., 2022). Like conspecific adults, *G. retiformis* juveniles in this study were typically dominated by *Cladocopium* taxa, but only at T0, although the cumulative abundance of all *Cladocopium* taxa remained higher in juveniles through time under ambient conditions – compared to the higher temperature and pCO_2 2050 and 2100 treatments (Figures 1, 2). At T1 and T2, *Durusdinium* (averaged across all taxa in that genus) were found at higher relative abundance (20–23%, Table 1), especially in the 2050 treatment, which was accompanied by a decrease in *Cladocopium* relative abundance (from 56% to as low as 2%, Table 1). This pattern was evident in both the T1 and T2 timepoints, which may be due to the extended duration of stress at both high temperature and pCO_2 or juvenile ontogeny and winnowing of symbiont communities.

As the average relative abundance of *Cladocopium* decreased through time (from 56% to as low as 2%, Table 1), this genus was

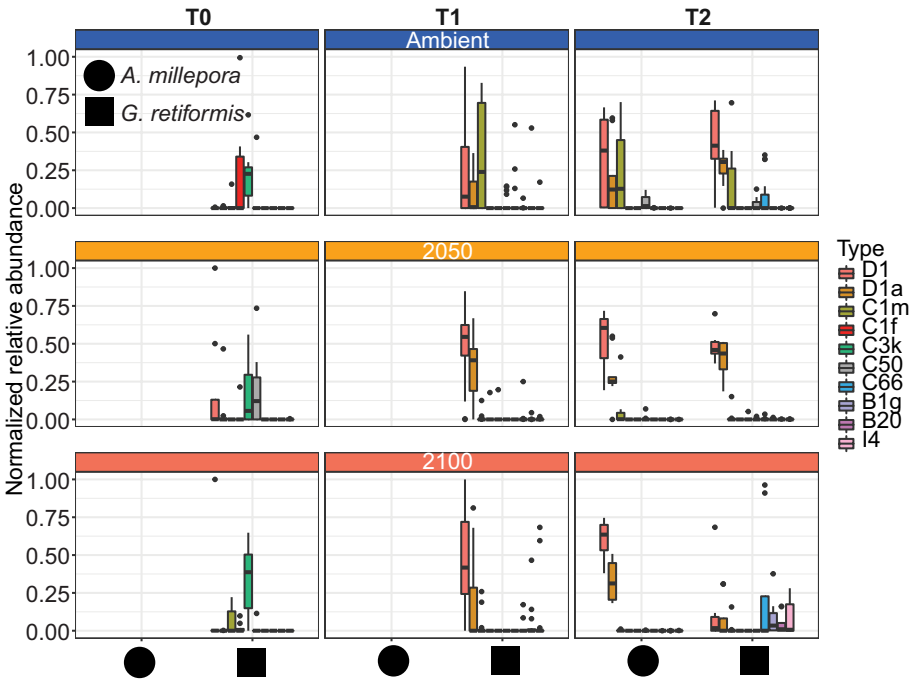

FIGURE 1
Effects of elevated temperature and pCO_2 on Symbiodiniaceae communities in coral juveniles of *Acropora millepora* and *Goniastrea retiformis*. Corals were sampled for ITS2 amplicon sequencing at 14 days post-settlement (T0; before exposure to treatment conditions), 10 days (T1) and four (*G. retiformis*) or five (*A. millepora*) weeks (T2) of exposure to 2050 (+1°C offset, pCO_2 685 ± 60ppm) and 2100 (+2°C offset, pCO_2 940 ± 60ppm) conditions. For *A. millepora*, only samples collected at T2 were sequenced, samples of *A. millepora* were not sequenced (NS) at T0 or T1 (see detailed information in Materials and Methods). The ten most abundant Symbiodiniaceae taxa (>4.2% relative abundance cut-off) across juveniles are shown here.

replaced by *Durusdinium* or other ASV-identified taxa (e.g., B1g, I4) in the 2050 and 2100 scenarios at T2 (Figure 1). This could suggest that *G. retiformis* may shuffle their symbiont communities towards more heat or high pCO_2 resistant taxa in the "shorter" term (up to 2050), taking on the classic shuffling pattern of *Cladocopium* to *Durusdinium* dominance. However, the future temperature and pCO_2 conditions projected for 2100 may represent a threshold in which this acclimatory shuffling mechanism breaks down, manifesting as the lowered relative abundances of *Cladocopium* and *Durusdinium* and increases in potentially "non-symbiotic" taxa (Figures 1, 2). We also cannot exclude that the distinct Symbiodiniaceae communities observed at T0 (i.e. before recruits were exposed to treatment conditions) across treatments may have influenced the symbiont community dynamics under 2050 and 2100 conditions at the later time points. Further, a limitation to this study is the lack of survival data collected. It is therefore not known with certainty if juveniles with sub-optimal symbiont communities experienced mortality before sampling. Therefore, we cannot conclusively say that the 2050 or 2100 treatment caused any impact or mortality over our sampling period. However, given the vast literature on the impacts of heat and acidification on coral juvenile survival as well as the impacts of these treatments specifically on other reef organisms (Botté et al., 2020; Uthicke et al., 2020), it is likely that the 2050 and 2100 conditions had an impact on growth and survival in this study. Some of the changes seen here, which we ascribed to potential shuffling, could be due to juveniles with sub-optimal symbiont communities dying. Regardless, we were interested in characterizing climate change impacts on the symbiont communities across time and species, even if it was not the result of differential mortality. Additional assessment of survival could help in indicating at what stress levels corals experience shuffling or if the observed shifts were a result of survival of the fittest.

G. retiformis juveniles sampled from the ambient treatment at T0 (i.e. before recruits were exposed to treatment conditions) were dominated by *Cladocopium* (as discussed above), but more specifically, by C3k and C1f and background ASVs like C1m (mean relative of <1% of samples) (Figure 2). Interestingly, these abundances varied across the three treatments despite the T0 sampling occurring before treatment exposure. This may be due to high flexibility in early life stages (Coffroth et al., 2001; Little et al., 2004) in combination with a smaller sample size at T0 (see Supplementary Material). These may represent potential symbiotic partnerships and may be relevant to the changes seen at the later time points.

In the ambient treatment, there were also changes in Symbiodiniaceae relative abundances over time, including an increase in *Durusdinium* (from 0 to 11–23%, Table 1). The shuffling (i.e. change in the relative abundance) of specific Symbiodiniaceae were also observed in the ambient treatment, including D1, D1a, and C1m (present in >50% of samples), as well as in background ASVs (C50, C66, and B1g), observed from T0 to T1 (Figures 1, 2). After four weeks (T2) under ambient conditions, juveniles were dominated by D1, D1a and C1m, with background ASVs including C50, C66, and I4 (Figures 1, 2). At T0, before exposure to 2050 and 2100 conditions, juveniles were

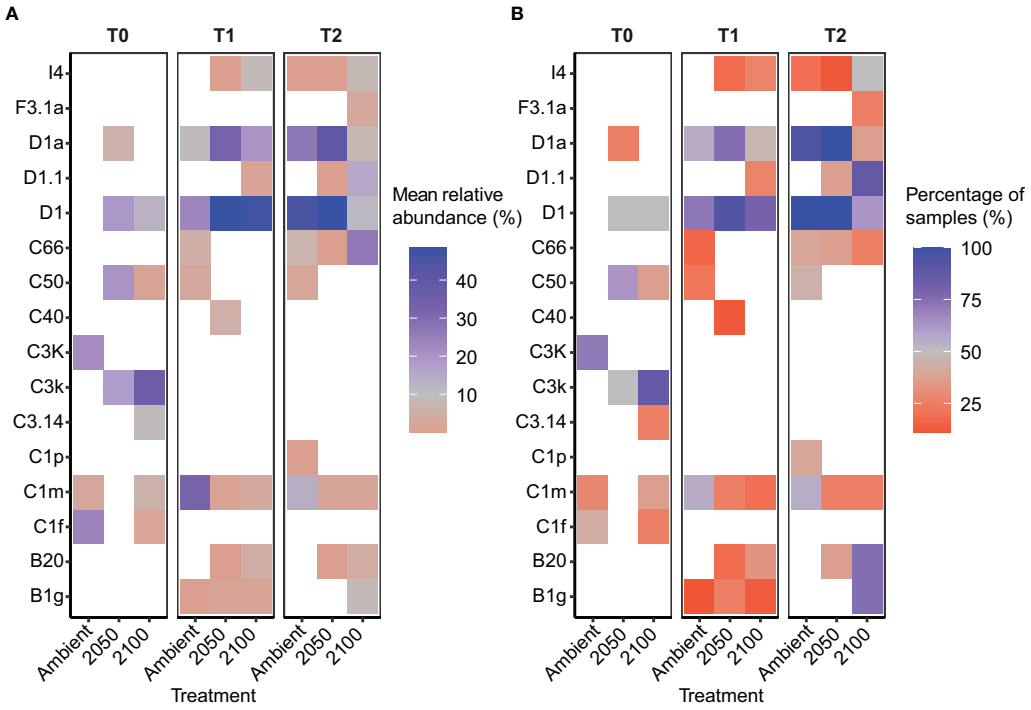

FIGURE 2
Relative abundance of the dominant Symbiodiniaceae taxa in *Goniastrea retiformis* juveniles over time and across climate treatments. **(A)** Mean relative abundance of the top Symbiodiniaceae taxa at T0 (before exposure to treatment conditions), T1 (10-day exposure), T2 (4-week exposure) under ambient, 2050 and 2100 conditions. **(B)** Proportion of coral juveniles associated with each dominant Symbiodiniaceae taxa under climate treatments over time (T0, T1, T2).

10.3389/fevo.2023.1113357

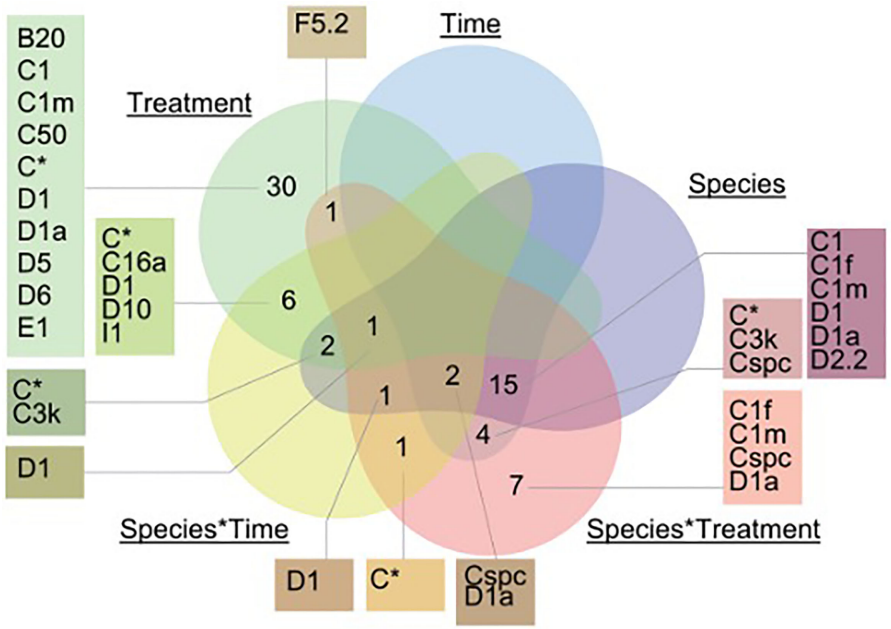

FIGURE 3
Venn diagram incorporating only ASVs that significantly changed in relative abundance between treatments, time and species. A generalized linear model was run to determine which factors (time, treatment, species, or their interactions) explained the greatest variation in ASV abundance using the package DESeq and DESeq2 (v.1.26.0). Specifically, species*time corresponds to: *A. millepora* (T2) and in *G. retiformis* (T0, T1, T2). There were no ASVs that were significantly associated with the time*treatment interaction and are not illustrated in the figure.

dominated by C50, D1, and C3k in 2050 treatments, and C3k and D1 in 2100 treatments, with background ASVs of D1a (2050), and C1m, C50, C1f, and C3.14 (2100) (Figure 1). After 10 days (T1) under 2050 and 2100 and 4 weeks (T2) at the 2050 treatment, *Cladocopium* relative abundances dropped and were replaced by *Durusdinium* ASVs, which were present across >75% of samples (Figure 2). By T2 in the 2100 treatment, more background types were represented in higher relative abundance, including D1.1, B1g, B20, I4, and F3.1a (Figure 1). This change toward *Durusdinium*-dominance may have been driven by juvenile age (or duration of temperature and pCO_2 stress exposure), although climate treatment was the main driver of the change in individual Amplicon Sequence Variants (ASVs). For example, a total of 70 ASVs were differentially abundant in relation to treatment or treatment*species (Figure 3). Significant changes by ASVs and time were only related to changes in ASV abundance when the climate treatment interaction was included. This suggests that while juvenile age and duration of climate exposure may result in changes in the relative abundance of ASVs within the Symbiodiniaceae communities, climate treatments likely represent the main driver of symbiont community changes in our study.

Changes in relative abundance of *Acropora millepora* juveniles

Acropora millepora juveniles (sequenced only at five weeks, T2, see Materials and Methods), were dominated by *Durusdinium* (D1 and D1a) across climate treatments (Figures 1, 4). ASVs associated with *Cladocopium* decreased in relative abundances with increasing climate stress (from 64% to as low as 0% in the T1 2100 treatment, Table 1, Figures 1, 4). For example, the average relative abundance of *Cladocopium* C1m decreased with increasing stress in the 2050 and 2100 treatments (from as high as 25% at T1 ambient to close to

TABLE 1 Relative abundance of the dominant *Cladocopium* and *Durusdinium* taxa across both species, timepoints and stress exposures (note no data was available for *A. millepora* for T0 and T1).

	All treatments		Ambient		2050		2100	
	Cladocopium	*Durusdinium*	*Cladocopium*	*Durusdinium*	*Cladocopium*	*Durusdinium*	*Cladocopium*	*Durusdinium*
T0	0.56 ± 0.04	0.13 ± 0.5	0.64 ± 0.17	0.00 ± 0.00	0.50 ± 0.11	0.25 ± 0.07	0.60 ± 0.04	0.13 ± 0.06
T1	0.02 ± 0.02	0.20 ± 0.14	0.04 ± 0.04	0.11 ± 0.09	0.01 ± 0.01	0.27 ± 0.16	0.00 ± 0.00	0.23 ± 0.19
T2	0.19 ± 0.2	0.23 ± 0.13	0.03 ± 0.02	0.23 ± 0.13	0.01 ± 0.01	0.24 ± 0.14	0.01 ± 0.01	0.06 ± 0.04

The dominant ASVs used are the same as Figure 1. Average relative abundance of the Cladocopium ASVs and Durusdinium ASVs grouped at the genus level. Over the sampling timepoints, there was a decrease in the relative abundance of *Cladocopium* and increase in relative abundance of *Durusdinium*.

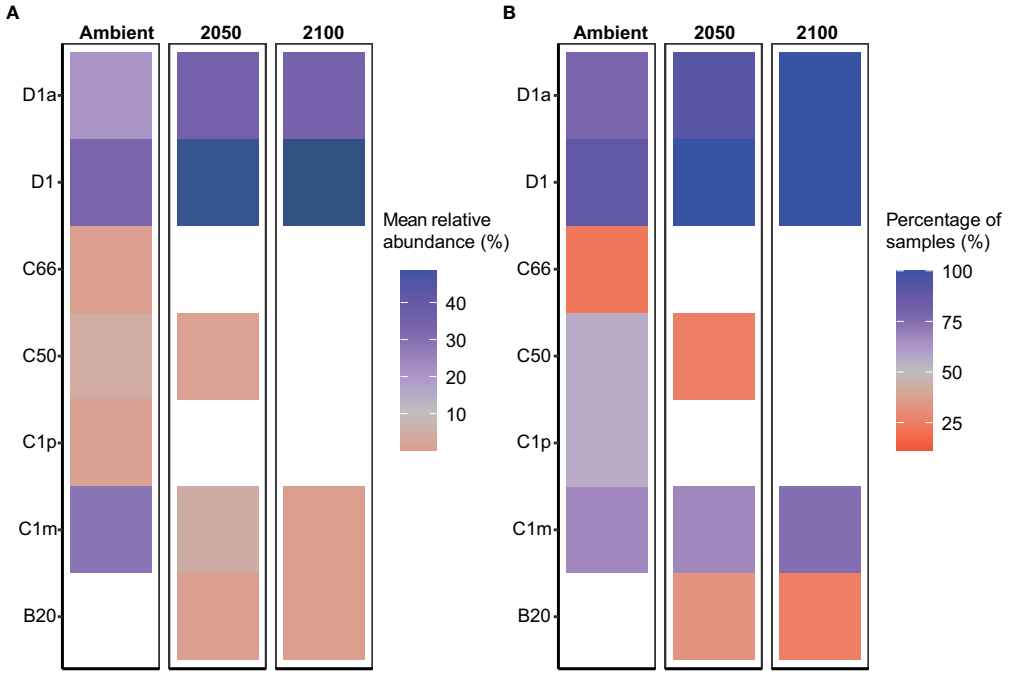

FIGURE 4
Relative abundance of the dominant Symbiodiniaceae taxa in *Acropora millepora* juveniles following 5-week exposure to climate treatments. **(A)** Mean relative abundance of the most abundant Symbiodiniaceae taxa under ambient, 2050 and 2100 conditions. Dark blue colours represent values >45%. **(B)** Proportion of coral juveniles associated with each dominant Symbiodiniaceae taxa under climate treatments.

0% in other treatments, Figure 4). Likewise, other background ASVs were more abundant in the ambient treatment juveniles compared to those under 2050 and 2100 conditions, with 2100 samples comprising very few background ASVs.

Our study examined the combined impacts of temperature and pCO_2. However, our results parallel studies that looked at these stressors singularly. For example, the dominance of *Durusdinium* in our study from the combined climate stressors was consistent with other studies conducted on *A. millepora* juveniles, which showed a change towards *Durusdinium*-dominance at higher temperatures (Abrego et al., 2012). Similar patterns were also reported in adult corals of the same species, with an increased abundance of *Durusdinium* observed in corals exposed to elevated sea surface temperatures and/or human disturbances (Oliver and Palumbi, 2011; Sully et al., 2019; Claar et al., 2020; Quigley and van Oppen, 2022). It is important to note that although community changes towards *Durusdinium* may increase host thermal tolerance or a more generalized stress tolerance, it may concomitantly decrease growth rates (Little et al., 2004). Hence, there may be limited benefits of hosting *Durusdinium* for the coral *A. millepora*. Finally, the increased relative abundance of D1 and D1a in conjunction with the decreased abundance of background types in both the high temperature and high pCO_2 2050 and 2100 treatments (for example, at T2, from <40% to >60%) suggests that *A. millepora* juveniles may have the ability to acclimate to these combined future climate conditions for at least short experimental periods. This demonstrated potential, if applicable in the wild, may promote greater survival under future climate scenarios, thereby increasing the opportunity for some coral species to survive through disturbance, like mass bleaching events combined with the impacts of acidification, to then go on to grow and reproduce and contribute to reef recovery.

Changes in the diversity of Symbiodiniaceae occurred across time, treatment, and coral species

Changes in the symbiont community in coral early life history stages have been observed in both field and lab-based experiments (Abrego et al., 2009; Quigley et al., 2017; Quigley et al., 2020a), in which the overall symbiont community diversity and composition can strongly influence host performance such as growth, survival and thermotolerance (Mieog et al., 2009). Endosymbiotic community diversity may also vary in response to environmental conditions, including temperature and nutrients (Gong et al., 2018). In our study, climate treatments did not impact diversity (as measured by the Shannon diversity index) within each coral species ($p > 0.001$; Figure 5). However, diversity in *G. retiformis* juveniles changed significantly over time, with an overall lower diversity at T1 compared to T2 (Lmer: $F_{2,97} = 11.2$, $p < 0.01$), though there were no significant differences between T0, and the later life stages. When comparing diversity between species at T2, mean diversity was higher in *A. millepora* compared to *G. retiformis* in juveniles under 2100 conditions (Lmer, species: $F_{1,54} = 6.0$, $p = 0.02$; species*treatment: $F_{2,54} = 3.4$, $p = 0.04$; *G. retiformis* 2100 – *A. millepora* 2100: $p = 0.03$). Taken together, these results suggest that at least at the final timepoint under 2100 conditions, Symbiodiniaceae communities in *A. millepora* were more diverse

10.3389/fevo.2023.1113357

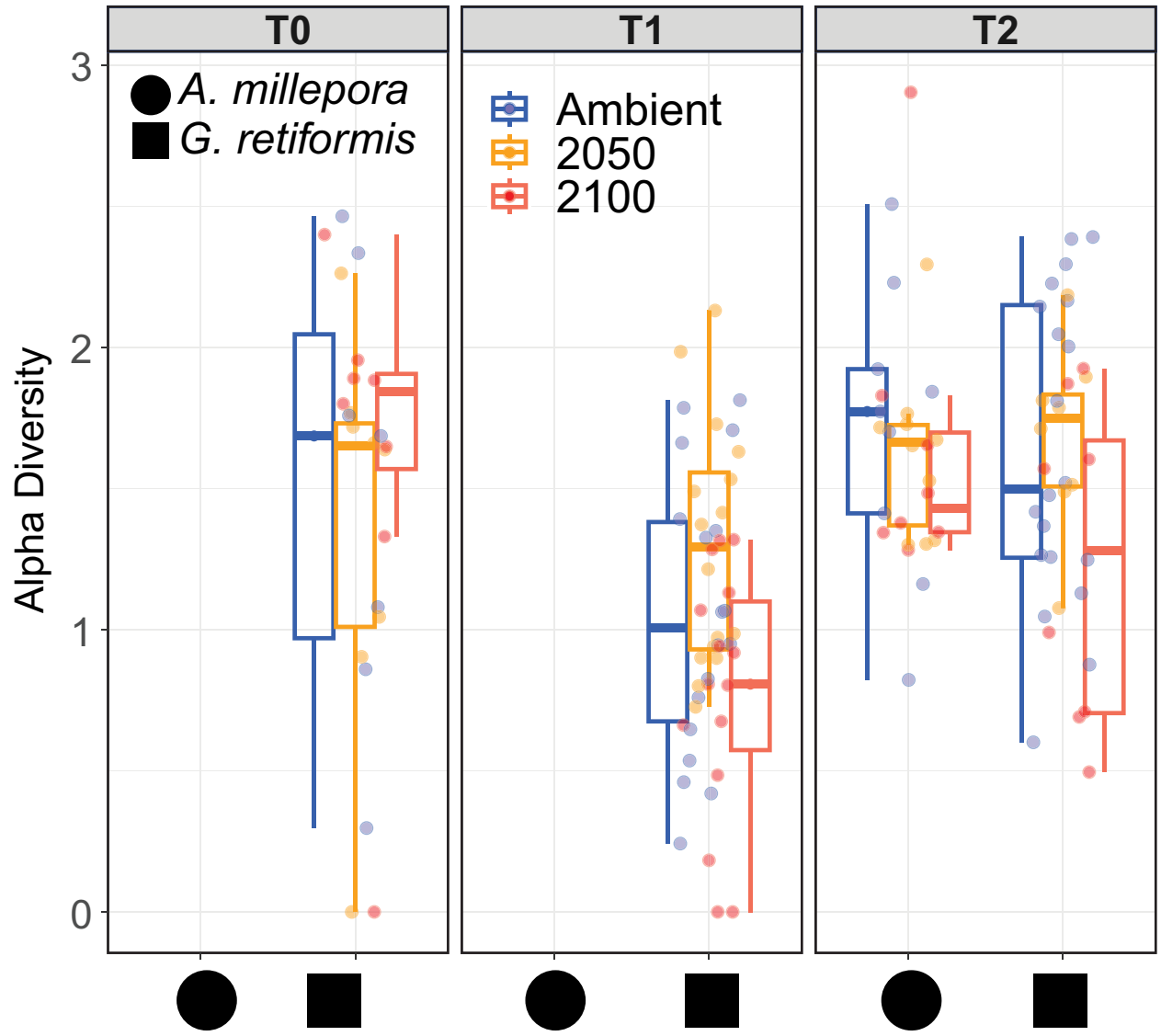

FIGURE 5
Shannon diversity index in *A. millepora* (circle) and *G. retiformis* (square) juveniles across temperature and pCO_2 treatments (ambient, 2050, 2100) and time (T0, T1, T2). The Shannon diversity metric was calculated using normalized ASVs abundances calculated for each individual juvenile using the R package Phyloseq. Samples of *A. millepora* were not sequenced (NS) at T0 and T1 for this species. Shannon diversity index differed significantly within each coral species ($p > 0.001$) and between species*conditions (species*treatment: $p = 0.04$) and over time for *G. retiformis* juveniles between T1 to T2 ($p < 0.01$). At T2 for 2100 conditions, *A. millepora* was significantly more diverse compared to *G. retiformis* ($p = 0.03$).

and more evenly distributed across individual juveniles compared to within *G. retiformis*, and importantly, they were shuffling towards a community of *Durusdinium* dominance.

Changes in specific Symbiodiniaceae taxa driven by coral species-specific responses to temperature and pCO_2

Durusdinium are of particular ecological interest due to their relative tolerance to stress compared to other symbionts (Morikawa and Palumbi, 2019). In our study, an increased abundance of *Durusdinium* (generally from 13% to 20–23%, Table 1) was observed through time (*G. retiformis*) and under climate stress (*G. retiformis* and *A. millepora*), and *Durusdinium* ASVs were the taxa most likely to change across climate treatments, including *D. glynnii* (15 ASVs to D1), and *D. trenchii* (9 ASVs to D1a). These shifts towards a *Durusdinium*-dominated community may be a consequence of the decrease in *Cladocopium* relative abundance, leaving available niches for *Durusdinium* through time or *via* competitive exclusion. *Cladocopium* ASVs also changed in abundance and included a total of 12 *Cladocopium* ASVs across our treatment conditions (Figure 4). The most common taxa that changed included C50 (4 ASVs), C1 (3 ASVs), and C1m (3 ASVs), mostly driven by climate treatment effects (Figure 3, Supplementary Figure 1). Interestingly, communities within the *G. retiformis*

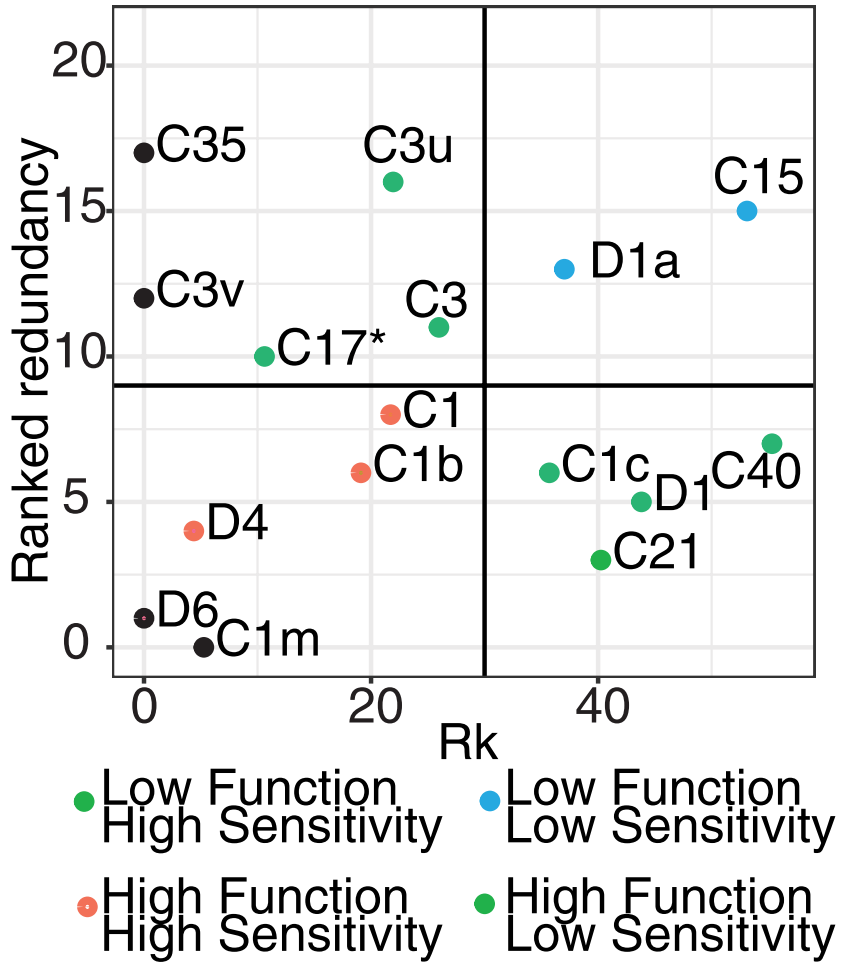

FIGURE 6
Risk metric quantifying the potential risk associated with the breakdown of host functioning due to Symbiodiniaceae loss. The metric included the 16 most highly abundant Symbiodiniaceae ASVs and included rankings of the likelihood of shifts (x-axis; R_k score) and functional redundancy of each taxon (y-axis). R_k values are from Swain et al. (2016) which measure the thermo-sensitivity of taxa. Redundancy rankings were calculated based on multiple health-associated measurements (e.g. Fv/Fm, chlorophyll content, lipid assessment) derived from 17 published experimental studies. The 16 ASVs were selected because they were the most abundant and were the ASVs which overlapped in both our study and those assessed for ranking. For each taxon, measurements were averaged across all studies per trait, with each function per taxa ranked from smallest to largest change, where a small change is indicative of greater redundancy and potential resilience of the host against stress. Final rankings were scored using a Borda Rank method and averaged to result in a relative ranking per function per taxa (from 1: important taxa for function – 21: less important taxa for function). Based on these two metrics, taxa were broken up into High (red points), Medium (green points), and Low (blue points) risk categories. For example, taxa in the High risk (lower left quadrat) identifies taxa which lost would have the greatest risk to impact host functioning due to their low redundancy and high functional importance. Taxa placed along the axis and colored in black only have one R_k value.

juveniles sampled from the 2100 treatment group changed over time from C50 (eight ASVs in T0 and T1) to C66 dominance (one ASV in T2 detected through outlier analysis). However, changes in C50 were more directly related to treatment effects whilst C66 changed by treatment*species interaction (Figure 3). While *Cladocopium* C66 has not been previously identified in *Goniastrea* adults (Leveque et al., 2019), it has been found at low abundance in corals (LaJeunesse et al., 2003). However, C66 has been reported from *A. tenuis* juveniles, with an increase of C66 over 71 days in the wild (Quigley et al., 2020a). This suggests that our T2 treatment may represent the initial establishment of a *Cladocopium* taxon containing the C66 marker and not an experimental artifact.

Further to consider is how different ASVs matching to *Cladocopium* species responded to different stress treatments (see Supplementary Figure 1). For instance, of the 4 ASVs designated C50, two reflected an increase in the relative abundances in response to increased thermal and pCO_2 stress in *A. millepora*, with increases in *G. retiformis* corresponding more to time (up to ~12.5%, Figure 1). This could be a factor of variable host–symbiont interactions between species, however this would require sequencing of *A. millepora* at earlier timepoints, which was not deemed feasible due to a lack of PCR bands. In addition, *Fugacium* sp. (formerly clade F) is recognized as being a potentially important thermally tolerant taxon (Cunning et al., 2015). While only one ASV matching *Fugacium* (F5.2) was identified as significantly changing in response to treatment factors, this change was seen in the species*treatment factor ($p = 0.025$). F5.2 was present in the greatest relative abundance in *G. retiformis* juveniles under ambient conditions and were alternatively at the lowest relative abundances in ambient *A. millepora*. This finding demonstrates the species-

specific nature of host–symbiont relationships and further emphasizes the need to investigate symbiosis establishment across multiple coral taxa.

The loss of specific Symbiodiniaceae taxa may impact coral host function

Symbiodiniaceae taxa are functionally diverse (Suggett et al., 2015; Swain et al., 2016) with different taxa performing diverse functions within the coral host (Muscatine, 1990). The loss or gain of particular taxa could, as a result, cause physiological changes in host functioning. This change of function may include changes to nutrient transfer (e.g. carbon translocation) or the increase or decrease in tolerance of the host to a stressor. To infer potential consequences on host functioning due to the taxonomic changes measured here, we developed a risk metric that incorporated 16 of the most highly abundant symbiont ASVs in our coral juveniles and their functional roles from the literature, to calculate a "risk" metric that would result from the loss of taxa relative to the redundancy of their functional roles (Figure 6). This metric also incorporates the metric R_k (*sensu* Swain et al., 2016, Supplementary Table 5), where a higher R_k value is indicative of increased thermal tolerance. This metric shows that *Cladocopium* ASVs vary in their sensitivity to high temperatures. For example, *Cladocopium goreaui* (C1) are more thermally-sensitive (R_k = 21.72) compared to C40 (R_k = 55.32), which are more tolerant. This was combined with relative abundance data from this study, for example, in ASVs like C40 that experienced dramatic changes in relative abundance between ambient and climate stress treatments (R_k shift = 55). Redundancy within juveniles for this taxon was also relatively low (redundancy rank = 6). Combined, this resulted in the assignment of this taxon to a "medium risk" category if lost (green points, Figure 6). This suggests that given C40's relatively high heat tolerance and potential ability to provide the coral host with greater stress resilience, the loss of this symbiont could be detrimental to host health given its low functional redundancy.

This same analysis was repeated for each of the 16 most highly abundant symbiont ASVs. *Durusdinium trenchii* (D1a), also generally known as a stress tolerant symbiont, had a correspondingly high R_k (37.03) and experienced relatively large changes in relative abundance between treatments. However, functional redundancy was high (~13), suggesting that there is a diminished risk to host health if this taxon is lost. Other ASVs like C1, C1b, and D4 have low thermal tolerance, experienced large changes in relative abundance, and had low functional redundancy, suggesting the loss of these ASVs are of greater risk to the host. Combined, this novel risk framework suggests that the loss or gain of different symbionts may not be functionally equivalent across these simulated future climate treatments and that each loss of particular symbionts may impact the host through downstream impacts on host function.

These outcomes may also be species-dependent, where some coral species may rely more heavily upon specific Symbiodiniaceae taxa to fulfill certain functions. It is also important to note that the majority of data for the R_k metric used in this risk assessment is derived from coral adults. Given we focus here on juveniles, we underscore those functions may be different across life-stages. Despite this, the use of the risk metric to understand the potential implications of loss and gain of symbiont taxa under future climate scenarios opens up the opportunity to better predict coral reef function in the future. The loss of high-functioning and low redundancy taxa, in particular, highlight the need to better protect reefs in order to minimize loss of these critical symbionts at critical early life stages.

A note on Symbiodiniaceae taxonomy

As alluded to in the Materials and Methods, Symbiodiniaceae taxonomy is challenging given the Symbiodiniaceae ITS2 gene is multicopy with high intragenomic variation (see Quigley et al., 2014 for full discussion). The choice of the DADA2 pipeline may therefore overinflate diversity but minimizes the chance of false-negatives that would be possible from the Symportal pipeline. To address these challenges, a workshop was convened to discuss strategies to move forward amongst experts in the field (Davies et al., 2022). In this work, the pros and cons of the ASV vs. DIV methods were presented, including how the methodology relates to how sequence and species diversity are being treated. Other work has undertaken formal comparisons of these two methods (during the review Quigley et al., 2019; published Quigley et al., 2022), and in both, we confirmed that the results are largely consistent between the ASV and DIV methods. However, and most importantly, we specifically chose the ASV method here for its superior ability to detect novel, low-abundance sequences (Davies et al., 2022).

Conclusion

Overall, we observed an increase in relative abundance of *Durusdinium* over time in relation to juvenile age and duration of climate stress exposure. In addition, we found a significant capacity for coral juveniles to take up D1 and D1a symbionts at treatments with increasing temperature and pCO_2, which generally corresponded with a decrease in *Cladocopium*. These results support the idea of "shuffling" algal symbiont communities for increased acclimation to stress, as seen in studies of adult corals. Longer-term observations of coral juveniles are required to understand the ontogenic consequences of temperature and pCO_2 on symbiosis as it may provide coral offspring with an increased capacity for heat tolerance and survival.

Data availability statement

The datasets presented in this study can be found in online repositories. The names of the repository/repositories and accession number(s) can be found in the article/Supplementary Material.

Author contributions

AT and KQ wrote manuscript. AT performed the lab work. KQ and NW developed the research idea; KQ and EM designed the experiment and sampling strategy and performed the experiment. AT ran the data analysis. NW and KQ provided funding. All authors contributed to the article and approved the submitted version.

Funding

Funding was provided by: AIMS@JCU, James Cook University, the Australian Institute of Marine Science.

Acknowledgments

This study was part of the Evolution21 project funded by AIMS and we are grateful to the AIMS SeaSim staff and volunteers who helped to collect the colonies, spawn the corals, and carry out the husbandry and experimental set-up and maintenance. The authors acknowledge the Gurambilbarra Wulgurukaba Traditional Owners of Magnetic Island, and pay our respects to their Elders, past, present, and emerging.

Conflict of interest

The authors declare that the research was conducted in the absence of any commercial or financial relationships that could be construed as a potential conflict of interest.

Publisher's note

Supplementary material

The Supplementary Material for this article can be found online at: https://www.frontiersin.org/articles/10.3389/fevo.2023.1113357/full#supplementary-material

References

Abrego, D., van Oppen, M. J. H., and Willis, B. L. (2009). Onset of algal endosymbiont specificity varies among closely related species of acropora corals during early ontogeny. *Mol. Ecol.* 18, 3532–3543. doi: 10.1111/j.1365-294X.2009.04276.x

Abrego, D., Willis, B. L., and van Oppen, M. J. H. (2012). Impact of light and temperature on the uptake of algal symbionts by coral juveniles. *PLoS One* 7, e50311. doi: 10.1371/journal.pone.0050311

Adams, L. M., Cumbo, V., and Takabayashi, M. (2009). Exposure to sediment enhances primary acquisition of *Symbiodinium* by asymbiotic coral larvae. *Mar. Ecol. Prog. Ser.* 377, 156–179. doi: 10.3354/meps07834

Ali, A., Kriefall, N. G., Emery, L. E., Kenkel, C. D., Matz, M. V., and Davies, S. W. (2019). Recruit symbiosis establishment and symbiodiniaceae composition influenced by adult corals and reef sediment. *Coral Reefs* 38, 405–415. doi: 10.1007/s00338-019-01790-z

Anthony, K., Hoogenboom, M. O., Maynard, J. A., Grottoli, A. G., and Middlebrook, R. (2009). Energetics approach to predicting mortality risk from environmental stress: a case study of coral bleaching. *Funct. Ecol.* 23, 539–550. doi: 10.1111/j.1365-2435.2008.01531.x

Anthony, K. R. N., Kline, D. I., Diaz-Pulido, G., Dove, S., and Hoegh-Guldberg, O. (2008). Ocean acidification causes bleaching and productivity loss in coral reef builders. *Proc. Natl. Acad. Sci.* 105, 17442–17446. doi: 10.1073/pnas.0804478105

Baird, A. H., Bhagooli, R., Ralph, P. J., and Takahashi, S. (2009). Coral bleaching: the role of the host. *Trends Ecol. Evol.* 24, 16–20. doi: 10.1016/j.tree.2008.09.005

Baker, D. M., Freeman, C. J., Wong, J. C. Y., Fogel, M. L., and Knowlton, N. (2018). Climate change promotes parasitism in a coral symbiosis. *ISME J.* 12, 921. doi: 10.1038/s41396-018-0046-8

Baker, A. C., Starger, C. J., McClanahan, T. R., and Glynn, P. W. (2004). Corals' adaptive response to climate change. *Nature* 430, 741. doi: 10.1038/430741a

Benjamini, Y., and Hochberg, Y. (1995). Controlling the false discovery rate: a practical and powerful approach to multiple testing. *J. R. Stat. society. Ser. B (Methodological)* 57 (1), 289–300. doi: 10.1111/j.2517-6161.1995.tb02031.x

Berkelmans, R., and van Oppen, M. J. H. (2006). The role of zooxanthellae in the thermal tolerance of corals: a "nugget of hope" for coral reefs in an era of climate change. *Proc. R. Soc. B: Biol. Sci.* 273, 2305–2312. doi: 10.1098/rspb.2006.3567

Borda, J.C.de (1781). M'emoire sur les' elections au scrutin. *Histoire l'Acad'emie Royale Des. Sci.*

Botté, E. S., Luter, H. M., Marangon, E., Patel, F., Uthicke, S., and Webster, N. S. (2020). Simulated future conditions of ocean warming and acidification disrupt the microbiome of the calcifying foraminifera marginopora vertebralis across life stages. *Environ. Microbiol. Rep.* 12, 693–701. doi: 10.1111/1758-2229.12900

Brown, B. E. (1997). Coral bleaching: causes and consequences. *Coral Reefs* 16, S129–S138. doi: 10.1007/s003380050249

Bushnell, B. (2017). *BBMap short read aligner, and other bioinformatic tools, version 37.33.*

Callahan, B. J., McMurdie, P. J., Rosen, M. J., Han, A. W., Johnson, A. J. A., and Holmes, S. P. (2016). DADA2: high-resolution sample inference from illumina amplicon data. *Nat. Methods* 13, 581–583. doi: 10.1038/nmeth.3869

Cantin, N., van Oppen, M., Willis, B., Mieog, J., and Negri, A. (2009). Juvenile corals can acquire more carbon from high-performance algal symbionts. *Coral Reefs* 28, 405–414. doi: 10.1007/s00338-009-0478-8

Claar, D. C., Starko, S., Tietjen, K. L., Epstein, H. E., Cunning, R., Cobb, K. M., et al. (2020). Dynamic symbioses reveal pathways to coral survival through prolonged heatwaves. *Nat. Commun.* 11, 1–10. doi: 10.1038/s41467-020-19169-y

Coffroth, M. A., Lewis, C. F., Santos, S. R., and Weaver, J. L. (2006). Environmental populations of symbiotic dinoflagellates in the genus *Symbiodinium* can initiate symbioses with reef cnidarians. *Curr. Biol.* 16, R985–R987. doi: 10.1016/j.cub.2006.10.049

Coffroth, M. A., Santos, S., and Goulet, T. (2001). Early ontogenetic expression of specificity in a cnidarian-algal symbiosis. *Mar. Ecol. Prog. Ser.* 222, 85–96. doi: 10.3354/meps222085

Cohen, A. L., and Holcomb, M. (2009). Why corals care about ocean acidification: uncovering the mechanism. *Oceanography* 22, 118–127. doi: 10.5670/oceanog.2009.102

Collins, M., Knutti, R., Arblaster, J., Dufresne, J.-L., Fichefet, T., Friedlingstein, P., et al. (2013). "Long-term climate change: projections, commitments and irreversibility," in *Climate change 2013-the physical science basis: contribution of working group I to the fifth assessment report of the intergovernmental panel on climate change* (Cambridge, UK and New York, USA: Cambridge University Press), 1029–1136.

Cunning, R., Silverstein, R. N., and Baker, A. C. (2015). Investigating the causes and consequences of symbiont shuffling in a multi-partner reef coral symbiosis under environmental change. *Proc. R. Soc B* 282, 20141725. doi: 10.1098/rspb.2014.1725

Davies, S., Gamache, M. H., Howe-Kerr, L. I., Kriefall, N. G., Baker, A. C., Banaszak, A. T., et al. (2022). Building consensus around the assessment and interpretation of symbiodiniaceae diversity. *PeerJ* 11, e15023. doi: 10.7717/peerj.15023

Fitt, W. K., Brown, B. E., Warner, M. E., and Dunne, R. P. (2001). Coral bleaching: interpretation of thermal tolerance limits and thermal thresholds in tropical corals. *Coral Reefs* 20, 51–65. doi: 10.1007/s003380100146

Foster, T., Falter, J. L., McCulloch, M. T., and Clode, P. L. (2016). Ocean acidification causes structural deformities in juvenile coral skeletons. *Sci. Adv.* 2, e1501130. doi: 10.1126/sciadv.1501130

Franklin, E. C., Stat, M., Pochon, X., Putnam, H. M., and Gates, R. D. (2012). GeoSymbio: a hybrid, cloud-based web application of global geospatial bioinformatics and ecoinformatics for *Symbiodinium*-host symbioses. *Mol. Ecol. Resour* 12, 369–373. doi: 10.1111/j.1755-0998.2011.03081.x

Gong, S., Chai, G., Xiao, Y., Xu, L., Yu, K., Li, J., et al. (2018). Flexible symbiotic associations of symbiodinium with five typical coral species in tropical and subtropical reef regions of the northern south China Sea. *Front. Microbiol.* 9, 2485. doi: 10.3389/fmicb.2018.02485

Hartig, F., and Hartig, M. F. (2021). *Package "DHARMa." R package version 0.3*, Vol. 3.

Hoegh-Guldberg, O., Mumby, P. J., Hooten, a J., Steneck, R. S., Greenfield, P., Gomez, E., et al. (2007). Coral reefs under rapid climate change and ocean acidification. *Science* 318, 1737–1742. doi: 10.1126/science.1152509

Hothorn, T., Bretz, F., Westfall, P., and Heiberger, R. M. (2008) *Multcomp: simultaneous inference for general linear hypotheses 2008*. Available at: http://CRAN.R-project.org/package=multcomp.

Howe-Kerr, L. I., Bachelot, B., Wright, R. M., Kenkel, C. D., Bay, L. K., and Correa, A. M. S. (2020). Symbiont community diversity is more variable in corals that respond poorly to stress. *Glob Chang Biol.* 26, 2220–2234. doi: 10.1111/gcb.14999

Hughes, T. P., Barnes, M. L., Bellwood, D. R., Cinner, J. E., Cumming, G. S., Jackson, J. B. C., et al. (2017a). Coral reefs in the anthropocene. *Nature* 546, 82–90. doi: 10.1038/nature22901

Hughes, T. P., Kerry, J. T., Álvarez-Noriega, M., Álvarez-Romero, J. G., Anderson, K. D., Baird, A. H., et al. (2017b). Global warming and recurrent mass bleaching of corals. *Nature* 543, 373–377. doi: 10.1038/nature21707

Hume, B. C. C., Smith, E. G., Ziegler, M., Warrington, H. J. M., Burt, J. A., LaJeunesse, T. C., et al. (2019). SymPortal: a novel analytical framework and platform for coral algal symbiont next-generation sequencing ITS 2 profiling. *Mol. Ecol. Resour* 19 (4), 1063–1080. doi: 10.1111/1755-0998.13004

Kuznetsova, A., Brockhoff, P. B., and Christensen, R. H. B. (2017). lmerTest package: tests in linear mixed effects models. *J. Stat. Softw* 82, 1–26. doi: 10.18637/jss.v082.i13

Lahti, L., Shetty, S., Blake, T., and Salojarvi, J. (2017). *Tools for microbiome analysis in r. version*, Vol. 1. 28.

LaJeunesse, T. C. (2001). Investigating the biodiversity, ecology, and phylogeny of endosymbiont dinoflagellates in the genus *Symbiodinium* using the ITS region: in search of a "species" level marker. *J. Phycol* 37, 866–880. doi: 10.1046/j.1529-8817.2001.01031.x

LaJeunesse, T. L. (2002). Diversity and community structure of symbiotic dinoflagellates from Caribbean coral reefs. *Mar. Biol.* 141, 387–400. doi: 10.1007/s00227-002-0829-2

LaJeunesse, T. C., Loh, W. K. W., Woesik, R., Hoegh-Guldberg, O., Schmidt, G. W., and Fitt, W. K. (2003). Low symbiont diversity in southern great barrier reef corals, relative to those of the Caribbean. *Limnol Oceanogr* 48, 2046–2054. doi: 10.4319/lo.2003.48.5.2046

LaJeunesse, T. C., Parkinson, J. E., Gabrielson, P. W., Jeong, H. J., Reimer, J. D., Voolstra, C. R., et al. (2018). Systematic revision of symbiodiniaceae highlights the antiquity and diversity of coral endosymbionts. *Curr. Biol.* 28, 2570–2580. doi: 10.1016/j.cub.2018.07.008

LaJeunesse, T. C., Smith, R. T., Finney, J., and Oxenford, H. (2009). Outbreak and persistence of opportunistic symbiotic dinoflagellates during the 2005 Caribbean mass coral "bleaching" event. *Proc. R. Soc. B: Biol. Sci.* 276, 4139–4148. doi: 10.1098/rspb.2009.1405

Lee, M. J., Jeong, H. J., Jang, S. H., Lee, S. Y., Kang, N. S., Lee, K. H., et al. (2016). Most low-abundance "background" symbiodinium spp. are transitory and have minimal functional significance for symbiotic corals. *Microb. Ecol.* 71, 771–783. doi: 10.1007/s00248-015-0724-2

Leveque, S., Afiq-Rosli, L., Ip, Y. C. A., Jain, S. S., and Huang, D. (2019). Searching for phylogenetic patterns of symbiodiniaceae community structure among indo-pacific merulinidae corals. *PeerJ* 7, e7669. doi: 10.7717/peerj.7669

Lewis, C. L., and Coffroth, M. A. (2004). The acquisition of exogenous algal symbionts by an octocoral after bleaching. *Science* 304, 1490–1492. doi: 10.1126/science.1097323

Little, A. F., van Oppen, M. J. H., and Willis, B. L. (2004). Flexibility in algal endosymbioses shapes growth in reef corals. *Science* 304, 1492–1494. doi: 10.1126/science.1095733

Love, M., Anders, S., and Huber, W. (2014). Differential analysis of count data–the DESeq2 package. *Genome Biol.* 15, 550. doi: 10.1186/s13059-014-0550-8

McIlroy, S. E., and Coffroth, M. A. (2017). Coral ontogeny affects early symbiont acquisition in laboratory-reared recruits. *Coral Reefs* 36, 927–932. doi: 10.1007/s00338-017-1584-7

McMurdie, P. J., and Holmes, S. (2013). Phyloseq: an r package for reproducible interactive analysis and graphics of microbiome census data. *PloS One* 8, e61217. doi: 10.1371/journal.pone.0061217

Meinshausen, M., Smith, S. J., Calvin, K., Daniel, J. S., Kainuma, M. L. T., Lamarque, J.-F., et al. (2011). The RCP greenhouse gas concentrations and their extensions from 1765 to 2300. *Clim Change* 109, 213–241. doi: 10.1007/s10584-011-0156-z

Mieog, J., van Oppen, M., Berkelmans, R., Stam, W., and Olsen, J. (2009). Quantification of algal endosymbionts (*Symbiodinium*) in coral tissue using real-time PCR. *Mol. Ecol. Resour* 9, 74–82. doi: 10.1111/j.1755-0998.2008.02222.x

Morikawa, M. K., and Palumbi, S. R. (2019). Using naturally occurring climate resilient corals to construct bleaching-resistant nurseries. *Proc. Natl. Acad. Sci. U.S.A.* 116, 10586–10591. doi: 10.1073/pnas.1721415116

Muscatine, L. (1990). The role of symbiotic algae in carbon and energy flux in reef corals. *Ecosyst. World: Coral Reefs* 25, 75–87.

Nitschke, M. R., Davy, S. K., and Ward, S. (2016). Horizontal transmission of *Symbiodinium* cells between adult and juvenile corals is aided by benthic sediment. *Coral Reefs* 35, 335–344. doi: 10.1007/s00338-015-1349-0

Oliver, T., and Palumbi, S. (2011). Do fluctuating temperature environments elevate coral thermal tolerance? *Coral Reefs* 30, 429–440. doi: 10.1007/s00338-011-0721-y

Padilla-Gamiño, J. L., Pochon, X., Bird, C., Concepcion, G. T., and Gates, R. D. (2012). From parent to gamete: vertical transmission of *Symbiodinium* (Dinophyceae) ITS2 sequence assemblages in the reef building coral *Montipora capitata*. *PLoS One* 7, e38440. doi: 10.1371/journal.pone.0038440

Pochon, X., Gates, R. D., Vik, D., and Edmunds, P. J. (2014). Molecular characterization of symbiotic algae (*Symbiodinium* spp.) in soritid foraminifera (*Sorites orbiculus*) and a scleractinian coral (*Orbicella annularis*) from St John, US virgin islands. *Mar. Biol.* 161, 2307–2318. doi: 10.1007/s00227-014-2507-6

Poland, D. M., and Coffroth, M. A. (2017). Trans-generational specificity within a cnidarian–algal symbiosis. *Coral Reefs* 36 (1), 119–129. doi: 10.1007/s00338-016-1514-0

Pollock, F. J., Katz, S. M., van de Water, J. A. J. M., Davies, S. W., Hein, M., Torda, G., et al. (2017). Coral larvae for restoration and research: a large-scale method for rearing *Acropora millepora* larvae, inducing settlement, and establishing symbiosis. *PeerJ* 5, e3732. doi: 10.7717/peerj.3732

Quigley, K. M., Bay, L. K., and van Oppen, M. J. H. (2020b). Genome-wide SNP analysis reveals an increase in adaptive genetic variation through selective breeding of coral. *Mol. Ecol* 29 (12), 2176–2188. doi: 10.22541/au.158921584.47783210

Quigley, K. M., Bay, L. K., and Willis, B. L. (2017). Temperature and water quality-related patterns in sediment-associated symbiodinium communities impact symbiont uptake and fitness of juveniles in the genus acropora. *Front. Mar. Sci.* 4. doi: 10.3389/fmars.2017.00401

Quigley, K. M., Davies, S. W., Kenkel, C. D., Willis, B. L., Matz, M. V., and Bay, L. K. (2014). Deep-sequencing method for quantifying background abundances of *Symbiodinium* types: exploring the rare symbiodinium biosphere in reef-building corals. *PLoS One* 9 (4), e94297. doi: 10.1371/journal.pone.0094297

Quigley, K., Ramsby, B., Laffy, P., Harris, J., Mocellin, V., and Bay, L. (2022). Symbioses are restructed by repeated mass coral bleaching. *Sci. Adv.* 8 (49), eabq8349. doi: 10.1126/sciadv.abq8349

Quigley, K. M., Randall, C. J., van Oppen, M. J. H., and Bay, L. K. (2020c). Assessing the role of historical temperature regime and algal symbionts on the heat tolerance of coral juveniles. *Biol. Open* 9 (1), bio047316. doi: 10.1242/bio.047316

Quigley, K. M., Strader, M. E., and Matz, M. V. (2018a). Relationship between acropora millepora juvenile fluorescence and composition of newly established symbiodiniumassemblage. *PeerJ* 6, e5022. doi: 10.7717/peerj.5022

Quigley, A. R. C., Torda, G., Bourne, D., and Willis, B. (2020a). Co-Dynamics of symbiodiniaceae and bacterial populations during the first year of symbiosis with acropora tenuis juveniles. *Microbiologyopen* 9, e959. doi: 10.1002/mbo3.959

Quigley, K. M., and van Oppen, M. J. H. (2022). Predictive models for the selection of thermally tolerant corals based on offspring survival. *Nat. Commun.* 13, 1–13. doi: 10.1038/s41467-022-28956-8

Quigley, K. M., Warner, P. A., Bay, L. K., and Willis, B. L. (2018b). Unexpected mixed-mode transmission and moderate genetic regulation of symbiodinium communities in a brooding coral. *Heredity* 121 (6), 524–536. doi: 10.1101/173591

Quigley, K. M., Willis, B. L., and Bay, L. K. (2016). Maternal effects and symbiodinium community composition drive differential patterns in juvenile survival in the coral acropora tenuis. *R Soc. Open Sci.* 3 (10), 160471. doi: 10.1098/rsos.160471

Quigley, K. M., Willis, B. L., and Kenkel, C. D. (2019). Transgenerational inheritance of shuffled symbiont communities in the coral montipora digitata. *Sci. Rep.* 9 (1), 13328. doi: 10.1038/s41598-019-50045-y

R Core Team (2013). *R core team. 2013. r: a language and environment for statistical computing* (Vienna, Austria: R Foundation for Statistical Computing).

Reich, H. G., Robertson, D. L., and Goodbody-Gringley, G. (2017). Do the shuffle: changes in *Symbiodinium* consortia throughout juvenile coral development. *PloS One* 12, e0171768. doi: 10.1371/journal.pone.0171768

Robison, J. D., and Warner, M. E. (2006). Differential impacts of photoacclimation and thermal stress on the photobiology of four different phylotypes of symbiodinium (Pyrrhophyta). *J. Phycol* 42, 568–579. doi: 10.1111/j.1529-8817.2006.00232.x

Rohwer, F., Seguritan, V., Azam, F., and Knowlton, N. (2002). Diversity and distribution of coral-associated bacteria. *Mar. Ecol. Prog. Ser.* 243, 1–10. doi: 10.3354/meps243001

Rouzé, H., Lecellier, G., Pochon, X., Torda, G., and Berteaux-Lecellier, V. (2019). Unique quantitative symbiodiniaceae signature of coral colonies revealed through spatio-temporal survey in moorea. *Sci. Rep.* 9, 7921. doi: 10.1038/s41598-019-44017-5

Rowan, R., Knowlton, N., Baker, A., and Jara, J. (1997). Landscape ecology of algal symbionts creates variation in episodes of coral bleaching. *Nature* 388, 265–269. doi: 10.1038/40843

Schoepf, V., Grottoli, A. G., Warner, M. E., Cai, W.-J., Melman, T. F., Hoadley, K. D., et al. (2013). Coral energy reserves and calcification in a high-CO2 world at two temperatures. *PLoS One* 8, e75049. doi: 10.1371/journal.pone.0075049

Sievers, F., Wilm, A., Dineen, D., Gibson, T. J., Karplus, K., Li, W., et al. (2011). Fast, scalable generation of high-quality protein multiple sequence alignments using clustal omega. *Mol. Syst. Biol.* 7. doi: 10.1038/msb.2011.75

Sievers, K. T., McClure, E. C., Abesamis, R. A., and Russ, G. R.. (2020). Non-reef habitats in a tropical seascape affect density and biomass of fishes on coral reefs. *Ecol Evol* 10 (24), 13673–13686.

Stat, M., and Gates, R. D. (2008). Vectored introductions of marine endosymbiotic dinoflagellates into Hawaii. *Biol. Invasions* 10, 579–583. doi: 10.1007/s10530-007-9167-0

Stat, M., Morris, E., and Gates, R. D. (2008). Functional diversity in coral–dinoflagellate symbiosis. *Proc. Natl. Acad. Sci.* 27, 9256–9261. doi: 10.1073/pnas.0801328105

Suggett, D. J., Goyen, S., Evenhuis, C., Szabó, M., Pettay, D. T., Warner, M. E., et al. (2015). Functional diversity of photobiological traits within the genus *Symbiodinium* appears to be governed by the interaction of cell size with cladal designation. *New Phytol.* 208, 370–381. doi: 10.1111/nph.13483

Suggett, D. J., Warner, M. E., and Leggat, W. (2017). Symbiotic dinoflagellate functional diversity mediates coral survival under ecological crisis. *Trends Ecol. Evol.* 32, 735–745. doi: 10.1016/j.tree.2017.07.013

Sully, S., Burkepile, D. E., Donovan, M. K., Hodgson, G., and van Woesik, R. (2019). A global analysis of coral bleaching over the past two decades. *Nat. Commun.* 10, 1264. doi: 10.1038/s41467-019-09238-2

Sun, Z., Huang, Y., Wang, Y., Zhao, Y., and Cui, Z. (2014). Potassium hydroxide-ethylene diamine tetraacetic acid method for the rapid preparation of small-scale PCR template DNA from actinobacteria. *Mol. Genetics Microbiol. Virol.* 29, 42–46. doi: 10.3103/S089141681401008X

Sun, Y., Jiang, L., Gong, S., Guo, M., Yuan, X., Zhou, G., et al. (2020). Impact of ocean warming and acidification on symbiosis establishment and gene expression profiles in recruits of reef coral acropora intermedia. *Front. Microbiol.* 11, 532447. doi: 10.3389/fmicb.2020.532447

Swain, T. D., Chandler, J., Backman, V., and Marcelino, L. (2016). Coral bleaching response index: a new tool to standardize and compare susceptibility to thermal bleaching. *Glob. Chang. Biol.* 22 (7), 2475–2488. doi: 10.1111/gcb.13276

Umeki, M., Yamashita, H., Suzuki, G., Sato, T., Ohara, S., and Koike, K. (2020). Fecal pellets of giant clams as a route for transporting symbiodiniaceae to corals. *PLoS One* 15, e0243087. doi: 10.1371/journal.pone.0243087

Uthicke, S., Patel, F., Karelitz, S., Luter, H. M., Webster, N. S., and Lamare, M. (2020). Key biological responses over two generations of the sea urchin echinometra sp. a under future ocean conditions. *Mar. Ecol. Prog. Ser.* 637, 87–101. doi: 10.3354/meps13236

Yorifuji, M., Harii, S., Nakamura, R., and Fudo, M. (2017). Shift of symbiont communities in *Acropora tenuis* juveniles under heat stress. *PeerJ* 5, e4055. doi: 10.7717/peerj.4055

Yuyama, I., and Higuchi, T. (2014). Comparing the effects of symbiotic algae (*Symbiodinium*) clades C1 and D on early growth stages of *Acropora tenuis*. *PLoS One* 9, e98999. doi: 10.1371/journal.pone.0098999

Yuyama, I., Nakamura, T., Higuchi, T., and Hidaka, M. (2016). Different stress tolerances of juveniles of the coral *Acropora tenuis* associated with clades C1 and D Symbiodinium. *Zool Stud.* 55. doi: 10.6620/ZS.2016.55-19

frontiers | Frontiers in Marine Science

TYPE Original Research
PUBLISHED 08 August 2023
DOI 10.3389/fmars.2023.1152647

OPEN ACCESS

EDITED BY
Diana Sofia Madeira,
University of Aveiro, Portugal

REVIEWED BY
Renato Crespo Pereira,
Fluminense Federal University, Brazil
Masahiro Nakaoka,
Hokkaido University, Japan

*CORRESPONDENCE
Colleen A. Burge
Colleen.Burge@wildlife.ca.gov;
caburge@ucdavis.edu

†PRESENT ADDRESSES
Sukanya Dayal,
Department of Biology and Marine Biology, University of North Carolina Wilmington, Wilmington, NC, United States
James Sanghyun Lee,
Front and Centered, Seattle, WA, United States
Colleen A. Burge,
California Department of Fish &Wildlife, UC Davis Bodega Marine Laboratory, Bodega Bay, CA, United States

‡These authors have contributed equally to this work and share first authorship

§These authors have contributed equally to this work and share last authorship

RECEIVED 28 January 2023
ACCEPTED 23 June 2023
PUBLISHED 08 August 2023

CITATION
Venkataraman YR, Shore A, Dayal S, Lee JS, Alidoost Salimi M, Crandall G, Loeher MM, Stoops M, Swanger M, Eisenlord ME, Van Alstyne KL, Fast MD, Burge CA and Groner ML (2023) Characterizing host-pathogen interactions between *Zostera marina* and *Labyrinthula zosterae*. *Front. Mar. Sci.* 10:1152647. doi: 10.3389/fmars.2023.1152647

Characterizing host-pathogen interactions between *Zostera marina* and *Labyrinthula zosterae*

Yaamini R. Venkataraman[1‡], Amanda Shore[2‡], Sukanya Dayal[3†], James Sanghyun Lee[4†], Mahsa Alidoost Salimi[5], Grace Crandall[6], Malina M. Loeher[7], Mark Stoops[8], Megan Swanger[6], Morgan E. Eisenlord[9], Kathryn L. Van Alstyne[10], Mark D. Fast[11], Colleen A. Burge[3,12*†§] and Maya L. Groner[11,13§]

[1]Biology Department, Woods Hole Oceanographic Institution, Woods Hole, MA, United States, [2]Department of Biology, Farmingdale State College, Farmingdale, NY, United States, [3]Institute of Marine & Environmental Technology, University of Maryland Baltimore County, University of Maryland Baltimore, Baltimore, MD, United States, [4]School of Marine and Environmental Affairs, University of Washington, Seattle, WA, United States, [5]School of Geography, Earth and Atmospheric Sciences, University of Melbourne, Victoria, VIC, Australia, [6]School of Aquatic and Fishery Sciences, University of Washington, Seattle, WA, United States, [7]Department of Aquatic Health Sciences, Virginia Institute of Marine Science, Gloucester Point, VA, United States, [8]University of North Carolina (UNC) Chapel Hill Institute of Marine Sciences, Morehead City, NC, United States, [9]Department of Ecology and Evolutionary Biology, Cornell University Corson Hall, Ithaca, NY, United States, [10]Shannon Point Marine Center, Western Washington University, Anacortes, WA, United States, [11]Hoplite Lab, Department of Pathology and Microbiology, Atlantic Veterinary College-University of Prince Edward Island (AVC-UPEI), Charlottetown, PE, Canada, [12]Department of Microbiology, University of Maryland Baltimore, Baltimore, MD, United States, [13]Bigelow Lab for Ocean Sciences, East Boothbay, ME, United States

Introduction: Seagrass meadows serve as an integral component of coastal ecosystems but are declining rapidly due to numerous anthropogenic stressors including climate change. Eelgrass wasting disease, caused by opportunistic *Labyrinthula* spp., is an increasing concern with rising seawater temperature. To better understand the host-pathogen interaction, we paired whole organism physiological assays with dual transcriptomic analysis of the infected host and parasite.

Methods: Eelgrass (*Zostera marina*) shoots were placed in one of two temperature treatments, 11° C or 18° C, acclimated for 10 days, and exposed to a waterborne inoculation containing infectious *Labyrinthula zosterae* (*Lz*) or sterile seawater. At two- and five-days post-exposure, pathogen load, visible disease signs, whole leaf phenolic content, and both host- and pathogen-transcriptomes were characterized.

Results: Two days after exposure, more than 90% of plants had visible lesions and *Lz* DNA was detectable in 100% percent of sampled plants in the *Lz* exposed treatment. Concentrations of total phenolic compounds were lower after 5 days of combined exposure to warmer temperatures and *Lz*, but were unaffected in other treatments. Concentrations of condensed tannins were not affected by *Lz* or temperature, and did not change over time. Analysis of the eelgrass transcriptome revealed 540 differentially expressed genes in response to *Lz* exposure, but not temperature. *Lz*-exposed plants had gene expression patterns

consistent with increased defense responses through altered regulation of phytohormone biosynthesis, stress response, and immune function pathways. Analysis of the pathogen transcriptome revealed up-regulation of genes potentially involved in breakdown of host defense, chemotaxis, phagocytosis, and metabolism.

Discussion: The lack of a significant temperature signal was unexpected but suggests a more pronounced physiological response to *Lz* infection as compared to temperature. Pre-acclimation of eelgrass plants to the temperature treatments may have contributed to the limited physiological responses to temperature. Collectively, these data characterize a widespread physiological response to pathogen attack and demonstrate the value of paired transcriptomics to understand infections in a host-pathogen system.

KEYWORDS

***Zostera marina*, *Labyrinthula zosterae*, eelgrass wasting disease, transcriptomics, host-pathogen interactions, marine disease**

Introduction

Despite occupying less than 0.1% of the ocean floor (primarily in estuaries and embayments), seagrasses provide numerous ecosystem services, including shoreline stabilization and protection from erosion, nutrient cycling, sediment retention, reduction of pathogens in the water column, and provision of critical nursery habitat for numerous invertebrate and fish species, many of which are of economic importance to the seafood industry (Nordlund et al., 2016; Lamb et al., 2017). Seagrass meadows are threatened by a wide range of global and local stressors associated with anthropogenic activity such as coastal development, increasing sea surface temperature, rising sea levels, sediment and nutrient runoff and disease (Orth et al., 2006; Sullivan et al., 2013). Consequently, over the past century, global seagrass beds have experienced approximately 19% loss in cover (Dunic et al., 2021).

Zostera marina, the most widely distributed seagrass species in the northern hemisphere (Short et al., 2007), is susceptible to infection with the protist *Labyrinthula zosterae (Lz)*, which causes eelgrass wasting disease (EWD). While chronic *Lz* infections are nearly ubiquitous in distribution, acute epidemics of wasting disease can cause declines in eelgrass populations, most notably in the 1930s when Atlantic eelgrass populations were nearly eliminated along the coasts of North America and Europe (Short et al., 1987). *Lz* is a pathogenic Labyrinthulomycete and can be transmitted through direct contact between healthy and infected blades within an eelgrass bed (Muehlstein, 1992) or through the water column (Groner et al., 2014; Groner et al., 2018). Upon infection, *Lz* targets chloroplasts of eelgrass leaves, compromising photosynthesis, and ultimately causing necrosis of eelgrass leaves, and in some cases, entire plants (Muehlstein, 1992). Non-lethal impacts of EWD include reductions in growth and below-ground storage of carbohydrates, which may impact seasonal resilience of eelgrass meadows (Graham et al., 2021). Strains of *Lz* vary in virulence, raising questions about mechanisms of virulence employed by this pathogen and potential costs associated with those mechanisms (Martin et al., 2016).

Eelgrass has a robust defense system which includes proteins and surface-associated metabolites like fatty acids and phenolics, *p*-coumaric acid, rosmarinic acid, and zosteric acid (Papazian et al., 2019). These compounds play a wide-range of roles including but not limited to signaling molecules, antioxidant activity, free radical scavenging activity, and regulators of auxin transport (Ma et al., 2016). Phenolic compounds which are produced in response to stress and pathogen presence can be also considered as defense-related secondary metabolites. Indeed, some phenolic compounds have been shown to inhibit growth of *Lz in vitro* (Vergeer and Develi, 1997) and concentrations of total phenols (% dry mass) are increased in diseased plants in the field (Groner et al., 2016). In terrestrial plants, phytohormones including abscisic acid (ABA), jasmonic acid (JA), and salicylic acid (SA) play significant roles in regulating defense responses against a great number of biotic and abiotic factors (Thaler et al., 2004; Tamaoki et al., 2013), however these hormones have not been well explored in marine plants such as eelgrass.

As with many marine diseases, EWD is sensitive to temperature (Tracy et al., 2019). Both EWD prevalence and severity are correlated with sea surface temperatures in the Salish Sea (WA, USA), and in the Isles of Scilly (UK), (Bull et al., 2012; Groner et al., 2021). Increased temperatures enhance the growth-reducing effects of EWD on eelgrass (Bull et al., 2012). These changes are likely driven by both the host and pathogen. *Lz* is also sensitive to temperature, with faster *in vitro* growth documented at 18°C compared to 11°C for a strain isolated from the Salish Sea (WA, USA) (Dawkins et al., 2018); similarly, increased disease severity was noted in eelgrass exposed to *Lz* and held at 18˚C compared to 11˚C (Agnew et al., 2022). Recent studies have correlated heatwaves

to substantial seagrass die-offs (Strydom et al., 2020; Groner et al., 2021), reduced restoration success (Aoki et al., 2020), and changes in fatty acid composition (Beca-Carretero et al., 2018), showing that seagrasses are sensitive to warming conditions.

To better understand the factors that contribute to *Lz* infection and provide insight on mechanisms of virulence and host defense, we characterized the production of defensive compounds in *Z. marina* and the transcriptional responses of both *Z. marina* and *Lz* following a controlled *Lz* challenge conducted at ambient and warm seawater temperatures. We hypothesize that both increased temperature and *Lz* infection will alter expression of genes related to immune function and stress response in *Z. marina*. More specifically, we hypothesize that phenolic and hormonal gene pathways will be enriched in response to presence of *Lz*, but we expected these responses may be reduced at warmer temperatures that could be stressful to *Z. marina*. Finally, we hypothesize that *Lz* will exhibit a change in gene expression in response to temperature, reflecting the association between EWD and warmer seawater temperatures found in nature (Brakel et al., 2019; Groner et al., 2021).

Materials and methods

Experimental design

Similarly sized eelgrass ramets were collected from False Bay, San Juan Island, WA (48.550° N, 123.008° W) on 29 July 2015. Epiphytes, grazers and damaged leaves were removed from ramets and they were held in flow-through 14°C, 0.2 µm filter-sterilized seawater at Friday Harbor Labs, WA, USA.

Eelgrass ramets were placed in one of two temperature treatments (target temperatures 11° or 18°C, actual temperatures ranged ± 1°C from target) on 3 Aug 2015 and allowed to acclimate to these treatments for 10 days. These temperatures represent typical summer sea surface temperatures found locally along coastal eelgrass beds at high and low tides, respectively. A constant exposure to 18°C would be unusually warm in this region. Each treatment was replicated eight times for a total of 16 experimental units. Each replicate unit contained four ramets. Experimental units were 4-L containers with 3500 mL of 0.2 µm filter-sterilized seawater. Experimental units were split into groups of eight that were clustered in a common cooler. Each cooler received flow-thru 0.2 µm filtered and UV-irradiated seawater. Seawater temperatures were continuously monitored and adjusted using Honeywell UDA2182 pH controller and Honeywell Durafet III electrodes. After flowing into the cooler, water was then piped into the 8 experimental units. Water temperatures were maintained by circulating it through chilled water set 1°C below target temperatures and, if necessary, heating it with aquatic heaters placed in the coolers (i.e. O'Donnell et al., 2013). Two temperature loggers (iButtons, Whitewater, WI) set to record every 30 min were placed in each cooler for independent confirmation of temperature. Full-spectrum lights were kept to a 12: 12 hr light: dark schedule with a mean light output of 161 ± 3 (mean ± SE) µmol/m^2/sec PAR below the water surface. To reduce algal blooms, which could clog plumbing and block light, tanks were treated daily with 0.67 ppm (final concentration) of Germanium dioxide (GeO_2; Markham and Hagmeier, 1982).

A 36-hr incubation with the pathogen inoculant was conducted after 10 days of temperature acclimation (Figure 1). Immediately prior to inoculation, all ramets were photographed, weighed, labelled with uniquely colored zip-ties, and pin-pricked at the sheath for later measurements of growth. All ramets within a replicate were placed in Whirlpaks with 98 mL of sterile seawater. Control treatments were inoculated with 2 mL of sterile seawater. *Lz* treatments were inoculated with 2 mL of inoculant for a final concentration of 2.5 x10^5 cells per mL (additional details in Supplementary Material). After adding the inoculate, the Whirlpaks were closed and floated in treatment containers to maintain target temperatures. 36 hours later, ramets were removed from Whirlpaks and placed back into treatment containers. The *Lz* strain used in this experiment, 8.16.D, has been used in several previous experiments, (e.g., Groner et al., 2014; Groner et al., 2018) and was isolated in 2011 from non-flowering adult *Zostera marina* shoots that were collected at Picnic Cove, Shaw Island, 48° 33.942' N, 122° 55.448' W).

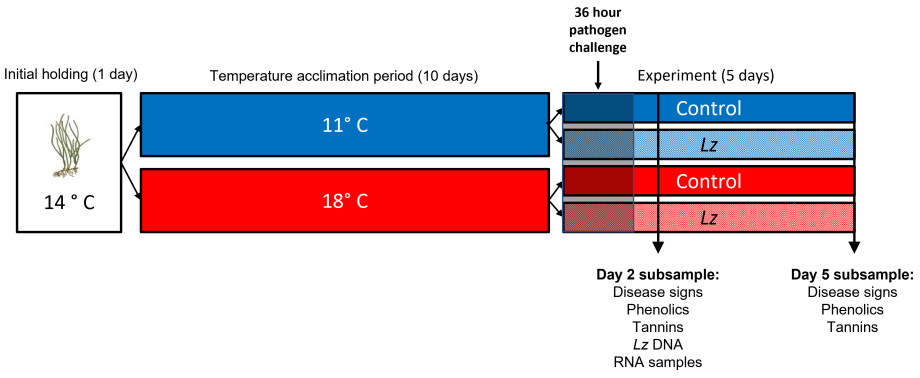

FIGURE 1
Timeline of experimental treatments and sampling. After collection and cleaning of plants to remove grazers, epiphytes and diseased tissue, eelgrass ramets were held at 14°C for 1d and then transferred in groups of 4 ramets to 11°C or 18°C for a 10d acclimation period. Each group of 4 ramets was replicated 8 times during the acclimation period. After that, the groups were equally divided into control and *Lz* – exposed treatments at each of the two temperatures. *Lz* or sham exposures occurred for 36 hr. Subsampling of plants occurred at days 2 and 5 post-*Lz* exposure.

Forty-eight hours after inoculation (experiment day 13), a random selection of half of the individuals (48 total) from each experimental unit were removed for sampling (Figure 1). Each of those individuals was photographed and weighed. Then the roots and shoots were frozen in liquid nitrogen for transcriptomic sampling. The oldest leaf was split lengthwise into two pieces. One half was frozen in liquid nitrogen for transcriptomic analysis, and the other was stored in 70% molecular grade ethanol at room temperature for subsequent measurement of *Lz* load using quantitative PCR (qPCR) as described in Groner et al. (2018). The second oldest leaf was frozen in liquid nitrogen for measurement of total phenolic compounds and condensed tannins. Five days after inoculation, the experiment was ended because the plants had severe disease signs. At this point, the remaining ramets were photographed and sampled (as described above) for measurement of visual disease signs (e.g., lesions with a distinct black border, *sensu* Groner et al., 2014) as well as phenol and tannin concentrations (Figure 1).

Measurement of total phenolic compounds and condensed tannins

Total phenolic compounds were measured in 96 well microplates using the methods described in Groner et al. (2018). Briefly, sampled eelgrass leaves were frozen (-20°C) and sent on dry ice to the Shannon Point Marine Center for analysis. Frozen tissues were lyophilized and ground to a fine powder in an SPEX mixer/mill (SPEX, Metuchen, NJ). Ground tissue (9-10 mg) was extracted overnight in 1 mL of HPLC-grade methanol, then diluted in ANSI Type I water (19 parts water to 1 part extract). Forty µL of 40% Folin-Ciocalteu's Reagent (Sigma F9252) was added to each 100 µL aliquot (n=3 per sample) of each of the diluted extracts, mixed for 5 min prior to the addition of 100 µL of 2N sodium carbonate. Samples were shaken for another 30 min in a 50°C chamber and then the absorbance of each cell was read at 765 nm. Concentrations were standardized using native standards from *Z. marina* collected from Ship Harbor WA, using caffeic acid as a secondary standard (Groner et al., 2016). The remaining methanolic extracts were used for measurements of condensed tannins, which were conducted with a sulfuric acid method (Bate-Smith and Rasper, 1969; Nitao et al., 2001) that was modified for use in a microplate reader. Condensed tannins (proanthocyanidins) were cleaved by the addition of 43% sulfuric acid in methanol (250 µL/well containing 100 µL of a methanol extract) for 30 min at 50°C for. Tannin cleavage produces red-colored chromophores (anthocyanins), which were then quantified spectrophotometrically at 550 nm using a Biotek Synergy multiplate reader. Cyanidin (Cayman Chemical, purity >98%) was used as a standard. All assessments were run in triplicate.

Quantification of *Lz* abundance

Samples (mean dry weight of leaf material = 7 mg) were preserved in 70% ethanol until DNA extractions were performed using a Qiagen DNeasy Plant Mini Kit following the manufacturer's instructions. Prior to DNA extractions, samples were removed from ethanol, patted dry, weighed and then transferred into a clean 1.5ml micro-centrifuge tube with one 3mm tungsten carbide bead (Qiagen) per tube. Samples were then placed on dry ice for 10-15 minutes and lysed using a Qiagen TissueLyser at a speed of 25 Hz for 5 minutes.

Presence of *Lz* DNA was detected and quantified using qPCR detection using primers and probe targeting the *Lz* ITS region (Bockelmann et al., 2013); Laby_ITS_Taq_f (5'- TTG AAC GTA ACA TTC GAC TTT CGT- 3') and the reverse primer Laby_ITS_Taq_r (5' –ACG CAT GAA GCG GTC TTC TT -3') were used, in addition to the TaqMan probe Laby_ITS_probe (5' FAM- TGG ACG AGT GTG TTT TG –MGB-NFQ 3'). qPCR reaction conditions and the standard curve (serial dilution between 1.37-1.37*10^4 cells) were as described by Groner et al., 2018 on run on the Applied Biosystems 7500 Fast Real-Time PCR System. For each qPCR plate, we aimed for R2 = 0.999 and an efficiency of 90-110%; the mean reaction efficiency was 105.5% +/- 1.5% (cross three total plates). We used a cut-off of 1.37 cells as our limit of detection (amplification of 1.37 cells was achieved in all reactions in each cell curve).

Statistical analyses of treatment effects on phenolic compounds, tannins, disease signs and *Lz* DNA

Independent and interactive effects of temperature and *Lz* exposure on concentrations of phenols, concentrations of tannins, presence of suspected disease signs and $\log_{10}$ transformed *Lz* DNA concentrations in leaf tissues were quantified for the time points when these measurements were taken (R v. 4.1.1). Linear regression was used to quantify treatment effects on total phenolic compounds, condensed tannins, and *Lz* DNA concentrations, while logistic regression was used to quantify treatment effects on the presence of disease signs (package lme4, Bates et al., 2015). In all models, the 4L container replicate was included as a random effect.

RNA extractions and transcriptome sequencing

Total RNA from four samples per treatment was extracted following the Qiagen RNeasy plant kit protocol; samples were chosen based on both quality of RNA and qPCR results. DNA was removed from extracted RNA using the Turbo DNA-free treatment according to the manufacturer's instructions (Ambion Inc., The Life Technologies Corporation™, Grand Island, NY). Removal of DNA was confirmed by using RNA (1 µl) as template in a qPCR targeting 18s ribosomal DNA as previously described (Burge and Friedman, 2012). RNA concentrations were quantified using the NanoDrop® ND-1000 (NanoDrop Technologies, Wilmington, DE). Samples were shipped to McGill University and Genome Quebec for library preparation and sequencing.

RNA quality was assessed prior to library preparation using an Agilent Bioanalyzer. The Illumina TruSeq stranded cDNA kit was used for library preparation and barcoding; quality assessment of libraries indicated that one sample was not of high enough quality for sequencing. The remaining samples were distributed across two sequencing lanes on an Illumina HiSeq 4000 platform (2x150 bp paired end reads).

Transcriptome assembly and annotation

Prior to *de novo* assembly, reads were quality screened (FastQC Version 0.11.4, Babraham Bioinformatics), and sequences were screened for remaining Illumina adapter sequences (Trimmomatic, Bolger et al., 2014). *De novo* assembly was carried out using reads from all fifteen samples using Trinity (Grabherr et al., 2011; Haas et al., 2013, Trinity RNASeq Github). Following transcriptome assembly, reads for each sample were matched back to gene isoforms.

A multi-step annotation process was used to annotate the transcriptome in order to separate isoform consensus sequences (or contigs) matching to *Z. marina* and those non-matching contigs ("non-host"). First, a database of annotations was created from the *Z. marina* genome (GCA_001185155.1) using a BLASTx search of the UniProtKB/Swiss-Prot database. The BLASTx algorithm (Altschul et al., 1990) was used to search the *Z. marina* database with a threshold E-value of 0.00001; each contig matching as *Z. marina* was filtered out. Similarly, the blastx algorithm was used to search the Swiss-Prot database with a threshold E-value of 0.00001 to form the non-*Zostera* annotation for subsequent analysis. Finally, to determine which non-host contigs have significant similarity to *Labyrinthula* and other closely related 'slime-mold' species, the blast algorithm was used to match non-host contigs against the recently added *Labyrinthula* sp. Ha genome (NCBI Accession # GCA_015227615.1) and also against the genomes of two other, better annotated genomes, a thraustochytrid, *Hondaea fermentalgiana* (NCBI Accession # GCA_002897355.1) and the amoeba model organism, *Dictyostelium discoideum* (NCBI Accession # GCF_000004695.1).

Gene ontology (GO) information was used to annotate both *Z. marina* and non-*Zostera* transcriptome data separately. Gene ontology IDs and associated GO Slim terms for biological processes, cellular components, and molecular function categories were downloaded from the UniProtKB/Swiss-Prot database. Swiss-Prot identifiers from BLASTx output were joined to gene ontology terms. Since assembly and annotation were conducted at the isoform level, transcriptome data was streamlined to conduct differential expression analysis on genes. Annotated sequences were sorted by contig name and e-value; contig names included a contig, gene, and isoform identifier. The isoform entry with the lowest e-value was retained for each gene. The final annotated dataset for both *Z. marina* and non-*Zostera* transcriptomes included only one entry per gene. Annotated genes were merged with count data to prepare for differential expression analysis. The data is deposited in the NCBI database in the SRA as Bioproject (PRJNA990835).

Analysis of *Zostera* and non-*Zostera* transcriptomes

Statistical differences in count data were conducted for *Z. marina* and non-*Zostera* annotated genes using EdgeR (Robinson et al., 2010; McCarthy et al., 2012; Chen et al., 2016). Briefly, we utilized EdgeR to filter and normalize the count data based on the library size and examine samples for outliers using MDS plots. Next, a multi-factorial model including estimated dispersion (i.e. estimate of biological variation) was used with multiple contrasts to calculate fold change, log CPM (counts per million), and raw and Benjamini-Hochberg adjusted p-values to correct for False Discovery Rate.

We tested for statistical differences using several contrasts followed by the primary questions of interest, respectively examining the relationships of the pathogen-by-temperature interaction, temperature alone, and pathogen exposure alone:

1) What genes are differentially expressed between Lz-exposed shoots at elevated temperatures? At ambient temperatures?
2) What genes are differentially expressed between elevated and ambient temperatures, irrespective of Lz-exposure?
3) What genes are differentially expressed between Lz-exposed and control shoots, irrespective of temperature?

Very few genes were differentially expressed in questions 1 and 2 (25 genes and 0 genes, respectively). Thus, for the remainder of the analysis we focused on the effect of *Lz* exposure alone. Differentially expressed genes were pooled into host and pathogen genes. Genes were considered differentially expressed based on FDR adjusted p-values from edgeR ($p < 0.05$).

To identify groups of *Z. marina* genes with similar expression patterns (eigengenes) and associate these patterns with experimental conditions, a Weighted Gene Co-expression Network Analysis (WGCNA) was conducted using the WGCNA package in R (version 1.69; Langfelder and Horvath, 2008). The WGCNA was only conducted for *Z. marina* genes, as transcriptome sequencing produced a high magnitude of information for *Z. marina* that was difficult to parse without additional analysis. After identifying significant modules, overrepresented biological process and molecular function GOterms were identified using the GO-MWU enrichment method (Wright et al., 2015). More details on WGCNA and GO-MWU analyses are available in the Supplemental Material.

Results

Disease progression and pathogen load

The inoculations were successful in transmitting *Lz* to the exposed plants. Two days after exposure, *Lz* concentrations in eelgrass tissue were 1.1 orders of magnitude greater in the 18°C treatment as compared to the 11°C treatment (with concentrations of $4.2 \pm 4.3 \times 10^4$ and $3.7 \pm 3.6 \times 10^3$ (mean ± SE) *Lz* cells/mg of eelgrass tissue, respectively) (Figure 2). These pathogen concentrations were

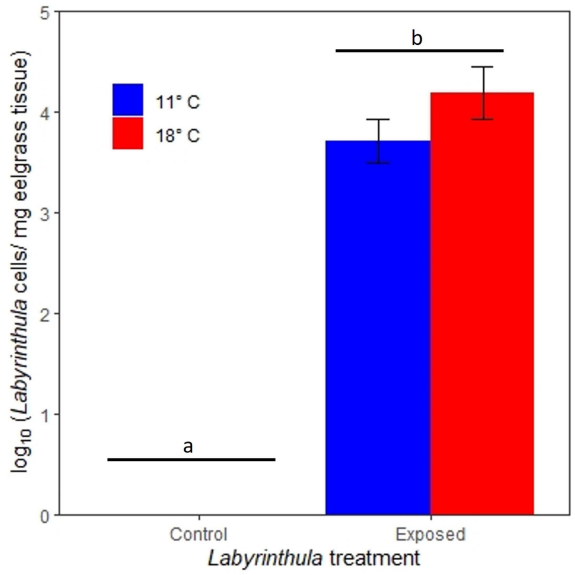

FIGURE 2
Lz cell equivalents (per mg eelgrass tissue) from qPCR analysis of eelgrass leaf tissue 2 days post-inoculation. Bars indicate standard errors. Letters and bars indicate significantly different treatments.

significantly higher than the control treatments, where no *Lz* was detected using qPCR (t value = 12.3, $p < 0.0001$) No other factors affected *Lz* abundance in our linear regression (all $p > 0.05$).

Visible disease signs were recorded in all treatments (Figure 3). Pathogen exposure was a significant predictor of disease signs on day 2 and a marginally significant predictor of disease signs on day 5. On day 2, the disease signs were recorded in 93.7 ± 8.8% (mean +/- SE) of the exposed plants and 28.8 ± 19.7% of the control plants (t = 2.1, p = 0.04). Neither temperature nor the temperature by exposure interaction were predictors of visual disease signs. These values increased on day 5 where disease signs were recorded in 100 ± 0% (mean +/- SE) of the exposed plants and 37.5 ± 17.7% of the control plants (t = 1.99, p = 0.07).

The concentrations of total phenolic compounds and condensed tannins were not impacted by temperature or *Lz* treatments on day 2 (Figure 4). By day 5, total phenolic compounds were significantly lower in the warmer exposed treatment, where they were 0.70 ± 0.17% of dry mass as opposed to ranging between 1.15 and 1.39% of dry mass in the other three treatments (t value = -3.298, $p < 0.001$ for the temperature by exposed interaction). There was no significant impact of temperature or *Lz* exposure on the concentration of condensed tannins in eelgrass leaves on day 5.

Transcriptome assembly and annotation

Trinity *de novo* assembly yielded 1,065,804 isoforms (767,296 potential genes) with an average read length of 654.71 bp (median of 349) and an N50 value of 1075. BLAST searches of the *de novo* assembly yielded 281,600 contigs matching the *Z. marina* genome. 784,204 contigs did not match the *Z. marina* genome and thus were categorized as 'non-host' contigs.

Differential expression analysis - host contigs

Of the 3,096 contigs identified as host genes and annotated, 540 genes were differentially expressed, with 338 genes with significantly higher expression levels in exposed blades and 202 genes with lower expression levels (Supplementary Table 1). The WGCNA identified thirteen module eigengenes comprised of genes with similar expression patterns for 3,096 *Z. marina* contigs (Figure 5A; Supplementary Table 2). Of these eigengenes, four - named "brown", "yellow", "blue", and "magenta" - were significantly

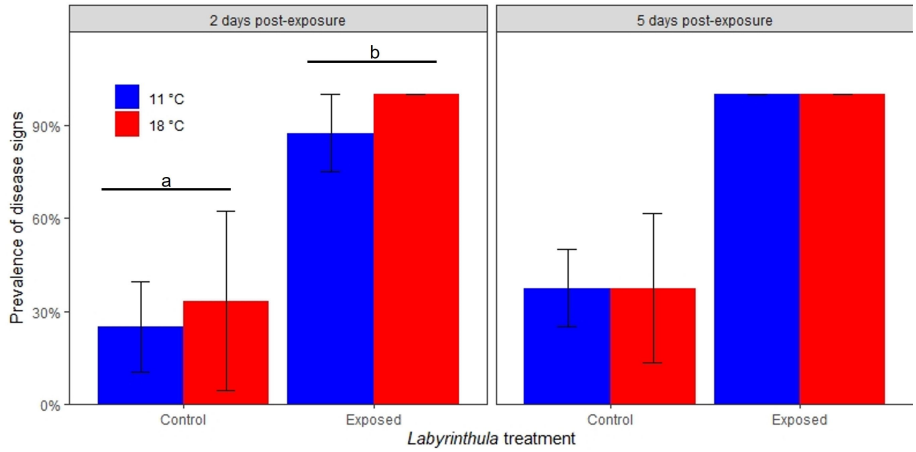

FIGURE 3
Prevalence of observed disease signs on eelgrass blades 2 and 5 days post-inoculation. Error bars indicate ± 1 standard error of the replicate mean. Letters and bars indicate significantly different treatments.

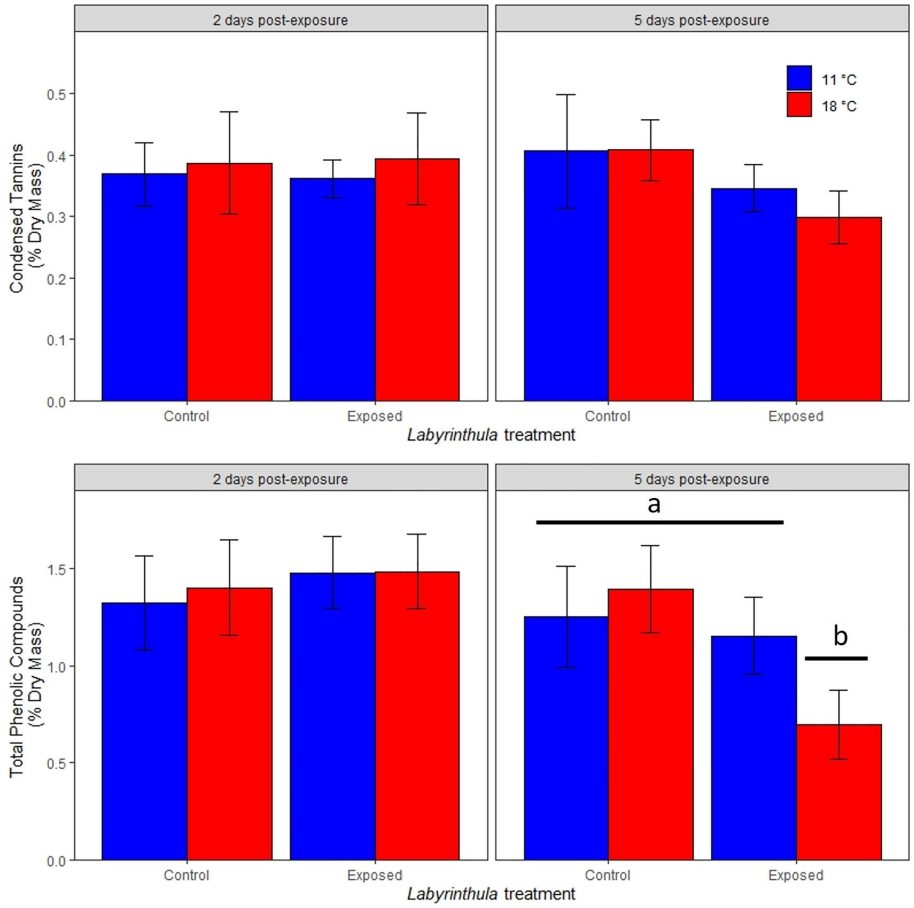

FIGURE 4
Effects of temperature and *Lz* treatment on condensed tannins and total phenolic compounds (as a percentage of eelgrass dry mass) 2 and 5 days post-inoculation. Data are means (± 1 SE). Letters and bars indicate significantly different treatments.

associated with *Lz* exposure (Figure 5B). These modules, labeled as color categories, are described in detail below.

The module eigengene "brown" was negatively correlated with *Lz* exposure, indicating lower module expression when eelgrass was exposed to *Lz*. (r^2 = -0.86, p= 3.3 x 10^{-5}) (Figure 5B) The module contained 194 differentially expressed genes (Figure 5C; Supplementary Table 2). Seven biological processes were significantly enriched, including response to fungus (GO:0009620), response to salt stress (GO:0009651), transposition (GO:0032197;GO:0032196), and cell wall organization or biogenesis (GO:0071555;GO:0045229;GO:0071554) (Table 1). Genes were also involved in responses to abscisic acid, jasmonic acid, and wounding (Supplementary Table 2). Additionally, 17 molecular functions were enriched in this module, including transferase activity, transferring glygosyl groups (GO:0016757), xenobiotic transmembrane transporter activity (GO:0042910), and transcription regulator activity (GO:0003700;GO:0140110) (Table 1).

The module eigengene "yellow" was positively correlated with *Lz* exposure (r^2 0.52, p= 0.049) and contained five differentially expressed genes (Figures 5B, C: Supplementary Table 2). While there were no significantly enriched GO terms in this module, common biological processes included proteolysis, cellular response to oxidative stress, response to osmotic stress, regulation of jasmonic acid metabolic process, and response to abscisic acid, and common molecular functions were binding of ATP, RNA, and metal ions (Supplementary Table 2).

The module eigengene "blue" was positively correlated with *Lz* exposure (r^2 = 0.99, p = 2.0 x 10^{-11}) (Figure 5B). The "blue" module contained 263 differentially expressed genes (Figure 5C; Supplementary Table 2). There were no enriched biological processes, but genes were involved in immune response, protein transport and ubiquitination, response to salt stress and oxidative stress, cell cycle, and abscisic acid-activated signaling pathway (Supplementary Table 2). Enriched molecular functions were double-stranded DNA binding (GO:0003690) and cyclic nucleotide-dependent protein kinase activity (GO:0004691; GO:0004690) (Table 1).

The module eigengene "magenta" was positively correlated with *Lz* exposure (r^2 = 0.52, p= 0.046) (Figure 5B). This module eigengene had the most variable expression of all significant modules (Figure 5C). The "magenta" module contained 60 differentially expressed genes (Figure 5C; Supplementary Table 2). Peptide biosynthetic process (GO:0006412;GO:0043043) and determination of adult lifespan (GO:0008340), and structural constituent of

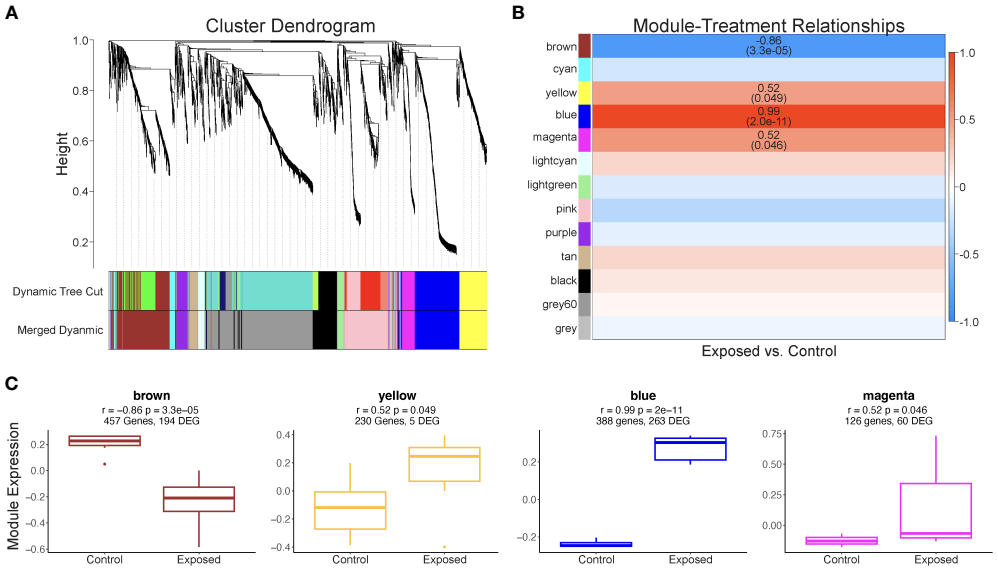

FIGURE 5
Results of *Z. marina* WCGNA analysis. **(A)** Cluster dendrogram of 3,096 genes used in WGCNA analysis. Modules were identified (Dynamic Tree Cut), then merged based on a cut height of 0.34 (Merged dynamic). All modules contain at least 30 genes. **(B)** Significant correlations between module eigengenes (rows) and *Lz* infection status (column). The R^2 value is provided for each significant correlation, with *P*-value in parentheses. Positive correlations are represented by red boxes, while negative correlations are represented by blue boxes, with the intensity of the color increasing with correlation strength. **(C)** Expression of module eigengenes significantly correlated *Lz* exposure for exposed and control eelgrass.

TABLE 1 Biological process and molecular function GOterms enriched within significant module eigengenes for *Z. marina*.

Module	GO ID	GOterm Name	GO Category	FDR	Number of Sequences
brown	GO:0006970	response to osmotic stress	Biological Process	0.07	74
brown	GO:0009620	response to fungus	Biological Process	0	17
brown	GO:0009651	response to salt stress	Biological Process	0	53
brown	GO:0015074	DNA integration	Biological Process	0.0916667	24
brown	GO:0032197; GO:0032196	transposition	Biological Process	0.0857143	11
brown	GO:0042538	hyperosmotic salinity response	Biological Process	0.0625	8
brown	GO:0071555; GO:0045229; GO:0071554	cell wall organization or biogenesis	Biological Process	0	35
brown	GO:0003677	DNA binding	Molecular Function	0.04	190
brown	GO:0004519; GO:0004518	nuclease activity	Molecular Function	0	52
brown	GO:0008170; GO:0008276	N-methyltransferase activity	Molecular Function	0.0766667	23
brown	GO:0008270	zinc ion binding	Molecular Function	0.0636364	110
brown	GO:0008757	S-adenosylmethionine-dependent methyltransferase activity	Molecular Function	0.0833333	36

(Continued)

TABLE 1 Continued

Module	GO ID	GOterm Name	GO Category	FDR	Number of Sequences
brown	GO:0016279; GO:0016278	protein-lysine N-methyltransferase activity	Molecular Function	0.0714286	15
brown	GO:0016757	transferase activity transferring glycosyl groups	Molecular Function	0	62
brown	GO:0016763	transferase activity transferring pentosyl groups	Molecular Function	0.0941176	12
brown	GO:0016779	nucleotidyltransferase activity	Molecular Function	0.090625	73
brown	GO:0016788	hydrolase activity acting on ester bonds	Molecular Function	0	139
brown	GO:0016891; GO:0004521; GO:0016893	endonuclease activity active with either ribo- or deoxyribonucleic acids and producing 5'-phosphomonoesters	Molecular Function	0	17
brown	GO:0018024	histone-lysine N-methyltransferase activity	Molecular Function	0.0125	11
brown	GO:0034061; GO:0003964	DNA polymerase activity	Molecular Function	0	34
brown	GO:0042054	histone methyltransferase activity	Molecular Function	0.0333333	16
brown	GO:0042910	xenobiotic transmembrane transporter activity	Molecular Function	0.0769231	13
brown	GO:0140097	catalytic activity acting on DNA	Molecular Function	0	56
brown	GO:0140110; GO:0003700	transcription regulator activity	Molecular Function	0	58
blue	GO:0003690	double-stranded DNA binding	Molecular Function	0.025	32
blue	GO:0004691; GO:0004690	cyclic nucleotide-dependent protein kinase activity	Molecular Function	0	9
magenta	GO:0006412; GO:0043043	peptide biosynthetic process	Biological Process	0	259
magenta	GO:0008340	determination of adult lifespan	Biological Process	0	10
magenta	GO:0003735	structural constituent of ribosome	Molecular Function	0	248
magenta	GO:0019843	rRNA binding	Molecular Function	0.05	64

ribosome (GO:0003735) and rRNA binding (GO:0019843) were significantly enriched biological process and molecular function terms in this module, respectively (Table 1). Other prominent biological processes included translation, cell redox homeostasis, and microtubule-based process (Supplementary Table 2).

Differential expression analysis - non-host contigs

Of the non-host contigs, 11.1% (87,550 out of 784,204) had significant matches to the Swiss-Prot database. Only 0.77% (5,959 out of 784,204) of non-host contigs had significant matches to the *Labyrinthula* sp. Ha genome. However, 42,601 non-host contigs (5.4% of total non-host contigs) had significant matches to a closely related thraustochytrid, *Hondaea fermentalgiana* (NCBI Accession # GCA_002897355.1). Thirty-two non-host contigs were differentially expressed; 30 up-regulated whereas two were down-regulated (Supplementary Table 3). Of the 32 differentially expressed non-host contigs, only 5 had significant similarity to the *Labyrinthula* sp. Ha genome; including arylsulfatase (SP_P08842), patatin-like phospholipase domain-containing protein (SP_Q8N8W4), 5-aminolevulinate synthase (SP_P08262), dynein heavy chain 10 (*dhcA*) (SP_Q8IVF4), and calponin-1 (SP_P`4318). In contrast, 20 differentially expressed non-host contigs had significant hits to the *H. fermentalgiana* genome

(Supplementary Table 3). Seven non-host contigs also had homology to genes found in the well-annotated genome of the slime-mold model organism, *D. discoideum*, including the dynein heavy chain *dhcA* (DDB_G0276355), dual specificity protein kinase *shkB* (DDB_G0288617), adenylate cyclase *sgcA* (DDB_G0276269), calponin homology containing protein *mp20* (DDB_G0292664), serine/threonine-protein kinase *roco5* (DDB_G0294533), beta-ketoadipyl-CoA thiolase (DDB_G0269588), and regulator of G-protein signaling 21 (DDB_G0273033) (Supplementary Table 3).

Of the differentially expressed genes that displayed significant similarity to either *Lz* or to related species *H. fermentalgiana* or *D. discoideum*, ten up-regulated non-host contigs were linked to chemotaxis and motility (i.e. actin binding proteins, tubulin beta-chain, and microtubule formation), 11 contigs to amino acid and lipid metabolism (i.e. peptidases and fatty acid synthesis enzymes), 4 contigs to transcription/translation, 3 contigs to transporter activity (i.e. ion channel and transporter subunits), and 4 contigs to other processes including respiration (i.e. cytochrome c oxidase subunits) and production of secondary metabolites (i.e. phytoene synthase) (Supplementary Table 3). Several non-host contigs were related to phagocytosis, such as patatin-like phospholipase domain containing protein (SP_Q8N8W4), beta-ketoadipyl-CoA thiolase (SP_O26884), leucine-rich repeat serine-threonine protein kinase 2 (*roco5*) (SP_Q1ZXD6), ATP-dependant RNA helicase (SP_Q0DB53), hypoxanthine-guanine phosphoribosyltransferase (SP_Q72454), pepsin A-1 (SP_Q03168), and dynein heavy chain 10 (*dhcA*) (SP_Q8IVF4).

Discussion

Exposure of eelgrass ramets to *Lz* resulted in rapid progression of EWD, with necrotic lesions forming within two days post-exposure and plant death occurring after five days. The temperature did not alter the pathogen load or progression of EWD in the *Lz* exposed plants. This may be due to the high concentration of pathogen in the exposure, which was higher than in previous studies with this *Lz* strain (Groner et al., 2014; Groner et al., 2018) and/or pre-acclimation of the plants to the temperature treatments prior to exposure. Analysis of the eelgrass transcriptome revealed changes in gene expression, with patterns consistent with increased defensive responses through altered regulation of genes associated with phytohormone biosynthesis, stress response, and immune function. Analysis of non-*Zostera* genes (likely *Lz* genes), revealed expression patterns suggestive of *Lz* disrupting host immune responses and undergoing phagocytosis. This study reveals the importance of specific pathways related to plant defense against pathogen presence, and provides molecular evidence to support previous phenotypic observations of host-pathogen interactions of eelgrass wasting disease.

Host responses

The genome of *Z. marina* allowed us to identify 3,096 host contigs, and we detected 540 differentially expressed host genes responding to *Lz* infection as opposed to increased temperature (Supplementary Table 1). We found expression changes in genes and/or pathways involved with immunity such as pathogen detection, defense-related cell-cell signaling, defense-related metabolite production, and apoptosis. We also detected genes potentially involved in salt stress. The occurrence of many differentially expressed defense-response related GO terms, including genes associated with microbial detection and defense response to bacterial or fungal pathogens, indicates that *Z. marina* is responding to *Lz* infection.

Plant innate immune system pathways are highly conserved and are initiated by recognition of pathogen-associated molecular patterns (PAMPs) and damage-associated molecular patterns (DAMPs) by membrane localized receptors (Choi and Klessig, 2016). Calcium signaling is a major pathway in pattern-triggered immunity, where binding of PAMPs and DAMPs to membrane receptors initiates the rapid release of calcium ions (Ca^{2+}) by receptor like kinases and their Ca^{2+} dependent protein kinases and mitogen activated protein kinases (Hou et al., 2018). For example, calcium/calmodulin-dependent protein kinase (CcaMK) genes have been found to play a role in maintaining endosymbionts and in pathogen resistance in tomato, by promoting accumulation of hydrogen peroxide (Wang et al., 2015). Genes related to calcium- and protein-kinases show up eight and 43 times, respectively, in the blue module. In particular, upregulation of the calcium/calmodulin-dependent protein kinase (CcaMK) type 1 (CaM kinase I) suggests the role of *Lz*-related PAMP/DAMP detection and may warrant further exploration.

Pathogen detection leads to the induction of signaling pathways to induce immune and defense responses. We found that the cAMP-dependent protein kinase catalytic subunit gamma is significantly upregulated with *Lz*-exposure. Changes in the abundance of cAMPs can affect the activity of other signaling pathways and cellular processes, such as protein kinases and transcription factors (Świeżawska et al., 2018), demonstrating that *Z. marina* may respond to *Lz* infection by altering upstream signal transduction.

Phytohormone production in plants is important for defense-related signaling and is turned on after PAMP/DAMP detection. For example, compounds such as jasmonic acid (JA), salicylic acid (SA), and abscisic acid (ABA) are involved in general activation of plant defense systems against pathogens (Thaler et al., 2004; Tamaoki et al., 2013). In particular, SA is used in defense against biotic factors such as insects, mites, fungi, and bacteria and JA is used in defense pathways against saprophytic microbes like *Lz* (Tamaoki et al., 2013; Zhang et al., 2020). ABA is triggered in response to both abiotic and biotic stressors, and has complex interactions with both JA and SA responses to infection (Fan et al., 2009). We found GO terms for SA, JA, and ABA phytohormones [GO:0080140, GO:0009695, GO:0009753, and GO:0009751] were highly represented in the blades experimentally exposed to *Lz*, although these gene ontologies were not significantly enriched. Gene expression patterns in this study were indicative of phytohormone signaling via enrichment of serine/threonine-protein kinase PCRK2 gene which is involved in the resistance to bacterial pathogens and salicylate biosynthesis during pathogenic infection (Sreekanta et al., 2015). Methylesterase 1 gene, which is

required during the conversion of methyl salicylate into SA was downregulated in exposed blades. These data suggest that *Z. marina* is altering production of these defense-related compounds. We found gene expression changes in two genes related to JA biosynthesis: chloroplastic rhomboid-like protein 11 (regulation of jasmonic acid metabolic process [GO:0080140]) and phospholipase A (defense response to fungus [GO:0050832]; jasmonic acid biosynthetic process [GO:0009695]). Phospholipase A is responsible for the release of linolenic acid from the chloroplast membrane during defensive signaling, which induces JA production (Yang et al., 2007; Mata-Pérez et al., 2015). The detection of differentially regulated genes in the JA pathway is particularly interesting, as the role of JA in seagrasses is unclear. A congener of *Z. marina, Z. muelleri*, lost genes encoding jasmonate methyltransferase, which converts JA into a volatile compound, methyl jasmonate, but maintain other genes along the JA pathway, including for jasmonate synthesis, and signaling (Lee et al., 2016). Although the JA-associated genes were not differentially expressed in our study, changes to expression in these genes suggests a role for the jasmonic acid pathway in responding to *Lz* infection.

Gene expression changes also indicated down-stream effects of phytohormone production. In maize roots, expression of CHC1 gene increases in response to SA or ABA, suggesting involvement of CHC1 in the SA signaling pathway in maize defense responses (Zeng et al., 2013). Upregulation of the probable clathrin heavy chain 1 gene (CHC1) ([GO:0005198]) in *Lz*-infected blades suggests a similar response in eelgrass. We detected gene expression changes in factors involved in stress signaling which either require ABA or interact with ABA to trigger defense responses. For example, the S-type anion channel SLAH3 is an anion channel that can be triggered by ABA during a stress response (Roelfsema et al., 2012), and was downregulated in response to *Lz* infection. The B3 domain-containing protein was also downregulated. This protein is a transcription factor for ABA and inhibits the production of ABA (Brady et al., 2003), so a decrease in expression of B3 could result in an increase in ABA production, indicating a greater stress response to *Lz* infection. One specific pathway in which ABA affects plant defense is in the callose pathway, which is involved in defense of fungal pathogens in plants. Specifically, ABA mutants displayed impaired resistance to necrotrophic fungi, and ABA addition to the infection site mimicked callose deposition and increased resistance to necrotrophic fungi (Mauch-Mani and Mauch, 2005). Therefore, it is not surprising to observe altered ABA expression in *Z. marina* infected with *Lz*, which has necrotic capabilities.

Additional immune responses in plants include the production of antimicrobial compounds and apoptosis of infected cells, the latter of which would be important for intracellular infections, such as with *Lz*. Upregulation of peroxisomal targeting signal 1 receptor indicates potential defenses at sites of pathogen entry. This gene is associated with concentrating antifungal glucosinolate derivatives in the peroxisome for eventual transport to sites of fungal infection entry (Bednarek et al., 2009). It would be valuable to assess whether these compounds can inhibit *Lz* as well. Differential expression of GDP-L-fucose synthase supports the role of apoptosis as an immune response to *Lz*. GDP-L-fucose plays a role in stomatal and apoptosis-related defense in *Arabidopsis*, indicating a similar role in *Z. marina* immunity (Zhang et al., 2019). Differential expression of EKC/KEOPS subunit genes, which are involved in apoptotic processes via telomere capping and elongation (Downey et al., 2006), also support the hypothesis that apoptosis is an important defense against *Lz*.

The production of phenolic compounds is another major immune response of plants. Many of phenolic metabolites detected in *Z. marina* have been implicated in *Z. marina* defense. These include flavonoids in sulfated and unsulfated form, as well as acids like caffeic, *p*-coumaric, ferulic, and zosteric, and rosmarinic acids, all of which are hydroxy, sulfoxy, or ester forms of cinnamic acid (Papazian et al., 2019). Resistance of *Z. marina* to *Lz* is hypothesized to depend upon phenolic acids, especially caffeic acid which has demonstrated activity against *Lz* in bioassays (Vergeer and Develi, 1997; Trevathan-Tackett et al., 2015). *Lz* has also been shown to induce production of total phenols in some cases (McKone and Tanner, 2009), and inhibit them in others, potentially as a mechanism to circumvent this defense. In addition, production of phenols in seagrasses are reduced at warmer temperatures (Vergeer et al., 1995). This is reflected in the reduced concentrations of phenols found five days post *Lz*-exposure in the warmer temperature treatment.

The shikimate pathway is the mechanism through which plants produce aromatic phenolic compounds in response to stress (Santos-Sánchez et al., 2019). Four genes - caffeic acid 3-O-methyltransferase, caffeoylshikimate esterase, 4-coumarate–CoA ligase-like 7, and cinnamoyl-CoA reductase - responsible for coding enzymes involved in the biosynthesis of different forms of cinnamic acids were differentially expressed in the exposed treatment, indicating a role for the shikimate pathway in *Lz* infection response. Caffeoylshikimate esterase (CSE), converts caffeoyl shikimate into caffeic acid, which has been shown to inhibit *Lz* growth *in vitro* (Vergeer and Develi, 1997; Vanholme et al., 2013). Another differentially expressed gene, caffeic acid 3-O-methyltransferase, is associated with converting caffeic acid into products associated with the lipid biosynthesis pathway. 4-coumarate-CoA is also associated with production of additional secondary compounds including isoflavonoids and furanocoumarins as phytoalexins (i.e., inhibitors of pathogen growth) (Hamberger and Hahlbrock, 2004). Cinnamoyl-CoA reductase is involved in the formation of phenolic compounds associated with the hypersensitive response (Lauvergeat et al., 2001). The hypersensitive response in plants is akin to the innate immune response in animals and is responsible for isolated apoptosis surrounding an infection in order to prevent further spread (Morel and Dangl, 1997).

Apart from individual roles in the shikimate pathway, all four differentially expressed genes in this pathway are also associated with lignin biosynthesis. The role of lignin is unclear in aquatic plants such as *Z. marina*. While it may be protective against microbial attack, it is typically concentrated in the slower growing rhizomes, and not in the blades (Klap et al., 2000), where gene expression was measured in this study.

In addition to genes involved in immune activation, hormone pathways, and phenolic production, the transcriptional patterns of *Lz* exposed plants and gene enrichment results suggest responses to environmental stress, including salt stress. Stress-related genes were significantly upregulated in the exposed treatment, indicating that

Lz infection may cause damage to cells in a way that triggers this response. The mitochondrial phosphate carrier protein 3 (MPT3) is induced under high salinity conditions (Zhu et al., 2012). Increased expression of the MPT3 gene suggests that *Z. marina* may be experiencing salt stress as *Lz* breaks through host physical barriers. Similarly, the sorting nexin 1 protein regulates the process of accumulating nitrous oxide, which is an important signaling molecule in responses to abiotic stressors, including salt stress (Li et al., 2018). Higher sorting nexin 1 protein gene expression implies that *Z. marina* may accumulate more nitrous oxide in an effort to respond to abiotic stress. Finally, the upregulation of the calcium/calmodulin-dependent protein kinase type 1 (CaM kinase I) gene suggests changing cytosol calcium concentrations, which is a known plant response to stressors such as anoxia, increases temperature, and increased salinity (White and Broadley, 2003). Changes in expression of genes associated with stress response in *Z. marina* may inform our understanding of how molecular functioning is altered upon exposure to environmental changes. This information can also shed light on how *Lz* infection cause stressful conditions for *Z. marina*.

Pathogen responses

By separating host from non-host contigs, we aimed to identify genes or pathways that may contribute to the virulence of *L. zosterae* during experimental infection of *Z. marina*. We found up-regulation of genes potentially involved in breakdown of host defense, chemotaxis and phagocytosis, and metabolism. Although an unannotated genome of another species of *Labyrinthula* (*Labyrinthula* sp. Ha) is newly available, very few contigs had significant matches to the current version of the genome, and only five of the differentially expressed genes from the non-host dataset had significant BLAST hits to this genome. However, the majority of the non-host contigs had significant matches to related slime-mold species including *Dictyostelium* species and *Hondaea fermentalgiana* (a thraustochytrid closely related to the genus *Labyrinthula*), suggesting that the identified non-host genes were likely from *Lz* inoculated in the infection treatment.

Zostera species (including *Z. marina*) produce high concentrations of a sulfate ester, zosteric acid, as a defense mechanism that protects blades from microbial biofouling (Grignon-Dubois et al., 2012; Vilas-Boas et al., 2017). We found a 24-fold up-regulation of a non-host contig that matched to the arylsulfatase gene (GBG30795.1) of *H. fermentalgiana*. Arylsulfatases are enzymes that break down sulfatides and organic sulfate esters. In other protists, arylsulfatases are produced in response to sulfate deprivation (Niedermeyer et al., 1987). However, for the fungal plant pathogen, *Colletotrichum gloeosporiodes*, arylsulfatase expression increases during penetration of host leaf tissue after experimental inoculation (Goodwin et al., 2000). In *Lz*, an increase in arylsulfatase expression may facilitate attachment by breaking down the anti-biofouling zosteric acid produced by the host. However, the potential role of arylsulfatases to facilitate protist pathogen attachment and colonization has yet to be investigated.

Initial studies describing EWD observed *Lz* directly penetrating mesophyll cell walls, damage suggestive of feeding on plant cell organelles such as chloroplasts, and moving rapidly through the host tissues (Muehlstein, 1992; Raghukumar, 2002). In support of these microscopic observations and supporting the role of plant consumption as a mechanism of pathogenesis, we identified several up-regulated genes that are likely involved in movement, i.e. chemotaxis and cytoskeleton rearrangement and organization, as well as phagocytosis. For example, contigs homologous to *shkB*, *sgcA* and *roco5* genes were all up-regulated after experimental inoculation of *Lz*. In *D. discoideum*, null mutants for *shkB* and *sgcA* have reduced chemotaxis and phagocytosis ability (Moniakis et al., 2001; Veltman and Van Haastert, 2006; Veltman et al., 2008), and null mutants for the *roco5* genes have slow or no motility (Sawai et al., 2007). Six up-regulated non-host contigs were homologous to genes that are up-regulated during phagocytosis and/or have gene products which are a part of the 'macropinocytosis proteome' of *D. discoideum* (Sillo et al., 2008; Journet et al., 2012). Additionally, in *D. discoideum*, dhcA proteins cluster to phagosomes and promote phagolysosome fusion (Rai et al., 2016), and lysosomal aspartic protease CatD, a ubiquitous hydrolytic enzyme with a protein of homology in *D. discoideum*, is known to be a lysosomal pepsin in the macropinosome and is involved with phagosome maturation (Vines and King, 2019).

Genes involved in amino acid and lipid metabolism were up-regulated among the non-host contigs. M42 peptidase, a co-catalytic metallopepsidase (cytosolic enzyme) described in bacteria and archaea (reviewed by Appolaire et al., 2016), was the most expressed non-host contig. M42 may play a role in pathogenesis in bacteria by using or modifying exogenous proteins including immunological antibacterial peptides. Other peptidases were up-regulated, such as Carboxypeptidase Y and an otubain-like ubiquitin thioesterase, and may be involved with the catabolism of both large and small peptides in *Lz*. Ethylmalony-CoA decarboxylase, polyketide synthase, beta-ketoadipyl-CoA thiolase, and patatin-like phosphatase domain-containing protein are all involved with fatty acid synthesis and may support membrane formation and increase membrane fluidity during cell division or for the extension of ectoplasmic nets of *Lz*. Up-regulation of these metabolism related contigs along with the up-regulation of genes associated with transcription and translation support increased metabolism and/or cellular proliferation.

Surprisingly, no genes potentially linked to the production of zoospores were up-regulated in this study. Other mechanisms of microbial virulence, such as toxin production, iron sequestration, and host immune invasion (Finlay and Falkow, 1997), were also not up-regulated in this study. Together the non-host transcriptome suggests the possible enzymatic degradation of plant cell defenses, supports the rapid dissemination of *Lz* cells within host tissue, and supports the voracious consumption of plant tissue by invading *Lz* cells as mechanisms of virulence in seagrass wasting disease. Time course experiments, with lower exposure concentrations (*sensu* Bower et al., 1989) would be useful in elucidating both the genes and virulence mechanisms involved in penetration vs. pathogenesis during this disease process.

Conclusion

With increased outbreaks of marine disease, continued influence of anthropogenic stressors, and rapidly changing oceans contributing to significant declines in seagrass meadows across the globe, there is an increasing need to understand host-pathogen dynamics across environmental scales. Given the rapid decline of *Z. marina* globally coupled with active restoration, we have increased need for understanding of host-pathogen dynamics and how this might impact future restoration. This study demonstrates the value of dual host-pathogen transcriptomics for understanding physiological consequences of disease across environmental gradients. While the *Lz* pathogen exhibited a limited repertoire of virulence approaches, including degradation of cell walls, consumption of intracellular materials and movement within the host, the eelgrass host exhibited a wide range of responses to infection, from cascading phytohormone signals, to altered production of phenols, increased PAMP/DAMP signaling and apoptosis. As our knowledge of *Lz* increases, biologically realistic inoculation experiments can be used to further understand the role of changing nearshore conditions in facilitating or repressing disease in this important coastal habitat-forming species.

Data availability statement

The RNAseq data presented in the study are deposited in the NCBI Short Read Archive repository, accession number PRJNA990835. Additional data presented in this study are available at FigShare (http://doi.org/10.6084/m9.figshare.22564528).

Author contributions

MG and CB obtained financial support, conceived of the experimental design, and implemented the experiment. MG led statistical analyses of phenolic and diagnostic data. YV, CB, and AS led the transcriptomics analysis, with help from all authors, and KA analyzed phenols and tannins in the samples. All authors contributed to the article and approved the submitted version.

Funding

This work was funded by a seed grant from the Canadian excellence research chair in support of aquatic epidemiology to MG, start-up funds provided to CB from the University of Maryland Baltimore County and the University of Maryland Baltimore, funding from the National Science Foundation (2109607; 1215977), as well as the University of Washington Friday Harbor Labs.

Acknowledgments

Michelle Herko, Rebecca Guenther and Connie Sullivan assisted in the execution of this experiment. N. Rivlin provided technical assistance and T. Bachvaroff bioinformatics assistance.

Conflict of interest

All authors declare that the research was conducted in the absence of any commercial or financial relationships that could be construed as a potential conflict of interest.

Publisher's note

Supplementary material

The Supplementary Material for this article can be found online at: https://www.frontiersin.org/articles/10.3389/fmars.2023.1152647/full#supplementary-material

References

Świeżawska, B., Duszyn, M., Jaworski, K., and Szmidt-Jaworska, A. (2018). Downstream targets of cyclic nucleotides in plants. *Front. Plant Sci.* 9, 1428. doi: 10.3389/fpls.2018.01428

Agnew, M. V., Groner, M. L., Eisenlord, M. E., Friedman, C. S., and Burge, C. A. (2022). Pacific oysters are a sink and a potential source of the eelgrass pathogen, *Labyrinthula zosterae*. *Aquacult Environ. Interact.* 14, 295–307. doi: 10.3354/aei00446

Altschul, S. F., Gish, W., Miller, W., Myers, E. W., and Lipman, D. J. (1990). Basic local alignment search tool. *J. Mol. Biol.* 215, 403–410. doi: 10.1016/S0022-2836(05)80360-2

Aoki, L. R., McGlathery, K. J., Wiberg, P. L., and Al-Haj, A. (2020). Depth affects seagrass restoration success and resilience to marine heat wave disturbance. *Estuaries Coast.* 43, 316–328. doi: 10.1007/s12237-019-00685-0

Appolaire, A., Colombo, M., Basbous, H., Gabel, F., Girard, E., and Franzetti, B. (2016). TET peptidases: a family of tetrahedral complexes conserved in prokaryotes. *Biochimie* 122, 188–196. doi: 10.1016/j.biochi.2015.11.001

Bates, D., Mächler, M., Bolker, B., and Walker, S. (2015). Fitting Linear Mixed-Effects Models Using lme4. *J. Statistical Software*. 67 (1), 1–48. doi: 10.18637/jss.v067.i01

Bate-Smith, E. C., and Rasper, V. (1969). Tannins of grain sorghum: luteoforol (leucoluteolinidin) 3',4,4',5,7-pentahydroxyflavan. *J. Food Sci.* 34, 203–209. doi: 10.1111/j.1365-2621.1969.tb00919.x

Beca-Carretero, P., Guihéneuf, F., Marín-Guirao, L., Bernardeau-Esteller, J., García-Muñoz, R., Stengel, D. B., et al. (2018). Effects of an experimental heat wave on fatty acid composition in two Mediterranean seagrass species. *Mar. Pollut. Bull.* 134, 27–37. doi: 10.1016/j.marpolbul.2017.12.057

Bednarek, P., Piślewska-Bednarek, M., Svatoš, A., Schneider, B., Doubský, J., Mansurova, M., Schulze-lefert, A., et al(2009). A glucosinolate metabolism pathway in living plant cells mediates broad-spectrum antifungal defense. *Science* 323, 101–106. doi: 10.1126/science.1163732

Bockelmann, A. C., Tams, V., Ploog, J., Schubert, P. R., and Reusch, T. B. (2013). Quantitative PCR reveals strong spatial and temporal variation of the wasting disease pathogen, *Labyrinthula zosterae* in northern European eelgrass (*Zostera marina*) beds. *PloS One* 8, e62169. doi: 10.1371/journal.pone.0062169

Bolger, A. M., Lohse, M., and Usadel, B. (2014). Trimmomatic: a flexible trimmer for illumina sequence data. *Bioinformatics* 30, 2114–2120. doi: 10.1093/bioinformatics/btu170

Bower, S. M., McLean, N., and Whitaker, D. J. (1989). Mechanism of infection by *Labyrinthuloides haliotidis* (Protozoa: labyrinthomorpha), a parasite of abalone (*Haliotis kamtschatkana*)(Mollusca: Gastropoda). *J. Invert Pathol.* 53, 401–409. doi: 10.1016/0022-2011(89)90106-7

Brady, S. M., Sarkar, S. F., Bonetta, D., and McCourt, P. (2003). The abscisic acid insensitive 3 (ABI3) gene is modulated by farnesylation and is involved in auxin signaling and lateral root development in *Arabidopsis*. *Plant J.* 34, 67–75. doi: 10.1046/j.1365-313X.2003.01707.x

Brakel, J., Jakobsson-Thor, S., Bockelmann, A. C., and Reusch, T. B. (2019). Modulation of the eelgrass–*Labyrinthula zosterae* interaction under predicted ocean warming, salinity change and light limitation. *Front. Mar. Sci.* 6, 268. doi: 10.3389/fmars.2019.00268

Bull, J. C., Kenyon, E. J., and Cook, K. J. (2012). Wasting disease regulates long-term population dynamics in a threatened seagrass. *Oecologia* 169, 135–142. doi: 10.1007/s00442-011-2187-6

Burge, C.A., and Friedman, C.S. (2012). Quantifying Ostreid herpesvirus (OsHV-1) copies and expression during transmission. *Microb Ecol.* 63 (3), 596-604. doi: 10.1007/s00248-011-9937-1

Chen, Y., Lun, A.A.T., and Smyth, G.K. (2016). "From reads to genes to pathways: differential expression analysis of RNA-Seq experiments using Rsubread and the edgeR quasi-likelihood pipeline." *F1000Research*. 5, 1438. doi: 10.12688/f1000research.8987.2

Choi, H. W., and Klessig, D. F. (2016). DAMPs, MAMPs, and NAMPs in plant innate immunity. *BMC Plant Biol.* 16, 232. doi: 10.1186/s12870-016-0921-2

Dawkins, P. D., Eisenlord, M. E., Yoshioka, R. M., Fiorenza, E., Fruchter, S., Giammona, F., et al. (2018). Environment, dosage, and pathogen isolate moderate virulence in eelgrass wasting disease. *Dis. Aquat Org* 130, 51–63. doi: 10.3354/dao03263

Downey, M., Houlsworth, R., Maringele, L., Rollie, A., Brehme, M., Galicia, S., et al. (2006). A genome-wide screen identifies the evolutionarily conserved KEOPS complex as a telomere regulator. *Cell* 124, 1155–1168. doi: 10.1016/j.cell.2005.12.04

Dunic, J. C., Brown, C. J., Connolly, R. M., Turschwell, M. P., and Cote, I. M. (2021). Long-term declines and recovery of meadow area across the world's seagrass bioregions. *Global Change Biol.* 27, 4096–4109. doi: 10.1111/gcb.15684

Fan, J., Hill, L., Crooks, C., Doerner, P., and Lamb, C. (2009). Abscisic acid has a key role in modulating diverse plant-pathogen interactions. *Plant Physiol.* 150, 1750–1761. doi: 10.1104/pp.109.137943

Finlay, B. B., and Falkow, S. (1997). Common themes in microbial pathogenicity revisited. *Microbiol. Mol. Biol. Rev.* 61, 136–169. doi: 10.1128/mmbr.61.2.136-169.1997

Goodwin, P. H., Li, J., and Jin, S. (2000). Evidence for sulfate derepression of an arylsulfatase gene of *Colletotrichum gloeosporioides* f. sp. *malvae* during infection of round-leaved mallow, *Malva pusilla*. *Physiol. Mol. Plant Pathol.* 57, 169–176. doi: 10.1006/pmpp.2000.0295

Grabherr, M. G., Haas, B. J., Yassour, M., Levin, J. Z., Thompson, D. A., Amit, I., et al. (2011). Full-length transcriptome assembly from RNA-seq data without a reference genome. *Nat. Biotechnol.* 29, 644. doi: 10.1038/nbt.1883

Graham, O. J., Aoki, L. R., Stephens, T., Stokes, J., Dayal, S., Rappazzo, B., et al. (2021). Effects of seagrass wasting disease on eelgrass growth and belowground sugar in natural meadows. *Front. Mar. Sci.* 8, 768668. doi: 10.3389/fmars.2021.768668

Grignon-Dubois, M., Rezzonico, B., and Alcoverro, T. (2012). Regional scale patterns in seagrass defences: phenolic acid content in *Zostera noltii*. *Estuar. Coast. shelf Sci.* 114, 18–22. doi: 10.1016/j.ecss.2011.09.010

Groner, M. L., Burge, C. A., Couch, C. S., Kim, C. J., Siegmund, G. F., Singhal, S., et al. (2014). Host demography influences the prevalence and severity of eelgrass wasting disease. *Dis. aquat org* 108, 165–175. doi: 10.3354/dao02709

Groner, M. L., Burge, C. A., Cox, R., Rivlin, N. D., Turner, M., Van Alstyne, K. L., et al. (2018). Oysters and eelgrass: potential partners in a high pCO_2 ocean. *Ecology* 99, 1802–1814. doi: 10.1002/ecy.2393

Groner, M. L., Burge, C. A., Kim, C. J., Rees, E., Van Alstyne, K. L., Yang, S., et al. (2016). Plant characteristics associated with widespread variation in eelgrass wasting disease. *Dis. aqaut org* 118, 159–168. doi: 10.3354/dao02962

Groner, M. L., Eisenlord, M. E., Yoshioka, R. M., Fiorenza, E. A., Dawkins, P. D., Graham, O. J., et al. (2021). Warming sea surface temperatures fuel summer epidemics of eelgrass wasting disease. *Mar. Ecol. Prog. Ser.* 679, 47–58. doi: 10.3354/meps13902

Haas, B. J., Papanicolaou, A., Yassour, M., Grabherr, M., Blood, P. D., Bowden, J., et al. (2013). *De novo* transcript sequence reconstruction from RNA-seq using the trinity platform for reference generation and analysis. *Nat. Protoc.* 8, 1494. doi: 10.1038/nprot.2013.084

Hamberger, B., and Hahlbrock, K. (2004). The 4-coumarate: CoA ligase gene family in arabidopsis thaliana comprises one rare, sinapate-activating and three commonly occurring isoenzymes. *PNAS* 101, 2209–2214. doi: 10.1073/pnas.0307307101

Hou, S., Jamieson, P., and He, P. (2018). The cloak, dagger, and shield: proteases in plant–pathogen interactions. *Biochem. J.* 475, 2491–2509. doi: 10.1042/bcj20170781

Journet, A., Klein, G., Brugière, S., Vandenbrouck, Y., Chapel, A., Kieffer, S., et al. (2012). Investigating the macropinocytic proteome of *Dictyostelium* amoebae by high-resolution mass spectrometry. *Proteomics* 12, 241–245. doi: 10.1002/pmic.201100313

Klap, V. A., Hemminga, M. A., and Boon, J. J. (2000). Retention of lignin in seagrasses: angiosperms that returned to the sea. *Mar. Ecol. Prog. Ser.* 194, 1–11. doi: 10.3354/meps194001

Lamb, J. B., Van De Water, J. A., Bourne, D. G., Altier, C., Hein, M. Y., Fiorenza, E. A., et al. (2017). Seagrass ecosystems reduce exposure to bacterial pathogens of humans, fishes, and invertebrates. *Science* 355, 731–733. doi: 10.1126/science.aal1956

Langfelder, P., and Horvath, S. (2008). WGCNA: an r package for weighted correlation network analysis. *BMC Bioinf.* 9, 559. doi: 10.1186/1471-2105-9-559

Lauvergeat, V., Lacomme, C., Lacombe, E., Lasserre, E., Roby, D., and Grima-Pettenati, J. (2001). Two cinnamoyl-CoA reductase (CCR) genes from *Arabidopsis thaliana* are differentially expressed during development and in response to infection with pathogenic bacteria. *Phytochemistry* 57, 1187–1195. doi: 10.1016/S0031-9422(01)00053-X

Lee, H., Golicz, A. A., Bayer, P. E., Jiao, Y., Tang, H., Paterson, A. H., et al. (2016). The genome of a southern hemisphere seagrass species (Zostera muelleri). *Plant Physiol.* 172, 272–283. doi: 10.1104/pp.16.00868

Li, T. T., Liu, W. C., Wang, F. F., Ma, Q. B., Lu, Y. T., and Yuan, T. T. (2018). SORTING NEXIN 1 functions in plant salt stress tolerance through changes of NO accumulation by regulating NO synthase-like activity. *Front. Plant Sci.* 9, 1634. doi: 10.3389/fpls.2018.01634

Ma, D., Li, Y., Zhang, J., Wang, C., Qin, H., Ding, H., et al. (2016). Accumulation of phenolic compounds and expression profiles of phenolic acid biosynthesis-related genes in developing grains of white, purple, and red wheat. *Front. Plant Sci.* 7, 528. doi: 10.3389/fpls.2016.00528

Markham, J. W., and Hagmeier, E. (1982). Observations on the effects of germanium dioxide on the growth of macro-algae and diatoms. *Phycologia* 21, 125–130. doi: 10.2216/i0031-8884-21-2-125.1

Martin, D. L., Chiari, Y., Boone, E., Sherman, T. D., Ross, C., Wyllie-Echeverria, S., et al. (2016). Functional, phylogenetic and host-geographic signatures of labyrinthula spp. provide for putative species delimitation and a global-scale view of seagrass wasting disease. *Estuaries Coasts* 39, 1403–1421. doi: 10.1007/s12237-016-0087-z

Mata-Pérez, C., Sánchez-Calvo, B., Begara-Morales, J. C., Luque, F., Jiménez-Ruiz, J., Padilla, M. N., et al. (2015). Transcriptomic profiling of linolenic acid-responsive genes in ROS signaling from RNA-seq data in *Arabidopsis*. *Front. Plant Sci.* 6, 122. doi: 10.3389/fpls.2015.00122

Mauch-Mani, B., and Mauch, F. (2005). The role of abscisic acid in plant–pathogen interactions. *Curr. Opin. Plant Biol.* 8, 409–414. doi: 10.1016/j.pbi.2005.05.015

McCarthy, D. J., Chen, Y., and Smyth, G. K. (2012). Differential expression analysis of multifactor RNA-seq experiments with respect to biological variation. *Nucleic Acids Res.* 40, 4288–4297. doi: 10.1093/nar/gks042

McKone, K. L., and Tanner, C. E. (2009). Role of salinity in the susceptibility of eelgrass *Zostera* marina to the wasting disease pathogen *Labyrinthula zosterae*. *Mar. Ecol. Prog. Ser.* 377, 123–130. doi: 10.3354/meps07860

Moniakis, J., Funamoto, S., Fukuzawa, M., Meisenhelder, J., Araki, T., Abe, T., et al. (2001). An SH2-domain-containing kinase negatively regulates the phosphatidylinositol-3 kinase pathway. *Genes Dev.* 15, 687–698. doi: 10.1101/gad.871001

Morel, J. B., and Dangl, J. L. (1997). The hypersensitive response and the induction of cell death in plants. *Cell Death differ* 4, 671–683. doi: 10.1038/sj.cdd.4400309

Muehlstein, L. K. (1992). The host-pathogen interaction in the wasting disease of eelgrass, *Zostera marina*. *Can. J. Bot.* 70, 2081–2088. doi: 10.1139/b92-258

Niedermeyer, I., Biedlingmaier, S., and Schmidt, A. (1987). Derepression of arylsulfatase activity by sulfate starvation in *Chlorella fusca*. *Z. für Naturforschung C*, 42 (5), 530–536, 42. doi: 10.1515/znc-1987-0507

Nitao, J. K., Birr, B. A., Nair, M. G., Herms, D. A., and Mattson, W. J. (2001). Rapid quantification of proanthocyanidins (condensed tannins) with a continuous flow analyzer. *J. Agric. Food Chem.* 49, 2207–2214. doi: 10.1021/jf001183b

Nordlund, L. M., Koch, E. W., Barbier, E. B., and Creed, J. C. (2016). Seagrass ecosystem services and their variability across genera and geographical regions. *PloS One* 11 (10), e0163091. doi: 10.1371/journal.pone.0169942

O'Donnell, M. J., George, M. N., and Carrington, E. (2013). Mussel byssus attachment weakened by ocean acidification. *Nat. clim Change* 3, 587–590. doi: 10.1038/nclimate1846

Orth, R. J., Carruthers, T. J., Dennison, W. C., Duarte, C. M., Fourqurean, J. W., Heck, K. L., et al. (2006). A global crisis for seagrass ecosystems. *Bioscience* 56, 987–996. doi: 10.1641/0006-3568(2006)56[987:AGCFSE]2.0.CO;2

Papazian, S., Parrot, D., Burýšková, B., Weinberger, F., and Tasdemir, D. (2019). Surface chemical defence of the eelgrass *Zostera marina* against microbial foulers. *Sci. Rep.* 9, 3323. doi: 10.1038/s41598-019-39212-3

Raghukumar, S. (2002). Ecology of the marine protists, the labyrinthulomycetes (Thraustochytrids and labyrinthulids). *Eur. J. Protistol.* 38, 127–145. doi: 10.1078/0932-4739-00832

Rai, A., Pathak, D., Thakur, S., Singh, S., Dubey, A. K., and Mallik, R. (2016). Dynein clusters into lipid microdomains on phagosomes to drive rapid transport toward lysosomes. *Cell* 164, 722–734. doi: 10.1016/j.cell.2015.12.054

Robinson, M. D., McCarthy, D. J., and Smyth, G. K. (2010). edgeR: a bioconductor package for differential expression analysis of digital gene expression data. *Bioinform* 26, 139–140. doi: 10.1093/bioinformatics/btp616

Roelfsema, M. R. G., Hedrich, R., and Geiger, D. (2012). Anion channels: master switches of stress responses. *Trends Plant Sci.* 17, 221–229. doi: 10.1016/j.tplants.2012.01.009

Santos-Sánchez, N. F., Salas-Coronado, R., Hernández-Carlos, B., and Villanueva-Cañongo, C. (2019). Shikimic acid pathway in biosynthesis of phenolic compounds. *Plant Physiol. aspects phenolic compounds* 1, 1–15. doi: 10.5772/intechopen.83815

Sawai, S., Guan, X. J., Kuspa, A., and Cox, E. C. (2007). High-throughput analysis of spatio-temporal dynamics in *Dictyostelium*. *Genome Biol.* 8, 1–15. doi: 10.1186/gb-2007-8-7-r144

Short, F., Carruthers, T., Dennison, W., and Waycott, M. (2007). Global seagrass distribution and diversity: a bioregional model. *J. Exp. Mar. Biol. Ecol.* 350, 3–20. doi: 10.1016/j.jembe.2007.06.012

Short, F. T., Muehlstein, L. K., and Porter, D. (1987). Eelgrass wasting disease: cause and recurrence of a marine epidemic. *Biol. Bull.* 173, 557–562. doi: 10.2307/1541701

Sillo, A., Bloomfield, G., Balest, A., Balbo, A., Pergolizzi, B., Peracino, B., et al. (2008). Genome-wide transcriptional changes induced by phagocytosis or growth on bacteria in *Dictyostelium*. *BMC Genomics* 9, 1–22. doi: 10.1186/1471-2164-9-291

Sreekanta, S., Bethke, G., Hatsugai, N., Tsuda, K., Thao, A., Wang, L., et al. (2015). The receptor-like cytoplasmic kinase PCRK 1 contributes to pattern-triggered immunity against *Pseudomonas syringae* in *Arabidopsis thaliana*. *New Phytol.* 207, 78–90. doi: 10.1111/nph.13345

Strydom, S., Murray, K., Wilson, S., Huntley, B., Rule, M., Heithaus, M., et al. (2020). Too hot to handle: unprecedented seagrass death driven by marine heatwave in a world heritage area. *Glob. Change Biol.* 26, 3525–3538. doi: 10.1111/gcb.15065

Sullivan, B. K., Sherman, T. D., Damare, V. S., Lilje, O., and Gleason, F. H. (2013). Potential roles of *Labyrinthula* spp. in global seagrass population declines. *Fungal Ecol.* 6, 328–338. doi: 10.1016/j.funeco.2013.06.004

Tamaoki, D., Seo, S., Yamada, S., Kano, A., Miyamoto, A., Shishido, H., et al. (2013). Jasmonic acid and salicylic acid activate a common defense system in rice. *Plant Signal Behav.* 8, e24260. doi: 10.4161/psb.24260

Thaler, J. S., Owen, B., and Higgins, V. J. (2004). The role of the jasmonate response in plant susceptibility to diverse pathogens with a range of lifestyles. *Plant Physiol.* 135, 530–538. doi: 10.1104/pp.104.041566

Tracy, A. M., Pielmeier, M. L., Yoshioka, R. M., Heron, S. F., and Harvell, C. D. (2019). Increases and decreases in marine disease reports in an era of global change. *Proc. R. Soc. B* 286, 20191718. doi: 10.1098/rspb.2019.1718

Trevathan-Tackett, S. M., Lane, A. L., Bishop, N., and Ross, C. (2015). Metabolites derived from the tropical seagrass *Thalassia testudinum* are bioactive against pathogenic *Labyrinthula* sp. *Aquat. Bot.* 122, 1–8. doi: 10.1016/j.aquabot.2014.12.005

Vanholme, R., Cesarino, I., Rataj, K., Xiao, Y., Sundin, L., Goeminne, G., et al. (2013). Caffeoyl shikimate esterase (CSE) is an enzyme in the lignin biosynthetic pathway in *Arabidopsis*. *Science* 341, 1103–1106. doi: 10.1126/science.1241602

Veltman, D. M., Keizer-Gunnik, I., and Van Haastert, P. J. (2008). Four key signaling pathways mediating chemotaxis in *Dictyostelium discoideum*. *J. Cell Biol.* 180, 747–753. doi: 10.1083/jcb.200709180

Veltman, D. M., and Van Haastert, P. J. (2006). Guanylyl cyclase protein and cGMP product independently control front and back of chemotaxing *Dictyostelium* cells. *Mol. Biol. Cell* 17, 3921–3929. doi: 10.1091/mbc.e06-05-0381

Vergeer, L. H. T., Aarts, T. L., and De Groot, J. D. (1995). The 'wasting disease'and the effect of abiotic factors (light intensity, temperature, salinity) and infection with *Labyrinthula zosterae* on the phenolic content of *Zostera marina* shoots. *Aquat. Bot.* 52, 35–44. doi: 10.1016/0304-3770(95)00480-N

Vergeer, L. H., and Develi, A. (1997). Phenolic acids in healthy and infected leaves of *Zostera marina* and their growth-limiting properties towards *Labyrinthula zosterae*. *Aquat. Bot.* 58, 65–72. doi: 10.1016/S0304-3770(96)01115-1

Vilas-Boas, C., Sousa, E., Pinto, M., and Correia-da-Silva, M. (2017). An antifouling model from the sea: a review of 25 years of zosteric acid studies. *Biofouling* 33, 927–942. doi: 10.1080/08927014.2017.1391951

Vines, J. H., and King, J. S. (2019). The endocytic pathways of *Dictyostelium discoideum*. *Int. J. Dev. Biol.* 63, 461–471. doi: 10.1387/ijdb.190236jk

Wang, J. P., Munyampundu, J. P., Xu, Y. P., and Cai, X. Z. (2015). Phylogeny of plant calcium and calmodulin-dependent protein kinases (CCaMKs) and functional analyses of tomato CCaMK in disease resistance. *Front. Plant Sci.* 6, 1075. doi: 10.3389/fpls.2015.01075

White, P. J., and Broadley, M. R. (2003). Calcium in plants. *Ann. Bot.* 9, 487–511. doi: 10.1093/aob/mcg164

Wright, R. M., Aglyamova, G. V., Meyer, E., and Matz, M. V. (2015). Gene expression associated with white syndromes in a reef-building coral. *Acropora hyacinthus. BMC Genomics* 16, 371. doi: 10.1186/s12864-015-1540-2

Yang, W., Devaiah, S. P., Pan, X., Isaac, G., Welti, R., and Wang, X. (2007). AtPLAI is an acyl hydrolase involved in basal jasmonic acid production and *Arabidopsis* resistance to *Botrytis cinerea*. *J. Biol. Chem.* 282, 18116–18128. doi: 10.1074/jbc.M700405200

Zeng, M. H., Liu, S. H., Yang, M. X., Zhang, Y. J., Liang, J. Y., Wan, X. R., et al. (2013). Characterization of a gene encoding clathrin heavy chain in maize up-regulated by salicylic acid, abscisic acid and high boron supply. *Int. J. Mol. Sci.* 14, 15179–15198. doi: 10.3390/ijms140715179

Zhang, L., Paasch, B. C., Chen, J., Day, B., and He, S. Y. (2019). An important role of l-fucose biosynthesis and protein fucosylation genes in *Arabidopsis* immunity. *New Phytol.* 222, 981–994. doi: 10.1111/nph.15639

Zhang, N., Zhou, S., Yang, D., and Fan, Z. (2020). Revealing shared and distinct genes responding to JA and SA signaling in arabidopsis by meta-analysis. *Front. Plant Sci.* 11, 908. doi: 10.3389/fpls.2020.00908

Zhu, W., Miao, Q., Sun, D., Yang, G., Wu, C., Huang, J., et al. (2012). The mitochondrial phosphate transporters modulate plant responses to salt stress via affecting ATP and gibberellin metabolism in *Arabidopsis thaliana*. *PloS One* 7, e43530. doi: 10.1371/journal.pone.0043530

frontiers | Frontiers in Ecology and Evolution

TYPE Original Research
PUBLISHED 09 April 2024
DOI 10.3389/fevo.2024.1347160

OPEN ACCESS

EDITED BY
Piero Calosi,
Université du Québec à Rimouski, Canada

REVIEWED BY
Athanasios Exadactylos,
University of Thessaly, Greece
Louis V. Plough,
University of Maryland, United States

*CORRESPONDENCE
Christian Bock
Christian.Bock@awi.de

RECEIVED 30 November 2023
ACCEPTED 21 March 2024
PUBLISHED 09 April 2024

CITATION
Bock C, Götze S, Pörtner HO and Lannig G (2024) Exploring the mechanisms behind swimming performance limits to ocean warming and acidification in the Atlantic king scallop, *Pecten maximus*.
Front. Ecol. Evol. 12:1347160.
doi: 10.3389/fevo.2024.1347160

Exploring the mechanisms behind swimming performance limits to ocean warming and acidification in the Atlantic king scallop, *Pecten maximus*

Christian Bock*, Sandra Götze, Hans O. Pörtner and Gisela Lannig

Integrative Ecophysiology, Alfred Wegener Institute Helmholtz Centre for Polar and Marine Research, Bremerhaven, Germany

Recently, we could show that scallops show limitations of muscular performance like a reduced force under ocean warming and acidification. However, the underlying mechanisms at the cellular level are not completely understood. Metabolomics has become a valuable tool to evaluate the responses of marine organisms to various stressors. In the present study we therefore used a semi-targeted, multi tissue NMR based metabolomic approach to analyze metabolite patterns in the Atlantic king scallop, *Pecten maximus*, that were long-term acclimated to different end of century conditions of ocean warming (OW), ocean acidification (OA) and their combination (OWA). We investigated tissue specific metabolic profiles and metabolite concentrations in frozen tissues from gills, mantle and phasic and tonic adductor muscle of *P. maximus* under present conditions using ^{1}H-HR-MAS NMR spectroscopy. A set of 33 metabolites revealed a clear tissue-specific pattern which can be attributed to the individual functions of the respective tissue type. We then evaluated the impact of OW, OA and OWA on the metabolic profiles of the different tissues. OW was the main driver of the changes in metabolites. In particular, energy-related metabolites seem to play an important role in the physiological response of scallops to OW and OWA. In combination with pathway analysis and network exploration we propose a possible correlation between metabolic changes in the adductor muscle and limited swimming performance of *P. maximus* under future climate. While the metabolic response of the phasic muscle seems to mainly depend on net consumption of energy related metabolites such as ATP and phospho-L-arginine, the tonic muscle seems to rely on metabolizing specific amino acids and beta-oxidation to account for the elevated energetic requirements under ocean warming and acidification.

KEYWORDS

bivalves, climate change, NMR spectroscopy, metabolite profiling, pathway and network analysis

1 Introduction

Increasing greenhouse gas emissions are not only responsible for the ongoing global warming trend, but as anthropogenic CO_2 has been taken up by the oceans (Bindoff et al., 2019; Licker et al., 2019), they also lead to a decrease in ocean pH through the marine carbonate system (Zeebe, 2012). This process known as "ocean acidification" (OA) is a global phenomenon and called the evil twin of warming, since both ocean warming and acidification are occurring in parallel. It is therefore important to investigate the influence of both factors on the physiology of marine organisms in order to be able to make realistic statements about climate-induced changes in marine ecosystems (Pörtner et al., 2014; Gattuso et al., 2018; Landrigan et al., 2020). Attempts to gain an understanding of the combined effects of elevated temperatures and PCO_2 levels on marine species in their ecosystem have been underway for some time (Doney et al., 2012; Byrne and Przeslawski, 2013), and the effects of these climate variables turned out to be context and species-dependent (Harvey et al., 2013). The combination of both factors has recently been reviewed (Baag and Mandal, 2022) and literature shows that ocean warming is the main driver affecting an organism's metabolism while the effects of acidification play more of an additive role (e.g. Pinsky et al., 2019; Matoo et al., 2021).

For water-breathing poikilotherms whose body temperature varies with environmental temperature, the concept of oxygen and capacity limited thermal tolerance highlights that, with increasing temperature, marine ectotherms experience progressive hypoxemia and finally, when reaching the critical temperature, rely on anaerobic ATP production to fuel the rising gap in energy demand, which is no longer supported by solely aerobic mitochondrial ATP production (Pörtner, 2002; Pörtner et al., 2017). Accordingly, since the aerobic power budget (excess of aerobic energy after maintenance costs are covered; Guderley and Pörtner, 2010; Pörtner et al., 2017) is limited and an organism cannot rely long-term on anaerobiosis, there are trade-offs between an organism's performance parameters (growth, exercise, reproduction) and there are bottlenecks in an organism's performance capacity under stressful (energy-demanding) environmental conditions such as ocean warming and acidification (OWA).

The impact of ocean acidification on marine life is manyfold (see reviews by e.g. Melzner et al., 2020; Doney et al., 2020; Findlay et al., 2022) and various calcifiers suffer from reduced growth and calcification rates even though the previously high level of concern about the fate of calcifiers in a future ocean no longer holds (see reviews by Zhao et al., 2020; Leung et al., 2022). Bivalves have a limited capacity for acid base regulation and are experiencing a drop in extracellular pH when exposed to OA (Lannig et al., 2010; Heinemann et al., 2012; Gazeau et al., 2014; Zhao et al., 2017) including the scallop *Pecten maximus* (Schalkhausser et al., 2013; Schalkhausser et al., 2014). Such studies indicate that OA impact and sensitivity differ between wild and aquaculture animals (Richards et al., 2015; Stapp et al., 2018). Among bivalves, scallops are unique due to their swimming (escape) behavior via jet propulsion through adductor muscle contractions (Guderley and Tremblay, 2016). The adductor muscle consists of two types that interact during swimming exercise (Pérez et al., 2008; Tremblay et al., 2012; Guderley and Tremblay, 2016). The striated phasic muscle, which is essentially responsible for swimming through claps, and the smaller smooth tonic muscle, which is mainly responsible for closing the shells and holding them closed (Chantler, 2006; Sun et al., 2018) During swimming, muscle contraction cannot solely be fueled by mitochondrial oxidative phosphorylation and is highly dependent on ATP generation from phosphate reserves like phospho-L-arginine (PLA) and anaerobic glycolysis (Guderley and Tremblay, 2016). In comparison to other bivalves like oysters or mussels that are able to colonize the intertidal zone, their active lifestyle gives scallops less flexibility to cope with changing environmental factors (Guderley and Pörtner, 2010; Ivanina and Sokolova, 2016; Götze et al., 2020).

1.1 Previous observations on scallops swimming performance

In previous studies, we investigated the influence of ocean warming and acidification on swimming performance of the king scallop, *Pecten maximus* (Schalkhausser et al., 2013, 2014). According to Schalkhausser et al. (2014) *P. maximus*' swimming ability was affected by warming more than by acidification (PCO_2 0.112 kPa). While the number of claps to exhaustion was similar for *P. maximus* between 10°C and 20°C, the force of the phasic adductor muscle was significantly reduced under long-term acclimation to 20°C. The time to exhaustion was reduced and the recovery period prolonged in warm-exposed *P. maximus*. Warming resulted in a significant decrease in hemolymph oxygen levels (extracellular partial pressure of O_2: P_eO_2). In combination with a significant increase in respiration rate at 20°C, the nearly 50% reduction in P_eO_2 indicated that *P. maximus* had surpassed its optimal temperature range and was exhibiting a progressive warming-induced mismatch between aerobic energy supply and demand (Pörtner et al., 2017). In a subsequent study on *P. maximus* exposed long-term to OW (20°C, 0.04 kPa PCO_2) and OWA (20°C, 0.112 kPa PCO_2; Bock et al., 2019), we investigated the availability of energy-rich phosphates, in particular PLA and inorganic phosphate (Pi) using *in vivo* ^{31}P NMR spectroscopy and calculated the mitochondrial maximum surplus oxidative flux of the phasic muscle. In both OW- and OWA-exposed scallops, PLA and maximum surplus oxidative flux of phasic muscle were reduced, which was attributed to the lower P_eO_2 in the haemolymph found in OW- and OWA-exposed scallops described in Schalkhausser et al. (2014).

The aim of the present study was to use state-of-the-art metabolomics and thereby elucidate the mechanisms at the cellular level which underpin the performance limitations on the organism-level in *P. maximus*. Metabolomics enables the holistic tracking of changing metabolic processes in response to an external stimulus such as environmental changes (Viant, 2008, for a recent review see Wishart, 2019). Metabolomics is believed to unravel the phenotype of an organism from the response to an external stimulus (Fiehn, 2002; Wishart et al., 2022). Using tissue samples from our previous experiments (see Schalkhausser et al., 2014), we applied a semi-untargeted metabolomics approach based on NMR

spectroscopy to a multi-tissue dataset for obtaining tissue specific insights into the metabolic response of *Pecten maximus*. In addition, metabolic responses of the adductor muscle were then related to whole-animal performance and capacity parameters (clapping response and oxygen consumption of *P. maximus* as described in Schalkhausser et al., 2014) to gain a more integrative understanding. To further support our interpretation of the data, a pathway analysis was complemented by a network exploration. This combination enables a better interpretation of the metabolite changes and the generation of testable experimental hypotheses. In particular, we focused on potential pathway modifications of the intermediary metabolism of the two adductor muscle types (phasic and tonic muscle). We propose a cellular mechanism that might explain the observed limitations in whole-animal performance of *P. maximus* under future climate change (Schalkhausser et al., 2014; Bock et al., 2019).

2 Materials and methods

2.1 Experimental design and tissue collection

All investigations were performed on tissue samples that were taken from our experiment described in Schalkhausser et al. (2014). Briefly, wild living Atlantic king scallop *Pecten maximus* with similar size were collected by SCUBA divers at Morlaix Bay (Baie de Morlaix, Les Grandes Fourches, France; 48°42′33.6″N, 3°55′59.30″W) and transported to the Alfred Wegener Institute (Bremerhaven, Germany). Animals were considered as typical from the sampling spot. After recovery from transportation for 2 weeks, scallops were cleaned from epibionts and randomly placed in recirculation aquarium systems and exposed to two different temperatures (10°C; C *vs.* 20°C; OW) and two different PCO_2 values (~0.04 kPa (400 µatm); OA *vs.* ~0.112 kPa (1,120 µatm); OWA) for at least 50 days. Three times per week scallops were fed live phytoplankton (DT´s Premium Reef Blend). Mortality was 9% for the C group, 0% for OA, 20% for OW and 9% in OWA group at the end of the experiment (Nov. 2011), but not statistically different between groups (see Schalkhausser et al., 2014). Scallops were dissected on ice, tissues (gills, mantle, phasic and tonic muscle of the adductor muscle) were freeze-clamped, shock-frozen in liquid nitrogen and stored at −80°C until present metabolite analyses were performed.

2.2 Metabolite analysis via NMR spectroscopy

Metabolite profiling of the different tissues was conducted using high resolution magic angle spinning nuclear magnetic resonance spectroscopy (^{1}H-HR-MAS NMR spectroscopy) using a wide-bore 400 MHz NMR spectrometer (9.4 T WB with Avance III HD electronics, Bruker Biospin, Germany) equipped with a triple tuned ^{1}H-^{13}C-^{31}P-HR-MAS NMR probe. All measurements were performed on frozen tissue samples similar to Podbielskie et al. (2016). Briefly, a sample was taken of the frozen organ of interest using a biopsy punch needle (3 mm diameter) and immediately placed in a standard zirconium HR-MAS rotor for untargeted metabolite profiling based on ^{1}H-NMR spectroscopy. A drop of D_2O (containing 0.05% TSP as standard) was added to the sample for lock and calibration purposes. All samples were measured at 4°C at a spinning rate of 3000 Hz using the Bruker acquisition software TopSpin 3.5pl. NMR parameters were as follows (see also Schmidt et al., 2017; Rebelein et al., 2018): pulse program: 1D-Carr-Purcell-Meiboom-Gill (CPMG) pulse train including f1 presaturation (Bruker protocol cpmgpr1d), 90° bp pulse length 8.4 µs, time domain 70,656, sweep width of 8802 Hz (22 ppm), acquisition time 4.01 s, relaxation delay 4 s, four dummy scans and 64–256 number of scans depending on the signal-to-noise ratio.

2.3 NMR processing

All NMR data were processed and analyzed using Chenomx NMR suite 8.4 professional suite (Chenomx Inc., Canada). Data were automatically zero-filled, processed with an exponential multiplication of 0.3 Hz, phase and base-line corrected using the automatic functions within Chenomx. The spectra were automatically shim-corrected and calibrated to the TSP standard. After completion of the processing procedure, all spectra from each individual tissue of the single experimental groups were overlaid within the Chenomx profiler. The superposition of the individual spectra allows a quick overview of the quality of the individual NMR spectra and the assessment of comparability. In this way, differences in the line widths and shifts of individual NMR signals can be specifically identified and different baselines between the spectra can be recognized. These factors are essential for an automatic evaluation of metabolite profiles. Shifts of NMR signals, just like different baselines between individual spectra, would lead to an erroneous determination of metabolite concentrations. Interestingly, there was no need for alignment shifts of NMR signals in individual spectra. Spectra that differed in baseline in comparison to the other NMR spectra were marked and later identified as potential outliers within MetaboAnalyst (MetaboAnalyst 5.0., see below). A standard metabolite profile from scallop gill tissue from our previous study (Götze et al., 2020) was overlaid to an example spectrum of each tissue and checked for consistency of the metabolite specific NMR peaks. A set of 33 metabolites was identified and was used for a targeted binning procedure on batches of spectra from each tissue within Chenomix. The water region (4.7–5.25 ppm) was excluded and removed from the spectra. Integrals of the metabolite specific bins were then automatically calculated in arbitrary units, normalized to integers and exported into a csv file. For further comparative statistical analysis, the csv files of the individual spectra were merged. For this, only those bins from the individual metabolites were used for the additional analysis that were distinct for the identification and quantification of the metabolite profiles, or showed a significant content, to get an unambiguous assignment of the metabolites. This included both the integral and the position of the bins in the spectrum that could be uniquely identified.

2.4 Statistics

All spectral data were analyzed for differences in spectral patterns and individual metabolites using the web-based analysis tool MetaboAnalyst (MetaboAnalyst 5.0). The entire analytic procedure followed the recommendation for metabolomic analysis as described in Chong et al. (2019) and corresponding YouTube tutorials of the same group. In a first step, the csv files of the metabolite specific bins were imported into MetaboAnalyst and normalized using pareto scaling as recommended. The data were checked for outliers using an operator controlled visual inspection of the particular heatmaps in combination with an unsupervised principal component analysis (PCA). Identified outliers were removed from the list before further analysis (4 samples for gill and 1 sample for tonic muscle). The identified outliers matched the spectra that had already been marked, as they had different baselines compared to the other NMR spectra (see above). Dendrograms of the data excluding the outliers were used to observe clusters of specific sample spectra between groups. Differences in patterns and classification discrimination between groups were determined by Partial Least Square-discriminant analysis (PLS-DA). Metabolites of interest were classified using the VIP (variance of importance) score of the PLS-DA. Classification and cross validation by permutation tests based on separation distance were performed in view of possible overfitting and meaning fullness of the PLS-DA. A significance analysis of microarray/metabolites (SAM) analysis was performed to identify significant different metabolites between groups. The delta value to control the false discovery rate (FDR) was set conservatively to the highest possible level (leading to a maximum FDR of 0.1). For the discussion we only considered those metabolites that showed definite significant changes in SAM. In addition, ANOVA combined with a *Post-Hoc* test (Fisher's) was used to underpin the results from the SAM analysis where possible. To better understand the interdependencies of the altered metabolites and a possible link to the observed limitations at the whole-animal level, a pathway analysis (PW analysis) was performed in combination with a network (NW) exploration in the muscle samples of control and warming exposed scallops. While the PW analysis establishes a connection to metabolic pathways on the basis of the altered metabolites, the NW exploration looks at the interaction of metabolites and their exchange and thus points to novel interactions. However, the two methods only allow two groups to be compared with each other. Due to its specific role in swimming performance, these analyses were therefore performed on the adductor muscle between the control group and warming. For the network exploration, the metabolite interactions between the control group and the respective experimental groups were also included for comparison. The pathway analysis was performed within MetaboAnalyst, similar to (Götze et al., 2020), to get an idea of the long-term induced changes in metabolic pathways limiting the swimming performance of the adductor muscle. Only those pathways with a significant impact >0.1 were taken into account. For network exploration a metabolite-metabolite interaction network based on STITCH ("search tool for interactions of chemicals") was used to elucidate potential linkages. STITCH is a searchable database that includes interactions for over 300,000 molecules and 1.6 million proteins. The similarity of chemical structures in combination with text mining are used to make predictions about relationships between molecules. For the network exploration the filter for nodes based on degree and a filter for nodes based on betweenness were adjusted for each exploration individually to reduce the complexity of the network and to identify those metabolites that can act as specific bottlenecks in the metabolic network (see figure legends for exact values). Both analyses were only performed on phasic and tonic muscle tissues to underline the particular interaction of the two tissues in relation to the observed changes in swimming performance of scallops under warming conditions.

3 Results

Figure 1 shows a comparative overview of ^{1}H-HR-MAS NMR spectra of the four tissues examined from *Pecten maximus* under control incubations. Although signal intensity varied between investigated tissue types, tissue-specific spectral patterns were quite similar. All large and medium sized signals are seen in each spectrum and there were no obvious additional signals that were observed in one or some tissues only. A set of 33 metabolites was automatically aligned to all spectra of tissue type. A closer look at the individual spectra, however, revealed tissue-specific differences between metabolite profiles with respect to signal intensity, and thus metabolite concentration. The spectrum from the mantle tissue biopsy showed the broadest line widths in relation to the standard (TSP). However, the quality was sufficient for a comparative approach between tissues (see Supplementary for example spectra of the different tissues). Figure 1 displays a multivariate comparison between the tissues by an unsupervised principal component analysis (PCA) and a supervised partial least square discriminant analysis (PLS-DA). Both analyses highlight significant differences in the metabolite profiles between the individual tissues, which were also evident in the visual comparison of the individual NMR spectra (see Supplementary), including differences between the two muscle types. The three principal components of the PCA explained 94.3% of the total variance (Figure 1A) and the three components of the PLS-DA produced a clear separation between the four tissue types. Interestingly, more than 70% were explained by the first component (Figure 1B). The clear separation is confirmed by the corresponding scree plot for the PCA. The cross validation as well as the permutation tests for the PLS-DA indicated a good prediction capability and meaningfulness (see Supplementary). The significantly different metabolite concentrations and the corresponding correlations between tissues after Anova analysis and *post hoc* test are shown in Table 1. Gills and mantle showed the highest concentrations of osmotically relevant metabolites such as imidazole, homarine and glycine, as well as of the two sugars (glucose and UDP glucose). In contrast, the two muscle tissues showed increased concentrations of the membrane-relevant metabolites choline and O-phosphocholine. L-arginine and carnitine were also significantly more concentrated in the two muscle types compared to gill and mantle. Interestingly, the tonic muscle showed metabolite concentrations that were not observed as prominently in the other tissues. These were high concentrations of hypotaurine, tyrosine, methionine, succinate and lactate, whereas

10.3389/fevo.2024.1347160

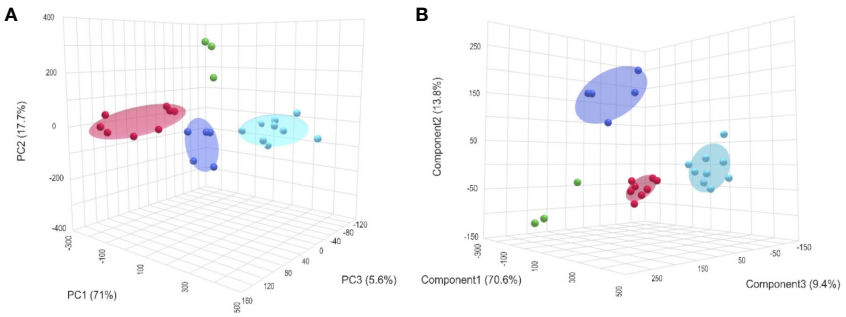

FIGURE 1
3D views of a PCA **(A)** and a PLS-DA **(B)** across the metabolite profiles of all four tissue types (gills = red; mantle = green; phasic muscle = blue and tonic muscle = cyan) of the king scallop, *P. maximus* exposed to control conditions (normocapnia at 10°C). The unsupervised PCA showed a clear separation of all four tissues and the supervised PLS-DA resulted in a distinct classification between tissues. The ellipsoids indicate the respective confidence areas (not available for mantle n=3).

TABLE 1 Summary of the results of the ANOVA test presenting the significant differences in metabolite concentrations between tissue types (gills (C_G), mantle (C_M), phasic (C_P) and tonic muscle (C_T)) of the king scallop, *P. maximus* exposed to control conditions (normocapnia at 10°C).

	f.value	p.value	−log10 (p)	FDR	Fisher's LSD
Tyrosine	598.23	1.7343e-20	19.761	5.7231e-19	C_T - C_G; C_T - C_M; C_T - C_P
Taurine	380.58	1,863E-15	17.73	3,074E-14	C_G - C_M; C_P - C_G; C_G - C_T; C_P - C_M; C_M - C_T; C_P - C_T
Leucine	323.79	9.8194e-18	17.008	1.0801e-16	C_M - C_G; C_P - C_G; C_G - C_T; C_P - C_M; C_M - C_T; C_P - C_T
Serine	225.78	3.9146e-16	15.407	3.2296e-15	C_G - C_M; C_G - C_P; C_T - C_G; C_T - C_M; C_T - C_P
Trimethylamine N-oxide	189.93	2.2606e-15	14.646	1,492E-11	C_G - C_M; C_P - C_G; C_G - C_T; C_P - C_M; C_M - C_T; C_P - C_T
Valine	184.55	3,022E-12	14.52	1.6621e-14	C_M - C_G; C_G - C_P; C_G - C_T; C_M - C_P; C_M - C_T; C_P - C_T
Imidazole	136.09	6.4237e-14	13.192	3.0283e-13	C_M - C_G; C_G - C_P; C_G - C_T; C_M - C_P; C_M - C_T
Homarine	83.469	7.8065e-12	11.108	3.2202e-11	C_M - C_G; C_G - C_P; C_G - C_T; C_M - C_P; C_M - C_T
Succinate	53.958	4.8391e-10	9.3152	1.7743e-09	C_T - C_G; C_T - C_M; C_T - C_P
Acetate	48.552	1.2757e-09	8.8942	4.2099e-09	C_M - C_G; C_P - C_G; C_P - C_M; C_M - C_T; C_P - C_T
Glycolate	44.7	2.6997e-09	8.5687	8.0991e-09	C_G - C_M; C_G - C_P; C_G - C_T; C_T - C_M; C_T - C_P
O-phosphocholine	43.079	3.7633e-09	8.4244	1.0349e-08	C_M - C_G; C_T - C_G; C_M - C_P; C_T - C_M; C_T - C_P
Trigonelline	32.673	4.2586e-08	7.3707	1,081E-04	C_G - C_M; C_G - C_P; C_G - C_T; C_M - C_P; C_M - C_T
Methionine	26.717	2.3098e-07	6.6364	5.4444e-07	C_G - C_M; C_G - C_P; C_T - C_G; C_T - C_M; C_T - C_P
Hypotaurine	23.891	5.7289e-07	6.2419	1.2604e-06	C_T - C_G; C_T - C_M; C_T - C_P
Glucose	23.643	6.2283e-07	6.2056	1.2846e-06	C_M - C_G; C_G - C_P; C_G - C_T; C_M - C_P; C_M - C_T
Alanine	23.328	6.9319e-07	6.1591	1.3456e-06	C_M - C_G; C_P - C_G; C_M - C_T; C_P - C_T
Glycine	22.798	8.3214e-07	6.0798	1.5256e-06	C_M - C_G; C_G - C_P; C_G - C_T; C_M - C_P; C_M - C_T
Dimeythylsulfone	22.257	1.0061e-06	5.9974	1.7474e-06	C_T - C_G; C_T - C_M; C_T - C_P
Glutamate	20.683	1.7838e-06	5.7487	2.9432e-06	C_M - C_G; C_P - C_G; C_P - C_M; C_M - C_T; C_P - C_T
Betaine	16.697	8.8916e-06	5.051	1.3972e-05	C_G - C_M; C_P - C_M; C_T - C_M
Carnitine	15.756	1.3503e-05	4.8696	2.0255e-05	C_P - C_G; C_T - C_G; C_P - C_M; C_T - C_M; C_P - C_T
Succinylacetone	15.168	1.7683e-05	4.7524	2.5371e-05	C_G - C_P; C_G - C_T; C_M - C_P; C_M - C_T
Threonine	11.387	0.00012061	3.9186	0.00016585	C_M - C_G; C_G - C_T; C_M - C_T; C_P - C_T
Isoleucine	10.501	0.00019983	3.6993	0.00026378	C_G - C_P; C_G - C_T; C_M - C_P; C_M - C_T

(Continued)

TABLE 1 Continued

	f.value	p.value	−log10 (p)	FDR	Fisher's LSD
UDP-glucose	9.631	0.00033613	3.4735	0.00042662	C_M - C_G; C_G - C_T; C_M - C_P; C_M - C_T; C_P - C_T
L-Arginine	9.5628	0.0003505	3.4553	0.00042839	C_P - C_G; C_P - C_M; C_P - C_T
Glutamine	8.1638	0.00085916	3.0659	0.0010126	C_M - C_G; C_P - C_G; C_P - C_T
Choline	5.1241	0.0081314	2.0898	0.009253	C_P - C_G; C_T - C_G; C_P - C_M
Lactate	4.8733	0.010006	1.9997	0.011007	C_T - C_G; C_T - C_P
ATP	3.5188	0.032878	1.4831	0.034999	C_G - C_T; C_M - C_T

ATP concentrations were lowest. The phasic muscle contained the highest concentrations of the amino acids alanine, glutamate and glutamine and of acetate, whereas the gill tissue exhibited the highest trigonelline levels. The mantle showed high concentrations of threonine and valine, but very low betaine concentrations compared to the other tissues.

The metabolic response to ocean acidification (OA), warming (OW) and the combination of both (OWA) did partially differ between tissue types. Figure 2 shows a graphical representation of the significant treatment-dependent metabolite changes of gill and phasic muscle tissues. According to the SAM technique, tonic and mantle tissue did not show any significant changes. In gill tissue only the energy related metabolite ATP changed in comparison to control conditions, with ATP levels showing a decrease under OW and OWA (Figure 2A). Most of the changes in concentration were observed in the phasic muscle. Here, eleven metabolites showed concentration changes. These were the essential amino acids leucine and threonine, but also amino acids involved in energy metabolism, such as L-arginine, alanine and glutamine and glutamate, which were lower in the warm groups compared to the control. Acetate and O-phosphocholine, which are utilized in membrane lipid metabolism, were also lower in the warming groups. O-phosphocholine was lowest in the OA group. A similar pattern was observed for lactate. In addition, succinylacetone showed decreased levels in the warming groups. However, glycolate showed increased concentrations under OW and OWA (Figure 2B).

3.1 Pathway and network analysis

A combination of pathway analysis and network correlation were performed on the phasic and tonic tissues from the adductor muscle in particular to get more insights of the metabolic mechanisms behind the swimming performance limits observed under ocean warming in comparison to control conditions. The metabolic pathways with the greatest impact identified in the PW analysis are listed in Table 2. The comparison between the metabolic profiles of the adductor muscle of control and OW-

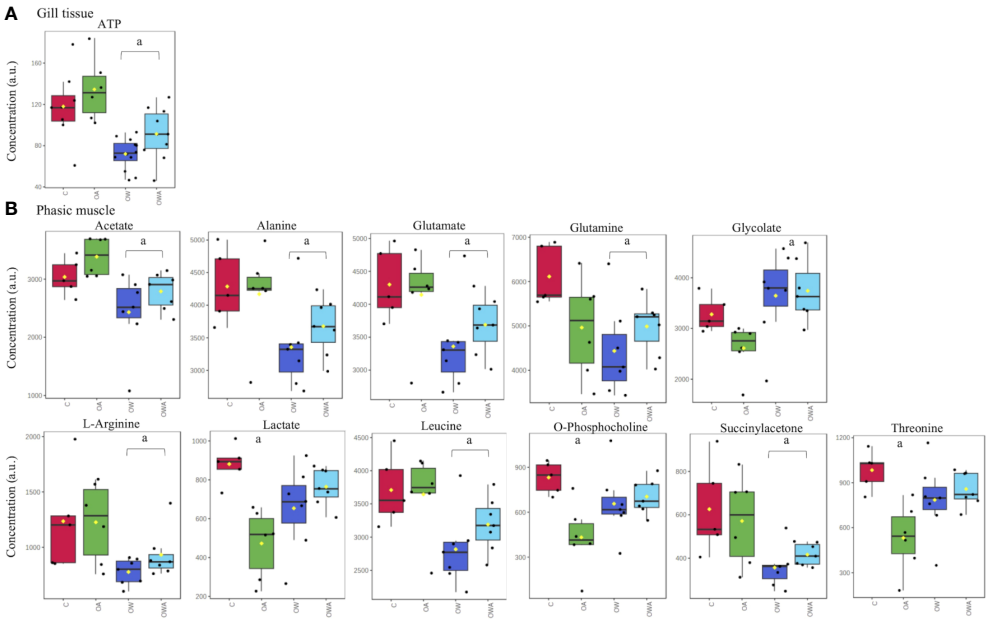

FIGURE 2
Changes in gill tissue **(A)** and phasic muscle **(B)** metabolite concentrations in *P. maximus* exposed to different treatments, controls (C: 10°C, 0.04 kPa PCO_2), ocean acidification (OA: 10°C, 0.112 kPa PCO_2), ocean warming (OW: 20°C, 0.04 kPa PCO_2) and combination of both (OWA: 20°C, 0.112 kPa PCO_2). Significant differences to control are marked with "a".

exposed scallops identified changes in four important pathways. All of them are directly related to arginine and energy metabolism. A Network (NW) exploration of metabolite–metabolite interactions is presented in Figure 3. The entire network consisted of 647 nodes, 2000 edges and 26 seeds (see insert on the left corner of Figure 3). A reduction of the network to the most important metabolites (nodes) and their connections (betweenness), highlights the central role of L-arginine, in addition to ATP, in the network. L-arginine is directly linked to oxygen, ATP and their degradation products, indicating a central role of L-arginine in energy supply during long-term acclimatization to warming in the adductor muscle. In addition, it is noteworthy that the amino acid L-methionine is in close proximity to L-arginine and ATP and that L-arginine is directly connected to carbon dioxide and sodium. In addition, network explorations from the phasic muscle under OA, OW and OWA were performed for comparison. The reduced networks confirmed the central role of L-arginine under OW and OWA, whereas under OA the metabolite phosphorylcholine was most connected (see Supplementary).

4 Discussion

In the present study, a retrospective metabolomic analysis using ^{1}H-HRMAS NMR spectroscopy was conducted using tissue samples of the king scallop, *Pecten maximus*, from long-term incubation experiments. Our aim was to gain a better understanding of the cellular mechanisms that respond to ocean warming (OW) and acidification (OWA) in scallops, and to relate the observed changes in metabolic pathways to the reduction in swimming performance (Schalkhausser et al., 2013, Schalkhausser et al., 2014; Bock et al., 2019).

4.1 Tissue-specific metabolite concentrations

Following our previously published targeted metabolomics approach we could identify a set of 33 metabolites for all tissues, similar to that defined in gill tissue of *P. maximus* (Götze et al., 2020). Similarly, Cappello et al. (2018) found only small differences between the metabolic profiles of mussel *Mytilus galloprovincialis* tissues (gills, phasic muscle and digestive gland). While a main set of metabolites is conserved across all tissue types, metabolite concentrations varied strongly between tissues indicating a differential prioritization of metabolic pathways in each organ.

In gills we found high concentrations of methionine and glycolate. Both metabolites have in common that they have antioxidant properties (methionine: Martínez et al., 2017; glycolate for mitochondria: Diez et al., 2021). The main function of gills is gas exchange making their large surface areas a target for (external and internal) fluctuations of oxygen radicals. In coastal environments, in particular in lagoons or tidal pools, oxygen levels can vary from hyperoxic during day time to hypoxic conditions during night time. Thus, it is not surprising that gills possess a higher concentration of metabolites associated with oxidative stress protection than muscle. Furthermore, gill tissue, which has an important role in osmo- and ion-regulation relies on organic osmolytes, such as compatible solutes like homarine, the sugars glucose and UDP-glucose, but also the amino acid glycine. The high imidazole concentration in gills can be explained by the strong emphasis on effective pH control (Götze et al., 2020). Other amino acids such as isoleucine, serine and valine are highly concentrated in gills due to their importance in protein synthesis and degradation under osmotic stress (Haider et al., 2019). Trigonelline was also found in high concentrations and is known as a plant alkaloid, but has also been found in a variety of marine invertebrates, including bivalves (Cappello et al., 2018; Poulin et al., 2018; Götze et al., 2020; Frizzo et al., 2021; Zhou et al., 2023). The exact function of alkaloids in animals is not yet clear, but trigonelline is supposed to have various biological functions. In crustaceans urinary trigonelline was shown to serve as a chemical sensor for predator–prey interaction (Poulin et al., 2018) but it also to play a role in glucose metabolism and inflammation (see review of Anthoni et al., 1991; Mathur and Kamal, 2012; Moreno et al., 2022). In the hard clam, *Mercenaria mercenaria*, increased trigonelline levels were found after animals were exposed to hypersaline stress and were discussed as an oxidative stress response (Zhou et al., 2023). Similarly, after acute warming (to 26°C) Götze et al. (2020) found a change in trigonelline levels in gills of *P. maximus* when additionally exposed to acute hypoxia and to the combination of hypoxia and hypercapnia. Liao et al. (2019) also reported increased levels of trigonelline under oxidative stress in OA-exposed scallop, *Patinopecten yessoensis*. However, whether the high trigonelline content is related to its putative role in oxidative stress remains speculative and requires further investigation. Interestingly, the tonic muscle shows similar concentrations in "gill-specific" metabolites such as glycolate and methionine, but also a very prominent serine concentration. Since the metabolite matrix of the tonic muscle is only poorly understood

TABLE 2 Major metabolic pathways identified by PW analysis contributing to the metabolic response of the adductor muscle (phasic and tonic muscle) of *P. maximus* to long-term exposures to ocean warming (OW: 20°C, 0.112 kPa PCO_2).

	Total	Expected	Hits	Raw p	–log10 (p)	Holm adjust	FDR	Impact
Arginine biosynthesis	14	0.097425	3	8.5e-05	4.0706	0.00697	0.00238	0.19289
D-Glutamine and D-glutamate metabolism	6	0.041754	2	0.00064455	3.1907	0.052208	0.009115	0.5
Alanine, aspartate and glutamate metabolism	27	0.18789	3	0.00065107	3.1864	0.052208	0.009115	0.3633
Arginine and proline metabolism	38	0.26444	2	0.026812	1.5717	1	0.22522	0.14046

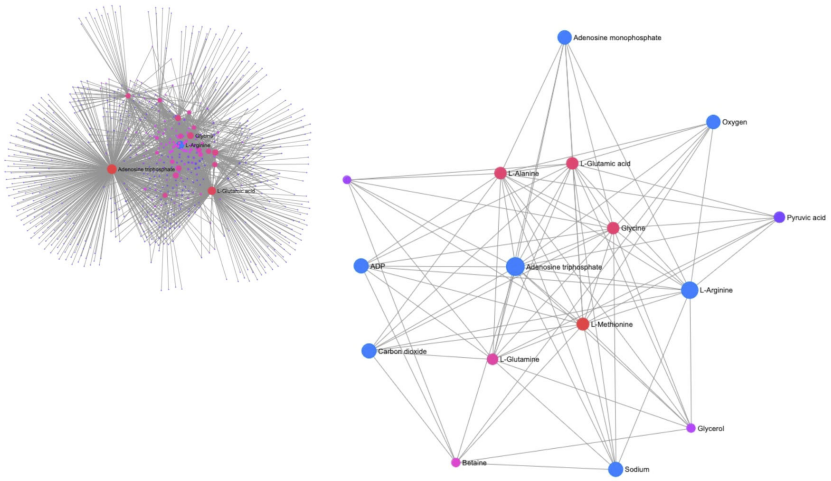

FIGURE 3
Plot of the metabolite-metabolite interaction network of phasic and tonic muscle tissue between control and long-term OW exposed *P. maximus*. The insert in the upper left corner shows the entire network, while the center presents a subnetwork reduced to metabolites with strong connections. Both ATP and L-arginine have a central role in the network. The interaction of L-arginine with ATP, ADP and AMP and with oxygen, carbon dioxide and sodium is marked by bigger blue circles. The filter for nodes based on degree were set to 15 and a filter for nodes based on betweenness were set to 5.

we can only assume that such metabolites in the tonic muscle have a function similar to that proposed for gills.

The metabolite spectrum of the mantle tissue is quite comparable to that of the gill tissue, exemplified by high concentrations of osmotically relevant metabolites, which indicate a role in osmo- and ion regulation as expected for a tissue in direct contact to seawater. However, the mantle spectra exhibited a lower quality due to a broader line width of the NMR signals. The generally poorer quality of ^{1}H-NMR spectra from mantle tissue is a phenomenon also observed in other NMR studies on tissue extracts from marine bivalves (e.g. Lannig et al., 2010). This was explained by the functional heterogeneity of the mantle tissue, e.g. between inner and outer mantle (Clark, 2020). However, despite this heterogeneity, small n numbers and lower NMR signal quality, distinct differences in metabolite concentrations were observed to those of the other tissues. The concentrations of the amino acids threonine, glycine and valine were highest in the mantle tissue compared to the other tissues. Other amino acids such as alanine, leucine and isoleucine also showed high concentrations in the mantle tissue, indicating a particular importance of amino acids in the mantle tissue. The main functions of the mantle lie in biomineralization and calcification. A high proportion of free amino acids, provided for biomineralization is therefore not surprising. It has been shown only recently that amino acids like serine and threonine are of particular importance for biomineralization and calcification processes in bivalves such as scallops (Yarra et al., 2016, Yarra et al., 2021).

The spectra of the two muscle types also show a characteristic picture in their metabolite profiles. In particular, both are characterized by prominent concentrations of the amino acid L-arginine. L-arginine is the precursor for PLA, which corresponds to phosphagen in vertebrate muscle. PLA is used as the main rapid energy reserve to provide ATP and for the formation of octopine in the muscle during exercise and recovery (Grieshaber, 1978). It is therefore the essential metabolite for spontaneous locomotion in the muscle of scallops and indeed, it was shown to vary depending on the lifestyle of different scallop species (Tremblay et al., 2012; Tremblay and Guderley, 2014). In addition, fumarate and carnitine could be detected in both muscle types. These metabolites are also important for energy provision in muscle. Fumarate (fumaric acid) is an intermediate in the Krebs cycle for the production of ATP, but is also involved in the biosynthesis of L-arginine. Carnitine is the shuttle for fatty acids into mitochondria where they are subsequently used for energy production through beta-oxidation. The relatively high content of both metabolites may indicate i) a pronounced biosynthesis of L-arginine and ii) a high proportion of beta-oxidation in the adductor muscle. Interestingly, Guderley et al. demonstrated that neither palmitoyl carnitine nor aspartate were oxidized in isolated muscle mitochondria of the tropic scallop, *Euvola ziczac* (Guderley et al., 1995). Therefore, the question arises why such high carnitine levels were found in the adductor muscle of *P. maximus* if fatty acids are apparently not used for energy production in muscle mitochondria. Yet, the studies of Guderley et al. were done on a tropical species and the rate of substrate use in mitochondria may differ in tropical and boreal species. Temperature is indeed an important factor for the utilization of a specific substrate in mitochondria in all species (Barbe et al., 2023). In addition to L-arginine, fumarate and carnitine, choline, glucose, homarine and some other amino acids also showed comparable concentrations in the two muscle types. However, there were also some fundamental differences. For example, acetate and the amino acids alanine, glutamine and glutamate were highest in phasic muscle, whereas in tonic muscle they were at similar levels as in gills. In tonic muscle ATP levels were lowest, but succinate, lactate and O-phosphocholine

levels were higher than those in other tissues. These differences can be explained by the specific function of each muscle type. The scallops' tonic muscle, the so-called slow-catch "smooth muscle", is mainly responsible for shell closure and prolonged contractures with little energy expenditure (Chantler, 2006; Sun et al., 2018). The phasic or glycolytic muscle is a fast twitching, striated muscle and mainly used during swimming. In line with a higher mitochondrial content in invertebrates' tonic compared to phasic muscle (Nguyen et al., 1997) the observed lower ATP content and elevated succinate levels in tonic muscle appear conceivable. O-phosphocholine is an intermediate for phosphatidylcholines, the key building blocks for cellular membranes, and its observed high levels might indicate that the tonic muscle has a high membrane conversion rate due to its higher mitochondrial content. It is also conceivable that the higher mitochondrial content of tonic muscle needs a higher cell membrane flexibility, as suggested in the theory of membranes as metabolic pacemaker (Hulbert and Else, 1999). The membrane pacemaker theory (MPT) developed for mammals has also been tested in bivalves, although the general applicability to bivalves may differ by species or phenotype and is not always obvious (Pernet et al., 2006, 2007; Sukhotin et al., 2017). However, the differences between individual MPT studies on molluscs could also be due to tissue type, lifestyle or different environmental histories of the species studied (Guderley et al., 2009). Further experiments would be necessary to elucidate the role of MPT for both muscle tissues in bivalves.

Finally, the tonic muscle showed the lowest taurine, TMAO and trigonelline concentrations between tissues. In addition, low concentrations were observed also in other osmotically relevant metabolites such as homarine, glycine and glucose, which were comparable to the phasic muscle. This simply shows that involvement in systemic osmoregulation is only of secondary importance for the tonic and partly also for the phasic muscle. For the amino acids the tonic muscle exhibited highest concentrations of serine and tyrosine, but lowest in alanine, glycine, leucine and threonine concentrations in comparison to the other tissues. The question, however, why these two amino acids were elevated in the tonic muscle and the others were deficient cannot be answered here.

4.2 Tissue-specific OA, OW and OWA related metabolite changes

Metabolite profiles after long-term acclimation to ocean acidification (OA), ocean warming (OW) and the combination of ocean warming and acidification (OWA) are tissue-specific. In gills, ATP levels decreased in the two warming groups indicating increased ATP demand in the warmth. Indeed, Schalkhausser observed an increased oxygen consumption after long-term acclimation (Schalkhausser et al., 2014) which may be mirrored in the lowering of ATP levels. Compared to other tissues, gills are an aerobic-active and mitochondria-rich tissue with a nearly 2-fold higher metabolism compared to, for example, mantle tissue (Stapp et al., 2017). In line with increased gill respiration rates determined in the blue mussel after long-term exposure to intermediate and high OA scenarios, the increased gill energy demand can be explained by increased cilia movements involved in water and food transport (Stapp et al., 2017).

The phasic muscle showed only a few changes in metabolite concentrations under OA but more prominent changes in both warming groups, OW and OWA. Glycolate, lactate, O-phosphocholine and threonine were all decreased in the phasic muscle of the OA group. The amino acids alanine, glutamine, glutamate, arginine and leucine, as well as acetate and succinylacetone also displayed lower concentrations in the OW and OWA groups. The observed decrease in O-phosphocholine under OA can be explained by its specific function as an essential constituent for membranes and their turnover. An increased turnover of cell membranes as visible in concentration changes of e.g. phosphocholine and its derivatives (also proposed by Rebelein et al., 2018 and Götze et al., 2020) could be induced by warming. In addition, bivalves are osmoconformers and OA as well as warming, similar to salinity fluctuations, were shown to induce osmotic changes in bivalve tissues (e.g. Morabito et al., 2013 for OA; Jiang et al., 2020; Georgoulis et al., 2022 for warming). Since muscle tissues have a lower content of organic osmolytes than gills (see above), the observed changes of phosphocholine in phasic muscle might indicate a remodeling of the cell membrane to compensate for cell volume changes and ensure cellular homeostasis. This is also indicated by the network exploration of phasic muscle under OA, in which the cell membrane-specific metabolite phosphorylcholine is at the center of the network together with lactate (see Supplementary). At the same temperature, a decrease in lactate levels might indicate metabolic depression under OA. A connection between lactate and metabolic depression was already suggested by Pörtner et al. (2014) in 1994. A depressive effect by the OA induced reduction in extracellular pH has been intensively discussed for different bivalve species (e.g. Thomsen and Melzner, 2010; Lesser, 2016 for blue mussels; Lannig et al., 2010 for oyster; Liu and He, 2012 for mussels, oysters and scallops). On the one hand, Liu and He (2012) reported decreased MO_2 levels under OA in the scallop *Chlamys nobilis* suggesting metabolic depression for scallops. On the other, one of our earlier organismal studies did not observe decreased MO_2 levels in *P. maximus* under OA, which argues against metabolic depression under the selected OA conditions for this species (Schalkhausser et al., 2014). The degree of metabolic depression will clearly be influenced by warming. In addition, lactate may be used as an extra energy source via the pyruvate shuttle under routine metabolism under OA conditions, when P_eO_2 levels are reduced in the hemolymph (Schalkhausser et al., 2014). However, it must be noted that the prominent NMR signals of lactate and threonine are close to each other in the NMR spectrum. In our semi-targeted binning analysis approach, it cannot be ruled out that nearby NMR signals may influence each other due to overlap, resulting in a misleading profile. The similar pattern of the two metabolites between the four groups could indicate this, so the results for lactate and threonine should be interpreted with caution. Indeed, threonine changes are not as expected for a proteinogenic amino acid, where one would expect that it changes in parallel to other proteinogenic amino acids between treatments, which is not the case.

The changes in amino acid levels under OW and OWA can all be explained by the increasing energy demand due to the higher temperatures, as all changing amino acids are involved to a greater or lesser extent in energy metabolism. In the particular case of L-arginine, the decrease in phasic muscle can be explained by PLA reduction and octopine formation. As shown above PLA is the main energy source for the fast-twitching phasic muscle to refuel ATP during swimming and escape responses. In our previous study, using *in vivo* ^{31}P-NMR spectroscopy we revealed a PLA decrease in resting phasic muscle of *P. maximus* following long term exposure to warming and OWA (Bock et al., 2019). In the present study, we obtained metabolic profiles via ^{1}H-HRMAS NMR spectroscopy. As in the case of lactate and threonine, the ^{1}H-NMR signals of L-arginine and PLA are very close to each other in the ^{1}H-NMR spectrum, therefore it was not possible to distinguish between PLA and L-arginine. The decreased L-arginine content under OW and OWA conditions may reflect the warming-induced increase in energy demand and dephosphorylation of PLA to fuel ATP, if octopine formation absorbed L-arginine. Unfortunately, we have only rudimentary information on the possible ^{1}H-NMR signals of octopine and have not found any data on octopine in the literature and databases. Therefore, an increase of octopine from L-arginine decomposition could not be verified in the NMR spectra from the phasic muscle of the OW and OWA groups. The decrease in acetate in the two warming groups could indicate that acetate is metabolized to fatty acids in order to obtain the required energy through beta-oxidation or to synthesize phospholipids (Zhukova, 1986) for the warming- induced rebuilding of cell membranes.

Finally, succinylacetone (SA) decreased in the phasic muscle under OW and OWA. This is a finding that to our knowledge has not been reported in the literature. SA is a metabolite in tyrosine metabolism and has signaling effects (Bechara et al., 2007). In vertebrates SA can inhibit the biosynthesis pathway of heme groups in mitochondria and it also can release iron in the liver and brain (Bechara et al., 2007). More importantly, SA can activate the biosynthesis of glutathione peroxidase and SOD (Rocha et al., 2000; Bechara et al., 2007). The production of reactive oxygen species is a well-known phenomenon in isolated mitochondria under heat stress, also in bivalves (e.g. Heise et al., 2003; Sokolova, 2023) and its importance was recently shown for the yesso scallop under OA (Liao et al., 2019). The observed increase of glycolate in phasic muscle of both warming groups would be in line with a strengthened antioxidative function of glycolate, compensating for the decrease in SA under these conditions. As described for gills the function of glycolate in marine animals is unclear and needs further investigations.

4.3 Link to organismal performance

The review of Guderley and Pörtner which focuses on scallops and fish, highlights the crucial role of energy availability under climate change for the aerobic power budget in marine ectotherms (Guderley and Pörtner, 2010). Energy availability depends on energy resources via food and/or stored energy reserves such as carbohydrates and lipids which are processed via aerobic and anaerobic metabolic pathways. Thereby, thermally induced hypoxemia which results from the mismatch between rising oxygen demand and increasingly limited supply via uptake (ventilatory capacity) and transport (cardiac circulatory capacity) is a main driver for temperature induced limitation in ectotherm performance (Pörtner, 2002, Pörtner and Lannig, 2009; Sokolova et al., 2012; Pörtner et al., 2017). Present observations in tissue-specific responses may indicate coordinated tissue changes balancing functional constraints for the sake of organism survival (Lannig et al., 2010; Tripp-Valdez et al., 2017; Götze et al., 2020).

In the following, we aim to interpret our previous results of *P. maximus*' swimming performance and oxidative capacity under ocean warming and acidification (Schalkhausser et al., 2014; Bock et al., 2019) together with the present metabolomics findings in tissue samples. The increased energy demand in ocean warming treatments indicated by elevated resting metabolic rates of *P. maximus* at 20°C compared to 10°C (Schalkhausser et al., 2014) is accompanied by and correlates with the observed decrease of ATP levels in gill tissue (see above). The decreased levels of L-arginine in phasic muscle of OW- and OWA exposed scallops may have followed the lowered levels of PLA (Bock et al., 2019) including absorption of L-arginine in octopine formation (Grieshaber, 1978). In addition, we showed a mainly OW-induced decrease in the phasic muscle's maximum oxidative flux of OW and OWA exposed *P. maximus* as well as the delayed replenishing of the phasic muscle's PLA pool in the warmth (Bock et al., 2019). All of this can be linked to the warming induced strong reduction in haemolymph P_eO_2 levels of OW- and OWA-exposed *P. maximus* (Schalkhausser et al., 2014) indicating that the warming induced hypoxemia does not allow for maximal and fast recovery of PLA levels, since PLA replenishment occurs upon aerobic recovery (Grieshaber, 1978; Kamp, 1993; Sokolova et al., 2000). Most metabolite changes in the warming groups were observed in the phasic muscle, which were mainly energy related, as confirmed by the pathway analysis and network exploration. A change in energy demand via the TCA cycle was also reported for the adductor muscle of *Argopecten irradians* under thermal stress (Song et al., 2022). In line with our conclusion, the authors suggested that stored energy reserves were mobilized under thermal stress. In addition, Song et al. reported the degradation of valine, leucine and isoleucine for *A. irradians* under thermal stress (Song et al., 2022), similar to our observations. According to the pathway analysis and network exploration, L-arginine plays a central role in the metabolite network for energy provision under long term acclimation to warming in the adductor muscle, which is decoupled from the impact of OA. In terms of energy metabolism, this is not surprising, as L-arginine-phosphate is the basis for providing phosphate groups to ADP for building ATP. However, its direct connection to oxygen as determined from the network analysis also shows its dependence on oxygen and supports our hypothesis that PLA cannot be sufficiently rebuilt due to the reduced oxygen content in the hemolymph. This in turn leads to a reduced support for the increased ATP demand under OW. Interestingly, the network exploration for the warming groups also displayed a direct

connection of L-arginine and ATP to methionine, sodium and CO_2. Furthermore, both muscle types exhibited significantly higher concentrations of carnitine in comparison to gills and mantle (see Table 1).

We therefore propose the following model of metabolic connectivity between the two muscle types, in accordance with the work by Pérez et al. (2008), who demonstrated the recuperation of the phasic muscle by the tonic muscle during swimming in scallops. Compared to the phasic muscle, for which energy must be provided immediately during swimming, the tonic muscle uses energy rather slowly and for a prolonged period. To accomplish their different tasks the phasic muscle requires fast ATP supply under performance and essentially uses PLA for ATP generation. Only during prolonged exercise at low speeds does it switch to aerobic utilization of carbohydrates and fatty acids to supply ATP, as is generally the case for contracting muscles (Hargreaves and Spriet, 2020). The tonic muscle provides ATP for a prolonged period of performance and therefore preferably utilizes beta-oxidation to generate ATP. This is reasonable, as carbohydrate oxidation has a higher rate of ATP synthesis than fatty acid oxidation; the latter, however, can obtain more energy per molecule in the long term (overall ATP generation of 130 ATP *vs* 36 ATP per molecule; Hargreaves and Spriet, 2020). Fatty acids are used as the predominant substrate, for example during fasting and hypoglycemia, to provide energy via beta-oxidation in the muscle (Longo et al., 2016; Talley and Mohiuddin, 2023). It is therefore quite conceivable that *P. maximus* make increased use of beta-oxidation for energy supply in times of increased energy requirements such as under OW and exercise in the tonic muscle. This view is supported by the increase of carnitine in the phasic and tonic muscle in comparison to control (see Figure 4), albeit not significant, and the high concentration of methionine in the tonic muscle (Table 1). The higher carnitine concentration may allow a higher shuttle of fatty acids into tonic muscle mitochondria and thus an increased beta-oxidation (see above). The connection to sodium and methionine in the network of L-arginine might confirm this, since sodium is essential for the transport of carnitine across membranes (Talley and Mohiuddin, 2023) and methionine, from which carnitine can be synthesized endogenously (Longo et al., 2016). The link to CO_2 might indicate the importance of beta-oxidation for energy provision in muscles under unfavorable conditions (Longo et al., 2016), such as OA, OW and the combination of both.

The decreased levels of proteinogenic amino acids in both warming groups in the adductor muscle (Figure 2) might indicate a switch to the use of proteins for energy production as also suggested by (Götze et al., 2020), since carbohydrates are limited. An ongoing depletion of carbohydrates during prolonged exercise together with lowered oxygen levels in the haemolymph would lead to a decrease in power output (Hargreaves and Spriet, 2020). Indeed, a decreased clapping force was observed in the warming groups, while the number of claps remained the same compared to control (Schalkhausser et al., 2014). Since the carbohydrate reserves in the phasic muscle of the warming groups (OW & OWA), just like the PLA level (Bock et al., 2019), are already reduced due to the higher energetic costs in the warmth, there is an earlier reliance on the tonic muscle during swimming (Pérez et al., 2008). Beta-oxidation, with its higher capacity but lower power output, can thus maintain the number of claps, but at the expense of a reduced clapping force. In addition, beta-oxidation can provide the energy during recovery from exercise in mammals (Hargreaves and Spriet, 2020), but the processes and pathways that metabolize fatty acids to provide ATP are much slower than carbohydrate pathways. If one assumes that due to the lower P_eO_2 levels in the haemolymph, the energy is rather provided by beta-oxidation and octopine is formed from L-arginine (Grieshaber, 1978), it becomes understandable why recovery after fatigue was prolonged in the scallops of the warming groups (OW & OWA) compared to control. To summarize, if the tonic muscle compensates for the reduced performance of the phasic muscle and if beta-oxidation is favored for energy production under systemic hypoxemia during OW and OWA, the observed organismic limitations of the scallops from the previous

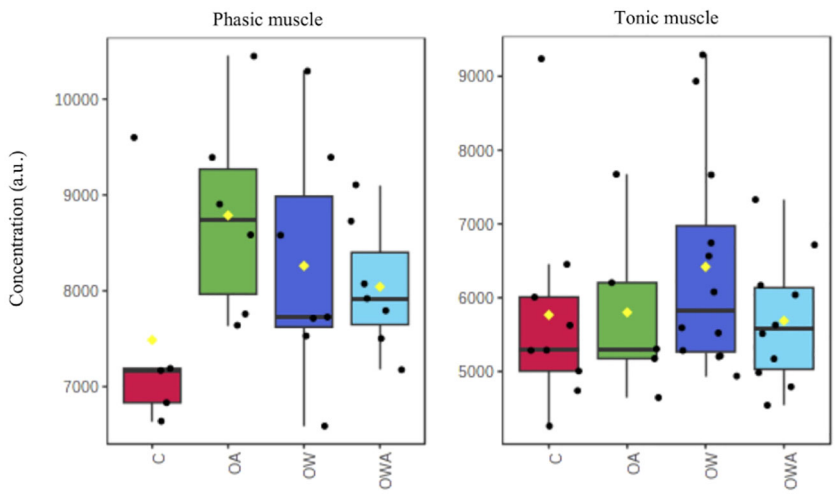

FIGURE 4
Changes in carnitine concentrations in phasic (left) and tonic muscle (right) tissue between treatments. Note, the differences are not significant.

studies can be explained. However, additional studies on the transport and flow of substrates fueling ATP production in the two muscle types will be needed to test this. Future experiments must show to what extent the energy is distributed in the body of the scallops under changing environmental conditions and whether additional energy requirements such as gonadal development will lead to a reduction in the energy budget and/or changes in energy distribution. This could have further consequences for the performance level of scallops from coastal and intertidal areas (Feidantsis et al., 2020).

5 Conclusions

The presented study of metabolite profiles of individual tissues showed distinct metabolite profiles, which are adjusted to the specific tasks of the organs. After long-term incubation under OA, OW and their combination OWA, metabolic profiles were largely different within the adductor muscle, between phasic and tonic muscles. These changes in metabolite concentrations mainly involved metabolic adjustments essential for the increased energy demand induced by warming and the associated hypoxemia. The proposed model for the interaction of the two muscle types of the adductor muscle can explain the observed performance limitations of scallops under OW and OWA. The tonic muscle apparently pursues a different strategy for energy provision than the phasic muscle, which for strong clapping essentially relies on PLA hydrolysis. This interplay is shifted to lower performance rates by organismic changes such as oxygen reduction in the hemolymph, especially under warming, and thus leads to the observed limitations in the swimming behavior of *P. maximus*.

Data availability statement

The datasets presented in this study can be found in online repositories. The names of the repository/repositories and accession number(s) can be found below: https://doi.pangaea.de/10.1594/PANGAEA.843533.

Ethics statement

Ethical approval was not required for the study involving animals in accordance with the local legislation and institutional requirements because an ethical approval by the German Council for Animal Care was not required for this study with bivalves.

Author contributions

CB: Conceptualization, Data curation, Formal analysis, Methodology, Validation, Visualization, Writing – original draft, Writing – review & editing. SG: Writing – review & editing. HP: Writing – review & editing. GL: Data curation, Validation, Visualization, Writing – review & editing.

Funding

The author(s) declare financial support was received for the research, authorship, and/or publication of this article. The project was supported by the research program "Changing Earth—Sustaining our Future" in the program-oriented funding periods (PoF IV subtopic 6.2—Adaptation of marine life: from genes to ecosystems) of the Helmholtz Association and is a contribution to the BMBF-funded project "Biological Impacts of Ocean Acidification" (BIOACID, FKZ 03F0608B) and the DFG funded project "TERSANE2".

Acknowledgments

We appreciate the technical assistance of Burgel Schalkhausser, F. Véliz Moraleda, Annette Tillman, Felicitas Wermter and Rolf Wittig. Furthermore, we would like to thank the biological technical assistant trainees from the AWI: Lara Holst, Caroline Otten, Imke Lüdecke, Sean Segert and Anna Klitsch for assisting during sample processing.

Conflict of interest

The authors declare that the research was conducted in the absence of any commercial or financial relationships that could be construed as a potential conflict of interest.

Publisher's note

Supplementary material

The Supplementary Material for this article can be found online at: https://www.frontiersin.org/articles/10.3389/fevo.2024.1347160/full#supplementary-material

References

Anthoni, U., Christophersen, C., Hougaard, L., and Nielsen, P. H. (1991). Quaternary ammonium compounds in the biosphere—An example of a versatile adaptive strategy. *Comp. Biochem. Physiol. B. Comp. Biochem.* 99, 1–18. doi: 10.1016/0305-0491(91)90002-U

Baag, S., and Mandal, S. (2022). Combined effects of ocean warming and acidification on marine fish and shellfish: A molecule to ecosystem perspective. *Sci. Total Environ.* 802, 149807. doi: 10.1016/j.scitotenv.2021.149807

Barbe, J., Roussel, D., and Voituron, Y. (2023). Effect of physiological hyperthermia on mitochondrial fuel selection in skeletal muscle of birds and mammals. *J. Therm. Biol.* 117, 103719. doi: 10.1016/j.jtherbio.2023.103719

Bechara, E. J. H., Dutra, F., Cardoso, V. E. S., Sartori, A., Olympio, K. P. K., Penatti, C. A. A., et al. (2007). The dual face of endogenous alpha-aminoketones: pro-oxidizing metabolic weapons. *Comp. Biochem. Physiol. C Toxicol. Pharmacol.* 146, 88–110. doi: 10.1016/j.cbpc.2006.07.004

Bindoff, N. L., Cheung, W. W. L., Kairo, J. G., Arístegui, J., Guinder, V. A., Hallberg, R., et al. (2019). "Changing ocean, marine ecosystems, and dependent communities," in *IPCC Special Report on the Ocean and Cryosphere in a Changing Climate*. Eds. H.-O. Pörtner, D. C. Roberts, V. Masson-Delmotte, P. Zhai, M. Tignor, E. Poloczanska, et al (Cambridge University Press, Cambridge, UK and New York, NY, USA), 447–587. doi: 10.1017/9781009157964.007

Bock, C., Wermter, F. C., Schalkhausser, B., Blicher, M. E., Pörtner, H. O., Lannig, G., et al. (2019). *In vivo* ^{31}P-MRS of muscle bioenergetics in marine invertebrates: Future ocean limits scallops' performance. *Magn. Reson. Imag.* 61, 239–246. doi: 10.1016/j.mri.2019.06.003

Byrne, M., and Przeslawski, R. (2013). Multistressor impacts of warming and acidification of the ocean on marine invertebrates' life histories. *Integr. Comp. Biol.* 53, 582–596. doi: 10.1093/icb/ict049

Cappello, T., Giannetto, A., Parrino, V., Maisano, M., Oliva, S., De Marco, G., et al. (2018). Baseline levels of metabolites in different tissues of mussel Mytilus galloprovincialis (Bivalvia: Mytilidae). *Comp. Biochem. Physiol. Part D Genomics Proteom.* 26, 32–39. doi: 10.1016/j.cbd.2018.03.005

Chantler, P. D. (2006). Scallop adductor muscles: structure and function. *Dev. Aquac. Fish Sci.* 35, 229–316. doi: 10.1016/S0167-9309(06)80031-1

Chong, J., Wishart, D. S., and Xia, J. (2019). Using MetaboAnalyst 4.0 for comprehensive and integrative metabolomics data analysis. *Curr. Protoc. Bioinf.* 68, e86. doi: 10.1002/cpbi.86

Clark, M. S. (2020). Molecular mechanisms of biomineralization in marine invertebrates. *J. Exp. Biol.* 223, jeb206961. doi: 10.1242/jeb.206961

Diez, V., Traikov, S., Schmeisser, K., Adhikari, A. K. D., and Kurzchalia, T. V. (2021). Glycolate combats massive oxidative stress by restoring redox potential in Caenorhabditis elegans. *Commun. Biol.* 4, 151. doi: 10.1038/s42003-021-01669-2

Doney, S. C., Ruckelshaus, M., Duffy, J. E., Barry, J. P., Chan, F., English, C. A., et al. (2012). Climate change impacts on marine ecosystems. *Ann. Rev. Mar. Sci.* 4, 11–37. doi: 10.1146/annurev-marine-041911-111611

Feidantsis, K., Giantsis, I. A., Vratsistas, A., Makri, S., Pappa, A. Z., Drosopoulou, E., et al. (2020). Correlation between intermediary metabolism, Hsp gene expression and oxidative stress related proteins in long-term thermal stressed Mytilus galloprovincialis. *Am. J. Physiol.: Regul. Integr. Comp. Physiol.* 319, R264–R281. doi: 10.1152/ajpregu.00066.2020

Fiehn, O. (2002). Metabolomics–the link between genotypes and phenotypes. *Plant Mol. Biol.* 48, 155–171. doi: 10.1023/A:1013713905833

Findlay, H. S. , Artoli, Y., Birchenough, S. N. R., Hartman, S., León, P., and Stiasny, M. (2022). Climate change impacts on ocean acidification relevant to the UK and Ireland. *MCCIP Sci. Rev.* 24. doi: 10.14465/2022.reu03.oac

Frizzo, R., Bortoletto, E., Riello, T., Leanza, L., Schievano, E., Venier, P., et al. (2021). NMR Metabolite Profiles of the Bivalve Mollusc *Mytilus galloprovincialis* Before and After Immune Stimulation With Vibrio splendidus. *Front. Mol. Biosci.* 8. doi: 10.3389/fmolb.2021.686770

Gattuso, J. P., Magnan, A. K., Bopp, L., Cheung, W. W. L., Duarte, C. M., Hinkel, J., et al. (2018). Ocean Solutions to Address Climate Change and Its Effects on Marine Ecosystems. *Front. Mar. Sci.* 5. doi: 10.3389/fmars.2018.00337

Gazeau, F., Alliouane, S., Bock, C., Bramanti, L., López Correa, M., Gentile, M., et al. (2014). Impact of ocean acidification and warming on the Mediterranean mussel (Mytilus galloprovincialis). *Front. Mar. Sci.* 1. doi: 10.3389/fmars.2014.00062

Georgoulis, I., Bock, C., Lannig, G., Pörtner, H. O., Feidantsis, K., Giantsis, I. A., et al. (2022). Metabolic remodeling caused by heat hardening in the Mediterranean mussel Mytilus galloprovincialis. *J. Exp. Biol.* 225, jeb244795. doi: 10.1242/jeb.244795

Götze, S., Bock, C., Eymann, C., Lannig, G., Steffen, J. B. M., and Pörtner, H. O. (2020). Single and combined effects of the "Deadly trio" hypoxia, hypercapnia and warming on the cellular metabolism of the great scallop *Pecten maximus*. *Comp. Biochem. Physiol. B Biochem. Mol. Biol.* 243-244, 110438. doi: 10.1016/j.cbpb.2020.110438

Grieshaber, M. (1978). Breakdown and formation of high-energy phosphates and octopine in the adductor muscle of the scallop, Chlamys opercularis (L.), during escape swimming and recovery. *J. Comp. Physiol. B* 126, 269–276. doi: 10.1007/BF00688937

Guderley, H., and Pörtner, H. O. (2010). Metabolic power budgeting and adaptive strategies in zoology: examples from scallops and fish. *Can. J. Zool.* 88, 753–763. doi: 10.1139/Z10-039

Guderley, H. E., Rojas, F. M., and Nusetti, O. A. (1995). Metabolic specialization of mitochondria from scallop phasic muscles. *Mar. Biol.* 122, 409–416. doi: 10.1007/BF00350873

Guderley, H. E., and Tremblay, I. (2016). "Swimming in scallops," in *Developments in Aquaculture and Fisheries Science*, vol. Vol. 40. (Elsevier, Amsterdam), 535–566. doi: 10.1016/B978-0-444-62710-0.00012-2

Guderley, H., Labbé-Giguere, S., Janssoone, X., Bourgeois, M., Pérez, H. M., and Tremblay, I. (2009). Thermal sensitivity of escape response performance by the scallop Placopecten magellanicus: Impact of environmental history. *J. Exp. Mar. Biol. Ecol.* 377, 113–119. doi: 10.1016/j.jembe.2009.07.024

Haider, F., Sokolov, E. P., Timm, S., Hagemann, M., Blanco Rayón, E., Marigómez, I., et al. (2019). Interactive effects of osmotic stress and burrowing activity on protein metabolism and muscle capacity in the soft shell clam Mya arenaria. *Comp. Biochem. Physiol. A Mol. Integr. Physiol.* 228, 81–93. doi: 10.1016/j.cbpa.2018.10.022

Hargreaves, M., and Spriet, L. L. (2020). Skeletal muscle energy metabolism during exercise. *Nat. Metabol.* 2, 817–828. doi: 10.1038/s42255-020-0251-4

Harvey, B. P., Gwynn-Jones, D., and Moore, P. J. (2013). Meta-analysis reveals complex marine biological responses to the interactive effects of ocean acidification and warming. *Ecol. Evol.* 3, 1016–1030. doi: 10.1002/ece3.516

Heinemann, A., Fietzke, J., Melzner, F., Böhm, F., Thomsen, J., Garbe-Schönberg, D., et al. (2012). Conditions of Mytilus edulis extracellular body fluids and shell composition in a pH-treatment experiment: Acid-base status, trace elements and δ11B. *Geochem. Geophys. Geosys.* 13 (1). doi: 10.1029/2011GC003790

Heise, K., Puntarulo, S., Pörtner, H. O., and Abele, D. (2003). Production of reactive oxygen species by isolated mitochondria of the Antarctic bivalve Laternula elliptica (King and Broderip) under heat stress. *Comp. Biochem. Physiol. C* 134, 79–90. doi: 10.1016/S1532-0456(02)00212-0

Hulbert, A. J., and Else, P. L. (1999). Membranes as possible pacemakers of metabolism. *J. Theor. Biol.* 199, 257–274. doi: 10.1006/jtbi.1999.0955

Ivanina, A. V., and Sokolova, I. M. (2016). Effects of intermittent hypoxia on oxidative stress and protein degradation in molluscan mitochondria. *J. Exp. Biol.* 219, 3794–3802. doi: 10.1242/jeb.146209

Jiang, Y., Jiao, H., Sun, P., Yin, F., and Tang, B. (2020). Metabolic response of *Scapharca subcrenata* to heat stress using GC/MS-based metabolomics. *PeerJ* 8, e8445. doi: 10.7717/peerj.8445

Kamp, G. (1993). "Intracellular reactions controlling environmental anaerobiosis in the marine annelid Arenicola marina, a fresh look at old pathways," in *Surviving hypoxia: mechanisms of control and adaptation*. Eds. P. W. Hochachka, P. L. Lutz, T. Sick, M. Rosental and G. van den Thillart (CRC, Boca Raton), pp 5 ± 17.

Landrigan, P. J., Stegeman, J. J., Fleming, L. E., Allemand, D., Anderson, D. M., Backer, L. C., et al. (2020). Human health and ocean pollution. *Ann. Glob. Health* 86, 151. doi: 10.5334/aogh.2831

Lannig, G., Eilers, S., Pörtner, H. O., Sokolova, I. M., and Bock, C. (2010). Impact of Ocean Acidification on Energy Metabolism of Oyster, Crassostrea gigas—Changes in Metabolic Pathways and Thermal Response. *Mar. Drugs* 8 (8), 2318–2339. doi: 10.3390/md8082318

Lesser, M. (2016). Climate change stressors cause metabolic depression in the blue mussel, Mytilus edulis, from the Gulf of Maine. *Limnol. Ocean.* 61, 1705–1717. doi: 10.1002/lno.10326

Leung, J. Y. S., Zhang, S., and Connell, S. D. (2022). Is Ocean Acidification Really a Threat to Marine Calcifiers?A Systematic Review and Meta-Analysis of 980+ Studies Spanning Two Decades. *Small* 18 (35), 2107407. doi: 10.1002/smll.202107407

Liao, H., Yang, Z., Dou, Z., Sun, F., Kou, S., Zhang, Z., et al. (2019). Impact of ocean acidification on the energy metabolism and antioxidant responses of the Yesso scallop (Patinopecten yessoensis). *Front. Physiol.* 9, 1967. doi: 10.3389/fphys.2018.01967

Licker, R., Ekwurzel, B., Doney, S. C., Cooley, S. R., Lima, I. D., Heede, R., et al. (2019). Attributing ocean acidification to major carbon producers. *Environ. Res. Lett.* 14, 124060. doi: 10.1088/1748-9326/ab5abc

Liu, W., and He, M. (2012). Effects of ocean acidification on the metabolic rates of three species of bivalve from southern coast of China. *Chin. J. Ocean. Limnol.* 30, 206–211. doi: 10.1007/s00343-012-1067-1

Longo, N., Frigeni, M., and Pasquali, M. (2016). Carnitine transport and fatty acid oxidation. *Biochim. Biophys. Acta* 1863, 2422–2435. doi: 10.1016/j.bbamcr.2016.01.023

Martínez, Y., Li, X., Liu, G., Bin, P., Yan, W., Más, D., et al. (2017). The role of methionine on metabolism, oxidative stress, and diseases. *Amino Acids* 49, 2091–2098. doi: 10.1007/s00726-017-2494-2

Mathur, M., and Kamal, R. (2012). Studies on trigonelline from Moringa oleifera and its *in vitro* regulation by feeding precursor in cell cultures. *Rev. Bras. Farmacogn.* 22, 994–100. doi: 10.1590/S0102-695X2012005000041

Matoo, O. B., Lannig, G., Bock, C., and Sokolova, I. M. (2021). Temperature but not ocean acidification affects energy metabolism and enzyme activities in the blue mussel, Mytilus edulis. *Ecol. Evol.* 00, 1–14. doi: 10.1002/ece3.7289

Melzner, F., Mark, F. C., Seibel, B. A., and Tomanek, L. (2020). Ocean acidification and coastal marine invertebrates: tracking CO_2 effects from seawater to the cell. *Ann. Rev. Mar. Sci.* 12, 499–523. doi: 10.1146/annurev-marine-010419-010658

Morabito, R., Marino, A., Lauf, P. K., Adragna, N. C., and La Spada, G. (2013). Sea water acidification affects osmotic swelling, regulatory volume decrease and discharge in nematocytes of the jellyfish Pelagia noctiluca. *Cell Physiol. Biochem.* 32, 77–85. doi: 10.1159/000356629

Moreno, R. I., Zambelli, V. O., Picolo, G., Cury, Y., Morandini, A. C., Marques, A. C., et al. (2022). Caspase-1 and Cathepsin B Inhibitors from Marine Invertebrates, Aiming at a Reduction in Neuroinflammation. *Mar. Drugs* 20, 614. doi: 10.3390/md20100614

Nguyen, P. V., Marin, L., and Atwood, H. L. (1997). Synaptic physiology and mitochondrial function in crayfish tonic and phasic motor neurons. *J. Neurophysiol.* 78, 281–294. doi: 10.1152/jn.1997.78.1.281

Pérez, H. M., Janssoone, X., and Guderley, H. (2008). Tonic contractions allow metabolic recuperation of the adductor muscle during escape responses of giant scallop Placopecten magellanicus. *J. Exp. Mar. Biol. Ecol.* 360, 78–84. doi: 10.1016/j.jembe.2008.04.006

Pernet, F., Tremblay, R., Comeau, L., and Guderley, H. (2007). Temperature adaptation in two bivalve species from different thermal habitats: energetics and remodelling of membrane lipids. *J. Exp. Biol.* 210, 2999–3014. doi: 10.1242/jeb.006007

Pernet, F., Tremblay, R., Gionet, C., and Landry, T. (2006). Lipid remodeling in wild and selectively bred hard clams at low temperatures in relation to genetic and physiological parameters. *J. Exp. Biol.* 209, 4663–4675. doi: 10.1242/jeb.02581

Pinsky, M. L., Eikeset, A. M., McCauley, D. J., Payne, J. L., and Sunday, J. M. (2019). Greater vulnerability to warming of marine versus terrestrial ectotherms. *Nature* 569, 108–111. doi: 10.1038/s41586-019-1132-4

Podbielski, I., Bock, C., Lenz, M., and Melzner, F. (2016). Using the Critical Salinity (Scrit) Concept to Predict Invasion Potential of the Anemone Diadumene Lineata in the Baltic Sea. *Mar. Biol.* 163, 227. doi: 10.1007/ s00227-016-2989-5

Pörtner, H. O. (2002). Climate variations and the physiological basis of temperature dependent biogeography: systemic to molecular hierarchy of thermal tolerance in animals. *Comp. Biochem. Physiol. A. Mol. Int. Physiol.* 132, 739–761. doi: 10.1016/s1095-6433(02)00045-4

Pörtner, H. O., Bock, C., and Mark, F. C. (2017). Oxygen-and capacity-limited thermal tolerance: bridging ecology and physiology. *J. Exp. Biol.* 220, 2685–2696. doi: 10.1242/jeb.134585

Pörtner, H.-O., Karl, D., Boyd, P., Cheung, W., Lluch-Cota, S. E., Nojiri, Y., et al. (2014). "Ocean systems," in *Climate Change 2014: Impacts, Adaptation, and Vulnerability. Part A: Global and Sectoral Aspects. Contribution of Working Group II to the Fifth Assessment Report of the Intergovernmental Panel on Climate Change*. Eds. C. B. Field, V. R. Barros, D. J. Dokken, K. J. Mach, M. D. Mastrandrea, T. F. Bilir, et al (Cambridge University Press, New York, NY), 411–484.

Pörtner, H. O., and Lannig, G. (2009). "Oxygen and capacity limited thermal tolerance," in *Fish Physiology: Hypoxia*, vol. Vol 27 . Eds. J. G. Richards, A. P. Farrell and C. J. Brauner (Burlington, MA: Academic Press, Elsevier Inc.), 143–191.

Poulin, R. X., Lavoie, S., Siegel, K., Gaul, D. A., Weissburg, M. J., and Kubanek, J. (2018). Chemical encoding of risk perception and predator detection among estuarine invertebrates. *Proc. Natl. Acad. Sci. U. S. A.* 115, 662–667. doi: 10.1073/pnas.1713901115

Rebelein, A., Pörtner, H. O., and Bock, C. (2018). Untargeted metabolic profiling reveals distinct patterns of thermal sensitivity in two related notothenioids. *Comp. Biochem. Physiol. A* 217, 43–54. doi: 10.1016/j.cbpa.2017.12.012

Richards, R. G., Davidson, A. T., Meynecke, J. O., Beattie, K., Hernaman, V., Lynam, T., et al. (2015). Effects and mitigations of ocean acidification on wild and aquaculture scallop and prawn fisheries in Queensland. *Aus. Fish. Res.* 161, 42–56. doi: 10.1016/j.fishres.2014.06.013

Rocha, M. E., Bandy, B., Costa, C. A., de Barros, M. P., Pinto, A. M., and Bechara, E. J. (2000). Iron mobilization by succinylacetone methyl ester in rats. A model study for hereditary tyrosinemia and porphyrias characterized by 5-aminolevulinic acid overload. *Free Radic. Res.* 32, 343–353. doi: 10.1080/10715760000300341

Schalkhausser, B., Bock, C., Pörtner, H.-O., and Lannig, G. (2014). Escape performance of temperate king scallop, *Pecten maximus* under ocean warming and acidification. *Mar. Biol.* 161, 2819–2829. doi: 10.1007/s00227-014-2548-x

Schalkhausser, B., Bock, C., Stemmer, K., Brey, T., Pörtner, H.-O., and Lannig, G. (2013). Impact of ocean acidification on escape performance of the king scallop, *Pecten maximus*, from Norway. *Mar. Biol.* 160, 1995–2006. doi: 10.1007/s00227-012-2057-8

Schmidt, M., Windisch, H. S., Ludwichowski, K. U., Seegert, S. L. L., Pörtner, H. O., Storch, D., et al. (2017). Differences in neurochemical profiles of two gadid species under ocean warming and acidification. *Front. Zool.* 14. doi: 10.1186/s12983- 017-0238-5

Sokolova, I. M. (2023). Ectotherm mitochondrial economy and responses to global warming. *Acta Physiol. (Oxf).* 237, e13950. doi: 10.1111/apha.13950

Sokolova, I. M., Bock, C., and Pörtner, H. O. (2000). Resistance to freshwater exposure in White Sea Littorina spp. I: Anaerobic metabolism and energetics. *J. Comp. Physiol. B.* 170, 91–103. doi: 10.1007/s003600050264

Sokolova, I. M., Frederich, M., Bagwe, R., Lannig, G., and Sukhotin, A. A. (2012). Energy homeostasis as an integrative tool for assessing limits of environmental stress tolerance in aquatic invertebrates. *Mar. Environ. Res.* 79, 1–15. doi: 10.1016/j.marenvres.2012.04.003

Song, J., Liu, B., and Wang, C. (2022). Metabolomic and Transcriptomic Responses of *Argopecten irradians concentricus* to Thermal Stresses. *Front. Mar. Sci*. 9. doi: 10.3389/fmars.2022.818083

Stapp, L., Parker, L., O'Connor, W. A., Bock, C., Ross, P. M., Pörtner, H. O., et al. (2018). Sensitivity to ocean acidification differs between populations of the Sydney rock oyster: role of filtration and ion-regulatory capacities. *Mar. Environ. Res.* 135, 103–113. doi: 10.1016/j.marenvres.2017.12.017

Stapp, L., Thomsen, J., Schade, H., Bock, C., Melzner, F., et al. (2017). Intra-population variability of ocean acidification impacts on the physiology of Baltic blue mussels (Mytilus edulis): integrating tissue and organism response. *J. Comp. Physiol. B Biochem. Syst. Environ. Physiol.* 187, 529–543. doi: 10.1007/ s00360-016-1053-6

Sukhotin, A., Fokina, N., Ruokolainen, T., Bock, C., Pörtner, H. O., and Lannig, G. (2017). Does the membrane pacemaker theory of metabolism explain the size dependence of metabolic rate in marine mussels? *J. Exp. Biol.* 220, 1423–1434. doi: 10.1242/jeb.147108

Sun, X., Liu, Z., Wu, B., Zhou, L., Wang, Q., Wu, W., et al. (2018). Differences between fast and slow muscles in scallops revealed through proteomics and transcriptomics. *BMC Genomics* 19, 377. doi: 10.1186/s12864-018-4770-2

Talley, J. T., and Mohiuddin, S. S. (2023). "Biochemistry, fatty acid oxidation," in *StatPearls* (StatPearls Publishing, Treasure Island (FL). Available at: https://www.ncbi.nlm.nih.gov/books/NBK556002/.

Thomsen, J., and Melzner, F. (2010). Moderate seawater acidification does not elicit long-term metabolic depression in the blue mussel Mytilus edulis. *Mar. Biol.* 157, 2667–2676. doi: 10.1007/s00227-010-1527-0

Tripp-Valdez, M. A., Bock, C., Lucassen, M., Lluch-Cota, S. E., Sicard, M. T., Lannig, G., et al. (2017). Metabolic response and thermal tolerance of green abalone ju- veniles (Haliotis fulgens: Gastropoda) under acute hypoxia and hypercapnia. *J. Exp. Mar. Biol. Ecol.* 497, 11–18. doi: 10.1016/j.jembe.2017.09.002

Tremblay, I., and Guderley, H. E. (2014). Scallops show that muscle metabolic capacities reflect locomotor style and morphology. *Physiol. Biochem. Zool.* 87, 231–244. doi: 10.1086/674107

Tremblay, I., Guderley, H. E., and Himmelman, J. H. (2012). Swimming away or clamming up: the use of phasic and tonic adductor muscles during escape responses varies with shell morphology in scallops. *J. Exp. Biol.* 215, 4131–4143. doi: 10.1242/jeb.075986

Viant, M. R. (2008). Environmental metabolomics using ^{1}H -NMR spectroscopy. *Methods Mol. Biol.* 410, 137–150. doi: 10.1007/978-1-59745-548-0_9

Wishart, D. S. (2019). Metabolomics for investigating physiological and pathophysiological processes. *Physiol. Rev.* 99, 1819–1875. doi: 10.1152/physrev.00035.2018

Wishart, D. S., Cheng, L. L., Copié, V., Edison, A. S., Eghbalnia, H. R., Hoch, J. C., et al. (2022). NMR and metabolomics—A roadmap for the future. *Metabolites* 12, 678. doi: 10.3390/metabo12080678

Yarra, T., Gharbi, K., Blaxter, M., Peck, L. S., and Clark, M. S. (2016). Characterization of the mantle transcriptome in bivalves: *Pecten maximus*, Mytilus edulis and Crassostrea gigas. *Mar. Genomics* 27, 9–15. doi: 10.1016/j.margen.2016.04.003

Yarra, T., Ramesh, K., Blaxter, M., Hüning, A., Melzner, F., and Clark, M. S. (2021). Transcriptomic analysis of shell repair and biomineralization in the blue mussel, Mytilus edulis. *BMC Genomics* 22, 437. doi: 10.1186/s12864-021-07751-7

Zhao, X., Guo, C., Han, Y., Che, Z., Wang, Y., Wang, X., et al. (2017). Ocean acidification decreases mussel byssal attachment strength and induces molecular byssal responses. *Mar. Ecol. Prog. Ser.* 565, 67–77. doi: 10.3354/meps11992

Zhao, L., Shirai, K., Tanaka, K., Milano, S., Higuchi, T., Murakami-Sugihara, N., et al. (2020). A review of transgenerational effects of ocean acidification on marine bivalves and their implications for sclerochronology. *Estuar. Coast. Shelf. Sci.* 235, 106620. doi: 10.1016/j.ecss.2020.106620

Zeebe, R. E. (2012). History of seawater carbonate chemistry, atmospheric CO_2, and ocean acidification. *Annu. Rev. Earth Planet. Sci.* 40, 141–165. doi: 10.1146/annurev-earth-042711-105521

Zhou, C., Xu, L., Song, H., Feng, J., Hu, Z., Yang, M., et al. (2023). Examination of the regulation of energy metabolism, antioxidant response, and ammonia detoxification in hard clam, Mercenaria mercenaria, under hypersalinity stress. *Aquaculture* 563, 738916. doi: 10.1016/j.aquaculture.2022.738916

Zhukova, N. V. (1986). Biosynthesis of non-methylene-interrupted dienoic fatty acids from [14C] acetate in molluscs. *Biochim. Biophys. Acta (BBA) Lipids Lipid Metab.* 878, 131–133. doi: 10.1016/0005-2760(86)90351-6

Frontiers in Marine Science

Explores ocean-based solutions for emerging global challenges

The third most-cited marine and freshwater biology journal, advancing our understanding of marine systems and addressing global challenges including overfishing, pollution, and climate change.

Discover the latest Research Topics

See more →

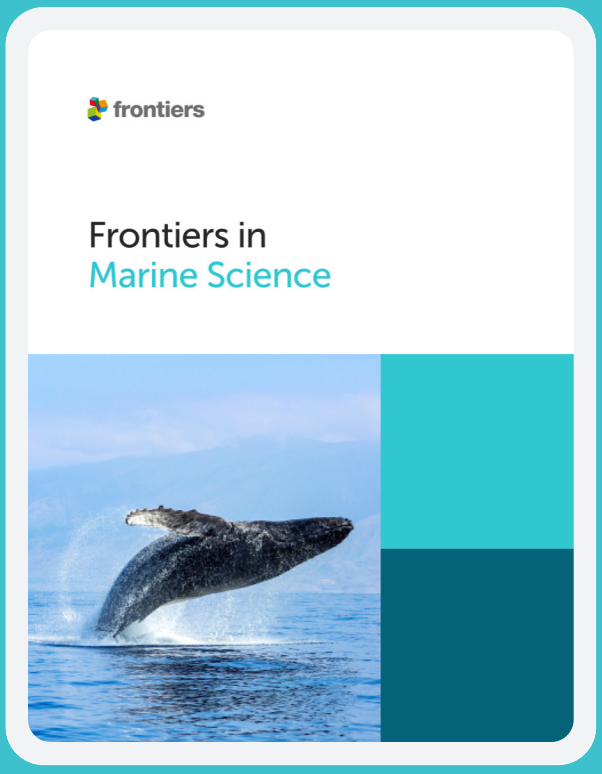

Frontiers

Avenue du Tribunal-Fédéral 34
1005 Lausanne, Switzerland
frontiersin.org

Contact us

+41 (0)21 510 17 00
frontiersin.org/about/contact